K.N. Mukhin

EXPERIMENTAL NUCLEAR PHYSICS

Volume 1

PHYSICS OF ATOMIC NUCLEUS

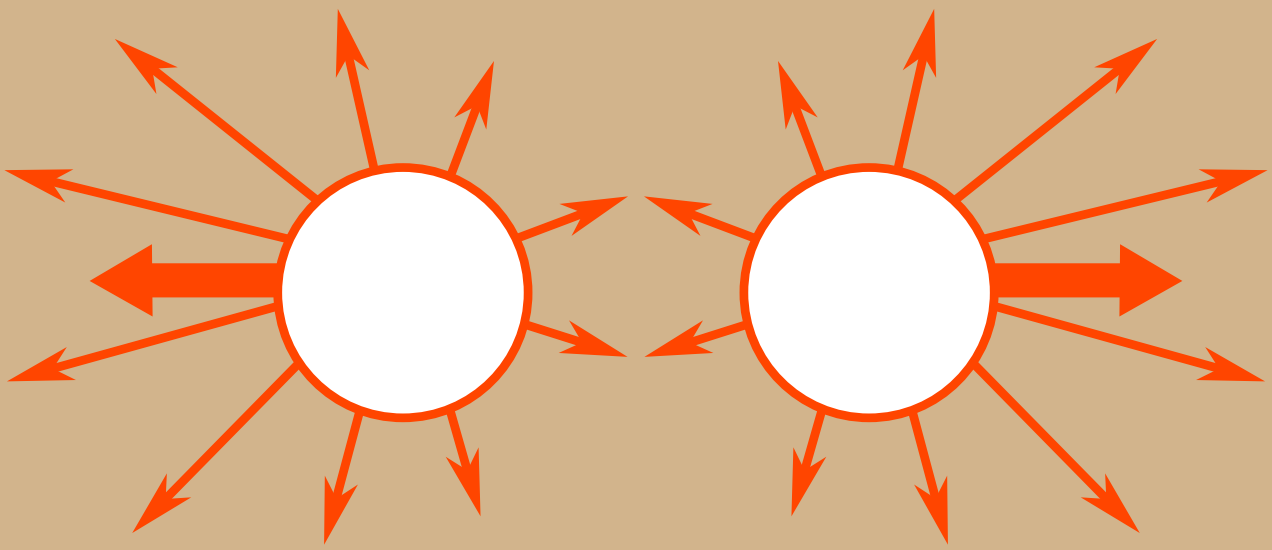

MIR PUBLISHERS MOSCOW

EXPERIMENTAL NUCLEAR PHYSICS

PHYSICS OF ATOMIC NUCLEUS

К. Н. Мухин

ЭКСПЕРИМЕНТАЛЬНАЯ ЯДЕРНАЯ ФИЗИКА

ТОМ I

ФИЗИКА АТОМНОГО ЯДРА

Энергоатомиздат Москва

K.N.Mukhin

EXPERIMENTAL NUCLEAR PHYSICS

Volume I

PHYSICS OF ATOMIC NUCLEUS

Mir Publishers
Moscow

Translated from Russian by
Ram S. Wadhwa, Ph.D.

First published 1987
Revised from the 1983 Russian edition

На английском языке

Printed in the Union of Soviet Socialist Republics

© Атомиздат, 1974
© Энергоатомиздат, 1983
© English translation, Mir Publishers, 1987

Contents

Preface to the English Edition 11
Preface to the Fourth Russian Edition 12
Introduction 15

PART ONE

Properties of Nuclei and Radioactive Radiation 26

Chapter 1. Properties of Stable Nuclei and Nuclear Forces 27

1.1. Mass Number A and Electric Charge Z of the Atomic Nucleus 27
1.2. Nuclear and Nucleonic Mass 29
1.2.1. Mass and Energy. Units of Measurement 29
1.2.2. Methods of Measuring the Nuclear Mass 32
1.2.3. The Mass of the Neutron 39
1.3. Nuclear Binding Energy of All Nucleons. Nuclear Stability 41
1.3.1. Binding Energy ε per Nucleon. Energy Surface 42
1.3.2. Beta-stable Nuclei and Properties of Nuclear Forces 44
1.3.3. Other Types of Nuclear Binding Energy. Separation Energy for a Nucleon 51
1.3.4. Nucleon-stable Nuclei and Properties of Nuclear Forces 53
1.4. Nuclear Radius 62
1.4.1. Estimation of the Radius of α-radioactive Nuclei from Their Lifetimes 62
1.4.2. Analysis of the Semiempirical Formula. Beta Decay of Mirror Nuclei 63
1.4.3. Investigation of Scattering of Fast Neutrons by Nuclei 64
1.4.4. Investigation of X-rays Emitted by Muonic Atoms 66
1.4.5. Measurement of Scattering of Fast Electrons by Nuclei 67
1.4.6. Comparison of Results 67
1.5. Spin and Magnetic Moment of Nucleons and Nuclei 69
1.5.1. Historical Background 69
1.5.2. Investigation of Hyperfine Structure 70
1.5.3. Methods of Determining Spin and Nuclear Magnetic Moment by Using External Fields 74
1.5.4. Determination of the Magnetic Moment of the Neutron 83
1.5.5. Results of Measurements of Spins and Magnetic Moments. Schmidt's One-nucleon Model 87
1.6. Parity. Law of Conservation of Parity 95
1.7. Quadrupole Electric Moment 101
1.8. Isotopic Spin 109
1.9. A Brief Resumé of Chapter 1 117

Chapter 2. Models of the Atomic Nucleus 120
2.1. The Liquid Drop Model 121
2.1.1. Weizsäcker's Semiempirical Formula for the Binding Energy and Mass of the Nucleus 122
2.1.2. Applicability of the Liquid Drop Model 125
2.1.3. Hypothetical Superdense Nuclei 129
2.2. Independent Particle Model 132
2.2.1. Drawbacks of the Liquid Drop Model 132
2.2.2 Nuclear Fermi Gas 133
2.3. Shell Model 135
2.3.1. Experimental Foundations of the Shell Model 136
2.3.2. Construction of the Shell Model 138
2.3.3. Experimental Consequences of the Shell Model and Its Applicability 145
2.3.4. Drawbacks of the Shell Model 147
2.4. Generalized Model of the Nucleus 149
2.4.1. Single-particle States in a Nonspherical Well 150
2.4.2. Rotational States 152
2.4.3. Vibrational Levels 154
2.4.4. Oscillations of All Nucleons in the Nucleus. Giant Resonances 155
2.4.5. Applicability of the Generalized Model 159
2.5. Superfluid Nucleus Model 160
2.6. A Brief Resumé of Chapter 2 163

Chapter 3. Radioactive Nuclear Transformations 166
3.1. Discovery and Basic Laws of Radioactive Transformations 166
3.1.1. Half-life 167
3.1.2. Laws of Radioactive Decay 169
3.2. Alpha Decay 173
3.2.1. Basic Experimental Results on Alpha Decay 173
3.2.2. Energy Consideration of Alpha Decay. Role of Conservation Laws 178
3.2.3. Mechanism of Alpha Decay. Tunnelling 186
3.2.4. The Role of Centrifugal Barrier 192
3.2.5. Basic Principles of the Theory of Alpha Decay 195
3.2.6. Parity-forbidden Alpha Transitions 200
3.3. Beta Decay 204
3.3.1. Three Types of Beta Decay. Properties of Beta-radioactive Nuclei 204
3.3.2. Nature of Beta Spectrum and the Neutrino Hypothesis 209
3.3.3. Experimental Verification of the Existence of Neutrino 211
3.3.4. Neutrino Mass 215
3.3.5. Concept of the Beta Decay Theory 217
3.3.6. Parity Nonconservation and C-invariance Violation in Beta Decay 230
3.3.7. A Review of the Beta Decay Theory 235
3.3.8. Beta Decay of Neutrons. The $(V-A)$-version of the Weak Interaction Theory 237
3.3.9. Isospin Selection Rules 244
3.4. Nuclear Gamma Radiation 244
3.4.1. Gamma Transition Probability and Selection Rules 247
3.4.2. Internal Conversion of Electrons 251
3.4.3. Nuclear Isomerism 253
3.4.4. Mössbauer Effect 258
3.4.5. Parity Violation in Gamma Transitions 274

3.5. New Types of Radioactivity 278
3.5.1. Proton Radioactivity 278
3.5.2. Double-proton Radioactivity 281
3.5.3. Neutron Radioactivity 282
3.5.4. Carbon Radioactivity 284
3.6. A Brief Resumé of Chapter 3 286

Chapter 4. Interaction of Particles and Radiation with Matter 289

4.1. General Description of the Interaction of Charged Particles, Neutrons and Gamma-quanta with Matter 289
4.2. Ionization Losses Due to Collisions of Charged Particles 291
4.2.1. Bohr's Formula for Specific Ionization. Relativistic Effects and the Density Effect 291
4.2.2. Dependence of Ionization Losses on the Medium 296
4.2.3. Relation Between Range and Energy 297
4.3. Dirac Monopole 299
4.4. Elastic Scattering of Particles 302
4.4.1. Momentum Scattering Diagram 303
4.4.2. Rutherford's Formula 307
4.4.3. Mott's Formulas (Basic Ideas) 311
4.4.4. Delta-electrons 313
4.4.5. Multiple Scattering 315
4.5. Radiation Losses for Electrons 319
4.6. Synchrotron Radiation 323
4.7. Cherenkov Radiation 325
4.8. Transition Radiation 333
4.9. Interaction of Neutrons with Matter 330
4.10. Interaction of Gamma Radiation with Matter 338
4.10.1. Photoeffect 338
4.10.2. Scattering of Gamma Radiation 342
4.10.3. Electron-positron Pair Formation 348
4.10.4. General Nature of Interaction of Gamma Radiation with Matter 351
4.11. A Brief Resumé of Chapter 4 352

PART TWO

Nuclear Interactions 355

Chapter 5. General Laws Governing Nuclear Reactions 355

5.1. Classification of Nuclear Reactions 355
5.2. Laws of Conservation of Electric Charge and Baryon Number 357
5.3. Energy and Momentum Conservation Laws 358
5.3.1. Reaction Energy 358
5.3.2. Energy Diagram for Nuclear Reactions. Endoergic Reaction Threshold 359
5.3.3. Momentum Diagram for Nuclear Reactions 364
5.4. Law of Conservation of Angular Momentum 368
5.4.1. General Remarks 368
5.4.2. The Role of Orbital Angular Momentum 368
5.5. Law of Parity Conservation 371
5.6. Law of Conservation of Isotopic Spin 373
5.7. A Brief Resumé of Chapter 5 375

Chapter 6. Interaction of Neutrons with Nuclei 376

6.1. Properties of Neutrons and Methods of Their Production 376
6.2. Types of Interaction of Neutrons with Nuclei 378
6.2.1. Radiative Capture of Neutrons 378
6.2.2. Reactions Involving the Formation of Protons 379
6.2.3. Reactions Involving the Formation of Alpha-particles 379
6.2.4. Fission Reactions 380
6.2.5. Reactions Involving the Formation of Two or More Nucleons 380
6.2.6. Inelastic Scattering of Neutrons 381
6.2.7. Elastic Scattering of Neutrons 381
6.3. Basic Experiments on the Investigation of Interaction of Neutrons with Matter 382
6.3.1. Slowing Down (Moderation) of Neutrons 383
6.3.2. Thermal Neutrons 390
6.3.3. Resonance Neutrons 393
6.3 4. Basic Principles of the Slowing-down Theory 397
6.3.5 Diffusion of Thermal Neutrons 402
6.4. Bohr's Theory of Nuclear Reactions 406
6.4.1. Compound Nucleus 406
6.4.2. Compound Nuclear Levels 407
6.4.3. Dispersive Nature of the Energy Distribution for a Compound Nucleus 411
6 4.4. Cross Section of a Nuclear Reaction. Breit-Wigner Formulas 412
6.5. Neutron Spectroscopy 420
6.5.1. Mechanical Monochromator Method 421
6.5.2. Mechanical Selector Method 423
6.5.3. Pulsed Accelerator Method 426
6.5.4. Diffraction of Slow Neutrons by a Crystal, or the Crystal Monochromator Method 428
6.5.5. Results of Measurements 431
6.6. Scattering of Fast Neutrons 435
6.7. On the Optical Model of Nuclear Interactions 440
6.8. Ultracold Neutrons 444
6.8.1. Refractive Index 444
6.8.2. Production and Properties of Ultracold Neutrons 446
6.8.3. Application of Ultracold Neutrons 449
6.9. A Brief Resumé of Chapter 6 452

Chapter 7. Nuclear Fission 455

7.1. Discovery and Basic Properties of Fission 455
7.2. First Experiments on Nuclear Fission 457
7.2.1. Measurement of the Kinetic Energy of Fission Fragments 457
7.2.2. Observation of the Fragment Tracks 459
7.2.3. Registration of Beta Radioactivity of Fragments 460
7.2.4. Detection of Fission Neutrons 460
7.3. Elementary Theory of Fission 461
7.3.1. Fission Energy 461
7.3.2. Fission Mechanism 463
7.4. Utilization of Fission Energy 470
7.4.1. Average Number ν of Secondary Neutrons Emitted During One Act of Fission 472
7.4.2. Delayed Neutrons 474
7.4.3. Fission Cross Section and Practical Realization of Nuclear Chain Reactions 477

7.4.4. Natural Nuclear Reactor 463
7.5. Supplementary Problems in Fission Physics 464
7.5.1. Properties of Fission Fragments 464
7.5.2. Mechanism of Formation and Emission Time of Fission Neutrons 468
7.5.3. Spectrum of Fission Neutrons 471
7.5.4. Emission of Instantaneous Gamma-quanta in Fission 483
7.5.5. Fast Particle Fission and Its Properties. Fission Asymmetry 484
7.5.6. Spontaneous Fission. Shape Isomers 486
7.5.7. Delayed Fission 503
7.5.8. Refined Data on Value of ν 506
7.5.9. Dependence of ν on the Mass and the Kinetic Energy of the Fission Fragment 509
7.5.10. Parity Violation in Fission. Asymmetry of Fission Fragment Escape 510
7.5.11. Distribution of Fission Energy 513
7.6. Basic Trends in Modern Atomic Power Engineering 513
7.7. A Brief Resumé of Chapter 7 519

Chapter 8. Reactions of Formation of Transuranic Elements 522

8.1. Neptunium, the First Transuranic Element. Methods of Its Investigation 522
8.2. Plutonium. Properties and Applications 524
8.3. Transuranic Elements with $Z > 94$ 526
8.3.1. Americium and Curium 526
8.3.2. Berkelium and Californium 527
8.3.3. Einsteinium and Fermium 528
8.3.4. Mendelevium 529
8.3.5. Nobelium, the 102nd Element 530
8.3.6. Lawrencium, the 103rd Element 534
8.3.7. Kurchatovium, the 104th Element 534
8.3.8. Elements with $Z = 105$-107 and 109 537
8.4. General Remarks About Transuranic Elements 538
8.5. A Brief Resumé of Chapter 8 544

Chapter 9. Nuclear Reactions Induced by Light Charged Particles 545

9.1. Some Features of Interaction of Charged Particles with Matter 545
9.1.1. Coulomb Interaction of Charged Particles with Nuclei 545
9.1.2. The Role of Centrifugal Barrier 547
9.1.3. Ionization Losses for Charged Particles. Yield of a Nuclear Reaction 548
9.2. Reactions Induced by Alpha-particles 551
9.2.1. Reactions of the (α, p) Type 552
9.2.2. Reactions of the (α, n) Type 555
9.3. Reactions Induced by Protons 556
9.3.1. Types of Proton-induced Reactions 556
9.3.2. Reactions of Protons with Lithium 558
9.3.3. The Reaction $^{14}_{6}C\ (p, n)\ ^{14}_{7}N$ and the Proof of Formation of a Compound Nucleus 562
9.3.4. Formation and Decay of the Compound Nucleus $^{64}_{30}Zn$ in Reactions $p + {}^{63}_{29}Cu$ and $\alpha + {}^{60}_{28}Ni$ 563
9.4. A Brief Resumé of Chapter 9 565

Chapter 10. Direct Interaction Reactions 567

10.1. General Properties of Direct Interaction Processes 567
10.2. Process of Partial Penetration of a Deuteron Into a Nucleus 569
10.3. Deuteron Stripping Reactions for $T_d \gg B_C$ 573
10.4. Deuteron Stripping Reactions for $T_d \geqslant B_C$. Butler's Analysis 575
10.5. Multinucleon Transfer Reactions. Clusters 581
10.6. A Brief Resumé of Chapter 10 583

Chapter 11. Nuclear Reactions Induced by Heavy Ions 585

11.1. Techniques of Operation with Heavy Ions 586
11.1.1. The T, ΔT Method and Its Applications 586
11.1.2. Other Methods of Identification of Nuclei and Determination of Their Lifetimes 587
11.2. A Review of Reactions Induced by Heavy Ions 589
11.3. Interaction of Heavy Ions with Nuclei at $T_{ion} < B_C$ 591
11.3.1. Rotational Spectra for Large Angular Momenta 591
11.3.2. Quasiatoms with Double Nuclei 594
11.4. Interaction of Heavy Ions with Nuclei for $T_{ion} \geqslant B_C$ 595
11.4.1. Elastic Scattering of Ions 595
11.4.2. Transfer Reactions 595
11.4.3. Complete Fusion Reactions 596
11.5. Interaction of Heavy Ions with Nuclei at Relativistic Energies 597
11.5.1. Problems in the Physics of Relativistic Ions 598
11.5.2. First Results. Cumulative Effect 599
11.5.3. Anomalous Nuclei 601
11.6. A Brief Resumé of Chapter 11 602

Chapter 12. Nuclear Reactions Induced by Gamma-quanta 604

12.1. Simplest Reactions Induced by Gamma-quanta 604
12.2. Direct Emission of Protons Induced by Gamma-quanta 605
12.3. Giant Electric Dipole Resonance 606
12.4. A Brief Resumé of Chapter 12 611

Chapter 13. Thermonuclear Reactions 612

13.1. Possibility of Self-sustained Fusion of Light Nuclei 612
13.2. Thermonuclear Reaction in the Sun and in a Hydrogen Bomb 614
13.3. The Problem of Controlled Thermonuclear Fusion 618
13.4. A Brief Resumé of Chapter 13 625

Appendix 626

I. Basic Formulas 626
II. Basic Constants and Units 628

Index 631

Preface to the English Edition

This book is based on the lectures on experimental nuclear physics delivered by the author for many years at various faculties of the Moscow Physical Engineering Institute. As was mentioned in the Preface to the Fourth Russian Edition, the main emphasis is laid on the description of basic experiments in nuclear physics and their interpretation on the basis of the symmetry of the laws of nature. A simple theoretical interpretation is also presented, which, however, cannot replace a serious theoretical source on nuclear physics.

The author believes, however, that an analysis of the basic concepts of the theory together with experiments will help generate a deeper understanding of the physics of the phenomena under consideration. Besides, such a presentation makes the book suitable for self-education.

The translation is based on the latest Russian edition (1983). Nevertheless, the material was updated for the present publication. The first volume is supplemented by information concerning the discovery of new types of radioactivity. The second volume contains new material on the discovery of intermediate vector bosons. Besides, redundant material and topics of no interest to English-speaking readers have been omitted. Misprints and errors noted in the Russian edition have been corrected.

Dedicated to the cherished memory of Igor Vasilyevich Kurchatov

Preface to the Fourth Russian Edition

This book is a revised version of a course of lectures on experimental nuclear physics delivered by the author at various faculties of the Moscow Physical Engineering Institute for over three decades. The book is intended for students of physical engineering and applied physics, and for engineers in atomic power industry, who want to supplement their knowledge in the field of nuclear physics. It can also be used by the physics students at universities.

The first and second editions of the book were published in 1963 and 1965 under the title *Introduction to Nuclear Physics*. The third edition was published in 1974 as a two-volume treatise *Experimental Nuclear Physics*. The present edition, also in two volumes, is being published under the same title. The first volume (*Physics of Atomic Nucleus*) is devoted to the problems of nuclear physics, including the properties of stable nuclei, nuclear models, alpha and beta decays, gamma radiation, passage of particles and radiation through matter, fundamentals of neutron and fission physics, nuclear reactions induced by light particles and heavy ions, thermonuclear reactions and reactions involving the formation of transuranic elements.

The second volume (*Elementary Particle Physics*) describes the basic properties of elementary particles and interactions in which they participate. Among the topics considered in this volume are: nucleon-nucleon interactions at low and high energies, deuteron theory, properties of nuclear forces, nucleon structure, properties of leptons, π-mesons, strange and charmed particles, physics of antiparticles and antinuclei, classification of particles and resonances. A brief account of the modern theory of electroweak interactions and quantum chromodynamics is also given.

Since the publication of the last edition of the book, a lot of new material has appeared. It was also felt that the old material needs to be revised and abridged. As a result, the book has undergone significant changes. New sections on the superfluidity model, giant resonances, nuclear reactions induced by heavy ions, multinucleon transfer reactions, parity violation in gamma transitions and fission, Dirac monopole, synchrotron and transient radiations, spontaneous fission from isomeric state and ultracold neutrons have been included in Vol. I. Some chapters (beta decay, thermonuclear reactions) have

been completely rewritten, while some others (fission physics, transuranic elements, etc.) have been considerably supplemented with new material.

The second volume has undergone a radical revision. The basic ideas about the nature of elementary particles and interactions have been revolutionized in the wake of recent discoveries. Now concepts have been introduced for really elementary particles. The theory of electroweak interactions, combining weak and electromagnetic interactions, has been constructed. Quantum chromodynamics which is capable of interpreting many features of strong interactions is being developed successfully. The main features of the "grand unification" of all three types of interactions have been outlined. These theoretical advances are based on a series of remarkable achievements of experimental physicists. In turn, this has been made possible by the creation of new unique accelerators and storage rings. An attempt has been made to describe all these aspects in the second volume of the book. New sections in this volume are devoted to the discovery of J/ψ-particle and other ψ-particles, the discovery of charmed particles, and the construction of the four-quark model, the discovery of Υ-mesons and the fifth quark, weak neutral currents and τ-lepton, and gluons.

Besides, some sections have been considerably revised and supplemented with new material on μ-catalysis, μ-nucleonic atoms, phase analysis of nucleon-nucleon, pion-nucleon, and pion-pion scattering, G-parity of mesons and the law of conservation of G-parity, etc.

In spite of the considerable revision and enlargement of the book, the author has endeavoured to adhere to the principles on which the previous editions of the book were based and which have stood the test of time:

1. The presentation of the material is based on the symmetry of the laws of nature and the conservation laws following from them.
2. To acquaint the reader with the thought-workshop of the experimental physicists, the ideas and schematics of the earlier instruments associated with discoveries in the field of nuclear physics are described.
3. The state-of-the-art is described for each problem.
4. The experimental material is discussed side-by-side with the basic theoretical concepts.
5. While deriving formulas, special care has been taken to reflect the physical significance of the phenomenon and the rapidity with which the results can be obtained. This aspect has been given preference over the mathematical elegance. Wherever possible, formulas have been reduced to numerical values.
6. A brief resumé is provided at the end of each chapter.

A word about the references. Naturally, it is impossible to give

any systematic classification of the literature. Hence the author has often quoted just the names of the physicists who obtained the given result for the first time, and the year in which this result was obtained. An exception has been made for the more recent results. In this case, the original articles are cited in the form of references in footnotes. Special care has been taken to indicate the review articles. The author is conscious of the fact that the desire to introduce the latest material is fraught with the danger of describing the results which may not stand the test of time. However, in view of the extreme care taken to select the appropriate material, it is hoped that the number of such cases will be very small.

In conclusion, the author expresses his sincere gratitude to A. P. Alexandrov, who recommended the publication of the first edition* of the book in 1963. He is also indebted to V.M. Kolobashkin for his persistent interest in the preparation of the manuscript, V.G. Kirillov-Ugryumov for a quite valuable and sincere criticism of the third edition, S.T. Belyaev, D.P. Grechukhin and B.A. Nikol'skii for valuable comments concerning new material in this edition. The author would like to place on record his deep sense of gratitude to I.I. Gurevich, whose numerous suggestions were extremely helpful in the preparation of the manuscripts of all the editions of the book. The important remarks and suggestions made by I.I. Gurevich while reviewing the manuscript of the present edition have led to a significant improvement of the quality of the book.

Suggestions for further improvement of the book will be received with gratitude.

---

* The manuscript of the book was first released in 1962 at the Moscow Physical Engineering Institute.

Introduction

Nuclear physics, which deals with the structure, properties and transformations of the atomic nucleus, is one of the most modern branches of science. Even at the end of the 19th century, the atomic nucleus had not been discovered and the atom was considered to be the smallest indivisible particle of matter. The discovery of cathode rays and X-rays in 1895 and of natural radioactivity in 1896 showed that the atomic structure of all elements has something in common. For example, all of them contain electrons which are emitted under certain conditions, and the heaviest elements exhibit the properties of alpha, beta and gamma radioactivities.

According to the first model of the atom proposed in 1904 by the English physicist Thomson, the atom is a positively charged sphere of radius 10^{-8} cm with electrons interspersed over its volume. This model seemed to be more or less satisfactory until it was found to contradict the results of experiments on the scattering of α-particles by thin foils of metals carried out in 1909. These experiments revealed that besides scattering at small angles corresponding to the Coulomb interaction of α-particles with a Thomson-type atom, some α-particles are scattered at very large angles (more than 90°). Thomson's model is quite unsuitable for explaining such scattering.

In 1911 Rutherford proposed a new model of the atom, according to which the atom consists of a central positively charged nucleus of a very small size (about 10^{-12} cm) with electrons distributed around it at comparatively large distances (about 10^{-8} cm). Since the mass of the electrons is very small, the entire mass of the atom is practically concentrated at the nucleus.

The nuclear model of the atom splendidly explained the experimental results on the scattering of α-particles and served as a giant leap in the quest for understanding the structure of matter. The year of creation of the nuclear model of the atom can be treated as the year of birth of nuclear physics. However, the nuclear model suffers from a significant drawback. Indeed, any model that lays claim to a correct representation of the structure of atom, which is a stable long-lived system, must itself be stable. Thus, the stability of the Thomson model was ensured by an equilibrium of the repulsive forces between electrons and the forces of their attraction towards the positively

charged sphere. The nuclear model of atom is reminiscent of the solar system in its structure. It is well known that the stability of the solar system is ensured by an equilibrium of the gravitational and centrifugal forces. It would seem that a similar situation must prevail in the nuclear model of the atom, if we assume that electrons revolve round the nucleus at such a distance and with such a speed that the centrifugal forces balance the forces of Coulomb attraction of the nucleus and prevent the electrons from falling into it. This conclusion, however, is not true since according to the laws of electrodynamics any accelerated charge (including an electron) moving uniformly in a circle around the nucleus must lose energy by radiation. Consequently, the energy of the system will decrease and hence the electrons will gradually move closer to the nucleus until they fall into it. The rotational frequency of electrons around the nucleus will keep on changing and so will the frequency of the radiation emitted by atoms. It is quite obvious that in this form the nuclear model of the atom contradicts two of the most significant experimental results, viz. the stability of atoms and the discrete nature of atomic spectra.

In order to overcome these difficulties, the Danish physicist Niels Bohr proposed in 1913 a new theory, viz. the quantum theory of atomic processes. Bohr postulated the existence of stationary electron orbits in the atom with definite values of angular momentum which is an integral multiple of Planck's constant ($\hbar = 1.05 \times 10^{-27}$ erg·s):

$$m_e v r = n\hbar,$$

where m_e is the electron mass, v is the electron velocity, r is the radius of the orbit, and n is an integer.

Each orbit lies at a quite definite distance ($r_n = n^2\hbar^2/Zm_e e^2$) from the nucleus ($Z$ is the charge of the nucleus) and is characterized by a quite definite energy state of the atom: $E_n = -(Z^2e^4m_e/2\hbar^2) \times (1/n^2)$. The orbit with the smallest radius corresponds to the lowest energy and is called the K-orbit. This is followed by the L-, M-, . . . orbits. When electrons move in these orbits, the atom is in a stable state. The emission or absorption of radiation by an atom is always caused by a transition of an electron from one orbit to another, and the radiation frequency is in one-to-one correspondence with the difference in the energies of the states participating in the transition:

$$\Delta E = h\nu,$$

where $h = 2\pi\hbar$.

With the help of simple calculations based on these assumptions, Bohr was able to theoretically obtain the spectral laws and the value of the Rydberg constant.

Bohr's theory was later modified and perfected: the motion of the nucleus about the common centre of mass was considered; circular orbits were replaced by elliptic orbits which lie in quite definite planes. All this led to a better understanding of the optical spectra of atoms and, in particular, allowed to explain the normal *Zeeman effect*.

Having put forth his famous postulates, Bohr took an extremely daring step. He abandoned the prevailing classical concepts and thus arrived at a correct description of the intra-atomic processes. However, certain difficulties still remained in Bohr's theory itself. It was not clear, for example, why the classical concepts must be renounced to describe atomic processes.

These difficulties were overcome only in 1926 when Heisenberg and Schrödinger proposed a quite new approach for describing microscopic phenomena. This approach was termed *quantum mechanics*. According to quantum mechanics, the trajectory of motion of electrons and other microscopic particles cannot be specified on account of the fact that the position and the velocity of a particle cannot be determined simultaneously.

The old model of the atom was replaced by a new one, in which the position of electrons in an atom cannot be specified exactly but has a certain probability given by a wave-function which is a solution of the wave equation. Quantum mechanics not only confirmed all the results of Bohr's theory but also explained why an atom does not emit energy in a stationary state. It also permitted a calculation of the intensities of spectral lines. Besides, quantum mechanics explained the diffraction of electrons, a phenomenon which was quite incomprehensible from the point of view of classical physics.

Quantum mechanics was subsequently used to explain nuclear processes as well. For example, Gamow and coworkers developed the quantum-mechanical theory of alpha decay in 1928.

Two important discoveries were made in 1919. A mass spectrometer was constructed by Aston and atomic masses were measured precisely. This led to the discovery of isotopes. Continuing his experiments on the scattering of α-particles, Rutherford discovered the splitting of the nitrogen nucleus accompanied by the escape of a positively charged particle with a charge $+e$ and a mass equal to that of the nucleus of the lightest isotope of hydrogen (equal to $1836.1m_e$). The experiment was repeated with other materials and in almost all the cases, the nuclei of these materials emitted hydrogen nuclei upon being bombarded by fast α-particles. Thus it was proved that nuclei contain the simplest hydrogen nuclei which were termed *protons* (p).

The discovery of the proton led to a comparatively simple model according to which the atomic nucleus consists of protons and electrons. The nucleus is supposed to contain A protons and $(A-Z)$

electrons, while Z electrons revolve round it at a distance of about 10^{-8} cm. This model provided a natural explanation of the fact that the atomic mass of the elements is proportional to the mass number A and the nuclear charge is proportional to the atomic number Z. However, the assumption that nuclei contain electrons led to unsurmountable theoretical difficulties: the properties of the nuclei could not be associated with the properties of the particles constituting them according to this model.

It is well known that besides mass and charge, elementary particles are also characterized by other properties, for example, the *intrinsic angular momentum* (*spin*) which is measured in units of $\hbar$, and the *magnetic moment*.

The existence of intrinsic angular momentum and magnetic moment in elementary particles, say, an electron, makes it possible to represent them as charged tops spinning about their axes. Unlike the classical top which can have any value of angular momentum, electrons have only one value of spin, viz. $\hbar/2$. Similarly, the magnetic moment of the electron also has only one value, viz. $M_B = e\hbar/2m_ec = 9.27 \times 10^{-21}$ erg/G, called the *Bohr magneton*. The magnetic moment of the electron is negative, i.e. its direction is opposite to that of spin.

The concept of electron spin was introduced in 1925 to explain the fine structure of atomic radiation. Later, in order to explain the hyperfine structure of optical spectra, it was assumed that atomic nuclei have a spin and a magnetic moment. In view of the fact that hyperfine splitting is extremely small, the nuclear magnetic moment must be lower than the electron magnetic moment by a factor of about 10^3.

Subsequent measurements revealed that the simplest nucleus, i.e. proton, has a spin $\hbar/2$ and a positive magnetic moment equal to $2.79\mu_B$ (where $\mu_B = e\hbar/2m_pc = M_B/1836 = 5.05 \times 10^{-24}$ erg/G), i.e. smaller than the electron magnetic moment by a factor of about 650. Measurements of the magnetic moments of other atomic nuclei have shown that their absolute values are close to the proton magnetic moment and differ considerably from the electron magnetic moment. This is a serious argument against the electron-proton model of the nucleus. The values of nuclear spins also point towards the incorrectness of such a model. For example, deuteron, whose nucleus should consist of two protons and one electron, according to this model can have only half-integral spin ($\hbar/2$ or $3\hbar/2$). The experimental value of the deuteron spin, however, is $\hbar$. On the basis of this and some other arguments it became clear that there are no electrons inside a nucleus. However, the nucleus cannot be composed of protons alone since in this case A will always be equal to Z. So there must exist some new particles which, together with protons, constitute the nucleus. These particles were soon discovered.

Continuing Rutherford's experiments, Bothe and Becker discovered in 1930 that upon being irradiated by α-particles, some light elements (Be, Li) emit instead of protons a radiation which is absorbed very weakly by lead. In 1932, Irène and Frédéric Joliot-Curie established that the new radiation knocks out recoil nuclei from light elements. It was naturally assumed that this radiation consists of high-energy γ-quanta. However, in order to correlate the results of experiments on absorption in lead and the creation of recoil nuclei, the γ-quanta had to be assigned higher values of energy and momentum than those obtained by irradiating light nuclei by α-particles.

These difficulties were overcome in 1932 by Chadwick who used the energy and momentum conservation laws to analyze the experimental results on the creation of nitrogen and hydrogen recoil nuclei by the new type of radiation. Chadwick concluded that the new radiation is a flux of neutral particles with a mass approximately equal to the proton mass. The new particle was called *neutron* (n).[1] The exact value of the neutron mass determined from the energy balance of nuclear reactions involving the creation or absorption of neutrons is $m_n = 1838.6m_e$. Thus, the neutron is heavier than the proton by $2.5m_e$, and heavier than the sum of proton and electron masses by $1.5m_e$. According to the well-known relation connecting mass and energy, each value M of mass in grams has an energy Mc^2 in ergs corresponding to it, where $c = 3 \times 10^{10}$ cm/s is the velocity of light. A particle at rest has the lowest energy called the *rest energy*. Since the neutron rest energy is higher than the sum of the proton and electron rest energies, a decay of the neutron into a proton and an electron is possible from the energy point of view. Such a decay was observed in 1950 by the Soviet physicists Spivak and Sosnovskii, the Canadian physicist Robson, and the American physicist Snell.

Thus, the neutron is an example of an unstable elementary particle. The present-day estimates put its half-life at about 10 min. Measurements of spin and magnetic moment revealed that, like the proton and electron, the neutron has a spin equal to $\hbar/2$, while its magnetic moment is negative and smaller than the electron magnetic moment by a factor of about 10^3 ($\mu_n = -1.91\mu_B$).

Soon after the discovery of neutron, Gapon and Ivanenko, as well as the German physicist Heisenberg, put forth a hypothesis about the proton-neutron structure of the nucleus. This model completely eliminated the difficulties associated with the proton-electron model and is widely accepted at present.

[1] The existence of neutron (and deuteron) was predicted by Rutherford who believed that, besides the nucleus containing only one proton and no electrons (the hydrogen nucleus contains just one *proton*), there must exist a nucleus containing a proton and an electron (i.e. a *neutron*), and a nucleus containing two protons and one electron (a *deuteron*).

According to this model, all nuclei contain two types of elementary particles or *nucleons*, viz. protons and neutrons. Different nuclei (at present, about 2000 nuclei, including those obtained artificially, are known to exist) differ in the number of neutrons and protons constituting them. Beta-stable nuclei have a quite definite ratio of the numbers of protons and neutrons contained in them.

Thus, light nuclei ($^4_2$He, $^7_3$Li, $^9_4$Be, $^{10}_5$B, $^{14}_7$N and so on) contain an equal, or nearly equal, number of protons Z and neutrons $(A-Z)$. Heavy nuclei ($^{208}_{82}$Pb, $^{226}_{88}$Ra, $^{238}_{92}$U) contain about 1.5 times more neutrons than protons.

The excess of neutrons in heavy nuclei is explained by the Coulomb repulsion of protons. For β-stable nuclei, the relation between Z and A is described by the empirical formula

$$Z = \frac{A}{(1.98+0.015A^{2/3})}.$$

Nuclei in which this relation is violated are found to be β-radioactive; neutron-rich nuclei emit an electron while the proton-rich nuclei emit a positron, i.e. an electron with a positive charge. The existence of the positron was predicted by Dirac in 1928 from an analysis of the relativistic quantum-mechanical equation for an electron. The positron was detected in 1932 by Anderson who studied cosmic rays with the help of a Wilson cloud chamber placed in a magnetic field. Under laboratory conditions, the positron was first detected by I. and F. Joliot-Curie, who in 1934 discovered artificial positron radioactivity while irradiating light nuclei by α-particles. Soon afterwards (in the same year), artificial electron radioactivity was discovered by Fermi who irradiated nuclei with neutrons.

In 1931, Pauli predicted the existence of yet another particle which he called a *neutrino* (ν). This is a neutral particle with a spin equal to $\hbar/2$ and a mass much smaller than the electron mass (or zero mass). The existence of this particle was necessitated by the energy consideration of the beta decay process. A neutrino must be emitted together with an electron or a positron to ensure the conservation of energy and angular momentum in such a process. For the same reason, the decay of a neutron is also accompanied by the emission of a neutrino (more precisely, an *antineutrino* $\tilde{\nu}$) and can therefore be expressed in the form

$$n \to p + e^- + \tilde{\nu}.$$

In view of its properties ($z = 0$, $m = 0$, $\mu \simeq 0$), a neutrino is extremely hard to detect. For this reason, scientists only had an indirect evidence of the existence of this particle for a very long time. It was only in 1953 that Reines and Cowan set up a direct experiment to detect a neutrino.

A very interesting type of radioactivity was discovered in 1938 by Alvarez. This is the so-called *e*-capture, i.e. a process involving the capture by the nucleus of an electron from an electron shell (most often the *K*-shell) of the same atom. Like beta decay, *e*-capture is accompanied by the emission of a neutrino.

The number of nuclei, both stable and radioactive, is very large indeed and continues to rise as new isotopes of known elements are obtained and new elements are synthesized. Thus, an element with $Z = 107$ was in 1976 synthesized in the USSR and an element with $Z = 109$ in 1982 in the FRG. Efforts are being continued to obtain elements with even higher values of Z.

The discovery of the neutron and the investigation of its interaction with matter led to one of the most significant achievements in nuclear physics. In 1938 Hahn and Strassmann discovered that when uranium is irradiated by neutrons, its nucleus is split into two parts having nearly equal masses (fission fragments). It was later shown that fission is accompanied by the emission of secondary neutrons and the liberation of a large amount of energy. In principle, these secondary neutrons can be used to continue the process of fission in new uranium nuclei with a subsequent emission of more neutrons, and so on. This leads to the possibility of a chain reaction which is accompanied by the release of a huge amount of energy.

The first nuclear reactor was commissioned in the USA under the supervision of the Italian physicist Enrico Fermi in December 1942. Four years later, this success was repeated independently in the USSR and the first nuclear reactor in Asia and Europe was commissioned in Moscow on the 25th of December, 1946.

Atomic energy is widely used in national economies of many countries at present. The problem to be solved in the coming years is to harness even more powerful sources of energy based not on heavy nuclei, but the light ones like hydrogen, deuterium, tritium, etc. Unlike the heavy nuclei for which the process of fission is favourable from the energy point of view, the structure of light nuclei is such that the process of synthesis, or fusion, is more favourable in their case. This process is accompanied by the liberation of thermonuclear energy. The investigation of fusion reactions for light nuclei has led to a quite definite result: it has been shown that thermonuclear energy is released instantaneously (during the explosion of a hydrogen bomb).

Controlled fusion reactions for light nuclei pose a much more complicated problem which has not been solved so far. However, the wide scope of experimental and theoretical investigations of this problem and its present status raise the hopes that it will be solved by the end of this century or at the latest by the beginning of the next century.

A very important branch of nuclear physics emerged in the beginning of the 1930s. At this time, Van de Graaff invented an electrostatic generator, Lawrence devised a cyclotron, while Cockroft and Walton devised a cascade accelerator tube. In 1932, Cockroft and Walton observed for the first time the splitting of lithium as a result of bombardment by accelerated particles (protons). This provided physicists with a powerful tool for transforming atomic nuclei. Subsequent technological advancements led to the production of accelerated electrons, deuterons, α-particles, and even the ions of heavier elements like nitrogen, oxygen, neon, titanium, chromium, etc.

The discovery of phase stability in 1944 by the Soviet scientist *Veksler, and independently in 1945 by the American physicist* McMillan, permitted a significant increase in the acceleration energy. At first proton accelerators up to energies of several hundred megaelectron-volts were constructed (in the USSR and abroad). Later, the acceleration energy was raised to several gigaelectron-volts. A 10-BeV proton accelerator was built in 1957 at the Joint Institute for Nuclear Research at Dubna, and the 30-BeV accelerators were installed in Switzerland at the end of 1959 and in the USA in 1960.

A proton accelerator with energy 76 BeV was commissioned in October 1967 near Serpukhov in the USSR. The construction of a 200-BeV accelerator was completed at Batavia (USA) in the year of 1972. After modification, the energy of this accelerator was increased to 400 BeV and later to 500 BeV. A similar 400-BeV accelerator was constructed in Switzerland in 1976. Considerable progress was made in the field of the acceleration of other particles. The Dubna accelerator was modified in 1970 to accelerate ions of elements from deuterium to neon up to an energy of 5 BeV/nucleon. The Bevalac accelerator set up at Berkeley (USA) in 1974 was able to accelerate oxygen ions up to 2 BeV/nucleon and iron ions up to 1.8 BeV/nucleon. Electron accelerators with energy 6 BeV and higher have been constructed in several countries, including the USSR (the energy of the Stanford accelerator in the USA is 21 BeV).

Accelerators operating on the principle of colliding electron-electron and electron-positron beams have also been constructed. A 2×31-BeV accelerator in which two proton beams undergo a head-on collision was constructed in Switzerland in 1971. An accelerator built in Brookhaven (USA) has an energy of 1×400 BeV. In 1981, a 2×270-BeV accelerator with colliding beams of protons and antiprotons was built at CERN (Switzerland). Later, the energy was brought up to 2×450 BeV.

Together with the technology of accelerating protons, methods were developed to extract them from the accelerator and to use for obtaining new particles in secondary processes. At present, these methods are being used for obtaining fast neutrons, antiprotons,

antideuterons, pions, K-mesons, γ-quanta, muons, neutrinos and other particles.

The advances in the field of accelerator technology have allowed scientists to embark on the solution of the most complicated problem in nuclear physics, viz. the problem of nuclear forces. The existence of stable nuclei consisting of neutrons and protons indicates that besides the Coulomb repulsion between protons, strong nuclear forces of attraction must exist between any pair of nucleons.

Information on the interaction of two nucleons can be gathered by studying the scattering of one of them by the other. Such experiments were carried out for protons and neutrons having various energies. Experiments with protons and neutrons having moderate energies showed that the range of nuclear forces is extremely small and is of the order of 10^{-13} cm. It was also shown that nuclear forces depend on the particle spin and, under identical conditions, $(n\text{-}p)$-, $(p\text{-}p)$- and $(n\text{-}n)$-forces are equal (the principle of charge independence of nuclear forces).

Quite significant properties of nuclear forces were obtained from an analysis of the angular and energy distributions of $(n\text{-}p)$- and $(p\text{-}p)$-scatterings at high kinetic energies ($T > 100$ MeV). In particular, an analysis of the angular distribution of scattered neutrons in $(n\text{-}p)$-interaction showed that the number of protons scattered in the forward direction is too large to be explained by the laws of conservation of energy and momentum without any additional assumptions concerning the interaction mechanism. However, the experimental results can be explained by assuming that a neutron and a proton can exchange charge during interaction. In this case, a fast neutron "acquires" the charge from a proton during interaction and continues to move forward (after undergoing a slight deflection during interaction) as a proton. This is the charge-exchange interaction which takes place together with the usual nuclear interaction.

It was naturally assumed that the charge exchange involves an exchange of certain particles, viz. nuclear field quanta, from one nucleon to the other. Such a hypothesis was put forth by the Soviet physicist Tamm in 1934 to explain the nature of nuclear forces. However, Tamm also showed that the light particles known at that time, viz. electrons and neutrinos, cannot serve as quanta of nuclear force field.

Tamm's idea was developed in 1935 by the Japanese physicist Yukawa who showed that the short-range character of nuclear forces and some other properties can be explained by assuming that during interaction nucleons exchange neutral or charged particles of mass $(200\text{-}300)m_e$. In order that these particles could serve as nuclear quanta, or carriers of nuclear forces, they must have nuclear activity, i.e. they must be generated copiously during nucleon-nucleon collisions and strongly absorbed by nuclei.

Muon, a particle with a mass of $207m_e$ and a lifetime of about 2×10^{-6} s was discovered in 1938 during studies of the composition of cosmic rays. An investigation of the properties of the muon revealed that it is a nuclear-passive particle and hence cannot be a nuclear quantum. The nuclear passivity and the short lifetime of the muon led to the prediction of heavier particles, viz. pions, in the cosmic radiation. These particles were indeed discovered in 1947 by Powell. An analysis of their properties showed that they exist in the form of π^+-, π^-- and π^0-mesons, have a mass equal to $273m_e$, zero spin, and a lifetime of about 10^{-8} s.[2] These particles were found to interact quite strongly with matter. Subsequently, it became possible to produce them in large amounts in accelerators and their interaction with nuclei and nucleons was studied at different energies. The results of these investigations indicate that π-mesons are really the quanta of nuclear forces between nucleons.

The 1950s were marked by the most significant achievements in the field of detection of particles, and this led to several important discoveries. With the help of emulsion cloud and bubble chambers which were invented in this period, new unstable particles were discovered in 1951-54 (first in the cosmic rays and then in accelerators). These include K-mesons with a mass of $966m_e$, and hyperons whose mass is higher than that of a proton. Large-sized liquid scintillators were able to register the interaction of a neutrino with a proton, thus providing experimental confirmation for the existence of this particle (1953-54). Finally, antiproton (1955) and antineutron (1956) were discovered with the help of Cherenkov and scintillation counters. At the same time, studies were undertaken to determine the structure of nucleons (1955), violation of parity in weak interactions was observed (1957), and the Mössbauer effect was discovered (1958).

The most interesting results obtained in the 1960s include the discovery of resonances, i.e. particles that are unstable with regard to strong interaction, the discovery of symmetry in the properties of strongly interacting particles and resonances (1961) culminating in the prediction of all the properties of Ω^--hyperon which was discovered soon afterwards (1964), the proof for the existence of the muon neutrino ν_μ which differs from the electron neutrino ν_e (1962), the discovery of the violation of combined parity in the decay of neutral K-mesons (1964), the creation of the quark model of hadrons (1964), the discovery of internucleon potential which is responsible for the violation of parity invariance (1964), the synthesis of transuranic elements with $Z = 104$ (1964) and $Z = 105$ (1968), the creation of a unified theory of weak and electromagnetic interactions (1967),

[2] The lifetime of π^0-mesons is about 10^{-16} s and their mass is approximately equal to $264m_e$.

and the discovery of antihelium-3 (1970). Among the most important achievements in the field of experimental techniques during this decade was the invention of spark and streamer chambers.

Among the notable achievements during the 1970s are the discovery of the last remaining (as it was assumed at that time) metastable antiparticle $\tilde{\Omega}^+$-hyperon (1971), investigation of inelastic scattering of ultrarelativistic electrons by protons which led to the formulation of the parton model of the nucleus, the proof of the existence of neutral currents in weak interactions (1973), the discovery of antitritium (1973), the discovery of the 106th (1974) and 107th (1976) elements, the discovery of J/ψ-particle (1974) and other ψ-particles (1975), the prediction and discovery of charmed mesons (1976) and baryons (1977), the discovery of Υ-meson and heavy τ-lepton (1977) and the discovery of gluons (1979).

The most important theoretical results of the 1970s are the development of the unified theory of weak and electromagnetic interactions, the creation of the four-quark model, and a successful development of quantum chromodynamics.

It is shown in the unified theory of weak and electromagnetic interactions that the role of quanta is shared by four vector bosons, viz. the massless photon, which is the electromagnetic-interaction quantum, heavy charged $W^{\pm}$-bosons which are responsible for weak charged currents, and the heavy neutral Z^0-boson which causes weak neutral currents. To discover $W^{\pm}$- and Z^0-bosons, the construction of a special accelerator with colliding beams of protons and antiprotons ($\tilde{p}p$-collider) for large energy was started at CERN.

Strong interaction between quarks is described in quantum chromodynamics. Strong-interaction quanta are called gluons. This interaction is sometimes termed truly strong interaction to distinguish it from the strong interaction between nucleons (and other hadrons), in which pions are involved. In this scheme, strong interaction is assumed to be a secondary manifestation of truly strong interaction.

The 1980s were marked by a splendid confirmation of the predictions of the theory of electroweak interactions: in 1982-83 at CERN, the $W^{\pm}$- and Z^0-bosons were discovered in the $\tilde{p}p$-collider with energy 2×270 BeV.

Attempts have been made in recent years to create the so-called "grand unification" theory, combining strong, electromagnetic and weak interactions into a single theory.

Part One

Properties of Nuclei and Radioactive Radiation

All atomic nuclei can be divided into two classes: stable and radioactive. *Stable nuclei remain unchanged over infinitely long periods* of time, while radioactive nuclei undergo spontaneous transformations.

The basic characteristics of a stable nucleus are its *mass number A*, *electric charge Z*, *mass M* (and *binding energy* ΔW), *radius R*, *spin* I, *magnetic moment* μ, *quadrupole electric moment Q*, *isotopic spin* T and *parity P of the wave-function.*

Radioactive nuclei are also characterized by the type of radioactive transformation (alpha or beta decay, spontaneous fission, etc.), half-life $T_{1/2}$, energy of emitted particles, etc.

The nucleus of an atom can be in various energy states. The state with the lowest energy is called the *ground* state while all the remaining states are called *excited* states. The ground state of a stable nucleus is stationary. The excited states of any nucleus (including a stable nucleus) are nonstationary (they undergo gamma transitions, etc.).

The characteristics mentioned above can be ascribed to the ground state as well as to any excited energy state of a nucleus. Generally speaking, their values are different for different states (except *A* and *Z* which have the same values for all the energy states of a given nucleus). If the characteristics of a nucleus are given without any mention of the state to which they correspond, the ground state is usually meant.

In the ideal case, the complete information about a nucleus must describe the structure and the characteristics of all its possible excited states (*levels*), the methods and probabilities of nuclear transition from one state to another, the probabilities of radioactive decay of the nucleus and the properties of the emitted particles, the cross sections and the nature of interactions of the nucleus with other nuclei and elementary particles, etc.

We shall consider in Chap. 1 only the ground states of nuclei. Chapters 2 and 3 describe the structure and properties of excited states. Chapter 4 and Part Two are devoted to the interaction of nuclei with elementary particles and other nuclei.

Chapter I

Properties of Stable Nuclei and Nuclear Forces

1.1. Mass Number A and Electric Charge Z of the Atomic Nucleus

The *mass number* A of a nucleus is determined by the number of nucleons (protons and neutrons) in it. The total number of nucleons in any ordinary nuclear reaction (not involving the creation of antiparticles) remains unchanged (the law of conservation of the number of nucleons). Hence the total mass number in such nuclear processes is conserved (see Sec. 5.2 for details).

A generalization of this statement to all particles and antiparticles leads to the law of conservation of the baryon charge (see Vol. II).

When expressed in atomic mass units (amu), the mass number gives an approximate value (to within 0.1-1%) of the mass of an atomic nucleus (see Sec. 1.2).

The *charge* Z of an atomic nucleus is defined by the number of protons in it (and hence by the number of electrons in the atomic shells). This number coincides with the atomic number of the element in the Periodic Table. The charge determines the chemical properties of all the isotopes of a given element. The most accurate measurements of the nuclear charge were made in 1913 by Moseley who established a simple relation between the frequency ν of the characteristic X-ray radiation and the charge Z:

$$\sqrt{\nu} = aZ - b.$$

Moseley found that the constants a and b do not depend on the element for a given series of radiation. This permitted him to arrange first the elements from ${}_{21}Ca$ to ${}_{30}Zn$ according to their atomic numbers, and then other elements as well.

Besides, Moseley's method helped in determining the position of certain elements, which had not been discovered by then, in the Periodic Table (${}_{43}Tc$, ${}_{61}Pm$, ${}_{85}At$, ${}_{87}Fr$)[1] and also confirmed the phenomenon of K-capture.

[1] These elements were not discovered for a long time since they only have radioactive isotopes. Hence ${}_{85}At$ and ${}_{87}Fr$ could be discovered only as a result of a detailed investigation of radioactive families. As regards ${}_{43}Tc$ and ${}_{61}Pm$, they are never encountered in nature since their half-lives are less than the age of the Earth, and they cannot be formed by radioactive transformations of neighbouring nuclei (among those found in nature) since the latter are stable. The elements ${}_{43}Tc$ and ${}_{61}Pm$ were obtained artificially in 1937-1940.

The nuclear charge was directly determined in 1920 by Chadwick from experiments on scattering of α-particles by foils prepared from a metal with a given Z (these experiments will be described in Chap. 4).

The electric charge occupies a special position among other charges (baryon, lepton, strange, etc.). As a matter of fact, it sort of performs two functions: it is responsible for the strength of electromagnetic interaction (it should be recalled that the fine-structure constant $\alpha = e^2/\hbar c$) and also participates in the conservation law. The electric charge is known to be conserved in all types of interactions (strong, electromagnetic, weak) considered in nuclear physics.

The law of conservation of electric charge was verified experimentally. The experiment involved an attempt to register the electromagnetic radiation corresponding to a transition of the atomic electrons to the K-shell in which a vacancy is due to the decay of an electron with a violation of the law of conservation of electric charge (for example, according to the scheme $e \to \nu_e + \gamma$).

The experiment was conducted in a deep well (about 400 m) with a NaI crystal scintillator which, in the case of K-electron decay, must register an X-ray photon from iodine with energy 33.2 keV. The experiment yielded the following lower bound of the electron lifetime: $\tau_e > 5 \times 10^{21}$ years. This means that the strength of the hypothetic interaction in which the law of conservation of electric charge is violated is smaller than the strength of weak interaction at least by a factor of 10^{28}.

The law of conservation of electric charge can be used to find the charge of a nucleus from the charge balance in nuclear reactions or radioactive transformations.

The electric sharge Z is an integral property of the nucleus and does not give any information about the distribution of charge over the volume of the nucleus. This information can be obtained from experiments on the scattering of fast electrons by nuclei (see Sec. 1.4.6).

An idea about the shape of the nucleus can be had by considering another electric property of the nucleus, viz. the *quadrupole electric moment* (see Sec. 1.7).

Since the nuclear charge Z is numerically equal to the number of protons in the nucleus and the mass number A is equal to the total number of nucleons (protons plus neutrons), the number $N = A - Z$ defines the number of neutrons in the nucleus.

Nuclei with the same mass number A are called *isobars*, those with the same charge Z are called *isotopes*, while nuclei containing the same number of neutrons $N = A - Z$ are called *isotones*. A specific nucleus (atom) with given A and Z is sometimes called a *nuclide*. We shall denote a nucleus containing A nucleons and Z protons by (A, Z), its mass by $M(A, Z)$, and the mass of the atom corresponding to it by

$M_{at}(A, Z)$. When the chemical symbol of an element has to be indicated, we shall denote the nuclear and atomic masses by M (^A_ZE) and M_{at} (^A_ZE). For example, the masses of a nitrogen nucleus and atom will be denoted by M ($^{14}_{7}$N) and M_{at} ($^{14}_{7}$N) respectively.

1.2. Nuclear and Nucleonic Mass

1.2.1. Mass and Energy. Units of Measurement

One of the most important characteristics of the atomic nucleus is its mass M. In nuclear physics, the mass of a nucleus (and atom) is measured in atomic mass units. One atomic mass unit (amu) is one twelfth of the mass of a neutral ^{12}C atom.[2] The value of the atomic mass unit can be easily expressed in grams. For this purpose, we take the reciprocal of the Avogadro number (N_A):

$$1 \text{ amu} = (1/12)(12/N_A) = 1/6.022 \times 10^{23} = 1.66 \times 10^{-24} \text{ g}.$$

According to Einstein's relation, each value of mass M in grams has a value of energy Mc^2 in ergs corresponding to it, where $c = 3 \times 10^{10}$ cm/s is the velocity of light in vacuum.[3] For example, the energy corresponding to 1 g mass is 9×10^{20} erg.

When the energy of a particle changes by ΔE, its mass changes by $\Delta M = \Delta E/c^2$. Thus, for example, if a particle, which is initially at rest and has a mass M_0 (called the *rest mass*) and hence an energy M_0c^2 (called the *rest energy*), is set in motion with a velocity v, the total energy of the moving particle, E, will be greater than its rest energy by its kinetic energy T:

$$E = M_0c^2 + T.$$

The mass of the particle increases by $\Delta M = T/c^2$ and will be equal to

$$M = M_0 + T/c^2$$

for the moving particle. It is shown in the theory of relativity that this new value of mass (called the *relativistic mass of the particle*)

---

[2] Earlier, the oxygen mass unit, equal to one sixteenth of the mass of a neutral atom of the oxygen isotope, ^{16}O, was used as the atomic mass unit.

The new mass unit differs only slightly from the old one: 1 amu ($^{12}_{6}$C) = 1.000317917±0.000000017 amu ($^{16}_{8}$O) ≃ 1.66×10^{-24} g, but is more convenient for measuring mass by mass-spectrometric doublets, since carbon forms many more compounds than oxygen.

[3] The exact value of the velocity of light in vacuum is $c = 299792458.0 \pm 1.2$ m/s.

can be simply expressed in terms of the rest mass M_0 and the velocity v of the particle

$$M = M_0 + T/c^2 = M_0\gamma = M_0/\sqrt{1-\beta^2}, \qquad (1.2.1)$$

where $\gamma = 1/\sqrt{1-\beta^2}$, $\beta = v/c$, hence

$$E = M_0c^2 + T = M_0c^2/\sqrt{1-\beta^2} = M_0c^2\gamma = Mc^2.$$

Thus, the relation between the mass and energy of a particle (or a system of particles) always has the form

$$E = Mc^2, \qquad (1.2.2)$$

where $E = M_0c^2 + T$ is the total energy and $M = M_0/\sqrt{1-\beta^2}$ is the relativistic mass. Hence we obtain the following expression for the relativistic kinetic energy:

$$T = E - M_0c^2 = Mc^2 - M_0c^2 = M_0c^2(\gamma - 1). \qquad (1.2.3)$$

For $\beta \ll 1$ ($v \ll c$), this expression becomes the classical formula $T = M_0v^2/2$.[4]

Sometimes, the relation between the total energy and the rest energy can be expressed more conveniently in the form

$$E = \sqrt{M_0^2c^4 + p^2c^2} \qquad (1.2.4)$$

instead of Eqs. (1.2.2) and (1.2.3). This formula is obtained from (1.2.2) by introducing the relativistic momentum of the particle:

$$p = Mv = M_0\beta c/\sqrt{1-\beta^2} = M_0\beta c\gamma. \qquad (1.2.5)$$

We also observe that the latter relation leads to a convenient expression for the velocity:

$$\beta = pc/E. \qquad (1.2.6)$$

Comparing Eqs. (1.2.1) and (1.2.4), we obtain a relation between the kinetic energy T and the momentum p in relativistic mechanics:

$$T(2M_0c^2 + T) = p^2c^2. \qquad (1.2.7)$$

If the kinetic energy of the particle is small in comparison with its rest energy, this formula assumes the classical form $T = p^2/2M_0$ (see Footnote 4).

If the particle under consideration is complex, i.e. consists of several particles, its rest energy must depend on the state of their intrinsic motion. The atomic nucleus is a complex system consisting of nucleons. Hence its rest energy is determined by the intrinsic mo-

[4] It can be easily shown that Eq. (1.2.3) should be used when $T > 0.1M_0c^2$. If $T < 0.1M_0c^2$, the formula $T = M_0v^2/2 = p^2/2M_0$ gives a fairly accurate value (about 95%).

tion of the nucleons. The higher the energy of intrinsic motion of nucleons, the higher the rest energy $\mathcal{E}_0$ of the nucleus and, consequently, the higher its rest mass $M_0 = E_0/c^2$.

The ground state of the nucleus corresponds to the lowest value of the energy and the rest mass.[6] The difference W between the energy E_0' of an excited state and the rest energy E_0 of the ground state is called the *excitation energy of the nucleus*:

$$W = E_0' - E_0.$$

The rest mass of the nucleus in the excited state is higher than the mass of the nucleus in the ground state by

$$\Delta M_0 = W/c^2$$

The rest energy (mass) of the nucleus is independent of the state of motion of the nucleus as a whole.

In mutual interactions of nuclei (*nuclear reactions*), the total energy E of interacting particles is conserved. Thus, for example, if the interaction of particles A and B leads to the formation of particles C and D ($A + B \to C + D$), the following energy balance equations must hold:

$$M_A c^2 + M_B c^2 + T_A + T_B = M_C c^2 + M_D c^2 + T_C + T_D \quad (1.2.8)$$

or

$$E = E_{01} + T_1 = E_{02} + T_2 = \text{const}. \quad (1.2.9)$$

Here $E_{01} = (M_A + M_B)c^2$ and $T_1 = T_A + T_B$ are the rest energy and the kinetic energy of the particles taking part in the reaction, and $E_{02} = (M_C + M_D)c^2$ and $T_2 = T_C + T_D$ are the same quantities for the particles formed as a result of the reaction.

The quantity

$$Q = E_{01} - E_{02} = T_2 - T_1 \quad (1.2.10)$$

is called the *reaction energy* (see Sec. 5.3.1 for details).

It can be seen from (1.2.10) that a nuclear reaction involves the transformation of a certain fraction of the rest energy into kinetic energy ($Q > 0$) or, conversely, of a part of kinetic energy into rest energy ($Q < 0$). In both cases, the mass of particles taking part in the nuclear reaction undergoes a change. Hence the correct formulation of energy balance requires a knowledge of the expression for the energy corresponding to one atomic mass unit:

$$1 \text{ amu} \to 1.66 \times 10^{-24} \times 9 \times 10^{20} \simeq 1.5 \times 10^{-3} \text{ erg}.$$

A more convenient unit of energy, called an *electron-volt* (eV), is usually employed in nuclear physics. One electron-volt corresponds

[6] This value is smaller than the sum of the masses of nucleons on account of their interaction (see Sec. 1.3)

to the energy gained or lost by a particle with a unit electric charge (say electron or proton) when it passes through a potential difference of 1 V. Obviously, in the CGS system of units,

$$1 \text{ eV} = (4.8 \times 10^{-10})/300 = 1.6 \times 10^{-12} \text{ erg}.$$

Larger units of measurement of energy are a kiloelectron-volt (keV), a megaelectron-volt (MeV), and a gigaelectron-volt (GeV or BeV):

$$1 \text{ keV} = 10^3 \text{ eV} = 1.6 \times 10^{-9} \text{ erg},$$
$$1 \text{ MeV} = 10^6 \text{ eV} = 1.6 \times 10^{-6} \text{ erg},$$
$$1 \text{ GeV} = 1 \text{ BeV} = 10^3 \text{ MeV} = 10^9 \text{ eV} = 1.6 \times 10^{-3} \text{ erg}.$$

It should be remembered that one atomic mass unit corresponds to an energy of 931.5 MeV[6], while the energy corresponding to the mass of one electron is 0.511 MeV. If the energy is measured in megaelectron-volts (MeV), the momentum is measured in MeV/c and the mass in MeV/c^2. However, the mass of a particle is expressed quite frequently in megaelectron-volts (MeV) directly.

1.2.2. Methods of Measuring the Nuclear Mass

The following methods are employed for determining the exact values of the nuclear mass: (a) mass spectrometry, (b) analysis of energy balance in nuclear reactions, (c) alpha decay balance, (d) beta decay balance, and (e) microwave radiospectroscopy.

We shall briefly describe these methods and give an estimate of their accuracy.

1.2.2a. Mass Spectrometry

The mass of a nucleus is equal to the difference between the mass of the atom and the total mass of Z electrons in the atomic shell (to within the binding energy of these electrons).

Mass spectrometers are employed for determining the mass of an atom. The principle of operation of a mass spectrometer, which was first proposed in 1907 by J.J. Thomson, is based on the focussing properties of electric and magnetic fields with respect to the charged particles with a given value of Ze/m moving in these fields. Atoms are neutral systems and must be ionized beforehand if their motion is to be influenced by an electric or a magnetic field. The first mass spectrometers with a sufficiently high resolution were constructed by Aston and Dempster in 1919. In Aston's mass spectrometer, ions from an ion source were emitted in a given direction but with differ-

[6] The exact value of this conversion factor is 931.5016 ± 0.0026 MeV.

ent velocities and the principle of velocity focussing was used. In Dempster's mass spectrometer, all the ions having the same velocity were emitted in a wide beam and direction focussing was employed.

Figure 1 shows the schematic of Dempster's mass spectrometer. Ions are produced in the ion source by bombarding the vapours of the substance under investigation by electrons. These ions are then accelerated to an energy $T = eV$ between the slit diaphragms D_1 and D_2, and enter the vacuum chamber in a fairly wide beam. The velocity v of the ions is determined by the relation[7]

$$eV = Mv^2/2. \tag{1.2.11}$$

The ions in the chamber are under the action of a uniform magnetic field H perpendicular to the plane of the orbit. This field causes an ion to perform circular motion. The radius of the circle can be found from the equality of the Lorentz force to the centrifugal force:

$$evH/c = Mv^2/r. \tag{1.2.12}$$

Eliminating the particle velocity v from the last two equations, we obtain a relation connecting V, M, H and r:

$$M = r^2H^2e/2Vc^2. \tag{1.2.13}$$

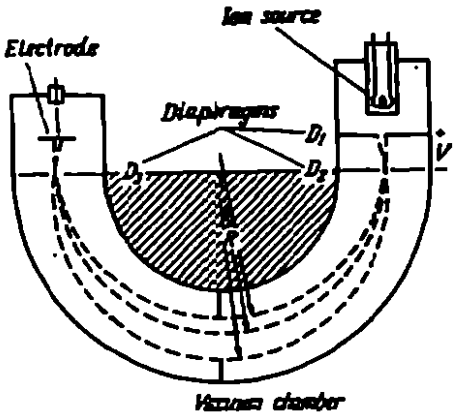

Fig. 1

This condition means that for a given magnetic field H, the radius r of the circular trajectory of an ion with mass M is controlled only by the value of the accelerating potential V. By smoothly varying the potential V, we can ensure that the radius r of the orbit coincides with the radius R of the vacuum chamber and the ions passing through the slit D_3 fall on the collecting electrode connected to an electrometer which shows an increase in the current. There is no need to create a directional ionic beam since the focussing action of the magnetic field on the trajectories of a given radius R is manifested in a fairly wide interval of the initial angles at which the ions are emitted from the source (dashed lines in Fig. 1).

Figure 2 shows a typical curve describing the dependence of the current I in the electrometer on the accelerating potential V (the scales for the left and right peaks on the ordinate axis differ by

[7] We assume the ions to be singly charged. For ions whose charge Z differs from unity, the left-hand side of Eq. (1.2.11) must contain an additional factor Z.

a factor of five). The ratio of the masses of the atoms under investigation can be determined from the positions of the peaks, since it follows from Eq. (1.2.13) that $V_1 : V_2 = M_2 : M_1$.

Dempster's spectrometer has a high resolving power. This can be seen from Fig. 2 which illustrates the analysis of potassium isotopes with mass numbers 41 and 39.

The mass spectrometers were subsequently modified and perfected. For example, a photographic plate was used instead of an electrometer as a detector. In this case, ions of different masses darken the photographic plate at different places (mass spectroscopy).

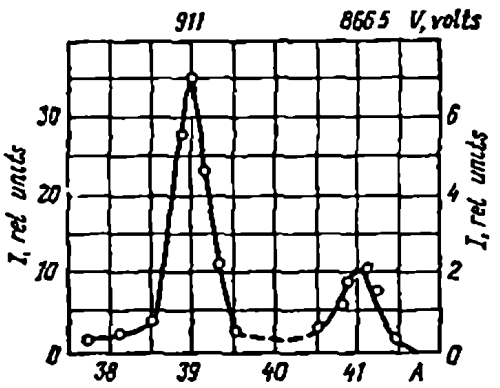

Fig. 2

Modern mass spectrometers employ the principle of double focussing (in direction and in velocity). The resolving power of such instruments is very high, and they can be used to measure mass differences with an error not exceeding 10^{-7}-10^{-8} amu. This gives a relative error $\delta M/M \simeq 10^{-8}$-$10^{-7}$ in the measurement of mass.

The development of mass-spectrometric techniques led to the confirmation of Soddy's statement made in 1910, according to which fractional atomic masses are due to the existence of isotopes. With the help of mass spectrometers, Aston and his coworkers investigated all the elements in the Periodic Table and found that almost everyone of them has several isotopes.

Table 1 shows the values of the masses of some light atoms together with the smallest errors of measurement to date.

Table 1

Isotope	Mass number	Atomic mass, amu	Isotope	Mass number	Atomic mass, amu
$^{1}_{1}H$	1	$1.00782522 \pm 4 \times 10^{-8}$	$^{7}_{4}Be$	7	$7.0169299 \pm 6 \times 10^{-7}$
$^{2}_{1}H$	2	$2.01410222 \pm 7 \times 10^{-8}$	$^{9}_{4}Be$	9	$9.0121828 \pm 6 \times 10^{-7}$
$^{3}_{1}H$	3	$3.01604972 \pm 16 \times 10^{-8}$	$^{11}_{5}B$	11	$11.00930533 \pm 3 \times 10^{-7}$
$^{3}_{2}He$	3	$3.01602970 \pm 16 \times 10^{-8}$	$^{12}_{6}C$	12	12.00000000
$^{4}_{2}He$	4	$4.00260326 \pm 27 \times 10^{-8}$	$^{14}_{7}N$	14	$14.00307440 \pm 13 \times 10^{-8}$
$^{7}_{3}Li$	7	$7.0160048 \pm 8 \times 10^{-7}$	$^{16}_{8}O$	16	$15.99491502 \pm 2 \times 10^{-7}$

It can be seen from the table that the mass of any atom (and nucleus) in atomic mass units is close to the mass number A. This

is due to the small value of the binding energy ΔW of any nucleus in comparison with its mass (see Sec. 1.3.2).

1.2.2b. Analysis of the Energy of Nuclear Reactions

The second method of determining the exact values of nuclear masses involves the application of the energy balance equation (1.2.8) for a nuclear reaction.

Suppose that we know the exact values of the masses of particles A, B and C and the kinetic energies of all the particles in Eq. (1.2.8). This gives the rest energy of particle D

$$M_D c^2 = (M_A + M_B - M_C)c^2 + T_A + T_B - T_C - T_D = (M_A + M_B - M_C)c^2 - Q, \quad (1.2.14)$$

and its mass

$$M_D = M_A + M_B - M_C - \Delta M,$$

where $\Delta M = Q/931.50$.

In actual practice, the determination of Q is reduced to the measurement of T_A and T_C, since $T_B = 0$ (the target nucleus is in a state of rest in a laboratory set-up) and T_D can be eliminated with the help of laws of conservation of energy and momentum. Exact measurements of energy are carried out with the help of magnetic analyzers which ensure $\Delta Q < 10$ keV. As a result, the mass is determined with an error

$$\delta M = \Delta Q/931.50 \simeq 10^{-5} \text{ amu}.$$

If Q is determined as a weighted average for a large number of measurements, the accuracy of mass measurement may be very high. As an example, let us consider the reaction

$$^2_1\text{H} + ^2_1\text{H} \rightarrow ^1_1\text{H} + ^3_1\text{H}, \quad (1.2.15)$$

for which the weighted average of the reaction energy is

$$Q = 4.0329 \pm 1.5 \times 10^{-4} \text{ MeV}.$$

In this case,

$$\Delta M \pm \delta M = (Q \pm \Delta Q)/931.50 = 4.329 \times 10^{-3} \pm 1.5 \times 10^{-7} \text{ amu}.$$

Thus, if the masses of the nuclei $^1_1$H and $^2_1$H are known with an error of the order of 10^{-7} amu, the mass of the nucleus $^3_1$H can be determined from the reaction (1.2.15) with the same accuracy.

Finally, it should be noted that the method of determining mass with the help of the energy balance equation for nuclear reactions can give accurate results only if:

(1) primary particles are fairly monochromatic,
(2) the energy of primary and secondary particles can be measured quite accurately, and
(3) it can be ensured that the parent and daughter nuclei are in their ground states.

1.2.2c. Alpha Decay Balance

The masses of the nuclei participating in the process of alpha decay can be determined from the energy balance equation for this process.

Alpha decay is the *process of spontaneous emission of a light* ${}_2^4\mathrm{He}$ *nucleus* (α-particle) *by a nucleus* (A, Z). The emission of an α-particle results in the formation of a nucleus with mass number $(A-4)$ and charge $(Z-2)$:

$$(A, Z) \rightarrow (A-4, Z-2) + {}_2^4\mathrm{He}. \qquad (1.2.16)$$

The necessary condition for the emission of an α-particle is that the mass of the parent nucleus should exceed the sum of the masses of the daughter nuclei:

$$M(A, Z) > M(A-4, Z-2) + M({}_2^4\mathrm{He}). \qquad (1.2.17)$$

If an α-particle is indeed emitted (see Sec. 3.2), this surplus (in units of energy) is realized as the alpha decay energy E_α:

$$E_\alpha = \{M(A, Z) - M(A-4, Z-2) - M({}_2^4\mathrm{He})\}c^2. \qquad (1.2.18)$$

It can be easily shown with the help of the laws of conservation of energy and momentum that the kinetic energy $T_\alpha \simeq (1-4/A)E_\alpha$ of the α-particle constitutes a considerable part of E_α, while the remaining energy is spent as the recoil energy of the daughter nucleus $T_{\mathrm{nuc}} \simeq 4E_\alpha/A$.

Equation (1.2.18) can be used to compute the exact value of the mass of one of the nuclei participating in alpha decay (parent or daughter nucleus) from the known values of the masses of the other nucleus and of ${}_2^4\mathrm{He}$, and by measuring the kinetic energy of the α-particle.

Modern methods of magnetic analysis of velocities of particles with a given Ze/M (cf. the "inverse" mass-spectrometric method) yield the values of kinetic energy of α-particles with an accuracy higher than ± 5 keV. This gives an absolute error $\delta M < 5 \times 10^{-6}$ amu for the mass.

1.2.2 d. Beta Decay Balance

A nucleus (A, Z), whose mass satisfies the condition

$$M(A, Z) > M(A, Z \mp 1) + m_e, \tag{1.2.19}$$

may undergo beta decay during which a positron (electron) and a neutrino (antineutrino) are emitted:

$$\left.\begin{aligned} (A, Z) &\to (A, Z-1) + e^+ + \nu, \\ (A, Z) &\to (A, Z+1) + e^- + \tilde{\nu} \end{aligned}\right\} \tag{1.2.20}$$

(see Sec. 3.3 for details of this and other types of beta decay). The energy of beta decay is given by

$$E_\beta = \{M(A, Z) - M(A, Z \pm 1) - m_e\} c^2. \tag{1.2.21}$$

Unlike alpha decay, which is a two-particle process, the beta decay energy is distributed among three particles, viz. a positron (electron), a neutrino (antineutrino) and the daughter nucleus:

$$\left.\begin{aligned} E_{\beta^+} &= T_{e^+} + E_\nu + T_{\text{nuc}} \\ E_{\beta^-} &= T_{e^-} + E_{\tilde{\nu}} - T_{\text{nuc}} \end{aligned}\right\}. \tag{1.2.22}$$

As a result, the energy spectrum of electrons (unlike the discrete spectrum of α-particles) is continuous and this complicates the measurement of E_β.

However, since T_{nuc} is small, it can be assumed that

$$E_\beta \simeq T_e + E_\nu = T_e^{\max}, \tag{1.2.23}$$

where $T_e^{\max}$ is the maximum energy of electrons (positrons) in beta decay (spectral limit). The spectral limit $T_e^{\max}$ can be measured by the method of magnetic analysis with an accuracy of ± 5 keV or higher.

Thus, an analysis of the beta decay balance equation (1.2.21) allows us to compute the mass with the same accuracy as by the method described above.

1.2.2e. Microwave Radiospectroscopy

The idea underlying this method is to measure the displacement of the rotational levels of a molecule due to a change in its mass.

It is well known that the structure of the rotational levels of a molecule depends on its moment of inertia which, in turn, depends on the reduced mass of the molecule, i.e. on the mass of the atoms in this molecule. If one of the atoms is replaced by an atom of another isotope of the same element, the reduced mass and the moment of inertia of the molecule will be slightly changed. This will lead to

a small displacement of the rotational levels. This displacement can be used to find the ratio of masses of the isotopes used in the experiment.

The energy E of transition between rotational levels is of the order of 10^{-5}-10^{-3} eV, which corresponds to the far infrared region of the optical spectrum and the microwave radiofrequency regions ($\lambda \simeq 10^{-1}$-10 cm). Since the condition $\Delta M \ll M$ is usually satisfied for the masses of the isotopes[8], $\Delta\omega \ll \omega$ and the energy shift $\Delta E = \hbar\Delta\omega$ of the rotational levels is so small that the resolving power of the optical method is not sufficient to measure it. Hence the measurement of $\Delta\omega$ is carried out by radiospectroscopic methods.

One version of the radiospectroscopic method involves the measurement of the absorption of a centimeter wave travelling in a waveguide[9] filled with the substance under investigation in gaseous form[10]. A resonant absorption of the wave is observed when its frequency coincides with the frequency of transition between rotational levels. By measuring ω_{res} and ω'_{res} in two experiments, we can find $\Delta\omega$ and compute the ratio of masses of the isotopes.

Although radiofrequency method is not used quite frequently, it has two advantages that make it a promising method for measuring mass. Firstly, it requires a very small amount of the substance under investigation and, secondly, it employs a high-accuracy resonance method of measurement.

The error in the measurement of mass ratio by this method is

$$\delta M/M \simeq 10^{-6}\text{-}10^{-5}.$$

Finally, it should be remarked that all the methods listed above have together provided about 2000 consistent values of nuclear masses, many of which are known with high accuracy.

To analyze the properties of atomic nuclei, it is very important to know the exact values of the masses of protons and neutrons, that is the particles constituting a nucleus. It can be seen from Table 1 that the mass of the hydrogen atom (and hence, the mass of the proton) has been determined up to seven decimal places with the help of modern mass-spectroscopic measurements. The approximate values for the masses of the hydrogen atom and the proton in various units are given below:

$$M_{at}\,(^1_1\mathrm{H}) = 1.007825\ \text{amu} = 938.79\ \text{MeV}/c^2 = 1837.2m_e,$$
$$m_p = 1.007276\ \text{amu} = 938.28\ \text{MeV}/c^2 = 1836.2m_e.$$

[8] Naturally, this condition is not satisfied for light elements.

[9] A waveguide is a metallic pipe whose diameter is comparable with the length of the wave propagating in it.

[10] Rotation is hampered in condensed media.

The methods of determining the mass of the neutron are described in the following section.

1.2.3. The Mass of the Neutron

Neutron is an electrically neutral particle, hence its mass cannot be determined by mass-spectroscopic methods. The first rough estimate of the mass of the neutron was made at the time of its discovery in 1932 by Chadwick. For this purpose, the results of experiments on neutron irradiation of hydrogen and nitrogen were analyzed with the help of the laws of conservation of momentum and energy.

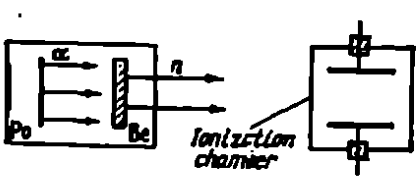

Fig. 3

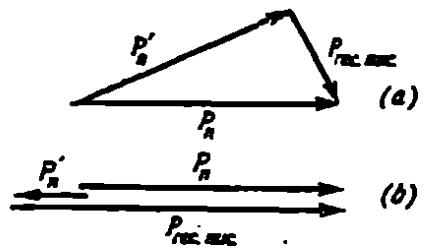

Fig. 4

In Chadwick's experiment (Fig. 3), the neutrons obtained by bombarding a beryllium target by α-particles from polonium were directed into the ionization chamber (see Sec. 6.1) which was alternately filled with hydrogen and nitrogen. The collisions of neutrons with the nuclei of the gas filling the chamber led to the formation of fast recoil nuclei. The ions left in the wake of these fast nuclei were registered by the ionization chamber as current pulses. The energy of a recoil nucleus depends on the energy of the neutrons and the nature of collision (Fig. 4).

Obviously (see Fig. 4*b*), the recoil nuclei will have the maximum energies for head-on collisions of neutrons with the hydrogen and nitrogen nuclei.[11] In this case, we can easily obtain the following relation between these energies and the masses of the neutron and the nuclei:

$$\sqrt{\frac{(T_{\mathrm{H}})_{\max} M(^{1}_{1}\mathrm{N})}{(T_{\mathrm{N}})_{\max} M(^{1}_{1}\mathrm{H})}} = \frac{M(^{1}_{1}\mathrm{N}) + m_n}{M(^{1}_{1}\mathrm{H}) + m_n}. \qquad (1.2.24)$$

Substituting the experimentally measured values of $(T_{\mathrm{H}})_{\max} = 5.7$ MeV and $(T_{\mathrm{N}})_{\max} = 1.2$ MeV into (1.2.24), we obtain the following expression for the mass of the neutron:

$$m_n \simeq 1 \text{ amu}.$$

[11] See Sec. 4.4.1 for details on elastic scattering.

The accuracy of measurements in this case was such that only an approximate equality of the proton and neutron masses could be established:

$$m_n \simeq m_p.$$

The exact value of the neutron mass can be determined from the energy balance of nuclear reactions involving neutrons. Such nuclear reactions may be reactions induced by neutrons or reactions leading to the formation of neutrons. The simplest reaction of the second type is the splitting of a deuteron under the action of γ-quanta:

$$\gamma + {}_1^2\mathrm{H} \rightarrow n + p. \qquad (1.2.25)$$

The law of energy conservation for this reaction can be written as follows:

$$E_\gamma + M({}_1^2\mathrm{H})c^2 = m_n c^2 + T_n + m_p c^2 + T_p, \qquad (1.2.26)$$

where E_γ is the energy of a γ-quantum, $M({}_1^2\mathrm{H})c^2$, $m_n c^2$ and $m_p c^2$ are the rest energies of the deuteron, neutron and proton respectively, T_n and T_p are the kinetic energies of the neutron and the proton (the deuteron is assumed to be at rest).

Gamma-quanta from ThC″ (${}_{81}^{208}\mathrm{Tl}$) having an energy of 2.62 MeV were used in the experiment. Measurements were carried out with the help of the Wilson cloud chamber and gave the value $T_p = 0.2$ MeV. It follows from simple considerations that $T_n \simeq T_p$. Indeed, it was established in Chadwick's experiment that $m_n \simeq m_p$. Besides, $|\mathbf{p}_n| \simeq |\mathbf{p}_p|$, since the momentum of a γ-quantum having an energy of 2.62 MeV is much smaller than that of a proton having an energy of 0.2 MeV.

Thus, all quantities in Eq. (1.2.26) are known with the exception of $m_n c^2$ which has to be determined. It can be easily seen that the accuracy with which the mass m_n of the neutron can be determined depends only on the accuracy with which the masses of the proton and deuteron and the energies of the γ-quanta and the proton are known. The approximate nature of the relations $|\mathbf{p}_n| \simeq |\mathbf{p}_p|$ and $T_n \simeq T_p$ does not affect the accuracy of the results since the error can be eliminated by repeating the calculation, using the mass of the neutron found in the previous calculation (the method of successive approximations). Thus, it was found that

$$m_n = 1.00866 \text{ amu}.$$

Another reaction which can be used for determining the mass of the neutron is the reaction involving the interaction of nitrogen with *slow (thermal) neutrons* (see Sec. 6.3.2) having an energy $T_n = 2.5 \times 10^{-2}$ eV:

This reaction leads to the formation of protons with energy $T_p = 0.585$ MeV. The energy balance equation for this reaction can be written as follows:

$$[M(^{14}_{7}\mathrm{N}) + m_n]c^2 = [M(^{14}_{6}\mathrm{C}) + m_p]c^2 + T_p + T_{^{14}_{6}\mathrm{C}},$$

or (after adding seven electron masses to each side)

$$m_n c^2 = [M_{at}(^{14}_{6}\mathrm{C}) - M_{at}(^{14}_{7}\mathrm{N})]c^2 + M_{at}(^{1}_{1}\mathrm{H})c^2 + T_p + T_{^{14}_{6}\mathrm{C}}.$$

The difference in the masses of the atoms $^{14}_{6}$C and $^{14}_{7}$N is known from mass-spectrometric measurements and is equal to 0.156 MeV in units of energy. The kinetic energy of the $^{14}_{6}$C atom can be calculated from the proportion $T_{^{14}_{6}\mathrm{C}}/T_p = m_p/M(^{14}_{6}\mathrm{C})$, which follows from the law of conservation of momentum:

$$\mathbf{p}_n = \mathbf{p}_p + \mathbf{p}_{^{14}_{6}\mathrm{C}},$$

in view of the fact that the neutron is slow ($p_n \simeq 0$). Calculations give the difference in the masses of a neutron and a hydrogen atom [$\Delta n = m_n - M_{at}(^{1}\mathrm{H}) = 0.782$ MeV], which can be used to determine the mass of the neutron.

The most accurate value of the neutron mass known to date is $m_n = 1.00866522 \pm 6 \times 10^{-8}$ amu, and the approximate value is $m_n \simeq 1.00867$ amu $= 939.57$ MeV $= 1838.7 m_e$. Thus, the mass of the neutron is larger than the proton mass by $2.5\, m_e$ (1.3 MeV). Hence the decay of a neutron into a proton and an electron[12] is allowed from the point of view of energy. This process will be analyzed in Chap. 3. The average value of the mass of a nucleon is

$$\overline{m}_N = (m_p + m_n)/2 \simeq 1.008 \text{ amu} \simeq 939 \text{ MeV}/c^2. \quad (1.2.28)$$

1.3. Nuclear Binding Energy of All Nucleons. Nuclear Stability

Knowing the exact values of the proton and neutron masses, we can compare the mass M of an atomic nucleus with the sum of masses of all the nucleons constituting this nucleus. It is found that the mass of a nucleus is always less than the sum of masses of all its neutrons and protons. This result is quite natural, since the nucleus is a tightly bound system of nucleons corresponding to the minimum energy.

The quantity

$$\Delta W = [Zm_p + (A - Z)m_n - M(A, Z)]c^2 \quad (1.3.1)$$

[12] In this process, an electron antineutrino $\tilde{\nu}_e$ is also emitted besides a proton and a neutron.

is called the *binding energy of the nucleus* relative to all the nucleons constituting it. The binding energy is a measure of energy which must be spent to split a given nucleus into all its constituent nucleons. It can be easily seen that the binding energy can be expressed in terms of the masses of neutral atoms. This is obvious from the fact that the atomic mass differs from the nuclear mass by a quantity equal to the mass of Z electrons (to within the electron binding energy):

$$\Delta W = [ZM_{at}({}^1_1\mathrm{H}) + (A - Z)m_n - M_{at}(A, Z)]c^2. \quad (1.3.2)$$

This version of the formula is more convenient since the masses of neutral atoms are usually given in tables instead of nuclear masses. The approximate values of the binding energy for some nuclei (in MeV) are:

$$\Delta W({}^{32}_{16}\mathrm{S}) \simeq 272, \quad \Delta W({}^{16}_{8}\mathrm{O}) \simeq 128,$$
$$\Delta W({}^{12}_{6}\mathrm{C}) \simeq 92, \quad \Delta W({}^{4}_{2}\mathrm{He}) \simeq 28.$$

1.3.1. Binding Energy ε per Nucleon. Energy Surface

The binding energy divided by the mass number A is called the *specific binding energy of a nucleon* in the nucleus or the *binding energy per nucleon:*

$$\varepsilon = \Delta W/A. \quad (1.3.3)$$

If the values of ε are calculated for all known nuclei and plotted as functions of A and Z in the (ε, A, Z)-space, a fairly smooth surface can be constructed from the obtained set of points $\varepsilon(A, Z)$. We shall call this surface the *energy surface.* To a very rough approximation, the energy surface is a warped ridge (Fig. 5) whose crest passes over the track of the most strongly bound (β-stable) nuclei, while the slopes pass over the region of β^-- and β^+-radioactive nuclei. The track of β-stable nuclei in the (A, Z) plane is determined by the formula

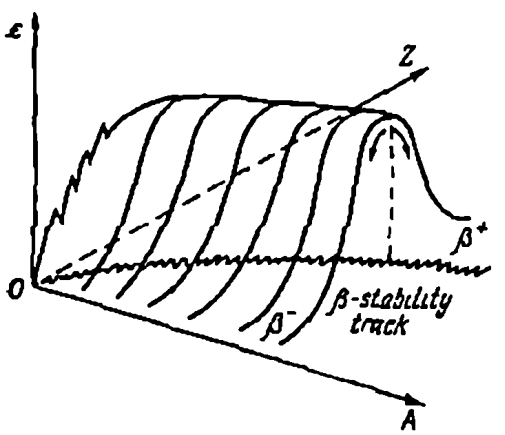

Fig. 5

$$Z = A/(1.98 + 0.015A^{2/3}) \quad (1.3.4)$$

(see Sec. 2.1). A more clear idea about the nature of the energy surface in relation to the properties of the nucleus can be obtained by considering its various sections.

The section of the energy surface by the plane A = const defines the values of ε for all nuclei, viz. isobars, with a given value of A (Fig. 6). It has the form of one (for odd A) or two (for even A) parabolas. In the first case, the values of $\varepsilon(A, Z)$ for even-odd (even Z, odd N) and odd-even (odd Z, even N) nuclei lie on the parabola. In the second case, the values of $\varepsilon(A, Z)$ for even-even nuclei (nuclei with even numbers of protons and neutrons) lie on the upper parabola, while the values of $\varepsilon(A, Z)$ for odd-odd nuclei lie on the lower

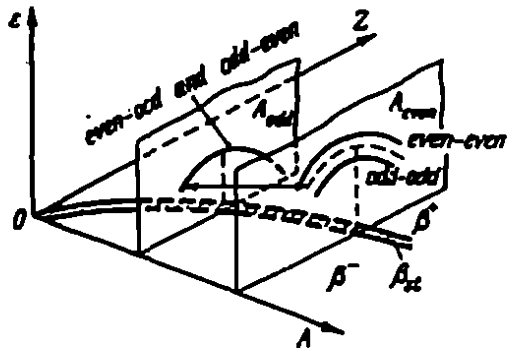

Fig. 6

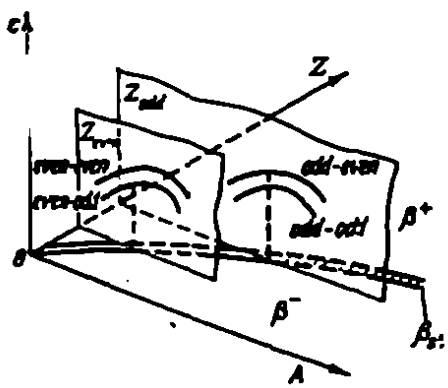

Fig. 7

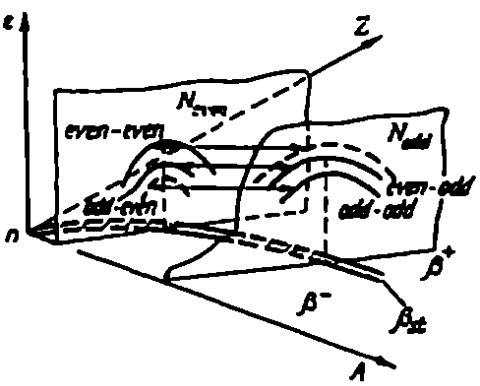

Fig. 8

parabola. The section of the energy surface by the plane Z = const (family of isotopes in Fig. 7) or $N = A - Z$ = const (family of isotones in Fig. 8) has the shape of two parabolas. On one of these parabolas lie the values of $\varepsilon(A, Z)$ for nuclei with even A, while the other parabola contains the corresponding values for nuclei with odd A. For even Z (or N), the parabola with even A lies above the parabola with odd A, while the situation is reversed for odd Z (or N). The vertices of the parabolas correspond to the values of ε for the

most stable (as a rule, β-stable) nuclei from a given family, while their branches correspond to the values of ε for β-radioactive nuclei.[13]

Thus, in the next (more accurate) approximation, the energy surface is a three-layered surface whose upper layer contains the values of ε for even-even nuclei, the middle layer for odd-even and even-odd nuclei, and the lower layer for odd-odd nuclei.

The sections listed above (A = const, Z = const, N = const) are quite convenient for a comparative analysis of β-stable and β-radioactive nuclei (see Sec. 1.3.4), but these sections cover only a comparatively small number of nuclei (about 25 at the most) in a narrow range of variation of Z and N (A and N, A and Z respectively). Hence they cannot provide information about the properties that are typical of most nuclei.

In order to obtain such information, we must construct a section which singles out a much larger class of nuclei based on a different property that is more convenient for analysis. This property is the β-stability of nuclei.

1.3.2. Beta-stable Nuclei and Properties of Nuclear Forces

Suppose that the energy surface is intersected by a vertical cylindrical surface passing through "the crest of the ridge" (Fig. 9). The section thus obtained will lie in the (A, Z) plane passing through the track of β-stable nuclei. This is the richest section in the sense that it contains information about the properties of some 350 β-stable nuclei. These include light and heavy nuclei, stable and α-radioactive nuclei, nuclei differing in spins, in the number of the nucleons contained in them (even-even, even-odd, odd-even, odd-odd), or in other properties. An analysis of this section provides the most extensive information on the properties of nuclei and nuclear forces. Let us consider these properties developing the cylindrical surface into a plane for the sake of convenience (Fig. 10).

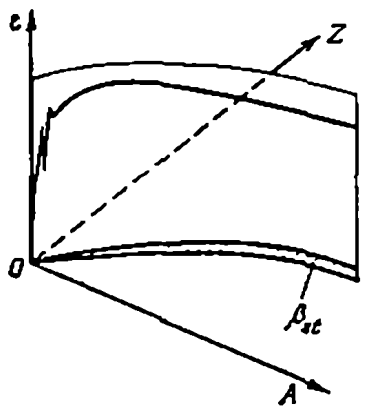

Fig. 9

It can be seen from the figure that ε (A) increases rapidly from ε = 0 for A = 1 to ε = 8 MeV for A = 16, passes through its maximum value ε_{max} = 8.8 MeV for $A \simeq 60$ (^{58}Fe and ^{62}Ni) and then

[13] There is an exception to this rule in the case of odd-odd nuclei among which only four are β-stable.

gradually decreases to $\varepsilon \simeq 7.6$ MeV for the heaviest element encountered in nature, viz. uranium. The average value $\bar{\varepsilon}$ is equal to 8 MeV and $\varepsilon \simeq \bar{\varepsilon} = 8$ MeV for most of the nuclei. Hence, to a first approximation, the binding energy of atomic nuclei can be expressed in terms of the mass number through the relation

$$\Delta W \simeq \bar{\varepsilon} A = 8A \text{ MeV} \simeq 0.0085A \text{ amu}. \qquad (1.3.5)$$

An analysis of the curve $\varepsilon(A)$ and of the relation (1.3.5) leads to the following conclusions concerning the properties of nuclei and nuclear forces:

(1) From the positive values of ΔW and ε for all nuclei (i.e. from the existence of the nuclei) it follows that nuclear forces are attractive in nature, the energy of attraction more than compensating the Coulomb repulsion between protons.

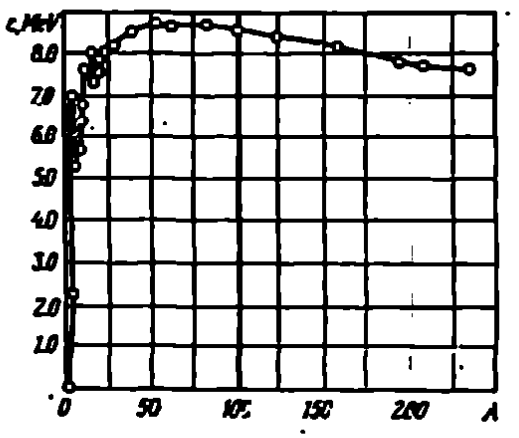

Fig. 10

(2) The large value of the average binding energy per nucleon $\bar{\varepsilon} = 8$ MeV means that the nuclear interaction is extremely strong. Thus, for example, the binding energy per nucleon in the ${}_2^4\text{He}$ nucleus ($\varepsilon \simeq 7$ MeV) is much higher than the Coulomb repulsion energy for the two protons[14] in this nucleus:

$$V_C = e^2/\delta = (4.8 \times 10^{-10})^2/(2 \times 10^{-13} \times 1.6 \times 10^{-6}) \simeq 0.7 \text{ MeV}.$$

As a matter of fact, it will be shown that the nuclear interaction is much stronger than the electromagnetic interaction (when compared for distances $\sim 10^{-13}$ cm) by 2-3 orders of magnitude.

(3) The linear dependence of ΔW on A implies a saturation of nuclear forces, i.e. the ability of a nucleon to interact not with all the nucleons surrounding it but just with a few of them. Indeed, if each nucleon in a nucleus interacted with all the $(A - 1)$ remaining nucleons, the total binding energy would be proportional to $A(A - 1) \simeq A^2$ and not to A. Saturation is closely related to the short-range nature of interaction.

(4) The existence of the ${}_1^2\text{H}$ nucleus consisting of a proton and a neutron having parallel spins and the absence of an analogous

[14] The distance $r = 2 \times 10^{-13}$ cm between protons can be obtained by comparing the dimensions of the nucleus with the number of nucleons in it (see Sec. 2.1).

nucleus in nature with antiparallel spins of the neutron and the proton indicate that the nuclear forces depend on spin.

(5) It follows from the relation $\Delta W \ll M(A, Z)$ that

$$M_{\text{nuc}} \simeq A \text{ amu}. \tag{1.3.6}$$

The accuracy of this equality is estimated as follows. From Eqs. (1.3.1) and (1.2.28) we get

$$M(A, Z) = Zm_p + (A-Z)m_n - \Delta W(A, Z) \simeq A\overline{m}_N - \Delta W(A, Z).$$

Hence

$$M(A, Z) \simeq (1.008 - 0.0085)A \text{ amu} = 0.9995A \text{ amu}$$

and the mass excess ΔM over the mass number A (also known as mass defect) will be given by

$$|\Delta M| = |M - A| = 0.0005 \text{ amu}. \tag{1.3.7}$$

Thus, the mass of a β-stable nucleus coincides, as a rule, with the mass number A to an accuracy of 99.9%. Some light nuclei, for which the mass defect ΔM is approximately equal to 1%, are an exception to this rule. For light nuclei ($A < 20$), the mass defect is usually positive ($\Delta M > 0$), while it has a negative value for $A > 20$ ($\Delta M < 0$).

(6) A comparison of the binding energies of two mirror nuclei (i.e. nuclei which are obtained from each other by replacing all the protons with neutrons and vice versa) showed that they coincide but for a correction term for the excess energy of Coulomb interaction in the case of the nucleus with an excess of protons. Thus, for example,

$$\Delta W({}_1^3\text{H}) - \Delta W({}_2^3\text{He}) = e^2/\delta \approx 0.75 \text{ MeV}$$

where e^2/δ is the energy of Coulomb repulsion between two protons in the ${}_2^3$He nucleus, and δ is their separation. This result can be interpreted as the charge symmetry of nuclear forces: $(p\text{-}p)_{nuc} = n\text{-}n$. A similar analysis of nuclear triplets in which three different pairs of nucleons, viz. n-n, p-p and n-p, are in identical states leads to the following hypothesis about the charge independence of nuclear forces:

$$n\text{-}n \equiv (p\text{-}p)_{nuc} \equiv n\text{-}p$$

(see Sec. 1.8 in this volume and Sec. 1.5.7 in Vol. II for details).

(7) The track of β-stable (the most stable) nuclei lies in the (A, Z) plane in such a way that $Z \simeq N \simeq A/2$ for light nuclei (symmetry effect), and $N \simeq 1.5Z$ (i.e. $Z \simeq A/2.5$) for heavy nuclei. The symmetry effect is explained by the fact that the proton and the neutron have spins equal to 1/2 and obey Pauli's exclusion principle. It is known from atomic physics that the exclusion principle forbids

two identical particles with half-integral spin to be in identical states. If we use the independent-particle model (see Chap. 2 for details of this model) and represent the possible states for nucleons as neutron and proton energy levels in a "dual" potential well (Fig. 11), then according to Pauli's exclusion principle the first neutron level can contain 0, 1 or 2 neutrons (with antiparallel spins). Similarly, the first proton level cannot contain more than two protons (also with antiparallel spins). The third and fourth neutrons (protons) must occupy the second neutron (proton) level, and so on.

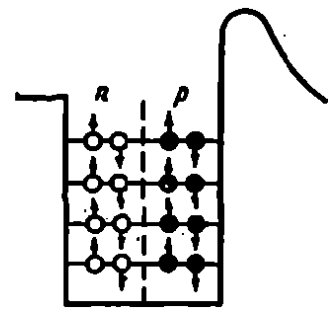

Fig. 11

Obviously, it is more favourable from energy point of view to fill both "halves" of the well to nearly the same height (energy). Otherwise, the higher-lying protons (neutrons) could go over to vacant lower levels in the neighbouring half of the well as a result of the mutual transformation $p \rightarrow n$ ($n \rightarrow p$), meaning thereby that the corresponding nucleus is not stable but β^+- (β^-)-radioactive.

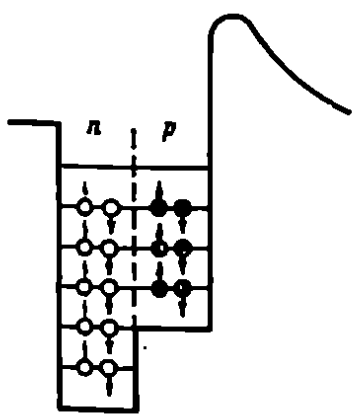

Fig. 12

In view of the charge symmetry of nuclear forces, the depth of both halves of the well is approximately the same (see Fig. 11) for light nuclei in which the Coulomb interaction is comparatively weak. Hence a symmetric filling of both types of levels ($N \simeq Z$) is favourable from the point of view of energy. On account of a relatively strong Coulomb interaction for heavy nuclei (unlike the nuclear interaction, which increases linearly with the atomic number A, the Coulomb interaction increases in proportion to A^2 or Z^2), the neutron half of the well is much deeper than the proton half. Hence the filling of levels in heavy nuclei by excess neutrons is more favourable from the energy point of view (Fig. 12).

The relation between Z and A in β-stable nuclei is determined by Eq. (1.3.4).

(8) The binding energy ε per nucleon in a nucleus is a measure of its stability. The value of ε is especially large in even-even nuclei (even Z and even N), which include the *α-particle-like nuclei* ^{12}C,

^{16}O, etc.[15]. This circumstance indicates an additional (pairing) interaction between two nucleons of the same type (see Sec. 1.3.4 for details) and an especially stable system of four nucleons (two protons and two neutrons, see Fig. 13).

Nuclei with an odd mass number, i.e. even-odd (even Z and odd N, see Figs. 14 and 15) and odd-even (odd Z and even N, see Figs. 16 and 17) nuclei have an unpaired neutron (proton) and hence a somewhat lower value of ε. Finally, the odd-odd nuclei (odd Z and

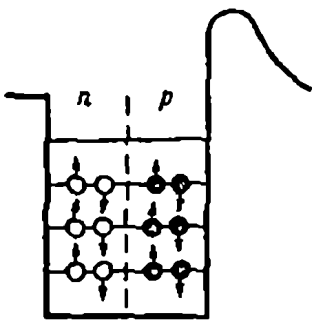

Fig. 13

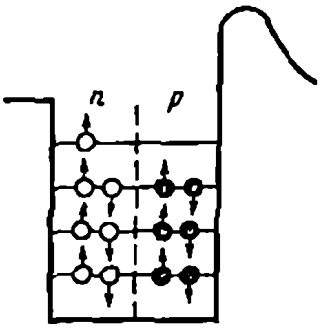

Fig. 14

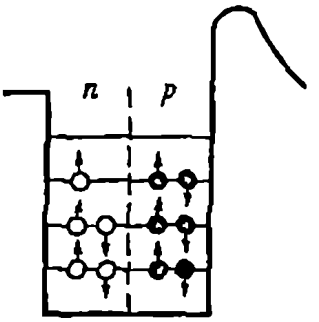

Fig. 15

odd N, see Fig. 18) are β-radioactive as a rule, since they have two unpaired nucleons, i.e. the lowest value of ε (only four such β-stable nuclei are known: $^{2}_{1}H$, $^{6}_{3}Li$, $^{10}_{5}B$ and $^{14}_{7}N$).

(9) A comparison of the values of ε for all even-even nuclei reveals that even against the background of α-particle-like nuclei with a high

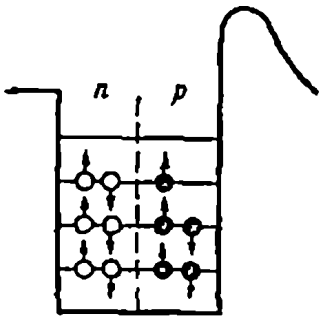

Fig. 16

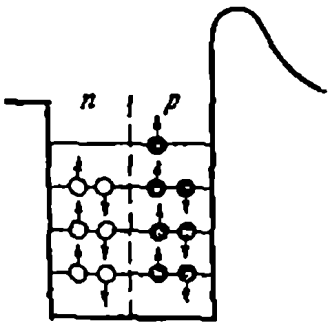

Fig. 17

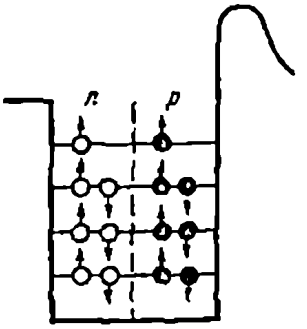

Fig. 18

stability, there are still higher values of ε for nuclei containing one of the following numbers of protons and (or) neutrons: 2, 8, 20, (28), 50, 82, 126 (the last number corresponds to neutrons only). These numbers are called *magic numbers* and the nuclei are called

[15] α-Particle-like nuclei are the ones containing $A = 4n$ nucleons, of which there are $Z = 2n$ protons and $N = 2n$ neutrons, n being an integer. These nuclei as if consist of several α-particles. These nuclei have some specific properties which are considered in the α-particle model of the nucleus (see Sec. 10.5).

magic nuclei. Nuclei having magic numbers of protons and neutrons are called *double magic nuclei*. The unusually high stability of magic nuclei is explained in the shell model of the nucleus which was the next step from the simple independent-particle model.

According to the shell model, the nucleon energy levels with close values of energy (small value of δE in Fig. 19) group together into series that are isolated from each other ($\Delta E \gg \delta E$) and are called *nucleon shells*. In accordance with Pauli's exclusion principle, each shell can contain a strictly limited number of nucleons of a given type (see the numbers on the left of Fig. 19). The filling of a shell corresponds to the formation of a magic nucleus (see the numbers on the right of Fig. 19). Nucleon shells for protons and neutrons are filled independently. A simultaneous filling of proton and neutron shells indicates the formation of the especially stable doublemagic nuclei.

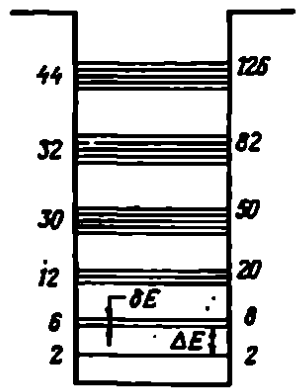

Fig. 19

Besides allowing for the existence of magic nuclei, the shell model also explains some other important properties of the atomic nucleus (see Chap. 2).

(10) For quite heavy nuclei (the right section of the ε vs. A curve in Fig. 20), the process of alpha decay is more favourable:

$$(A, Z) \to (A - 4, Z - 2) + {}_2^4\mathrm{He}. \qquad (1.3.8)$$

This follows from an analysis of the energy of alpha decay:

$$\begin{aligned} E_\alpha &= \{M(A, Z) - M(A-4, Z-2) - m_\alpha\}c^2 \\ &= \Delta W(A-4, Z-2) + \Delta W({}_2^4\mathrm{He}) - \Delta W(A, Z) \\ &= (A-4)\varepsilon_{A-4} + 4\varepsilon({}_2^4\mathrm{He}) - A\varepsilon_A \\ &= 4\{\varepsilon({}_2^4\mathrm{He}) - \varepsilon_{A-4}\} + A\{\varepsilon_{A-4} - \varepsilon_A\} \\ &\simeq 4\{\varepsilon({}_2^4\mathrm{He}) - \varepsilon_{A-4}\} + A(d\varepsilon/dA)\,dA. \qquad (1.3.9) \end{aligned}$$

In order to estimate E_α numerically, we choose $A = 220$ and consider the dependence of ε on A as A varies from 200 to 240. It follows from Fig. 20 that

$$\varepsilon({}_2^4\mathrm{He}) = 7.1 \text{ MeV}, \quad \varepsilon(220) \simeq \varepsilon(216) = 7.7 \text{ MeV},$$
$$d\varepsilon/dA \simeq \Delta\varepsilon/\Delta A = -0.33/40 = -1/120 \text{ MeV},$$
$$dA = -4.$$

(The mass number decreases by four units as a result of alpha decay.) Substituting this value into (1.3.9), we get

$$E_\alpha = 4\,(7.1 - 7.7) + 220 \times 4/120 \simeq 5 \text{ MeV}.$$

Although this is a very rough estimate, it gives the correct order of magnitude of the energy of alpha decay (see Sec. 3.2 for a more accurate estimate).

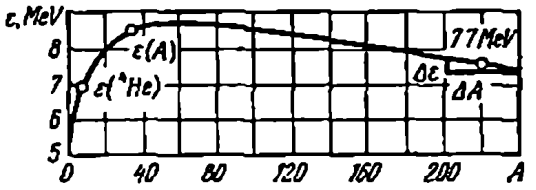

Fig. 20

Obviously, alpha decay is not possible in the case of light nuclei [16] since for the left branch of the curve (see Fig. 20)

$$d\varepsilon/dA > 0, \text{ while } \{\varepsilon(^4_2\text{He}) - \varepsilon_{A-4}\} < 0$$

and

$$E_\alpha < 0.$$

(11) For heavy nuclei (A, Z) corresponding to the right branch of the ε vs. A curve, the process of *fission* into two roughly equal in mass

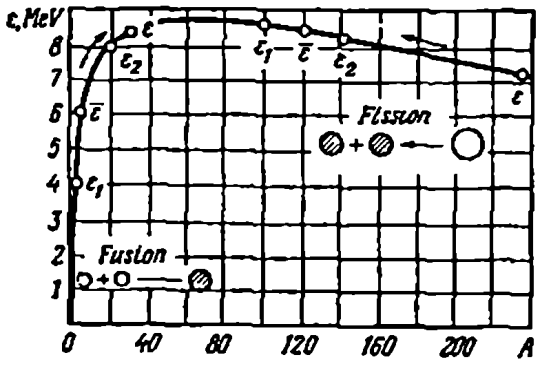

Fig. 21

nuclei (A_1, Z_1) and (A_2, Z_2), called the *fission fragments*, is more favourable from the point of view of energy (Fig. 21).

[16] Naturally, this conclusion is no longer valid if the light nucleus is in a highly excited state (see, for example, Sec. 3.2.6).

For light nuclei (A_1, Z_1) and (A_2, Z_2) belonging to the left side of the ε vs. A curve, the processes of *fusion* (synthesis) into a single heavier nucleus (A, Z) is more favourable from energy point of view:

$$A = A_1 + A_2, \qquad Z = Z_1 + Z_2.$$

The proof of these statements follows from a comparison of the masses of all three nuclei.

These masses can be written in the following form with the help of Eq. (1.3.1):

$$M = Zm_p + (A - Z)m_n - \varepsilon A,$$
$$M_1 = Z_1 m_p + (A_1 - Z_1)m_n - \varepsilon_1 A_1,$$
$$M_2 = Z_2 m_p + (A_2 - Z_2)m_n - \varepsilon_2 A_2.$$

This gives the following expression for the energy liberated in the case of fission of heavy nuclei:

$$Q_{fis} = (M - M_1 - M_2)c^2 = \varepsilon_1 A_1 + \varepsilon_2 A_2 - \varepsilon A = A(\bar{\varepsilon} - \varepsilon), \quad (1.3.10a)$$

where $\bar{\varepsilon} = (\varepsilon_1 A_1 + \varepsilon_2 A_2)/(A_1 - A_2)$ is the average value of ε for the nuclei (A_1, Z_1) and (A_2, Z_2). It can be seen from Fig. 21 (right side) that $\bar{\varepsilon} > \varepsilon$, i.e. $Q_{fis} > 0$.

Similarly, for the fusion of light nuclei, we have

$$Q_{fus} = (M_1 + M_2 - M)c^2 = A(\varepsilon - \bar{\varepsilon}), \quad (1.3.10b)$$

where $\varepsilon > \bar{\varepsilon}$, i.e. $Q_{fus} > 0$ (see the left side of Fig. 21). At present, both these processes (fission of heavy nuclei and fusion of light nuclei) are used to obtain energy (the process of fusion is realized so far only in the form of the explosion of a thermonuclear bomb).

(12) Estimates of the values of Q_{fis} by Eq. (1.3.10a) for various nuclear fragments show that the fission energy for heavy nuclei decreases rapidly with increasing ratio A_1/A_2 (and Z_1/Z_2) from $Q_{fis} \simeq 200$ MeV for $A_1 \simeq A_2$ to $Q_{fis} \simeq 30$ MeV for $A_1/A_2 \simeq 15$. The positive value of Q_{fis} for $A_1 \gg A_2$ allows in principle the existence of radioactive processes accompanied by the escape of nuclei heavier than ^{4}He. One such process, viz. natural radioactivity of carbon, was discovered in 1984 (see Sec. 3.5.4).

For example, the binding energy of the $^{32}_{16}S$ nucleus with respect to two $^{16}_{8}O$ nuclei is

$$\Delta W_{2^{16}_{8}O}(^{32}_{16}S) = [2M(^{16}_{8}O) - M(^{32}_{16}S)]c^2 = \Delta W(^{32}_{16}S) - 2\Delta W(^{16}_{8}O) \simeq 16 \text{ MeV}.$$

Similarly,

$$\Delta W_{8^{4}_{2}He}(^{32}_{16}S) = \Delta W(^{32}_{16}S) - 8\Delta W(^{4}_{2}He) \simeq 48 \text{ MeV},$$

and *so on*. Naturally, the binding energy in all these cases is less than $\Delta W(^{32}_{16}S) = 272$ MeV.

In some cases, the binding energy of the nucleus with respect to some of its constituents becomes very small. This is the case, for example, when a light nucleus emits a neutron.

Thus, the binding energy of $^{9}_{4}Be$ with respect to its disintegration into a neutron and two helium nuclei $^{4}_{2}He$ is equal to about 2 MeV, although the binding energy of the $^{9}_{4}Be$ nucleus with respect to all its nine nucleons is

$$\Delta W(^{9}_{4}Be) \simeq 58 \text{ MeV}.$$

Nuclei of heavy elements, for example uranium, have a very high binding energy with respect to all its nucleons. However, if the binding energy for $^{238}_{92}U$ is calculated with respect to $^{4}_{2}He$ and $^{234}_{90}Th$, we obtain a negative value:

$$\Delta W_{^{234}_{90}Th + ^{4}_{2}He}(^{238}_{92}U) = [M(^{234}_{90}Th) + M(^{4}_{2}He) - M(^{238}_{92}U)]c^2 = -4.25 \text{ MeV}.$$

This means that the uranium nucleus is an unstable system with respect to disintegration into an α-particle ($^{4}_{2}He$ nucleus) and $^{234}_{90}Th$. Indeed, uranium is found to be alpha-active. Apparently, the quantity $\Delta W_{(A-4,\,Z-2)+^{4}_{2}He}(A, Z)$ coincides with the alpha decay energy E_α introduced above [see Eqs. (1.2.18) and (1.3.9)] up to the sign:

$$\varepsilon_\alpha = \Delta W_{(A-4,\,Z-2)+^{4}_{2}He}(A, Z) = -E_\alpha(A, Z). \qquad (1.3.11)$$

Similarly, it follows from Eq. (1.3.10a) that heavy nuclei, for example uranium, have a negative binding energy with respect to the nuclei (A_1, Z_1) and (A_2, Z_2) satisfying the condition $A_1 + A_2 = A$, $Z_1 + Z_2 = Z$, $A_1 \simeq A_2$ and $Z_1 \simeq Z_2$:

$$\Delta W_{(A_1,\,Z_1)+(A_2,\,Z_2)}(A, Z) = [M(A_1, Z_1) + M(A_2, Z_2) - M(A, Z)]c^2 = -Q_{\text{fis}}(A, Z) < 0. \qquad (1.3.12)$$

The binding energy of $^{238}_{92}U$ with respect to the nuclei $^{234}_{90}Th$ and $^{4}_{2}He$ is the energy which must be spent to detach an α-particle from the uranium nucleus. Hence it can be called the *separation energy* (or

binding energy) ε_α *of an α-particle* for the uranium nucleus. The concept of *separation energy* ε_N *for a nucleon* is widely used in nuclear physics (not to be confused with the binding energy per nucleon $\varepsilon = \Delta W/A$). In analogy with the above, the separation energy of a nucleon, say neutron, for the nucleus (A, Z) is defined as

$$\varepsilon_n = \{m_n + M(A-1, Z) - M(A, Z)\}c^2. \quad (1.3.13)$$

The physical meaning of the neutron separation energy is that this is the energy which must be imparted to a nucleus (A, Z) in order to separate a neutron from it. Obviously, if the reverse process of fusion of a nucleus $(A-1, Z)$ and a neutron is considered, the nucleus (A, Z) is formed and the energy liberated is equal to the energy ε_n of separation of the neutron from the nucleus (A, Z). In this case, it is sometimes called the *energy of adhesion* to the nucleus $(A-1, Z)$.

The binding (seperation) energy ε_p of a proton in the nucleus is defined in a similar manner:

$$\varepsilon_p = \{m_p + M(A-1, Z-1) - M(A, Z)\}c^2. \quad (1.3.14)$$

It can be easily seen that

$$\left.\begin{aligned} \varepsilon_\alpha &= \Delta W(A, Z) - \Delta W(A-4, Z-2) - \Delta W({}^4_2\mathrm{He}), \\ \varepsilon_n &= \Delta W(A, Z) - \Delta W(A-1, Z), \\ \varepsilon_p &= \Delta W(A, Z) - \Delta W(A-1, Z-1). \end{aligned}\right\} \quad (1.3.15)$$

Unlike ε, the values of ε_n and ε_p fluctuate strongly from nucleus to nucleus. Thus, for example, $\varepsilon_n({}^2_1\mathrm{H}) = \varepsilon_p({}^2_1\mathrm{H}) = 2.22$ MeV, $\varepsilon_n({}^{13}_7\mathrm{N}) = 20.3$ MeV, $\varepsilon_p({}^{11}_6\mathrm{C}) = 20.8$ MeV, $\varepsilon_p({}^{13}_7\mathrm{N}) = 1.9$ MeV (see Sec. 1.3.4 for details).

1.3.4. Nucleon-stable Nuclei and Properties of Nuclear Forces

So far, we have considered the properties of β-stable nuclei. The binding energy per nucleon $\varepsilon = \Delta W/A$ is the highest in these nuclei. In other words, its values lie on the crest of the ridge of the energy surface (see Fig. 5). The projection of the crest onto the (A, Z) plane is the track of the β-stable isotopes which is defined by Eq. (1.3.4):

$$Z = A/(1.98 + 0.015A^{2/3}).$$

Let us now descend from the crest of the ridge along the slope, i.e. descend from the track of β-stable nuclei in the plane (A, Z). As we slide down the crest to the right, we shall depart from the track towards an excess [in comparison with Eq. (1.3.4)] of Z, while to the left we move towards a Z-deficiency. The first region corresponds to the values of A and Z for β^+-radioactive nuclei, and the second for β^--radioactive nuclei.

Properties of β-radioactive nuclei which differ from those of β-stable nuclei are discussed in detail in Sec. 3.3. Here we shall consider such properties that are common to both types of nuclei.

Beta decay of nuclei occurs under the influence of weak beta forces. Hence it proceeds very slowly in comparison with the typical nuclear lifetime $\tau_{nuc} \simeq 10^{-23}$ s which is characteristic for strong (nuclear) interaction. The shortest lifetime for weak decay of known β-radioactive nuclei is $\tau \simeq 10^{-2}$ s, while for known elementary particles it is about 10^{-13} s. But even this smallest value is about 10^{10} times as high as the nuclear lifetime.

Thus, over an extremely long time (on the nuclear scale) $\tau \gg \tau_{nuc}$, a β-radioactive nucleus retains all its individual (characteristic for the given nucleus) properties (mass, nuclear composition, system of levels, properties of these levels, nuclear transformations like alpha decay, fission, etc.). Just like a β-stable nucleus, a β-radioactive nucleus has $\varepsilon > 0$, $\varepsilon_p > 0$ and $\varepsilon_n > 0$, i.e. it is a *bound nucleon system* called the *nucleon-stable nucleus* which does not spontaneously emit protons and neutrons[17]. Thus, an analysis of the properties of β-active nuclei must provide information no less important than the β-stable nuclei. Hence it is expedient to consider jointly the properties of all nucleon-stable nuclei (both β-stable and β-active).

The range of existence of nucleon-stable nuclei is much wider than that of β-stable nuclei. It extends to the boundary of proton stability $\varepsilon_p = 0$ on the side of β^+-radioactive nuclei and to the boundary of neutron stability $\varepsilon_n = 0$ on the side of β^--radioactive nuclei. The exact position of these boundaries is not known so far, and their determination is associated with one of the most interesting problems concerning nucleon-stable nuclei: how far can we slide down the crest of the ridge on the energy surface without the risk of falling into an abyss with $\varepsilon < 0$?

This question is closely linked with several other questions. How many β-radioactive nuclei have been discovered so far? What are their properties (including nuclear) and how do they vary with the departure of the values of A and Z for these nuclei from the relation (1.3.4)? How many nucleon-stable nuclei can be expected to be discovered within the nucleon stability range? Can their properties be predicted? What are specific features of nuclei near the nucleon stability boundaries? Finally, what is a nucleon-unstable nucleus? Does this concept have a physical meaning?

The answers to these questions can be obtained in two ways. The first involves an individual analysis of the properties of nuclei already discovered and a semiempirical extrapolation to the neighbouring unknown nuclei. The second approach involves the use of

[17] Delayed neutrons and protons (see Sec. 3.3) are emitted not from the ground state, but the excited state of the nucleus in the wake of beta decay.

theoretical models of the atomic nucleus for analysis and predictions. The latter method permits a more extensive extrapolation (right up to the boundaries of nucleon stability). We shall briefly consider both these methods.

For the individual analysis, let us again turn to the intersection of the energy surface by the planes $Z = \text{const}$ (see Fig. 7) and $N = \text{const}$ (see Fig. 8), and study the change in the properties of the nucleus in two specific cases.

Table 2 contains the values of ε, ε_n, ε_p, E_β, $T_{1/2}^{(\beta)}$ and some other characteristics of some isotopes of carbon, i.e. nuclei isolated by the section $Z = 6$.

Table 2

Nucleus	$^{9}_{6}C^{4}$	$^{11}_{6}C^{5}$	$^{12}_{6}C^{6}$	$^{13}_{6}C^{7}$	$^{14}_{6}C^{8}$	$^{15}_{6}C^{9}$	$^{16}_{6}C^{10}$
Type of radioactivity	β^+	β^+	Stable	Stable	β^-	β^-	β^-
E_β, MeV	2.2	1.0	—	—	0.15	9.8	8.0
$T_{1/2}^{(\beta)}$	19 s	20 min	—	—	5730 yrs	2.4 s	?
ε, MeV	6.0	6.6	7.7	7.5	7.5	7.1	6.9
ε_n, MeV	—	13.1	18.7	4.9	8.2	1.2	4.3
ε_j, MeV	4	8.7	16	17.5	20.8	—	—
P_n, MeV	?	—	5.6	—	3.3	—	3.1
ε_{2n}, MeV	?	—	32	—	13	—	5.5
$\bar{\varepsilon}_n$, MeV	?	—	16	—	6.5	—	2.75

At present seven isotopes of carbon are well studied, starting from the nucleus $^{10}_{6}C$ containing 6 protons and 4 neutrons up to the nucleus $^{16}_{6}C$ containing 6 protons and as many as 10 neutrons (Fig. 22).[18]

[18] Several other isotopes of carbon have been discovered recently but their properties have not been thoroughly investigated so far.

Isotopes with a neutron deficiency exhibit β^+-radioactivity while those having an excess of neutrons are β^--radioactive. The beta decay energy increases and the half-life decreases as we move away (on either side) from the β-stable isotopes ^{12}C and ^{13}C. The binding energy ε per nucleon changes rather insignificantly (by about 10% of the

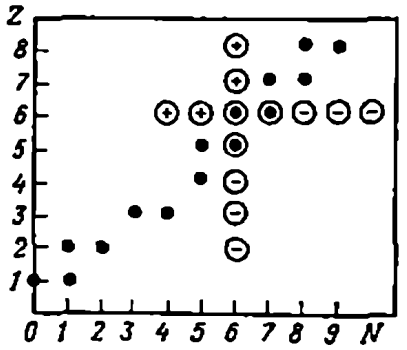

Fig. 22

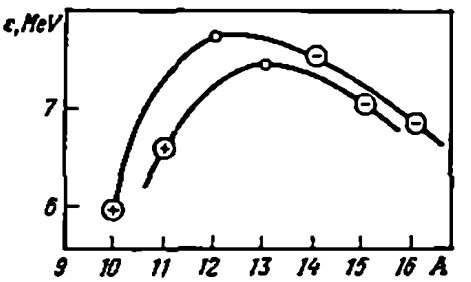

Fig. 23

average value of ε) for all these nuclei. The ε vs. A curve clearly reveals the above-mentioned effect of dependence of ε on the evenness or oddness of the numbers Z and N (Fig. 23). The values of ε for even-even nuclei lie on the upper parabola and those for even-odd nuclei lie on the lower parabola.

The dependence of ε_n and ε_p on mass number A is much more pronounced (Figs. 24 and 25). It can be seen from the figures that as the

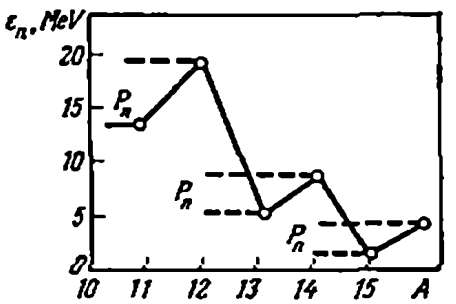

Fig. 24

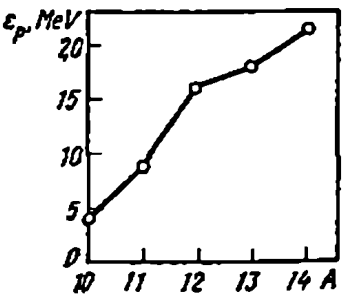

Fig. 25

number of neutrons increases, the neutron separation energy decreases (on the average) and the proton separation energy increases. Both these results are quite expected: the more the ratio of A to Z deviates for a given nucleus from the equilibrium ratio, the weaker its bond with the last excess nucleon and the stronger the bond with the last deficient nucleon. For a neutron-unstable nucleus the value of ε_n must decrease to $\varepsilon_n \leqslant 0$. The nonmonotonic nature of variation of ε_n with increasing number of neutrons, which makes it difficult to predict the value of N corresponding to $\varepsilon_n = 0$, is worth noting.

This effect is a manifestation of the above-mentioned (Sec. 1.3.2) pairing interaction of neutrons. An odd neutron interacts only with the remaining nucleus as a whole, while an even neutron interacts with the entire remaining nucleus as well as with the odd neutron. Hence ε_n for an even neutron is higher than for an odd neutron.

A quantitative estimate of the pairing interaction can be made by introducing the concept of *pairing energy* P_n of a neutron:

$$P_n = \varepsilon_n(A, Z) - \varepsilon_n(A-1, Z), \qquad (1.3.16)$$

where $Z = \text{const}$ and $A - Z = N$ is even.

In physical sense, the pairing energy of a neutron is the energy of formation of a pair of neutrons in the nucleus. The values of P_n for even-even isotopes of carbon are given in the seventh row of Table 2. Usually, the pairing energy P_n is of the order of 2-3 MeV and is known to depend on the shape of the nucleus. The energy P_n decreases as the number of nucleons approaches a magic number, i.e. as the shape of the nucleus approaches spherical symmetry.

The last two rows of the table contain the values of ε_{2n} and $\bar{\varepsilon}_n = \varepsilon_{2n}/2$. The quantity ε_{2n}, viz. the energy of separation of a pair of neutrons, is, by definition, equal to

$$\varepsilon_{2n} = \{2m_n + M(A-2, Z) - M(A, Z)\}c^2, \qquad (1.3.17)$$

where $Z = \text{const}$ and $N = A - Z$ is even. The separation energy of a pair of neutrons is convenient in that it is free of fluctuations due to pairing interaction (it changes monotonically). The average separation energy $\bar{\varepsilon}_n = \varepsilon_{2n}/2$ is introduced for reducing ε_{2n} to a single-nucleon scale.

Figure 22 shows all the investigated carbon isotopes (circles) as well as all β-stable light nuclei (dots). It can be seen from this figure that an investigation of the section of the energy surface by the plane $Z = 6$ leads to an estimate of the "horizontal width" of the region of known nucleon-stable nuclei in the region of small values of Z. In order to estimate its "vertical width", we must consider the section of the energy surface by the plane $N = \text{const}$.

Table 3 presents the characteristics of seven well-known isotonic nuclei with $N = 6$ (see Fig. 22).

We shall not analyze this table in detail since it lists results analogous to those contained in Table 2 if we replace the neutron by the proton everywhere (ε_p, P_p, ε_{2p} and $\bar{\varepsilon}_p$ behave in the same way as ε_n, P_n, ε_{2n} and $\bar{\varepsilon}_n$ in Table 2). In analogy with P_n, the quantity

$$P_p = \varepsilon_p(A, Z) - \varepsilon_p(A-1, Z-1) \qquad (1.3.18)$$

for even Z and constant $N = A - Z$ is called the *proton pairing energy*. The quantity

$$\varepsilon_{2p} = \{2m_p + M(A-2, Z-2) - M(A, Z)\}c^2 \qquad (1.3.19)$$

Table 3

Nucleus	$^{8}_{2}He^{6}$	$^{8}_{3}Li^{6}$	$^{10}_{4}Be^{6}$	$^{11}_{5}B^{6}$	$^{12}_{6}C^{6}$	$^{13}_{7}N^{6}$	$^{14}_{8}O^{6}$
Type of radioactivity	β^-	β^-	β^-	Stable	Stable	β^+	β^+
E_β, MeV	14	13.6	0.55	—	—	1.2	1.8
$T_{1/2}$	0.12 s	0.17 s	2.5×10^{6} yrs	—	—	10 min	72 s
ε, MeV	3.9	5.0	6.5	6.9	7.7	7.2	7.0
ε_{p}, MeV	?	?	?	11.2	16	1.9	4.6
ε_{n}, MeV	?	?	6.8	11.5	18.7	20.3	?
P_p, MeV	?	—	?	—	4.8	—	2.7
ε_{2p}, MeV	?	—	?	—	27.2	—	6.6
$\bar{\varepsilon}_p$, MeV	?	—	?	—	13.6	—	3.3

for Z = even and $N = A - Z$ = const is called the *separation energy of two protons*, while $\bar{\varepsilon}_p = \varepsilon_{2p}/2$ *is called the average separation energy of a proton.*

Nuclei whose properties are considered in Table 3 are arranged in a vertical line in Fig. 22 for $N = 6$. It can be seen from the figure that this line nearly reaches the N-axis. The lightest nucleus $^{8}_{2}He$ on this line has three times more neutrons than protons.

The "cross" obtained from isotopes with $Z = 6$ and isotones with $N = 6$ gives an estimate of the range of known nucleon-stable nuclei for small Z and N. It can be seen from the figure that the number of nucleon-stable nuclei for small values of Z and N is about 3-4 times larger than the number of β-stable nuclei (the number of β-radioactive nuclei is 2-3 times larger than the number of β-stable nuclei).

Similarly, we can intersect the energy surface by planes Z = const (or N = const) for all values of Z (or N).

In the region of large values of Z, we get besides the characteristics listed above (ε, ε_p, ε_n, P_n, P_p, ε_{2n}, ε_{2p}, E_β and $T_{1/2}^{(\beta)}$) additional information in the form of the energy E_α of alpha decay and the energy $E_{sp.\,fs.}$ of spontaneous fission, as well as the half-lives $T_{1/2}^{(\alpha)}$ and $T_{1/2}^{sp.\,fs.}$.

Figure 26 shows the general form of the (Z, N) plane filled with all the known nucleon-stable nuclei. The narrow hatched strip shows the track of β-stable nuclei, while the broken solid lines show the boundaries of known β^+- and β^--radioactive nuclei.[19]

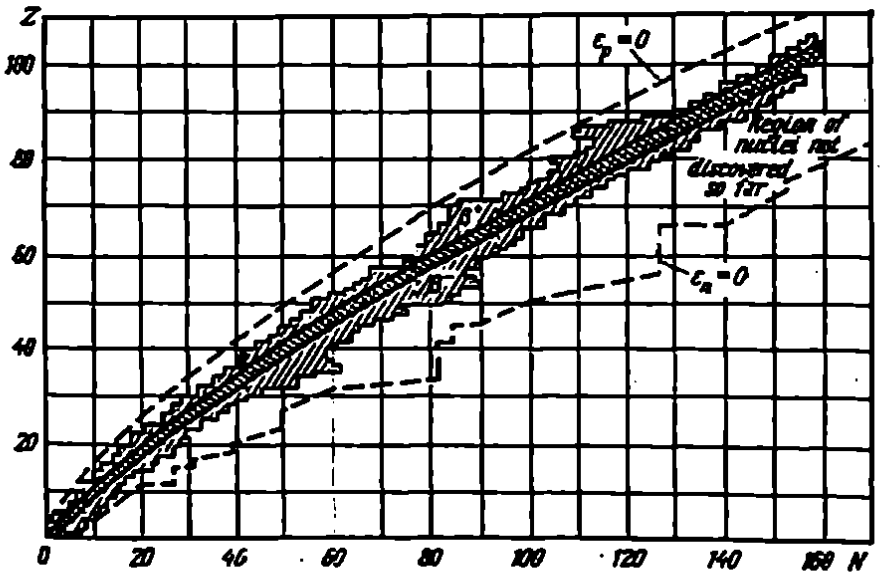

Fig. 26

The figure shows that the width of the region of nucleon-stable nuclei does not vary uniformly with increasing Z and N. An especially large number of nuclei (about 25) lie on the sections corresponding to magic numbers (for example, $Z = 50$, 82) and in the regions which were investigated in great detail for some reason or the other (heavy radioactive elements and fission fragments). In all, about 2000 nucleon-stable nuclei are known at present.

A comparison of ε, ε_n, ε_p, ε_α, $T_{1/2}^{(\beta)}$, $T_{1/2}^{(\alpha)}$, $T_{1/2}^{sp.\,fs.}$, E_β, E_α, $E_{sp.\,fs.}$ and other characteristics for these nuclei allows us to draw several conclusions about their properties and about the change of these properties with a variation of Z and N, as well as about cer-

[19] Figure 26 is of an arbitrary nature. The track of β-stable nuclei is shown approximately, while the strip of β-radioactive nuclei has gaps corresponding to nuclei that have not been discovered so far.

tain new properties of nuclear forces, for example, pairing interaction. However, the regularities that can be noticed from a comparison of data presented in Tables 2 and 3 are purely empirical in nature. In fact they describe only the properties of the nucleus under consideration and can, at best, be used to predict roughly some properties of a couple of neighbouring unknown nuclei (for example, the regut larities concerning the variation of ε_{2n} and ε_{2p}).

In order to explain the observed regularities and also to predic new nuclei over a wide range of variation of Z and N, we require theoretical laws based on the model concepts concerning the structure of the atomic nucleus.

We have already used the independent-particle model and the shell model to explain the high stability of nuclei with $Z = N$, with even values of Z and N, or with magic values of Z and N. (These models are discussed in detail in Chap. 2.) Other regularities among those listed above (dependence of ε on A and Z, the laws of alpha decay and nuclear fission, the relation between A and Z in β-stable nuclei, etc.) are explained by the liquid drop model of the nucleus, which is also described in Chap. 2.

In this model, we can obtain the following semiempirical formula for the nuclear binding energy:

$$\Delta W(A, Z) = \alpha A - \beta A^{2/3} - \gamma Z^2/A^{1/3} - \zeta (A/2 - Z)^2/A + \delta A^{-3/4}, \qquad (1.3.20)$$

where α, β, γ, ζ and δ are coefficients among which $\delta = 0$ for nuclei with odd A and γ can be expressed in terms of the nuclear radius R:

$$\gamma Z^2/A^{1/3} = 3 (Ze)^2/5R. \qquad (1.3.21)$$

The semiempirical formula with balanced coefficients can be used to compute the value of $\Delta W(A, Z)$ from A and Z with an error not exceeding 10-20 MeV. A combination of the liquid drop and shell models increases the accuracy of the formula to such an extent (1-2 MeV) that it can be used to estimate the values of ε_n and ε_p, each of which is a difference of two large quantities of the type ΔW.

Thus, all nuclear parameters given in Tables 2 and 3 can be computed for known nuclei and predicted for unknown nuclei with a high degree of accuracy. It should be noted that these predictions concern not only an increase in the number of isotopes of known elements with $1 \leqslant Z \leqslant 109$, but are also applicable to superheavy elements that have not been discovered so far. A noncritical list of these predictions is given below:

(1) Besides the known nucleon-stable nuclei (about 2000), there must exist at least as many nuclei in nature with $\varepsilon > 0$. The predicted pattern of nucleon stability boundaries is shown in Fig. 26 by dashed lines.

(2) The neutron-rich nuclei near the neutron stability boundary $\varepsilon_n = 0$ must be β^--radioactive (with a small half-life $T_{1/2}^{(\beta)}$ and a large beta decay energy E_β) and emit delayed neutrons, neutron pairs, and even neutron triplets (see Sec. 3.5.3 for details). It is possible that they have anomalously large dimensions and for them a high reaction yield with a simultaneous escape of two neutrons will be observed. This conclusion has been drawn by taking into consideration the properties of already discovered nuclei with a large excess of neutrons, for example, $^8_2$He, $^6_2$He. The neutron separation energy for these nuclei is very low, and this points towards their "porosity", i.e. large dimensions (cf. properties of deuteron, Sec. 1.3.2, Vol. II). Besides, $\varepsilon_{2n} < \varepsilon_n$ for these nuclei.

(3) The existence of nuclei with a large excess of neutrons (like $^8_2$He and $^{11}_3$Li) led certain physicists to believe that there can be nucleon-stable neutron nuclei, i.e. nuclei consisting of neutrons only. However, experiments aimed at discovering a nucleus consisting of two neutrons (bineutron) or four neutrons (tetraneutron) were unsuccessful.

At present, it is assumed that neutron nuclei may be formed due to collisions of heavy nuclei with an energy of tens of MeV per nucleon. In this case, the powerful Coulomb impact in the colliding nuclei must excite a giant dipole resonance displacing the protons with respect to neutrons (see Sec. 12.3). In principle, this may lead to a congregation of neutrons into a neutron nucleus. The possibility of the existence of neutron nuclei in the superdense state of nuclear matter also cannot be ruled out (see Sec. 2.1.3).

(4) Neutron-deficient nuclei near the proton stability boundary must be β^+-radioactive (with a small $T_{1/2}^{(\beta)}$ and a large E_β) and may emit delayed protons from the excited state of the nucleus formed after β^+-decay or e-capture (if $W > \varepsilon_p$). In principle, they can also emit protons from an isomeric state (if $W > \varepsilon_p$) and have proton radioactivity (if $\varepsilon_p < 0$) or two-proton radioactivity if $\varepsilon_p > 0$ but $\varepsilon_{2p} < 0$ (see Sec. 3.5 for details).

(5) In the region of very remote transuranic elements, there may exist "stability islets", i.e. nuclei with a relatively very low probability of alpha and beta decays and spontaneous fission. These islets may be located in the region of new predicted magic numbers $Z = 114$, $N = 184$ and $Z = 164$.

(6) Nuclei beyond the nucleon stability boundaries $\varepsilon_n = 0$, $\varepsilon_p = 0$ are nucleon-unstable, i.e. exist for a very short nuclear time $\tau_{nuc} \simeq 10^{-22}$ s. However, just like ordinary nuclei, these nuclei can also be characterized by parameters such as mass, charge, spin, and also by velocity, energy, emission angle, etc.

1.4. Nuclear Radius

The first estimates of the size of the atomic nucleus were obtained by Rutherford in his experiments on the scattering of α-particles. In order to match the experimental results with the theory, he had to assume that a considerable part of the mass of an atom is concentrated in its central part, viz. the nucleus, which can be represented as a sphere of radius $\simeq 10^{-12}$ cm.

The size of the nucleus was subsequently determined in several ways, for example, by

(1) estimating the radius of α-radioactive nuclei from the alpha decay constant λ;

(2) analyzing the semiempirical formula for the mass and binding energy of the nucleus;

(3) investigating the scattering of fast neutrons by nuclei;

(4) investigating the X-rays from μ-atoms; and

(5) measuring the scattering of fast electrons by nuclei.

We shall briefly describe each of the above methods and compare the results obtained with their help.[20]

1.4.1. Estimation of the Radius of α-radioactive Nuclei from Their Lifetimes

The last elements of the Periodic Table are known to be α-radioactive and according to the empirical Geiger-Nuttall law, the lifetime of α-radioactive nuclei is in one-to-one correspondence with the energy T_α of the emitted α-particles:

$$\ln \tau + A \ln T_\alpha = B. \tag{1.4.1}$$

The coefficients A and B in Eq. (1.4.1) are such that a small difference in the energy of α-particles (from 9 to 4 MeV) corresponds to an enormous variation in the lifetime of the nuclei (from 10^{-7} s to 10^{10} years). This feature of the alpha decay is due to the quantum-mechanical effect of the passage of α-particles through a Coulomb potential barrier (see Sec. 3.2.3). Since one of the boundaries of the barrier coincides with the radius R of the nucleus, the theoretical expression for the lifetime of a nucleus undergoing alpha decay contains R which can be found by comparing the experimental results on the determination of lifetime of α-radioactive nuclei.

It was found that the radii of all α-radioactive nuclei lie between 8.4×10^{-13} and 9.8×10^{-13} cm and are described quite well by the formula $R = r_0 A^{1/3}$, where $r_0 = (1.45\text{-}1.5) \times 10^{-13}$ cm.[21]

[20] A more detailed description of these methods will be given in the appropriate sections of this book.

[21] Sometimes, the quantity 10^{-13} cm (femtometer) is called a fermi (fm) and hence $R = (1.45\text{-}1.5) A^{1/3}$ fm.

1.4.2. Analysis of the Semiempirical Formula. Beta Decay of Mirror Nuclei

It was mentioned in Sec. 1.3.4 that one of the terms in the semiempirical formula (1.3.20) for the binding energy

$$\Delta W(A, Z) = \alpha A - \beta A^{2/3} - \gamma Z^2/A^{1/3} - \zeta (A/2 - Z)^2/A + \delta A^{-3/4} \qquad (1.4.2)$$

can be expressed in terms of the nuclear radius R [Eq. (1.3.21)] as follows:

$$\gamma Z^2/A^{1/3} = 3(Ze)^2/5R \quad \text{or} \quad \gamma = 3e^2/5r_0. \qquad (1.4.3)$$

Initially, the nuclear radius R was found from an analysis of alpha decay of a small number of heavy nuclei. However, it later turned out that the semiempirical formula with the value of γ obtained from this analysis correctly describes the binding energy not only of heavy nuclei, but of all the remaining nuclei as well. Thus, a comparison with the experiment shows that the formula is universal in nature and hence the assumptions made while deriving it were correct (see Sec. 2.1.1). In particular, the relation between the coefficient γ and the nuclear radius R was correctly assumed.

This means that the arguments used for deriving the semiempirical formula can be applied in reverse order and the value of the nuclear radius can be obtained from a comparison of the experimental and theoretical results.

Such a comparison can be made in a very elegant manner for mirror pairs of nuclei connected through the condition of beta decay.

Suppose that, as a result of β^+-decay, a nucleus (A, Z) is transformed into its mirror nucleus $(A, Z-1)$. For the mirror nuclei, the number of neutrons $N = A - Z$ for one nucleus must be equal to the number of protons $(Z-1)$ in the other nucleus: $A - Z = Z - 1$, i.e. $A = 2Z - 1$. For such a relation between A and Z, however, the δ-term in formula (1.4.2) is equal to zero, and all the remaining terms except γ-terms are equal for both nuclei.[22]

Hence the difference in the binding energies of the nuclei (A, Z) and $(A, Z-1)$ is

$$\Delta E = \Delta W(A, Z-1) - \Delta W(A, Z) = \gamma \frac{2Z-1}{A^{1/3}} = \gamma A^{2/3} = \frac{3}{5}\frac{e^2}{r_0} A^{2/3}. \qquad (1.4.4)$$

[22] The ζ-terms are identical, since under the condition $A = 2Z - 1$ we have for the nuclei (A, Z) and $(A, Z-1)$

$$\zeta \frac{(A/2-Z)^2}{A} = \zeta \frac{[A/2-(Z-1)]^2}{A} = \frac{\zeta}{4A} = \text{const}.$$

Thus, the value of r_0 can be found from the slope of the experimental straight line

$$y = kx, \qquad (1.4.5)$$

where $y = \Delta E_{exp}$, $k = \frac{3}{5}\frac{e^2}{r_0}$ and $x = A^{2/3}$ (Fig. 27). The values of ΔE_{exp} can be found from the masses of the nuclei $\Delta E = M(A, Z) - M(A, Z-1) + m_n - m_p$, or from the beta decay energy $\Delta E = E_{\beta^+} + m_n + m_e - m_p = E_{\beta^+} + 1.8$ MeV.

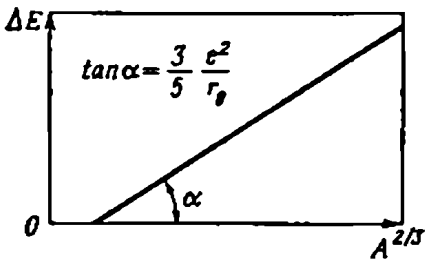

Fig. 27

These methods have led to the following value of r_0:

$$r_0 = (1.2\text{-}1.3) \times 10^{-13} \text{ cm}.$$

By using the most up-to-date value of γ in the semiempirical formula (1.4.2), the value of r_0 was found to be

$$r_0 = 1.2 \times 10^{-13} \text{ cm}.$$

1.4.3. Investigation of Scattering of Fast Neutrons by Nuclei

The nuclear radii can be determined quite accurately by studying the interaction of fast neutrons with atomic nuclei. The interaction probability is characterized in nuclear physics by effective cross section σ, which is defined as follows for fast neutrons. Let N be the flux of neutrons impinging on a thin 1-cm² target (so that the target nuclei do not overlap (shade) one another, Fig. 28*a*). The effective cross section of interaction of a neutron and a nucleus is then defined as

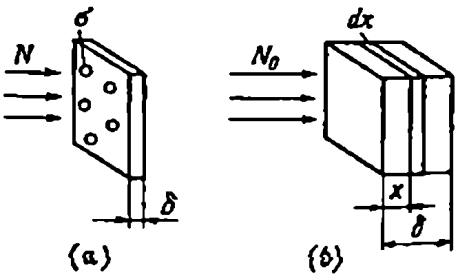

Fig. 28

$$\sigma = dN/Nn\delta, \qquad (1.4.6)$$

where dN is the number of interactions, n is the concentration of nuclei in the target and δ is the target thickness. It follows from the expression (1.4.6) that the relative fraction dN/N of the neutrons that have interacted is equal to the relative fraction $dS = \sigma n \delta$ of the target area occupied by all the nuclei if we assign σ the physical meaning of the nuclear cross sectional area.

In the case of a thick target, the flux density varies with the depth x. Obviously, to estimate the number of neutrons passing through

the target, we must write down the differential equation for a thin layer dx of the target at the depth x:

$$dN = -N(x)\, n\sigma\, dx. \tag{1.4.7}$$

Here, $N(x)$ is the number of neutrons reaching the target layer at the depth x, and dx is the layer thickness (see Fig. 28*b*).

The solution of Eq. (1.4.7) is obtained in the form

$$N(x) = N_0 \exp(-n\sigma x), \tag{1.4.8}$$

where N_0 is the primary neutron flux.

Thus, in order to determine the cross section of interaction of fast neutrons with nuclei, it is sufficient to measure in a special experiment the attenuation $N(\delta)/N_0$ of the intensity of a neutron beam passing through a target of thickness δ:

$$\sigma = -\ln [N(\delta)/N_0]/n\delta. \tag{1.4.9}$$

In order to determine the nuclear radius, we must express σ in terms of R.

It seems at first glance that the effective cross section, which has the physical meaning of the nuclear cross sectional area, must be equal to πR^2. This would indeed be true if the interaction of fast neutrons ($T_n = 10$ MeV) with nuclei were reduced to the inelastic scattering considered above. However, in actual practice there exists another process of interaction for fast neutrons, viz. the elastic diffraction scattering of a de Broglie neutron wave by nuclei (see Sec. 6.6 for details). The effective cross section of this process is also equal to πR^2. Thus, the total effective cross section of interaction of fast neutrons with nuclei will be

$$\sigma = 2\pi R^2. \tag{1.4.10}$$

Hence, the experiments on the attenuation of a neutron beam can provide information about the radius of the target nuclei.

Experiments were carried out with neutrons having energy of 14 and 25 MeV. These led to the value

$$R = r_0 A^{1/3}$$

for the nuclear radius, where $r_0 = 1.4 \times 10^{-13}$ cm.

Similar results were obtained in experiments on the scattering of 90-MeV neutrons ($r_0 = 1.37 \times 10^{-13}$ cm). A slightly smaller value ($r_0 = 1.28 \times 10^{-13}$ cm) was obtained in experiments on absorption of very fast neutrons ($T_n = 1.4$ BeV) by nuclei.

Thus, the methods of determining the radii of nuclei by studying their interaction with neutrons lead to the following result:

$$R = r_0 A^{1/3},$$

where $r_0 = (1.3\text{-}1.4) \times 10^{-13}$ cm.

1.4.4. Investigation of X-rays Emitted by Muonic Atoms

A new elementary particle, called muon (μ), was discovered in 1938 in cosmic rays. An investigation of the properties of muons revealed that they can be positively or negatively charged, have a mass equal to $207m_e$, and disintegrate into an electron and two neutrinos[23] in about 2×10^{-6} s.

A subsequent detailed analysis of the properties of the negative muon showed that it behaves in the same way as an electron. In particular, when a muon, decelerated to a certain velocity, appears in the vicinity of an atomic nucleus, it is captured on one of the Bohr orbits. This leads to a system which is similar to the ordinary atom and is called a μ-*atom*. The radius of the muon orbit is 207 times (the ratio of the muon mass to the electron mass) smaller than the radius of the corresponding Bohr orbit for an electron. For example, the radius of the K-orbit of a μ-atom of lead is

$$(r_K)_{\mu^-} = \frac{\hbar^2}{Z\mu e^2} \simeq \frac{10^{-54}}{82 \times 207 \times 9 \times 10^{-28} \times 23 \times 10^{-20}} = 3 \times 10^{-13} \text{ cm}. \quad (1.4.11)$$

Here, $\hbar = 1.05 \times 10^{-27}$ erg·s is Planck's constant, $Z = 82$ is the charge of the lead nucleus, $\mu = 207m_e = 207 \times 9 \times 10^{-28}$ g is the muon mass, and $e = 4.8 \times 10^{-10}$ CGS units is the electron charge.

Muonic atoms have the same properties as ordinary atoms. In particular, transitions of muons from one orbit to another are accompanied by the emission of X-rays. The energy of these X-rays can be measured experimentally and calculated theoretically. Since the radius of a muon orbit is very small, the calculated value of the energy of the emitted radiation depends strongly on the assumption concerning the nuclear radius. Hence the radius of the atomic nucleus can be found from the experimental values of the radiant energy.

This method gives the most accurate results for nuclei with large Z, since they have muon orbits of very small radii. For example, calculations show that as the assumed value of the nuclear radius R changes from 0 to $1.3 \times \sqrt[3]{208} \times 10^{-13}$ cm, the energy of radiation emitted by a μ-atom of lead changes from 16 to 5.5 MeV.

Measurement of the radiant energy of the μ-atoms of lead and a comparison of the result obtained with a theoretical value give $R_{Pb} = 1.17 \times 10^{-13} \times 208^{1/3}$ cm for the radius of this nucleus.

---

[23] More precisely, according to the schemes $\mu^+ \to e^+ + \nu_e + \tilde{\nu}_\mu$ and $\mu^- \to e^- + \tilde{\nu}_e + \nu_\mu$.

1.4.5. Measurement of Scattering of Fast Electrons by Nuclei

The de Broglie wavelength for an electron with energy $T_e \gg m_e c^2$ is

$$\lambda = \frac{\hbar}{p} \simeq \frac{\hbar c}{T_e} = \frac{6.62 \times 10^{-27} \times 3 \times 10^{10}}{1.6 \times 10^{-6} T_e} = \frac{1.24 \cdot 10^{-10}}{T_e} \qquad (1.4.12)$$

(where λ is in centimetres and T_e is in MeV), and becomes comparable with the dimensions of atomic nuclei for $T_e = 100$ MeV. Hence an idea about the radius of the atomic nucleus can be had from experiments on elastic scattering of fast electrons by nuclei, i.e. from the results of the angular distribution of scattered electrons. Experiments were carried out with electrons accelerated in a synchrotron to energies of the orders of tens (in first experiments) and hundreds (in the most accurate experiments conducted by Hofstadter) megaelectron-volts. The results of the experiments were compared with the calculations employing Dirac's equation under the assumption of a uniform charge distribution in nuclei with different radii. It was found that the best agreement of formula $R = r_0 A^{1/3}$ with experimental results is obtained at different values of r_0 for different nuclei (from 1.32×10^{-13} cm for $^{40}_{20}$Ca to 1.18×10^{-13} cm for $^{197}_{79}$ An).

Thus, experimental investigation of scattering of fast electrons gives the following values of the nuclear radius:

$$R = r_0 A^{1/3},$$

where $r_0 = (1.2\text{-}1.3) \times 10^{-13}$ cm (see Sec. 3.2, Vol. II for details)

1.4.6. Comparison of Results

Let us now compare the results obtained by different methods. All the experiments confirmed the correctness of the assumption that the nucleus has a nearly spherical shape. For the nuclear radius, however, different values are obtained:

$$R = r_0 A^{1/3}, \qquad (1.4.13)$$

where

$$r_0 = (1.2\text{-}1.5) \times 10^{-13} \text{ cm}.$$

Considering that the value of $r_0 = (1.45\text{-}1.5) \times 10^{-13}$ cm obtained from an analysis of alpha decay is somewhat exaggerated (see Sec. 3.2.3), there still remains some discrepancy between the values $r_0 = (1.3\text{-}1.4) \times 10^{-13}$ cm and $r_0 = (1.2\text{-}1.3) \times 10^{-13}$ cm, which are obtained by quite reliable methods. Apparently, this discrepancy can be explained as follows.

When the electromagnetic properties of the nucleus (radiation from a μ-atom, scattering of fast electrons, etc.) are investigated, the results of experiments are compared with calculations based on certain assumptions concerning the radius R of the sphere containing the nucleons (to be more precise, protons). Hence, the investigations of electromagnetic properties of the nucleus lead to the experimental value of the nuclear radius ($R \simeq 1.2 \times 10^{-13} A^{1/3}$ cm) in *this very sense.*

In experiments on the scattering of fast neutrons by nuclei, the nuclear interaction of neutrons with a nucleus is investigated. Hence in such experiments we measure not the nuclear radius but a somewhat larger quantity, viz. the range of nuclear interaction. In this connection, the terms "electric" and nuclear radii are used for atomic nucleus.

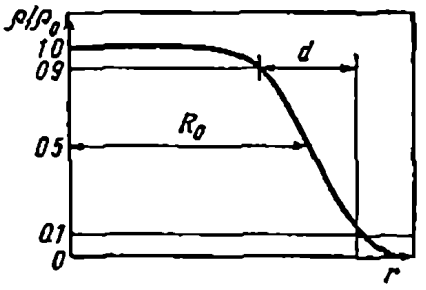

Fig. 29

Finally, it should be noted that the high accuracy of the present-day experiments on the scattering of fast electrons ($T_e > 500$ MeV) by nuclei not only helps to determine the average value of the region occupied by protons, but also provides an estimate of the charge density distribution over the nucleus. It was found that the experimental results are in best agreement not with a uniform distribution of charge in the nucleus, but with a distribution of the type

$$\rho = \frac{\rho_0}{1+\exp\left[(r-R_0)/\delta\right]} \qquad (1.4.14)$$

(Fermi model). According to this formula, the charge density is constant inside the nucleus and smoothly decreases to zero near its boundary (Fig. 29). The quantity R_0 determines the distance from the centre of the nucleus to the point where the charge density is reduced to half its value, while $\delta \simeq 0.55 \times 10^{-13}$ cm is the rate of attenuation of charge density with distance from the centre of the nucleus. Experiment shows that $R_0 = 1.08 \times 10^{-13} A^{1/3}$ cm for all the investigated nuclei. The charge density (from $0.9\rho_0$ to $0.1\rho_0$) starts decreasing at the same distance ($d = 4.4\delta = 2.4 \times 10^{-13}$ cm) for all nuclei, and hence the region of constant charge density diminishes with decreasing Z and completely disappears for $Z \leqslant 6$.

1.5. Spin and Magnetic Moment of Nucleons and Nuclei

1.5.1. Historical Background

In just the same way as the spin and intrinsic (spin) magnetic moment were associated with an electron to account for the fine structure of spectral lines, the hyperfine structure was explained by assuming that the nucleus has a spin as well as a magnetic moment.

The fine structure of optical spectra is due to the interaction of the intrinsic (spin) magnetic moment μ_s of an electron with the magnetic field H_l produced by the orbital motion of electrons in an atom. The interaction energy

$$U = -\mu H_l \tag{1.5.1}$$

is different for different orientations of μ_s relative to H. The number $2s + 1$ of possible orientations is determined by the spin s.

Quantitative agreement between this statement and experimental results is obtained for the following values of spin and magnetic moments of an electron:

$$\left.\begin{aligned} &s = 1/2 \text{ (in Planck's constants } \hbar), \\ &\mu_s = \frac{e\hbar}{2m_e c} = M_B = 9.27 \times 10^{-21} \text{ erg/G (Bohr magneton)}, \\ &l = 0, 1, 2, \ldots \text{ (in Planck's constants } \hbar), \\ &\mu_l = lM_B. \end{aligned}\right\} \tag{1.5.2}$$

The values of spin s and spin magnetic moment μ_s of an electron were later obtained theoretically by considering Dirac's relativistic quantum-mechanical equation for an electron (see Sec. 5.1, Vol. II).

The fine structure of spectral lines is due to the interaction of magnetic moments of all outer (valence) electrons with the magnetic field of the atom.[24] The pattern of interaction is quite simple for atoms with only one electron in their outer shells. In this case, there are only two ($2s + 1 = 2$) orientations of μ_s relative to H, i.e. each spectral line splits into two closely spaced lines. The splitting of the D-line of sodium into two lines with wavelengths 5890 and 5896 Å is a typical example of such a simple fine structure.

The outer shell of an atom usually contains not one but several electrons which contribute to the angular momentum and magnetic moment of the atom. Hence the following quantities are used as the basic vector characteristics of electron shells:

(1) the total spin $S = s_1 + s_2 + \ldots$ of all valence electrons and

[24] The electrons of closed shells do not produce a magnetic moment since their total angular momentum is equal to zero.

the magnetic moment μ_S corresponding to it;

(2) the total orbital angular momentum $\mathbf{L} = \mathbf{l}_1 + \mathbf{l}_2 + \ldots$ of all valence electrons and the magnetic moment μ_L corresponding to it;

(3) the total angular momentum $\mathbf{J} = \mathbf{L} + \mathbf{S}$ of the electrons and the magnetic moment μ_J corresponding to it.

The fine structure in this case is much moro complicated than for monovalent atoms although its physical nature remains the same, i.e. the interaction of the magnetic moment of valence electrons with the magnetic field of the orbital motion of electrons is responsible for the fine structure.

A similar scheme was also proposed for explaining the hyperfine splitting of optical spectral lines.

In 1928, Pauli put forth the hypothesis that the nucleus has a spin I and a magnetic moment μ_I. The interaction of the magnetic moment of the nucleus with the magnetic field of the electrons (which is slightly different for different orientations of the nuclear spin) causes an additional splitting of the spectral lines. To explain the extremely small magnitude of this splitting (which is about 10^3 times smaller than the fine splitting), Pauli proposed that the magnetic moment of the proton should be taken equal to one Bohr magneton μ_B:

$$|\mu_p| = \frac{e\hbar}{2m_p c} = \frac{m_e}{m_p} M_B = \mu_B = 5.05 \times 10^{-24} \text{ erg/G}, \quad (1.5.3)$$

while the magnetic moment of the nucleus should be taken as an integral multiple of the Bohr magneton:

$$\mu_I = \gamma \mu_B, \quad (1.5.4)$$

where γ is an integer.

Pauli's concept of interaction between the nuclear magnetic moment and the magnetic field of the atom was later found to be valid in all respects except that γ need not be an integer. This concept essentially forms the basis of all the methods for determining nuclear spin and magnetic moment. We shall now consider these methods.

1.5.2. Investigation of Hyperfine Structure

The spin of a nucleus can be determined in three ways from an analysis of the hyperfine structure of spectral lines: by counting the number of lines in hyperfine splitting, by measuring the spacing between them, or by comparing their intensities.

The essence of these methods can be easily understood by analyzing the energy U of interaction between the nuclear magnetic moment μ and the average magnetic field $\overline{H}_e$ of electrons at the point where the nucleus is situated:

$$U = -\mu\overline{H}_e. \tag{1.5.5}$$

Let us find how μ and $\overline{H}_e$ are related to the vectors J, I and $F = J + I$. It is known from atomic physics that the magnetic moment μ_l due to the orbital motion of electrons is antiparallel to the orbital angular momentum l and is equal to

$$\mu_l = \frac{e}{2m_e c} l. \tag{1.5.6}$$

Considering that l is measured in units of $\hbar$, we obtain the following expression for the numerical value of the magnetic moment:

$$\mu_l = l\frac{e\hbar}{2m_e c} = lM_B, \tag{1.5.7}$$

where l is the orbital quantum number and $M_B = 9.27 \times 10^{-21}$ erg/G is the Bohr magneton. Similarly, the magnetic moment of an electron due to its spin s is antiparallel to it and, as mentioned above, is given by

$$\mu_s = \frac{e}{m_e c} s = 2\frac{e}{2m_e c} s. \tag{1.5.8}$$

The numerical value of the spin magnetic moment is

$$\mu_s = 2s\frac{e\hbar}{2m_e c} = 2sM_B = M_B, \tag{1.5.9}$$

where $s = 1/2$ is the spin quantum number.

Thus, the following relation holds between the magnetic moment of an electron, measured in Bohr magnetons, and its angular momentum M, measured in units of $\hbar$:

$$\mu = gM. \tag{1.5.10}$$

The coefficient g is called the *gyromagnetic ratio*. It can be seen from Eqs. (1.5.7) and (1.5.9) that $g_l = 1$ for the orbital motion of electrons and $g_s = 2$ for spin. This leads to the noncollinearity of the resultant magnetic moment vector

$$\mu_j = \mu_s + \mu_l$$

of an electron and its total angular momentum vector $j = l + s$. The same is true for vectors $\mu_J = \mu_S + \mu_L$ and $J = L + S$ which characterize the overall effect of all the electrons in an atom (Fig. 30).

The interaction between the magnetic moments μ_S and μ_L leads to the precession of the resultant vector $\mu_J = \mu_S + \mu_L$ about the resultant vector J. Apparently, in this case, $\bar{\mu}_\perp = 0$ and the average value of the vector μ_J coincides with the value of its component $\bar{\mu}_J = \mu_\parallel$ which is parallel to vector J. Thus, the average magnetic field created by the electrons is

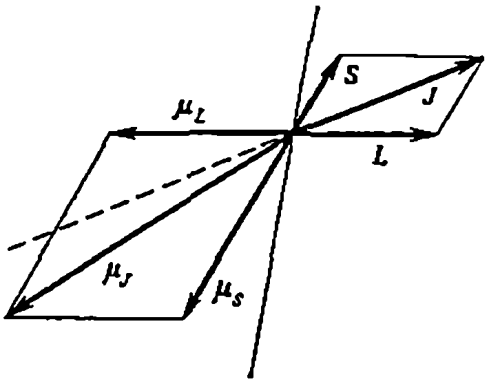

Fig. 30

$$\bar{\mathbf{H}}_e = -a\frac{\mathbf{J}}{|\mathbf{J}|}. \quad (1.5.11)$$

The value of constant a, which determines the absolute magnitude of the electron field, can be computed by using quantum-mechanical methods.

Similarly, the magnetic moment μ_{nuc} of the atomic nucleus can also be expressed in terms of its spin:

$$\mu_{nuc} = \mu\frac{\mathbf{I}}{|\mathbf{I}|}. \quad (1.5.12)$$

The energy of interaction between the nuclear magnetic moment and the magnetic field of electrons is then given by

$$U = -\mu_{nuc}\bar{\mathbf{H}}_e = \mu a\frac{\mathbf{JI}}{|\mathbf{J}|\,|\mathbf{I}|} \quad (1.5.13)$$

The value of JI is obtained from the relation

$$\mathbf{F}^2 = (\mathbf{J}+\mathbf{I})^2 = \mathbf{J}^2 + \mathbf{I}^2 + 2\mathbf{JI},$$

$$\mathbf{JI} = \frac{\mathbf{F}^2 - \mathbf{J}^2 - \mathbf{I}^2}{2} \approx \frac{\hbar^2}{2}[F(F+1) - J(J+1) - I(I+1)], \quad (1.5.14)$$

while $|\mathbf{J}|\,|\mathbf{I}|$ is the product of the moduli of vectors J and I:

$$|\mathbf{J}|\,|\mathbf{I}| = \sqrt{J(J+1)\,I(I+1)}\,\hbar^2.$$

Finally, we get

$$U = \frac{\mu a}{2}\frac{\{F(F+1) - J(J+1) - I(I+1)\}}{\sqrt{J(J+1)\,I(I+1)}}, \quad (1.5.15)$$

where F has $2I + 1$ or $2J + 1$ values for given I and J (the smallest value of I and J is taken). For a fixed J (for a given atomic energy level), the interaction energy U has the same number of values.[25]

[25] The value of I determines the nuclear spin and hence remains constant for any value of J.

From an analysis of Eq. (1.5.15), we can indicate the following three methods of determining the nuclear spin:

1. If $J > I$, the number of hyperfine splitting lines is equal to $2I + 1$, and the nuclear spin can be determined by counting the number of hyperfine splitting lines for a completely resolved spectrum.

2. If $J < I$, the nuclear spin can be determined by using another method employing the interval rule which consists in the following.

Since all the lines of a given hyperfine splitting correspond to identical values of J and I, the difference in energies for two states F and $F - 1$ is[20]

$$\Delta U = \mu a F / \sqrt{J(J+1)\, I(I+1)}. \qquad (1.5.16)$$

Consequently, the ratio of intervals between adjacent levels can be written as

$$F : (F-1) : (F-2) : \ldots = (J+I) : (J+I-1) : (J+I-2) : \ldots \qquad (1.5.17)$$

3. In some cases, the nuclear spin cannot be determined by either of the methods described above. An example of this kind is the hyperfine splitting of each of the sodium doublet lines: $\lambda_1 = 5390$ Å corresponding to a transition between the levels $1^2S_{1/2}$ and $2^2P_{1/2}$ and $\lambda_2 = 5896$ Å corresponding to a transition between $1^2S_{1/2}$ and $2^2P_{3/2}$. Both lines split into two hyperfine components with $\Delta\lambda_1 = 0.021$ Å and $\Delta\lambda_2 = 0.023$ Å. In both cases, the hyperfine structure of the spectral lines is due to the splitting of the $2^2S_{1/2}$ level, since the splitting of the $2^2P_{1/2}$ and $2^2P_{3/2}$ levels is very small.

The number of splitting components is equal to two, and hence neither of the methods mentioned above can be used for determining the nuclear spin. This is so because $2 = 2J + 1$ and hence $I > J$, which rules out the first method. The second method is inapplicable because there are only two lines and hence there is only one interval ΔU between them.

In such cases the nuclear spin I can be determined by comparing the intensities of the spectral components of hyperfine splitting. The intensity of a spectral line is proportional to the number $2F + 1$ of components into which a level splits in a magnetic field.

Equation (1.5.16) for the energy of interaction between the nuclear magnetic moment and the magnetic field of electrons can be used for calculating the nuclear magnetic moment μ from the results of measurements of the absolute value of the separation U between lines.

[20] This relation is valid if the hyperfine splitting is small in comparison with the splitting of two atomic states with different values of J.

These calculations, however, require the knowledge of the quantity a which characterizes the magnetic field of electrons at the location of the nucleus. This quantity can be determined quite accurately only for the simplest atomic systems, e.g. hydrogen and hydrogen-like atoms, halogens and alkali-earth elements. These calculations show that the field of electrons is about 10^5-10^6 Oe. For electrons in their ground state, this field is 1.3×10^5 Oe for $_3$Li and 2.1×10^6 Oe for $_{55}$Cs.

In the general case, a cannot be calculated with an error of less than 10%. Hence the values of the nuclear magnetic moment from the hyperfine structure are also not very accurate. However, this method can be used for determining the sign of the nuclear magnetic moment from the position of the sublevels into which a level splits. The rule for hydrogen-like atoms is especially simple: if the magnetic moment is positive, a sublevel with a larger F will be at a higher position than the one with a smaller F.

Finally, it should be mentioned that the Mössbauer effect can be used for measuring the hyperfine structure of *nuclear* levels, and hence for determining the intrinsic magnetic field of an atom from the value of its nuclear magnetic moment. This method can also be used for determining the magnetic moments of the excited states of an atomic nucleus (see Sec. 3.4.4e).

1.5.3. Methods of Determining Spin and Nuclear Magnetic Moment by Using External Fields

In these methods, the nuclear magnetic moment μ_{nuc} interacts with the magnetic field $\overline{H}_e$ of electrons as well as with the external field H. The interaction energy is

$$U = -\mu_{nuc}(\overline{H}_e + H). \tag{1.5.18}$$

The external field may be uniform, nonuniform or high-frequency field. We shall consider the methods corresponding to these cases.

1.5.3a. Zeeman Effect and Paschen-Back Effect

Suppose that H in Eq. (1.5.18) denotes a uniform external magnetic field. Then, depending on the ratio of $\overline{H}_e$ to H, three different situations may arise: the strong field case, the weak field case and the intermediate case. We shall consider the first two cases in detail.

A field H is *strong* if the energy of its interaction with the electron shells is much higher than the energy of interaction of electron shells with the nuclear magnetic moment:

$$M_J H \gg \mu_{nuc}\overline{H}_e. \tag{1.5.19}$$

Similarly, a *weak* field H satisfies the following condition:

$$M_J H \ll \mu_{nuc} \overline{H}_e. \qquad (1.5.20)$$

Considering that $\mu_{nuc}/M_J \simeq 10^{-3}$ and $\overline{H}_e \simeq 10^5$-$10^6$ Oe, we obtain the following estimate for the order of magnitude of strong fields:

$$H \gg \frac{\mu_{nuc}}{M_J} \overline{H}_e \simeq 10^2\text{-}10^3 \text{ Oe}.$$

For weak fields, we get $H \ll 10^2$-10^3 Oe.

In the first case, the strong external fields disturb the coupling between the nuclear magnetic moment and the magnetic moment of valence electrons. The electron shell and the nuclear moment are

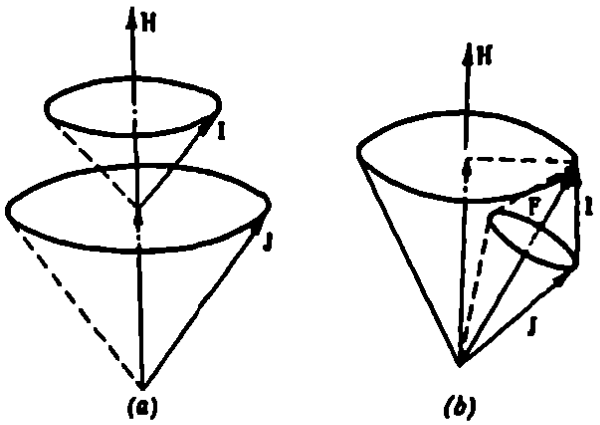

Fig. 31

independently oriented with respect to the external field H in accordance with their intrinsic angular momenta J and I (Fig. 31*a*).

In an external field, vectors J and I acquire $2J + 1$ and $2I + 1$ different orientations respectively. These orientations are characterized by different projections J_z and I_z:

$$\left.\begin{aligned} &J, J-1, J-2, \ldots, -(J-2), -(J-1), -J, \\ &I, I-1, I-2, \ldots, -(I-2), -(I-1), -I. \end{aligned}\right\} \qquad (1.5.21)$$

Each projection has a definite value of additional interaction energy corresponding to it:

$$\left.\begin{aligned} U_J &= -\mu_J H = -\frac{\mu_J}{J} JH = -\frac{\mu_J H}{J} J_z, \\ U_I &= -\mu_I H = -\frac{\mu_I}{I} IH = -\frac{\mu_I H}{I} I_z. \end{aligned}\right\} \qquad (1.5.22)$$

The energy differences corresponding to adjacent values of projections are

$$\Delta U_J = \mu_J H/J, \quad \Delta U_I = \mu_I H/I. \tag{1.5.23}$$

Since $\mu_J \gg \mu_I$, the interaction energy is determined only by the orientations of vector J, each of these orientations has $2I + 1$ closely spaced sublevels corresponding to it (Fig. 32). The nuclear spin I can be determined from the number $2I + 1$ of sublevels. This phenomenon is called the *Paschen-Back effect*.

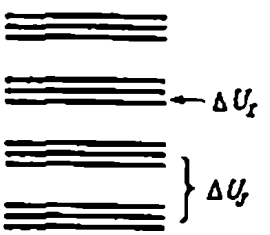

Fig. 32

In the second case, the weak external field cannot break the coupling between vectors J and I and the resultant vector $\mathbf{F} = \mathbf{J} + \mathbf{I}$ is oriented in the external field (see Fig. 31b) with $2F + 1$ values of the projections for each possible value of F. The total number of various states[27] calculated for all possiblo values of F is obviously equal to $(2J + 1)(2I + 1)$. The magnitude of splitting in this case is determined by the quantity $\mu_F \simeq \mu_J$. Knowing J, we can find the nuclear spin I from the number of splitting $2F + 1 = (2J + 1) \times (2I + 1)$. This phenomenon is called the *Zeeman effect*.

1.5.3b. Method of Deflection of Molecular Beams

The deflection of molecular beams in a nonuniform magnetic field is used for determining μ_{nuc} in an experiment similar to the one conducted by Stern and Gerlach. The idea behind the Stern and Gerlach experiment is the application of a transverso magnetic field of such a high degree of nonuniformity that it is felt even within the size of one magnetic dipole, i.e. on the atomic level. The atomic magnetic moment will then be subjected to a ponderomotive force whose value will depend on the orientation of the moment:

$$\mathbf{F} = (\boldsymbol{\mu}\nabla)\,\mathbf{H} = \mu_x \frac{\partial \mathbf{H}}{\partial x} + \mu_y \frac{\partial \mathbf{H}}{\partial y} + \mu_z \frac{\partial \mathbf{H}}{\partial z}.$$

[27] In order to obtain the total number of projections of F for all possible values of its quantum number $F = J + I, J + I - 1, \ldots, |J - I|$, we must take the sum $\sum_{|J-I|}^{J+I} (2F_i + 1)$. This gives the value $(2J + 1)(2I + 1)$.

In the particular case, when the field H and its gradient grad H are directed along the z-axis, we get

$$F = \mu_z \frac{\partial H}{\partial z} = \mu \frac{\partial H}{\partial z} \cos(\mu H). \qquad (1.5.24)$$

When a beam passes through the magnetic field H, the magnetic dipoles will assume $2J + 1$ different orientations and different values of the force of interaction F will correspond to each orientation. Hence dipoles with different orientations of μ will deviate differently from their initial direction. Consequently, the beam is split into several beams and the magnitude of splitting will be proportional to the field gradient and the dipole magnetic moment.

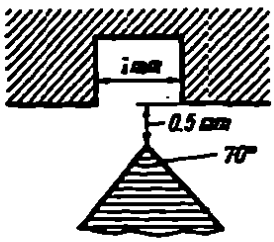

Fig. 33

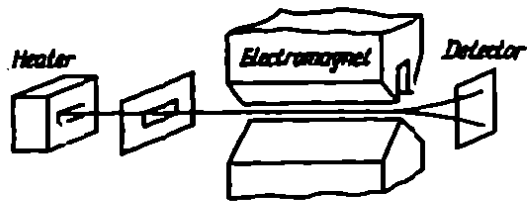

Fig. 34

Stern and Gerlach carried out their experiments in 1921 with neutral silver atoms for which $J = S = s_e$ $(L = 0)$.

Experiments for determining the nuclear magnetic moment are much more complicated, the effect being about 10^3 times weaker than in the Stern-Gerlach experiment due to the smallness of the magnetic moment of nucleus. Besides, the problem becomes extremely complicated since this very weak effect has to be observed against a background of the effect caused by the magnetic moment of electron shells, which is about 10^3 times stronger.

These difficulties were overcome as follows. In order to increase the effect an electromagnet with a special type of pole tips (Fig. 33) was constructed. This ensured a much stronger nonuniformity of the magnetic field with a gradient of (2-5) $\times$ 10^5 Oe/cm. To reduce the strong background effect investigations were made not on atoms but on molecules with mutually compensated magnetic moments of electrons (for example, H_2, H_2O).

Figure 34 shows the schematic diagram of the experiment. The molecular beam is obtained with the help of a heater with a narrow slit (0.01-0.1 mm) through which it enters a vacuum chamber with several diaphragms (one of these is shown in the figure). After passing between the poles of an electromagnet which generates a strongly nonuniform field, the beam hits a screen or detector. For prop-

er formation of the beam, the mean free path of the molecules in the heater must be more than the slit width. Calculations show that this can be attained at a gas (or vapour) pressure of about 1 mm Hg in the heater. Depending on the nature of the substance used for investigation, such a pressure can be attained at quite different temperatures (from liquid air temperature for gases to 1000 °C for solids).

The pressure in the vacuum chamber is maintained at such a value that the mean free path of the molecules is several times more than the size of the apparatus. This ensures that the molecules reach the detector without collisions. Detection is made by any of the following methods:

(1) vapour condensation methods (Stern-Gerlach experiment involving the condensation of silver vapours);

(2) chemical registration method, for example, reduction (or oxidation) reactions for detecting hydrogen (or oxygen);

(3) surface ionization mechanism on an incandescent detector filament (for alkali metals); and

(4) increasing the pressure in a closed vessel with a slit through which the molecular beam enters the chamber. The pressure is measured with the help of a Pirani gauge which operates on the principle that the temperature of an incandescent filament changes with gas pressure. The temperature of the filament is determined by measuring its resistance.

Measurements have shown that in spite of the large value of $\partial H/\partial Z$, the experimentally observed deflection of the beam is so small (about 0.04 mm) that it is comparable with the spread due to the Maxwell velocity distribution. Hence the actual splitting is not observed in such experiments and a careful measurement of the density of molecular distribution in the beam has to be made for determining the magnetic moment. Another difficulty in the experiment is that nuclear magnetic moments of two atoms in a molecule can be oriented in different ways relative to each other. This severely complicates the analysis of results.[28]

Nevertheless, Stern, Estermann and Frisch succeeded in measuring the magnetic moment of a proton, which was found to be about $2.5\mu_N$.[29] This value differs sharply from the value $1\mu_B$ which could be expected in analogy with the magnetic moment of an electron. We shall discuss this question in greater detail at a later stage (see Sec. 1.5.5).

It was mentioned above that the small magnitude of the splitting is a serious drawback of the method of molecular beams in highly

[28] This difficulty is not encountered when a neutron beam is split by the Stern-Gerlach method (see Sec. 1.5.4).

[29] At present, the magnetic moment of the proton is taken as $\mu_p = (2.7928456 \pm 0.0000011)\,\mu_N$.

nonuniform strong magnetic fields. There is a simple method of increasing this effect but it seems impracticable at first glance. This method involves the application of a weak external magnetic field in which the coupling between vectors J and I is preserved and the resultant vector $\mathbf{F} = \mathbf{J} + \mathbf{I}$ is oriented in the field with $2F + 1$ orientations. Since J is usually known, the nuclear spin I can be found by counting the total number of splitting components which is equal to $(2J + 1)(2I + 1)$ in this case. It is important to note that the deflecting force in the weak field method is proportional to the atomic magnetic moment which is 10^3 times the nuclear moment. Hence the deflection is found to be much more pronounced than in the strong field method.[30] (Naturally, in this case we must take atoms with $\mu_J \neq 0$ instead of molecules.)

The weak field method is unsuitable for determining the nuclear magnetic moment since the deflection depends on the magnetic moment of the atom and not the nucleus.

This method was used for determining the nuclear spins of potassium, cesium and other elements.

1.5.3c. Magnetic Resonance and Other RF Methods

The *magnetic resonance method*, or the *radiofrequency method*[31], proposed by Rabi is a particularly accurate method of determining the nuclear magnetic moments.

Rabi's method involves a forced reorientation of the nuclear spin I (and the magnetic moment μ_I) by a resonance high-frequency (HF) electromagnetic field and the computation of μ_I from the resonance frequency ω_{res} of the field. The schematic diagram of the instrument is shown in Fig. 35.

Here, $\mathbf{H}_1$, $\mathbf{H}_2$ and $\mathbf{H}_3$ are three identically directed constant magnetic fields generated by electromagnets *A*, *B* and *C*. The field $\mathbf{H}_2$ is uniform, while $\mathbf{H}_1$ and $\mathbf{H}_3$ are strongly nonuniform. The fields $\mathbf{H}_1$ and $\mathbf{H}_3$ are absolutely identical but have opposite gradients:

$$\partial H_3/\partial z = -\partial H_1/\partial z.$$

A narrow beam of molecules or atoms moving from a heater to a detector (in the form of a Pirani gauge) passes through all three magnetic fields which interact with the magnetic moments of atoms and nuclei and orient them according to the possible values of the

---

[30] The smaller value of H in the case of weak fields does not nullify the advantage, since the weak field is only 10-10^2 times weaker than the strong field.

[31] The method is called so because it involves the application of high-frequency electromagnetic fields of the radiofrequency range.

The effect of one of these fields (rotating against the Larmor precession) is averaged over time, while the effect of the other field (rotating in the same direction as that of the Larmor precession) at $\omega_{HF} = \omega_L$ is sort of "accumulated" with time. This cumulative effect is shown in Fig. 36 where two positions of the vectors μ and H_t can be seen at instants t and $t - T/2$ (after a half-period). It is clear from the figure that the mutual orientation of vectors μ and H_t (angle θ) does not change with time.

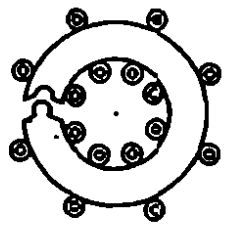

Fig. 37

It is borne out by simple calculations that for quite large HF-field regions and quite low velocities of particles in the beam, the mutual orientation of μ and H_t can be preserved over 10^2-10^3 periods T. This means that during this time the interaction between μ and H_t will tend to change the orientation of vector I in a certain direction (towards increasing or decreasing values of angle θ). As a result of this action, a part of magnetic dipoles will be reoriented while leaving the region.

Knowing the frequency ν_{res}, at which the reorientation of magnetic dipoles takes place, we can calculate the gyromagnetic ratio γ from the formula

$$\omega_{res} = 2\pi\nu_{res} = \omega_L = \mu H/\hbar I = \gamma\mu_B H/\hbar. \qquad (1.5.27)$$

The occurrence of resonance is established with the help of the nonuniform fields H_1 and H_2 which displace the dipoles in opposite directions. Since the fields H_1 and H_2 are absolutely identical but have opposite direction of gradients, the action of both fields will be mutually compensated in the absence of the reorienting HF field, and the beam will return to its original course after passing through the two fields (see Fig. 35). However, if a partial reorientation of nuclear magnetic dipoles takes place due to the resonance action of the HF field, the displacement of dipoles in field H_2 will not compensate the displacement caused by field H_1 and hence the particles will deviate from their initial direction (dashed line in Fig. 35).

Figure 37 shows the cross section of electromagnet A (from Fig. 35) which was used for generating the nonuniform field H_1 (or H_2). The electromagnet is made of an iron pipe about 50 cm long with a cut along its element in the shape of two coaxial cylinders for which the field strength of the electromagnet can be calculated. The slit has an operational width of 1 mm. A copper tube is wound around the pipe and a current of about 100 A is passed through this winding. The strength of the field at 800 ampere-turns is equal to 10^4 Oe and

$\partial H/\partial z = 8 \times 10^4$ Oe/cm. For an overall length of the traversed path of about 1 m, the beam is deflected by about 0.05 mm. Hence the experiment was conducted with extremely narrow beams (about 0.01 mm) of very high intensity (10^{10}-10^{11} particles/cm^2).

The field H_2 is produced by an electromagnet having ground and polished plane-parallel poles. The poles must be prepared with utmost care in order to obtain a strictly uniform field, which must single out a direction for the orientation of dipoles in space but must not displace them.

The oscillating field H_1 was created with the help of the current-carrying loop shown in Fig. 38. As a high-frequency current passes

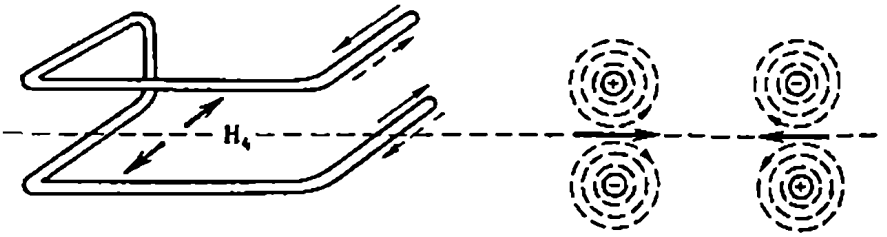

Fig. 38

through the loop, coaxial magnetic fields are generated around the conductors, and their resultant produces the oscillating field H_1 in the path of the particles.

The resonance condition $\omega_{HF} = \omega_L$ can be realized either by changing the frequency ν_{HF} of the field H_1 or by changing the Larmor precession frequency ω_L (i.e. by changing the constant field H_2). By using (1.5.27), we can easily calculate that for $H_2 \simeq 10^4$ Oe,

$$\nu_{res} = \gamma\mu_B H/2\pi\hbar = 0.8\gamma \times 10^7 \text{ Hz}.$$

Putting $\gamma = 1$, we get $\nu_{res} \simeq 10^7$ Hz and $\lambda = c/\nu \simeq 30$ m. Thus, the field H_1 can be produced with the help of RF generators.

The magnetic resonance method was used to obtain for the first time the exact value of the magnetic moment of the proton

$$\mu_p = 2.792845\mu_B,$$

as well as the exact values of the magnetic moments of atomic nuclei.

Besides the method described above, other versions of the magnetic resonance method are also used. Basically, these methods differ in the ways of detecting the reorientation of magnetic moments in a resonance field. In one of the methods, for example, the reorientation is determined by emission or absorption of radiation quanta which accompanies the reorientation of the dipoles. In another method,

the e.m.f. induced by precessing nuclear spins in a coil placed near the sample under investigation is measured. Both methods do not require narrow beams or nonuniform fields.

1.5.4. Determination of the Magnetic Moment of the Neutron

In principle, Rabi's method of deflection of beams in magnetic fields is also suitable for determining the magnetic moment of the neutron. However, nuclear reactors were not available in the 1930s (when the magnetic moment of the neutron was measured for the first time) for obtaining neutrons with a high flux density. Hence a somewhat modified form of Rabi's method was used for determining the magnetic moment of the neutron. In this method, neutrons are made to pass successively through two ferromagnetics that have been magnetized to saturation. Narrow beams are not required in this method.

The essence of the method lies in the following. Nuclear scattering is the main process of interaction as neutrons pass through a medium (with a small absorption cross section). As a result of scattering, neutrons deviate from their initial direction (leave the beam) and hence their number N in the beam decreases with thickness δ of the medium according to the law

$$N = N_0 \exp(-n\sigma\delta), \qquad (1.5.28)$$

where N_0 is the initial number of neutrons, n is the concentration of nuclei in the medium and σ is the scattering cross section.

It was shown by Bloch in 1936 that if a ferromagnetic is magnetized to saturation and used as the medium, the neutron magnetic moment must lead to an additional effect (besides the nuclear attraction) due to its electromagnetic interaction with the oriented magnetic dipoles of the ferromagnetic. The interaction of magnetic dipoles depends on their mutual orientation (parallel dipoles repel each other while antiparallel dipoles attract each other). Hence the sign of the additional effect will be different for neutrons with different orientations of spin (and hence of the magnetic moment) relative to the direction of magnetization of the ferromagnetic ($\uparrow\!\!\downarrow$ or $\downarrow\!\!\uparrow$).

For neutrons with one direction ($\uparrow$) of spins, the magnetic interaction leads to an increase in the scattering cross section ($\sigma = \sigma_0 + \Delta\sigma$), while for the opposite direction ($\downarrow$), the scattering cross section decreases ($\sigma = \sigma_0 - \Delta\sigma$). The long-range nature of electromagnetic forces makes this effect quite significant ($\Delta\sigma/\sigma \simeq 0.1$). If the initial neutron beam is not polarized, i.e.

$$N = \overset{\uparrow}{N}_0 + \overset{\downarrow}{N}_0, \quad \overset{\uparrow}{N}_0 = \overset{\downarrow}{N}_0 = N_0/2,$$

the number of neutrons after scattering by a magnetized ferromagnetic with upward orientation ($\uparrow\uparrow$) will be

$$N_1(\uparrow\uparrow) = \overset{\uparrow}{N}_1(\uparrow\uparrow) + \overset{\downarrow}{N}_1(\uparrow\uparrow) = \overset{\uparrow}{N}_0 \exp[-n(\sigma_0 + \Delta\sigma)\delta]$$
$$+ \overset{\downarrow}{N}_0 \exp[-n(\sigma_0 - \Delta\sigma)\delta] = (N_0/2)\{\exp[-n(\sigma_0 + \Delta\sigma)\delta] + \exp[-n(\sigma_0 - \Delta\sigma)\delta]\}, \quad (1.5.29)$$

where $\overset{\uparrow}{N}_1(\uparrow\uparrow) < \overset{\downarrow}{N}_1(\uparrow\uparrow)$.[32]

Thus, the passage of neutrons through a ferromagnetic must enrich the beam in neutrons with a certain orientation of spin and magnetic moment. For the neutrons, the ferromagnetic behaves as a polarizer through which neutrons with a certain direction of the magnetic moment predominantly pass.

If such a partially polarized neutron beam is then passed through a second ferromagnetic with the same orientation of the magnetization vector ($\uparrow\uparrow\ \uparrow\uparrow$), the number of neutrons after the second scattering will be

$$N_2'(\uparrow\uparrow\ \uparrow\uparrow) = \overset{\uparrow}{N}_2(\uparrow\uparrow\ \uparrow\uparrow) + \overset{\downarrow}{N}_2(\uparrow\uparrow\ \uparrow\uparrow) = \overset{\uparrow}{N}_0 \exp[-2n(\sigma_0 + \Delta\sigma)\delta]$$
$$+ \overset{\downarrow}{N}_0' \exp[-2n(\sigma_0 - \Delta\sigma)\delta] = (N_0/2)\exp(-2n\sigma_0\delta)$$
$$\times \{\exp(-2n\delta\Delta\sigma) + \exp(+2n\delta\Delta\sigma)\}. \quad (1.5.30)$$

For opposite orientations of the magnetization vectors ($\uparrow\downarrow$), the number of transmitted neutrons will be

$$N_2(\uparrow\downarrow) = \overset{\uparrow}{N}_2(\uparrow\downarrow) + \overset{\downarrow}{N}_2(\uparrow\downarrow) = \overset{\uparrow}{N}_0 \exp[-n(\sigma_0 + \Delta\sigma)\delta]$$
$$\times \exp[-n(\sigma_0 - \Delta\sigma)\delta] + \overset{\downarrow}{N}_0 \exp[-n(\sigma_0 - \Delta\sigma)\delta]$$
$$\times \exp[-n(\sigma_0 + \Delta\sigma)\delta] = N_0 \exp(-2n\sigma_0\delta). \quad (1.5.31)$$

It can be easily seen that if $\Delta\sigma \neq 0$, i.e. if the neutron has a magnetic moment, we get

$$\frac{N_2(\uparrow\uparrow\ \uparrow\uparrow)}{N_2(\uparrow\uparrow\ \downarrow\downarrow)} = \frac{\exp(-2n\delta\Delta\sigma) + \exp(2n\delta\Delta\sigma)}{2} > 1. \quad (1.5.32)$$

Thus, the second ferromagnetic behaves as an analyzer: it allows different number of neutrons to pass through for different orientations of its magnetization vector.

Experiments have revealed that such an effect takes place in actual practice, thereby indicating that the neutron does possess a magnetic moment.

[32] The description takes into account the fact that the spin and magnetic moment of the neutron are antiparallel (see below).

The magnetic resonance method was used for measuring the neutron magnetic moment. Figure 39 is a schematic diagram of the experimental set-up.

Fast neutrons from a cyclotron are slowed down in a moderator and made to pass through a cadmium collimator Cd followed by a ferromagnetic polarizer in which the beam is partially polarized. This polarization can be detected from the change in the number of neutrons registered by a detector upon a change in the orientation of a ferromagnetic analyzer. In the space between the polarizer and

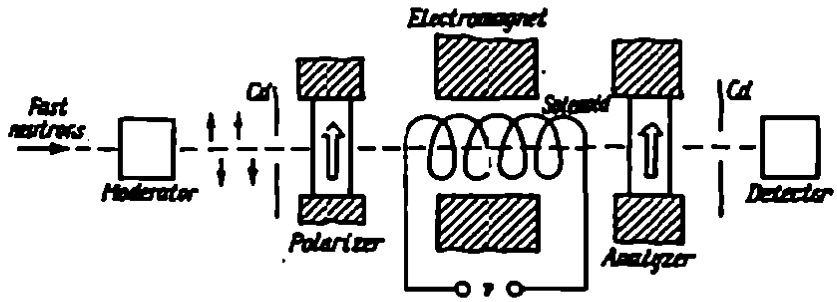

Fig. 39

analyzer, the neutrons are subjected to a constant transverse magnetic field of strength $H = 7 \times 10^3$ Oe, created by an electromagnet, and to a longitudinal HF field created by a solenoid.

In the experiment, the detector signal was measured with varying generator frequency ν. A sharp decrease in the number of transmitted neutrons was observed at $\nu_{res} = 2 \times 10^7$ Hz. Substituting this value into the formula for the Larmor frequency

$$\omega_L = \mu H/\hbar s = \gamma \mu_B H/\hbar, \qquad (1.5.33)$$

we get

$$|\gamma| = 2\pi\hbar\nu_{res}/\mu_B H \simeq 3.8.$$

The apparatus described above can be used for determining not only the magnitude, but also the sign of γ. For this purpose, we must replace the electromagnet and the HF solenoid by another solenoid which produces a weak constant longitudinal magnetic field $H \simeq 10$ Oe. This magnetic field causes a slow precession of the neutron magnetic dipoles, thus turning the direction of polarization over the length of the solenoid by a small angle φ (Fig. 40). Choosing the value of H in such a way that the angle of rotation is less than π, we can fix the direction of precession (and hence the sign of γ) by turning the analyzer. The experiment revealed that γ has a negative

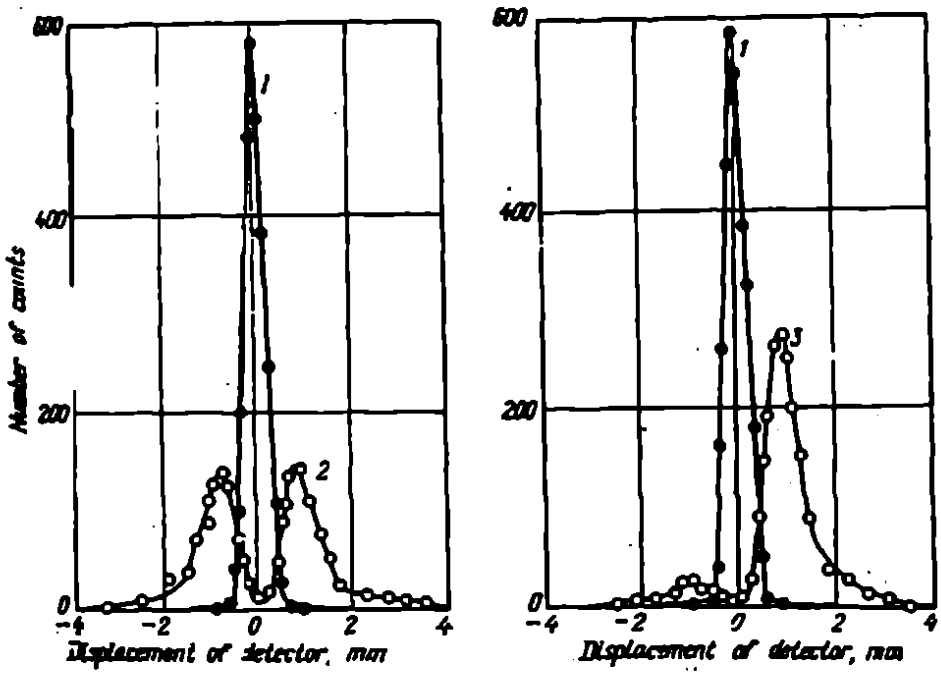

Fig. 42

The values of polarization, obtained by this method, are $P = 80$-90% with an error of about 10%.

The degree of polarization of a neutron beam can be determined more accurately (with an accuracy of about 99%) by directly measuring the intensity of its components which are split in a strong nonuniform magnetic field (Stern-Gerlach experiment on neutrons). Figure 42 shows the results of one such experiment. Here curve *1* corresponds to an unsplit beam, curve *2* to a split nonpolarized beam ($P = 0$) and curve *3* to a split polarized beam (with polarization $P = 80\%$). The splitting of a beam into two components is the most direct evidence of the fact that the neutron has a spin $s_n = 1/2$ $(2s + 1 = 2)$.

1.5.5. Results of Measurements of Spins and Magnetic Moments. Schmidt's One-nucleon Model

The values of spins and approximate magnetic moments of some nuclei are given in Table 4. We shall analyze these data starting with nucleons, i.e. proton and neutron. These have identical spins 1/2 and their magnetic moments are

$$\mu_p \simeq 2.79\mu_B \quad \text{and} \quad \mu_n \simeq -1.91\mu_B. \qquad (1.5.34)$$

Table 4

Nucleus	I in $\hbar$	μ in μ_B	Nucleus	I in $\hbar$	μ in μ_B
n	1/2	−1.91	$^{12}_{6}C$	0	0
p	1/2	+2.79	$^{13}_{6}C$	1/2	+0.7
$^{2}_{1}H$	1	+0.86	$^{14}_{7}N$	1	+0.4
$^{3}_{1}H$	1/2	+3	$^{15}_{7}N$	1/2	−0.28
$^{3}_{2}He$	1/2	−2.1	$^{16}_{8}O$	0	0
$^{4}_{2}He$	0	0	$^{17}_{8}O$	5/2	−1.9
$^{6}_{3}Li$	1	+0.82	$^{35}_{17}Cl$	2	+1.3
$^{7}_{3}Li$	3/2	+3.3	$^{115}_{49}In$	9/2	+5.5
$^{9}_{4}Be$	3/2	−1.2	$^{204}_{82}Pb$	0	0
$^{10}_{5}B$	3	+1.8	$^{209}_{83}Bi$	9/2	+4.1

Since the spins of the neutron and proton are equal to 1/2, the values of their magnetic moments can be written in a form similar to (1.5.9):

$$\mu_p = 2s \times 2.79\mu_B = 5.58s\mu_B, \tag{1.5.35}$$

$$\mu_n = -2s \times 1.91\mu_B = -3.82s\mu_B. \tag{1.5.36}$$

The coefficient 5.58 (−3.82) expresses the connection between the numerical value of the intrinsic magnetic moment of the proton (neutron) in nuclear magnetons μ_B and the numerical value of its spin in units of $\hbar$. This factor is called the *gyromagnetic ratio* γ_s. Thus, in analogy with (1.5.10), we can write the following relation for a nucleon:

$$\mu = \gamma_s s, \tag{1.5.37}$$

where $(\gamma_s)_p = 5.58$ and $(\gamma_s)_n = -3.82$.

It was mentioned above that the difference of the proton magnetic moment from one nuclear magneton is an astonishing result. Even more astonishing is the fact that the uncharged neutron has a magnetic moment. Obviously, a complete explanation of this fact is possible only in quantum chromodynamics. However, some ideas concerning the possibility that nucleons may have anomalous magnetic moments can also be considered in the framework of the classical phenomenological concepts of strong interaction described in this book.

If, for example, we assume that the neutron (at least for some part of its lifetime) is a complex formed by a central positive charge and an equal negative charge at the periphery, such a system will have a negative magnetic moment as it rotates about its axis. Similarly, by introducing the concept of a positive peripheral charge, we can explain the anomalously large value of the proton magnetic

moment. Nearly identical deviations of the magnetic moments of protons and neutrons from their Dirac values ($\Delta\mu_n = \mu_n - 0 = -1.91\mu_B$, $\Delta\mu_p = \mu_p - 1 = 1.79\mu_B$ and $|\Delta\mu_n| \simeq |\Delta\mu_p|$ point towards the similar nature of these peripheral charges.

Investigations carried out in the 1950s and 1960s on the nature of nuclear forces and the structure of nucleons lend credibility to such concepts about neutrons and protons. The results of such investigations lead to the conclusion that a real nucleon is surrounded by a cloud ("sheath") of continuously emitted and absorbed virtual π-mesons (see Sec. 1.2, Vol. II for details).

It can be assumed that with a certain probability ω the neutron is a complex system consisting of an "ideal" proton p_0 (with a unit magnetic moment $\mu_{p_0} = 1\mu_B$) and a negative π-meson revolving around it[28] ($n = p_0 + \pi^-$), while the probability of its behaving as an "ideal" neutron with zero magnetic moment ($\mu_{n_0} = 0$) is $1 - \omega$. In this model, the averaged magnetic moment of the neutron will be

$$\mu_n = (1 - \omega)\,\mu_{n_0} + \omega\,(\mu_{p_0} - \mu_\pi) = [(1 - \mu_\pi)\,\omega]\,\mu_B, \quad (1.5.38)$$

where μ_π is the magnetic moment created by the orbital motion of a π-meson.

Similarly, assuming that ω is the probability that a proton consists of an ideal neutron and a positive π-meson ($p = n_0 + \pi^+$) while $1 - \omega$ is the probability of its being an ideal proton p_0, we obtain

$$\mu_p = \omega\,(\mu_{n_0} + \mu_\pi) + (1 - \omega)\,\mu_{p_0} = [1 + (\mu_\pi - 1)\,\omega]\,\mu_B. \quad (1.5.39)$$

Assuming, for example, that $\mu_\pi = 7\mu_B$ (the orbital magnetic moment of a π-meson with $l = 1$ must be equal to $m_p\mu_B/m_\pi \simeq 7\mu_B$) and equating (1.5.39) to the experimental value $(1 + 6\omega)\,\mu_B = 2.79\mu_B$, we obtain $\omega \simeq 0.3$. Substituting this value into (1.5.33), we obtain the following theoretical value for the neutron magnetic moment:

$$\mu_n = (1 - \mu_\pi)\,0.3\mu_B = -1.8\,\mu_B \simeq \mu_n^{exp}.$$

Let us now consider the spins and magnetic moments of nuclei. In the first place, the simple relation between the spin and the mass number is worth noting. All nuclei with even A have integral spin, while nuclei with odd A have half-integral spin. This invalidates the proton-electron model of the nucleus. Thus, if the nitrogen nucleus consisted of 14 protons and 7 electrons, its spin would be half-integral ("the *nitrogen catastrophe*"). The order of magnitude of nuclear magnetic moments, which does not exceed a few magnetons,

[28] It has been shown theoretically that the π-meson "cloud" has a nonzero angular momentum. For details on virtual and real π-mesons, nuclear forces and the structure of nucleons, see Sec. 1.2 Chaps. 3 and 6, Vol. II.

points to the same fact. If the nucleus contained electrons, its magnetic moments would be of the order of the Bohr magneton for electrons, i.e. would be about 10^3 times higher.

An analysis of the values of nuclear spins and magnetic moments leads to the conclusion that the spins and magnetic moments of neutrons and protons in the nucleus are almost completely neutralized on account of their mutual arrangement inside the nucleus. Indeed, the maximum spin of the nucleus does not exceed a few units, which is much smaller than $A/2$, a value that would be expected if the spins of all nucleons were parallel and were added arithmetically. The same is true for magnetic moments as well.

The neutralization of spins and magnetic moments can be followed quite clearly by considering the four lightest nuclei in the Periodic Table, viz. ${}_1^2\mathrm{H}$, ${}_1^3\mathrm{H}$, ${}_2^3\mathrm{He}$ and ${}_2^4\mathrm{He}$. The first of these, deuteron, is the simplest atomic nucleus consisting of one proton and one neutron. The spin ($s = 1$) and the magnetic moment ($0.86\mu_B$) of the deuteron are obtained by adding the spins and magnetic moments of the proton and the neutron:

$$\left.\begin{aligned} s_n + s_p &= 1/2 + 1/2 = 1 = I_{{}_1^2\mathrm{H}}, \\ \mu_p + \mu_n &= 2.8 - 1.9 = 0.9 \simeq \mu_{{}_1^2\mathrm{H}}. \end{aligned}\right\} \qquad (1.5.40)$$

In the deuteron nucleus, the spins of the neutron and proton do not cancel out, but are rather added; the neutron and the proton may form a bound system, viz. a deuteron, only when their spins are parallel.[34] There are no nuclei in which the neutron and proton spins are antiparallel. This result is a consequence of the spin dependence of nuclear forces (see Sec. 1.5.2, Vol. II for details).

The phenomenon of spin compensation in nuclei starts manifesting itself in the tritium nucleus ${}_1^3\mathrm{H}$. The spin (1/2) and the magnetic moment (about $3\mu_p$) of tritium are obtained from the spins and magnetic moments of two neutrons and one proton by adding them under the assumption that the spins of two neutrons are antiparallel and hence cancel out. In this case the magnetic moments of both the neutrons also cancel out and the nuclear spin and magnetic moment are determined by the spin and magnetic moment of the unpaired proton.

A similar situation holds for the ${}_2^3\mathrm{He}$ nucleus whose spin (1/2) and magnetic moment ($\mu_{{}_2^3\mathrm{He}} \simeq -2.1\mu_B$) nearly coincide with the corresponding values for an unpaired neutron (1/2 and $-1.9\mu_B$).

[34] This circumstance is a convincing argument that the spin of the neutron is equal to 1/2 and not 3/2. Indeed, if the neutron spin were 3/2, the spin of the deuteron (1) would be obtained as the difference between the spins of the neutron and the proton. In this case, it would be impossible to reconcile the magnetic moment of the deuteron with the magnetic moments of nucleons (see also Sec. 1.5.4).

The spin compensation is manifested most clearly in the $^4_2$He nucleus which has zero spin and zero magnetic moment. Both pairs of similar nucleons in this nucleus are arranged in such a way that their spins and magnetic moments cancel out and we get zero spin and zero magnetic moment as a result.

Total compensation of spins and magnetic moments is observed not only in the $^4_2$He nucleus but also in all even-even nuclei which invariably have $I = 0$, $\mu = 0$ (no hyperfine splitting is observed experimentally in their case).[35] In this connection, it could be natural to assume that the spin and magnetic moment of odd nuclei which differ from the even-even nuclei in one additional (or deficient) nucleon are determined by the spin and magnetic moment of this nucleon. It can be seen from the above description that this assumption is confirmed by taking the example of $^3_1$H and $^3_2$He whose spins and magnetic moments are determined by the unpaired nucleons.

An anomalous situation is observed, however, when the spin and magnetic moment of a neutron are compared with the values for the $^{13}_6$C nucleus which differs from the even-even nucleus $^{12}_6$C only in an additional neutron. The $^{13}_6$C nucleus has the same spin as the neutron but their magnetic moments differ not only in magnitude, but also in sign ($0.7\mu_B$ and $-1.91\mu_B$ respectively).

A similar conclusion can be drawn about the $^{15}_7$N nucleus which has one unpaired proton, but has a negative magnetic moment.

This anomaly can be overcome by assuming that the additional nucleon participates in the orbital motion, thus generating additional spin and magnetic moment. In analogy with Eq. (1.5.7), the magnetic moment corresponding to the proton orbital angular momentum l is $\mu_l = l\mu_B$, so that the gyromagnetic ratio $(\gamma_l)_p = 1$. The orbital motion of neutrons does not create a magnetic moment since the neutron has no charge. Consequently, $(\gamma_l)_n = 0$.

Schmidt used these concepts in 1937 to develop a simple one-nucleon model for nuclear spin and magnetic moment. According to this model, the angular momentum and magnetic moment of an odd nucleus are determined by the total angular momentum and total magnetic moment of the unpaired nucleon[36]:

$$\mathbf{I} = \mathbf{l} + \mathbf{s} \quad \text{and} \quad \boldsymbol{\mu} = \gamma_l \mathbf{l} + \gamma_s \mathbf{s}. \tag{1.5.41}$$

The calculation of I is carried out by the usual laws of addition of quantum-mechanical vectors. The difference between γ_l and γ_s, leading to nonparallelism between I and μ, must be taken into

[35] It should be recalled that in this chapter we consider the ground states of nuclei. Excited states of even-even nuclei may have a nonzero angular momentum (see Sec. 2.4).

[36] Schmidt's idea about the orbital motion of nucleons in a nucleus is used in the nuclear shell model (see Chap. 2).

account. The resultant vector μ precesses about the vector I and its average value coincides with its component parallel to I (Fig. 43). It is this averaged value of the magnetic moment (sometimes it is called the *effective magnetic moment*) that is manifested in various experiments. In an external magnetic field, μ_{eff} has $2I+1$ possible projections, the largest of these characterizing the numerical value of the magnetic moment. Since μ_{eff} is parallel to I, its numerical value can be expressed through the relation $\mu_{eff} = \gamma_I I$, where γ_I is the gyromagnetic ratio.

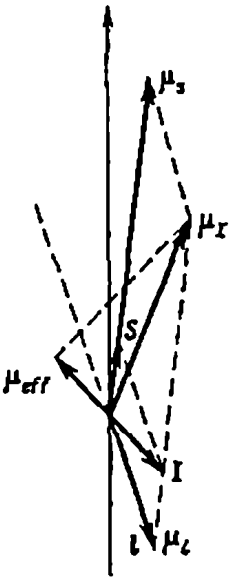

Fig. 43

In order to determine the effective magnetic moment of a nucleon (henceforth we shall call it just the magnetic moment of a nucleon), we must calculate the scalar product of the vectors μ and I. We shall skip these calculations[37] and write the final result for γ_I:

$$\gamma_I = \gamma_l \pm (\gamma_s - \gamma_l)/(2l+1) \quad \text{for} \quad I = l \pm 1/2. \tag{1.5.42}$$

Thus, we get for the proton

$$\left.\begin{aligned} \mu &= (I + 2.29)\,\mu_B && (I = l + 1/2), \\ \mu &= [1 - 2.29/(I+1)]\, I\mu_B && (I = l - 1/2), \end{aligned}\right\} \tag{1.5.43}$$

and for the neutron

$$\left.\begin{aligned} \mu &= -1.91\mu_B && (I = l + 1/2), \\ \mu &= [1.91/(I+1)]\, I\mu_B && (I = l - 1/2). \end{aligned}\right\} \tag{1.5.44}$$

It can be seen from (1.5.43) and (1.5.44) that the sign of the nucleon magnetic moment is determined by the mutual orientation of s and l, as well as by the value of l. In particular, $\mu = -0.26\mu_B$ when the proton is in the $p_{1/2}$ state ($l = 1$, $I = 1/2$) instead of $+2.79\mu_B$ when it is in the s state. The corresponding value for the neutron is $+0.64\mu_B$ (instead of $-1.91\mu_B$).[38]

---

[37] See, for example, E Fermi, *Nuclear Physics*, University of Chicago, Chicago and London, 1974.

[38] Sometimes a proton (neutron) in the s state is called an s-proton (s-neutron), a p state proton (neutron) is called a p-proton (p-neutron), and so on.

These values are in quite good agreement with the experimental values of the magnetic moments of the $^{13}_{7}N$ and $^{13}_{6}C$ nuclei considered above by way of examples. Hence it can be stated that according to Schmidt's model the spin and magnetic moment of the nucleus $^{15}_{7}N$ ($^{13}_{6}C$) are determined by the unpaired proton (neutron) in the $p_{1/2}$ state.

Many more examples can be cited where μ_{exp} is close to the calculated value. Such a situation is encountered in nearly-magic nuclei when the number of protons (neutrons) is equal to $N_{mag} \pm 1$ (^{17}O, ^{19}F, ^{35}S, ^{207}Pb).

However, there are very few cases in which such a good agreement occurs. As a rule, the experimental values of the magnetic moments

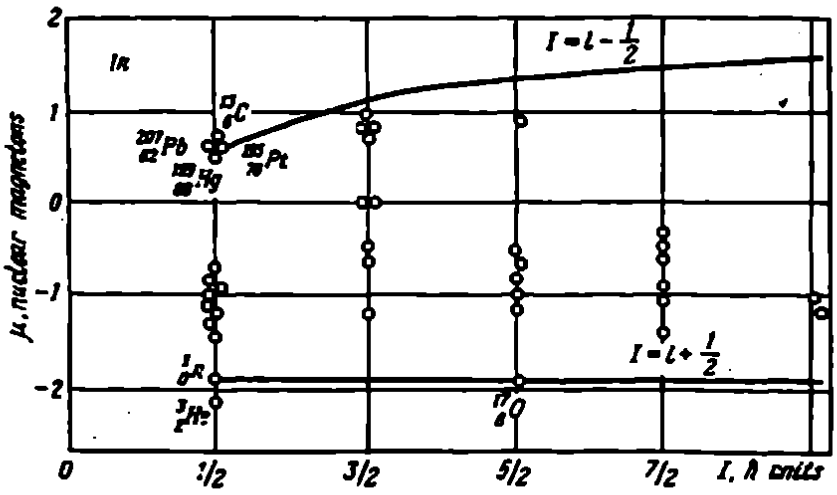

Fig. 44

of odd nuclei differ significantly from the theoretical results obtained with the help of Eqs. (1.5.43) and (1.5.44) and represented by the so-called Schmidt curves. The experimental values of the magnetic moment for even-odd (Z even) and odd-even ($A - Z$ even) nuclei are compared with the Schmidt curves in Figs. 44 and 45.

It can be seen from these figures that for most nuclei the magnetic moments really differ considerably from the calculated values. However, it follows from the same figures that the Schmidt curves correctly represent the general tendency of variation of magnetic moments for odd nuclei. Nearly all the values of magnetic moments lie between the Schmidt curves and are noticeably closer to one of these (the middle region in Fig. 45 practically does not contain

any point).[39] The magnetic moments of odd-even nuclei increase with spin (or orbital angular momentum) while for even-odd nuclei no such dependence is observed. All this confirms the correctness of Schmidt's basic idea about the role of orbital motion of a nucleon in the formation of the nuclear spin and magnetic moment, i.e. about the one-particle origin of these quantities.

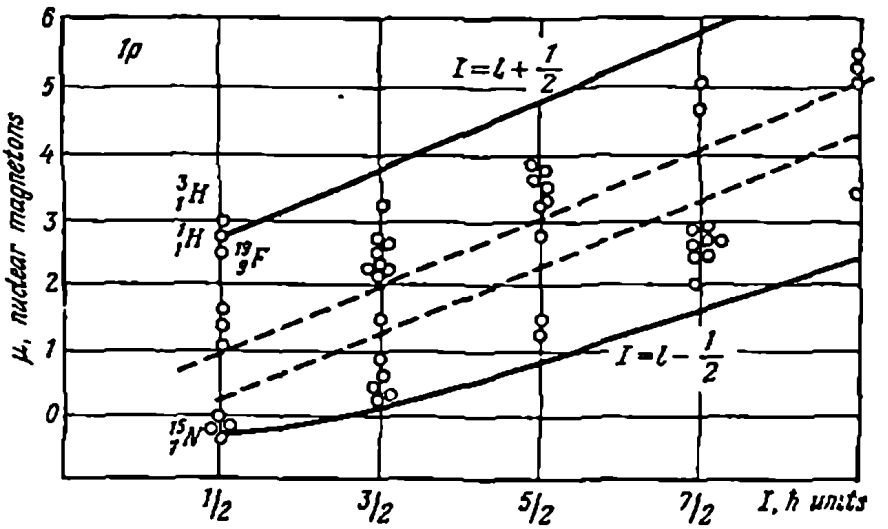

Fig. 45

The discrepancy between the experimental values of nuclear magnetic moments and the Schmidt curves is a measure of the inaccuracy of this model. This inaccuracy may be due to the erroneous assumption that the bound nucleons in a nucleus have the same values of magnetic moments as the free nucleons.[40] Another possible reason for the inaccuracy of Schmidt's model may be the basic assumption that only one unpaired nucleon contributes to the spin and magnetic moment.

This model was further developed into its modern version of the nuclear shell model which considers, unlike one particle in Schmidt's model, several particles in the field of remaining nucleons which are unfilled shells and hence produce neither spin nor magnetic moment

[39] This allows us to use Schmidt's model for choosing the correct value of l for an unpaired nucleon from two possible values for a given I ($l = I - 1/2$ and $l = I + 1/2$). The value of l for the unpaired nucleon must be known for constructing the nuclear shell model.

[40] Assuming that the magnetic moments of nucleons in a nucleus lie in the interval $1 \leqslant \mu_p \leqslant 2.79\mu_N$, $-1.91\mu_N \leqslant \mu_n \leqslant 0$, we obtain a better agreement with the model. In particular, this explains the reason behind the absence of any experimental values of magnetic moments in the middle of Fig. 45 (the dashed lines correspond to the value $\mu_p = 1\mu_N$).

(see Chap. 2). The nuclear spin and magnetic moment are determined by all the outer nucleons which do not form closed shells. In particular, the nuclear magnetic moment is determined as the projection of the vector sum of the magnetic moments of all the outer nucleons onto the direction of the nuclear spin. In the shell model, such calculations can be made for a large number of light nuclei, and the results are in better agreement with the experiment than in the case of Schmidt's model.

1.6. Parity. Law of Conservation of Parity

Historically, the concept of parity of a wave-function appeared at the birth of quantum mechanics (Wigner, 1927). It is well known that the first achievements of quantum mechanics were associated with electromagnetic and strong interactions (structure of the atom, theory of alpha decay) which are described by the Schrödinger equation. The Hamiltonian of this equation has the form

$$H = -\sum \frac{\hbar^2}{2m_i}\left(\frac{\partial^2}{\partial x_i^2}+\frac{\partial^2}{\partial y_i^2}+\frac{\partial^2}{\partial z_i^2}\right)+U(x_i, y_i, z_i), \quad (1.6.1)$$

where the first term is the kinetic energy operator for the system of particles while the second term describes their potential energy.

It can be easily seen that both terms in the Hamiltonian are symmetric with respect to the operation of mirror reflection, i.e. with respect to the inversion of coordinates:

$$x_i \to -x_i, \quad y_i \to -y_i, \quad z_i \to -z_i,$$
$$r \to r, \quad \theta \to \pi - \theta, \quad \varphi \to \pi + \varphi.$$

Indeed, the first term has mirror symmetry since ∂x, ∂y and ∂z appear in it as squares. The second term is symmetric since the potential is a function of the mutual arrangement of particles only and thus cannot change due to inversion of coordinates.

Naturally, the wave-function ψ, which is the solution of the mirror symmetric Schrödinger equation, must also be symmetric with respect to the reflection operation. This means that the probability $W(V, t)$ of finding a particle in a volume V at an instant t must not depend on whether the measurements are made in the right-handed (x, y, z) or left-handed $(-x, -y, -z)$ system of coordinates:

$$W(V, t) = \int_V |\psi(x, y, z)|^2 dV = \int_V |\psi(-x, -y, -z)|^2 dV. \quad (1.6.2)$$

Proceeding to the limit $V \to 0$, we get

$$|\psi(x, y, z)|^2 = |\psi(-x, -y, -z)|^2, \quad (1.6.3)$$

odd and some even, the parity of this state will be indefinite[42]. In this case, parity conservation leads to the conservation of the relative fraction of partial components with definite values of parity.

Parity conservation imposes certain restrictions on nuclear processes. Hence it is very important to determine the parity of a nuclear system. Quite frequently, the problem of determining the parity of a complex system may be solved by decomposing it into subsystems. Let us consider, for example, a system of two noninteracting particles A and B. The wave-function of such a system can be represented as the product of four wave-functions:

$$\psi_{A+B} = \psi_A \psi_B \psi_{l_A} \psi_{l_B},$$

where ψ_A and ψ_B are the wave-functions describing the intrinsic state (motion with respect to the centre of inertia of the subsystems) of each particle (which itself may be a complex system), while ψ_{l_A} and ψ_{l_B} are the wave-functions of the relative motion of A and B. (These wave-functions give an idea of the law of motion for the centres of inertia of the subsystems A and B.) Since the "parity test" is reduced to the coordinate inversion and a comparison of the signs of the functions $\psi(x, y, z)$ and $\psi(-x, -y, -z)$ it is quite obvious that when these operations are carried out successively on ψ_A, ψ_B, ψ_{l_A}, and ψ_{l_B}, we obtain the following rule for the parity of a complex system:

$$P_{A+B} = P_A P_B P_{l_A} P_{l_B}.$$

Thus, the parity of a complex system is equal to the product of the parities of composite parts and the parities of the wave-functions describing their motion relative to their common centre of inertia.

It has been proved in quantum mechanics that the relative motion of two particles is described by a wave-function of the type

$$\psi_l = R(r) P_l^m(\cos\theta) e^{im\varphi}, \qquad (1.6.7)$$

where $P_l^m(\cos\theta)$ is the Legendre associated function. The structure of this function is such that when $\cos\theta$ is replaced by $-\cos\theta$, it acquires a multiplier $(-1)^{l-m}$ where l is the orbital angular momentum and m is its projection on the polar axis.

---

[42] A plane wave is the simplest example of a wave-function with indefinite parity. However, the interaction of a plane wave with the nucleus leads to a state with a definite parity. For example, if the particles are slow, the interaction takes place with $l = 0$ and hence the parity of the resulting state is the product of the parities of interacting particles.

As a result of mirror reflection, the polar coordinates of a point change as follows:

$$r \to r,$$

$$\theta \to \pi - \theta, \quad \cos(\pi - \theta) \to -\cos\theta,$$

$$\varphi \to \pi + \varphi, \quad \exp(im\varphi) \to \exp[im(\pi + \varphi)] \to (-1)^m \exp(im\varphi).$$

Hence $\psi_l = R(r) P_l^m(\cos\theta) \exp(im\varphi)$ is transformed into $R(r) \times (-1)^{l-m} P_l^m(\cos\theta) \exp(im\varphi) (-1)^m = (-1)^l \psi_l$.

The parity of a wave-function relative to the motion is given by

$$P_l = (-1)^l.$$

Thus, the parity of the system $A + B$ is[43]

$$P_{A+B} = P_A P_B (-1)^{l_A} (-1)^{l_B}. \tag{1.6.8}$$

If the intrinsic parities of the subsystems A and B are known, the parity of the complex system will be determined. If A and B themselves are complex systems whose intrinsic parities are known, the same arguments can be applied to them. Ultimately, a complex system (atomic nucleus) can be represented (for example, in the shell model) as an aggregate of nucleons that move relative to one another but do not interact so that the parity of the system will be equal to the product of intrinsic parities of nucleons by $(-1)^{\Sigma l_i}$, where l_i is the orbital number determining the nature of motion of a given nucleon.

Since the number of nucleons is usually conserved in ordinary nuclear processes, the intrinsic parity of a nucleon can be chosen arbitrarily, say, positive. Then the parity state of a nucleon will be even or odd depending on whether its motion is described by a wave-function with even or odd l. For example, s-proton and s-neutron ($l = 0$) will be even, p-proton and p-neutron ($l = 1$) will be odd, and so on. Thus, the parity of a system of noninteracting nucleons is determined by the sum of all l. If $\sum l$ is even, the system will be even, and if $\sum l$ is odd, the system will be odd.

Thus, for example, it has been shown in the shell model (see Chap. 2) that the $^7_3$Li nucleus is formed when the potential well is filled by four nucleons in the s state ($l = 0$) and three nucleons in the p state ($l = 1$). Hence the intrinsic parity of the $^7_3$Li nucleus in the ground state is $(-1)^3 = -1$.

---

[43] The wave-function of the system $A + B$ is often represented in the form $\psi_{A+B} = \psi_A \psi_B \psi_{l_{AB}}$, where $\psi_{l_{AB}}$ is the wave-function of the relative motion of A and B (one of these systems is assumed to be fixed). All the arguments given above remain valid and the parity of $\psi_{l_{AB}}$ is determined by the factor $(-1)^{l_{AB}}$.

The parity of the wave-function is as important a property of the nucleus as its spin. All electromagnetic and strong interaction processes (for example, emission of γ-quanta, alpha decay, nuclear reactions) proceed in such a way that the overall parity of the system of interacting particles does not change after the interaction (specific examples in which the law of parity conservation has been applied can be found in Secs. 3.2, 3.4, 9.3 and 10.4).

Hence each energy state of the atomic nucleus (ground as well as excited state) is characterized, besides its energy and spin (angular momentum for the excited state), by its parity as well. The parity of a nuclear energy level is specified as a superscript (by a plus or minus sign) above the value of its spin (see, for example, Figs. 51 and 53).

It was mentioned above that the law of parity conservation was first formulated for electromagnetic and strong interactions. Its validity for various processes of this kind was experimentally verified several times. Perhaps that is the reason why it was assumed for a long time (up to 1956) that parity is conserved in all, including weak, interactions.

It is also possible that the protracted existence of this general misconception was facilitated by the subconscious desire to assume that the space surrounding us (which, in accordance with the laws of conservation of momentum and angular momentum, is homogeneous and isotropic) has mirror symmetry and is not twisted or helical.

Whatever may be the case, the first version of the theory of beta decay formulated by Fermi in 1934 was based on parity conservation. As a matter of fact, it was shown theoretically in 1956 and proved experimentally in 1957 that parity is not conserved in weak interactions. In view of this, the theory of beta decay was reviewed soon after this discovery (see Secs. 3.3.5 and 3.3.6). It is remarkable that the initial incorrect version of the theory existed for about a quarter of a century and was not disputed by even one of the many experiments conducted during this period. It turned out that *none* of these experiments was sensitive to the additional effects that follow from the correct theory.

The basic characteristics of the atomic nucleus, viz. its mass and the energy level structure (as also the very fact of the existence of the nucleus) are determined by strong interaction, while the processes involving gamma transitions are described by electromagnetic interaction. Parity is conserved in both these interactions. However, the nucleons comprising the nucleus participate not only in strong and electromagnetic interactions but also in weak interactions in which parity is not conserved.

In other words, the interaction potential V must also contain the $V_{\text{par. noncons.}}$ term which violates parity.

Hence the wave-function ψ of the nucleus can be written in its most general form as follows:

$$\psi = \psi_{reg} + F\psi_{irreg}, \tag{1.6.9}$$

where the second term characterizes the part of the state with opposite parity ($P\psi_{irreg} = -P\psi_{reg}$).[44]

The regular part ψ_{reg} of the wave-function describes processes in which parity is conserved, while the irregular part ψ_{irreg} describes phenomena associated with parity nonconservation law. Coefficient F serves as a measure of the nonconservation.

Since the weak-interaction constant is small, the coefficient F must be much smaller than unity. It can be approximately estimated from dimensional analysis:

$$F \approx \frac{g_w}{\hbar c \delta^2} \simeq 10^{-7}, \tag{1.6.10}$$

where $g_w = 1.4 \times 10^{-49}$ erg·cm^3, $\hbar \simeq 10^{-27}$ erg·s, $c = 3 \times 10^{10}$ cm/s and $\delta = 2 \times 10^{-13}$ cm (δ is the distance between nucleons in the nucleus).

Theoretically, the perturbation theory method is used to determine the quantity F by investigating the potential $V_{par.\ noncons.}$ violating parity. An experimental estimate of F can be obtained from experiments on comparative analysis of the probabilities of processes that are allowed and forbidden by the law of parity conservation.

Depending on the nature of these experiments, the effects caused by parity violation can be of the order F^2 (for example, in alpha decay, see Sec. 3.2.8) or of the order F (in electromagnetic transitions, see Sec. 3.4.5).

Since F is extremely small, these experiments are extremely difficult to perform. Their success depends on fulfilling certain special conditions, for example, the suppression of effects allowed by the law of parity conservation. Under normal conditions, it can be assumed that $F \approx 0$.

A special manifestation of parity nonconservation in strong interactions is observed in the fission of polarized heavy nuclei (see Sec. 7.5.10).

1.7. Quadrupole Electric Moment

One of the most important characteristics of the atomic nucleus is its electric charge Z which gives the number of protons in the nucleus and the magnitude of the Coulomb potential and also determines

[44] Obviously, in the form (1.6.9) the wave-function ψ does not satisfy the law of conservation of parity, since

$$P\psi = \pm\psi_{reg} \mp F\psi_{irreg} \neq \pm\psi.$$

the chemical properties of the nucleus. However, the charge Z cannot give a complete idea about the electric properties of the nucleus, since it does not tell anything about the properties of the nucleus that depend on the distribution of nucleons inside the nucleus. Charge Z is the simplest integral characteristic of the electrical properties of the nucleus.

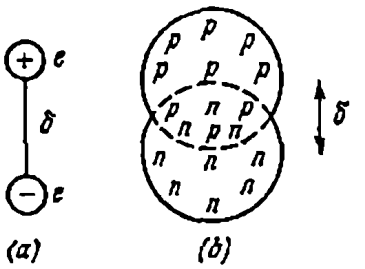

Fig. 46

The dipole moment is a more complicated characteristic. It should be recalled that an electric dipole is a system of two equal and opposite charges e separated by a certain distance δ. The dipole moment of such a system is equal to $D = e\delta$ (Fig. 46*a*). Since the nucleus contains protons and neutrons, i.e. particles having charge $+e$ and 0, noncoincidence of the centres of inertia of the proton and neutron "fluids" in the nucleus will result in a dipole moment $D = Ze\delta$ whose magnitude is equal to the product of the charge and the distance between the centres of inertia of the fluids[45] (see Fig. 46*b*). To be more exact, the projection D_z of the dipole moment on the z-axis is an integral of the form

$$D_z = \int z\rho_Z(r)\,dr, \tag{1.7.1}$$

where $\rho_Z(r)$ is the charge distribution with respect to the centre of inertia of the nucleus and dr is a volume element near the point r.

We shall show that the dipole moment of nuclei in the ground state is equal to zero. Indeed, the charge distribution $\rho_Z(r)$ can be represented in the form

$$\rho_Z(r) = \sum_{1}^{Z} eP_i(r), \tag{1.7.2}$$

where $P_i(r)$ is the probability of ith proton being located at the point $r(x, y, z)$ (in an element dr near the point r). This probability can be expressed in terms of the wave-function $\psi(r_1, r_2, \ldots, r_Z, \ldots, r_A)$ of the state of the system

$$P_i(r) = \int |\psi(r_1, r_2, \ldots, r_A)|^2 dr_1\, dr_2, \ldots, dr_A. \tag{1.7.3}$$

[45] A dipole can be formed not only from a positive and a negative charge, but also from a positive (negative) charge and a neutral particle. When placed in an electric field, such a system has the property of a dipole to align with the electric field (the positive charge rotates relative to the centre of the dipole when placed in the electric field).

Here, the integration is carried out over all r_k except r_i which is equal to r. Hence

$$D_z = \sum_{i=1}^{Z} \int ez_i \,|\, \psi(r_1, \ldots, r_A) \,|^2 d\tau, \tag{1.7.4}$$

where $d\tau$ is the volume element for all coordinates $r_1, r_2, \ldots, r_A$. According to the law of parity conservation, however, $|\psi(r_1, \ldots, r_A)|^2 = |\psi(-r_1, \ldots, -r_A)|^2$ and since z is an odd function, the integrand is also an odd function and the integral vanishes. The dipole moments of nuclei in the ground state are equal to zero.[46]

The following two generalizations can be obviously drawn from the above result:

(1) The electric dipole moment is equal to zero not only for the ground state of the nucleus (which is always nondegenerate), but also for all nondegenerate excited states.

(2) The above conclusion concerning the electric dipole moment is completely valid for all static electric moments of odd order.[47]

The problem concerning the existence of an electric dipole moment in elementary particles is quite interesting. Let us assume that a certain elementary particle, say, neutron, has an electric dipole moment D. As a quantum-mechanical vector, this moment D can have only a longitudinal projection onto the direction of the spin s (the transverse projection averages out). Hence the direction of vector D must coincide with the direction of vector a:

$$\mathbf{D} = h\mathbf{s}. \tag{1.7.5}$$

If the quantum-mechanical system has mirror symmetry, Eq. (1.7.5) must hold when x, y, z are replaced by $-x, -y, -z$. But $\mathbf{D} = e\mathbf{r}$ and s has the dimensions of angular momentum:

$$[\mathbf{pr}] = m\left[\left(\frac{d\mathbf{r}}{dt}\right)\mathbf{r}\right].$$

Hence

$$\left.\begin{aligned} \mathbf{D}(-x, -y, -z) &= -\mathbf{D}(x, y, z), \\ \mathbf{s}(-x, -y, -z) &= \mathbf{s}(x, y, z), \end{aligned}\right\} \tag{1.7.6}$$

[46] This result is also obvious from the fact that parity invariance requires a uniform distribution of all protons and neutrons over the volume of the nucleus. In other words, there should be no displacement of all protons relative to all neutrons (since the existence of regions in the nucleus with the predominance of one type of nucleons would render the nucleus nonsymmetric with respect to the operation of mirror reflection). The absence of such a displacement means that the electric dipole moment is equal to zero.

[47] An identical conclusion can be also drawn for all even-order static magnetic moments.

and the relation (1.7.5) will be satisfied only if $k = 0$. Hence the law of parity conservation means that the dipole moment is equal to zero.

The converse, however, is not true since the equality $k = 0$ holds not only when parity is conserved, but also when invariance with respect to time inversion is observed. Indeed, replacement of t by $-t$ gives

$$\mathbf{D}(-t) = \mathbf{D}(t), \quad \mathbf{s}(-t) = -\mathbf{s}(t). \tag{1.7.7}$$

In other words, if the system has the property of t-invariance, we must have $k = 0$ in (1.7.5).

Thus, the electric dipole moment in a quantum-mechanical system can be nonzero only when the law of parity conservation and invariance with respect to time inversion are simultaneously violated. This circumstance makes the dipole moment of particles (and complex systems) a "touchstone" for verifying the t-invariance of various interactions. The magnitude of D indicates the extent to which t-invariance is violated in any interaction. Until 1964, it was assumed that t-invariance is satisfied in all interactions including weak interaction for which parity is not conserved as was found in 1957. This was confirmed in experiments which were conducted with an error of less than 1% (see Sec. 3.3.8 in this book and Sec. 7.6.1, Vol. II).

A slight violation of t-invariance (0.1%) was observed in 1964 in the decay of K_2^0-mesons (see Sec. 7.6.4, Vol. II) whose mechanism is not clear so far. A change in the electric dipole moment indicates the type of interaction (weak, electromagnetic, strong, or some other new type) responsible for this violation. Hence over the last few years there has been a sharp increase in the interest towards exact measurement of the dipole moment of elementary particles (in particular, the neutron and the electron). Within experimental errors, the results of measurements carried out so far agree with the values $\mathbf{D}_n = \mathbf{D}_e = 0$.[48]

A more complicated electric property of the nucleus than the dipole electric moment is its quadrupole electric moment which is a measure of the deviation of charge distribution from spherical symmetry.

The simplest model of a quadrupole is a pair of equal and opposite dipoles D separated by a certain distance d (Fig. 47*a*). Such a system has a quadrupole moment $Q = 2Dd = 2e\delta d$. Since the quadrupole moment Q is proportional to δ and d, its value (referred to a unit charge) is measured in units of area.

While referring to the quadrupole electric moment of the nucleus, the intrinsic (internal) quadrupole moment Q_0 of the nucleus is

[48] The latest and most accurate result has been obtained by Lobasbev *et al.*: $d_n = (2.3 \pm 2.3) \times 10^{-25}$ *e* cm (*Phys. Lett.*, *B*, 102, 13 (1981)).

distinguished from the observed quadrupole moment Q. The intrinsic quadrupole moment Q_0 of the nucleus is defined as an integral of the type

$$Q_0 = \int (3\zeta^2 - r^2)\,\rho_z\,dV, \tag{1.7.8}$$

where r (ξ, η, ζ) is the distance from the centre of inertia of the nucleus, ζ is the projection of r onto the ζ-axis which coincides with the symmetry axis of the nucleus, and ρ_z is the density distribution

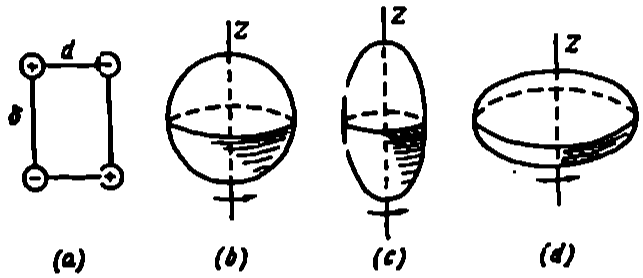

Fig. 47

of charge Z. Integration is carried out over the entire volume of the nucleus. Since $r^2 = \xi^2 + \eta^2 + \zeta^2$, $3\overline{\zeta^2} = \overline{r^2}$ for spherically symmetric distribution, $3\overline{\zeta^2} > \overline{r^2}$ for distribution elongated along the ζ-axis, while $3\overline{\zeta^2} < \overline{r^2}$ for a flattened distribution. Hence $Q_0 = 0$ for a spherically symmetric charge (for example, in the case of magic nuclei, see Sec. 2.3)[45], $Q_0 > 0$ for charge distribution which is elongated along the ζ-axis, while $Q_0 < 0$ for a flattened (with respect to the ζ-axis) charge distribution (see Figs. 47*b*, *c*, *d*, respectively).

The intrinsic quadrupole moment Q_0 can be determined from the experimental data for the cross section of Coulomb excitation[46] of rotational levels of nuclei and the probability of gamma transitions between these levels.

The observed quadrupole electric moment Q is determined with respect to the z-axis which coincides with a chosen direction in space:

$$Q = \int (3z^2 - r^2)\,\rho_z\,dV. \tag{1.7.9}$$

---

[45] Earlier, all nuclei with $I = 0$ were considered spherically symmetric. It has now been established that some nuclei with $I = 0$ have a nonspherical equilibrium form.

[46] The *Coulomb excitation of nucleus* is its excitation by the electromagnetic (mainly electric) field of a fast charged particle whose energy is not sufficient to allow it to penetrate the nucleus.

It can be concluded from the nature of variation of the sign of Q_0 that in the interval between two magic numbers nuclei successively assume the following form: spherically symmetric, oblate, spherically symmetric, prolate, strongly prolate, prolate, spherically symmetric (Fig. 50).

The large values of the intrinsic quadrupole moments, which assume values of up to 10-20 times the square of their radii, are worth noting. This means that the nuclear quadrupole moments are

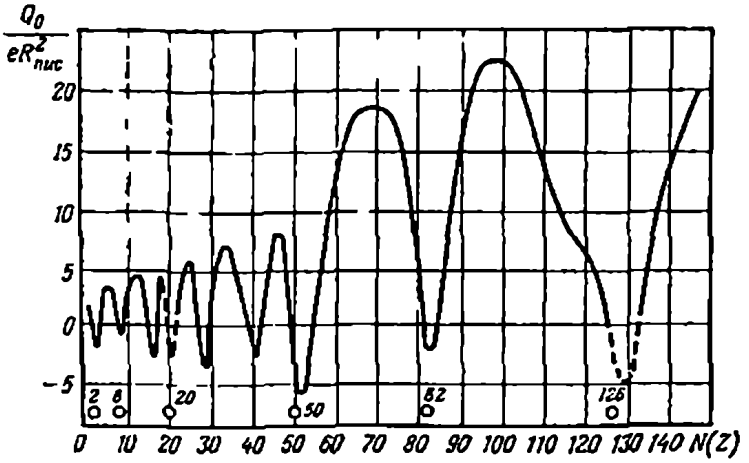

Fig. 49

caused by the collective motion of many nucleons in the nucleus (see Sec. 2.4).

The quadrupole moment also gives very important additional information about the nuclear forces.

The positive quadrupole moment of a deuteron indicates that the distribution of charge (and hence of the nuclear matter) in it is

Fig. 50

stretched along the axis coinciding with the direction of spin of the deuteron. This points towards a connection between the deuteron axis (the lino "passing" through the neutron and the proton) and its spin. In other words, the nuclear forces are the strongest and form a bound system (deuteron) only when the spins of both the nucleons are directed along its axis. Thus, nuclear forces are generally noncentral since they depend not only on the distance between the particles, but also on the mutual spin orientation and the line on which the particles are "located". This type of interaction is called *tensor interaction*.

1.8. Isotopic Spin

It was shown in Sec. 1.3.4 that the properties of isobar nuclei with a given mass number A undergo a considerable change with a change in the ratio of the protons Z and neutrons $N = A - Z$ in them. Such nuclei have different masses and binding energies, different electric charges and magnetic moments; some of these nuclei are β-stable while others are β-radioactive, and so on.

At first glance, the outlined differences between the isobar nuclei appear to be so numerous and significant that the mass number A seems to be the only common feature of these nuclei. This, however, is not true. A more detailed analysis of isobar nuclei shows that they form groups of nuclei with similar nuclear properties.

It turns out that in many cases a replacement of one or more protons by a corresponding number of neutrons leads only to a change in the weak and electromagnetic properties of the nucleus without affecting its main characteristics which are due to strong nuclear interactions.

As an example, let us consider the nuclei ${}^3_1\mathrm{H}$ and ${}^3_2\mathrm{He}$, which differ in their weak properties: one of these nuclei (${}^3_1\mathrm{H}$) is β-radioactive, while the other is β-stable. Their electromagnetic properties are also different (they have electric charges equal to 1 and 2 respectively, and their magnetic moments are equal to $+2.98\mu_B$ and $-2.13\mu_B$). However, these two nuclei are quite similar with respect to strong interaction, which determines the main part of the nuclear binding energy.

It is found (as was mentioned in Sec. 1.3.2) that the difference in the binding energies of the ${}^3_1\mathrm{H}$ and ${}^3_2\mathrm{He}$ nuclei, which is equal to

$$\Delta W({}^3_1\mathrm{H}) - \Delta W({}^3_2\mathrm{He}) = 8.48 - 7.72 = 0.76 \text{ MeV},$$

coincides with the energy of Coulomb repulsion between two protons in the ${}^3_2\mathrm{He}$ nucleus if we assume that they are separated by a distance $r = 1.9 \times 10^{-13}$ cm (this is a fair assumption):

$$\Delta U_C = \frac{e^2}{r} = \frac{(4.8 \times 10^{-10})^2}{1.9 \times 10^{-13} \times 1.6 \times 10^{-6}} = 0.76 \text{ MeV}.$$

Thus, the binding energies of the two nuclei, caused by the nuclear attraction only, are equal:

$$\Delta W({}^3_1\mathrm{H}) = [\Delta W({}^3_2\mathrm{He})]_{\text{nuc}}.$$

A similar conclusion can also be drawn about other mirror nuclei (A, Z) and $(A, A - Z)$, i.e. pairs of nuclei that can be obtained from each other by replacing all protons with neutrons and vice versa. This conclusion is experimentally confirmed not only for the ground state (the binding energies coincide after a correction has

been made for the difference in the Coulomb energies), but also for excited states.

Figure 51 shows the energy level diagram for two mirror nuclei ${}^{7}_{3}\mathrm{Li}$ and ${}^{7}_{4}\mathrm{Be}$, whose ground state energies differ by

$$\Delta E = \Delta U_{\mathrm{C}} - \Delta m_{N}, \qquad (1.8.1)$$

ΔU_{C} being the difference in the Coulomb energies of the two nuclei, and Δm_N, the difference in the masses of the nucleons ($m_N > m_p$). It can be seen from the figure that the spins and parities of the corresponding levels are identical while their energies are quite close.

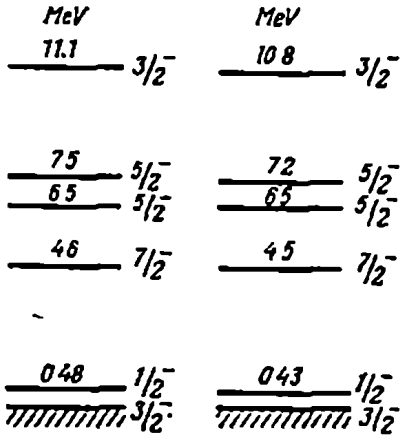

Fig. 51

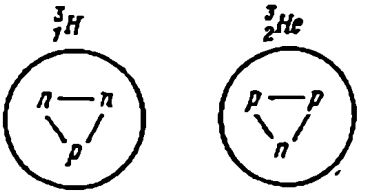

Fig. 52

Mirror nuclei differ from each other in that all (p-p) bonds are replaced by (n-n) bonds, while the number of (n-p) bonds remains unchanged.

Figure 52 shows a schematic comparison of two simplest mirror nuclei ${}^{3}_{1}\mathrm{H}$ and ${}^{3}_{2}\mathrm{He}$. It can be seen from this figure that the ${}^{3}_{1}\mathrm{H}$ nucleus does not contain any (p-p) bond, has one (n-n) bond and two (n-p) bonds; the number of (n-p) bonds in the ${}^{3}_{2}\mathrm{He}$ nucleus is also two, but it has one (p-p) bond and no (n-n) bond.

The similarity in the level structures of mirror nuclei can be explained if we assume that elementary (p-p) and (n-n) interactions are identical. This assumption is called the *hypothesis of charge symmetry of nuclear forces.*

An analysis of the properties of mirror nuclei helps in establishing a similarity between (p-p) and (n-n) nuclear interactions, but does not enable us to compare them with the (n-p) interaction. In order to compare all three types of (N-N) interactions (n-n, p-p and n-p), we must consider triplets of nuclei which differ only in an additional pair of nucleons of different type. Among light nuclei, the triplet ${}^{10}_{4}\mathrm{Be}$, ${}^{10}_{5}\mathrm{B}$ and ${}^{10}_{6}\mathrm{C}$ has this property.

Each of these nuclei can be roughly represented as a combination of a common group $4p + 4n$ and a pair of nucleons: n-n, n-p or p-p.

Arguing in the same way as for the pair ${}^3_1\mathrm{H}$ and ${}^3_2\mathrm{He}$, we arrive at the conclusion that the binding energy and the structure of levels of each nucleus (after making necessary corrections for the difference in their Coulomb energies and the mass difference of the nucleons) must be determined ultimately by the properties of the specific types of $(N$-$N)$ interaction. For n-$p = (p$-$p)_{\text{exc}} = n$-n, the levels of all three nuclei must have similar parameters.

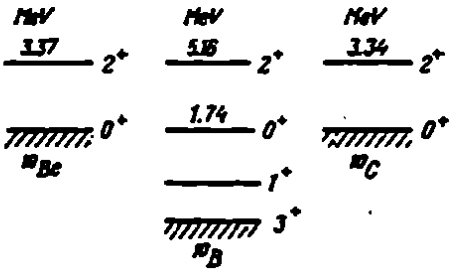

Fig. 53

The diagram for the first levels of the nuclei ${}^{10}_4\mathrm{Be}$, ${}^{10}_5\mathrm{B}$ and ${}^{10}_6\mathrm{C}$ is shown in Fig. 53. It can be seen that the introduction of corrections by $\Delta U_C - \Delta m_N$ leads to a situation when the ground states of the nuclei ${}^{10}_4\mathrm{Be}$ and ${}^{10}_6\mathrm{C}$ coincide with the second excited state of the nucleus ${}^{10}_5\mathrm{B}$. These three nuclei have the same moment and parity 0^+. It can also be easily verified that the third excited state of the nucleus ${}^{10}_5\mathrm{B}$ is separated from the second by an energy

$$\Delta E = 5.16 - 1.74 = 3.42 \text{ MeV},$$

which is close to the excitation energy of the other two nuclei (3.37 and 3.34 MeV respectively). These three levels also have the same moment and parity 2^+.

Thus, a comparison of the structure of energy levels for the nuclear triplet ${}^{10}_4\mathrm{Be}$, ${}^{10}_5\mathrm{B}$ and ${}^{10}_6\mathrm{C}$ leads to the conclusion that all three types of elementary interactions of nucleons are identical:

$$(p\text{-}p)_{\text{exc}} = n\text{-}n = n\text{-}p.$$

The assumption about such an extensive symmetry of nuclear forces (the inclusion of n-p interaction into consideration) is called the *hypothesis of charge independence of nuclear forces.*

It should be noted that the coincidence of the parameters of the *ground* states of the nuclei ${}^{10}_4\mathrm{Be}$ and ${}^{10}_6\mathrm{C}$ with an *excited* state of the nucleus ${}^{10}_5\mathrm{B}$ does not undermine the significance of the obtained result, since the specific properties of the excited state (short lifetime due to a high probability of gamma transition into a less excited state) are determined not by strong interaction, but by electromagnetic interaction which need not be taken into account when considering the manifestation of nuclear forces.

Another important remark concerns the spin dependence of nuclear forces. It is well known that a neutron and a proton with parallel spins form a nucleus (deuteron), while the same proton and neutron

with antiparallel spins do not have a bound state (see Sec. 1.5.2, Vol. II for details on the spin dependence of nuclear forces). Thus, the properties of (*N-N*) interaction strongly depend on the spin orientation of the interacting nucleons. This means that when (*n-n*), (*p-p*) and (*n-p*) interactions are compared, they must be considered in identical spin and spatial (meaning the orbital angular momentum *l*) states.

Finally, the third remark concerns the experimental confirmation of the hypothesis of the charge independence of nuclear forces.

As a matter of fact, the above arguments concerning the comparison of levels of isobar nuclei is not a direct proof of the charge independence of nuclear forces in the strict sense, since it involves a comparison of the properties of complex nucleon systems rather than the elementary processes of (*N-N*) interactions of various types.

A direct proof of the validity of the hypothesis of the charge independence of nuclear forces was obtained in direct experiments on (*p-p*) and (*n-p*) scattering (see Sec. 1.5.5, Vol. II) and indirect experiments on (*n-n*) scattering[52] (comparison of (*n-p*) scattering with the scattering of a neutron by a deuteron). Quantum-mechanical treatment of the results of these experiments led to the conclusion that the potential well has the same form for all three elementary processes.

Thus, we shall assume that nuclear forces have the property of charge independence, i.e. purely nuclear interactions (without Coulomb interaction) between any nucleons (*p-p*, *n-n*, *n-p*) *in identical spatial and spin states* are identical. In other words, we shall assume that neutron and proton are identical particles (except for the electromagnetic interaction).

The identity of the nuclear properties of the neutron and proton can be described with the help of a formal but very convenient parameter called the *isotopic spin vector* T, whose value is the same for both nucleons and is equal to 1/2. The vector T is defined in an auxiliary (formal) isotopic space.

One of the projections of the vector, $T_\zeta = +1/2$, describes a proton, while the other projection, $T_\zeta = -1/2$, describes a neutron. The number of projections $2T + 1 = 2$ is equal to the number of nucleons with identical nuclear properties (Fig. 54).

Since the nature of interaction is independent of the type of nucleon (i.e. of the projection T_ζ), the nuclear interaction of a nucleon is determined only by the value of the vector T and not by its projection (which characterizes the difference in electromagnetic properties). Thus, the nuclear interaction is invariant to rotation in the isotopic

[52] It is not possible to carry out direct experiments on (*n-n*) scattering in view of the absence of a neutron target and colliding neutron beams.

space. This property is called *isotopic invariance*. The situation is analogous to the invariance of interaction with respect to rotation in ordinary three-dimensional space, which leads to the law of conservation of angular momentum. Consequently, the law of conservation of isotopic spin must be obeyed in nuclear interactions.

Operations on vectors T are carried out in the same way as on ordinary quantum-mechanical vectors. Thus, for example, the $(p\text{-}p)$ interaction is characterized by the vector $T = 1$, since $(T_\zeta)_p = +1/2$; $(T_\zeta)_{2p} = +1$, and of the two values 0 and 1 of the sum $T_1 + T_2$, only the second is possible. The $(n\text{-}n)$ interaction is characterized by the same vector $T = 1$ but with another projection $(T_\zeta)_{2n} = -1$; the $(n\text{-}p)$ interaction can be characterized by $T = 0$ and $T = 1$, since for this case $T_\zeta = 0$ and hence both values 0 and 1 are possible for the sum $T_1 + T_2$. Analysis shows that one of these interactions (for $T = 1$) is identical to $(p\text{-}p)$ and $(n\text{-}n)$ interactions, while the other (for $T = 0$) differs from them (for example, it gives rise to a bound state, viz. deuteron, for $\Delta W = 2.22$ MeV)[43].

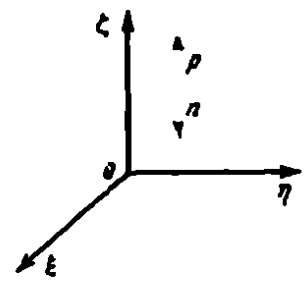

Fig. 54

Thus, it is found that a system of two nucleons may be in any of three states with identical nuclear properties, each state being characterized by the same value of the isotopic spin vector $T = 1$ $(2T + 1 = 3)$, or in one state with different properties (deuteron), characterized by the value $T = 0$ $(2T + 1 = 1)$.

The concept of isotopic spin can be easily generalized to the atomic nucleus (A, Z). Obviously,

$$T_\zeta = \frac{Z-N}{2} = \frac{2Z-A}{2} \tag{1.8.2}$$

and

$$T \geqslant \left|\frac{Z-N}{2}\right|. \tag{1.8.3}$$

where

$$|T_{max}| = A/2.$$

[43] The fact that $(n\text{-}p)_{T=0} \neq (n\text{-}p)_{T=1}$ is not surprising, since these interactions differ in the spin states while the nuclear forces depend on spin. The difference between $(n\text{-}p)_{T=0}$ and $(n\text{-}p)_{T=1}$ essentially expresses the spin dependence of nuclear forces.

Analysis of light nuclei (in which the role of electromagnetic interaction is comparatively insignificant and the isotopic invariance is manifested clearly) shows that the ground states of the nuclei are usually characterized by the minimum value of

$$T = \left| \frac{2Z - A}{2} \right|, \qquad (1.8.4)$$

corresponding to the highest symmetry of the wave-function, i.e. to the lowest energy.

Thus, the isotopic spin T of the nucleus ^3_2He is equal to $(4-3)/2 = 1/2$. The number of projections of the vector $T = 1/2$ is equal to $2T + 1 = 2\,(1/2) + 1 = 2$. Consequently, there must be another nucleus with identical properties. This is the ^3_1H nucleus with the same value $T = 1/2$ but with a different projection (T_ζ (^3_2He) $= +1/2$, while T_ζ (^3_1H) $= -1/2$). Similarly, the nuclei ^7_3Li and ^7_4Be also have an isotopic spin $T = 1/2$ (although the values $T = 1/2$, 3/2, 5/2 and 7/2 are possible for them in principle).

The nuclei $^{14}_6C^8$ and $^{14}_8O^6$ have isospin projections T_ζ equal to -1 and $+1$ respectively. Hence $T = 1$ and $2T + 1 = 3$, i.e. there must exist another isobar nucleus with $T = 1$ and $T_\zeta = 0$, having identical properties, viz. the excited state of the nucleus $^{14}_7N^7_{exc}$ with an excitation energy of 2.3 MeV (see Fig. 55, top). The nuclei $^{14}_6C^8_{gr}$ and $^{14}_8O^6_{gr}$ in the ground state together with the nucleus $^{14}_7N^7_{exc}$ in the excited state form an isotriplet with $T = 1$. The ground state of the nucleus $^{14}_7N^7_{gr}$ has a higher spin symmetry (the last two nucleons have parallel spins) and is characterized by the isospin $T = 0$ (Fig. 55, bottom), i.e. is an isosinglet.

In some cases, the isotopic analogue may have even higher excitation energy. By way of an example, let us consider the triplet of nuclei $^{12}_5B^7_{gr}$, $^{12}_6C^6_{exc}$ and $^{12}_7N^5_{gr}$, in which the nucleus $^{12}_6C^6_{exc}$ is characterized by an excitation energy of 15 MeV. Such a large difference in energy between the ground state and the excited analogue state of the nucleus $^{12}_6C^6$ is due to the fact that these two states have different spatial symmetries (Fig. 56). The ground state of the nucleus $^{12}_6C^6_{gr}$ has a higher spatial symmetry than the excited state of the $^{12}_6C^6_{exc}$ nucleus which must be similar to the nuclei $^{12}_5B^7_{gr}$ and $^{12}_7N^5_{gr}$ whose symmetry is uniquely determined by the Pauli exclusion principle. The nuclei $^{12}_5B^7_{gr}$, $^{12}_7N^5_{gr}$ and $^{12}_6C^6_{exc}$ also form an isotopic triplet ($T = 1$), while the nucleus $^{12}_6C^6_{gr}$ in the ground state forms an isotopic singlet ($T = 0$). Deuteron (^2_1H) and α-particle (^4_2He) are the simplest of isotopic singlets.

Investigation of nuclear reactions shows that like (N-N) interactions, they obey the law of conservation of isotopic spin, and this leads to certain selection rules with respect to the isotopic spin. In this connection, nuclear levels must be characterized not only by energy, angular momentum and parity, but also by isotopic spin.

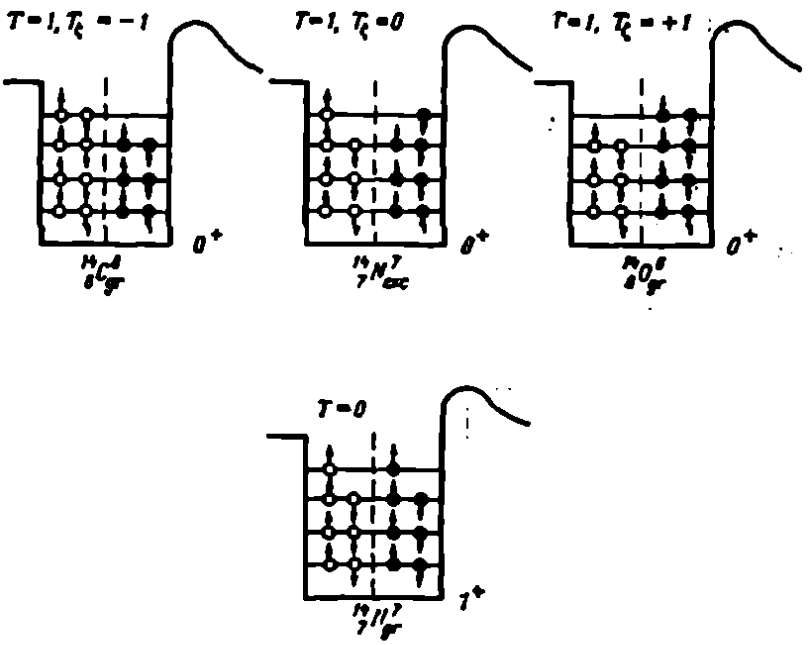

Fig. 55

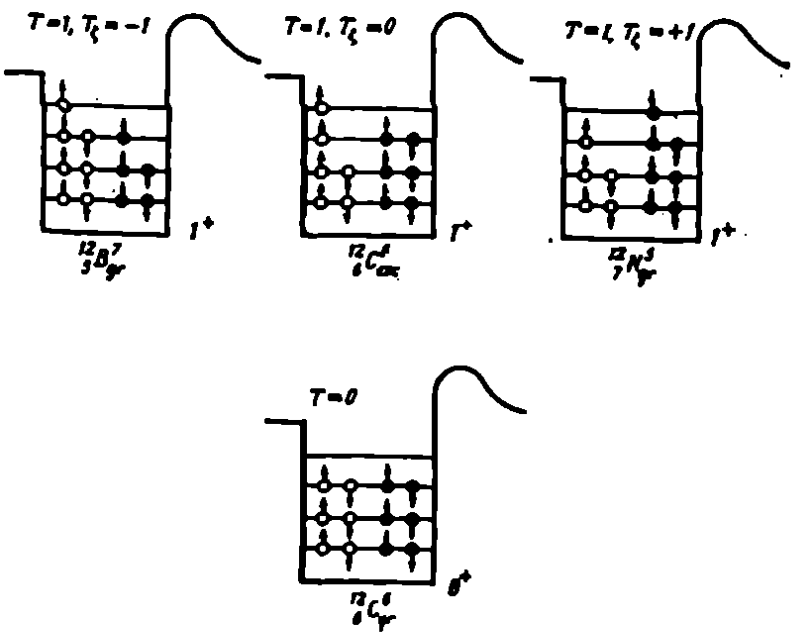

Fig. 56

The value of T of a nuclear level is indicated on the diagrams along with the values of spin and parity.

The law of conservation of isotopic spin imposes certain restrictions on nuclear processes. Thus, an α-particle (T = 0) can be emitted by a nucleus only if its initial and final states have the same isotopic spin. It should be recalled that isotopic relations are valid if electromagnetic interaction is not taken into account. Hence they are manifested most clearly in light nuclei where the role of electromagnetic forces is comparatively insignificant.

However, isotopic analogues for comparatively heavy nuclei were also discovered long ago. While investigating the reaction $^{51}_{23}V\ (p, n)\ ^{51}_{24}Cr$, Anderson and Wong[54] discovered in 1961 practically monoenergetic neutrons against a background of continuous neutron spectrum. These monoenergetic neutrons correspond to the formation of a narrow level in the high excitation region of the nucleus $^{51}_{24}Cr$. The energy and angular distribution of the continuous spectrum of neutrons are in accordance with the predictions of the statistical model of a compound nucleus. At proton energies $T_p > 10$ MeV, direct (nonevaporative) neutrons were observed and their energy was measured with the help of the time-of-flight technique.

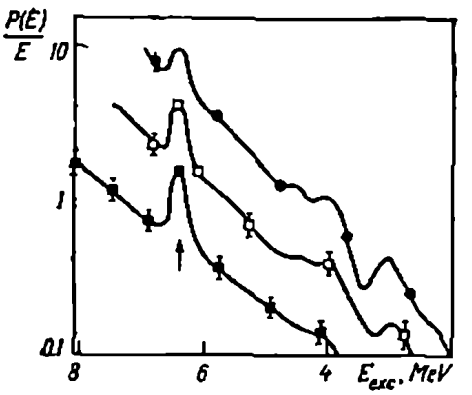

Fig. 57

The neutron spectrum $P(E)/E$, transformed to the centre-of-inertia system and referred to the energy E of the emitted neutrons, is shown in Fig. 57 as a function of the excitation energy E_{exc} of the nucleus $^{51}_{24}Cr$. The three curves in the figure correspond to three different proton energies: 10.8 (black circles), 12.0 (light squares) and 13.3 MeV (black squares). It can be seen from the figure that all three curves have a distinct peak for the same excitation energy $E_{exc} = 6.5$ MeV of the nucleus. It was found that the reaction energy Q^* for this excitation energy is equal to the difference in the Coulomb energies of the nuclei $^{51}_{23}V$ and $^{51}_{24}Cr$: $Q^* = \Delta U_C$, and $E_{exc} = \Delta U_C - |Q|$.

The result obtained here can be interpreted by using the shell model of the atomic nucleus, which should be quite satisfactory in the neighbourhood of number 28 (see Sec. 2.3). From the point of view of the shell model, the reaction $^{51}_{23}V^{28}\ (p, n)\ ^{51}_{24}Cr^{27}$ is reduced to a transformation of the 28th neutron into 24th proton, both of which occupy the same level $1f_{7/2}$. Hence, by isotopic invariance,

[54] J.D. Anderson and C. Wong, *Phys. Rev. Lett.*, 7, 250 (1961).

the energies of both nuclei due to strong interaction must be the same, and the difference between them boils down just to the correction for the difference between the Coulomb part ΔU_C of the interaction and the difference Δm_N in the masses of the nucleons:

$$\Delta E = \Delta U_C - \Delta m_N. \tag{1.8.5}$$

Let us find the value of E_{exc}. By definition,

$$E_{exc} = |Q^*| - |Q|.$$

where Q is the energy of reaction involving the formation of the ^{51}V nucleus in the ground state, and Q^* represents the same quantity for the excited state (for the reaction under consideration, $Q < 0$). However,

$$|Q^*| = M^*_{Cr} + m_n - M_V - m_p = \Delta E + \Delta m_N = \Delta U_C.$$

Hence

$$E_{exc} = \Delta U_C - |Q|. \tag{1.8.6}$$

The value of ΔU_C has been estimated to be about 8 MeV, while the computed value of $|Q|$ is about 1.5 MeV. Their difference coincides with the value $E_{exc} = 6.5$ MeV. Thus, the peaks observed in the neutron spectrum indeed correspond to the formation of the analogue state in the ^{51}V nucleus.

Similar analogue states were also observed in heavier nuclei including uranium. They are characterized by a small width of the neutron peaks (less than or equal to 50 keV) and a high excitation energy (8-12 MeV) of the daughter nucleus.

1.9. A Brief Resumé of Chapter 1

In Chapter 1, we have considered the basic properties of stable atomic nuclei, viz. charge Z, mass M, binding energy ΔW, radius R, spin I, magnetic moment μ, parity P of the wave-function, electric quadrupole moment Q, and isotopic spin T. The following conclusions can be drawn from an analysis of these characteristics.

1. The atomic nucleus with a charge Z and a mass number A consists of A nucleons, i.e. Z protons and $A - Z$ neutrons, which are bound by nuclear forces. There are no electrons in the nucleus.

2. The proton is a particle with a charge $+e$, mass $m_p = 1836m_e$, spin $s_p = 1/2$ and magnetic moment $\mu_p = 2.79\mu_B$. The neutron has zero charge, mass $m_n = 1838.6m_e$, spin $s_n = 1/2$ and magnetic moment $\mu_n = -1.91\ \mu_B$.

The fact that $m_n > m_p + m_e$ indicates that it is possible for a neutron from the energy point of view to undergo beta decay.

The difference between the experimental values of μ_p and μ_n and the theoretical values ($\mu_p^{theor} = 1\mu_B$, $\mu_n^{theor} = 0$) can be explained by assigning a definite structure (size and distributed charge) to the nucleons.

3. Nuclei are nearly spherical in shape. The radius of an atomic nucleus is given by $R = r_0 A^{1/3}$, where $r_0 = (1.2\text{-}1.3) \times 10^{-13}$ cm. The nuclear interaction radius is slightly larger: $R_{int} = 1.4 \times 10^{-13} A^{1/3}$ cm.

The shape of heavy and some light nuclei is not quite spherical. They are prolate in the direction of spin. The electric quadrupole moment Q is a measure of the nonsphericity of the nucleus.

The electric dipole moment of nuclei in the ground state is equal to zero.

4. The stability of the nucleus is determined by its binding energy $\Delta W(A, Z)$, i.e the amount by which the sum of the masses of all the nucleons constituting a nucleus exceeds the mass of the nucleus itself:

$$\Delta W(A, Z) = [Zm_p + (A - Z)m_n - M_{nuc}(A, Z)]c^2.$$

The exact values of the masses of nuclei (as well as the mass of the proton) are determined with the help of mass spectrometers, the instruments in which the electric and magnetic fields are employed to focus moving charged particles. The exact value of the neutron mass was obtained from an analysis of nuclear reactions involving neutrons.

The binding energy (and mass) of a nucleus with given A and Z can be calculated from the semiempirical formula

$$\Delta W(A, Z) = \alpha A - \beta A^{2/3} - \gamma \frac{Z^2}{A^{1/3}} - \zeta \frac{(A/2 - Z)^2}{A} + \delta A^{-3/4}$$

(where α, β, γ, ζ and δ are coefficients) which follows from the liquid drop model of atomic nucleus. This model is based on the concept that a nucleus is a spherical drop of charged incompressible superdense nuclear fluid.

5. From the binding energy of various nuclei it follows that even-even nuclei are the most stable, while odd-odd nuclei are the least stable. Nuclei containing a magic number of nucleons (2, 8, 20, (28), 50, 82, 126) are extraordinarily stable.

6. A comparison of binding energies for light and heavy nuclei shows that it is advantageous from the energy point of view for the light nuclei to fuse and for the heavy nuclei to disintegrate into parts (fission reaction).

7. The charge Z and mass number A of stable nuclei satisfy the relation $Z = A/(1.98 + 0.015A^{2/3})$. Deviations from this relation point towards a tendency to β^- or β^+ radioactivity on the part of the nucleus.

8. The spins and magnetic moments of nucleons in a nuclei tend to compensate each other, and a complete compensation is observed in even-even nuclei ($I = 0$ and $\mu = 0$). The spins and magnetic moments of the remaining nuclei have comparatively small values:

$$\left(|I_{nuc}| \ll A\frac{\hbar}{2}, \quad |\mu_{nuc}| \ll |A\mu_N| \right),$$

which indicates that they have a single-particle origin.

Nuclei with even A have integral spin, while those with odd A have half-integral spin. While calculating the spin and magnetic moment of nuclei, we must take into account the spins and magnetic moments of the nucleons, as well as additional mechanical and magnetic moments due to their orbital motion in the nucleus.

9. In the case of mirror symmetry the wave-function of a system of particles has a definite parity (positive or negative). In strong (nuclear) and electromagnetic interactions, the law of conservation of parity is obeyed

The parity P_{A+B} of a system consisting of two noninteracting particles A and B is

$$P_{A+B} = P_A P_B (-1)^l,$$

where P_A and P_B denote the intrinsic parities of the particles, and l is the orbital quantum number. The intrinsic parity of a nucleon is positive.

The law of parity conservation is violated in weak interactions. This violation must also be manifested in the form of some (very weakly expressed) specific features of strong and electromagnetic processes.

10. The following properties of nuclear forces were established from an analysis of various properties of the atomic nucleus:

(a) a high intensity (on account of a high binding energy per nucleon, $s = \Delta W/A \simeq 8$ MeV);

(b) a short range (from the size of the nucleus);

(c) saturation (from the linear dependence of the binding energy on the mass number: $\Delta W \simeq 8A$ MeV)

(d) spin dependence (from the existence of the nucleus ${}^3_1\mathrm{H}$ with $I = 1$ and the nonexistence of an analogous nucleus with $I = 0$);

(e) tensor (noncentral) nature (from the existence of the quadrupole electric moment for deuteron);

(f) charge independence.

11. Systems of nucleons with identical nuclear properties are characterized by the same value of isospin T. In strong interactions (including nuclear reactions), the law of conservation of isospin is obeyed.

Chapter 2

Models of the Atomic Nucleus

At present, there is no complete theory which could describe all the properties of the atomic nucleus and answer all the questions concerning its structure and properties, such as:

(1) Which nuclei are stable and which are radioactive? What are the types of radioactivity, half-life, spectral composition and angular distribution of particles escaping from radioactive nuclei?

(2) What are the magnitudes of the radius, mass, binding energy, spin, magnetic moment, parity, quadrupole electric moment and other characteristics of a nucleus?

(3) How are the energy states distributed in the nucleus? What values of energy, spin, magnetic moment, parity, etc. correspond to them?

(4) What are the probabilities of transitions from higher (excited) states to lower states for various mechanisms of these transitions and as functions of level parameters?

(5) How do the cross sections of interaction of various particles with different nuclei vary with energy?

Since there is no complete theory of the atomic nucleus, the answers to these questions can be sought with the help of various nuclear models. Each model is constructed on the basis of some selected properties of the nucleus which are assumed to be the main properties for constructing the given model. Other properties of the nucleus are not considered in this model. Naturally, the model constructed on such a principle has a limited applicability. However, within the range of its applicability, each model provides some interesting results.

In this chapter, we shall consider some models of the atomic nucleus based on quite different (sometimes even apparently contradictory) properties of the nucleus. The liquid drop model described in Sec. 2.1 is based on the assumption of strong nucleonic interaction. This model belongs to the class of collective models (it considers the interaction of large ensembles of nucleons). In the Fermi gas model described in Sec. 2.2, it is assumed that nucleons in the nucleus do not interact with one another. In the shell model considered in Sec. 2.3, the motion of the nucleons is treated as independent, but a strong spin-orbital interaction is assumed. Both these models be-

long to the class of single-particle models, since they describe the motion of an individual particle in the self-consistent field of all the remaining particles. Section 2.4 is devoted to the generalized model of the atomic nucleus which describes the motion of individual particles in a self-consistent field as well as the collective motion of a large group of nucleons (rotation and deformation of a nucleus without any change in its volume). Finally, Sec. 2.5 considers the superfluid model of the nucleus which is based on the pairing interaction of nucleons with opposite projections of moments.

Besides these models, we shall separately consider in Sec. 6.7 the optical model in which the interaction of nucleons with the nucleus is treated as the passage of a nucleon wave through an absorbing and refracting medium. In this model, the nucleus is characterized by an optical potential (which is generally complex), and hence the optical model essentially belongs to the class of single-particle models. This model is considered separately since it describes the absorption and scattering of nucleons, i.e. the processes of interaction of an external nucleon with the nucleus.

2.1. The Liquid Drop Model

To explain the anomalous scattering of α-particles, Rutherford proposed as early as in 1911 that the atom contains a spherical nucleus with a radius of about 10^{-13} cm. Later, the radius of these nuclei was estimated from an analysis of the empirical relation between the lifetime of α-active nuclei and the energy of the α-particles emitted by them. It was found that for all α-active nuclei,

$$R = r_0 A^{1/3}, \tag{2.1.1}$$

where $r_0 = (1.45\text{-}1.5) \times 10^{-13}$ cm, and A is the mass number. We assume that the law $R \propto A^{1/3}$ is valid not only for α-active nuclei but for all other nuclei as well. Then the mass of any nucleus will be proportional to its volume ($A \propto R^3$) and hence all nuclei have the same concentration of nucleons

$$n = \frac{A}{V} = \frac{A}{(4/3)\pi R^3} = \frac{A}{(4/3)\pi (1.5 \times 10^{-13})^3 A} \simeq 10^{38} \text{ nucleon/cm}^3, \tag{2.1.2}$$

the same density

$$\rho = n m_N = 10^{38} \times 1.66 \times 10^{-24} \simeq 10^{14} \text{ g/cm}^3 \tag{2.1.3}$$

and the same value of the mean distance between nucleons

$$\delta = \sqrt[3]{V/A} = \sqrt[3]{10^{-38}} \simeq 2 \times 10^{-13} \text{ cm}. \tag{2.1.3a}$$

The validity of this assumption was later confirmed by various methods of determining the radii of atomic nuclei (see Sec. 1.4).

The fact that the density of nuclear matter is constant for all nuclei points towards its incompressibility. This property indicates a similarity between the nuclear matter and a liquid. This analogy also follows from the above-mentioned linear dependence of the binding energy ΔW on the mass number A which can be compared with the linear dependence of the energy of vaporization of a liquid on its mass.

The property of saturation of nuclear forces, which follows from the fact that the binding energy per nucleon $\varepsilon = \Delta W/A$ is nearly constant, makes the analogy even more complete since the same property is also possessed by the chemical forces binding the molecules of a liquid. On the basis of these concepts, the liquid drop model of the nucleus was constructed, according to which the nucleus is a spherical drop of an incompressible superdense nuclear fluid.

The liquid drop model of the nucleus was developed by Bohr, Wheeler and Frenkel. This model was able to explain a large number of phenomena. It also led to a semiempirical formula for the binding energy and mass of the nucleus, explained several properties of fission of heavy nuclei and the laws of alpha decay. Besides, this model led to a qualitative idea of the structure of first excited states in even-even nuclei, and enabled to predict the masses and binding energies of some new nuclei.

2.1.1. Weizsäcker's Semiempirical Formula for the Binding Energy and Mass of the Nucleus

It was shown above that to first approximation the binding energy of a nucleus is proportional to its mass number A. Introducing the proportionality constant α, we can express the binding energy in the following form:

$$\Delta W = \alpha A, \quad \varepsilon = \Delta W/A = \alpha$$

In this form of notation, it is assumed that all the A nucleons in the nucleus are equivalent. As a matter of fact, this is not true since the nucleons at the surface of the nuclear "drop" are in a special position because they are attracted only from one (internal) side. Hence the binding energy of the nucleus is less than αA by an amount proportional to the surface area of the drop, i.e. $A^{2/3}$ (surface tension):

$$\Delta W = \alpha A - \beta A^{2/3},$$

where β is the proportionality factor.

Further, we must take into account the Coulomb repulsion of protons, which is proportional to Z^2 [Coulomb forces do not possess the property of saturation, and each of the Z protons interacts with each of the remaining $Z - 1$ protons; hence the Coulomb repulsion

is proportional to $Z(Z-1) \sim Z^2$ and inversely proportional to r (i.e. $\propto A^{-1/3}$). This factor also leads to a decrease in the binding energy

$$\Delta W = \alpha A - \beta A^{2/3} - \gamma \frac{Z^2}{A^{1/3}},$$

where γ is the proportionality factor.

Finally, the formula must reflect the observed tendency towards symmetry in the structure of atomic nuclei. This symmetry is explicitly manifested in light nuclei which, as a rule, consist of nearly equal numbers of protons and neutrons. This means that nuclei with $Z = A/2$ are the most stable and hence have the highest binding energy ε per nucleon. Deviation from the equality $Z = A/2$ to either side leads to a decrease in the binding energy and must be taken into account in the formula for ε through a term of the type $\zeta\ (1/2 - Z/A)^2$ with minus sign, ζ being the proportionality factor.

Accordingly, we must add a term of the type[1] $-\zeta \frac{(A/2 - Z)^2}{A}$ to the formula for ΔW. The liquid drop model cannot explain the introduction of this term to the semiempirical formula.

It was mentioned in Sec. 1.3 that the effect of symmetry is due to the fact that the neutron and the proton have spin $s_N = 1/2$ and obey the Pauli exclusion principle. The role of the latter can be taken into account in the independent particle model.

When the symmetry is taken into consideration, the formula for binding energy assumes the following form:

$$\Delta W = \alpha A - \beta A^{2/3} - \gamma \frac{Z^2}{A^{1/3}} - \zeta \frac{(A/2-Z)^2}{A}. \qquad (2.1.4)$$

Since the nuclear mass is expressed in terms of the binding energy through the relation $\Delta W = Zm_p + (A - Z)\, m_n - M(A, Z)$, formula (2.1.4) can be also used for calculating the masses of the nuclei

$$M(A, Z) = Zm_p + (A - Z)\, m_n - \alpha A + \beta A^{2/3} + \gamma Z^2/A^{1/3} + \zeta (A/2 - Z)^2/A. \qquad (2.1.5)$$

The coefficients α, β, γ and ζ were found by comparison with known binding energies[2] (from a comparison of the measured values of atomic masses). The value of γ can be found by directly calculating the electrostatic energy of mutual repulsion of the Z protons in the

[1] In heavy nuclei, this equality is violated in favour of neutrons on account of a large number of protons. But since this effect is taken into account by the term $\gamma Z^2/A^{1/3}$, the effect of symmetry must be taken into consideration for the heavy nuclei also through the term $\zeta \frac{(A/2-Z)^2}{A}$.

[2] Obviously, formula (2.1.5) can also be used to calculate the atomic mass if m_p in the first term on the right-hand side is replaced by $M(1H)$.

ly shown that

$$\varepsilon_n(A, Z) = \Delta W(A, Z) - \Delta W(A-1, Z), \quad (2.1.12)$$

$$\varepsilon_p(A, Z) = \Delta W(A, Z) - \Delta W(A-1, Z-1), \quad (2.1.13)$$

$$\varepsilon_{2n}(A, Z) = \Delta W(A, Z) - \Delta W(A-2, Z), \quad (2.1.14)$$

where $A - Z$ is even;

$$\varepsilon_{2p}(A, Z) = \Delta W(A, Z) - \Delta W(A-2, Z-2), \quad (2.1.15)$$

where Z is even;

$$P_n(A, Z) = \Delta W(A, Z) + \Delta W(A-2, Z) - 2\Delta W(A-1, Z) = 2\varepsilon_n - \varepsilon_{2n}, \quad (2.1.16)$$

where $A - Z$ is even; and

$$P_p(A, Z) = \Delta W(A, Z) + \Delta W(A-2, Z-2) - 2\Delta W(A-1, Z-1) = 2\varepsilon_p - \varepsilon_{2p}, \quad (2.1.17)$$

where Z is even.[4]

Naturally, the relative error in the values of ε_n, ε_p and other above-mentioned parameters, each of which is a small difference between two large quantities, is much higher than the error in the computation of ΔW. However, we can use Levi's narrow-band formulas (in Z and N) to calculate the values of ΔW (the total number of parameters in these formulas is equal to 81) with an error of 0.5-1 MeV, and thus obtain the values of ε_n, ε_p and other difference quantities to within 10-20%.

Since the energy of alpha decay,

$$E_\alpha = \{M(A, Z) - M(A-4, Z-2) - M({}^4_2\mathrm{He})\}c^2 = \Delta W(A-4, Z-2) + \Delta W({}^4_2\mathrm{He}) - \Delta W(A, Z),$$

is also expressed in terms of $\Delta W(A, Z)$, the semiempirical formula can be used to analyze some general laws of alpha decay (see Sec. 3.2).

The collective nature of the motion of particles in the incompressible nuclear fluid must lead to surface oscillations of the shape of the drop (without a change in its volume). The simplest of these are the quadrupole and octupole oscillations. In the case of quadrupole oscillations, the excited drop attains the form of an ellipsoid,

[4] See remarks to Tables 2 and 3 in connection with the evenness of Z and $A - Z$ in formulas (2.1.14)-(2.1.17).

while for octupole oscillations, it becomes pear-shaped. The energy of oscillations is

$$E = n\hbar\omega, \tag{2.1.18}$$

where $n = 1; 2, \ldots$, and $\hbar\omega$ is an octupole or quadrupole quantum. Since the quadrupole quantum is characterized by a spin and parity 2^+, while the corresponding value for the octupole quantum is 3^-, the value $n = 1$ must correspond to the nuclear levels with parameters 2^+ and 3^-, as is indeed observed for some even-even nuclei. The first excited states of even-even nuclei also include close levels with parameters 0^+, 2^+ and 4^+, which can be associated with quadrupole oscillations for $n = 2$. No quantitative agreement, however, is observed between the frequency of oscillations and the energy of levels (see Sec. 2.4).

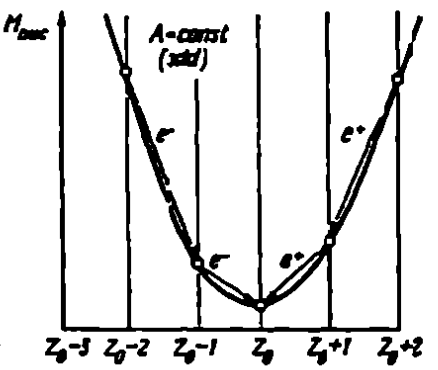

Fig. 58

The liquid drop model of the nucleus leads to a semiquantitative fission theory (see Sec. 7.3).

This model can be also used for deriving a condition linking A and Z for all β-stable nuclei.

Indeed, formula (2.1.11) gives a dependence of the nuclear mass $M_{нас}$ on its charge for a fixed A. This dependence is parabolic (Fig. 58). It was mentioned above that the most stable nucleus has the smallest mass. Hence the value of Z_0 corresponding to this nucleus can be determined by finding the minimum of the curve. Differentiating (2.1.11) with respect to Z for a fixed A and equating the derivative to zero, we obtain

$$Z = \frac{A}{1.98 + 0.015A^{2/3}}. \tag{2.1.19}$$

which can be used to calculate Z_0 for the β-stable isobar from a known value of A. A comparison of this formula with experiment shows that it gives quite accurate values of Z_0, differing from the actual values by not more than $\Delta Z = \pm 1$.

If A is odd and $\delta = 0$, the function $M(Z)$ is single-valued and, generally speaking, each value of A has only one value of Z_0 corresponding to the stable isobar. The isobar nucleus $Z = Z_0 + 1$ on the right branch of the parabola has a higher value of mass and must be transformed into the stable isobar with $Z = Z_0$ as a result of β^+-transition if the inequality (1.2.19) is satisfied. Similarly, the isobar nucleus with $Z = Z_0 - 1$ on the left branch of the parabola also has a higher mass value and if this excess satisfies the inequality

(1.2.19), the nucleus is transformed into a stable nucleus with $Z = Z_0$ by emitting an electron.[5] The situation is the same for isobar nuclei $(A, Z_0 + 2)$ and $(A, Z_0 - 2)$, which can be transformed into the nuclei $(A, Z_0 + 1)$ and $(A, Z_0 - 1)$ respectively, and so on.

For an even mass number A, the function $M(Z)$ is double-valued since the δ-term has different values for even-even and odd-odd nuclei. Owing to this circumstance, the dependence of M on Z is described for an even constant A by two parabolas arranged one above the other (Fig. 59*a*). The lower parabola corresponds to the more stable

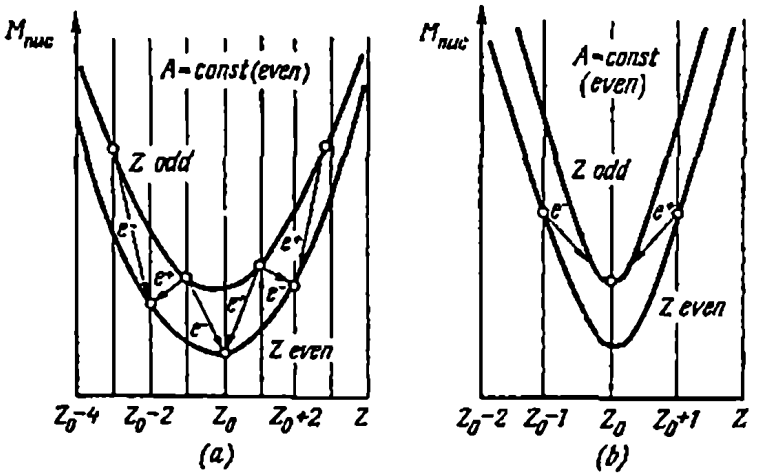

Fig. 59

nuclei with an even Z, while the upper parabola corresponds to less stable nuclei with an odd Z. It can be seen from Fig. 59*a* that since neighbouring nuclei on the same parabola differ by two units on the Z-scale, several (up to three) stable isobars can exist for even-even nuclei. This is so because a transition of the nucleus with a charge $Z_0 + 2$ (or $Z_0 - 2$) *into the nucleus with charge* $Z_0 + 1$ (or $Z_0 - 1$) is forbidden from the energy point of view, while a double beta decay[6] with a direct transition from $Z_0 + 2$ ($Z_0 - 2$) into Z_0 is impossible (or highly improbable). On the contrary, since each nucleus on the upper parabola has a corresponding lighter nucleus on the lower parabola differing in charge from this nucleus by ± 1, all odd-odd nuclei must be unstable; the only exceptions are the four nuclei mentioned above: ${}^2_1\mathrm{H}$, ${}^6_3\mathrm{Li}$, ${}^{10}_5\mathrm{B}$ and ${}^{14}_7\mathrm{N}$.

This is due to the fact that the isobar nuclei are arranged on parabolas in this case in accordance with the diagram shown in Fig. 59*b*. Obviously, the even-even isobars must be unstable in this case.

[5] See Sec. 3.3.1 for details.
[6] See Sec. 5.4.2, Vol. II for details on double beta decay.

An example of this kind is the even-even nuclei $^{14}_{6}C$ and $^{14}_{8}O$ which lie above the odd-odd nucleus $^{14}_{7}N$.

The liquid drop model can also be used for calculating the energy of beta decay

$$E_\beta = \{M(A, Z) - M(A, Z+1) - m_e\} c^2$$
$$= (m_n - m_p - m_e) c^2 + \Delta W(A, Z+1) - \Delta W(A, Z). \quad (2.1.20)$$

2.1.3. Hypothetical Superdense Nuclei

The model of the nucleus based on the concept of a nuclear fluid allows in principle far-reaching analogies with an ordinary liquid. In particular, it can be assumed that a phase transition to another state can take place in the nuclear fluid just like in an ordinary liquid.

Phase transitions in an ordinary liquid (say, water) take place upon a change in temperature or pressure. It is well known that ice and water have different densities and are characterized by different bonding forces between molecules. Similarly, it can be assumed that as a result of compression, the nuclear fluid can in principle be transformed into another phase with a different density and binding energy.

The mechanism of phase transition in the nuclear fluid was proposed in 1971 by Migdal[7] who considered the polarization of the nucleon medium under the action of the π-mesonic field existing in it. The polarization of the medium leads to a new mechanism of interaction between pions, viz. the exchange of excitations in the medium. The main types of these excitations are the low-energy excitations like the nucleon-hole in the Fermi filling (as well as Δ-resonance-hole).

The dispersion law for π-mesons in the medium can be written as follows:

$$\omega^2 = k^2 + m_\pi^2 + \Pi(\omega, k), \quad (2.1.21)$$

where $\Pi(\omega, k)$ is the polarization operator including all the processes of polarization of the medium (in vacuum, $\Pi(\omega, k) = 0$ and $\omega^2 = k^2 + m_\pi^2$, i.e. Eq. (2.1.21) is transformed into the equation of motion for a free π-meson).

An analysis of Eq. (2.1.21) shows that when the nucleon density ρ exceeds a certain critical value ρ_{cr}, the pion spectrum may acquire an additional branch with $\omega^2 < 0$, which gives an increasing solution of the type $\psi \sim \exp(\gamma t)$, where $\gamma > 0$. Thus, the nuclear matter with density $\rho > \rho_{cr}$ must be unstable relative to the creation of π^+-, π^-- and π^0-mesons. This can be graphically interpreted as the disintegration of a proton into a neutron and a π^+-meson with $l_\pi = 1$, or the decay of a neutron in a similar manner:

$$p \to n + \pi^+, \qquad n \to p + \pi^-. \quad (2.1.22)$$

[7] A.B. Migdal, *Zh. Eksp. Teor. Fiz.*, **61**, 2209 (1971).

Since both the processes are accompanied by flip of spin and isospin, we can speak of the propagation of a spin-isospin wave in the nucleonic medium.

Detailed investigation has shown that the nucleon-nucleon interaction described above is of atttactive nature and its strength increases with decreasing distance between nucleons, i.e. with increasing density of the nuclear matter. If this attraction exceeds the repulsion between nucleons at small distances, the energy of the nucleonic system starts to decrease and a new phase state of the nuclear matter, which is stable from the energy viewpoint and has a periodic spin structure, may appear in principle. This state is called superdense.

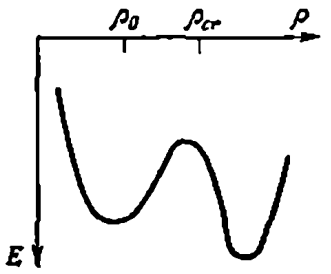

Fig. 60

Another new concept is closely related with the idea of superdense nuclei. It is well known that π-mesons are bosons. Hence the instability of the superdense nuclear matter relative to the creation of π-mesons must lead to their accumulation in a state that is advantageous from the energy viewpoint, i.e. to a pion condensation. The interaction of the π-condensate with the nucleonic medium leads to a change in the equation of state of the nuclear matter. Hence it is very important to study the properties of the π-condensate, i.e. of the $(\pi\text{-}\pi)$ interaction in the nucleon medium. The initial experimental data for constructing the theory of π-condensate in the nucleonic medium are the π-π scattering parameters for vacuum, which can be obtained by studying reactions of the type $\pi + N \to \pi + \pi + N$ (see Sec. 6.3.6, Vol. II).

The role of the π-condensate in the formation of the superdense phase of the nuclear matter can be visualized with the help of Fig. 60. The first peak in this figure corresponds to ordinary nuclear matter with density ρ_0. With increasing density, the energy rapidly increases due to repulsion at short distances. However, if the density increases beyond the critical value ρ_{cr}, the resulting π-condensate makes the nuclear matter more compliant to compression. Beginning from $\rho = \rho_{cr}$, the increase of energy with density becomes slower (point of inflection), and is then replaced by a decrease. The creation of π-mesons and a further decrease in energy will continue until the onset of many-particle repulsion between π-mesons. As a result, the energy curve acquires a new peak corresponding to the superdense state with $\rho > \rho_0$.

Theoretical calculations for the masses of the new type of nuclei indicate two possibilities: (a) the existence of superdense nuclei with $Z \simeq N$ and values of A similar to those for ordinary nuclei; (b) the

existence of neutronic nuclei with $N \gg Z$ and $A > 10^4$ (for example, with $Z \simeq 100$ and $A > 10^4$).

At present, the accuracy of calculations is not sufficiently high to yield the value of the critical density ρ_{cr}. Apparently, this value lies in the interval

$$0.6\rho_0 < \rho_{cr} < 2\rho_0.$$

In other words, we cannct rule out the possibility that the ordinary nuclear matter is in a superdense state.

The energy of the superdense state can be higher or lower than the energy of the normal state. Hence, in principle four different versions

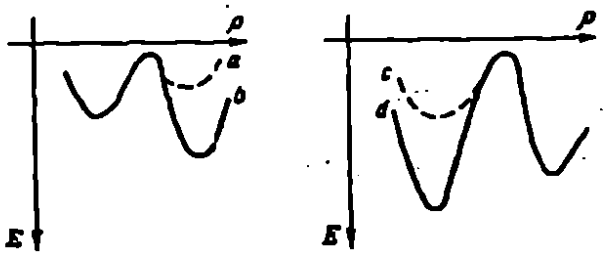

Fig. 61

are possible for the dependence of energy on density, each version having its own specific features (Fig. 61). Thus, for example, if $\rho_{cr} > \rho_0$ (which is more probable than $\rho_{cr} < \rho_0$), the superdense nuclei must be unstable with respect to a transition to the normal state if version (a) holds; for version (b), the nuclei will be stable.

Experimental investigations aimed at discovering superdense nuclei are being made at present. The idea behind one such experiment is to bombard the nuclei by heavy ions that have been accelerated to relativistic energies. At the moment of collision, a strong condensation of the nucleons can be expected (twofold due to the overlapping of nuclei plus additional effect due to the shock wave which must appear if the velocity of propagation exceeds $v \simeq 0.2c$, the velocity of sound in the nuclear matter). Such experiments were conducted at Berkeley by using Ar ions accelerated to $E = 1.62$ BeV/nucleon. It was proposed to identify the superdense nuclei by their anomalously large momenta and to register them with the help of a lexane detector. The experiments failed to give any positive results.

In other experiments, attempts were made to observe the backward scattering of protons with $T_p = 800$ MeV from superdense nuclei (in analogy with the backward scattering of α-particles in Rutherford's experiments). These experiments led to the value 10^{-6} as the upper bound of the concentration of superdense nuclei.

Attempts were also made to detect the superdense nuclei from the anomalously large values of the energy ε_n of attachment of neutrons. Thus, if $\varepsilon_n > 140$ Mev, the neutron capture reactions can be accompanied by the creation of π^0-mesons which can be easily detected from the γ-quanta of disintegration with an energy of 70 MeV ($\pi^0 \rightarrow 2\gamma$). These experiments were also unsuccessful.

The assumption that the nuclear matter has a superdense phase requires a further evolution of the liquid drop model of the nucleus. In particular, to reduce the rigidity of the nucleus with increasing density, we must introduce a term of the type $\varepsilon_\pi(\rho)A$ into the semiempirical formula for binding energy to take into account the pion condensation energy. The dependence of this term on density is inverse to that of the term $\varepsilon_N(\rho)A$.

2.2. Independent Particle Model

2.2.1. Drawbacks of the Liquid Drop Model

In the previous section, we have described several achievements of the liquid drop model of the nucleus. This model gives a fairly correct idea about the mass, binding energy and other parameters of the nucleus, and leads to the energy conditions for alpha and beta decay. This model can be used to obtain a correct qualitative idea of the distribution, spin and parity of several first levels in even-even nuclei, to construct a qualitative fission theory, and so on.

However, even for the range of aspects covered by it, this model is not quite consistent. We mentioned in Sec. 2.1.1 that it is not possible to obtain a semiempirical formula for the binding energy and the nuclear mass just with the help of the liquid drop model. It was found that the three-term formula based on the analogy between the nuclear matter and a liquid drop does not accurately describe the dependence of the nuclear mass on charge Z and mass number A. It is necessary to introduce a fourth term to take into account the symmetry, and a fifth term (δ-term) which has different forms for odd and even nucleons in the nucleus. The introduction of these terms into the semiempirical formula essentially indicates a departure from the liquid drop model.

The liquid drop model is also unable to give quantitative data on the excited states of the nucleus. An attempt to match the frequency of the surface waves of a liquid drop of the nuclear matter with the position of the nuclear levels proved futile. The model is also unable to describe one of the basic features of nuclear fission, viz. its asymmetry.

Besides, there is a wide range of problems that are left untouched by the liquid drop model. These include the individual character-

istics of the ground and excited states of nuclei (binding energy, spin, magnetic moment and parity), some properties of alpha and beta decays, the disposition of isomer nuclei relative to other nuclei, the abundance of various nuclei in nature, etc.

It was found that the properties listed above, as well as some other properties, have a specific dependence on the number of nucleons in the nucleus, viz. the periodicity of variation. Thus, for example, it was shown in Sec. 1.5 that all even-even nuclei in the ground state have zero spins and magnetic moments, and a high binding energy. The specific role of the magic numbers of nucleons (2, 8, 20, 50, 82, 126) was mentioned in Sec. 1.3. Experiments have shown that nuclei with such a number of protons or neutrons (*magic nuclei*) are especially stable (see Sec. 2.3 for details). The *double magic nuclei* having a magic number of protons and a magic number of neutrons (for example, $^{4}_{2}He^{2}$, $^{16}_{8}O^{8}$, $^{40}_{20}Ca^{20}$ and $^{208}_{82}Pb^{126}$) are the most stable ones.

The periodicity in the variation of the properties of nuclei with the number of nucleons contained in them is reminiscent of the change in the properties of atoms with the number of electrons in them. Like magic nuclei, atoms containing a certain number of electrons (2, 10, 18, 36, 54, 86) are especially stable (inert gases).

The modern model of the atom is based on the assumption that electrons move independently in a central potential field. Hence, we can assume that the above-mentioned periodicity in the properties of nuclei can also be explained by the independent particle model, although the very idea of using this model to describe the properties of the nucleus which consists of strongly interacting nucleons seems to be controversial at first glance.

We shall consider below two independent particle models: the simplest nuclear Fermi gas model and the more complex nuclear shell model. The problem of the applicability of the independent particle model to the nucleus is discussed simultaneously with the consideration of its versions.

2.2.2. Nuclear Fermi Gas

The Fermi gas model is the simplest independent particle model of the nucleus. Instead of the complex pattern of superpositions of individual nucleon-nucleon interactions, this model considers the motion of noninteracting nucleons in the field of an averaged potential well of width $R = r_0 A^{1/3}$. The depth U_0 of the well which must contain nucleons within the radius R of the nucleus can be found from the following simple argument.

The ground state of a nucleus corresponds to the lowest state of the Fermi gas at absolute zero, when all the lowest states are filled

with nucleons (degenerate Fermi gas). The total number of neutrons is

$$N = \int_0^{p_{max}} \frac{dN}{dp} dp, \qquad (2.2.1)$$

where

$$\frac{dN}{dp} = 2\,\frac{4\pi p^2 V}{(2\pi\hbar)^3}$$

is the density of states in the Fermi statistics (p is the neutron momentum, $V = 4\pi R^3/3 = 4\pi r_0^3 A/3$ is the volume of the nucleus, and

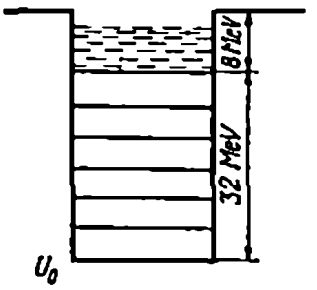

Fig. 62

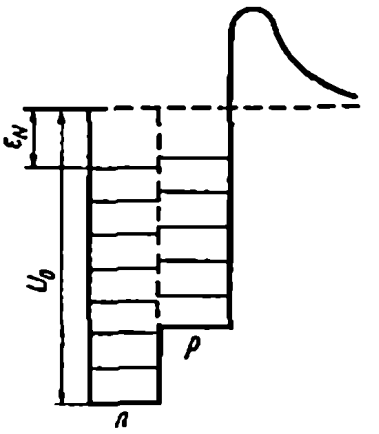

Fig. 63

p_{max} is the maximum momentum of a neutron during the filling of states; the factor 2 takes into account two directions of the spin).

As a result of integration, we get

$$N = \frac{V p_{max}^3}{3\pi^2\hbar^3}. \qquad (2.2.2)$$

For a symmetric nucleus with $N = A/2$ and

$$p_{max}^{(n)} = \sqrt[3]{\frac{9}{8}\pi}\,\frac{\hbar}{r_0} = 1.3 \times 10^{-14}\ \text{erg·s/cm}, \qquad (2.2.3)$$

where the value 1.2×10^{-13} cm has been taken for r_0.

This gives the following expression for the maximum kinetic energy of a neutron:

$$T_{max} = \frac{p_{max}^2}{2m_n} = 32\ \text{MeV}. \qquad (2.2.4)$$

Since the average binding energy of a neutron in the nucleus is 8 MeV, the depth of the potential well is $U_0 = 32 + 8 = 40$ MeV (see Fig. 62). The proton well of a symmetric nucleus has identical para-

meters. (It is assumed that the Coulomb repulsion of protons can be neglected for a symmetric, i.e. light, nucleus.)

If a nucleus is nonsymmetric ($N > Z$), then

$$T_{max}^{(n)} > T_{max}^{(p)} \text{ and } U_0^{(n)} > U_0^{(p)},$$

since an additional repulsive Coulomb interaction exists between protons (Fig. 63; see also Figs. 11 and 12, and their explanation in the text).

It can be easily shown that the average energy of the nucleons in a nucleus is

$$\bar{T}_N = \int_0^{T_{max}} T \frac{dN}{dT} dT \simeq 20 \text{ MeV}.$$

The values of U_0 and $\bar{T}_N$ both agree with analogous results obtained from other premises (see Sec. 1.3, Vol. II). Thus, the independent particle model unexpectedly gives a plausible description of the atomic nucleus which turns out to be similar to a liquid as well as a gas.

This dual nature of the atomic nucleus should not be considered contradictory, since a degenerate nuclear Fermi gas differs significantly from ordinary Fermi gas at absolute zero. In the first case $T_{max} \simeq V_0$, i.e. the state of the nucleons does not change as a result of collisions with other nucleons (see Sec. 2.3.2 for details), and they behave like independent particles. In the second case, $V_0 \simeq 10^3 T_{max}$, i.e. the "frozen" particles of the ordinary gas are bound relatively much more strongly and hence at absolute zero the ordinary gas exhibits the properties of a condensed medium.

The range of applicability of the Fermi gas model is not very wide. This model can be applied to explain qualitatively the effect of symmetry and saturation, as well as the properties of nuclei associated with the momentum distribution of nucleons inside a nucleus. The latter is quite important for considering processes whose characteristics depend on the internal motion of the nucleons. An example of such a process is the creation of π-mesons as a result of interaction between a nucleon and a nucleus. The threshold of this reaction is considerably lowered if the external nucleon collides with a nucleon of the nucleus moving towards it (see Sec. 6.1.3, Vol. II).

2.3. Shell Model

We have mentioned in Secs. 1.3 and 1.7 that nuclei containing a magic number of nucleons (2, 8, 20, 50, 82, 126)[6] have an anomalously

[6] Obviously, the number 126 can only characterize the number of neutrons contained in the nucleus.

high binding energy (i.e. they are especially stable) and zero electric quadrupole moment (i.e. they are spherically symmetric). This periodicity in the properties of nuclei, which is similar to the periodic variation of the properties of atoms, lends credibility to the assumption that the nucleus has a shell structure like the atom.

The corresponding nuclear model is called the *shell model.*

Before describing the shell model, let us recall and systematize the facts highlighting the special properties of nuclei with a magic number of nucleons. We shall supplement these facts by some other empirical results.

2.3.1. Experimental Foundations of the Shell Model

2.3.1a. Regularities in the Variation of Binding Energy

The existence of especially stable nuclei can be judged from the binding energy. Stable nuclei have the highest binding energy. The additional nucleons attached to them must be weakly bound (the adhesion energy of nucleon is low).

Consider the series of nuclei ${}_1^1H$, ${}_1^2H$, ${}_2^3He$, and ${}_2^4He$, each of which is obtained by coupling a nucleon to the previous nucleus. The binding energy of this nucleon to the first three nuclei is 2.2, 5.5 and 20.6 MeV, i.e. increases rapidly as the last nucleus is approached.

However, if this construction is continued and another nucleon (proton or neutron) is attached to the nucleus ${}_2^4He$, its binding energy will be negative in both cases and the resulting nucleus (${}_3^5Li$ or ${}_2^5He$) will be unstable. Thus, the nucleus ${}_2^4He$ with two protons and two neutrons (i.e. *double magic nucleus*) is especially stable. This conclusion is also supported by the fact that ${}_2^4He$ nuclei (in the form of α-particles) are emitted in radioactive decay.

It is difficult to verify the special stability of nuclei with 8, 20, 50, 82 or 126 particles, since all nuclei with even numbers of protons and neutrons are more stable than nuclei with odd mass numbers or nuclei with odd numbers of protons and neutrons. However, if the comparison is restricted only to even-even nuclei, the special stability of nuclei containing a magic number of nucleons becomes apparent.

Besides, the high stability of magic nuclei is manifested in a decrease (by a factor of 10 to 100) in the neutron capture cross section for these nuclei.

2.3.1b. Abundance of Isotopes

The special stability of nuclei containing a magic number of nucleons also follows from their higher abundance in nature. Let us consider some examples.

1. The last stable nucleus with $Z = N$ is the double magic nucleus $^{40}_{20}Ca$. Its content in the natural mixture of calcium isotopes is 97%. The preceding nucleus with $Z = N$ ($^{36}_{18}Ar$) has a relative abundance of 0.3%, while the next one ($^{44}_{22}Ti$) is not found in nature at all.

2. On the average, about three or four isotones with a given even N are found in nature. Their number, however, increases to five ($^{32}_{16}S$, $^{37}_{17}Cl$, $^{38}_{18}Ar$, $^{39}_{19}K$ and $^{40}_{20}Ca$) at $N = 20$, to six at $N = 50$, and to seven at $N = 82$.

3. Among various isotopes of a given element, the most abundant is the one with the average value of mass. Exceptions are observed for isotopes with $N = 50$ and $N = 82$ ($^{138}_{56}Ba$, $^{139}_{57}La$, $^{88}_{38}Sr$, $^{140}_{58}Ce$, etc.).

4. Tin $_{50}Sn$ has the largest number of stable isotopes (ten), three of these having odd values of A.

2.3.1c. Regularities of Alpha and Beta Decay

1. It is well known that all three radioactive families existing in nature terminate at $_{82}Pb$. Among the nuclei encountered in nature, those with $Z \leqslant 82$ are, as a rule, stable.

2. According to the semiempirical formula, the energy of emitted α-particles must increase with Z. Experiments show that an exception to this rule are the polonium nuclei ($Z = 84$), which emit α-particles having a higher energy than those emitted by nuclei following polonium.

3. Two polonium isotopes $^{210}_{84}Po$ and $^{212}_{84}Po$ emit long-range α-particles. Generally, α-particles with the highest energy (in comparison with the neighbouring nuclei) are emitted by radioactive nuclei with $N = 128$, $Z = 84$ and $N = 84$, which are transformed into the nuclei with $N = 126$, $Z = 82$ and $N = 82$ respectively. For example, the activity of an isotope of neodymium ($^{144}_{60}Nd$), an element in the middle of the Periodic Table, was discovered. The half-life of $^{144}_{60}Nd$ was found to be 5×10^{15} years, and the maximum energy of the α-particles emitted by it was 1.8 MeV.

4. Similarly, the highest energy of beta decay is observed in beta transitions to magic nuclei, while the β-particles emitted by magic nuclei have the lowest energy.

As an example, we can consider the chain of beta transformations $^{97}_{36}Kr \xrightarrow{\beta^-} {}^{97}_{37}Rb \xrightarrow{\beta^-} {}^{97}_{38}Sr$; in the first link of this chain, the energy re-

leased in beta decay is $\Delta E_\beta = 3.6$ MeV, while in the second link, $\Delta E_\beta = 0.27$ MeV.

5. The double magic nucleus $^{16}_{8}O$ is the final nucleus in two cascade processes of emission of delayed nucleons:

$$^{17}_{7}N \xrightarrow{\beta^-} {}^{17}_{8}O^* \xrightarrow{n} {}^{16}_{8}O; \qquad (2.3.1)$$

$$^{17}_{10}Ne \xrightarrow{\beta^+} {}^{17}_{9}F^* \xrightarrow{p} {}^{16}_{8}O. \qquad (2.3.2)$$

In both cases, the beta decay leads to the formation of excited magic nuclei $^{17}_{8}O^9$ and $^{17}_{9}F^8$ containing $N_{mag} + 1 = 9$ neutrons and $Z_{mag} + 1 = 9$ protons respectively. The separation energy of the ninth nucleon in these nuclei is so low that it turns out to be less than their excitation energy. This leads to the emission of nucleons that are delayed by the half-life of the preceding beta transition:

$$T^{(n)}_{1/2} = T^{(\beta^-)}_{1/2}, \quad T^{(p)}_{1/2} = T^{(\beta^+)}_{1/2}.$$

2.3.2. Construction of the Shell Model

We have mentioned that the phenomena listed above cannot be explained in the framework of the liquid drop model which is based on the assumption of strong interaction between the particles in the nucleus.

Magic numbers point towards the existence of some internal structure of the nucleus and a regular distribution of particles over the energy levels or orbits of the nucleus in a manner identical to the distribution of atomic electrons. It can be assumed that the aggregate of particles on one energy level or several closely spaced levels forms a nuclear shell whose gradual filling leads to the formation of especially stable nuclei (in analogy with the formation of inert gases as a result of filling of atomic shells).

2.3.2a. Principles of the Construction of the Shell Model

The periodic system of elements, first proposed by Mendeleev, is based on the specific nature of interaction of electrons with the nucleus. There is a central Coulomb attraction field (force centre in an atom), and the electrons moving in this field interact weakly with each other. The atomic levels are occupied by electrons in accordance with the Pauli exclusion principle.

At first glance, it seems that it is impossible to construct a shell model for the nucleus. Indeed, two of three conditions necessary for

such a model are not satisfied for the nucleons in the atomic nucleus. Unlike the atom, the nucleus does not have an isolated force centre and the nucleons (unlike the electrons) are strongly interacting particles.

The concentration of nucleons in the atomic nucleus is $n \simeq 10^{38}$ nucleons/cm^3 (see Sec. 2.1), while the mutual interaction cross section of nucleons at an energy of 25 MeV (the average energy of motion of nucleons in the nucleus) is $\sigma = 0.3 \times 10^{-24}$ cm^2 (see Sec. 1.5.2, Vol. II). Hence the mean free path of a nucleon in the nucleus is

$$\lambda = 1/n\sigma = 1/10^{38} \times 0.3 \times 10^{-24} \simeq 0.3 \times 10^{-13} \text{ cm}, \tag{2.3.3}$$

i.e. less than the nuclear radius. Hence it would appear meaningless to speak of any regular (orbital) motion of nucleons in the nucleus. However, it was found that the very fact that the interaction between nucleons is a strong and short-range interaction allows us to construct a spherically symmetric potential in whose field the nucleons move independently of each other.

Indeed, it will be shown in Sec. 1.3, Vol. II that the high efficiency and the small radius of interaction between two nucleons can be described by using a narrow (about 10^{-13} cm) and deep (about 30 MeV) potential well (nucleonic well) which can be assumed to be rectangular to a first approximation.

In the atomic nucleus, the nucleons move rapidly with respect to one another at distances comparable with the width of the nucleonic well. Hence the interaction of a nucleon with the nucleus can be described with the help of a mean field which is independent of time and which is represented by the total potential well formed by the superposition of several adjoining nucleonic potential wells. On account of the close proximity of the nucleons and the small radius of nuclear interaction, the mean potential must be nearly uniform (should not change much) inside the nucleus and must rapidly drop to zero at the boundary of the nucleus. Since the nucleus has a spherical shape to first approximation, the potential must be spherically symmetric.

According to quantum mechanics, the nucleons moving in the field of this potential can be in different energy states. The complete filling of all lower levels corresponds to the ground state. A collision between two nucleons is reduced to a redistribution of energy between them, and consequently one of the nucleons must lose a part of its energy and go over to a lower energy level. This, however, is not possible since all the lower levels are completely filled and no additional nucleons can be accomodated on them on account of the Pauli exclusion principle. Thus the mean free path of a nucleon between two collisions turns out to be much longer than that expected from

(2.3.3), and we can assume that the nucleons in the nucleus practically do not interact with one another.[9]

Thus, we have all the premises for constructing the shell model of the nucleus: noninteracting particles, viz. neutrons and protons, which have half-integral spin and obey the Pauli exclusion principle, move in a spherical potential field. To a first approximation, the potential is the same for protons and neutrons, since Coulomb repulsion between the protons becomes significant only in heavy nuclei. This conclusion is confirmed by the identical values of magic numbers for protons and neutrons. Owing to spherical symmetry, the orbital angular momentum l is an integral of motion and the same value of energy corresponds to all $2l + 1$ orientations of l (due to the isotropy of the field). In accordance with the Pauli exclusion principle, $2(2l + 1)$ nucleons of a given type can occupy this energy level (the factor 2 appears due to two spin orientations). Thus it becomes possible to construct a nuclear model in which nucleons are distributed in a definite way over the energy shells.

The simplest version of the shell model is the single-particle model for nuclei with an odd mass number A. In this model, it is assumed that all nucleons with the exception of the last odd one form a spherically symmetric inert core with zero angular momentum and magnetic moment, and all the basic properties of the nucleus are determined by the last odd nucleon. In the more complicated versions of the shell model, a complete shell is taken as the neutral core, and mutual interaction between all the remaining nucleons is taken into consideration.

2.3.2b. Specific Schemes for the Shell Model

To determine the position of the particle levels, certain parameters are specified for the potential well: its width is taken equal to the diameter of the nucleus and the depth is determined from the condition that the binding energy of a neutron in the nucleus is approximately equal to 8 MeV (the parameters of the potential well do not change significantly with a change in the value of A). Solving the Schrödinger equation for a particle in such a potential well, we obtain a series of eigenvalues and corresponding eigenfunctions, describing various states of the particle in this potential well.

A rectangular well can be used to describe the potential to a first approximation. The solution of the Schrödinger equation in this case gives the following sequence of states (Table 5):

[9] This discussion is valid only for nucleons in an unexcited nucleus. For a nucleon entering the nucleus from outside and exciting it by an energy equal to or more than ε_N (the binding energy of a nucleon), collisions become possible on account of the existence of vacant higher levels. In this case, formula (2.3.3) is valid but the shell model is inapplicable.

Table 5

States	1s	1p	2s 1d	1f 2p	1g 2d 3s	1h 2f 3p
l	0	1	0 2	3 1	4 2 0	5 3 1
$N=2(2l+1)$	2	6	2 10	14 8	18 10 2	22 14 6
$\sum N$	2	8	10 20	34 40	58 68 70	92 106 112

Here, the states (levels) are arranged in increasing order of energy, and are characterized by the quantum number n (which determines the number of nodes of the wave-function) and orbital quantum number l. According to the Pauli exclusion principle, each level can accomodate $N = 2(2l + 1)$ nucleons of each type (protons and neutrons).

As the shape of the potential well changes, the levels are displaced along the energy scale (sometimes, this displacement disrupts the level sequence) and combine to form groups of closely spaced energy levels separated by large energy gaps. These groups of closely spaced energy levels can be compared with nuclear shells. In the correct model, the total occupation number ($\sum N$) for a shell must coincide with a magic number. The large energy gap between shells makes magic nuclei exceptionally stable and renders the addition of the next nucleon to such a nucleus difficult.

The most natural change in the shape of a rectangular potential well, which brings this shape close to the real potential, is a rounding-off of its corners. Calculations show that this operation does not change the level sequence, but combines the following states into groups: 2s and 1d; 1f and 2p; 1g, 2d and 3s; 1h, 2f and 3p (these groups are shown in Table 5). Thus the shells for a rectangular well with rounded-off edges are closed at numbers 2, 8, 20, 40, 70 and 112. A comparison with the magic numbers (2, 8, 20, 50, 82 and 126) shows that this scheme gives correct values only for the first three magic numbers.

A more radical change in the shape of the potential well leads to the correct values for all magic numbers, although the corresponding model does not explain other experimental regularities.

The model proposed in 1949 by Goeppert-Mayer and Jensen, which takes into account the spin-orbital coupling, turned out to be the

most successful. In this model, the self-consistent potential is taken in the form

$$V(r) + U(r)\ (sl), \tag{2.3.4}$$

where $V(r)$ is a Saxon-Woods type potential, i.e. has the shape of a potential well with a flat bottom and a blurred edge (Fig. 64), or a harmonic-oscillator type potential, and $U(r) \propto (1/r)\,\partial V/\partial r$. The energy of a state with a given l assumes two values depending on the mutual orientation of the spin s and the orbital angular momentum l of the nucleon, the parallel orientation corresponding to the lower energy value (i.e. higher interaction energy).[10] Thus, a splitting of levels with a given l into two sublevels with given $i = l \pm 1/2$ is observed. Instead of one state np, we get two states $np_{3/2}$ and $np_{1/2}$, instead of nd, we get $nd_{5/2}$ and $nd_{3/2}$, and so on, the state with higher value of i having the lower energy.[11] This splitting is small for small values of l, increases with l (as $2l + 1$ approximately), and becomes so significant for $l \geqslant 4$ that it moves apart two sublevels ($l + 1/2$ and $l - 1/2$) into different shells.[12]

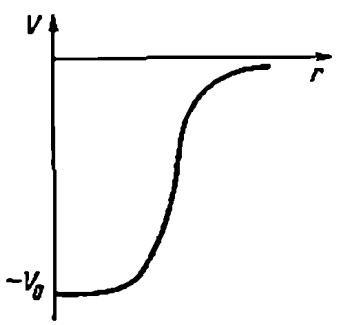

Fig. 64

Figure 65 shows the splitting and the corresponding redistribution of levels for the simplest (single-particle) shell model. Table 6 presents the distribution of states over shells, taking into account the spin-orbital shift, the occupation number $m = 2l + 1$ of each state and the occupation numbers N characterizing the closure of shells.

It can be seen from this table that all the shells are closed for the experimental values of magic numbers.

The distribution of nuclei over shells is carried out by comparing the number of nucleons contained in them and the spin values with

---

[10] The correctness of the assumption concerning a strong spin-orbital interaction is confirmed (besides the success of the shell model) by the existence of polarization of high-energy protons upon scattering.

[11] This type of interaction is observed in heavy atoms and differs from the scheme of electron interaction in light atoms (Russel-Saunders scheme). According to the Russell-Saunders scheme, the interaction between electrons is stronger than the spin-orbital coupling of an electron. In this case the spins and orbital angular moments of all electrons are separately added to form resultant vectors $\mathbf{S} = \sum \mathbf{s}_i$ and $\mathbf{L} = \sum \mathbf{l}_i$, which interact weakly with each other.

[12] Even for $l = 3$, the splitting of the $1f$ state into $1f_{7/2}$ and $1f_{5/2}$ is so significant that sometimes an increased stability of nuclei with $N = 28$ is observed. Hence one refers to a subshell with this value of total occupation number.

Table 6

Shell	State	$m = 2l + 1$	$N = \sum m$
I	$1s_{1/2}$	2	2
II	$1p_{3/2}1p_{1/2}$	4+2=6	8
III	$1d_{5/2}2s_{1/2}1d_{3/2}$	6+2+4=12	20
IV	$1f_{7/2}2p_{3/2}1f_{5/2}2p_{1/2}1g_{9/2}$	8+4+6+2+10=30	50
V	$1g_{7/2}2d_{5/2}2d_{3/2}3s_{1/2}1h_{11/2}$	8+6+4+2+12=32	82
VI	$1h_{9/2}2f_{7/2}2f_{5/2}3p_{3/2}3p_{1/2}1i_{13/2}$	10+8+6+4+2+14=44	126

the occupation numbers and the quantity l characterizing a given state. The following assumptions, which are confirmed experimentally, are made in this case (some of these assumptions were considered in Sec. 1.5.5).

1. The total angular momentum of a system consisting of an even number of protons and an even number of neutrons is equal to zero.

2. The total angular momentum of a system consisting of an odd number of nucleons is determined by the angular momentum $I = s + l$ of the unpaired nucleon.

3. The total angular momentum of an odd-odd system whose unpaired nucleons are in identical states is equal to double angular momentum of a nucleon.

4. The energy of a level (with a given n) increases with l.

5. The spin-orbital interaction energy for a state corresponding to a parallel arrangement of l and s is higher than for an antiparallel arrangement.

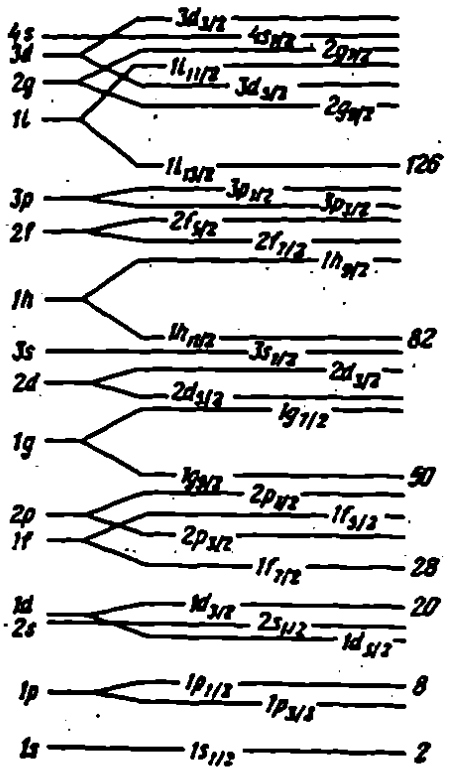

Fig. 65

The correctness of ascribing a state to a nucleus is checked by calculating the magnetic moment and comparing this value with the experimental value. The magnetic moment of nuclei having one nucleon in excess of a filled shell is calculated by formulas (1.5.43) and (1.5.44), which gives a good agreement with the experiment. For other (light) nuclei, the magnetic moment is calculated by tak-

ing into account the contribution of all the nucleons besides those in the filled shell (see Sec. 1.5.5) and also satisfactorily fits the experimental results.

Table 7

Nucleus (nucleon)	Spin	State	μ_{exp}	μ_{theor}
n	1/2	$1s_{1/2}$	−1.91	—
p	1/2	$1s_{1/2}$	+2.79	—
$^2_1$H	1	$(1s_{1/2})^2$	+0.86	+0.88
$^3_1$H	1/2	$(1s_{1/2})^3$	+2.98	+2.79
$^3_2$He	1/2	$(1s_{1/2})^3$	−2.13	−1.91
$^4_2$He	0	$(1s_{1/2})^4$	0	0

Nuclei belonging to the I shell are listed in Table 7. The nucleons in these nuclei occupy the same state $1s_{1/2}$ which is completely filled for the last nucleus $^4_2$He (for $i = 1/2$, $2i + 1 = 2$, i.e. two protons and two neutrons can occupy this state).

The filling of shell II begins with the addition of a fifth nucleon. However, it was mentioned in Sec. 2.3.1a that the nuclei $^5_2$He and $^5_3$Li are unstable. The nucleus $^6_3$Li is encountered in nature, but its position in the shell classification is determined by the irregularity in the filling of shells (similar to that observed in the filling of electron shells) and hence will not be considered (see Sec. 2.4.1). The remaining nuclei in the second shell (except $^{11}_5$B for which the computation of μ_{theor} gives ambiguous results) are listed in Table 8.

Table 8

Nucleus	Spin	State	μ_{exp}	μ_{theor}
$^7_3$Li	3/2	$(1s_{1/2})^4 (1p_{3/2})^3$	3.26	3.07
$^9_4$Be	3/2	$(1s_{1/2})^4 (1p_{3/2})^5$	−1.18	−1.14
$^{10}_5$B	3	$(1s_{1/2})^4 (1p_{3/2})^6$	1.80	1.88
$^{12}_6$C	0	$(1s_{1/2})^4 (1p_{3/2})^8$	0	0
$^{13}_6$C	1/2	$(1s_{1/2})^4 (1p_{3/2})^8 1p_{1/2}$	0.70	0.64
$^{14}_7$N	1	$(1s_{1/2})^4 (1p_{3/2})^8 (1p_{1/2})^2$	−0.40	−0.40
$^{15}_7$N	1/2	$(1s_{1/2})^4 (1p_{3/2})^8 (1p_{1/2})^3$	−0.28	−0.24
$^{16}_8$O	0	$(1s_{1/2})^4 (1p_{3/2})^8 (1p_{1/2})^4$	0	0

It can be seen from this table that the spins of the first four nuclei, which are formed by the filling of the state $1p_{3/2}$, are indeed multiples of 3/2 (or are equal to zero) as expected from the rules mentioned above.

The spins of the last four nuclei are multiples of 1/2 (or are equal to zero), since these nuclei are formed by the filling of the state $1p_{1/2}$. Besides, as in the case of the shell I, a good agreement between μ_{exp} and μ_{theor} is observed here also.

Similarly, we can accomodate about ten nuclei in shell III. However, the computation of μ_{theor} becomes more difficult as the nuclei become more complex. Nevertheless, it can be stated that the shell model does not contradict the experimental results for higher occupation numbers also. Thus, for example, it is known that among the nuclei containing $28 < N < 50$ nucleons of one type, there is not a single nucleus with spin $I = 7/2$; the nuclei of shell V do not contain any nucleus with spin $I = 9/2$, and so on. Conversely, $^{209}_{83}$Bi with one proton in excess of the closed shell indeed has a spin corresponding to the state of this 83rd nucleon (9/2), and so on.

2.3.3. Experimental Consequences of the Shell Model and Its Applicability

Experimental values of magic numbers, spins and magnetic moments of nuclei (as well as some other characteristics like the electric quadrupole moment) are used for constructing the shell model of the nucleus. Hence the agreement between the experimental and theoretical values of these quantities cannot serve as a criterion for the correctness of the model. However, some consequences of the model can be independently compared with the experiment. These include two phenomena which will be considered in detail in Chap. 3, viz. the distribution of the isomer nuclei and the selection rules for beta decay.

Isomers are nuclei with metastable energy levels, i.e. levels with a fairly long lifetime. It will be shown in Sec. 3.4.3 that the existence of long-lived isomers is associated with the existence of a weakly excited state of the nucleus, which differs considerably from the ground state in the value of the angular momentum ($\Delta I \geqslant 4$). It is obvious from Table 6 that a sharp difference in the angular momenta of close (adjoining) states is observed at the end of shell IV, where the last two states differ by $\Delta I = 9/2 - 1/2 = 4$. Hence the nuclei formed by the occupation of state $2p_{1/2}$ (i.e. having this state as the ground state) will have the state $1g_{9/2}$ as the nearest excited state from which a transition is hampered.

Thus, for occupation numbers $N > 20 + 8 + 6 + 4 = 38$, nuclei must exhibit isomeric properties.[13] This boundary coincides with the experimental boundary (see Fig. 127 and Table 21). The condition

[13] The nature of the isomeric transition ($M4$) corresponds to the difference in the parities of the states between which the transition takes place.

for the existence of isomeric states is preserved right up to the end of shell ($N = 50$), although it appears at first glance that isomerism should be exhibited only by the nuclei corresponding to the filling of the state $2p_{1/2}$. This fact is explained by the alternation of the levels $2p_{1/2}$ and $1g_{9/2}$ during the filling of shell IV.

Similarly, it can be shown that among the nuclei of shell V, isomerism must be observed after the filling of the first two states ($N > 50 + 8 + 6 = 64$), since the filling of the next three states takes place alternately and one of these states ($1h_{11/2}$) differs significantly from all the remaining states in the value of its angular momentum.

The second conclusion that can be drawn from the shell model concerns the selection rules for beta decay. It will be shown in Sec. 3.3 that the selection rules are associated with a change in the parity and spin of the nucleus in the process of beta decay. The shell model can predict this variation and hence the nature of the beta transition (allowed or forbidden, the extent to which a transition is forbidden, i.e. the theoretical value of the mean lifetime τ).

The predicted value of τ is in a good agreement with the experimental value.

As an example, let us consider two beta transitions:

$$^{17}_{9}\mathrm{F} \xrightarrow{\beta^+} {}^{17}_{8}\mathrm{O} \text{ and } {}^{123}_{50}\mathrm{Sn} \xrightarrow{\beta^-} {}^{123}_{51}\mathrm{Sb}. \qquad (2.3.5)$$

In the first case, the beta decay is reduced to a transformation of the ninth proton in the ^{17}F nucleus to the ninth neutron of the ^{17}O nucleus. According to the shell model, both these nucleons are in the state $1d_{5/2}$. Hence the transition $^{17}\mathrm{F} \rightarrow {}^{17}\mathrm{O}$ does not involve a change of the total or orbital angular momenta of the transforming nucleus. Consequently, the spin and parity of the nuclei also remain unchanged ($\Delta I = 0$, $P_i/P_f = 1$).

According to the theory of beta decay (see Sec. 3.3), such beta transitions should belong to the allowed transitions which are characterized by the experimental parameter

$$\log F\tau \simeq 3\text{-}5,$$

where F is a known function of the beta decay energy E_β and τ is the mean lifetime of the β-radioactive nucleus. Experiment confirms this conclusion of the shell model. The value of $(\log F\tau)_{exp}$ obtained experimentally for the beta decay of the ^{17}F nucleus is 3.36.

In the second case, the 73rd neutron occupying the state $1h_{11/2}$ in the nucleus $^{123}_{50}$Sn is transformed into the 51st proton occupying the state $1g_{7/2}$ in the nucleus $^{123}_{51}$Sb. For such a transition, the total and orbital angular momenta of the nucleon change by 2 and 1 respectively. Hence the nuclei $^{123}_{50}$Sn and $^{123}_{51}$Sb must differ in spin by 2 units and must have opposite parities: $\Delta I = 2$, $P_i/P_f = -1$. According to the theory of beta decay, such beta transitions are for-

bidden. The quantity log $F\tau$ must have a value of about 9 for such transitions. The experimental value for the beta decay of $^{123}_{50}Sn$ was found to be

$$\log (F\tau)_{exp} = 9.1.$$

The single-particle shell model correctly predicts the transition of electric quadrupole moment through zero (with a sign inversion) at a magic number of nucleons (but does not permit a computation of its value).

The shell model also explains why forbidden alpha transitions are encountered most frequently in nuclei with odd mass numbers.

It follows from general considerations that the probability of formation of an α-particle inside an α-emitting nucleus must increase from the centre to the periphery.[14] Hence it can be assumed that α-particles emitted by the nucleus and carrying away a considerable amount of energy from it are formed near its surface from the peripheral nucleons (having the highest energy). The creation of α-particles near the surface of an odd nucleus is less probable than for an even nucleus, since odd nuclei have one peripheral nucleon which must be coupled with a nucleon from the inner shell. The creation of an α-particle in an odd-odd nucleus having two peripheral nucleons should be even less probable.[15]

Later on, we shall also consider some other phenomena which can be explained within the framework of the shell model.

2.3.4. Drawbacks of the Shell Model

In spite of the resounding success of the shell model, its significance should not be overestimated. The range of applicability of this model is quite limited: it can be used to explain the phenomena related to certain properties of spherical nuclei (mainly, light nuclei) in the ground state and in weakly excited states. Even in this narrow range, however, discrepancies are observed between theoretical and experimental data. Let us consider some of these discrepancies.

1. When levels in a potential well are being filled by nucleons, some discrepancies are observed between the predicted and experimental values of spin. For example, in the shell model, the spin of the nucleus $^{6}_{3}Li$ is determined by the angular momenta of the third proton and the third neutron. Both these nucleons are in the state $1p_{3/2}$. Consequently, according to the rules formulated in Sec. 2.3.2b, the shell model predicts $I_{theor} = 3$ for $^{6}_{3}Li$. However, the experimentally observed value I_{exp} for this nucleus is equal to unity.

[14] The probability of finding an α-particle outside an α-radioactive nucleus is nonzero, and the range of an α-particle inside the nucleus is very small.

[15] In a heavy (α-radioactive) nucleus $Z < N = A - Z$ and the last neutron and proton (in the order of filling) are in different states.

Similarly, the nucleus $^{19}_{9}F$ with its ninth proton in the state $d_{5/2}$ must have a spin $I = 5/2$, but $I_{exp}(^{19}_{9}F) = 1/2$. The experimental value of spin for $^{23}_{11}Na$ is equal to 3/2, although the eleventh proton of this nucleus is in the state $1d_{5/2}$ and hence we should expect the value 5/2 for $I_{theor}(^{23}_{11}Na)$, and so on.

This drawback of the model was usually overcome by stating that the filling of levels was not regular (as had been established earlier in atomic physics for the filling of certain electron shells). Such an explanation, however, does not always sound convincing.

2. Several even-even nuclei belonging to the middle of level occupation have a pronounced structure of rotational levels. This experimental fact is in contradiction to the model based on the assumption that the self-consistent potential, and hence the nucleus, is spherically symmetric.[16]

3. The shell model gives drastically reduced values of quadrupole electric moments for nuclei corresponding to the occupation of the middle of shells. Obviously, the quadrupole moment Q of a single-particle type must be approximately equal to eR^2, where R is the radius of the nucleus. However, experimental values of Q lie between 10 and 20 times this value.

4. For the same nuclei (from the middle of nuclear shells) the model predicts much lower values of the probabilities of the $E2$-type gamma transitions corresponding to the emission of electric γ-quanta carrying an angular momentum $l = 2$ in comparison to the experimentally observed values (see Sec. 3.4 for details of gamma transitions).

The reasons behind these drawbacks of the shell model should be sought in the assumptions on which this model is based. It should be recalled that three such assumptions were made by us: (1) spherical symmetry of the potential; (2) the absence of interaction between nucleons, and (3) the validity of the Pauli exclusion principle for nucleons.

Since there are no grounds for doubting the validity of the exclusion principle, the observed discrepancies between the shell model and experiment can be attributed to the violation of the first two assumptions. Hence the most natural and economical (in terms of new parameters of the theory) way of overcoming the drawbacks of the shell model is to introduce nonsphericity associated with the interaction.

The model of the nucleus taking into account these two factors is called the *generalized model* (sometimes it is also called the collective model).

---

[16] According to quantum mechanics, a spherically symmetric nucleus does not have any rotational degrees of freedom.

2.4. Generalized Model of the Nucleus

The generalized model of the nucleus was developed in the works of Rainwater, A. Bohr and Mottelson, Hill and Wheeler. The idea behind this model is very simple.

The self-consistent spherically symmetric potential used in the shell model is the result of mutual interaction of nucleons. Hence it cannot be absolutely rigid and invariable, and must depend on the motion and interaction of individual nucleons. The nature and intensity of this dependence are determined by the number n of nucleons in excess of the filled shells.

For nuclei with filled or nearly filled shells, the spherically symmetric potential has a fairly high stability to the perturbing action

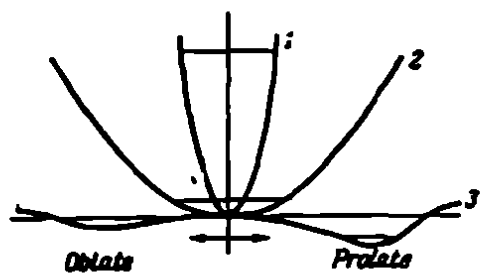

Fig. 66

of the additional nucleons. So the potential, and hence the shape of the nucleus, remains spherically symmetric if a small number of nucleons are added to such nuclei. The excited states of these nuclei are determined by single-particle levels in a spherically symmetric potential and by quadrupole oscillations about the equilibrium spherically symmetric shape of the nucleus.

The high stability of the nuclear shape with respect to the spherically symmetric equilibrium state means that the potential energy curve for the nucleus steeply rises with increasing deformation (see curve *1*, Fig. 66). The first vibrational level in such a potential well must correspond to a very high excitation energy (comparable with the energy of single-particle states).

As the number of nucleons in excess of the filled shells increases, the effect of the individual motion of nucleons on the self-consistent potential becomes more pronounced. A centrifugal pressure due to the excess nucleons is created at the walls of the nucleus. Consequently, the rigidity of the potential is reduced, and this leads to a lower stability of the spherical shape of the nucleus and a decrease in the energy of the vibrational levels (see curve *2*, Fig. 66).

Finally, for a sufficiently large number of excess nucleons, the spherically symmetric shape of the nucleus may become unstable

(see curve *3*, Fig. 66), i.e. the potential energy minimum will correspond to a nonspherical nucleus with a nonzero equilibrium deformation.

According to quantum theory, a nonspherical nucleus is capable of rotation. Hence it must have a rotational degree of freedom, i.e. rotational spectra of levels. The vibrational degrees of freedom are also retained in nonspherical nuclei, but the frequency of vibrations (energy of vibrational levels) must decrease. Finally, the nature of single-particle levels must change in a nonspherical potential. Thus the system of levels in a nonspherical nucleus is determined by single-particle motion as well as the collective (rotational and vibrational) motion of nucleons outside the closed shells.

As the number of nucleons in excess of the filled shells increases, the collective interaction strengthens and finally, this interaction becomes so strong that it starts affecting the closed core of the nucleus, which consists of several closed shells. This effect can be interpreted as a sort of tidal wave running around the closed nuclear core under the action of the external "rotating" nucleons. In this case, practically the entire nucleus will be deformed and thus experience particularly strong rearrangements of energy to the tune of 3-20 MeV.

Thus, it is clear from the pattern described above that the introduction of nonsphericity by taking into account the nucleonic interaction must lead to the following results:

1. Single-particle states, differing from the states observed for a spherical well, must appear in a nonspherical potential well.
2. In a nucleus with a small excess of nucleons over the filled shells, vibrational levels may appear as a result of interaction between the excess nucleons and the surface of the nucleus.
3. Rotational levels must appear in a nucleus having a large excess of nucleons over the closed shells.
4. Vibrations of all the nucleons are possible as a result of a very strong excitation of the nucleus. The energy of these vibrations may be about 10 MeV.

Let us consider these new degrees of freedom of the nucleus.

2.4.1. Single-particle States in a Nonspherical Well

In a nonspherical field, the total angular momentum i is not conserved, and hence the $(2i + 1)$-fold degeneracy of the level is removed. However, if the field is axially symmetric, the projection i_z of the vector i onto the symmetry axis is conserved. This leads to a double degeneracy of each sublevel with a given value of $|i_z|$ (in accordance with the two values of projection, viz. $+i_z$ and $-i_z$). Thus, the level i splits into $(2i + 1)/2$ sublevels that are displaced

relative to one another. The extent of displacement depends on the sign and nonsphericity parameter $\delta = \Delta R/R$ of the nucleus, which can be calculated from the values of its quadrupole electric moment Q.

The computation of single-particle levels for a nonspherical nucleus was first made by Nilsson who used the potential well of an oscillator with axial symmetry and a strong spin-orbital coupling:

$$V(r) = \frac{1}{2}M[\omega^2(x^2 + y^2) + \omega_z^2 z^2] + C\mathbf{ls} + Dl^2. \qquad (2.4.1)$$

Here, $\omega^2 = \omega_0^2(1 - 2\delta/3)$; $\omega_z^2 = \omega_0^2(1 - 4\delta/3)$; C, D, ω_0 are constants, and δ is the deformation parameter.

The results of calculations are shown in Fig. 67 (for a small number of levels and a small δ). It can be seen from the figure that the level $p_{3/2}$, on which four nucleons can be accommodated in a spherical well ($\delta = 0$), splits into two sublevels for $\delta \neq 0$, corresponding to two pairs of possible projections of vector $\mathbf{l} = 3/2$: $\pm 1/2$ and $\pm 3/2$.

Both sublevels have a negative parity, since $l = 1$ for the state p. Two nucleons can be accommodated on each sublevel. For $\delta > 0$, the sublevel with $l_z = \pm 1/2$ is first filled, followed by the sublevel with $l_z = \pm 3/2$. For $\delta < 0$, the order of filling is reversed.

Similarly, the $d_{5/2}$ level splits into three sublevels corresponding to three pairs of possible projections of vector $\mathbf{l} = 5/2$: $\pm 1/2$, $\pm 3/2$ and $\pm 5/2$. All sublevels have a positive parity ($l = 2$). Once again, two nucleons can occupy each sublevel. The filling of levels for $\delta > 0$ proceeds in increasing order of $|l_z|$. For $\delta < 0$, the state with $l_z = \pm 5/2$ is first filled, followed by the level with $l_z = \pm 1/2$, and finally, the level with $l_z = \pm 3/2$ is filled.

Confining ourselves to these few examples of level splitting in the shell model, let us find out the features that distinguish Nilsson's scheme from the shell model for explaining the nuclear spin.

It was mentioned at the end of the previous section that the spins of nuclei $^{6}_{3}$Li, $^{19}_{9}$F, $^{23}_{11}$Na etc. cannot be correctly explained by the shell model. From the point of view of Nilsson's scheme, this result can be naturally expected, since these nuclei have nonzero electric quadrupole moments Q, i.e. they are nonspherical in shape. We shall use Nilsson's scheme to determine the spins of these nuclei.

It is known from experiment that for all these nuclei $Q > 0$, i.e. the nonsphericity parameter $\delta = \Delta R/R$ for these nuclei is positive. Hence we must consider the right half of Nilsson's scheme for these nuclei. The $^{6}_{3}$Li nucleus has one (i.e. third) unpaired proton and one (also third) unpaired neutron. Both these nucleons occupy the sublevel with characteristics $1/2^-$, and so the spin and parity of the $^{6}_{3}$Li nucleus must be equal to 1^+. This conclusion is consistent with the experimental results.

The spin of the nucleus $^{19}_{9}$F must be determined by the ninth proton

occupying the sublevel $1/2^+$. Hence the spin and parity of the nucleus $^{19}_{9}F$ must be equal to $1/2^+$. Finally, the spin and parity of the nucleus $^{23}_{11}Na$ are determined by the eleventh proton occupying the sublevel $3/2^+$. Hence the spin and parity of the nucleus $^{23}_{11}Na$ must also be equal to $3/2^+$. Both these predictions are confirmed by experiment. The spins and parities of other nonspherical nuclei, corresponding to the filling of higher levels (not shown in Fig. 67) of Nilsson's scheme, are explained in a similar way.

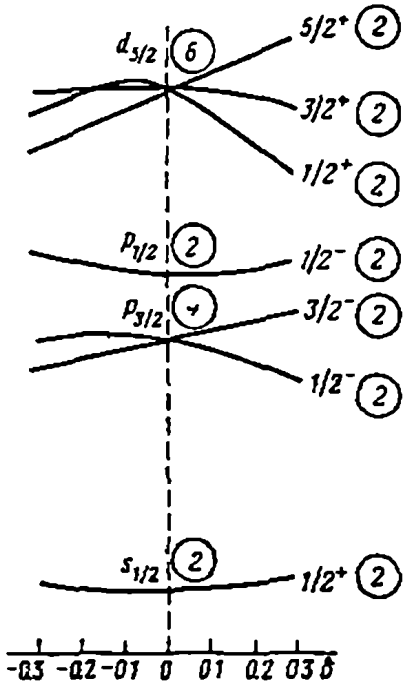

Fig. 67

2.4.2. Rotational States

The observed spin value of a nonspherical nucleus having axial symmetry (ellipsoid of revolution) is the projection of the sum of total angular momenta Σi of the nucleons in the nucleus onto the symmetry axis of the nucleus. This projection is denoted in Fig. 48 by K. This vector coincides with the spin of the nucleus in the ground state, i.e. $K = I_0$. For an even-even nucleus, $I_0 = K = 0$.

If a nonspherical nucleus is in an excited state, its spin (angular momentum) may differ from I_0 firstly because the quantity Σi and hence the value of K changes, and secondly because the nucleus can rotate around an axis perpendicular to the axis of symmetry. If the rotational moment of the nucleus is equal to Ω, its total angular momentum in the excited state will be

$$\mathbf{I} = \mathbf{K} + \Omega. \tag{2.4.2}$$

We shall consider the excited states of the rotational band. In this case, $K = \text{const}$ and the energy of the rotational state is given by

$$E_{\text{rot}} = \frac{\Omega^2}{2J_{\text{eff}}} = \frac{I^2 - K^2}{2J_{\text{eff}}} = \frac{\hbar^2}{2J_{\text{eff}}}[I(I+1) - K(K+1)], \tag{2.4.3}$$

here J_{eff} is the effective moment of inertia, viz.

$$J_{\text{eff}} \simeq J_0 (\Delta R/R)^2. \tag{2.4.4}$$

Here, J_0 is the moment of inertia of a rigid body of the same shape as the nucleus.[17]

If we are considering an even-even nucleus and transitions to the ground state ($K = 0$), then

$$E_{rot} = \hbar^2 I (I + 1)/2J_{eff}, \qquad (2.4.5)$$

where I can assume only even values: $I = 0, 2, 4, 6, \ldots$ (due to the symmetry of deformation about a plane perpendicular to the axis of symmetry of the nucleus). Hence the energy of rotational levels can assume the following values:

$$E_0 = 0, \quad E_1 = 3\hbar^2/J_{eff}, \quad E_2 = 10\hbar^2/J_{eff},$$
$$E_3 = 21\hbar^2/J_{eff}, \quad E_4 = 36\hbar^2/J_{eff}, \quad E_5 = (55/3)\ (\hbar^2/J_{eff}),$$

and so on.

Thus,

$$E_1 : E_2 : E_3 : E_4 : E_5 : \ldots = 1 : 10/3 : 7 : 12 : 55/3 : \ldots \qquad (2.4.6)$$

As an example, let us consider the system of rotational levels of the nucleus $^{238}_{92}U$ (Fig. 68). It can be seen from the figure that the angular momenta and parities of the levels exactly correspond to the rules of their sequence for rotational levels, and $E_1 : E_2 : E_3 : E_4 : E_5 = 1 : 3.32 : 6.92 : 11.7 : 17.6$. which is nearly identical to that predicted by the above-mentioned regularity (2.4.6).

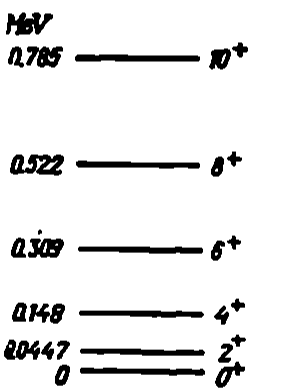

Fig. 68

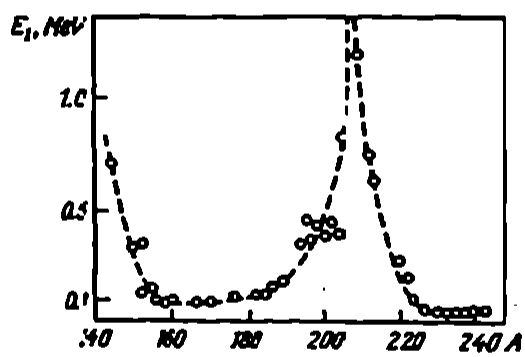

Fig. 69

The scale of excitation energy for the first rotational level E_1 is about 40-50 keV for heavy nuclei ($A \simeq 240$) and about 80-90 keV for rare-earth nuclei ($A = 150$-160). Near the magic numbers $E_1 \to \infty$, since spherical nuclei do not have any rotational states (Fig. 69).

[17] Formula (2.4.4) means that not all the nucleons of a nucleus but only some of them participate in rotation (see Sec. 2.5, superfluidity of the nuclear fluid).

Comparing the values of E_1 with the expression $E_1 = 3\hbar^2/J_{eff}$, we can estimate the effective moment of inertia for the corresponding nuclei. In turn, a comparison of the obtained values of J_{eff} for an ellipsoidal nucleus with the moment of inertia J_0 of a rigid body of the same shape, i.e. comparing

$$J_0 = \frac{2}{5} MR^2 \text{ and } J_{eff} = J_0 \left(\frac{\Delta R}{R}\right)^2$$

where R is the mean radius of the ellipsoid, we can find the value of the deformation parameter $\delta = \Delta R/R$ of the nucleus. The comparison gives $J_0/J_{eff} \simeq 2.5$, whence $\delta \simeq 0.35$. Such large values of the deformation parameter of nonspherical nuclei are consistent with the large values of the quadrupole electric moment and a high probability of $E2$-transitions.

Before concluding the analysis of the rotational degree of freedom, we can mention that it can be used for obtaining a better agreement between experimental and theoretical values of magnetic moments if the latter are calculated from the formula

$$\mu = g_K K + g_\Omega \Omega, \qquad (2.4.7)$$

where g_K and g_Ω are coefficients.

2.4.3. Vibrational Levels

Unlike rotational levels which appear due to a large excess (deficiency) of nucleons over filled shells, the vibrational (oscillatory) levels appear at a comparatively small (about 10) excess or deficit of such nucleons. Vibrational levels are characterized by equidistant levels

$$E = n\hbar\omega, \quad n = 1, 2, \ldots \qquad (2.4.8)$$

and a definite sequence of spins and parities. For example, a quantum of the most probable quadrupole vibrations has the value 2^+ for its total angular momentum and parity. Hence the first excited oscillatory state ($n = 1$) must also be characterized by the value 2^+, the second state corresponding to the excitation of two quanta ($n = 2$) must be a degenerate triplet with the states 0^+, 2^+ and 4^+.

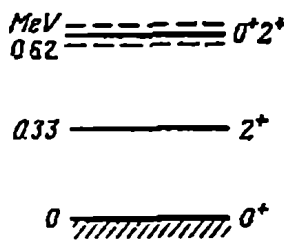

Fig. 70

Figure 70 depicts a typical level scheme for oscillatory spectra. The scale of energy excitation for the first oscillatory level (about 0.3 MeV) is small as compared with the distance between single-par-

ticle levels. This can be explained by a weak binding of external nucleons and a large value of their total mass:

$$\omega = \sqrt{\frac{k}{N m_N}} \tag{2.4.9}$$

(here, k is the modulus of elasticity and N is the number of excess nucleons).

2.4.4. Oscillations of All Nucleons in the Nucleus. Giant Resonances

Giant resonances of different multipolarities, which can be treated as different types of oscillations of all the nucleons in the nucleus, are the most clearly expressed characteristics of collective excitation of the nucleus. The main features of giant resonances are as follows:

1. Giant resonances are observed for many nuclei, i.e. they exhibit general properties of the nuclear matter and not the specific features of a given nucleus.

2. The position of a giant resonance on the scale of nuclear excitation energy varies smoothly with the mass number A (approximately as $A^{-1/3}$ for all open giant resonances).

3. The width Γ of giant pulses is large (several megaelectron-volts) and varies smoothly with mass number.

4. These resonances cover a considerable part of the energy-weighted sum rule (EWSR) for the corresponding multipole transitions.[16]

A graphic representation of giant resonances can be obtained through the liquid drop model and the shell model. From the point of view of the liquid drop model, giant resonances of different multipolarities are different types of collective motions of all the nucleons in a nucleus, for example, a uniform expansion and subsequent compression of the nucleus for monopole resonance, a displacement of all protons relative to neutrons for dipole resonance, and so on. From the point of view of the shell model, giant resonances are strongly correlated coherent particle-hole excitations accompanied by a jump of many nucleons from a filled shell, corresponding to the ground state of the nucleus, to higher vacant shells.

The type of a resonance (dipole, quadrupole, etc.) and its nature (electric or magnetic) are determined by the change in the angular momentum L and parity P of the nucleus. For electric resonances, $P_i/P_f = (-1)^L$, while for magnetic resonances $P_i/P_f = (-1)^{L+1}$ (cf. classification of γ-multipoles in Sec. 3.4).

---

[16] See Sec. 12.3 for details of the sum rule.

2.4.4d. Monopole Resonances $E0$ (0^+)

The existence of isoscalar monopole type resonance ($E0$, $\Delta T = 0$) at an excitation energy (MeV)

$$W = 80A^{-1/3} \tag{2.4.16}$$

was revealed in 1975 during a study of inelastic scattering spectra of deuterons with an energy of 80 MeV by ^{40}Ca, ^{90}Zr and ^{208}Pb and a comparison with the spectra of inelastic scattering of α-particles with an energy of 96 MeV. Subsequently the existence of this resonance was confirmed in 1977 during the investigation of inelastic scattering of α-particles by lead. These investigations showed that the contribution to the cross section for $W = 80A^{-1/3}$ MoV and $W = 63A^{-1/3}$ MeV (quadrupole resonance) depends on the scattering angle, thereby

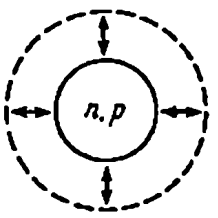

Fig. 75

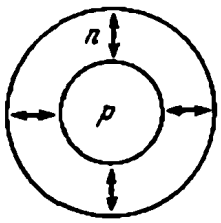

Fig. 76

indicating the existence of two different types of multipoles. Since the reaction of inelastic scattering of α-particles is improbable at $\Delta T = 1$, the new type multipolarity must be isoscalar. Figure 75 shows a graphic scheme of isoscalar monopole resonance.

There are certain indications concerning the existence of giant isovector monopole resonance whose mechanism is schematically shown in Fig. 76.

In view of the transverse nature of electromagnetic radiation, γ-quanta cannot excite a giant monopole resonance.

2.4.4e. On the Possibility of Excitation of Giant Resonances by Ions of Heavier Nuclei

The main difficulties of identifying giant resonances excited in the reactions of inelastic scattering of light particles ($A \leqslant 4$) are associated with the existence of a high level of nonresonance background whose elimination leads to significant errors. The situation is improved if heavier ions are used for exciting giant resonances. In 1980, the excitation of monopole, quadrupole and octupole resonances by ^{6}Li ions with an energy of 93 MeV in a number of nuclei were inves-

tigated at the Kurchatov Atomic Energy Institute.[21] A much better effect-to-background ratio was observed in the region of excitation of monopole and quadrupole resonances.

2.4.4f. Magnetic and Gamow-Teller Resonances

In recent years, giant isoscalar magnetic resonances $M0$, $M1$ and $M2$ have been reported. The excitation of these resonances is accompanied by a rearrangement of magnetic moments (for example, as a result of spin flip of a nucleon, $\Delta S = 1$). The excitation of magnetic resonances is schematically depicted in Fig. 77, where isoscalar magnetic dipole resonances are shown. It can be seen from the figure that nucleons with upward and downward spins move in opposite phases.

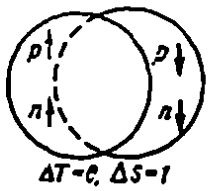

Fig. 77

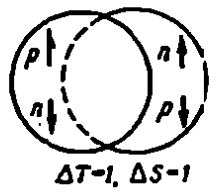

Fig. 78

In 1979, it was reported that Gamow-Teller giant resonance (dipole, isovector, magnetic, $I^P = 1^+$) had been observed in the (p, n) charge exchange reaction. The schematic diagram for this resonance is shown in Fig. 78. Gamow-Teller resonances are characterized by the flipping of spin ($\Delta S = 1$) and isospin ($\Delta T = 1$). At present, Gamow-Teller resonance has been observed in more than 20 nuclei from ^{7}Li up to ^{208}Pb. Theoretically, the existence of such a resonance was predicted in 1972 at the Kurchatov Atomic Energy Institute by Gaponov and coworkers.

2.4.5. Applicability of the Generalized Model

The range of application of the generalized model is shown conventionally (by dashed circles) in Fig. 79. The wide band depicts the domain of all known β-stable and quite long-lived ($\tau > 1$ min) β-radioactive nuclei. The vertical and horizontal lines passing through magic numbers indicate the range of application of the shell model. The hatched regions contain nuclei with large values of electric quadrupole moment. It is clear from the figure that these regions are concentrated within the circles. It can be expected that other nuclei observed in these regions will also be nonspherical.

[21] N.I. Venikov *et al.*, Preprint IAE 3352/2, Moscow, 1980 (in Russian).

Finally, let us summarize the results obtained with the help of the generalized model.

1. Correct values of spins were obtained for some nuclei.
2. The existence of rotational levels in nonspherical nuclei midway through the filling of shells was explained.
3. The vibrational spectra of some nuclei were explained.

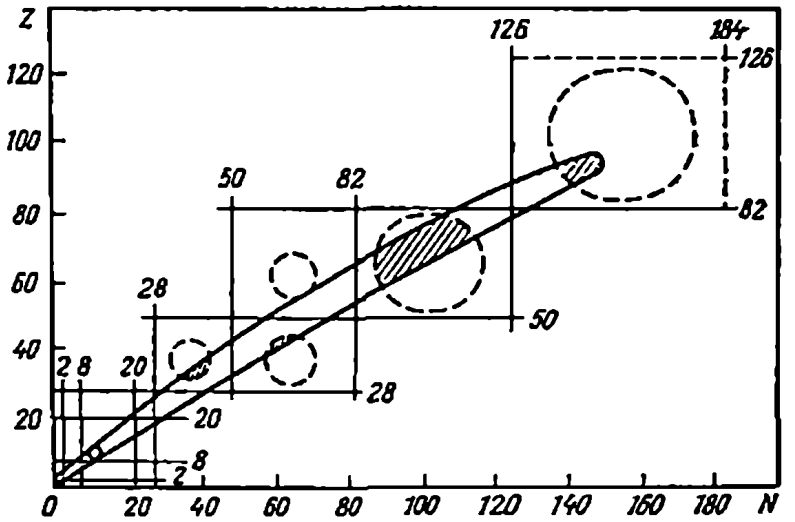

Fig. 79

4. Large values of quadrupole electric moments and enhanced probability of $E2$-transitions for nonspherical nuclei were accounted for.
5. A better agreement was obtained between calculated and experimental values of magnetic moments of nuclei.
6. A graphic representation of the essence of giant resonances was given.

2.5. Superfluid Nucleus Model

The success of the shell model and generalized model of the nucleus notwithstanding, several regularities in the properties of the nucleus remain unexplained even if residual interaction is taken into account. Firstly, it is the difference in the masses and binding energies of even-even, odd and odd-odd nuclei as mentioned in Sec. 1.3.2. It should be recalled that this difference is accounted for by introducing the δ-term into the semiempirical formula for the binding energy (see Sec. 2.1.1). Secondly, the first level of nonrotational excited states of even-even nuclei is far removed (by about 1 MeV) from the ground state (the energy gap). At the same time, the first level for odd and odd-odd nuclei is separated from the ground state by just

a few tens of keV. Thirdly, it was mentioned in Sec. 2.4.2 that in order to describe correctly the rotational spectrum of deformed nuclei, we must introduce an effective moment of inertia $J_{eff} = J_0 \times (\Delta R/R)^2$, which is smaller than the value of J_0 for a rigid body, thus indicating that rotation has a superfluid nature. The moment of inertia of odd nuclei is considerably higher than that of even-even nuclei (this difference cannot be attributed to the addition of another nucleon). Fourthly, the experimental value of the density of single-particle levels in deformed odd nuclei is twice the value calculated with the help of Nilsson's potential (or any other potential).[22]

To explain these and some other features, the superfluid model of the nucleus was proposed. This model is based on the isolation of short-range pairing forces from the residual interaction, and on taking these forces into account while considering the structure of the nucleus.

It was mentioned in Sec. 1.3.4 that the pairing interaction is the attraction between two (paired) nucleons of the same type having identical values of energy E and total angular momentum I, but different signs of the projection of the total angular momentum I onto the symmetry axis of the nucleus. In even-even nuclei, all nucleons are paired and the spins of these nuclei are equal to zero (total neutralization of spins, see Sec. 1.5.5). In order to excite an even-even nucleus, we must break the bond between a pair of nucleons, i.e. supply a sufficient amount of energy to the nucleus. In other words, in even-even nuclei, an energy gap must exist between the ground state and the first excited state (of nonrotational type).

A similar energy gap also exists in the electron spectra of metals and is responsible for their superconductivity. On the basis of this analogy, Bogolyubov indicated in 1958 for the first time the possibility of the existence of superfluidity of nuclear matter. The theory of superfluid state of the nucleus was constructed in 1959 by Belyaev, and independently by Solov'ev.

As in the independent particle model, a mean self-consistent field is introduced in the superfluid model. This field can be determined by the same potentials as before, for example, Nilsson's potential. However, the analogy between the two models ends here. In the independent particle model, the properties of the nucleus are determined by accommodating noninteracting nucleons on single-particle levels constructed for the mean field. Since such a description is found to be inaccurate, an attempt is made to correct it by mixing configurations, i.e. by considering the superposition of many single-particle states (but without taking into account correlations since it complicates matters).

---

[22] The average density of levels does not depend on the shape of the potential, but is determined just by the density of the nuclear matter.

In the superfluid model, a two-particle potential is considered. From the very beginning, the term responsible for residual interaction is isolated in this potential besides the terms that contribute to the self-consistent potential. In turn, this term can be further divided into two terms responsible for short-range pairing forces and long-range multipole forces respectively.

The isolated residual interaction is quite strong, and hence it is difficult to compute its value.[23] However, for the residual interaction in the form of a strong paired attraction of nucleons with identical I and E but opposite I_ζ, it is possible to carry out a special transformation which converts a system of interacting nucleons into a system of practically noninteracting quasiparticles (superpositions of particles and holes) for which a new energy spectrum of other single-particle states is observed. The energy of these states is given by

$$E_\nu = \sqrt{(\varepsilon_\nu - \lambda)^2 + \Delta_\nu^2}, \tag{2.5.1}$$

where ε_ν is the energy of a nucleon with quantum numbers ν in the single-particle model, λ is the energy of the last nucleon (it is approximately equal to the Fermi energy), and Δ is the energy-gap parameter in the spectrum of quasiparticles, its magnitude being of the same order as the pairing energy.

It follows from theory that the excited states of nuclei with even A are characterized by an even number of quasiparticles. The first excited state has an energy

$$E_0 + E_\nu + E_{\nu'}, \tag{2.5.2}$$

where E_0 is the energy of the ground state (this value differs from tho initial value in the single-particle model), while E_ν and $E_{\nu'}$ are determined by formula (2.5.1).

It can be seen from formula (2.5.1) that $E_0 + E_\nu + E_{\nu'} \geqslant E_0 + 2\Delta$, i.e. the energy spectrum of nuclei with even Δ must indeed have an energy gap of width

$$\Delta E \geqslant 2\Delta. \tag{2.5.3}$$

The excited states of nuclei with an odd A are characterized by an odd number of quasiparticles, including one. Hence in this case

$$E = E_0 + E_\nu, \tag{2.5.4}$$

where E_ν assumes several values. Therefore, the energy spectrum of nuclei with an odd A does not have an energy gap, i.e. differs radi-

[23] The methods of the perturbation theory are not applicable in this case.

cally from the spectra of nuclei with an even A. The displacement of the ground-state energy and a change in the nature of the spectrum lead to a change in the level density in deformed odd nuclei. Other features of energy spectra can be explained by taking into account the multipole forces.

2.6. A Brief Resumé of Chapter 2

In this chapter, some models of the atomic nucleus have been considered, viz. liquid drop model. Fermi gas model, shell model, generalized model and superfluid model. Each of these models is based on the assumption that certain properties of the nucleus are of fundamental importance, while the remaining properties are secondary. Hence each model can be used only within some preset limits.

The liquid drop model is based on the assumption that nucleons interact strongly with one another. According to this model, the atomic nucleus is a spherical drop of a superdense incompressible charged nuclear fluid. The main achievement of this model is a semiempirical formula for the binding energy of the atomic nucleus:

$$\Delta W(A, Z) = \alpha A - \beta A^{2/3} - \gamma \frac{Z^2}{A^{1/3}} - \zeta \frac{(A/2-Z)^2}{A} + \delta A^{-3/4}.$$

This relation can be used to estimate not only the binding energy and the nuclear mass, but also certain other parameters of the nucleus, for example the separation energy of a nucleon. The liquid drop model was used for constructing a qualitative theory of fission of heavy nuclei, for obtaining a relation between A and Z for β-stable nuclei, for explaining some properties of alpha decay, etc.

The liquid drop model leads to a smooth dependence of the properties of the nucleus on the number of nucleons contained in it. However, experiments indicate that several nuclear properties (binding energy, abundance in nature, spin, magnetic moment, electric quadrupole moment, etc.) vary periodically with the number of nucleons. Thus, for instance, among light nuclei those containing an equal number of protons and neutrons are more stable, other conditions remaining the same. Even-even nuclei are more stable than even-odd, odd-even, or odd-odd nuclei. Besides, all even-even nuclei have zero spins and magnetic moments in the ground state. Nuclei containing 2, 8, 20, (28), 50, 82 or 126 nucleons (magic nuclei) are especially stable, even in comparison with even-even nuclei, and have zero electric quadrupole moments.

Such periodic properties of the nucleus are described in the independent particle model. The simplest independent particle model is the Fermi gas model in which the motion of noninteracting nucleons is considered in the field of an averaged potential well. This model can explain the simplest periodic properties of nuclei (symmetry in the number of protons and neutrons, dependence of stability of the nucleus on the evenness or oddness of the nucleons contained in it, and zero spins and magnetic moments of even-even nuclei). The existence of magic nuclei is explained by the shell model of the nucleus, constructed in analogy with the model of electron shells in the atom.

The simplest single-particle version of the shell model of the nucleus considers the motion of an unpaired nucleon in a spherically symmetric uniform potential field created by the interaction of the remaining nucleons. The solution of the Schrödinger equation for this potential by taking into account the strong spin-

orbital interaction leads to a certain sequence of energy levels that are grouped near some energy values. A level is characterized by its energy, total angular momentum j and orbital number l. In accordance with the Pauli exclusion principle, each level can accommodate $2j+1$ nucleons. A complete occupation of the group corresponds to the completion of a shell containing a magic number of nucleons. The distribution of nuclei over shells is carried out by comparing the mass number, spin and other properties of the nucleus with the level parameters.

More complex versions of the shell model consider the residual interaction of nucleons in an incomplete shell.

The shell model only describes the properties of the ground state and the weakly excited states of spherical nuclei. In this respect, it correctly describes a large number of experimental regularities, viz. magic numbers, spins and magnetic moments of light nuclei, electric quadrupole moments of magic nuclei, isomerism islands, selection rules for beta decay, etc. However, the shell model is quite unsuitable for describing nonspherical nuclei, and gives absolutely incorrect values of electric quadrupole moments and even spins of these nuclei.

The properties of nonspherical nuclei were explained by Nilsson who constructed a single-particle model with a nonspherical (elliptic) potential. This model satisfactorily describes the spins and some other properties of odd nonspherical nuclei with mass numbers $150 \leqslant A \leqslant 186$ and $A \geqslant 222$.

Later, a more correct approximation was constructed in the form of the generalized model of the nucleus which takes into account the effect of collective motion of nucleons on the mean field parameters. According to this model, the collective motion of nucleons outside the filled shells leads to a change in the shape of the nucleus (without a change in its volume) and its orientation in space. The former corresponds to the volume and surface oscillations of the nuclear matter, while the latter accounts for the rotation of the nucleus (for nonspherical nuclei).

The deformation of the nucleus first increases with the number of nucleons in an incomplete shell, then decreases as the shell nears completion, and finally disappears when a complete filling has taken place.

As a result of deformation, a spherical nucleus is transformed into an ellipsoid of revolution capable of rotating about an axis perpendicular to its symmetry axis. However, unlike a rigid body, the rotation of the atomic nucleus is considered hydrodynamically and hence the moment of inertia of the nucleus is found to be less than the moment of inertia of a rigid body of the same mass and shape. The generalized model gives a qualitative explanation of the change in the quadrupole moments of nuclei with a change in Z and $N = A - Z$, and correctly explains the structure of the first excited rotational states for even-even nuclei with a quite large A. The arrangement of the energy levels of such nuclei corresponds to the intervals rule following from the nature of rotation of a deformed nucleus described above.

For very high excitations, a quite extensive rearrangement of the entire nucleus may take place. This is manifested in the appearance of broad levels ($\Gamma \simeq 1$-5 MeV) at excitation energies of 5 to 20 MeV, i.e. in the appearance of giant monopole, dipole, quadrupole and octupole resonances.

None of the models considered above can explain the dependence of the nuclear mass on the evenness or oddness of the number of protons and neutrons in the nucleus. These models are also unable to explain the wide energy gap (about 1 MeV) in the vicinity of the ground state for nonrotational levels of even-even nuclei, the anomalously low moment of inertia of even-even nuclei and some other properties. To explain these properties, the superfluid nuclear model was proposed. This model is based on the isolation of pairing attractive forces between nucleons, having the same energy and total angular momentum, but opposite angular momentum projections, from the residual interaction of nucleons.

Each of the model considered in this chapter is based on certain premises which seem contradictory in some cases. In spite of this, all these models correctly describe many properties of the nucleus. This indicates that all the models considered above are different aspects of some basic principle behind the structure of the nuclear matter. This basic principle is the assumption concerning the independence of motion, i.e. a weak interaction between nucleons in the nucleus. Thus, the basic model of the nucleus is the independent particle model in which the nucleons are assumed to be noninteracting. An analysis of different forms of residual interaction of nucleons leads to different versions of the shell model, as well as the superfluid and generalized models. The liquid drop model, whose construction was based on the assumption of strong interaction between nucleons, is also consistent with the basic principle, since the phenomena described by this model (for example, fission) are based on the collective motion of all nucleons of the nucleus as a whole, and thus are covered by the generalized model.

Chapter 3

Radioactive Nuclear Transformations

All unstable nuclei, as well as nuclei in excited states, undergo spontaneous transformations leading to a change in their composition and/or internal energy of the nucleus. Such spontaneous nuclear processes are called radioactive processes since they follow the laws of radioactive decay. Among well-known radioactive processes are alpha decay, beta decay (including *e*-capture), gamma radiation, spontaneous fission of heavy nuclei, emission of delayed protons and neutrons, and delayed fission. Besides, many less familiar forms of radioactive processes have been observed in the recent past: proton decay, carbon radioactivity, emission of delayed proton and neutron pairs, etc.

Many of the processes listed above are described in this chapter. The entire material is divided into five sections. Section 3.1 describes the basic regularities of radioactive processes; Secs. 3.2-3.4 deal with the "old" types of radioactivity, viz. alpha decay, beta decay and gamma radiation; and Sec. 3.5 is devoted to "new" types of radioactivity, which also include (for the sake of convenience) the well-known processes of delayed nucleon emission. For the same reason, the description of spontaneous and delayed fission has been included in Chap. 7.

3.1. Discovery and Basic Laws of Radioactive Transformations

The radiation from radioactive nuclei was first analyzed in experiments on the deflection of radiation in electric and magnetic fields, as well as on its absorption in matter. As a result of these experiments, it was established that radioactive substances emit three types of radiation.

(1) Alpha radiation, consisting of heavy positively charged particles that move at a velocity of about 10^9 cm/s and are absorbed by an aluminium foil few microns thick. It was later shown by spectral analysis that these particles are nothing but helium nuclei $^4_2$He.

(2) Beta radiation consists of light negatively charged particles moving at velocities close to the velocity of light and absorbed by an

aluminium foil about 1 mm thick. These particles turned out to be electrons.

(3) Gamma radiation is a highly penetrating radiation that is not deflected by an electric or a magnetic field. By nature, this is a hard electromagnetic radiation with an even shorter wavelength than X-rays. It was later established that the atomic nucleus (Rutherford's discovery in 1911) is the source of all three types of radiation.

3.1.1. Half-life

A detailed investigation of radioactivity led Rutherford in 1902 to the discovery of an isotope of the radioactive gas radon (Rn) which belongs to the group of noble gases. Radon is released as a result of alpha decay of radium. A significant feature of this gas is that its activity $A(t)$ decreases noticeably with time t.

After a passage of time $T_{1/2} = 3.8$ days, this activity is reduced to half: $A(T_{1/2}) = A_0/2$. After another 3.8 days, i.e. $T_{1/2}$, the activity is again halved, i.e. is reduced to one-fourth of its initial value: $A(2T_{1/2}) = A_0/2^2$; and so on. Hence, after a time t the initial activity A_0 becomes

$$A(t) = A_0/2^{t/T_{1/2}}. \qquad (3.1.1)$$

Naturally, this phenomenon was interpreted as a decrease in the initial number N_0 of radioactive atoms according to a similar law:

$$N(t) = N_0/2^{t/T_{1/2}}. \qquad (3.1.2)$$

The time $T_{1/2}$ in which the initial number N_0 of radioactive atoms is reduced to half is called *half-life*.[1]

Extensive investigations of radioactive elements showed that the value of $T_{1/2}$ is different for different elements but is always the same for a given isotope.

The range of variation of $T_{1/2}$ is very broad. At present, α-radioactive materials with half-lives varying from 3×10^{-7} s (for $^{212}_{84}Po$) to 5×10^{15} years (for $^{144}_{60}Nd$) are known. The intervals over which $T_{1/2}$ varies for beta decay and gamma radiation are also very broad. A direct measurement of the decrease in radioactivity with time is possible only for substances having a conveniently measurable half-lives. For example, it is not difficult to measure half-lives from several seconds to several hours and even days. In this case, an ionization chamber or a counter is used for measuring the activity of the sample at various instants of time and a curve of the type shown in

[1] The subscript 1/2 will be omitted sometimes

of radium showed that 1 g of radium undergoes about 3.7×10^{10} disintegrations per second; this corresponds to a half-life

$$T_{1/2} = \frac{0.69}{dN/dt}\frac{N_A}{A} = \frac{0.69}{3.7\times 10^{10}}\frac{6.025\times 10^{23}}{226}$$
$$= 5 \times 10^{10}\ \text{s} \simeq 1600\ \text{years}.$$

It follows from Eq. (3.1.4) that the process of radioactive decay is described by an exponential function. Hence at any instant of time t (however remote from the initial moment), there always exist undecayed nuclei with lifetime longer than t. Conversely, all the nuclei that have undergone disintegration by this instant lived for a time less than t. Nuclei disintegrating at the instant t have a lifetime exactly equal to t. The number of these nuclei will be

$$dN(t) = \lambda N(t)\,dt = \lambda N_0 \exp(-\lambda t)\,dt.$$

We can calculate the average lifetime τ of a given radioactive nucleus by calculating the average value of t:

$$\tau = \bar{t} = \frac{\int_0^\infty t\,dN(t)}{\int_0^\infty dN(t)} = \frac{N_0\int_0^\infty \lambda t \exp(-\lambda t)\,dt}{N_0} = \frac{1}{\lambda}\int_0^\infty \exp(-x)\,x\,dx = \frac{1}{\lambda}. \tag{3.1.6}$$

The average lifetime τ of a radioactive nucleus is the reciprocal of the disintegration constant λ. This result is quite natural, since the disintegration constant has the physical meaning of the disintegration probability, i.e. the fraction of disintegrations taking place per unit time. Apparently, the initial number of nuclei decreases in time τ by a factor of e.

If, in turn, the nuclei N_2 appearing as a result of radioactive disintegration of nuclei N_1 are also radioactive, we must write a system of two differential equations to describe these two successive transformations instead of the single differential equation (3.1.3):

$$\left.\begin{aligned} \frac{dN_1(t)}{dt} &= -\lambda_1 N_1(t), \\ \frac{dN_2(t)}{dt} &= \lambda_1 N_1(t) - \lambda_2 N_2(t), \end{aligned}\right\} \tag{3.1.7}$$

where λ_1 and λ_2 are the disintegration constants of nuclei N_1 and N_2 respectively. The first differential equation is analogous to Eq. (3.1.3) and describes the radioactive decay of the primary (parent) substance. The second differential equation describes the change in the quantity of the secondary (daughter) substance and its right-hand side consists of two terms. The first term describes the increment of

the radioactive nuclei of the secondary substance due to the disintegration of the primary substance and is therefore exactly equal to $\lambda_1 N_1$, i.e. to the number of disintegrating nuclei of the primary substance. The second term accounts for the number of disintegrating nuclei of the secondary substance.

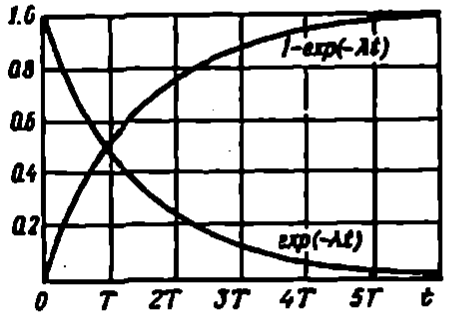

Fig. 81

The system of equations describing the mutual transformation of three, four or more substances can be written in an exactly similar manner. We shall consider the simplest (but the most important from the point of view of practical application) case of two substances, described by the system of equations (3.1.7).

Solving this system of equations we obtain the following result:

$$\left.\begin{aligned} N_1(t) &= N_{10}\exp(-\lambda_1 t),\\ N_2(t) &= N_{20}\exp(-\lambda_2 t)+\frac{\lambda_1 N_{10}}{\lambda_2-\lambda_1}[\exp(-\lambda_1 t)-\exp(-\lambda_2 t)], \end{aligned}\right\} \quad (3.1.8)$$

where N_{10} and N_{20} are the values of $N_1(t)$ and $N_2(t)$ at $t = 0$. Expressions (3.1.8) are considerably simplified if $T_1 \gg T_2$ ($\lambda_1 \ll \lambda_2$) and time periods $t \ll T_1$ are considered. In this case

$$\left.\begin{aligned} N_1(t) &\simeq N_{10},\\ N_2(t) &\simeq N_{20}\exp(-\lambda_2 t)+\frac{\lambda_1 N_{10}}{\lambda_2}[1-\exp(-\lambda_2 t)]. \end{aligned}\right\} \quad (3.1.9)$$

If $N_{20} = 0$, we get

$$N_2(t) \simeq \frac{\lambda_1}{\lambda_2} N_{10}[1-\exp(-\lambda_2 t)]. \quad (3.1.10)$$

To estimate the value of $N_2(t)$, we can use the graphic method (Fig. 81) of constructing the curves $\exp(-\lambda t)$ and $[1-\exp(-\lambda t)]$. In view of the special properties of functions $\exp(-\lambda t)$, it is very convenient to construct the ordinates of the curves for values of t corresponding to T, $2T$, ... (Table 9).

Relation (3.1.10) and Fig. 81 show that the amount of radioactive daugther material increases with time and approaches its limiting value for $t \gg T_2$ ($\lambda_2 t \gg 1$):

$$\lim_{t\to\infty} N_2(t) = \lambda_1 N_0/\lambda_2 = \text{const}. \quad (3.1.11)$$

Table 9

t	$\exp(-\lambda t)$	$1-\exp(-\lambda t)$
0	1	0
$1T$	$1/2=0.5$	0.5
$2T$	$1/2^2=0.25$	0.75
$3T$	$1/2^3=0.125$	0.875
. . . . .	. . . . .	. . . . .
$10T$	$1/2^{10}\simeq 0.001$	~ 0.999

For example, it can be seen from Table 9 that this equality is satisfied with an accuracy of about 99.9% for $t > 10T$. Usually, this equality is written in the form

$$\lambda_1 N_1 = \lambda_2 N_2 \qquad (3.1.12)$$

and is called the *secular equation*. The physical meaning of the secular equation is quite clear. Since in accordance with (3.1.3) λN is equal to the number of disintegrations per unit time, the relation $\lambda_1 N_1 = \lambda_2 N_2$ indicates that the number of disintegrations $\lambda_2 N_2$ of the daughter material is equal to the number of disintegrations of the parent substance, i.e. to the number $\lambda_1 N_1$ of the nuclei of the daughter substance formed as a result of this disintegration.

The secular equation is widely used for determining the half-lives of long-lived radioactive substances. This equation can be used for comparing two interconvertible substances, the half-life of the second substance being much smaller than that of the first ($T_2 \ll T_1$) under the condition that this comparison is made at the instant $t \gg T_2$ ($T_2 \ll t \ll T_1$).

The transformation of radium into radon is an example of successive disintegration of two radioactive substances. It is well known that $^{226}_{88}$Ra emits α-particles with a half-life $T_1 \simeq 1600$ years and is transformed into radioactive radon gas ($^{222}_{86}$Rn) which itself is radioactive and emits α-particles with a half-life $T_2 \simeq 3.8$ days. In this example, $T_1 \gg T_2$ and hence for an instant $t \ll T_1$ the solution of Eq. (3.1.7) can bo written in the form (3.1.9). Choosing $T_{Rn} \ll t \ll T_{Ra}$, we obtain the secular equilibrium condition

$$\lambda_{Ra} N_{Ra} = \lambda_{Rn} N_{Rn}$$

or

$$N_{Ra}/T_{Ra} = N_{Rn}/T_{Rn}. \qquad (3.1.13)$$

This condition means that starting from a sufficiently large t ($t \gg T_{Rn}$), the number of disintegrating Rn nuclei is equal to the num-

ber of Rn nuclei created as a result of disintegration of radium. For example, relation (3.1.13) is satisfied with an accuracy of 99.9% for $t > 40$ days ($t > 10T_{Rn}$).

Three of the four quantities appearing in Eq. (3.1.13) can be measured directly: N_{Ra} and N_{Rn} by precision weighing and λ_{Rn} by determining the half-life of Rn whose value 3.8 days is quite convenient for measurements. Thus, the fourth quantity λ_{Ra} can be calculated. This computation gives the half-life of radium $T_{Ra} \simeq 1600$ years, which is in agreement with the results on measurement of T_{Ra} by absolute counting of the emitted α-particles.

The radioactivity of Ra and Rn was chosen as a standard for comparing the activities of various radioactive materials. The unit of radioactivity was chosen as the activity of 1 g of radium or of the amount of radon in equilibrium with it.[4] This unit was called a curie (Ci). The amount of radon in equilibrium with 1 g of radium can be easily found from the following simple arguments.

It is well known that 1 g of Ra undergoes about 3.7×10^{10} disintegrations per second. Consequently,

$$\lambda_{Rn} N_{Rn} = \lambda_{Ra} N_{Ra} = 3.7 \times 10^{10},$$

where N_{Ra} is the number of Ra nuclei in 1 g of the substance, and N_{Rn} is the number of Rn nuclei in equilibrium with 1 g of Ra. This gives $N_{Rn} = 3.7 \times 10^{10}/\lambda_{Ra}$.

In order to find the expression for N_{Rn} in terms of mass, we must calculate the number of Rn nuclei in 1 g:

$$C_{Ra} = N_A/A_{Rn} = 6.025 \times 10^{23}/222,$$

where N_A is the Avogadro number and A_{Ra} is the atomic mass of Rn. Dividing N_{Rn} by C_{Ra}, we obtain the mass of radon whose activity corresponds to 1 Ci: $N_{Rn} = 6.5 \times 10^{-4}$ g.

3.2. Alpha Decay

3.2.1. Basic Experimental Results on Alpha Decay

The main characteristics of α-radioactive nuclei and the particles emitted by them are the half-life $T_{1/2}$, kinetic energy T_α and the range R.

---

[4] In view of the refinement of experimental techniques, the activity of 1 g of radium expressed in terms of the number of disintegrations per second keeps on undergoing modification with the passage of time, and this leads to considerable difficulties when this quantity is used as the unit of radioactivity. Hence the unit of radioactivity is now considered to be the value 3.700×10^{10} disintegrations per second, which is just approximately equal to the activity of 1 g of radium.

The half-life $T_{1/2}$ can be measured directly from the decrease in activity with time, or determined from the number of disintegrations per unit time or from the secular equilibrium.

The range of α-particles in different media is measured by different methods: with the help of a Wilson cloud chamber for gases, a bubble chamber for liquids, and photographic emulsion for solids. Different composite methods employing filters made of thin films or foils and counters are also used.

In the first experiments, the energy of α-particles was determined from their range.

A transition from range to energy is carried out with the help of empirical or theoretical formulas connecting the range and the energy of α-particles for a given medium (see Sec. 4.2.3). In the first approximation, the range of α-particles in air (in cm) is connected with energy (in MeV) through a power function of the type

$$R \simeq 0.3 T_\alpha^{3/2}. \qquad (3.2.1)$$

Exact measurements of the energy of α-particles are carried out with the help of the magnetic analysis in which the energy of the α-particles is compared with the energy of α-particles chosen as a standard.[5]

A magnetic spectrometer is an instrument similar in construction to a mass spectrometer. The main part of the instrument is an electromagnet which focuses α-particles of different energies at different points. Very thin films of α-active materials are used as the sources of α-particles, and detectors are chosen in the form of photographic plates or counters. The resolving power of magnetic spectrometers is very high and attains values of 5 keV (or even less) in the best instruments. This allows the detection of weak fine-structure lines against a background of high-intensity lines which correspond to the main group α-particles with close energies.

Another widely used method of investigating α-particles is the ionization chamber method, in which the electron current created by the ionizing action of α-particles is measured. Usually the chamber is equipped with a pulse analyzer. The resolving power of ionization chambers is weaker than that of magnetic spectrometers, and is about 25 keV for the best chambers. However, it is a much more high-transmission method, since it can use up to 50% of the emitted α-particles. In this connection, the ionization chamber method can be used to analyze minute quantities (a few dozens of nuclei) of α-active substances.

---

[5] For example, the energy of α-particles emitted by $^{214}_{84}Po$ is equal to .6804±0.0009 MeV.

Measurements of the ranges and energies of α-particles, as well as the half-lives for various α-active nuclei, led to the discovery of the following regularities and properties of alpha decay.

1. Geiger and Nuttall established in 1911 that for all α-active elements of the three radioactive families, the disintegration constant λ for an α-active nucleus and the range R_α of the α-particles emitted by it are connected through the relation

$$\log \lambda = A \log R_\alpha + B, \qquad (3.2.2)$$

where the constant A is the same for all three radioactive families, and the constants B differ by about 5% from one another.

Since the range and the energy of an α-particle are connected through a power function, the Geiger-Nuttall law can be written in a different form:

$$\log \lambda = A' \log T_\alpha + B', \qquad (3.2.3)$$

where A' and B' are similar to A and B.

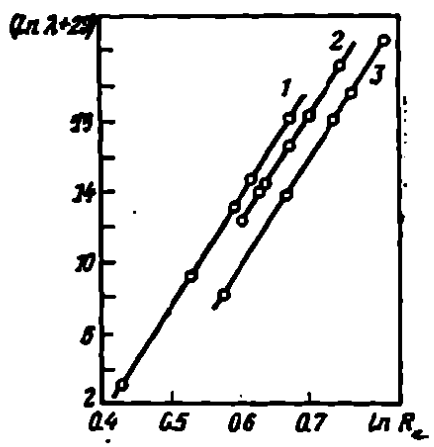

Fig. 82

The Geiger-Nuttall law is graphically shown in Fig. 82. In logarithmic coordinates, it is approximately represented by three parallel straight lines. Line *1* corresponds to the uranium family, line *2* to the thorium family, and line *3* to the actinouranium family. The significance of the Geiger-Nuttall law lies in that it can be used for finding the disintegration constants for nuclei to which the method of direct determination of the half-life cannot be applied (for example, for long-range α-particles).

At present, the more accurate formula (3.2.37) is used instead of (3.2.3). We shall derive this formula later.

2. It is worth noting that the range of possible values of the α-particle energy is very narrow, while their half-lives vary over a very wide range. Measurements have shown that with a very few exceptions, the energy T_α of α-particles and the half-lives $T_{1/2}$ for all α-active nuclei known to date lie in the intervals

$$4 \text{ MeV} \leqslant T_\alpha \leqslant 9 \text{ MeV}; \quad 10^{16} \text{ years} \geqslant T_{1/2} \geqslant 10^{-7} \text{s}. \qquad (3.2.4)$$

The average value of energy is approximately equal to 6 MeV.

3. A clear demarcation of all nuclei in the periodic system of elements into two groups is observed, viz. the α-radioactive and α-stable nuclei. As a rule, the α-radioactive nuclei have charges $Z > 82$.

(heavier than lead), and the energy of α-particles increases with increasing charge Z of the nucleus. The exceptions to this rule are some rare-earth nuclei (like $^{144}_{62}$Sm), $^{190}_{78}$Pt, as well as some artificially obtained nuclei with a large neutron deficiency.

The energy of α-particles is much lower for rare-earth elements, and their half-life is much longer than for heavy elements (for example, $^{144}_{60}$Nd has $T_\alpha = 1.8$ MeV and $T_{1/2} = 5 \times 10^{15}$ years).

4. A comparison of the alpha decay energy E_α of various isotopes of the same element reveals that the energy decreases regularly with increasing mass number (Fig. 83). An especially clear pattern is ob-

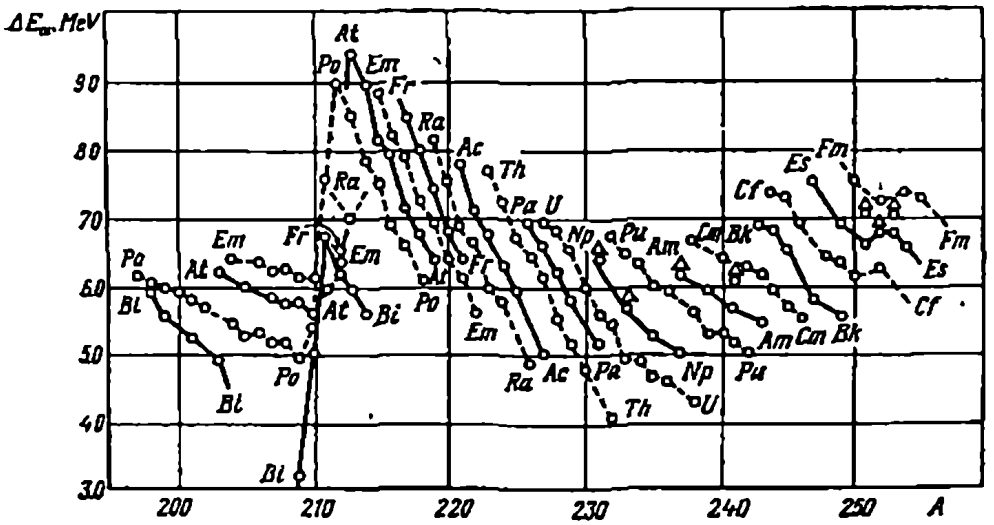

Fig. 83

served for even-even nuclei. A detailed analysis of this regularity shows that it is valid for $A > 215$ and $A < 209$, but is violated for the intermediate values. This regularity helps in predicting the energy of α-particles for unknown isotopes of a given element.

5. The application of accurate methods of measuring the energy of α-particles led to the discovery of the *fine structure* of α-spectra. It was found that the α-particles emitted by a nucleus usually do not have just the same value of the kinetic energy, but have values lying in a small interval.

As an example, we can consider the nucleus ThC ($^{212}_{83}$Bi) having the composition of the spectrum of emitted α-particles shown in Table 10. It was observed that the largest number of fine-structure lines is found in the α-spectra of nuclei whose daughter nuclei have a clearly defined nonsphericity, and that α-particles with lower energy are emitted at a lower intensity, other conditions remaining the same.

6. There are two cases of alpha decay which are interesting in that the nuclei (ThC′ and RaC′) emit, besides the main group of α-parti-

Table 10

Alpha-particle Group	T_α, MeV	Composition, %*	Alpha-particle Group	T_α, MeV	Composition, %*
α_0	6.066	27.2	α_3	5.622	~0.15
α_1	6.047	69.9	α_4	5.603	1.1
α_2	5.765	1.7	α_5	5.481	~0.016

* The difference in the sum of the percentage composition from 100% is due to different degrees of accuracy of experiments carried out for α-particles of different groups. Such a disparity will be also observed in some other tables.

cles, a small number of *long-range* α-particles with a high energy. Table 11 presents the composition of α-particles for the ThC′ nucleus.

Table 11

Alpha-particle Group	T_α, MeV	Composition, %	Alpha-particle Group	T_α, MeV	Composition, %
α_0	8.78	100	α_2	10.422	0.002
α_1	9.492	0.0035	α_3	10.543	0.018

The RaC′ nucleus emits an even smaller number of long-range α-particles, but they have 12 different values of kinetic energy (Table 12).

Table 12

Alpha-particle Group	T_α, MeV	Composition, %
α_0	7.680	100
α_1	8.277	4×10^{-4}
α_2	8.939	4×10^{-4}
α_3	9.065	2.2×10^{-3}
α_4	9.313	4×10^{-4}
α_5	9.489	1.4×10^{-4}
α_6	9.657	4×10^{-4}
α_7	9.779	1.1×10^{-4}
α_8	9.905	4×10^{-4}
α_9	10.074	1.7×10^{-4}
α_{10}	10.146	4×10^{-4}
α_{11}	10.328	1.1×10^{-4}
α_{12}	10.526	2×10^{-4}

It should be noted that both the cases correspond to the isotope nuclei of the same element, viz. polonium: $^{212}_{84}$Po (ThC′) and $^{214}_{84}$Po (RaC′).

The regularities and properties mentioned above will be considered in detail in Secs. 3.2.2 and 3.2.3.

3.2.2. Energy Consideration of Alpha Decay. Role of Conservation Laws

Alpha decay is one of the nuclear processes occurring under the action of a strong interaction. Hence all the known conservation laws must be obeyed for allowed alpha transitions, including the law of conservation of parity P and the law of conservation of isotopic spin T.

Each of these laws imposes certain restrictions on allowed alpha transitions. Thus, it follows from the law of conservation of isotopic spin that an α-radioactive nucleus (A, Z) and the daughter nucleus $(A-4, Z-2)$ formed as a result of alpha decay must have the same isotopic spin T (since the isospin T_α of an α-particle is equal to zero). From the laws of conservation of parity P and total angular momentum I it follows that the parity and spin of initial (P_i and I_i) and final (P_f and I_f) nuclei must be connected with the orbital angular momentum l_α of the α-particle through the following relation:

$$|I_i - I_f| \leqslant l_\alpha \leqslant I_i + I_f, \qquad P_i/P_f = (-1)^{l_\alpha} \tag{3.2.5}$$

(since $P_\alpha = +1$ and $I_\alpha = 0$)[6], and so on. Let us consider in detail the laws of conservation of energy and momentum.

In accordance with (1.3.11), the condition for a possible alpha decay from the point of view of energy is written as follows:

$$\varepsilon_\alpha = [M(A-4, Z-2) + M(^4_2\mathrm{He}) - M(A, Z)]\,c^2 < 0 \tag{3.2.6}$$

or

$$M(A, Z) > M(A-4, Z-2) + M(^4_2\mathrm{He}).$$

The mass (energy) of the parent nucleus must exceed the sum of the masses (energies) of the product nucleus and the α-particle emitted by the parent nucleus. The excess energy of the parent nucleus is released during alpha decay in the form of kinetic energy:

$$E_\alpha = |\varepsilon_\alpha| = [M(A, Z) - M(A-4, Z-2) - M(^4_2\mathrm{He})]\,c^2 = T_\alpha + T_{\mathrm{nuc}}. \tag{3.2.7}$$

[6] Alpha transitions which are forbidden by parity considerations will be discussed in Sec. 3.2.6.

which is distributed between the α-particle and the daughter nucleus in such a way that the momentum conservation law is not violated:

$$\mathbf{P}_\alpha + \mathbf{P}_{\text{nuc}} = \mathbf{P}(A, Z).$$

Assuming that the disintegrating nucleus is at rest, we obtain $|\mathbf{P}_\alpha| = |\mathbf{P}_{\text{n.c}}|$, whence $T_{\text{nuc}} = T_\alpha M_\alpha / M_{\text{nuc}}$ or

$$E_\alpha = T_\alpha + T_{\text{nuc}} = T_\alpha \left(1 + \frac{M_\alpha}{M_{\text{nuc}}}\right) \text{ and}$$
$$T_\alpha = E_\alpha \frac{M_{\text{nuc}}}{M_{\text{nuc}} + M_\alpha}. \tag{3.2.8}$$

Thus, most of the kinetic energy released in the process of alpha decay is taken away by the α-particle and only an insignificant part (about 2% for heavy α-radioactive nuclei) goes to the daughter nucleus. In the alpha decay of the nucleus ThC ($^{212}_{83}$Bi) considered above, $T_\alpha = 6.086$ MeV, $T_{\text{nuc}} = 0.117$ MeV and $E_\alpha = T_\alpha + T_{\text{nuc}} = 6.203$ MeV.

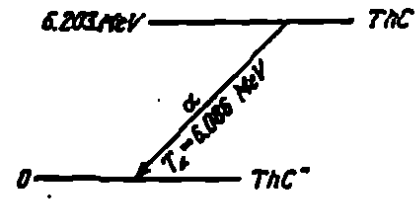

Fig. 84

The most convenient way of considering the alpha decay is to use the energy level diagrams. The energy state of a system is marked by a horizontal line whose height characterizes the energy in megaelectron-volts. Since the total energy of the nucleus is very high (about $931A$ MeV, A being the mass number), and only an insignificant part is released in the process of alpha decay (about 10 MeV), the sum of the rest energies of the daughter nucleus and the α-particle is taken as the zero value of energy for the sake of convenience:

$$[M(A-4, Z-2) + M(^4_2\text{He})]\, c^2.$$

Figure 84 shows a simplified energy level diagram for the alpha decay of ThC nucleus.

The upper level in this diagram is equal to $E_\alpha = |\varepsilon_\alpha| = 6.203$ MeV and corresponds to the energy state of the ThC ($^{212}_{83}$Bi) nucleus before the alpha decay. The lower energy level is equal to zero and corresponds to the energy state of the system consisting of the daughter nucleus and an α-particle (both having zero kinetic energy). The lower level is labelled only by the symbol of daughter nucleus ThC'' ($^{208}_{81}$Tl) and the appurtenance of the α-particle to this level is indicated by an arrow pointing downwards to the left. The energy of the emitted α-particle is usually shown near the arrow [although this energy can be easily calculated from the difference in the energy levels in accordance with formula (3.2.8)].

The diagram shown in Fig. 84 corresponds to the simplest case of alpha decay, when the emitted α-particles have a quite definite unique value of energy. This, however, is not the only possible scheme. It was mentioned above that alpha spectra frequently contain groups of α-particles with lower (fine structure of alpha spectra) and sometimes even higher (long-range α-particles) energies as compared to the main group of α-particles. Let us consider the energy interpretation of these properties of alpha decay.

While considering the processes of alpha decay, we have assumed so far that both nuclei (initial and final) are in the ground state. In

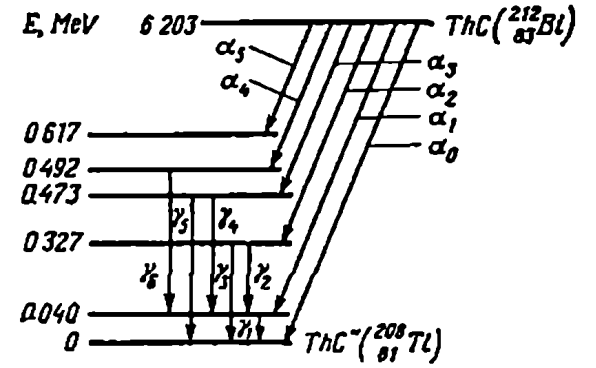

Fig. 85

actual practice, each of these nuclei has its own system of excited states which are characterized by certain values of energy E, total angular momentum I, parity P and isospin T. In principle, alpha transitions between these states are also possible (if they are not forbidden by the conservation laws).

The emission of the main group of α-particles with a definite energy (see Fig. 84) corresponds to the energy transitions between the ground states of the initial and final nuclei. However, if a transition is accomplished to an excited state of the final nucleus (or, conversely, from an excited state of the initial nucleus), the energy of the α-particles will be lower (or higher) than the normal value. The first case corresponds to the emergence of a fine structure of alpha spectra, while the second leads to the appearance of long-range α-particles. Figure 85 shows the energy scheme illustrating the emergence of a fine structure in the alpha spectrum of the ThC nucleus. In addition to the ground state of the final nucleus, which (together with the rest energy of the α-particle) has zero value of energy, the figure shows five excited states with energies 0.040, 0.327, 0.473, 0.492 and 0.617 MoV respectively. If, for example, an alpha decay is accompanied by the formation of the final nucleus in the fourth excited state, the kinetic energy E_α, released in this case will be 6.203—0.492 =

5.711 MeV. According to formula (3.2.8), the energy imparted to the α-particle will be

$$T_{\alpha_1} = E_{\alpha_1} \frac{M_{\text{nuc}}}{M_{\text{nuc}} + M_\alpha} = 5.711 \frac{208}{212} = 5.603 \text{ MeV}.$$

The energies of other α-particles from the fine-structure spectrum are obtained in a similar way (see Table 10).

The correctness of this scheme for the fine structure in alpha spectra is confirmed by experiments on the registration of the gamma radiation accompanying an alpha decay.[7] It was found that the energy of these γ-quanta exactly coincides with the difference in the energy states of the final nucleus.[8] For example, the following values of energy have been registered for γ-quanta accompanying the alpha decay of ThC: 0.040, 0.287, 0.327, 0.433, 0.452 and 0.473 MeV. It can be easily seen that all these values can be obtained by subtracting the energy of one level of the final nucleus from that of another level of the same nucleus. This means that the γ-quanta accompanying an alpha decay are emitted as a result of a transition of the final nucleus from some excited state to the ground state or to a less excited state.

Some fine-structure lines in the alpha spectrum are very weak. For example, there are only 0.15% α-particles with energy 5.622 MeV in the spectrum of ThC, and those with energy 5.481 MeV constitute just 0.016%. Naturally, it is very difficult to register such weak lines against the background of a large number of main α-particles. Hence a special method of $(\alpha - \gamma)$-coincidence is used to register such particles.

The essence of the coincidence method (which is used extensively in experimental nuclear physics) as applied to the problem under consideration lies in the following. The alpha decay is registered by two detectors. One detector measures the energy of α-particles with a rather low accuracy (about 95%), while the other registers the energy of γ-quanta. The pulses from both detectors are fed to a special electronic circuit which is activated only when the pulses arrive simultaneously. This means that if the time resolution of the circuit is quite high and the detectors are aligned appropriately, only such α-particles will be registered which are accompanied by a simultaneous emission of the γ-quanta corresponding to them. In other words, the electronic circuit can select rare events against a high background. This method can be used to register lines whose intensity is 10^4 times weaker than that of the fundamental spectral line.

[7] See Secs. 3.4 and 4.10 of the methods of registration of γ-quanta.

[8] As a matter of fact, the final nucleus receives a very small amount of recoil energy $T_{\text{nuc}} \simeq 10^{-4} E_\gamma$ during the emission of a gamma quantum. As a result, the energy E_γ of the γ-quantum is somewhat lower than the difference in the energies of the corresponding levels. This difference (which is of no consequence for the question under consideration) is discussed in detail in Sec. 3.4.4.

The fine structure of alpha spectra is encountered frequently. The largest number of fine-structure lines are observed in alpha spectra corresponding to transitions to the excited levels of a nonspherical nucleus. This is due to the fact that such nuclei have low excitation energy levels associated with the rotation of the nucleus. It is transitions to these levels (located close to the ground state) that generate α-particles with close energy values, which must be emitted with comparable probabilities in accordance with the Geiger-Nuttall law.

The investigation of the fine structure of alpha spectra is interesting since it can be used to construct the energy level diagram for the daughter nuclei formed in the process of decay.

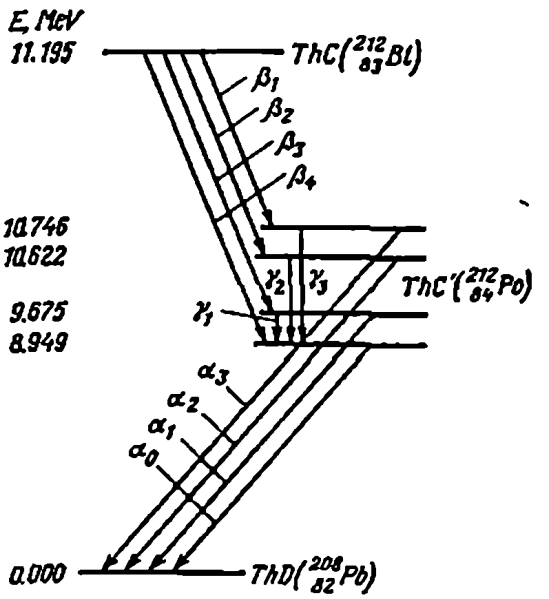

Fig. 86

Similarly, the energy level diagram for long-range α-particles formed in alpha decay is also important, since its investigation provides information about the structure of the levels of the parent nucleus. The basic scheme of the formation of long-range α-particles is as simple as the emergence of fine structure. Their emission is due to a transition from an excited state of the parent nucleus to the ground state of the daughter nucleus.

Figure 86 shows the scheme of emission of long-range α-particles by the ThC′ nucleus ($^{212}_{84}$Po). This nucleus is created as a result of the beta decay of ThC nucleus ($^{212}_{83}$Bi), and depending on the nature of beta transition, the nucleus may be formed in the ground state or an excited state (cf. similar situation in the onset of a fine structure in alpha spectra). Long-range α-particles are those emitted from the

excited state of the nucleus ThC′. Table 13 contains the energy values for α-particles, the energy released during beta decay[9], the percentage of α- and β-particles, and the energy of the γ-quanta accompanying an alpha decay.

For simplicity, only one group of long-range α-particles, viz. α_1-particles with energy $T_{\alpha_1} = 9.492$ MeV, is included in Table 13. We see that the energy level diagram for the ThC′ nucleus shown

Table 13

Alpha-particle Group	Energy, MeV	Content, %	Alpha-particle Group	Energy, MeV	Content, %
α_0	8.780	100	β_2	1.520	5
α_1	9.492	0.0035	γ_1	0.729	—
β_1	2.250	40			

in Fig. 86 is confirmed by a comparison of the energies released during α_1-, β- and γ-transitions of nuclei.

The extremely low intensity (10^{-3}%) of long-range α-particles seems incomprehensible at first glance. This is absolutely out of tune with the relatively high fraction (1-10%) of beta transitions to the corresponding excited states of the nucleus ThC′.

As a matter of fact, the excitation in the ThC′ nucleus can be removed in two ways, viz. the emission of a long-range α-particle or of γ-quanta, the probability of the second process being much higher than that of the first one. Hence, the disintegration constants corresponding to these two processes are in relation $\lambda_{\alpha_{l.r.}} \ll \lambda_\gamma$.

Then, in accordance with Eq. (3.1.3), the radioactive transformation of the ThC′ nuclei will be described by the formula

$$dN = -(\lambda_\gamma + \lambda_{\alpha_{l.r.}}) N\, dt, \qquad (3.2.9)$$

where N is the number of radioactive nuclei at the instant t, and dN is the decrease in this number in time dt as a result of both radioactive processes.

But the number dN of nuclei disintegrating in time dt is equal to the total number of γ-quanta and long-range α-particles released during this period:

$$dN = dN_\gamma + dN_{\alpha_{l.r.}}. \qquad (3.2.10)$$

[9] We shall show in Sec. 3.3 that the energy released in beta transition does not coincide with the kinetic energy of the β-particle but is equal to its maximum value.

explained by the liquid drop model of the nucleus and another model, viz. the shell model, is required for this purpose (see Chap. 2).

The curve shown in Fig. 87 explains the existence of a practical boundary for alpha decay in heavy nuclei at $Z = 82$, α-activity in rare-earth nuclei, long-range α-particles for two isotopes of Po, and a lower boundary for the possible values of the kinetic energy of α-particles. All these features of alpha decay are due to the fact that

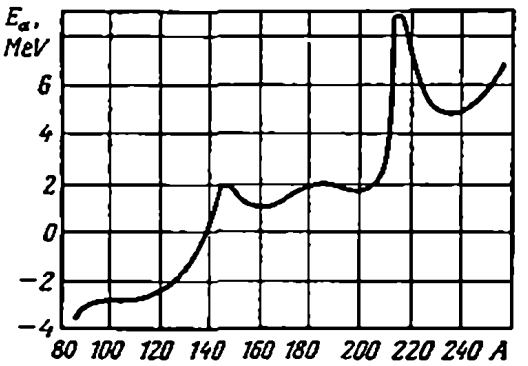

Fig. 87

in accordance with the Geiger-Nuttall law, alpha decay can be experimentally detected only when the alpha decay energy is sufficiently high.

Another experimental regularity, viz. a decrease in the energy of the α-particles of various isotopes of the same element with increasing mass number, is also explained by the liquid drop and the shell models of the nucleus.

It is found that if the derivative $(\partial T_\alpha/\partial A)_Z$ is calculated with the help of formulas (3.2.8), (2.1.10) and (3.2.12), we obtain a negative value of this derivative for A and Z corresponding to α-active nuclei. Hence the kinetic energy of α-particles from different isotopes of the same element decreases with increasing A. A departure from this regularity in the interval $209 < A < 215$ also cannot be explained by the liquid drop model. This departure is manifested in the region of nuclei containing 126 neutrons and, like the number 82, 126 also has special properties in the shell model.

3.2.3. Mechanism of Alpha Decay. Tunnelling

An analysis of alpha decay from the energy point of view helped in explaining a number of experimental regularities of this process. Only the nature of the Geiger-Nuttall law cannot be explained with the help of the energy level diagram for alpha decay.

According to the energy level diagram, alpha decay becomes possible when $\varepsilon_\alpha < 0$, i.e. when the energy of the original nucleus is

higher than the sum of energies of the product nucleus and the α-particle. But then why does not the alpha decay occur instantaneously (i.e. during the time $\tau \simeq R/v$, where R is the radius of the nucleus and v is the velocity of the α-particle)? The answer to this question was obtained from Rutherford's experiments on the scattering of α-particles from ThC′ ($^{212}_{84}$Po) by heavy radioactive nuclei, the results of which were interpreted by Gamow and by Henry and Condon.

Rutherford in 1927 established that α-particles from ThC′ with an energy $T_\alpha = 8.8$ MeV are scattered by heavy α-radioactive nuclei (which emit α-particles with a lower energy) according to the

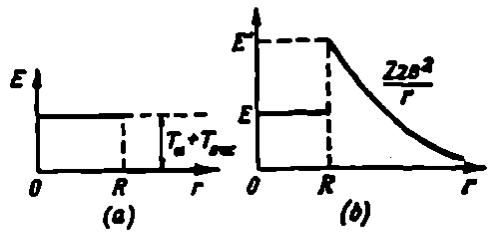

Fig. 88

Coulomb law. No scattering anomaly indicating the nuclear nature of interaction between ThC′ α-particles and the target nuclei was observed.

The results of Rutherford's experiment are schematically shown in Fig. 88. Figure 88*a* indicates the pattern of alpha decay: the distance r between the daughter nucleus and an α-particle is plotted along the abscissa axis, and hence $r < R$ corresponds to the state of the system before alpha decay and $r \gg R$ (R is the nuclear radius) corresponds to the after-decay period. The energy of the system is plotted along the ordinate axis. As usual, the sum of the rest masses of the daughter nucleus and the α-particle is taken as the zero energy. The level E corresponds to the energy of the original α-radioactive nucleus, and its value is less than 8.8 MeV (for example, $E \simeq 4$ MeV for uranium). Alpha decay corresponds to an increase in the value of r and a transition of the system from the energy state E to the zero state. The energy E is released as the kinetic energy of the α-particle and the daughter nucleus.

Figure 88*b* shows the scattering of the α-particles from ThC′ ($T_\alpha = 8.8$ MeV). The first stage of scattering (approaching of the nucleus by an α-particle) involves a decrease in the value of r and an increase in the energy of the system according to the Coulomb law from zero to the value E' which must be higher than 8.8 MeV at $r = R$ according to Rutherford's experiment. Thus, the system energy at $r \simeq R$ is higher than its initial value (E), as well as its final value (0).

The potential energy curve has a peak at $r = R$, called the *Coulomb potential barrier*. Hence it is not surprising that alpha decay does not occur instantaneously. What is surprising is the fact that it does occur at all, since the overcoming of a Coulomb barrier of height $E' > 8.8$ MeV by an α-particle with a kinetic energy of 4 MeV is forbidden in classical physics. However, it was shown by Gamow, and Henry and Condon in 1928-29 that the explanation of Rutherford's experiment lies in the effect of overcoming the potential barrier which is not feasible from the point of view of classical physics. Actually, in the world of microscopic particles (electrons, nucleons, α-particles) whose motion is described by quantum mechanics rather than by classical physics, there exists a possibility of *tunnelling*, i.e. the passage of a particle through a potential barrier.

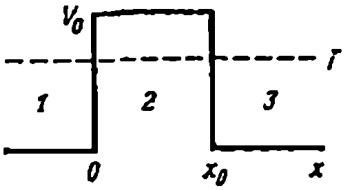

Fig. 89

This problem was formulated in quantum mechanics as follows. We consider a one-dimensional rectangular potential barrier of the form shown in Fig. 89.

It can be seen from the figure that the potential V assumes the following values:

$$V = \begin{cases} 0 & \text{for } x < 0 \text{ and } x > x_0, \\ V_0 & \text{for } 0 \leqslant x \leqslant x_0. \end{cases}$$

Suppose that a particle of mass m moves from left to right with a kinetic energy $T < V_0$. What is the probability of this particle penetrating the potential barrier V_0?

It is well known that the motion of microscopic particles in quantum mechanics is described by the *wave-function* ψ, the square of whose modulus characterizes the probability density of the particle being at this place. The wave-function ψ is the solution of the Schrödinger equation

$$\Delta\psi + (2m/\hbar^2)(E - V)\psi = 0. \qquad (3.2.13)$$

Here, ψ is the wave-function of the coordiantes (x, y, z), E is the total energy and V is the potential energy of the particle. The equation is simplified for the one-dimensional case:

$$\partial^2\psi/\partial x^2 + (2m/\hbar^2)(E - V)\psi = 0,$$

and can be written as follows for various regions shown in Fig. 89:

$$\partial^2\psi/\partial x^2 + (2m/\hbar^2)E\psi = 0 \quad (V = 0 \text{ and } T = E)$$

for region *1*,

$$\partial^2\psi/\partial x^2 + (2m/\hbar^2)\ (E - V)\ \psi = 0 \quad (V > E) \qquad (3.2.14)$$

for region *2*, and

$$\partial^2\psi/\partial x^2 + (2m/\hbar^2)\ E\psi = 0 \quad (V = 0 \text{ and } T = E)$$

for region *3*.

The solution is sought in the form $\psi(x) \propto \exp(ikx)$ for regions *1* and *3* and in the form $\psi(x) \propto \exp(kx)$ for the region *2*, where k is a real number.

Then the characteristic equation for regions *1* and *3* can be written as $-k^2 + 2mE/\hbar^2 = 0$, whence $k = \pm\sqrt{2mE}/\hbar$ and

$$\psi_1(x) = A\exp[i\sqrt{2mE}\,x/\hbar] + B\exp[-i\sqrt{2mE}\,x/\hbar],$$

where the first term $\psi_1^A = A\exp(i\sqrt{2mE}\,x/\hbar)$ corresponds to an incident wave, and the second term $\psi_1^B = B\exp[-i\sqrt{2mE}x/\hbar]$ represents a wave reflected at the boundary for $x = 0$. Similarly,

$$\psi_3(x) = a\exp(i\sqrt{2mE}\,x/\hbar) + b\exp(-i\sqrt{2mE}\,x/\hbar).$$

Here, $b = 0$, since the wave moves to the right in region *3*.

The characteristic equation for region *2* has the form

$$k^2 = (2m/\hbar^2)\ (V - E),$$

whence

$$k = \pm\sqrt{2m(V-E)}/\hbar$$

and

$$\psi_2(x) = \alpha\exp(\sqrt{2m(V-E)}\,x/\hbar) + \beta\exp(-\sqrt{2m(V-E)}\,x/\hbar).$$

The penetrability of the barrier, i.e. the fraction of particles passing from region *1* to region *3*, is the ratio of the probability flux densities of the transmitted and incident waves:

$$D = \frac{v_3|\psi_3|^2}{v_1|\psi_1^A|^2} = \frac{a^2}{A^2} \qquad (3.2.15)$$

(the velocities of the particle in regions *1* and *3* are assumed to be equal, $v_1 = v_3$).

The coefficient A characterizing the incident wave can be put equal to unity without any loss of generality. The remaining four coefficients B, a, α and β are obtained from the boundary conditions imposed on the functions and their derivatives:

$$\left.\begin{aligned} \psi_1(0) &= \psi_2(0), \quad \psi_1'(0) = \psi_2'(0), \\ \psi_2(x_0) &= \psi_3(x_0), \quad \psi_2'(x_0) = \psi_3'(x_0). \end{aligned}\right\} \qquad (3.2.16)$$

Solving Eqs. (3.2.14) and substituting the values thus obtained into Eq. (3.2.15), we obtain the following expression for the barrier penetrability D:

$$D = \exp\left[-\frac{2}{\hbar}\sqrt{2m(V-E)}\,x_0\right]. \qquad (3.2.17)$$

That the result should have this form is shown by the following simple arguments. The wave-function in regions *1* and *3* is of oscillatory nature, while in the region *2* it is exponential. Since the concentration of particles can only decrease upon passing through the

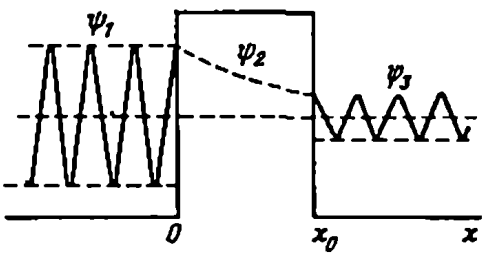

Fig. 90

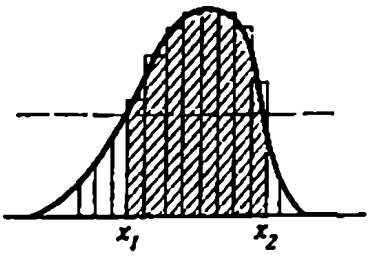

Fig. 91

barrier, the coefficient α must be much smaller than β and $\psi_2 \simeq \beta \exp[-\sqrt{2m(V-E)}\,x/\hbar]$ (Fig. 90).

The barrier penetrability is equal to the ratio of fluxes at the barrier boundaries:

$$D = \frac{v_2 |\psi_2(x_0)|^2}{v_1 |\psi_1^A(0)|^2},$$

where we use $\psi_2(x)$ at $x = x_0$ (at the end of region *2*). Since $v_1 = v_3$ (the incident and transmitted particles have the same energy) and $|\psi_1^A|^2 = A^2 = 1$, we get

$$D = |\psi_2(x_0)|^2 \propto \exp\left[-\frac{2}{\hbar}\sqrt{2m(V-E)}\,x_0\right]. \qquad (3.2.18)$$

This result can be easily extended to a barrier of arbitrary shape (Fig. 91), which can be split into several rectangular barriers. The overall effect of these barriers can be expressed in the form

$$D = \exp\left[-(2/\hbar)\int_{x_1}^{x_2}\sqrt{2m(V-E)}\,dx\right]. \qquad (3.2.19)$$

For the three-dimensional case, the barrier penetrability is given by

$$D = \exp\left[-(2/\hbar)\int_{r_1}^{r_2}\sqrt{2m(V-E)}\,dr\right]. \qquad (3.2.20)$$

As an example, let us consider the simplest case of a Coulomb potential $V_C = Zze^2/r$ acting between two charged particles with charges Z and z, for example between an α-particle and a nucleus in the case of alpha decay ($z = 2$). In this case, the expression (3.2.20) assumes the following form:

$$D = \exp\left[-\frac{2}{\hbar}\int_R^{r_T}\sqrt{2m\left(\frac{Zze^2}{r}-E\right)}\,dr\right], \qquad (3.2.21)$$

where $E = T$ is the kinetic energy of the α-particle, R is the radius of the nucleus, $r_T = Zze^2/T$ is the turning point which can be found from the condition $V_C(r_T) = T$, and m is the mass of the α-particle[11] (Fig. 92).

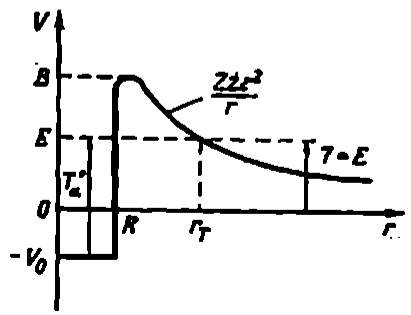

Fig. 92

It should be noted that the potential energy curve shown in Fig. 92 falls below the total energy level E in the region $r < R$, and above this level in the region $R < r < r_T$, so that the kinetic energy of the α-particle inside the nucleus is higher than outside it: $T_\alpha > T = E$.

The integral in (3.2.21) can be evaluated and we obtain the following result for the barrier penetrability:

$$D = \exp(-2g\gamma), \qquad (3.2.22)$$

where

$$g = \frac{R}{\lambda_B}, \quad \gamma = \sqrt{\frac{B}{T}}\arccos\sqrt{\frac{T}{B}} - \sqrt{1-\frac{T}{B}}.$$

$B = V_C(R) = Zze^2/R$ is the height of the Coulomb barrier, and $\lambda_B = \hbar/p_B = \hbar/\sqrt{2mB}$ is the de Broglie wavelength corresponding to the kinetic energy of the particle, equal to the barrier height ($T = B$).[12]

The height B of the Coulomb barrier (in MeV) can be easily obtained from the simple formula

$$B = \frac{Zze^2}{R} \approx \frac{Zz}{A^{1/3}}. \qquad (3.2.23)$$

Approximate values of B for different nuclei and particles are given in Table 14.

[11] Strictly speaking, we should use the reduced mass $\mu = mM/(m+M)$ in the radicand, where M is the mass of the nucleus; but since $m \ll M$, we get $\mu \approx m$.

[12] See formula (9.1.6).

Table 14

Nucleus	B_p, MeV	B_α, MeV	Nucleus	B_p, MeV	B_α, MeV
$^{4}_{2}He$	2.5	5	$^{118}_{50}Sn$	10	20
$^{16}_{8}O$	3.5	7	$^{238}_{92}U$	15	30

The value of $\lambda\!\!\!^{-}_T$ for nucleons having a kinetic energy T is determined from the formula

$$\lambda\!\!\!^{-}_T = \frac{\hbar}{\sqrt{2mT}} \simeq \frac{10^{-27}}{\sqrt{2\times 1.66\times 10^{-24}\times 1.6\times 10^{-6}T}} \simeq \frac{4.5\times 10^{-13}}{\sqrt{T}} \text{ cm}, \tag{3.2.24}$$

where T is in MeV.

The mass difference must be taken into account for other particles. The value of the function $\gamma = \sqrt{B/T}$ arccos $\sqrt{T/B} - \sqrt{1 - T/B}$ is usually taken from the graph (Fig. 93).

3.2.4. The Role of Centrifugal Barrier

We have considered above the simplest case of potential barrier when charged particles with the orbital angular momentum $l = 0$ interact. In a more general case, the α-particle may escape from a nucleus with $l \neq 0$.

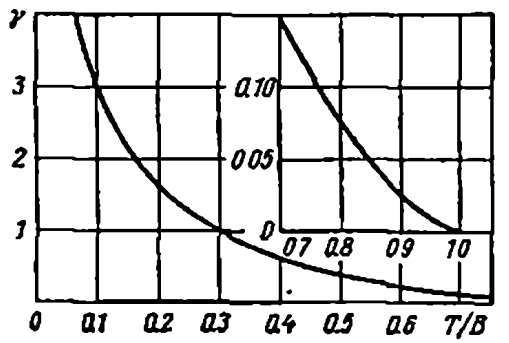

Fig. 93

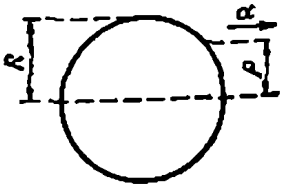

Fig. 94

This is so because the impact parameter ρ for α-particles escaping from the nucleus must not exceed the nuclear radius, i.e. $\rho \leqslant R$ (Fig. 94). However, according to quantum mechanics,

$$|l| = p\rho = \hbar\sqrt{l(l+1)},$$
$$\rho = (\hbar/p)\sqrt{l(l+1)} = \lambda\!\!\!^{-}\sqrt{l(l+1)}. \tag{3.2.25}$$

Hence, $\lambda\sqrt{l(l+1)} \leqslant R$ or $l \leqslant R/\lambda$. Using the formula $R = 1.4 \times 10^{-13} \times A^{1/3}$ cm for a heavy nucleus, we obtain $R \simeq 10^{-12}$ cm. In order to compute λ, we use formula (3.2.24) which assumes the form $\lambda = (2.25 \times 10^{-12})/\sqrt{T}$ for an α-particle, T being in MeV and λ in cm. If the kinetic energy of the α-particle is taken equal to its average value for radioactive nuclei, $\overline{T}_\alpha = 6$ MeV, we get $\lambda \simeq 10^{-12}$ cm. Hence, $l \leqslant 10$.

The possible values of l are determined by the selection rules (3.2.5) for angular momentum and parity, which follow from the corresponding conservation laws.

If $l \neq 0$ is allowed by the selection rules, we must take, besides the Coulomb potential, a centrifugal potential in the form

$$V_c = \hbar^2 l(l+1)/2mr^2. \qquad (3.2.26)$$

This quantum-mechanical formula for centrifugal potential can be written in analogy with the corresponding classical concepts. In classical mechanics, the centrifugal force is given by

$$-\partial V_c/\partial r = mv^2/r = m^2v^2r^2/mr^3 = |l|^2/mr^3,$$

where m is the mass of the particle, v its velocity, r the radius of motion (and the impact parameter), and $|l|$ the modulus of the orbital angular momentum.

In quantum mechanics, however, orbital angular momentum is a quantity which is quantized and assumes the following values:

$$|l|^2 = \hbar^2 l(l+1).$$

Consequently,

$$-\partial V_c/\partial r = \hbar^2 l(l+1)/mr^3,$$

whence

$$V_c = \frac{\hbar^2 l(l+1)}{2mr^2}.$$

The value of V_c at $r = R$ is called the height of the centrifugal barrier $B_c = \hbar^2 l(l+1)/2mR^2$. It can be easily seen that the classical condition $\rho \leqslant R$ (which leads to the set of possible values of l: $l \leqslant R/\lambda$) is equivalent to the condition $T \geqslant B_c$. In other words, the centrifugal barrier does not prevent α-particles with $l \leqslant R/\lambda$ from escaping (above-barrier effect). Conversely, the case $\rho > R$ ($l > R/\lambda$) corresponds to the condition $T < B_c$, when the centrifugal barrier impedes the escape of α-particles with $l > R/\lambda$ (under-barrier effect).

It is important to note that the existence of the centrifugal barrier is associated not with the charge, but rather with the nature of motion of the particle and with the existence of a nonzero orbital

angular momentum of this particle. Hence the centrifugal barrier must also be taken into consideration for the interaction of neutral particles (for example, neutrons) with nuclei.

Thus, in the general case of alpha decay, when $l \neq 0$, the potential of interaction of an α-particle with the nucleus is given by

$$V = V_C + V_c = Zze^2/r + \hbar^2 l(l+1)/2mr^2 \qquad (3.2.27)$$

(Fig. 95), while V in the expression for D is replaced by $V_C + V_c$:

$$D_{l\neq 0} = \exp\left[-\frac{2}{\hbar}\int_R^{r_T} \sqrt{2m(V_C + V_c - T)}\, dr\right]. \qquad (3.2.28)$$

This leads to an increase in the integral and a decrease in the barrier penetrability D: $D_{l\neq 0} < D_{l=0}$.

However, the effect of the centrifugal barrier cannot be strong. Firstly, it was shown that the orbital angular momentum l of the α-particles emitted by a nucleus is comparatively small: $l \leqslant R/\lambda \simeq 10$.

Secondly, the value of the centrifugal barrier which can be estimated at its highest point (for $r = R$) by the formula

$$B_c = \frac{\hbar^2 l(l+1)}{2m_\alpha R^2} = \frac{10^{-54} l(l+1)}{8 \times 1.66 \times 10^{-24} \times 10^{-24} \times 1.6 \times 10^{-6}} \simeq \frac{l(l+1)}{20} \text{ MeV} \qquad (3.2.29)$$

does not exceed 5 MeV even for the maximum value $l = 10$. On top of this, if we consider that the centrifugal potential decreases much faster than the Coulomb potential with increasing distance r, it becomes clear that the difference between $D_{l\neq 0}$ and $D_{l=0}$ cannot be too large (both the quantities have the same order of magnitude).

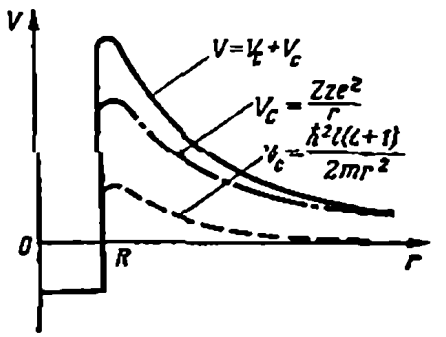

Fig. 95

The quantity $D_{l\neq 0}$ can be estimated for $l \leqslant 6$ with the help of the following formula:

$$D_{l\neq 0} = D_{l=0} \exp\left[-2.027 l(l+1) Z^{-1/2} A^{-1/6}\right].$$

According to this formula, the probability of emission of an α-particle with $l = 5$ by a heavy nucleus is lower than the probability of emission of an α-particle with $l = 0$ by a factor of 13 (5.5 for $l = 4$). Thus, α-particles with different l should be observed in alpha spectra with comparable intensities. This conclusion is confirmed experimentally.

The converse statement is also true. The interaction of α-particles (and other charged particles) with nuclei occurs with comparable probabilities for $l = 0$ as well as $l \neq 0$ right up to a certain value l_{cr} (see Sec. 5.4.2 for details). In this respect, the centrifugal barrier is manifested much more strongly in the interaction of neutral particles with nuclei. On account of the centrifugal barrier, slow neutrons can interact with nuclei only for $l = 0$.

3.2.5. Basic Principles of the Theory of Alpha Decay

The barrier penetrability D introduced above has a physical meaning of the probability that an α-particle inside the nucleus near its surface overcomes the potential barrier and leaves the nucleus. In order to obtain the experimentally measurable disintegration constant λ, we must also take into account the probability P of the formation of an α-particle from the protons and neutrons in the nucleus, and the frequency ν of collisions of the α-particle with the walls of the nucleus:

$$\lambda = P\nu D. \tag{3.2.30}$$

The calculation of P is reduced to determining one of the coefficients a_i in the expression

$$\psi_{nuc} = \sum_i a_i \varphi_i. \tag{3.2.31}$$

where ψ_{nuc} is the nuclear wave-function and φ_i are the wave-functions of certain nucleonic configurations. To be more specific, $P = |a_\alpha|^2$, where a_α is the coefficient of the wave-function φ_α describing the α-particle configuration involving two protons and two neutrons.

The estimation of P is a complicated and as yet unsolved problem in nuclear dynamics. A comparison with experiment (see below) shows that even-even nuclei in the ground state and in weakly excited states have identical values of P which can be taken equal to unity.

The collision frequency ν is the reciprocal of the time $\tau = 2R/v$ taken by an α-particle to cross the nucleus:

$$\nu = 1/\tau = v/2R, \tag{3.2.32}$$

where v is the velocity of the α-particle and R is the radius of the nucleus.

The quantity $k = P\nu$ is often called the pre-exponential factor. In the simplest interpretation given above, the pre-exponential factor is

$$k = \nu = v/2R. \tag{3.2.33}$$

In another estimate obtained by Landau, the pre-exponential factor is equated to the frequency of an oscillator for which the distance between levels is equal to the average separation δ between the levels of the nucleus under consideration. In this case, the factor k is given by

$$k = \delta/2\pi\hbar. \tag{3.2.34}$$

Both the estimates lead to the numerical factor $k \simeq 10^{20}$.

Thus, taking the pre-exponential factor into consideration, the probability of alpha decay can be written as

$$\lambda = k \exp\left[-\frac{2}{\hbar}\int_R^{r_T} \sqrt{2m(V-T)}\,dr\right] = k \exp[\varphi(T)], \tag{3.2.35}$$

whence

$$\ln \lambda = \ln k + \varphi(T). \tag{3.2.36}$$

With the help of simple transformations, we can reduce this equation to a more convenient form for experimental verification:

$$\log \lambda = A\sqrt{T_\alpha} + B, \tag{3.2.37}$$

where A and B are constants which vary insignificantly with the nuclear charge Z. It can be seen from this relation that a small variation of the kinetic energy T corresponds to a very large variation of λ. Analysis shows that for values of T_α encountered in α-particles of natural radioactive elements, formula (3.2.37) is identical with the Geiger-Nuttall law: $\log \lambda = A \log T_\alpha + B$.

The weak dependence of T_α on λ explains the existence of the lower boundary for the kinetic energy of α-particles. A change in T_α by just 10% changes the alpha disintegration constant by a factor of 10^3. For $T_\alpha < 2$ MeV, the half-life becomes so large that it is practically impossible to detect alpha activity. This also explains why there are practically no α-radioactive nuclei with $Z < 82$, when $\Delta E_\alpha \simeq 2$ MeV (see Fig. 87).

The alpha decay theory connects not only the disintegration constant λ with the kinetic energy T_α, but also the charge Z and radius R of the nucleus. All these constants are quite well known for a very large number of α-radioactive nuclei whose number has grown considerably over the last few years due to a large number of artificially obtained nuclei. Hence the alpha decay theory can be verified more accurately at present than with the help of the Geiger-Nuttall law.

Firstly, we can use Eq. (3.2.35) to estimate the radius of α-radioactive nuclei. Indeed, it can be seen from (3.2.35) that the quantity R varies very weakly upon a variation of λ, and hence the radius R can be estimated quite accurately from the value of λ.[13] Calculations made for a large number of α-radioactive nuclei have led to the following formula for determining the radius (in cm) of α-radioactive nuclei:

$$R = (1.45\text{-}1.5) \times 10^{-13} A^{1/3}.$$

This value of nuclear radius is larger than that obtained by other methods. This is so because measurement of quadrupole moments (see Sec. 1.7) shows that most of the α-radioactive nuclei are not spherically symmetric (as it was assumed in the theory of alpha decay), but have an ellipsoidal form with the ratio of semi-major and semi-minor axes as high as 1.3. Since the barrier penetrability for a non-spherical nucleus has different values at different parts of the nucleus and is especially large at the "edges", estimates of the nuclear radius obtained from alpha decay give an exaggerated value.

By using the obtained dependence of mass number A on radius R, we can verify the alpha decay theory by comparing λ, Z and T_α. In Fig. 96 theoretical curves are compared with experimental points for alpha transitions between the ground states of even-even nuclei. The figure reveals a good agreement between theoretical curves and experimental points. Such alpha transitions are called *allowed* transitions. If similar curves are constructed for other nuclei or for other alpha transitions in even-even nuclei, the experimental value of the disintegration constant is found to be several orders of magnitude lower than the theoretical value. In contrast to allowed transitions, such transitions are called *forbidden* transitions, and the ratio of the experimental half-life to the theoretical half-life is called *forbiddenness factor*:

$$F = T_{\text{exp}}/T_{\text{theor}}.$$

(Notice the arbitrariness in the term "forbidden" transitions. As a matter of fact, the "forbidden" transitions discussed here are allowed by all the conservation laws, see Sec. 3.2.6).

The forbiddenness factor F is equal to 10^2 on the average for odd-even and even-odd nuclei, and 10^3 for odd-odd nuclei. "Forbidden" transitions may be encountered among alpha transitions of the same nucleus. In this case, the "forbidden" alpha transitions violate the law of monotonic increase in the disintegration constant with the α-particle energy. This violation is manifested in that the highest intensity of the fine-structure spectrum of α-particles does not correspond to particles with the highest energy.

[13] For the same reason, Eq. (3.2.35) cannot be used for the inverse operation i.e. the estimation of λ from R.

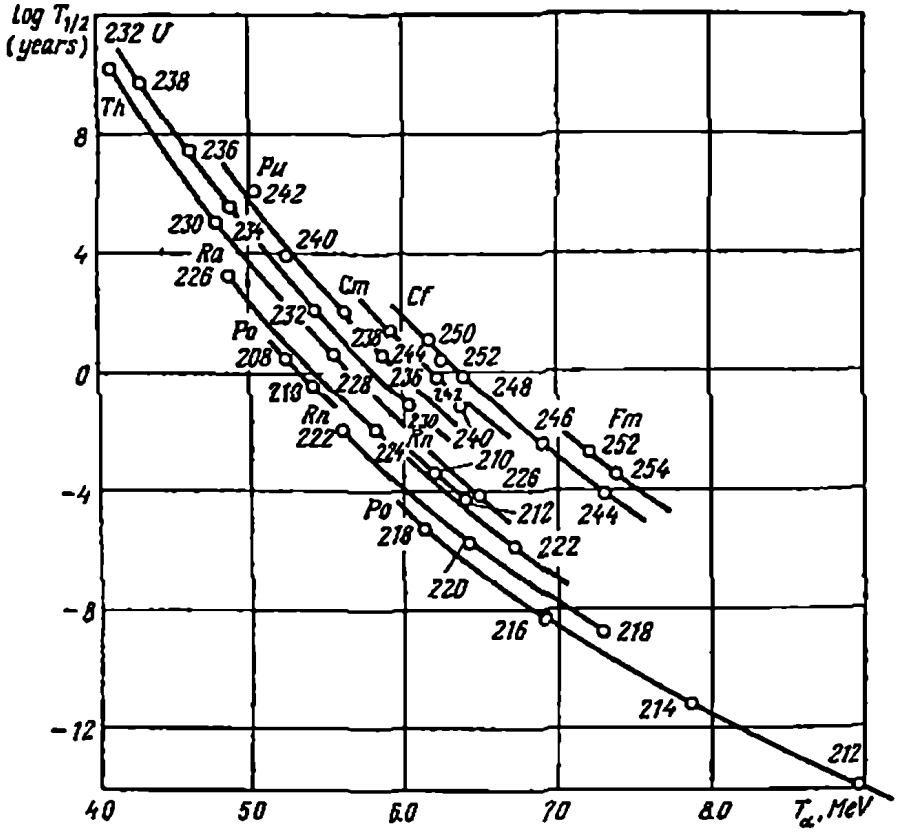

Fig. 96

As an example, Fig. 97 contains a scheme of alpha transitions of the nucleus $^{241}_{95}$Am. It can be seen from this scheme and Table 15 that all these alpha transitions are allowed by spin, parity and isospin. Consequently, it would appear that the relative probability

Table 15

Alpha-particle Group	P_1/P_i	l_α	ω, %
α_0	−1	1, 3, 5	0.4
α_1	−1	1, 3, 5	0.2
α_2	+1	0, 2, 4	85
α_3	+1	2, 4, 6	13

of alpha transition should decrease monotonically with increasing subscript of the α-particle. In actual practice, α-particles with the lowest energy have the highest probability of emission, while alpha transitions with a higher energy are forbidden.

The probability of alpha decay may be considerably lower than the theoretical value due to different reasons. One of these reasons is that the elementary theory does not consider the probability of formation of an α-particle and it was assumed that the nucleus contains α-particles in ready-made form. However, if we assume that an α-particle is formed in the nucleus at the instant of alpha decay, the probability of its formation must be different for different nuclei. Thus, for example, according to the shell model (see Sec. 2.3), the probability of formation of an α-particle in a nucleus with an odd number of nucleons must be lower than in nuclei with even number of nucleons.

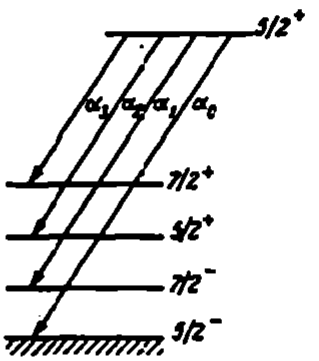

Fig. 97

Similarly, we can explain the nonmonotonicity in the probability of alpha transitions in the above example involving the $^{241}_{95}$Am nucleus. Apparently, α_0- and α_1-transitions are "forbidden" since they involve a more serious reconstruction of the nucleus (for example, a change in parity) than α_2- and α_3-transitions.

Another possible reason behind a decrease in the probability of alpha decay in comparison to the theoretical value is that the elementary theory of alpha decay does not take into consideration the momentum carried away by the α-particle. In this case, the difficulty lies in the fact that the high values of the forbiddenness factor F observed experimentally cannot be explained simply by an increase in the barrier height due to the centrifugal potential (whose role was shown to be insignificant), and we must take into consideration much more complicated phenomena. Such phenomena include, for example, the effect of the radiation field of the daughter nucleus on the escaping α-particle. In this case, the connection between the alpha decay probability and the orbital angular momentum l carried away by the α-particle must be manifested because different values of l correspond to the formation of the daughter nucleus in different states. Different types of radiation are emitted upon transitions from these states.

The theory of alpha decay is modified in other respects also. For example, the effect of the electron shell of α-radioactive nuclei on the probability of alpha decay is taken into account (decrease in the barrier height). All these attempts were successful to a certain extent, but the theory of alpha decay is still far from perfection.

3.2.6. Parity-forbidden Alpha Transitions

If the spin and parity of the parent and daughter nuclei do not obey relations (3.2.5), the corresponding alpha transition is forbidden by the parity conservation law and cannot be observed under ordinary conditions. However, it was mentioned in Sec. 1.6 that the prohibition imposed by the law of parity conservation is not absolute even though it leads to a drastic decrease in the probability of the corresponding process. It can be easily seen that in the case of alpha decay this decrease must be about $F^2 \simeq 10^{-14}$.

Indeed, according to Eq. (1.6.9), the wave-function of any energy state of the nucleus can be written in the form

$$\psi = \psi_{reg} + F\psi_{irreg},$$

where $F \simeq 10^{-7}$, while ψ_{reg} and ψ_{irreg} have different parities. If an alpha transition from a given level is forbidden, it means that ψ_{reg} does not satisfy the parity conservation law. But then this law must be satisfied by ψ_{irreg}, and hence an alpha transition from a forbidden level is allowed with a probability

$$|F\psi_{irreg}|^2 \sim F^2 \simeq 10^{-14}.$$

Of course, an alpha decay with such a low probability can be detected against a background of allowed alpha transitions with close energies only when certain special conditions are satisfied (past history of the formation of levels, favourable relations for the probabilities of competing processes, and so on). As an example, we consider the alpha decay of ^{16}O.

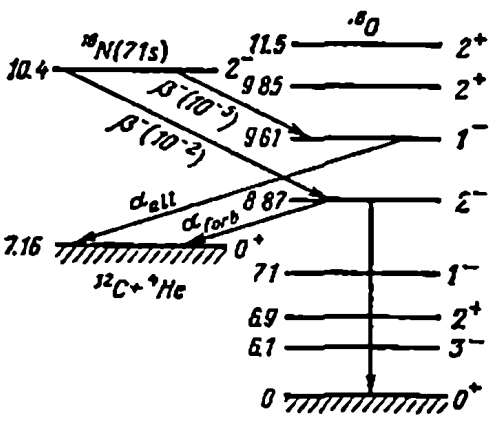

Fig. 98

Figure 98 shows the scheme of alpha, beta and gamma transitions for ^{16}N and ^{16}O nuclei. The energy of separation of an α-particle from the nucleus ^{16}O is $\varepsilon_\alpha = 7.16$ MeV. Hence alpha transitions from levels 11.5 MeV (2^+), 9.85 MeV (2^+), 9.61 MeV (1^-) and 8.87 MeV (2^-) are allowed from the energy point of view. Transitions from the first three levels are allowed by the laws of conservation of momentum and parity, and lead to the emission of α-particles with energies of 3.25, 2.01 and 1.83 MeV respectively. An estimation of the barrier penetrability for these alpha transitions leads to the value $\Gamma_{\alpha\,all.} \simeq 10^4$ eV, i.e. $\tau_{\alpha\,all.} \simeq 10^{-19}$ s. This time is so short that alpha decay takes place without any competition with gamma transitions ($\Gamma_\alpha > \Gamma_\gamma$).

Alpha transition from the level 8.87 MeV (2^-) is parity-forbidden, but still does occur due to an impurity introduced into this energy state by closely situated levels with the same momentum but opposite parity (2^+). It is this contribution that determines $F_l\psi_{\text{irreg}}$ (8.87 MeV). The amplitude of the impurity F_l is calculated by the methods of the perturbation theory for each lth level 2^+ according to the formula

$$F_l = \frac{(l,\ 2^+ | V_{\text{par. noncons.}}\ 8.87;\ 2^-)}{E_l - 8.87}. \qquad (3.2.38)$$

Taking into account the value of F_l obtained above, we get for the probability of a forbidden alpha transition $\Gamma_{\alpha\ \text{forb.}} \simeq 10^{-10}$ eV or $\tau_{\alpha\ \text{forb.}} \simeq 10^{-6}$ s. Thus, indeed $\tau_{\alpha\ \text{all.}}/\tau_{\alpha\ \text{forb.}} = 10^{-19}/10^{-6} = 10^{-14}$, which seems hopeless at first glance from the point of view of experimental observation of forbidden alpha transitions.

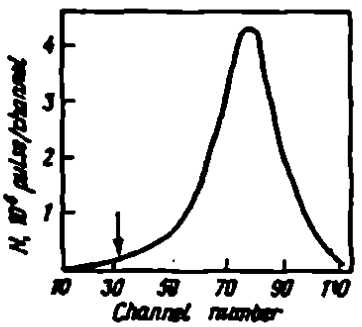

Fig. 99

In actual practice, the situation is much more satisfactory since the levels 9.61 and 8.87 MeV are formed as a result of the preceding beta decay of the ^{16}N nucleus ($T_{1/2}$=7.1 s), the beta transition to the level 8.87 MeV occurring with a partial probability 10^{-2} and to the level 9.61 MeV with a partial probability 10^{-4}. Thus, these levels of the ^{16}O nucleus are formed on the average after τ_β (8.87) $= 7 \times 10^2$ s and τ_β (9.61) $= 7 \times 10^4$ s respectively. Since both these values of τ_β are much higher than $\tau_{\alpha\ \text{all.}}$ as well as $\tau_{\alpha\ \text{forb.}}$, they determine the relative frequency of emission of α-particles (delayed α-particles). Moreover, it is found that the forbidden α-particles must be seemingly emitted about 10^8 times more frequently than the allowed particles. This, however, is not true since the above arguments do not take into consideration another factor, viz. the competing gamma transitions which are quite significant for the level 8.87 MeV (on account of a comparatively large value of $\tau_{\alpha\ \text{forb.}} \simeq 10^{-6}$ s). It turns out that $\Gamma_{\alpha\ \text{forb.}}/\sum\Gamma_\gamma = 10^{-10}/3 \times 10^{-3} \simeq 3 \times 10^{-8}$, and this gives the following expression for the ratio of the numbers of allowed and forbidden α-particles:

$$N_{\alpha\ \text{all.}}/N_{\alpha\ \text{forb.}} = 10^{-3}/3 \times 10^{-8} \simeq 3 \times 10^4.$$

This value is also quite high, but if we consider that the peak of the energy spectrum of allowed α-particles is considerably displaced with respect to the forbidden alpha line (Fig. 99) shown by an arrow in the figure, the ratio is found to be about (1-2) $\times 10^2$ in the region

of the forbidden alpha line. In other words, the background is "just" 100-200 times stronger than the effect. Such a weak effect is difficult, but not impossible, to detect.

The experiment was carried out as follows.[14] The target was chosen in the form of gaseous ^{15}N under a pressure of 1 atm, irradiated by deuterons with energy 3 MeV. As a result of the reaction

$$d + {}^{15}N \rightarrow {}^{16}N + p,$$

gaseous ^{16}N was formed and released from the target volume through thin capillaries into a small (about 2 cm^3) chamber which served as a low pressure detector (about 7 mm Hg). Alpha-particles left the chamber through thin windows and entered the detector. After preamplification, pulses from the detector were supplied to a 4 × 128-channel analyzer. The energy of α-particles was determined to within 10 keV.

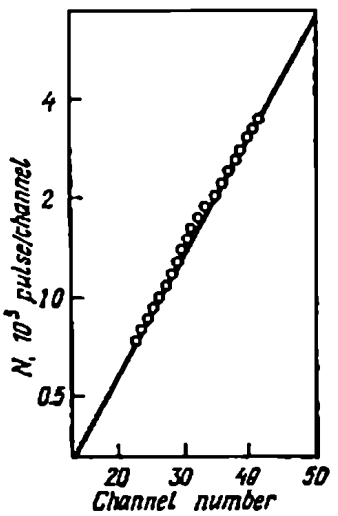

Fig. 100

The general form of the α-particle spectrum is shown in Fig. 99 where the channel number is plotted on the abscissa axis, and the pulse count per channel on the ordinate axis. The total number of registered particles was 1.3×10^8. The arrow indicates the region (channel No. 32) where forbidden α-particles must arrive. In this region, the number of counts per channel was about 1.5×10^5.

In order to distinguish a weak effect (about 10^3 counts per channel) against this background, an exponential approximation of the experimental curve was carried out for all the channels between 13 and 53, with the exception of channels Nos. 30-34 (Fig. 100). All the experimental points (including those obtained for channels Nos. 30-34) were then plotted on this curve. It can be seen from the figure that these last five points lie somewhat higher than the approximation curve.

The difference ΔN between the experimental values of the count and those given by the approximation curve is plotted in Fig. 101. This figure clearly shows the contribution of the forbidden α-particles for all five channels with numbers between 30 and 34 (and even for two neighbouring channels with numbers 28 and 29). Thus, we can assume that the existence of alpha transitions that are forbidden by parity has been proved experimentally.

[14] H. Hattig, K. Hünchen and H. Wäffler, *Phys Rev. Lett.*, 25, 14, 941 (1970).

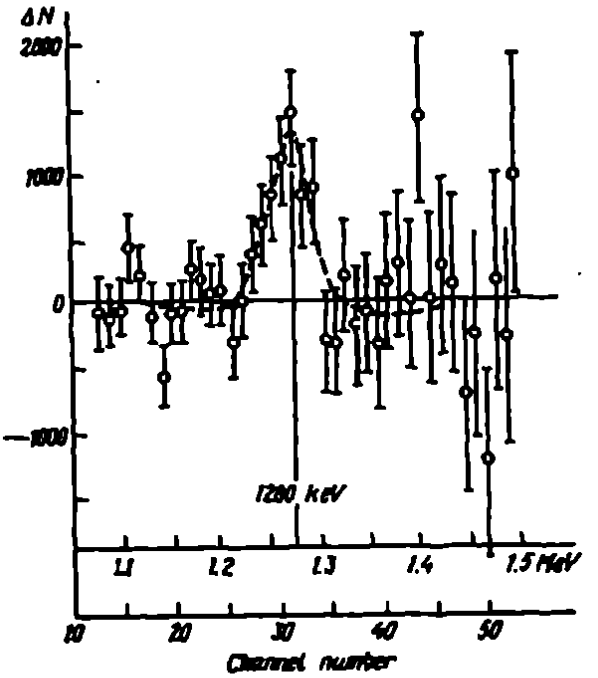

Fig. 101

The experimental results led to the estimation of $\Gamma_{\alpha\,forb.}^{exp}$ (8.87) according to the following obvious formula:

$$\frac{N_\alpha(8.87)}{N_\alpha(9.61)}=\frac{Y_\beta(8.87)}{Y_\beta(9.61)}\,\frac{\Gamma_\alpha(8.87)\,[\Gamma_\alpha(9.61)+\Sigma\,\Gamma_\gamma(9.61)]}{\Gamma_\alpha(9.61)\,[\Gamma_\alpha(8.87)+\Sigma\,\Gamma_\gamma(8.87)]},$$

where N_α (8.87) and N_α (9.61) are the numbers of registered α-particles emitted from levels 8.87 and 9.61 MeV respectively, $Y_\beta(8.87)/Y_\beta(9.61)$ is the ratio of yields of β-particles in transitions to levels 8.87 and 9.61 MeV, and $\Sigma\,\Gamma_\gamma$ (8.87) is the total radiation width for the level 8.87 MeV. Considering that $\Gamma_\alpha(8.87)\ll\Sigma\,\Gamma_\gamma$ (8.87) and $\Gamma_\alpha(9.61)\gg\Sigma\,\Gamma_\gamma(9.61)$, we finally obtain

$$\Gamma_\alpha(8.87)=\frac{N_\alpha(8.87)}{N_\alpha(9.61)}\,\frac{Y_\beta(9.61)}{Y_\beta(8.87)}\sum\Gamma_\gamma(8.87). \qquad (3.2.39)$$

Substituting into this formula the experimentally obtained values $N_\alpha(8.87)=7.100\pm1.800$, $N_\alpha(9.61)=1.3\times10^8$ and the values $Y_\beta(8.87)=(1.0\pm0.2)\times10^{-3}$, $Y_\beta(9.61)=(1.19\pm0.10)\times10^{-4}$ and $\sum\Gamma_\gamma(8.87)=2.7\pm0.5$ MeV known from other experiments, we find $\Gamma_{\alpha\,forb.}^{exp}=(1.8\pm0.8)\times10^{-10}$ eV. This value is in good agreement with the theoretical value $\Gamma_{\alpha\,forb.}^{theor}$.

3.3. Beta Decay

3.3.1. Three Types of Beta Decay. Properties of Beta-radioactive Nuclei

Beta decay is the process of spontaneous transformation of an unstable nucleus into an isobar nucleus with charge differing by $\Delta Z = \pm 1$ following the emission of an electron (positron) or the capture of an electron. The half-life of β-radioactive nuclei varies from 10^{-2} s to 2×10^{15} years. The energy of beta decay lies between 18 keV (for ${}^{3}_{1}\mathrm{H}$) and 16.6 MeV (for ${}^{12}_{7}\mathrm{N}$).

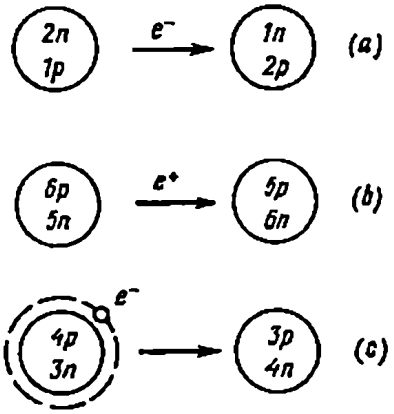

Fig. 102

There are three types of beta decay, viz. β^--decay, β^+-decay and *e*-capture (or *K*-capture).

If we do not take into consideration the beta decay of the neutron, the simplest example of the electron beta decay is the beta decay of tritium:

$$ {}^{3}_{1}\mathrm{H} \xrightarrow[12 \text{ years}]{\beta^-} {}^{3}_{2}\mathrm{He}. $$

This process is schematically shown in Fig. 102*a*. The beta decay of tritium is ultimately reduced to the transformation of one neutron into a proton.

It was shown in Sec. 1.3 that the energy condition for the possibility of the β^--decay of a nucleus with mass number A and charge Z is written as follows:

$$ M(A, Z) > M(A, Z+1) + m_e. \qquad (3.3.1) $$

The mass of the parent (β^--radioactive) nucleus must be higher than the sum of the masses of the daughter nucleus and the electron. This condition can be expressed in terms of the masses of the atoms if we add Zm_e to the left- and right-hand sides of the inequality (3.3.1):

$$ M_{\mathrm{at}}(A, Z) > M_{\mathrm{at}}(A, Z+1). \qquad (3.3.2) $$

The energy liberated in the process of β^--decay is [15]

$$ E_{\beta^-} = [M_{\mathrm{at}}(A, Z) - M_{\mathrm{at}}(A, Z+1)]c^2. \qquad (3.3.3) $$

For the example considered above, $E_{\beta^-} = 0.018$ MeV.

[15] This equality and other similar equalities are valid to within the binding energy of electrons in atoms.

An example of the positron beta decay is the disintegration of the $^{11}_{6}C$ nucleus, accompanied by the emission of a positive electron, viz. a positron:[18]

$$^{11}_{6}C \xrightarrow[20.4\ \text{min}]{\beta^+} {}^{11}_{5}B.$$

In this case, the β^+-decay of the $^{11}_{6}C$ nucleus is reduced as if to the transformation of a proton into a neutron (see Fig. 102*b*). Naturally, this transformation must be treated as conditional, since the mass of the proton is less than that of the neutron and consequently the positron decay of a free proton is impossible. However, for a proton bound in a nucleus, such a transformation is possible since the missing energy is supplied by the nucleus.

The energy condition for the β^+-decay is written in analogy with the β^--decay condition as follows:

$$M(A, Z+1) > M(A, Z) + m_e. \qquad (3.3.4)$$

Adding $(Z+1)m_e$ to both sides of this inequality and going over from nuclear masses to atomic masses, we can write (3.3.4) in the following form:

$$M_{at}(A, Z+1) > M_{at}(A, Z) + 2m_e. \qquad (3.3.5)$$

The energy liberated during β^+-decay is

$$E_{\beta^+} = [M_{at}(A, Z) - M_{at}(A, Z-1) - 2m_e]c^2. \qquad (3.3.6)$$

The value of E_{β^+} for β^+-decay of the nucleus $^{11}_{6}C$ is $\simeq 1$ MeV.

The third type of beta radioactivity, viz. electron capture (ϵ-capture) involves the capture of an electron by the nucleus from its own electron shell. The nature of ϵ-capture was disclosed during the investigation of the X-rays accompanying it. It was found that the X-ray radiation accompanying an ϵ-capture corresponds to the transition of electrons to the vacancy in the electron shell of the atom $(A, Z-1)$ formed as a result of the ϵ-capture. The phenomenon of ϵ-capture is quite significant for heavy nuclei whose K-shells are quite close to the nucleus. Besides the capture of an electron from the K-shell (K-capture), capture from L-shell (L-capture), M-shell (M-capture), etc. are also observed.

The specific nature of the ϵ-capture process (i.e. capture, and not emission, of an electron by the nucleus) is manifested in that the disintegration constant λ is weakly dependent on external conditions in the case of ϵ-capture. This is due to the fact that the ϵ-capture probability is proportional to the density of electrons in the nucleus (i. e. to the quantity $|\psi_e|^2$ for the centre of the nucleus), which depends on the strength of the chemical bond.

[18] See. Sec. 5.1, Vol. II for the discovery and properties of positrons.

An example of light K-radioactive nucleus is the nucleus $^{7}_{4}Be$ which captures a K-electron and is transformed into the nucleus $^{7}_{3}Li$:

$$^{7}_{4}Be \xrightarrow[53.6\ days]{K} {}^{7}_{3}Li.$$

Figure 102c shows the e-capture of $^{7}_{4}Be$.

The energy condition for the possibility of K-capture is written in the following form:

$$M(A, Z) < M(A, Z+1) + m_e. \tag{3.3.7}$$

Adding the mass of Z electrons to both sides, we get

$$M_{at}(A, Z) < M_{at}(A, Z+1). \tag{3.3.8}$$

The energy released during K-capture is given by

$$E_K = [M_{at}(A, Z+1) - M_{at}(A, Z)]\, c^2. \tag{3.3.9}$$

The value of E_K for the example under consideration is 0.864 MeV.

Comparing the inequalities (3.3.2), (3.3.5) and (3.3.8), we arrive at the following conclusions.

1. Since the nucleus (A, Z) is β^--radioactive in the case when $M_{at}(A, Z) > M_{at}(A, Z+1)$, and K-radioactive when $M_{at}(A, Z) < M_{at}(A, Z+1)$, there must not exist, generally speaking, two stable neighbouring isobars. Exceptions are possible only when the corresponding transitions are forbidden due to a large difference in the total angular momenta of the two nuclei (see Sec. 3.3.5d).

2. When the inequality (3.3.5) is satisfied, the inequality (3.3.8) is automatically satisfied, and hence transitions between corresponding nuclei are possible via β^+-decay as well as through K-capture. As an example, we can consider the nucleus $^{52}_{25}Mn$ which is transformed into the nucleus $^{52}_{24}Gr$ as a result of β^+-decay in 35% of cases and as a result of K-capture in 65% of cases.

3. For some nuclei (A, Z), the condition (3.3.5) with respect to the isobar $(A, Z-1)$ and the condition (3.3.2) with respect to the isobar $(A, Z+1)$ may be satisfied simultaneously. In this case, the nucleus (A, Z) will simultaneously undergo all three types of beta transformations. An example is the nucleus $^{64}_{29}Cu$ which emits an electron in 40% of cases, undergoes an electron capture in 40% of cases, and emits a positron in 20% of cases (Fig. 103).

4. For the mass ratio of isobars $(A, Z-1)$, (A, Z) and $(A, Z+1)$ indicated in the above example, when successive beta transformations of the type $(A, Z-1) \xrightarrow{\beta^-} (A, Z) \xrightarrow{\beta^-} (A, Z+1)$ are forbidden, the possibility of a double beta decay [if $M_{at}(A, Z-1) > M_{at}(A, Z+1)$] must be taken into consideration, when the nucleus $(A, Z-1)$ is directly transformed into the nucleus $(A, Z+1)$

by simultaneously emitting two electrons. This possibility will be discussed in Sec. 5.4.2, Vol. II.

5. In the case of β^- (β^+)-decay of a nucleus with a large excess (deficiency) of neutrons, the daughter nucleus may be formed in an excited state whose excitation energy W exceeds the separation energy ε_N of a neutron (proton). In this case, the daughter nucleus emits a delayed (by the beta decay duration) neutron (proton).

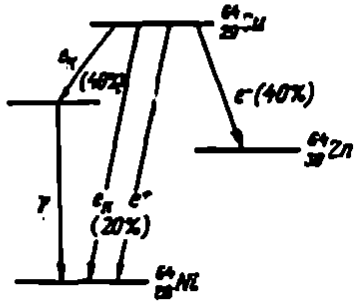

Fig. 103

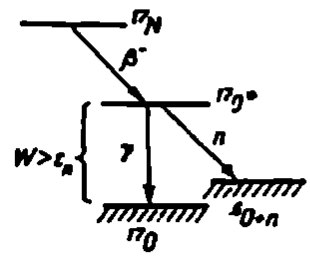

Fig. 104

Figure 105 shows schematically the emission of delayed protons by the excited nucleus ${}^{17}_{9}F^*$ formed as a result of β^+-decay of ${}^{17}_{10}Ne$:

$$ {}^{17}_{10}Ne \xrightarrow[T_{1/2}=0.1\ s]{\beta^+} {}^{17}_{9}F^* \xrightarrow[T_{1/2}=0.1\ s]{p} {}^{16}_{8}O + p. \qquad (3.3.10) $$

A similar scheme of delayed neutron emission by the excited nucleus ${}^{17}_{8}O^*$ formed during β^--decay of ${}^{17}_{7}N$ is shown in Fig. 104:

$$ {}^{17}_{7}N \xrightarrow[T_{1/2}=4.1\ s]{\beta^-} {}^{17}_{8}O^* \xrightarrow[T_{1/2}=4.1\ s]{n} {}^{16}_{8}O + n. \qquad (3.3.11) $$

It is interesting to note that in both these cases, the final nucleus is the double magic nucleus ${}^{16}_{8}O^8$ characterized by a low adhesion energy ε_N of the ninth nucleon. This circumstance ensures the validity of the inequality $W > \varepsilon_N$. Delayed protons and neutrons will be discussed in detail in Secs. 3.5 and 7.4.2 respectively.

6. A comparison of the beta decay energies E_β and half-lives $T_{1/2}$ (β) shows that β-radioactive nuclei can be roughly divided into several groups with approximately identical values of the quantity

$$ \log F(E_\beta)\tau. \qquad (3.3.12) $$

where

$$ F(E_\beta) \sim (1 + E_\beta/m_e c^2)^5 \text{ for } E_\beta \gg m_e c^2, $$

and

$$ \tau = T_{1/2}(\beta)/\ln 2. $$

The interpretation of the continuous nature of the energy spectrum of beta decay electrons caused at first a great deal of difficulties. It appeared that like the process of alpha decay in which α-particles having definite energy values are emitted, beta decay must also lead to the emission of monochromatic electrons whose energies are determined in accordance with (3.3.1) by the energy states of the parent nucleus and the daughter nucleus:[17]

$$T_e = E_{\beta^-} = E_1 - E_2 - m_e c^2. \qquad (3.3.14)$$

Such an assumption, however, is not in agreement with the continuous nature of the experimentally observed spectrum of beta decay electrons.

The following hypotheses were put forth to explain the observed disparity between the electron energy and the energy liberated in beta decay:

1. A beta transition is accomplished to various excited states of the daughter nucleus, and the excitation energy is then released in the form of gamma radiation. If the number of levels is very large, a practically continuous spectrum of electrons and γ-quanta should be observed according to this mechanism. However, it was shown experimentally that the spectrum of γ-quanta accompanying a beta decay has a discrete nature and in some cases the beta decay is not accompanied by the emission of γ-quanta at all.

2. Monochromatic electrons with energy E_β are emitted in the process of beta decay, but a part of their energy is lost due to interaction with the electron shells of the same atom as well as the neighbouring atoms (in the target, in the counter walls, and so on)

In order to verify this hypothesis, Ellis and Wooster conducted in 1927 a calorimetric experiment to determine the total energy of beta decay electrons. A thick-walled copper calorimeter contained a β-sample [18] RaE ($^{210}_{83}$Bi) wrapped in a lead foil which was opaque to electrons. The total energy of beta decay electrons was liberated in the lead foil shielding the sample and could be measured. If the assumption made above were correct, the energy would be equal to the maximum energy in the RaE beta spectrum (1.2 MeV). However, measurements showed that the liberated energy is close to the average value of energy for the beta spectrum of RaE:

$$T_{exp} \simeq 0.33 \text{ MeV}.$$

3. The law of conservation of energy is not obeyed in a beta decay process. This hypothesis was widely discussed but was regarded as implausible.

[17] This equality is valid to within T_{nuc}, the kinetic energy of the recoil nucleus ($T_{nuc} \ll T_e$).

[18] This sample is chosen because the beta decay of RaE is practically not accompanied by gamma radiation.

4. In addition to the electron with energy T_e, another particle is emitted in the process of beta decay, viz. the neutrino ν which takes away an energy equal to $E_\beta - T_e$ so that the total energy of the electron and the neutrino is equal to the beta decay energy E_β. This hypothesis, which was first put forth by Pauli in 1931, is widely accepted at present and has been experimentally confirmed.

The properties of the neutrino can be easily predicted. In view of the charge conservation law and the fact that a neutrino does not ionize the atoms of the medium through which it passes, it can be concluded that the charge of the neutrino must be equal to zero. The mass of the neutrino also must be zero (or in any case much smaller than the electron mass, see Secs. 3.3.3 and 3.3.4). This is due to the fact that neutrino carries away most of the beta decay energy. The absence of ionization indicates that the magnetic moment of the neutrino is equal to zero or has an extremely low value[19]. The spin of the neutrino must be half-integral. This is so because the spin of the atomic nucleus (integral or half-integral) is determined, as it was shown in Sec. 1.5, by the mass number A. During beta decay, the value of A does not change and hence the spin of the nucleus must remain the same. However, the electron leaving as a result of beta decay carries away a spin $\hbar/2$, and this should change the spin of the nucleus. The contradiction can be removed by assigning a half-integral spin to the neutrino. Theoretical calculations made for the shape of the beta spectrum under various assumptions concerning the spin of the neutrino show that its spin must be equal to $\hbar/2$. These arguments are valid for β^--as well as β^+-decay.

3.3.3. Experimental Verification of the Existence of Neutrino

The specific properties of the neutrino ($z_\nu = 0$, $m_\nu \simeq 0$, $\mu_\nu \simeq 0$) make the experimental detection of this particle extremely difficult. An estimate of the interaction cross section of the neutrino with the nucleus gives a value $\sim 10^{-44}$ cm^2. This corresponds to the mean free path in a condensed medium ($n = 10^{23}$ cm^{-3}) given by

$$l = 1/n\sigma = 1/10^{23} \times 10^{-44} = 10^{22} \text{ cm} = 10^{17} \text{ km},$$

while the corresponding value in the nuclear matter ($n = 10^{38}$ cm^{-3}) is

$$l = 1/n\sigma = 1/10^{38} \times 10^{-44} = 10^{6} \text{ cm} = 10 \text{ km}$$

(i.e. 10^{13} times more than the nuclear dimensions).

Obviously, such a weak effect caused by the neutrino can be detected only when there is a high-intensity flux of these particles. Hence

[19] According to the most accurate estimates, $\mu_\nu < 10^{-9}\mu_B$; the exact value of the neutrino mass and its other properties are discussed in detail in Sec. 5.4, Vol. II.

the existence of neutrino was confirmed only indirectly in early experiments.

Leipunskii was the first to set up in 1936 an experiment to detect the effect associated with the existence of a neutrino.

The idea behind the experiment lies in comparing the energy spectra of electrons and recoil nuclei formed during beta decay. If the process of beta decay is not accompanied by the emission of a neutrino, the momenta of the electron and the recoil nucleus must satisfy the following simple relation:

$$p_e + P_{\text{rec. nuc.}} = 0. \tag{3.3.15}$$

Hence

$$|p_e| = |P_{\text{rec. nuc.}}|. \tag{3.3.16}$$

If, however, a neutrino is emitted during the beta decay, we get in accordance with the momentum conservation law

$$p_e + p_\nu + P_{\text{rec. nuc.}} = 0 \tag{3.3.17}$$

and

$$|p_e| \neq |P_{\text{rec. nuc.}}|. \tag{3.3.18}$$

Since both the momenta (p_e and $P_{\text{rec.nuc.}}$) refer to charged particles, it is possible to measure them in principle.

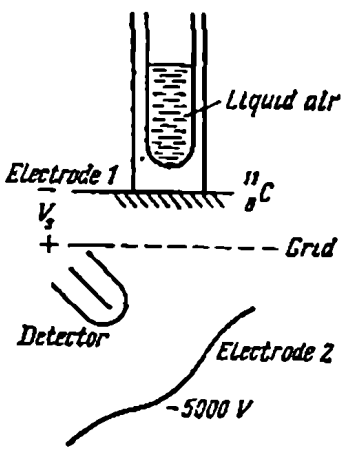

Fig. 109..

Figure 109 is a schematic of Leipunskii's experiment. The β^+-decay of the carbon isotope $^{11}_{6}C$ was investigated in it:

$$^{11}_{6}C \xrightarrow[20.4\ \text{min}]{\beta^+} {}^{11}_{5}B.$$

With the help of liquid air, $^{11}_{6}C$ is adsorbed on electrode *1*. As a result of beta decay, the atom $^{11}_{5}B$ receives recoil energy and leaves the substrate in the form of an ion (the electronic work function of the substrate is higher than the ionization potential). The escaping ions fall in the region between electrode *1* and a grid to which a stopping potential V_s is applied. Ions, whose energy exceeds the grid potential, pass into the region between the grid and electrode *2* with a high accelerating potential. The ions accelerated in this region knock out secondary electrons from electrode *2*. These secondary electrons are registered by a detector. The energy distribution of the recoil nuclei can be determined by observing the dependence of the detector count on the stopping potential on the grid. It was shown by the

experiment that this energy distribution does not correspond to the beta decay without a neutrino.

To obtain quantitative results, it was proposed by Alikhanov and Alikhanyan to use the K-capture of an electron by the $^{7}_{4}$Be nucleus. Like beta decay, the K-capture also must be accompanied by the emission of a neutrino. This is so because the mass number A of the nucleus does not change as a result of the K-capture. Consequently, in accordance with Sec. 1.5, the spin of the nucleus must also remain unchanged. However, the capture of an electron with half-integral spin by the nucleus must change the spin of the latter. This discrepancy is removed by assuming that K-capture is accompanied by the emission of a neutrino. Only two particles are formed during K-capture: the recoil nucleus and the neutrino. Hence energy will be distributed strictly in a definite way between these two particles. In other words, the recoil nuclei formed in this case must be monoenergetic.[20]

The energy of the recoil nucleus $^{7}_{3}$Li formed during the K-capture of $^{7}_{4}$Be can be easily calculated. The total energy liberated during K-capture is

$$E_K = [M_{at}(^{7}_{4}\mathrm{Be}) - M_{at}(^{7}_{3}\mathrm{Li})]\,c^2 = 0.864 \text{ MeV}.$$

Most of this energy is carried away by the neutrino. Indeed, it follows from the law of momentum conservation that

$$p_\nu = p_{\text{rec. nuc.}} = \sqrt{2M_{\text{rec. nuc.}} T_{\text{rec. nuc.}}},$$

$$T_{\text{rec. nuc.}} = \frac{p^2_{\text{rec. nuc.}}}{2M_{\text{rec. nuc.}}} = \frac{p^2_\nu}{2M_{\text{rec. nuc.}}} = \frac{E^2_\nu}{2M_{\text{rec. nuc.}}c^2}$$

$$= \frac{(E_K - T_{\text{rec. nuc.}})^2}{2M_{\text{rec. nuc.}}c^2} \simeq \frac{E^2_K}{2M_{\text{rec. nuc.}}c^2} = \frac{0.864^2 \text{ MeV}^2}{2 \times 7 \times 931 \text{ MeV}} \simeq 57.3 \text{ eV}.$$

The experiment must involve the measurement of the energy of the recoil nucleus and a comparison of T_{exp} with the calculated value. Because of the outbreak of war, this experiment could not be set up. An absolutely analogous experiment was carried out by Allen (USA) in 1942 (Fig. 110).

A thin layer of $^{7}_{4}$Be is deposited on a platinum plate (source). As a result of K-capture, $^{7}_{4}$Be atoms are transformed into $^{7}_{3}$Li atoms which leave the plate in the form of ions on account of the recoil energy. Positive $^{7}_{3}$Li ions are accelerated between the source and grid 1 by a potential difference $V \simeq -$ (100-200) V and retarded by an alternating stopping potential between grids 1 and 2. Ions

[20] When a particle at rest disintegrates into two, there are two unknown velocities which satisfy two equations, viz. the law of conservation of momentum and the law of conservation of energy. This system of equations has a unique solution.

with a definite energy are counted with the help of a photomultiplier having a Geiger counter at the outlet (the accelerating potential between grid 2 and the photomultiplier is equal to 3.6 kV).

A comparison of the number of ions impinging on the photomultiplier for different values of the stopping potential showed that the maximum energy of the recoil atoms is about 48 eV. The agreement with the expected value (57 eV) can be considered quite satisfactory, especially if we consider that a part of the ion energy is absorbed at the source. This result was confirmed by the results of later experiments which gave a value 56.6± 1.0 eV for $T_{\text{rec. nuc.}}$.

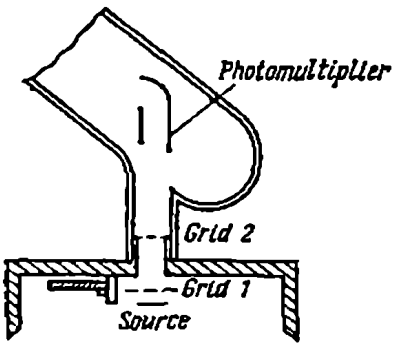

Fig. 110

Strictly speaking, the experiments described above cannot serve as the experimental verification of the existence of neutrino, since they are not based on the observation of an effect caused directly by a free neutrino. The result of Allen's experiment essentially proves that the assumption concerning the existence of a particle with the properties of neutrino is in accord with the conservation laws.

A direct experiment on detecting the interaction of a free neutrino with matter was set up only in 1953 by Cowan and Reines (see Sec. 5.4.3, Vol. II). The interaction cross section of the neutrino was found to be about 10^{-43} cm^2.

Thus, the hypothesis that a neutrino is emitted during beta decay was experimentally proved. Accordingly, the beta decay of the nucleus (A, Z) can be represented as follows:

$$(A, Z) \rightarrow (A, Z \mp 1) + e^{\pm} + \nu, \qquad (3.3.19)$$

A more detailed investigation of the properties of the neutrino shows that besides the neutrino ν, there also exists an antineutrino $\tilde{\nu}$ which differs from the former in the nature of its interaction with matter. Neutrino and antineutrino are a particle and an antiparticle, and hence $m_{\tilde{\nu}} = m_{\nu}$, $s_{\tilde{\nu}} = s_{\nu}$ and $\tau_{\tilde{\nu}} = \tau_{\nu}$. It is assumed that β^--decay is accompanied by the emission of an antineutrino, while a neutrino is emitted in the processes of β^+-decay and e-capture.

Neutrinos and antineutrinos emitted in the process of beta decay are called *electron neutrino* and *antineutrino* and are denoted by ν_e and $\tilde{\nu}_e$. Accordingly, the β^+-decay and e-capture are described as

follows:

$$(A, Z) \rightarrow (A, Z+1) + e^- + \tilde{\nu}_e, \quad (3.3.20)$$

$$(A, Z) \rightarrow (A, Z-1) + e^+ + \nu_e, \quad (3.3.21)$$

$$(A, Z) \xrightarrow{e} (A, Z-1) + \nu_e. \quad (3.3.22)$$

It was shown in 1962 that besides electron neutrino and antineutrino, there also exist *muon neutrino* (ν_μ) and *muon antineutrino* ($\tilde{\nu}_\mu$). The emission of these particles accompanies the decay of $\pi^\pm$-mesons:

$$\pi^+ \rightarrow \mu^+ + \nu_\mu, \quad (3.3.23)$$

$$\pi^- \rightarrow \mu^- + \tilde{\nu}_\mu \quad (3.3.24)$$

(see Sec. 5.6, Vol. II for detailed properties of ν_e, $\tilde{\nu}_e$, ν_μ and $\tilde{\nu}_\mu$).

Finally, τ-leptons were discovered in 1975. The disintegration of these particles is accompanied by the emission of the third type of neutrinos and antineutrinos:

$$\tau^- \rightarrow \pi^- + \nu_\tau, \quad \tau^+ \rightarrow \pi^+ + \tilde{\nu}_\tau, \text{ etc.} \quad (3.3.25)$$

(see Sec. 5.8, Vol. II).

3.3.4. Neutrino Mass

According to formula (3.3.19), the energy balance equation for beta decay can be written as follows:

$$E_\beta = T_e + T_\nu + m_\nu c^2 + T_{\text{rec. nuc.}}. \quad (3.3.26)$$

Neglecting $T_{\text{rec. nuc.}}$, which is a very small quantity, we get

$$E_\beta \simeq T_e + T_\nu + m_\nu c^2 \quad (3.3.27)$$

or

$$E_\beta \simeq T_e^{\max} + m_\nu c^2. \quad (3.3.28)$$

This relation can be used for estimating the rest mass of the neutrino (antineutrino)[21]. It is equal to the difference in the beta decay energy (calculated from the masses of the parent and daughter nuclei) and the maximum kinetic energy of electrons:

$$m_\nu c^2 = E_\beta - T_e^{\max} \quad (3.3.29)$$

The most accurate estimate can be obtained by comparing the values of E_β and $T_e^{\max}$ for light radioactive nuclei having low values of E_β and $T_e^{\max}$.

[21] As particle and antiparticle, ν and $\tilde{\nu}$ must have the same mass.

The first estimates of the neutrino mass (actually, the antineutrino mass) were made by Hanna and Pontecorvo in 1949, who obtained a value $m_{\tilde{\nu}_e} < 1$ keV. Later, this result was progressively refined and Tret'yakov *et al.* (Institute of Theoretical and Experimental Physics, Moscow) in 1976 obtained a record value for the upper bound of the neutrino mass:

$$m_{\tilde{\nu}_e} < 35 \text{ eV} = 0.7 \times 10^{-4}\, m_e. \qquad (3.3.30)$$

As a result of a progressive decrease in the upper bound of $m_{\tilde{\nu}_e}^{\exp}$ on the one hand, and theoretical considerations on the other hand (see Sec. 5.4, Vol. II), the most probable value for the neutrino mass was assumed to be $m_{\nu_e} \equiv 0$. However, arguments have been put forth in recent years in favour of the version $m_{\nu_e} \neq 0$ (see Sec. 5.4.5, Vol. II). At the same time, the measuring techniques for beta spectra were developed to such an extent that it became possible to estimate not only the upper bound of the neutrino mass, but lower bound as well.

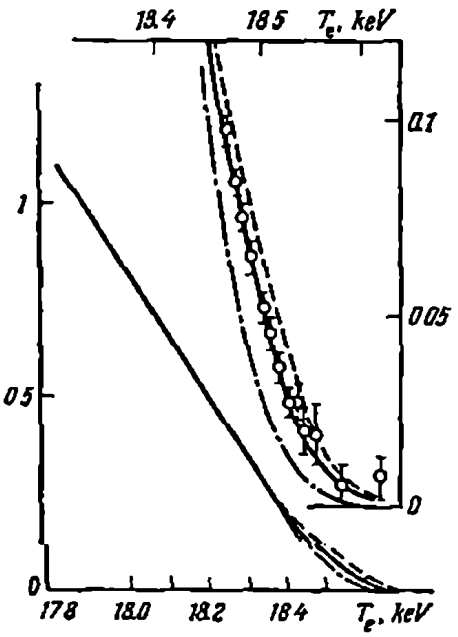

Fig. 111

Lyubimov *et al.* (Institute of Theoretical and Experimental Physics, Moscow) published in 1980 a paper [22] wherein it was indicated that the mass of the neutrino lies in the interval

$$28 \leqslant m_{\nu_e} \leqslant 41 \text{ eV} \quad \text{(with 99\% reliability)}. \qquad (3.3.31)$$

Measurements were made with the help of a new type of beta spectrometer with an iron-free toroidal magnetic field and a proportional detector. This spectrometer has a large solid angle for the particle capture and the background is an order of magnitude lower than in other spectrometers used in this kind of research.

The high-quality parameters of the beta spectrometer allowed precision measurements of the right end of the beta spectrum of tritium which is sensitive to the neutrino mass. Figure 111 shows

[22] V.A. Lyubimov *et al.*, *Phys. Lett.*, 94B, 266 (1980)

the experimental beta spectrum of tritium near its end, and the best approximation (solid line) corresponding to $m_{\nu_e} = 37$ eV. The dashed curve corresponds to $m_{\nu_e} = 0$, and the dot-and-dash curve to $m_{\nu_e} = 80$ eV.

In this experiment, the source of β-particles was not tritium but tritiated valine ($C_5H_{11}NO_2$) which was deposited on an aluminium substrate in the form of a thin (2×10^{-4} cm) layer containing 2 μg/cm² valine. Generally, the shape of the ^3H spectrum may depend on the source material. Hence the authors carried out a special analysis of their results and obtained an estimate for the neutrino mass that is independent of the chemical composition of the source material:

$$14 \leqslant m^2_{\nu_e} \leqslant 46 \text{ eV} \quad \text{(with 99\% reliability).} \qquad (3.3.32)$$

This estimate is valid under the assumption that there are no neutrino oscillations (see Sec. 5.4.5, Vol. II). The result has not been confirmed so far by independent investigations.

3.3.5. Concept of the Beta Decay Theory

3.3.5a. Historical Background

In recent years, the theory of weak interactions underwent radical transformations. From the nonrenormalizable four-fermion theory of local (contact) weak interaction, it was transformed into a unified renormalizable electroweak interaction theory in which weak and electromagnetic interactions are described with the help of a massless photon and three heavy intermediate vector bosons $W^{\pm}$ and Z^0. At present, this theory has been accepted by theoretical physicists and confirmed experimentally to a considerable extent. Only the heavy vector bosons (80-90 BeV) and some other particles predicted by the theory remain to be discovered. However, there is no doubt that these particles will be discovered as soon as the accelerators with appropriate energy are put into operation.[23]

As is always true of a good theory, the new theory practically did not affect the achievements of the old theory in the low-energy region $E \ll M_W$, attained as a result of several hundred experiments in the field of nuclear and elementary particle physics. On the other hand, the old theory was gradually developed to such a level of perfection that it was able to predict many new effects. In view of such a close relation between the old theory and experiment, we

[23] The discovery of W-bosons at CERN was reported in the beginning of 1983.

consider it appropriate for a course in experimental nuclear physics to retain the semihistorical way of the presentation, starting from the original version of the beta decay theory developed by Fermi, and gradually going over to more perfect versions (five types of interactions, parity violation, discovery of neutral currents, partial conservation of the vector current, Cabibbo's diagram, the success of the quark model, etc.). Some of these questions will be discussed in this section, while the remaining ones will be considered in Sec. 10.1, Vol. II. An idea about the modern Weinberg-Salam theory of electroweak interactions will be given in Sec. 10.2 Vol. II.

3.3.5b. The Fermi Theory

It is well known that there are no electrons in the nucleus. In Sec. 1.5.5 we showed that the hypothesis concerning the existence of electrons inside the nucleus is not in accord with the experimentally known values of the spins and magnetic moments of nuclei. Another argument against the existence of electrons in the nucleus is the large lifetime of β-radioactive nuclei, which cannot be explained by the existence of a potential barrier (a high barrier penetrability on account of small mass). Finally, the existence of electrons in the nucleus is countered by the uncertainty relation $\Delta p \Delta r \simeq \hbar$ which indicates that the momentum of an electron in the nucleus must be about

$$\Delta p \simeq \hbar/\Delta r = 10^{-27}/10^{-13} = 10^{-15} \text{ erg·s/cm.}$$

This corresponds to an electron energy

$$T \simeq \Delta pc = 3 \times 10^5 \text{ erg} \simeq 20 \text{ MeV,}$$

which is far in excess of the energy of beta decay electrons. Such a difference in the kinetic energies of the particles inside the nucleus can be explained in principle by enormous forces of attraction between the nucleus and the electrons, but this assumption is refuted by the experimental observations. In particular, a weak interaction between electrons and neutrons is indicated by the experiment.

Thus, there are no electrons in the nucleus. They are created at the moment of beta decay as a result of the transformation of a neutron into a proton according to the scheme

$$n \to p + e^- + \tilde{\nu} \tag{3.3.33}$$

The electron thus created cannot remain inside the nucleus and escapes from it. An antineutrino accompanies the electron. The β^+-decay proceeds similarly, accompanied by the release of a neutrino. Thus, beta decay is similar, to a certain extent, to the process

of radiation in which a photon is also created at the instant of emission.

The fact that beta decay involves the emission of electrons, i.e. particles constituting the atom, from the nucleus, stems from the following considerations:

(1) the mass and charge of the β^--particles are identical to those of atomic electrons;

(2) β^+-particles are annihilated by the atomic electrons;

(3) atomic electrons are captured by the nuclei; and

(4) Pauli's exclusion principle is valid for a mixed ensemble of particles containing atomic electrons and β^--particles (β^--particles emitted by the nucleus are not captured at the atomic electron levels occupied by electrons).

The theory of beta decay was formulated in 1934 by the Italian physicist Enrico Fermi in analogy with quantum electrodynamics. However, Fermi explained the beta decay by introducing a new type of forces, viz. weak interaction. According to quantum electrodynamics, the process of emission and absorption of photons is treated as the result of interaction of a charge with the electromagnetic field surrounding it. Photons as such are not present in the atom but are created right at the instant of emission. The charge is the source of photons.

In the Fermi theory, the beta decay is considered to be the result of interaction of a nucleon in the nucleus with the electron-neutrino field: the nucleon is transformed (from neutron to proton, and vice versa), resulting in the creation of an electron (positron) and an antineutrino (neutrino). Nucleons are the source of light particles. As in electrodynamics, it is assumed here that the laws of conservation of parity and angular momentum are satisfied in this case.

The exceptionally weak nature of the interaction responsible for beta decay allows the use of the perturbation theory methods. According to this theory, the probability P of the transition of a system (say, the atomic nucleus) from the initial to the final state is given by

$$P = \frac{2\pi}{\hbar} \left| \int \psi_f^* H' \psi_i \, d\tau \right|^2 \frac{dn}{dE}, \qquad (3.3.34)$$

where ψ_i and ψ_f are the wave-functions of the initial and final states of the system (the asterisk indicates that a complex conjugate is used), H' is the perturbation operator responsible for the transition, dn/dE is the density of the final states, and $d\tau$ is a volume element.

In the case under consideration, the wave-function ψ_i coincides with the wave-function ψ_{N_i} of the initial state of a nucleon, and $\psi_f = \psi_{N_f}\psi_e\psi_\nu$, where ψ_{N_f} is the wave-function of the final state of the nucleon, ψ_e is the electron wave-function and ψ_ν is the wave-function of the neutrino (antineutrino).

Since all particles participating in beta decay are fermions, each of them must be represented by a four-component wave-function, i.e. the bispinor

$$\begin{pmatrix} \psi_1 \\ \psi_2 \\ \psi_3 \\ \psi_4 \end{pmatrix}.$$

Two components of the bispinor indicate the spin state of the particle, while the remaining two indicate the two possible energy values $E = \pm \sqrt{m^2c^4 + p^2c^2}$ for a given momentum p (see Sec. 5.1, Vol. II for details). The operator H' is a complex combination of these bispinors and four γ-matrices. The structure of γ-matrices is similar to that of the well-known two-row Pauli spin matrices σ used for describing spin and isospin:

$$\gamma_1 = \begin{pmatrix} \hat{0} & \sigma_x \\ -\sigma_x & \hat{0} \end{pmatrix}; \qquad \gamma_2 = \begin{pmatrix} \hat{0} & \sigma_y \\ -\sigma_y & \hat{0} \end{pmatrix};$$

$$\gamma_3 = \begin{pmatrix} \hat{0} & \sigma_z \\ -\sigma_z & \hat{0} \end{pmatrix}; \qquad \gamma_4 = \begin{pmatrix} \hat{1} & \hat{0} \\ \hat{0} & -\hat{1} \end{pmatrix};$$

$$I = \begin{pmatrix} \hat{1} & \hat{0} \\ \hat{0} & \hat{1} \end{pmatrix}; \qquad 0 = \begin{pmatrix} \hat{0} & \hat{0} \\ \hat{0} & \hat{0} \end{pmatrix}, \tag{3.3.35}$$

where $\sigma_x = \begin{pmatrix} 0 & 1 \\ 1 & 0 \end{pmatrix}$;

$$\sigma_y = \begin{pmatrix} 0 & -i \\ i & 0 \end{pmatrix}; \qquad \sigma_z = \begin{pmatrix} 1 & 0 \\ 0 & -1 \end{pmatrix};$$

$$\hat{1} = \begin{pmatrix} 1 & 0 \\ 0 & 1 \end{pmatrix}; \qquad \hat{0} = \begin{pmatrix} 0 & 0 \\ 0 & 0 \end{pmatrix}.$$

Let us recall some properties of γ- and σ-matrices:

$$\sigma_i^2 = 1; \quad |\sigma|^2 = \sigma_x^2 + \sigma_y^2 + \sigma_z^2 = 3;$$

$$\sigma_i\sigma_j - \sigma_j\sigma_i = 2i\sigma_k, \qquad \sigma_i\sigma_j = -\sigma_j\sigma_i = i\sigma_k$$

(cyclic permutation of i, j, k is carried out);

$$\gamma_i^2 = 1; \qquad \gamma_i\gamma_k = -\gamma_k\gamma_i. \tag{3.3.36}$$

In the same way as from Pauli matrices we can construct operators for spin flipping, for transformation of a neutron into a proton, and others (see Sec. 1.5.9, Vol. II), γ-matrices can be used for constructing

operators which transform all the four components of a bispinor according to certain rules (annihilation and creation operators for particles with a given energy and spin).

The Fermi theory considers a vector version of weak interaction, which has an operator similar to the one used in the theory of electromagnetic interactions. However, this version of the theory was unable to interpret all allowed beta transformations, i.e. those having a high probability (for example, it cannot explain the beta decay of ^{6}He). This necessitated a certain modification of the Fermi theory.

3.3.5c. Five Types of Interaction. Rough Model of Beta Decay

It is possible to construct 256 linearly independent types of interaction from four bispinors. The imposition of Lorentz invariance reduces this number to five covariant types of interactions:

$$\left.\begin{array}{lll} \text{scalar interactions } S & \Delta P = 0, & \Delta I = 0; \\ \text{vector interactions } V & \Delta P = 0, & \Delta I = 0; \\ \text{tensor interactions } T & \Delta P = 0, & \Delta I = 0, \pm 1; \\ \text{axial-vector interactions } A & \Delta P = 0, & \Delta I = 0, \pm 1; \\ \text{pseudoscalar interactions } P & \Delta P \neq 0, & \Delta I = 0. \end{array}\right\} \quad (3.3.37)$$

Each of these interactions has a definite form of the perturbation operator H_i' corresponding to it, which preserves parity and angular momentum in weak interactions. The parity and angular momentum of the initial and final states vary in accordance with the selection rules on the right (see Sec. 3.3.5d for details).

Thus, in the general case (but still assuming the validity of the law of parity conservation in weak interactions) the perturbation operator H' can be written in the form

$$H' = \sum_{i=1}^{5} C_i H_i' \quad (3.3.38)$$

where i runs through values corresponding to the five versions mentioned above, each of which is characterized by a complex coefficient C_i. In accordance with the law of parity conservation, H' does not change sign upon a coordinate inversion

The total number of parameters (10) is too large to be determined from the existing experimental data. However, by making a number of additional assumptions concerning the structure of weak interaction, we can drastically reduce the number of parameters (without contradicting the experiment). We shall discuss this question in the general form in Sec. 3.3.5g, but for the present, we consider

a quite rough model of beta decay which also leads to a number of results that are in accord with the experiment and, besides, facilitates a transition to more complicated theoretical concepts.

Let us consider all the factors appearing in (3.3.34) turnwise. In order to simplify the line of arguments radically, we shall assume that ν and e are described by one-component wave-functions and the perturbation operator is equal to a constant $H' = g$. In view of the very weak interaction of the neutrino with nucleons, its wave-function can be written in the form of a plane wave:

$$\psi_\nu = \frac{1}{\sqrt{V}} \exp\left[\frac{i}{\hbar}(p_\nu r)\right]. \tag{3.3.39}$$

A similar approximation

$$\psi_e = \frac{1}{\sqrt{V}} \exp\left[\frac{i}{\hbar}(p_e r)\right]$$

is also valid for electrons if we neglect the effect of the Coulomb field of the nucleus (this assumption is valid for light nuclei and electrons with kinetic energy $T_e > 200$ keV)[24]. Under this assumption, $p_\nu = p_e \simeq m_e c$ and $pr/\hbar \simeq \frac{m_e c R}{\hbar} \simeq 1/100$, i.e. $\psi_e(r) \simeq \psi_e(0) = 1/\sqrt{V}$ and $\psi_\nu(r) = \psi_\nu(0) = 1/\sqrt{V}$. This gives

$$\int \psi_f^* H' \psi_i \, d\tau = \frac{g}{V} \int \psi_{N_f}^* \psi_{N_i} \, d\tau = \frac{g}{V} M, \tag{3.3.40}$$

where g is a constant characterizing the strength of beta interaction (in the same way as the electric charge e characterizes the strength of Coulomb interaction), and M is the nuclear matrix element determined by the properties of the wave-functions of initial and final states of the nucleon.

The weak-interaction constant g is determined experimentally from a comparison of certain outcomes of the beta decay theory with experiment (see Sec. 3.3.5e). The matrix element

$$M = \int \psi_{N_f}^* \psi_{N_i} \, d\tau \tag{3.3.41}$$

is the larger, the higher the degree of overlapping of wave-functions of the initial and final states of the nucleon. It these two states are identical, $M = 1$ $\left(\text{since } \int \psi^* \psi \, d\tau = 1\right)$. The sharper the difference between the two wave-functions, the lower the value of M.

An integral of type (3.3.41) is the simplest form of notation for the matrix element. In a more rigorous analysis, each of the five versions of the theory has its own form of notation for the matrix element. In all versions of the theory, however, the matrix element is deter-

[24] See Sec. 3.3.5e for the Coulomb correction.

mined by the properties of wave-functions of the initial and final states of the nucleus and assumes a maximum value around unity for allowed transitions (for example, $|M|^2 = 2$ for beta decay of ^{14}O, $|M|^2 = 1$ and $|M|^2 = 3$ for two types of beta decay of neutrons, and so on). Allowed transitions are subject to certain conditions (selection rules) which must be satisfied by the initial and final states of the nucleus (the values of spin and parity of the nucleus).

The expression dn/dE indicates the number of states[26] for the waves ψ_e and ψ_ν, when the momentum values lie in the interval between p and $p + dp$:

$$dn = 4\pi p^2 V dp/(2\pi\hbar)^3 = Vp^2 dp/2\pi^2\hbar^3.$$

Taking both particles (e and $\tilde{\nu}$) into consideration, we get

$$dn/dE = V^2 p_e^2 dp_e p_\nu^2 dp_\nu/4\pi^4\hbar^6 dE_e. \qquad (3.3.42)$$

Substitution of (3.3.40) and (3.3.42) into Eq. (3.3.34) and integration over all possible values of p_e and p_ν (these values are determined from the laws of energy and momentum conservation in beta decay) yields the emission probability and hence the lifetime τ of the nucleus for beta decay. This period is found to be connected with the beta decay energy through the relation

$$F(\varepsilon_0)\tau = 2\pi^3\hbar^7 c/g^2 (mc)^5 |M|^2, \qquad (3.3.43)$$

where $\varepsilon = (m_e c^2 + T_e)/m_e c^2$; $\varepsilon_0 = [m_e c^2 + (T_e^{max})]/m_e c^2$, while the quantity $F(\varepsilon_0)$ can be calculated. In particular, $F(\varepsilon_0) \sim \varepsilon_0^5$ for sufficiently large ε_0, i.e. $\varepsilon_0^5\tau \simeq$ const.

It is interesting to note that the dependence $F(\varepsilon_0)\tau \simeq \varepsilon_0^5\tau \simeq$ const can be readily obtained from dimensions. Indeed, the beta decay probability must be proportional to the square of the weak-interaction constant, i.e.

$$1/\tau \propto g^2. \qquad (3.3.43a)$$

The dimensions of the left-hand side of this formula are $[T]^{-1}$, while the right-hand side has dimensions $[E]^2[L]^6$ as follows from (3.3.43). We equalize them, using the system of units in which $\hbar = c = 1$. In this system, $[T] = [L]$ since $t = l/c$; $[L] = [M]^{-1}$ since $\lambda = \hbar/mc$; and $[M] = [E]$ since $E = Mc^2$. Hence $[L] = [T] = [E]^{-1}$. Thus the left-hand side of formula (3.3.43a) has dimensions $[E]$, while the dimensions of the right-hand side are $[E]^{-4}$. Equalizing the dimensions, we obtain the formula $1/\tau \propto \varepsilon_0^5$, i.e. $\tau\varepsilon_0^5 =$ const.

[26] It is well known that the quantity $dn = 4\pi p^2 V dp/(2\pi\hbar)^3$ is obtained by assuming an equiprobable distribution over all volume elements in the phase space. When applied to the case under consideration, this indicates equiprobabilities of all possible energy distributions between three particles (e, ν and the recoil nucleus) in beta decay.

3.3.5d. Allowed and Forbidden Transitions. Selection Rules

Among the quantities appearing in formula (3.3.43), $F(\varepsilon_0)$ can be determined experimentally, and $|M|^2$ must be close either to unity (for allowed transitions) or to zero (for forbidden transitions). Hence the theory of beta decay predicts that the product of two experimentally measurable characteristics of beta decay, viz. $F(\varepsilon_0)$ and τ, must be nearly constant for allowed as well as for forbidden transitions, the constant in the latter case being much larger than in the former case. The lowest value of $F\tau$ must be obtained for especially simple processes of beta decays, for example beta decay of the neutron and tritium, in which the matrix element $|M|^2$ assumes its highest possible value. This is due to the fact that the wave-functions of the initial and final states of a free neutron and proton are identical, while for the mirror nuclei ${}^3_1\mathrm{H}$ and ${}^3_2\mathrm{He}$ they are very similar.

The values of $\log F\tau$ for several cases of beta transitions between light nuclei are listed in Table 17. It can be seen that in spite of the vast difference in half-lives of the nuclei being compared, the quantity $F\tau$ (called the reference half-life) has the same order of magnitude (about 10^3 s) in all cases. Such transitions are called *superallowed* (preferentially allowed, unconditionally allowed, facilitated) transitions.

For medium nuclei in the Periodic Table, the matrix elements for allowed transitions must be smaller than for the light nuclei considered in Table 17. This is due to the fact that there are more neu-

Table 17

Beta transition	Half-life	$(T_e)_{max}$, MeV	$\log F\tau$
${}^3_1\mathrm{H} \xrightarrow{\beta^-} {}^3_2\mathrm{He}$	12.46 years	0.019	3.05
${}^6_2\mathrm{He} \xrightarrow{\beta^-} {}^6_3\mathrm{Li}$	0.82 s	3.22	2.91
${}^{11}_6\mathrm{C} \xrightarrow{\beta^+} {}^{11}_5\mathrm{B}$	20.42 min	0.99	3.59
${}^{18}_9\mathrm{F} \xrightarrow{\beta^+} {}^{18}_8\mathrm{O}$	1.78 hours	0.64	3.57

trons than protons in medium nuclei, and hence the levels occupied by the last neutron of the parent nucleus and the last proton of the daughter nucleus are different (see Sec. 2.3.3). Consequently, the wave-functions of the parent and daughter nuclei will be quite

different and the matrix element $|M|^2$ must be much smaller than unity. A comparison of half-lives and the energies of beta decay for these nuclei shows that $F\tau \simeq 10^8$ s. Such values of $F\tau$ correspond, for example, to the transitions

$$^{91}_{42}\mathrm{Mo} \xrightarrow{\beta^+} {}^{91}_{41}\mathrm{Nb}\ (6 \times 10^3\ \mathrm{s}) \text{ and}$$

$$^{169}_{68}\mathrm{Er} \xrightarrow{\beta^-} {}^{169}_{69}\mathrm{Tm}\ (2 \times 10^5\ \mathrm{s}).$$

Transitions characterized by the values $F\tau \simeq 10^8$ s are called *allowed* or normally allowed transitions.

It was mentioned above that the initial and final states of a nucleus must satisfy definite conditions for allowed (superallowed) transitions. These conditions require the compliance of the laws of conservation of angular momentum and parity and are called *selection rules* for allowed transitions. There are two types of selection rules, viz. the Fermi rules and the Gamow-Teller rules.

According to the Fermi selection rules, allowed transitions include beta transitions that leave the total angular momentum and parity of the nucleus unchanged: $\Delta I = 0$, $P_i/P_f = 1$. In the Gamov-Teller selection rules, the parity of the nucleus remains unchanged ($P_i/P_f = 1$), while the change in the angular momentum satisfies the condition $\Delta I = 0, \pm 1$ (with the exception of the (0-0) transition).

In the rigorous theory, the selection rules follow from the properties of transformation of operators and orthogonality of wave-functions with different angular momenta. However, these rules can also be obtained in a simple and graphic manner.

The parity selection rule clearly follows from the fact that for different intrinsic parities P_i and P_f, expression (3.3.41) becomes equal to zero.

The following simple arguments lead to the angular momentum selection rule.

According to quantum mechanics, the angular momentum l is a quantized quantity which assumes the values

$$|l| = \hbar\sqrt{l(l+1)}, \tag{3.3.44}$$

where $l = 0, 1, 2, \ldots$.

However, in accordance with classical mechanics, $|l| = p\rho$, where p is the momentum and ρ is the impact parameter for a particle. Hence

$$\rho = (\hbar/p)\sqrt{l(l+1)}. \tag{3.3.45}$$

In the process of beta decay, an electron and a neutrino escape from the nucleus. Consequently, they must obey the condition $\rho < R$, where R is the radius of the nucleus. Substituting into Eq. (3.3.45)

the value of p, corresponding to the energy of beta decay ($E \simeq 1$ MeV), we obtain

$$\rho = (\hbar/p)\sqrt{l(l+1)} \simeq (\hbar c/E)\sqrt{l(l+1)}$$
$$= (10^{-27} \times 3 \times 10^{10}/1.6 \times 10^{-6})\sqrt{l(l+1)}$$
$$= 2 \times 10^{-11}\sqrt{l(l+1)}\ \text{cm},$$

whence it can be seen that l must be equal to zero for $\rho < R$. Thus, for allowed transitions in beta decay, the electron and the neutrino are emitted with $l = 0$. Emission of e and ν with $l \neq 0$ is improbable and corresponds to forbidden transitions.

Two possibilities should be taken into consideration for allowed transitions.

(1) e and ν are emitted with antiparallel spins ($\uparrow e$, $\downarrow \nu$). Then the total angular momentum carried away by both particles is

$$\underbrace{s_e + s_\nu}_{0} + \underset{0}{l_e} + \underset{0}{l_\nu} = 0 \qquad (3\,3.46)$$

(spin orientation of the nucleon undergoing transformation is preserved). Consequently, the angular momentum of a nucleus does not change as a result of beta decay: $\Delta I = 0$. This result is in accord with the Fermi selection rule for angular momentum in the case of allowed transitions;

(2) e and ν are emitted with parallel spins ($\uparrow e$, $\uparrow \nu$), so that the total angular momentum carried away by both particles is

$$\underbrace{s_e + s_\nu}_{1} + \underset{0}{l_e} + \underset{0}{l_\nu} = 1 \qquad (3.3.47)$$

(the spin flip takes place). The total angular momentum of the nucleus can change by $\Delta I = 0, \pm 1$ (with the exception of the (0-0) transition). This result is in accord with the Gamow-Teller selection rule for angular momentum.

A comparison of spins and parities of nuclei among which beta transitions are allowed shows that they indeed satisfy the Fermi or Gamow-Teller selection rules (or both of them simultaneously).

As an example of a purely Fermi transition, we can consider the beta decay of ${}^{14}_{8}O$ [$(0^+\text{-}0^+)$ transition]. An example of a purely Gamow-Teller transition is the beta decay of the nucleus ${}^{6}_{2}He$ [$(0^+\text{-}1^+)$ transition]. The beta decay of neutron [$(1/2^+\text{-}1/2^+)$ transition] is an example of mixed transition. Forbidden transitions (with large values of $F\tau$) are characterized by a violation of the selection rules. Moreover, the constant $F\tau$ is the larger, the larger the violation. For example, the beta transition ${}^{137}_{55}Cs \xrightarrow{\beta^-} {}^{137}_{56}Ba$, accompanied by a varia-

tion of I by $\Delta I = 7/2 - 3/2 = 2$ corresponds to $F\tau = 4 \times 10^9$ s. For the beta transition ${}^{11}_{6}C \xrightarrow{\beta^-} {}^{11}_{7}N$, $F\tau$ is of the same order (10^7). In this case, $\Delta I = -1$, but the nuclei ${}^{14}_{6}C$ and ${}^{14}_{7}N$ have different parities ($P_i/P_f = -1$). For the transition ${}^{10}_{4}Be \xrightarrow{\beta^-} {}^{10}_{5}B$, which is accompanied by a variation of I by $\Delta I = 3$, the value of $F\tau \simeq 5 \times 10^{12}$ s, while the transition ${}^{40}_{19}K \xrightarrow{\beta^-} {}^{40}_{20}Ca$ for which I changes by $\Delta I = 4$ is characterized by the value $F\tau = 10^{18}$ s.[26]

3.3.5e. The Shape of Beta Spectrum. Curie Plot

The correctness of the beta decay theory can be also verified by comparing the results of experiments for determining the shape of beta spectrum with the corresponding theoretical formulas:

$$N(E_e)dE_e \propto pE\,(E_0 - E_e)^2 C\,(Z_0 p)\,dE_e, \tag{3.3.48}$$

or

$$N(\varepsilon)\,d\varepsilon \propto \varepsilon\sqrt{\varepsilon^2 - 1}\,(\varepsilon_0 - \varepsilon)^2 C\,(Z,\ p)\,d\varepsilon, \tag{3.3.49}$$

where E, E_0, ε and ε_0 have the same values as in formulas (3.3.42) and (3.3.43). These formulas can be easily derived from Eq. (3.3.42) if we use the obvious relations

$$\left.\begin{aligned} &E_e^2 = m_e^2c^4 + p_e^2c^2, \quad E_\nu^2 = m_\nu^2c^4 + p_\nu^2c^2, \\ &E_e + E_\nu = E_0 \end{aligned}\right\} \tag{3.3.50}$$

and

$$\left.\begin{aligned} &E_e dE_e = c^2 p_e dp_e, \quad E_\nu dE_\nu = c^2 p_\nu dp_\nu, \\ &dE_e = -\,dE_\nu = dE \end{aligned}\right\} \tag{3.3.51}$$

to go over from momenta to energies under the assumption that $m_\nu = 0$. (The formula assumes a different form if $m_\nu \neq 0$.) Besides, a more exact analysis must take into account the correction for the influence of the Coulomb field $C\,(Z, p)$ of the nucleus which distorts the spectral shape (increases the number of electrons in the soft spectral region and that of positrons in the hard region). The Coulomb correction factor can be written as

$$C(Z, p) = \frac{|\psi_e(0)|^2_{\text{in}}}{|\psi_e(0)|^2},$$

where $|\psi_e(0)|^2_{\text{in}}$ is the square modulus of the wave-function of electrons at the centre of the nucleus, taking into account the Coulomb

[26] See Sec. 3.3.9 for anomalously large values of $F\tau$ for some Fermi transitions.

interaction, while $|\psi_e(0)|_0^2$ is the same quantity but without taking into account the Coulomb interaction.

A comparison of the theoretical spectrum with the experimental one is difficult in view of the fact that most of the beta spectra represent the cumulative effect of β-particles emitted during transitions to the ground state as well as to excited states of the daughter nucleus. Hence such a comparison can be carried out only in *the vicinity of the right-hand spectral boundary, where the electron* energy has its highest value, which corresponds to a transition to the ground state.

For convenience in comparison, the quantity $(N(E)/C(Z, p)pE)^{1/2}$ is usually plotted. It can be seen from (3.3.48) that this quantity is proportional to E:

$$(N(E)/C(Z, p)pE)^{1/2} \propto (E_0 - E). \tag{3.3.52}$$

Thus, we obtain a straight line intersecting the energy axis at $E = E_0$ (Curie plot). Experiments confirm the linearity of the Curie plot over a significant region for many nuclei. A fine analysis of the Curie plot near the maximum electron energy can be used to answer the question concerning the neutrino mass (see Sec. 3.3.4).

3.3.5f. Beta Interaction Constant

It was shown above that an analysis of the experimental values of $F\tau$ and of the shape of beta decay spectrum points towards the correctness of the basic principles of the simple theory of beta decay. This allows us to calculate the beta interaction constant g. The value of g is estimated with the help of the relation (3.3.43) in which we put $|M|^2 \simeq 1$ for allowed transitions, while the values of F and τ are taken from the experiment. The following estimate was obtained in this way:

$$g \simeq 10^{-49} \text{ erg} \cdot \text{cm}^3. \tag{3.3.53}$$

The extremely small magnitude of g points towards the extremely weak nature of beta interaction. Beta forces are incomparably *weaker than nuclear or Coulomb forces, and are only stronger than* the gravitational forces. The weak nature of beta interactions explains the relatively large values of half-lives for β-radioactive nuclei.

The simplified theory of beta decay described above is unable to explain certain fine effects, for example, the angular correlation between the momenta of electrons and antineutrinos. A more rigorous theory is required for this purpose.

3.3.5g. Alternative Versions of the Beta Decay Theory

We have shown above that the basic assumptions of the theory are satisfied by five versions listed in (3.3.37). Each of them is characterized by its own selection rules for allowed transitions. For scalar (S) and vector (V) versions of the theory, allowed transitions are determined by the Fermi selection rules, while the Gamow-Teller selection rules are applicable to the tensor (T) and axial-vector (A) versions. The pseudoscalar (P) version is not suitable for describing allowed transitions, since in this case only such transitions are allowed for which $\Delta I = 0$ and the parity of the nucleus changes.

As was mentioned above, the beta decay theory was initially constructed under the assumption that parity is conserved in weak interactions, and that the interaction operator H' is determined by the relation (3.3.38) with five complex coefficients C_i, i.e. ten real parameters.

Assuming that weak interactions are invariant to time reversal (see Sec. 3.3.8d and Sec. 7.6.1, Vol. II for details), the coefficients C_i become real, i.e. the number of parameters is reduced to five. In order to find out as to which of the five versions corresponds to reality we must determine the values of these parameters.

It follows from selection rules that we can put $C_P = 0$ while describing allowed transitions. This leaves four parameters, viz. C_S, C_V, C_A and C_T.

The statistical nature of the energy spectrum (the absence of an interference term of the type $1/T_e$) means that of the two possible versions of the Fermi interaction (S and V) and of the two possible versions of the Gamow-Teller interaction (T and A), one version must be predominant. This indicates that only two of the four admissible versions can be operative simultaneously: ST or SA, or VT or VA. A thorough analysis of the shape of beta spectra reduced this choice to just two possible versions, viz. ST and VA. However, this result failed to reduce the number of parameters of the theory.

A more unambiguous choice of the plausible version is possible from an analysis of the shape of beta spectrum for forbidden beta transitions. It is shown by theoretical considerations that the shape of the spectrum for forbidden transitions differs from that for allowed transitions and is also different for different versions of the theory.

Another possibility of experimentally choosing the version of the theory involves the investigation of angular correlations for beta decay. Theoretical analysis shows that the beta decay probability depends on the angle between the electron momentum p_e and the neutrino momentum p_ν, the function describing this angular correlation being different for different versions.

will have the same orientation if the magnetic moments of electrons are polarized. This is a fairly simple task since the magnetic moments of electrons are about 10^3 times larger than the nuclear magnetic moments, and hence magnetic fields of a few hundred oersteds are sufficient for their polarization (at the same temperature of about 0.01 K).

Ultralow temperatures are obtained by *adiabatic demagnetization* of paramagnetic materials (Debye, 1926) cooled to about 1 K in liquid helium evaporating at a low pressure. Cooling in the process of adiabatic demagnetization is due to the *magnetocaloric effect*, in which the demagnetization of a paramagnetic in the absence of heat flow from outside occurs at the expense of the internal energy, i.e. the energy of thermal motion. The paramagnetic is first magnetized *isothermally* (to remove the heat liberated during magnetization). This method can be used to obtain temperatures of about 0.001 K, while the nuclear paramagnetism makes it possible to attain temperatures as low as 10^{-7}-10^{-6} K.

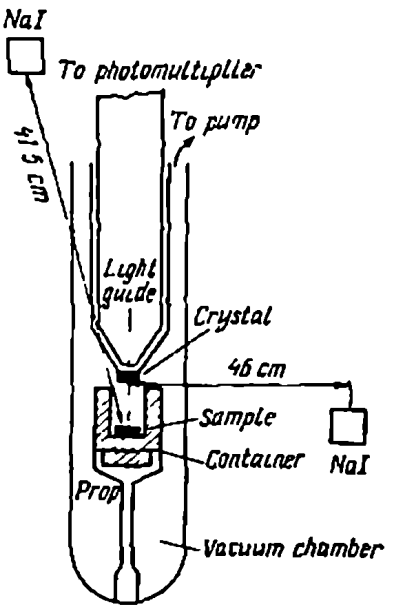

Fig. 112

A schematic diagram of Wu's experiment is shown in Fig. 112. The sample under investigation is a thin (0.05 mm) film of the β-radioactive isotope ^{60}Co (several microcurie) deposited on a single crystal of cerium-magnesium nitrate. The sample is at the bottom of a container made of the same material and fixed to a heat-insulating prop in a glass vacuum chamber. An anthracene crystal of thickness 1.6 mm, placed inside the chamber at a distance of 2 cm, was used as the electron counter. Scintillations created in the crystal by electrons are directed to a photomultiplier through a long (about 120 cm) light guide whose lower end abuts the crystal through a glass window in the vacuum chamber.

Preliminary cooling of the vacuum tube was carried out with the help of a coaxial Dewar flask whose outer part was filled with liquid nitrogen and the inner part (connected to a pump) with liquid helium.

Measurements are made as follows. Gaseous helium is introduced into the vacuum chamber (for bringing the container in thermal contact with the surrounding medium), and cerium-magnesium nitrate is magnetized with the help of a special magnet. The gas is

then pumped out and the sample is adiabatically demagnetized, which leads to a further cooling of the container and the sample. The magnet is then removed and replaced by the polarizing solenoid which can be used to orient the electron (and hence nuclear) magnetic moments upwards or downwards.

The polarization of ^{60}Co is measured in terms of anisotropy of gamma radiation accompanying the beta decay. Two gamma counters made of a NaI crystal were used for this purpose.

The results of measurements are shown in Fig. 113, where the abscissa and ordinate axes represent the time of measurement and the ratio of counting rates N_c and N_w for "cold" and "warm" samples.

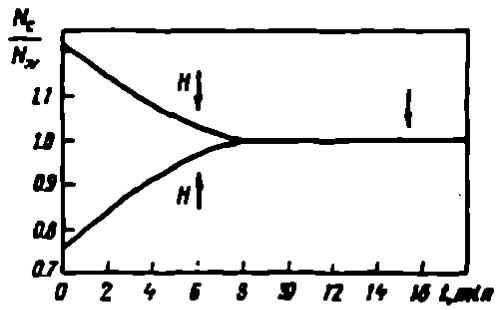

Fig. 113

Arrows indicate the two directions of the polarizing magnetic field and the instant at which gas is let in for warming. Comparing Figs. 112 and 113, it can be easily seen that the electrons are emitted predominantly in a direction opposite to the spin of the nucleus, the asymmetry gradually decreases with time and disappears completely in about 8 minutes. This is due to a decrease in the nuclear polarization as ^{60}Co is warmed by the heat liberated during beta decay, as well as by heat received from the surrounding objects. This conclusion is confirmed by the fact that the disappearance of asymmetry of beta decay is accompanied by a loss in the anisotropy of gamma radiation.

According to the results of the experiment conducted by Wu *et al.*, the angular distribution of beta decay electrons relative to the direction of nuclear spin can be written as follows:

$$f(\theta) = A(1 + \alpha \cos \theta), \qquad (3.3.55)$$

where $\alpha < 1$. Electrons escape predominantly against the nuclear spin,[29] thereby indicating the absence of mirror symmetry in the beta decay process or the nonconservation of parity.

[29] Experiments with ^{60}Co give a value $\alpha > 0$, i.e. the positrons in the process of β^+-decay fly along the nuclear spin.

Such a conclusion can be explained as follows. According to Sec. 1.6, if the parity conservation law is observed, the following condition is satisfied for the squared modulus of the wave-function:

$$|\psi(x, y, z)|^2 = |\psi(-x, -y, -z)|^2,$$

or, in spherical coordinates,

$$|\psi(r, \theta, \varphi)|^2 = |\psi(r, \pi-\theta, \pi+\varphi)|^2.$$

Thus, the probabilities of finding a particle at an angle θ or $180 - \theta$ are equal, and hence the function $f(\theta)$ describing the angular distribution of beta decay electrons cannot contain a term with $\cos\theta$ if the law of parity conservation is obeyed.

Besides beta decay and the disintegration of K-mesons, there are a whole lot of other phenomena involving weak interactions. A comparison of half-lives characterizing these processes with theoretical values shows that the constant g for them is very close to the constant g for beta and K-decays. Hence it can be expected that parity is not conserved in these processes as well. We shall discuss these processes in Vol. II.

It can be easily shown that besides the parity conservation law invariance with respect to charge conjugation is also violated in weak interactions.

There exists a theorem in relativistic field theory, called the CPT theorem and proved by Lüders and Pauli, according to which the laws of nature are invariant relative to the product of three discrete transformations C, P and T, i.e.

$$CPT = 1. \tag{3.3.56}$$

The transformation C indicates the operation of charge conjugation (replacement of a particle by an antiparticle), P is the space inversion, or a transformation to the mirror image (replacement of x, y, z by $-x$, $-y$, $-z$), while T is the time reversal (replacement of t by $-t$).

The nonconservation of parity (in weak interactions) indicates the absence of P-invariance, i.e. the presence of a pseudoscalar term of the type $(s_n p_e)$ in the weak-interaction Hamiltonian, which changes sign upon a P-transformation:

$$P(s_n p_e) = -s_n p_e \tag{3.3.57}$$

(since the expression $s_n p_e$ contains coordinates x, y, z to an odd power). However, this term is invariant under a T-transformation[39]:

$$T(s_n p_e) = s_n p_e$$

[39] Obviously, three-term expressions like $s_n [p_e p_\nu]$ are sensitive to T-transformation (see Sec. 3.3 8d).

(since time t appears to an even power in the expression $s_n p_e$). Hence

$$P\hat{T}\,(s_n p_e) = -\,s_n p_e, \tag{3.3.58}$$

i.e. weak interaction is noninvariant to the product of P- and T-transformations. However according to CPT theorem, a PT-transformation is equivalent to a C-transformation. Thus, the invariance to charge conjugation is violated in weak interactions.

It has not been possible to verify the violation of C-invariance in nuclear beta decay in a direct experiment with antinuclei, since it is not possible to set up such experiments. However, such a direct verification was obtained in experiments on comparing two cascade charge-conjugation schemes for the decay of a particle (π^+) and an antiparticle (π^-):

$$\pi^+ \to \mu^+ \to e^+, \quad \pi^- \to \mu^- \to e^-.$$

These decays are weak processes. The comparison showed that $\mu^+(e^+)$ and $\mu^-(e^-)$ have different polarizations.

3.3.7. A Review of the Beta Decay Theory

The proof of parity violation in weak interactions required a review of the beta decay theory. In the new theory, the operator H' must be written in the most general form

$$H' = \sum_{i=1}^{5} (C_i H_i' + C_i' H_i''), \tag{3.3.59}$$

where i runs through values corresponding to five types of interaction (S, V, T, A and P) listed in (3.3.37). Each term is characterized by a complex coefficiet C_i (or C_i'). The first five terms $\sum C_i H_i'$ do not change sign upon a coordinate inversion, while a reversal of sign is observed for the five second terms $\sum C_i' H_i''$. This leads to the appearance of pseudoscalar terms of the type $I_{nuc} p_e$ in the expression for the square of modulus of the matrix element, describing the beta decay probability.

It follows from Eq. (3.3.59) that the most general theory of beta decay contains 20 parameters, i.e. twice as many as in the classical theory. It would appear that this should lead to a worsening of the situation concerning the choice of the operative versions of the theory. Fortunately, this does not correspond to the actual state of affairs since experiments on beta decay of polarized nuclei provided

fresh information about the longitudinal polarization of beta decay products. According to this information, $C_i = C_i'$, and hence the actual number of parameters in the new theory is tho same as in the old one.[31]

The longitudinal polarization of the beta decay products of polarized nuclei is obvious from the following clear arguments. Figure 114 shows the beta decay of ^{60}Co employed by Wu *et al.* in their experiment. It can be seen from this scheme that the beta transition is accompanied by a change in spin by $\Delta I = 1$ (while the parity of the nucleus remains the same). In other words, this transformations is guided by the A-version.

The experiment on the investigation of angular correlation mentioned above showed that A-version is characterized by the escape of

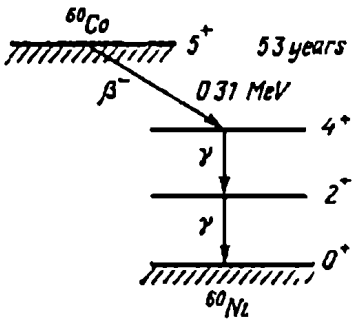

Fig. 114

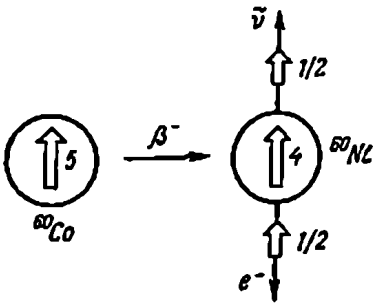

Fig. 115

an electron and an antineutrino in opposite directions (for the V-version, they fly in the same direction). A comparison of this result with that obtained from Wu's experiment (preferred escape of electrons against the nuclear spin) leads to the pattern of decay of ^{60}Co shown in Fig. 115. Here, single arrows represent the momenta of e and $\tilde{\nu}$, while double arrows indicate the spin of all the particles participating in beta decay (the numbers indicate the value of spin in units of $\hbar$). It can be clearly seen from the figure that the law of conservation of angular momentum requires the electron to be polarized against momentum (left-hand longitudinal polarization), and the antineutrino to be polarized along momentum (right-hand longitudinal polarization).[32]

Quito important results were obtained in the beta decay theory from investigations of the beta decay of neutrons.

---

[31] See Sec. 3.3.8d for a more detailed description.

[32] See Sec. 5.4.4, Vol. II for details on the magnitude and sign of the longitudinal polarization of e^-, e^+, ν and $\tilde{\nu}$.

3.3.8. Beta Decay of Neutrons. The $(V-A)$-version of the Weak Interaction Theory

3.3.8a. Half-life. Electron Spectrum

Beta transition between two simplest mirror "nuclei", viz. the neutron and the proton, belongs to "superallowed" transitions for which $F\tau \simeq 10^3$ s.

Since the difference between the neutron and proton masses is known, we can calculate the limiting energy of the beta spectrum of the neutron, as well as the function F and thus theoretically predict the half-life τ of the free neutron. This value was estimated to be $\tau \simeq 30$ min. Such half-lives can be easily measured for radioactive nuclei. Nevertheless, it is extremely difficult to observe the beta decay of a free neutron experimentally. This is because it is impossible to construct a fixed neutron target for successive measurements of its radioactivity by usual methods. Free neutrons are always in motion and once stopped, they are no longer free. Even the slowest neutrons formed as a result of deceleration of fast neutrons to energy of thermal motion of atoms of the medium[33] have a velocity $v \simeq 2 \times 10^5$ cm/s at room temperature. Entering a beta radiation detector of linear dimensions $l \simeq 10$ cm, such a neutron leaves it after a period

$$\Delta t = l/v = 10/(2 \times 10^5) = 5 \times 10^{-5} \text{ s}.$$

Hence the probability of a beta decay being registered turns out to be

$$P = 5 \times 10^{-5}/30 \times 60 = 3 \times 10^{-8},$$

and therefore high-intensity neutron beams must be used for successfully conducting the experiment. Hence experimental investigation of beta decay of neutrons became possible only after nuclear reactors with high densities of thermal neutrons were constructed.

The first experiments on the measurement of half-life of beta decay of the neutron were conducted simultaneously in the USSR (Spivak and Sosnovskii), the USA (Snell) and Canada (Robson) in 1950.

The experimental set-up used by Spivak and Sosnovskii is schematically shown in Fig. 116. There are two spherical electrodes 1 and 2 with a high potential difference (20 kV). A proportional counter with a window covered by a thin film is contained inside electrode 2. The operation of the counter is monitored with the help of α-particles emitted by an alpha gun. A beam of thermal neutrons (shown by the

[33] See Sec. 6.3 for detailed properties of thermal neutrons. Even slower neutrons (cold and ultracold) are described in Secs. 6.5.4 and 6.8.

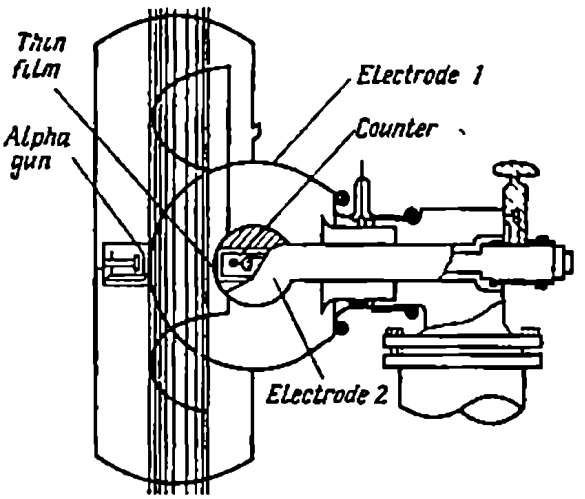

Fig. 116

hatched region in the figure) is passed through the apparatus. Protons formed as a result of the beta decay of neutrons and having comparatively low energy (about 100 eV) are deflected by the 20-kV electric field towards the inner electrode, and a part of these protons is registered by the proportional counter. Knowing the shape and size of the instrument, we can calculate the half-life of the neutron from the number of registered protons and the known value of the intensity of thermal neutron beam. The neutron half-life was found to be 12.5 min.

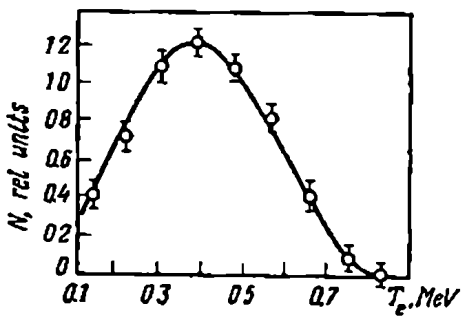

Fig. 117

Similar results were obtained by Snell and Robson. Moreover, in Robson's method, the magnetic analysis was used for measuring the energy spectrum of electrons released during the beta decay of neutrons. Unlike the beta spectra of heavy nuclei, this spectrum has a symmetric shape (Fig. 117).

Later, Spivak and his coworkers refined tho result of their measurements:

$$T_{1/2}\,(n) = 11.7 \pm 0.3 \text{ min.}$$

Christensen *et al.*[34] obtained in 1972 a somewhat lower value of

[34] Christensen *et al.*, *Phys. Rev.*, D5, 1628 (1972).

$T_{1/2}(n)$, equal to 10.61±0.16 min. Finally, Spivak *et al.*[34] made fresh measurements and obtained the following result:

$$T_{1/2}(n) = 10.13 \pm 0.09 \text{ min.}$$

The most straightforward (although for the time being hypothetical) method of measuring the neutron half-life is a direct measurement of the decrease in the number of ultracold neutrons in a closed volume with totally reflecting walls ("neutron bottle")[34].

3.3.8b. $(F\tau)_{exp}$ and $\lambda = |g_{GT}/g_F|$

The exact value of $T_{1/2}$ and, consequently, of $(F\tau)_{exp}$ for the neutron led to an estimation of the Gamov-Teller interaction constant g_{GT}. This possibility is associated with the fact that beta transition for the neutron occurs between the states $(1/2^+ \to 1/2^+)$ for which both the Fermi interaction and the Gamow-Teller interaction are allowed. The fact that the neutron and the proton are mirror particles leads to the exact values of the matrix element in both cases: $(|M_F|^2 = 1;\ |M_{GT}|^2 = 3)$. Hence the experimental constant $F\tau$ for the neutron decay is expressed in terms of g_F which is known from expression (3.3.54), as well as in terms of g_{GT} :

$$(F\tau)^{(n)}_{exp} = \frac{2\pi^3\hbar^7 c}{(mc)^5 (g_F^2 + 3g_{GT}^2)}. \qquad (3.3.60)$$

A comparison of this relation with the analogous expression for purely Fermi transitions 0+-0+ (for which the matrix element is $|M_F|^2 = 2$) yields

$$(F\tau)^{(n)}_{exp}/(F\tau)^{0^+-0^+}_{exp} = 2g_F^2/(g_F^2 + 3g_{GT}^2). \qquad (3.3.61)$$

Calculations show that $|g_{GT}|$ is somewhat larger than $|g_F|$. Two values of $\lambda = |g_{GT}/g_F|$, obtained by using two most accurate values of $T_{1/2}(n)$, are

$$|g_{GT}/g_F| = \begin{cases} 1.244 \pm 0.011 \text{ (Christensen)}, \\ 1.279 \pm 0.006 \text{ (Spivak)}. \end{cases} \qquad (3.3.62)$$

3.3.8c. Angular Correlations

In order to choose a version of the weak interaction theory, it is very important to conduct experiments for finding various correlations between the electron momentum $\mathbf{p}_e$, the antineutrino momentum $\mathbf{p}_{\tilde{\nu}}$ and the neutron spin $\mathbf{s}_n$ in the neutron beta decay. In the

[34] L.N. Bondarenko *et al.*, *Pis'ma Zh. Eksp. Teor. Fiz.*, 28, 5, 329 (1978).
[35] Calculations show that total internal reflection must be observed for ultracold neutrons ($T_n < 10^{-7}$ eV). See Sec. 6.8 for details.

general form, the neutron beta decay probability is defined by the expression

$$W(E, \mathbf{p}_e, \mathbf{p}_{\tilde{\nu}}) = F(E)\left[1 + a\frac{v}{c}(\mathbf{p}_e\mathbf{p}_{\tilde{\nu}}) + A\frac{v}{c}(\mathbf{s}_n\mathbf{p}_e) + B(\mathbf{s}_n\mathbf{p}_{\tilde{\nu}}) + D\frac{v}{c}\mathbf{s}_n[\mathbf{p}_e\mathbf{p}_{\tilde{\nu}}]\right], \quad (3.3.63)$$

where $F(E)$ is the function characterizing the spectral shape, v is the electron velocity, while a, A, B and D are coefficients.

The most reliable experiments on the determination of electron-antineutrino correlation were carried out by Vladimirskii *et al.* and reported in a number of works [37]. These measurements were taken with the help of electron and proton spectrometers and led to

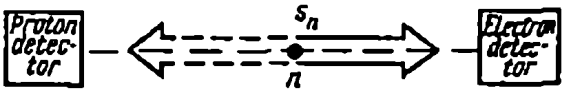

Fig. 118

the energy values and directions of velocities of electrons and protons, which in turn helped in establishing the direction of escape of the antineutrino. To reduce the background, triple coincidences (from the proton counter and two beta detectors) were used[38]. The following value was obtained for a:

$$a = -0.091 \pm 0.039. \quad (3.3.64)$$

First experiments aimed at establishing angular correlations of electrons and antineutrinos with the neutron spin were carried out by Telegdi in 1958. The neutrons were polarized with the help of a magnetic mirror made of cobalt (see Sec. 1.5.4). A nearly complete polarization (0.9) was attained for a grazing angle of 0°8′.

To measure the angular distribution of electrons, the number of (e-p) coincidences resulting from the beta decay of neutrons was registered for two different orientations of the neutron spin. The experimental set-up is schematically shown in Fig. 118. Measurements gave the following distribution for electrons:

$$f(\theta) = 1 + A\frac{v_e}{c}\cos\theta, \quad (3.3.65)$$

where $A \simeq -0.1$.

[37] V.K. Grigor'ev *et al.*, *Yadernaya Fizika*, 6, 329 (1967).

[38] One of the beta detectors is placed at the focus of the electron trajectories, while the other is at the terminal point.

The antineutrino angular distribution was measured with the help of a device capable of registering coincidences of electrons and protons flying in a certain direction (Fig. 119). In accordance with the momentum conservation law, the antineutrinos resulting from beta decay must escape upwards in such a geometry of the apparatus. Measurements of the number of $(e\text{-}p)$ coincidences for two spin orientations of the neutrons (upwards and downwards) led to the following result:

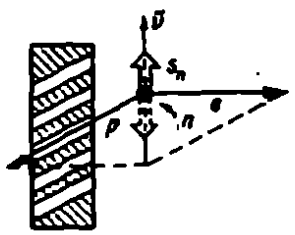

Fig. 119

$$\varphi(\theta) = 1 + B\cos\theta, \quad (3.3.66)$$

where $B \simeq 1$. The up-to-date values[29] of coefficients A and B are:

$$A = -0.118 \pm 0.010, \qquad B = 0.995 \pm 0.035. \quad (3.3.67)$$

3.3.8d. The $(V-A)$-version. Admixtures of Other Versions

The obtained values of the coefficients A and B confirm the nonconservation of parity in beta decay and the predominance of V- and A-versions of interaction. These values are also in accord with the right-hand longitudinal polarization of the antineutrino. Besides, the relative magnitude and signs of coefficients A and B indicate that V- and A-interactions are in opposite phases. This result can be graphically illustrated with the help of the following arguments.

Both A- and V-versions are allowed for the beta decay of the neutron. It was mentioned above that the A-version is characterized by the escape of an electron against the spin of the nucleus and an antineutrino along the spin, while in the V-version both the particles fly opposite to the nuclear spin (Fig. 120). In the former case, e^- and $\tilde{\nu}$ take away total spin equal to unity (it should be recalled that $l_e = l_{\tilde{\nu}} = 0$), i.e. the nuclear spin flip takes place in the process of beta decay. In the latter case, e^- and $\tilde{\nu}$ do not carry away spin. Both the diagrams are in accord with the signs of longitudinal polarization of the electron and antineutrino.

It can be easily seen that the "sum of the diagrams" [$(V + A)$-version] corresponds to a strong correlation for $\mathbf{p}_e$ and $\mathbf{s}_n$, and to a weak correlation for $\mathbf{p}_{\tilde{\nu}}$ and $\mathbf{s}_n$. This is inconsistent with experimental observations. However, the "difference of diagrams" [$(A - V)$-

[29] See B.G. Erozolimskii *et al.*, *Usp. Fiz. Nauk*, 116, 1, 145 (1975).

version] gives the correlation actually observed in experiments. These arguments are correct to within the sign of weak potential relative to the strong potential. The relative sign of both potentials can be determined from interference experiments of weak nucleon scattering type, which led to $-(A - V)$, i.e. $(V - A)$-version.

Finally, we reiterate that the available experimental material is insufficient for an independent determination of all the coefficients

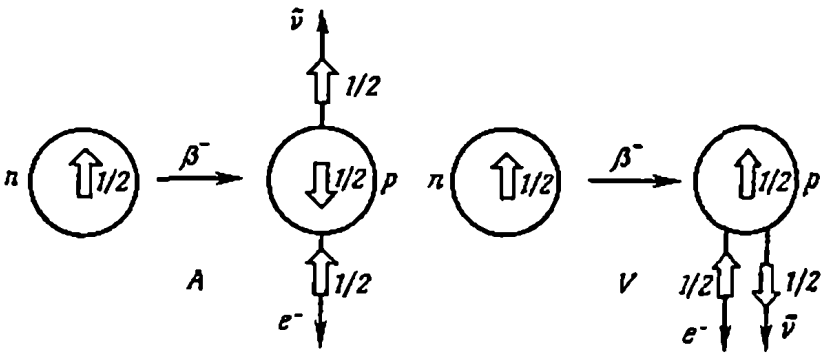

Fig. 120

in expression (3.3.59). Strictly speaking, the $(V - A)$-version does not contradict any of the modern experiments which, however, do not permit a complete elimination of the admixtures of other versions. These versions may be present in significant proportions (up to 15% of T-version in A and up to 40% of S-version in V).

Hence the conclusion about the $(V - A)$-version of weak interaction is based to a considerable degree on the assumption that the t-invariance and the two-component theory of the neutrino are valid (i.e. there is a 100% longitudinal polarization of neutrino and antineutrino). As was mentioned earlier, it follows from the first assumption that all the coefficients $C_k = |C_k| \exp(i\varphi_k)$ and $C'_k = |C'_k| \exp(i\varphi'_k)$ must be real, while the second assumption means that they are equal pairwise. Thus, the validity of both the assumptions for the $(V - A)$-version leads to the following relations:

$$\left.\begin{aligned} &\varphi_V - \varphi'_V = 0, \quad \varphi_A - \varphi'_A = 0, \\ &\varphi_V - \varphi_A = 180°, \quad \varphi'_V - \varphi'_A = 180°, \\ &|C_V| = |C'_V|, \quad |C_A| = |C'_A|. \end{aligned}\right\} \tag{3.3.68}$$

The t-invariance was experimentally verified while measuring the triple correlation in beta decay of neutrons. If the experiment is set up in such a way that the three vectors s_n, p_e and $p_{\tilde{\nu}}$ are mutually perpendicular, these vectors are transformed upon a change $t \to -t$ into a mirror triple of vectors which (after a rotation through 180° relative to s_n) differs from the original set only in the

spin orientation (Fig. 121). Thus, in the case of t-invariance, there must be a symmetry in the emission of e and $\tilde{\nu}$ relative to the change in the direction of the neutron spin s_n. In other words, the weak-

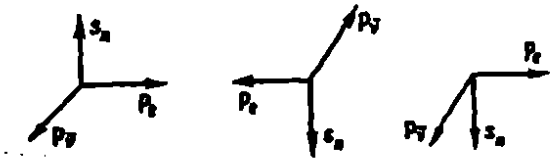

Fig. 121

interaction Hamiltonian must not contain a term with a scalar triple product of the type $Ds_n [p_e p_{\tilde{\nu}}]$, i.e. the coefficient D of such a triple product must be equal to zero.

The schematic diagram of a possible experimental set-up is shown in Fig. 122. The geometry of the instrument is such that it selects events for which p_n, p_e, p_p and $p_{\tilde{\nu}}$ lie in the same plane. In this case, s_n is perpendicular to this plane and the vector product $[p_e p_{\tilde{\nu}}]$ is parallel or antiparallel to s_n. Consequently, a reversal of s_n should lead to a sign reversal of the scalar triple product $s_n [p_e p_{\tilde{\nu}}]$. The coefficient D can be estimated from the difference in the results of measurements carried out for two spin orientations. The most accurate measurements[40] for this coefficient gave the value $D = 0.01 \pm 0.01$, which speaks in favour of the t-invariance[41].

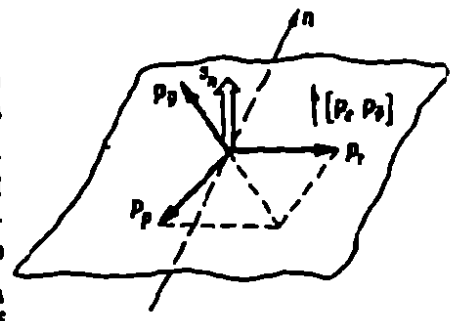

Fig. 122

The conclusion about the 100% longitudinal polarization is based on the fact that the mass of ν_e ($\tilde{\nu}_e$) is identically equal to zero. The latest data show (see Sec. 3.5.4) that $m_{\nu_e}^{exp} \neq 0$, but its value is so small that this result should not affect the conclusion under discussion.

---

[40] See Footnote 39.

[41] In 1964, a 0.1%-violation of CP-parity was observed in the decay of neutral K-mesons, which indicates (if we assume that the CPT theorem is valid) a violation of t-invariance in this process. For details, the reader is referred to Sec. 7.6.4, Vol. II.

The following results are obtained from an analysis of the experimental data:

$$\left.\begin{aligned} &\varphi_V - \varphi'_V = 0 \pm 48^\circ, \quad && \varphi_A - \varphi'_A = 0 \pm 13^\circ, \\ &\varphi_V - \varphi_A = 180 \pm 31^\circ, \quad && \varphi'_V - \varphi'_A = 180 \pm 31^\circ, \\ &|C_V|^2/|C'_V|^2 = 1 \pm 0.2, \quad && |C_A|^2/|C'_A|^2 = 1 \pm 0.015. \end{aligned}\right\} \quad (3.3.69)$$

It can be seen that the accuracy with which the $(V - A)$-version of the weak interaction theory is verified is not very high, although the validity of this version is also indicated by the fact that it is of a fairly universal nature. Besides the beta decay, the $(V - A)$-version of the theory also describes the $(\mu\text{-}e)$-decay, muon capture by a proton, as well as some other weak interaction processes. The accuracy of this description will be discussed in Sec. 10.1, Vol. II.

3.3.9. Isospin Selection Rules

Recently, quite a few (over ten) Fermi $(0^+\text{-}0^+)$ transitions have been observed with anomalously large values of $F\tau \simeq 10^9\text{-}10^{10}$ s (including transitions involving heavy nuclei). A comparison of these beta transitions with known superallowed $(0^+\text{-}0^+)$ beta transitions ($F\tau \simeq 10^3$ s) shows that the large values of $F\tau$ are associated with the *isospin selection rules. It can be shown in the exact theory* of beta decay that the Fermi matrix element has the following selection rules for isospin:

$$\Delta T = 0 \text{ and } \Delta T_z = \pm 1.$$

It was found that these selection rules are obeyed for $(0^+\text{-}0^+)$ transitions with $F\tau \simeq 10^3$ s, and are violated $(\Delta T = 1)$ *for anomalous* transitions. Thus, the restriction imposed by the isospin selection rules is quite strong (even for heavy nuclei). A similar conclusion (the small value of the Fermi matrix element for $\Delta T = 1$) was also drawn for a number of mixed beta transitions of the type $I \to I \neq 0$.

However, such an analysis cannot be made for the Gamow-Teller *transitions which have similar isospin selection rules for forbidden* transitions:

$$\Delta T = 0, \pm 1; \qquad \Delta T_z = \pm 1.$$

3.4. Nuclear Gamma Radiation

Gamma radiation is the *spontaneous emission of γ-quanta by the nucleus.* By emitting γ-quanta, the nucleus goes over from an excited state to a stato with a lower energy (radiative transition). There are single radiative transitions when the nucleus emits a single quantum

and at once goes over to the ground state (Fig. 123*a*), or cascade transitions when the excitation is removed by a successive emission of several γ-quanta (see Fig. 123*b*).

Gamma radiation is a short-wave electromagnetic radiation of nuclear origin. The energy of nuclear γ-quanta usually varies from 10 keV to 5 MeV ($10^{-8} \geqslant \lambda_\gamma \geqslant 2 \times 10^{-11}$ cm).

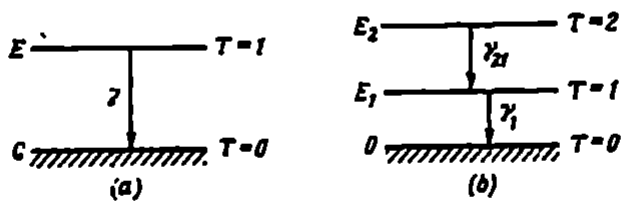

Fig. 123

The energy E_γ of a γ-quantum is determined by the difference in the nuclear energy levels E between which the radiative transition occurs. According to the laws of conservation of energy and momentum, we have

$$E = E_\gamma + T_{\text{nuc}}, \qquad 0 = \mathbf{p}_\gamma + \mathbf{p}_{\text{nuc}}, \tag{3.4.1}$$

where T_{nuc} and $\mathbf{p}_{\text{nuc}}$ are the kinetic energy and momentum of the recoil nucleus respectively. From here, we can easily obtain an estimate for T_{nuc}:

$$T_{\text{nuc}} = \frac{E_\gamma^2}{2M_{\text{nuc}}c^2} \simeq \frac{E^2}{2M_{\text{nuc}}c^2}. \tag{3.4.2}$$

This gives $T_{\text{nuc}} \simeq 0.1\text{-}10$ eV $= (10^{-6}\text{-}10^{-5})E$ for $E \simeq 0.1\text{-}1$ MeV and for nuclei with $A \simeq 10^2$. Thus, the γ-quantum carries away an overwhelming part of the nuclear excitation energy. From the above discussion it is obvious that the γ-quantum spectrum is discrete.

There are different reasons for which a nucleus may turn out to be in an excited state. For example, an alpha or beta decay can leave the nucleus in an excited state. An alpha decay is usually followed by the emission of low-energy γ-quanta ($E_\gamma < 0.5$ MeV), since an alpha decay followed by the creation of a highly excited daughter nucleus ($W > 0.5$ MeV) is hindered because of a low barrier penetrability for low-energy α-particles. The energy of γ-quanta emitted by a daughter nucleus after the beta decay may be higher and attains values up to 2-2.5 MeV. This is due to the fact that the probability of beta decay is determined by a weaker energy function ($F \propto E_\beta^5$) than the alpha decay probability.

In both the examples considered above, the nucleus emitting γ-quanta has a comparatively low excitation energy which is not

sufficient for the emission of a nucleon. This result can be also extended to many other processes leading to the creation of nuclei with an excitation energy lower than the separation energy of a nucleon. These processes include various nuclear reactions involving a nucleus in an excited state as a product. In these cases the excitation energy of the daughter product is smaller than the separation energy of a nucleon (or some other particle), and the emission of γ-quanta is the only possible way of removing the excitation (if we do not take into account the processes of internal conversion and the formation of $(e^+\text{-}e^-)$-pairs).

If the excitation energy of the daughter nucleus is equal to (or higher than) the nucleon separation energy, the emission of γ-quanta may dominate when the emission of nucleons is hindered due to some reasons. In Part Two of this book, we shall consider the radiative capture of slow neutrons, when the nuclear excitation due to the capture of a neutron is removed by the emission of two or three γ-quanta. The emission of γ-quanta in this case is more probable than the separation of the neutron, since the latter requires the concentration of the entire excitation energy at one nucleon which has to be near the nuclear boundary. This phenomenon is improbable since the binding energy carried by the neutron is distributed immediately after capture among all the nucleons in the nucleus.

The emission of γ-quanta by nuclei excited to energies much higher than the separation energy for a particle is associated with the forbiddenness in parity and angular momentum for the escape of nucleons (or other particles), making the emission of γ-quanta relatively more probable. An example of this type is the emission of γ-quanta with energy 17 MeV as a result of the reaction ${}^{7}_{3}\mathrm{Li} + p \rightarrow {}^{8}_{4}\mathrm{Be} + \gamma$ (see Sec. 9.3.2).

The γ-quanta emitted by the nucleus during a transition to a lower energy state may carry away different angular momenta l. The radiation carrying angular momentum $l=1$ is called the dipole radiation, for $l = 2$ it is called the quadrupole radiation, for $l = 3$ the octupole radiation, and so on.[42] Each of these radiations is characterized by a definite angular distribution. Gamma-quanta of different multipolarities are the result of different types of "oscillations" of the nuclear fluid, viz. electric ($E1$ dipole radiation, $E2$ quadrupole radiation, and so on) and magnetic ($M1$ dipole radiation, $M2$ quadrupole radiation, and so on).

The first type of processes are caused by a redistribution of the electric charges in the nucleus, while the second type of processes are due to a redistribution of the spin and orbital magnetic moments. The redistribution of neutrons for which $Z = 0$ must also lead to

[42] There is no radiation with $l = 0$ due to the transverse nature of electromagnetic waves.

the emission of electric γ-quanta, since the motion of a neutron is accompanied by the emergence of charged recoil nuclei.

A more clear idea about the mechanism of gamma transition can be formed on the basis of a specific model of the nucleus. Thus, in the single-particle model, the emission of the γ^l-multipole is associated with the transition of a nucleon between two single-particle levels differing in their angular momenta by $\Delta I = l$.

3.4.1. Gamma Transition Probability and Selection Rules

In view of the small magnitude of the electromagnetic interaction constant $\alpha = e^2/\hbar c = 1/137 \ll 1$, the probability P of radiative transition can be calculated by the time-dependent perturbation theory methods:

$$P = \frac{2\pi}{\hbar} |M|^2 \frac{dn}{dE}. \qquad (3.4.3)$$

Here, $M = \int \psi_f^* H' \psi_i d\tau$ is the matrix element of the Hamiltonian H' of interaction between the electromagnetic field on the one hand, and charges and magnetic moments on the other hand; dn/dE is the density of the final states; ψ_f and ψ_i are the wave-functions of the final and initial states of the nucleus respectively.

The electromagnetic theory can be used to write the expressions for H' and dn/dE. Hence the probability P can be estimated by using some model of the nucleus (for example, the shell model) to obtain ψ_i and ψ_f. The following very rough conclusions can be drawn from the results of the theory.

The radiation field of the moving charges can be represented as a series of spherical functions. If the dependence on the coordinates and angles is neglected, we are left with the factor R/λ in the first term of the series (corresponding to the dipole radiator and the quantum with moment $l \simeq 1$), where R is the nuclear radius and λ is the wavelength of the emitted radiation. The second term ($l = 2$) corresponds to $(R/\lambda)^2$, and the lth term to $(R/\lambda)^l$. For normal values of $E_\gamma \simeq 1$ MeV for nuclei in the middle of the Periodic Table ($A \simeq 10^2$), we have

$$\frac{R}{\lambda} = \frac{RE}{2\pi\hbar c} = \frac{6 \times 10^{-13} \times 1.6 \times 10^{-6}}{2\pi \times 10^{-21} \times 3 \times 10^{10}} \simeq 10^{-3}\text{-}10^{-2}, \qquad (3.4.4)$$

i.e. the series converges rapidly.

Since P is proportional to $|M|^2$, we obtain for γ-quanta with multipolarity l

$$P_l \propto (R/\lambda)^{2l} \propto A^{2l/3} E^{2l}. \qquad (3.4.5)$$

Thus, as l increases by unity, the radiation intensity decreases by a factor of about $P_{l+1}/P_l \propto (R/\lambda)^2 \simeq 10^5$. This means that the first nonzero term in the series (which may not correspond to $l = 1$ due to the selection rules) is the decisive one.

The same conclusion can be drawn regarding magnetic multipoles. For the same values of l, however, the intensity of magnetic radiation is $(d/\mu)^2$ times lower than that of the electric field, where d and μ are the electric and magnetic moments of the nucleus. This is due to different structures of H' for electric and magnetic transitions. In the former case, H' contains the electric nuclear moments, while in the latter case, it contains nuclear magnetic moments. For $A \simeq 10^2$, the quantity $(d/\mu)^2$ is approximately equal to

$$\left(\frac{eR}{e\hbar/m_N c}\right)^2 = \left(\frac{m_N cR}{\hbar}\right)^2 \simeq 10^2\text{-}10^3. \qquad (3.4.6)$$

The set of possible values of l_E and l_M is determined by the angular momentum and parity selection rules. According to the first selection rule, there must exist the following relation between the angular momentum l carried away by the γ-quantum, and the angular momenta I_i and I_f of the initial and final states of the nucleus:

$$|I_i - I_f| \leqslant l \leqslant I_i + I_f. \qquad (3.4.7)$$

According to the second selection rule, the angular momenta l_E and l_M of the electric and magnetic gamma radiation must be connected with the parities P_i and P_f of the initial and final states through the relations

$$P_i/P_f = (-1)^{l_E}, \qquad P_i/P_f = (-1)^{l_M+1}. \qquad (3.4.8)$$

It follows from these relations, for example, that the $E1$-transition is possible only between nuclear states with different parities, while the parities of the nuclear states must be the same for the $M1$-transition. In both the cases, the nuclear angular momenta must satisfy the relation $\Delta I = 0, \pm 1$ (with the exception of the (0-0) transitions).

The parity selection rules can be obviously obtained by considering the structure of the matrix element

$$M = \int \psi_f^* H' \psi_i \, d\tau.$$

In the case of the $E1$-transition, H' in this matrix element contains the electric dipole moment which is transformed as a polar vector upon coordinate inversion. For the $M1$-transition, H' contains the magnetic dipole moment having the properties of an axial vector.

Taking into account all the above-mentioned features of the gamma radiation, viz.

(1) a decrease in the gamma transition probability with increasing l;

(2) a relatively small probability of magnetic transitions in comparison with electric transitions for the same value of l; and

(3) angular momentum and parity selection rules, we arrive at the following conclusion.

The dominating role in the radiative transition between two nuclear states with given P_i, P_f and ΔI is played by electric and/or magnetic multipoles with the lowest values of l_E and l_M satisfying the angular momentum and parity selection rules:

$$l = |\Delta I| \quad \text{and} \quad l = |\Delta I| + 1. \tag{3.4.9}$$

One of these multipoles must be electric, and the other magnetic.

Table 18 describes the main gamma transitions for some values of

Table 18

$\frac{P_i}{P_f}$	$\lvert \Delta I \rvert$			
	0	1	2	3
−1	$\underline{E1}$, $M2$	$\underline{E1}$, $M2$	$\underline{M2}$, $E3$	$\underline{E3}$, $M4$
+1	$\underline{M1}$, $E2$	$\underline{M1}$, $E2$	$\underline{E2}$, $M3$	$\underline{M3}$, $E4$

$|\Delta I|$ when the parities of the initial and final states are the same or different. Naturally, the following transitions must be excluded from the list of possible transitions: (0-0) transition for $|\Delta I| = 0$; (0-1) and (1-0) transitions (at $l = 2$) for $|\Delta I| = 1$; (0-2) and (2-0) transitions (at $l = 3$) for $|\Delta I| = 2$, and so on.

As a rule, one of the two main gamma transitions considerably predominates over the other due to a strong dependence of the gamma radiation probability on l (the dominant transition is underlined in the table).[43]

In order to obtain a rough estimate of the absolute values of half-lives $T_{1/2}$ for different gamma transitions, we can use the Weisskopf formula obtained on the basis of the single-particle model of the nucleus under the assumption that the gamma transition is caused by the transition of one nucleon from one single-particle state into another (cf. (3.4.5))

$$W_{El} \propto E^{2l+1}A^{2l/3}, \qquad W_{Ml} \propto E^{2l+1}A^{(l-1)2/3}. \tag{3.4.10}$$

[43] When the $M1$-transition is the lowest allowed level, the probability of the other principal transition $E2$ also turns out to be of the same order.

Table 19

l	$E_\gamma = 0.1$ MeV		$E_\gamma = 1.0$ MeV		$E_\gamma = 10$ MeV	
	Electric	Magnetic	Electric	Magnetic	Electric	Magnetic
1	10^{-13} s	10^{-11} s	10^{-16} s	10^{-14} s	10^{-19} s	10^{-17} s
2	10^{-8} s	10^{-4} s	10^{-11} s	10^{-9} s	10^{-16} s	10^{-14} s
3	10 s	10^3 s $\simeq$ 15 min	10^{-6} s	10^{-4} s	10^{-13} s	10^{-11} s
4	10^8 s $\simeq$ 3 years	10^{10} s $\simeq$ 300 years	10^{-1} s	10 s	10^{-10} s	10^{-8} s
5	10^{15} s $\simeq$ 10^8 years	10^{17} s $\simeq$ 10^{10} years	10^4 s $\simeq$ 3 h	10^6 s $\simeq$ 10 days	10^{-7} s	10^{-5} s

Table 19 shows approximate values of $T_{1/2}$ for electric and magnetic transitions for $l = 1$-5, and three values of energy $E_\gamma = 0.1$ MeV, 1.0 MeV and 10 MeV, calculated with the help of these formulas for the nucleus with $A = 125$.

Besides the spin and parity selection rules, gamma transitions must satisfy the selection rules for isospin. For gamma radiation of any multipolarity, these rules have the following form:

$$\Delta T = 0, \pm 1 \quad \text{and} \quad \Delta T_\zeta = 0. \tag{3.4.11}$$

The experimental data available to date do not contradict these rules. For some nuclei, it was shown that the gamma transition from a level with T = 2 to a level with T = 0 occurs not directly, but in a cascade-like manner through an intermediate level with T = 1 (see Fig. 123*b*).

Gamma radiation is studied experimentally in the secondary processes accompanying the propagation of γ-quanta through matter, viz. photoelectric effect, Compton effect, and formation of electron-positron pairs (see Sec. 4.10). All these processes involve electrons the magnitude and direction of whose momenta can be used to form an idea about the energy and direction of the γ-quanta inducing them.

For example, the recoil electrons appearing in the Compton effect can be analyzed with the help of the Wilson cloud chamber with a magnetic field. This method was first proposed in 1927 by the Soviet physicist Skobel'tsyn and played a very important role in the experimental investigation of the Compton effect and the photoelectric effect. However, in view of its low resolving power and moderate statistical accuracy, this method is rarely used for analyzing Compton electrons (although magnetic field chambers are used quite widely for investigating other problems).

The statistical accuracy of the Wilson chamber can be improved by using a light-material plate in the chamber. When the plate is irradiated by γ-quanta, more Compton electrons are produced than in the gas contained in the chamber. The energy of the γ-quanta inducing electrons can be estimated from the upper limit of the electron spectrum. The resolving power is again not very high (it is possible to distinguish between two monochromatic lines E_1 and E_2 with $\Delta E = E_2 - E_1 \simeq 150$ keV).

In another method, the recoil electrons are analyzed with the help of a conventional magnetic beta spectrometer, in which the source of electrons is a plate of a light material irradiated by γ-quanta. In this case also, the resolving power is not quite sufficient.

The method of investigation of electrons appearing in the photoelectric effect is a lot more accurate. Here the energy of the electrons is uniquely determined by the energy of the γ-quanta (and the electron binding energy in the atom). In this method, thin foils of heavy materials (like lead) serve as the source of photoelectrons.

Of late, scintillation counters are used quite successfully in gamma spectrometry (see Sec. 3.3.6) in view of their high efficiency. Besides, semiconductor detectors (made of silicon and germanium) are also used because of their high resolving power. The gamma spectrometry based on the Mössbauer effect has an absolutely unique resolving power (see Sec. 3.4.4e).

3.4.2. Internal Conversion of Electrons

Besides the emission of γ-quanta, there is another mechanism for the loss of excitation energy, viz. the emission of internal conversion electrons. It is shown by the theory that the nuclear excitation energy in this process is directly (without an intermediate emission of a γ-quantum) transferred to an orbital electron (overlapping of nuclear and electron wave-functions). In this mechanism, obviously, monoenergetic electrons will be emitted, whose energy is determined by the energy of nuclear transition and the type of electron shell. The process of internal conversion has the highest probability for K-electrons. In this case,

$$T_e = E - I_K, \tag{3.4.12}$$

where T_e is the kinetic energy of electrons and I_K is the ionization potential for the K-electrons.

However, if the energy E released during a nuclear transition is less than the binding energy of the K-electron, the K-conversion becomes impossible from the energy point of view and an L-conversion is observed. From the very nature of the phenomenon it follows

An astonishing result of these experiments was the existence of not two but three values of half-life for the β-particles emitted by the nuclei $^{80}_{35}Br$ and $^{82}_{35}Br$:

$$\left.\begin{aligned} &^{80}_{35}Br \xrightarrow{\beta^-} {}^{80}_{36}Kr \\ &^{82}_{35}Br \xrightarrow{\beta^-} {}^{82}_{36}Kr \end{aligned}\right\} \begin{aligned} &\tau_1 = 18 \text{ min}, \\ &\tau_2 = 4.4 \text{ h}, \\ &\tau_3 = 34 \text{ h}. \end{aligned} \qquad (3.4.16)$$

Thus, one of the two radioactive isotopes of bromine must be assigned two values of half-life. In order to find out which isotope has which lifetimes, γ-quanta were used for irradiating bromine.

The corresponding reactions lead to the formation of radioactive bromine isotopes $^{78}_{35}Br$ and $^{80}_{35}Br$, and are accompanied by the emission of neutrons:

$$^{79}_{35}Br + \gamma \rightarrow {}^{78}_{35}Br + n, \quad {}^{81}_{35}Br + \gamma \rightarrow {}^{80}_{35}Br + n. \qquad (3.4.17)$$

Both the bromine isotopes formed in this way are radioactive and disintegrate according to the following schemes:

$$\left.\begin{aligned} &^{78}_{35}Br \xrightarrow{\beta^+} {}^{78}_{34}Se \\ &^{80}_{35}Br \xrightarrow{\beta^-} {}^{80}_{36}Kr \end{aligned}\right\} \begin{aligned} &\tau_1 = 6.4 \text{ min}, \\ &\tau_2 = 18 \text{ min}, \\ &\tau_3 = 4.4 \text{ h}. \end{aligned} \qquad (3.4.18)$$

In this case also, three values of half-life are observed instead of two.

A comparison of the experimental data reveals that in both cases, identical periods (18 min and 4.4 h) are observed with the same isotope ($^{80}_{35}Br$) which, consequently, must be assigned these values of half-life.

The existence of two values of half-life for the same nucleus can be understood by assuming that the nucleus $^{80}_{35}Br$ is formed in two different isomer states, viz. the ground state and a long-lived (metastable) excited state.[46]

The processes associated with the nucleus $^{80}_{35}Br$ from the instant of its formation up to the moment when it emits an electron are schematically shown in Fig. 125*a*. The nucleus $^{80}_{35}Br$, formed out of the nucleus $^{79}_{35}Br$ as a result of neutron capture, is in a highly excited state at the moment of its creation (this state is marked by an asterisk in the figure). The excitation is removed as the nucleus successively goes over to lower energy states with a simultaneous emission of γ-quanta and/or internal conversion electrons which carry away the surplus energy. If there is a metastable state, transitions may occur in two different ways (marked in the figure as I and II). As a result of transitions taking place in the first case, the nucleus goes over to the

[46] Weizsäcker in 1936 explained the origin of isomerism as being due to the existence of metastable nuclear states.

ground state quite rapidly (10^{-12} s approx.), whence β-particles with a half-life $\tau_1 = 18$ min are emitted. In the second case of transition, the nucleus rapidly passes into a long-lived metastable state $^{80}_{35}Br^m$, whence it goes slowly into the ground state with a period $\tau_2 = 4.4$ h and then emits a β-particle. Thus, in the second case the beta decay becomes possible only after the final transition of the nucleus from the metastable state to the ground state, which occurs

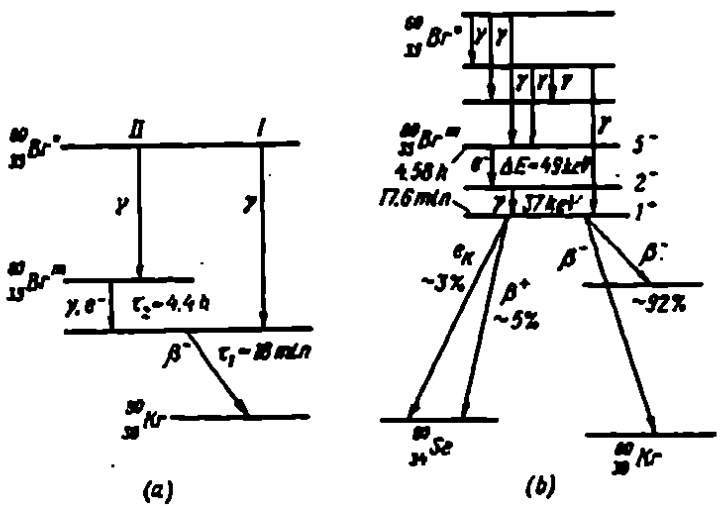

Fig. 125

with a period of 4.4 h. Hence the beta decay corresponding to it will also be characterized by a period of 4.4 h. Since β-particles are emitted in both cases from the same energy level, their energy spectra will be identical.

The nuclear isomerism has been investigated quite extensively at present. The condition for the existence of nuclear isomerism is the presence of an energy level near the ground state, differing strongly from the latter in its angular momentum ($|\Delta I| \geqslant 4$). It was mentioned above that gamma transitions between such levels must be severely hindered and hence the corresponding lifetimes may be of the order of several hours, days, or even years. It is these levels that play the role of metastable states of the isomer nuclei.

There are two ways in which excitation can be removed from a metastable nuclear state. The first of these was illustrated above by considering the example of $^{80}_{35}Br^*$. Figure 125*b* shows a detailed scheme of decay of the nucleus $^{80}_{35}Br^*$ with more exact values of the half-lives. The nucleus goes over from the metastable state to the ground state by emitting γ-quanta or internal conversion electrons. After this, β-particles are emitted from the ground state with the same energy spectrum as for β-particles emitted during the normal

beta transition. However, since the lifetime of the metastable state is longer than the half-life of beta radiation, we observe the second (longer) half-life for beta decay.

The second way is observed when a β-particle can be emitted directly from the metastable state. This is possible if the probability of radiative transition is comparable with that of the emission of a β-particle. The energy spectra of both types of β-particles must be different. This is due to the fact that in these cases, the beta transitions occur between different energy states. Not only are the original states (ground state in the first case and the metastable state in the

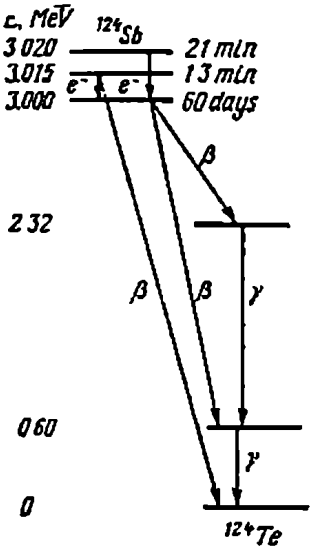

Fig. 126

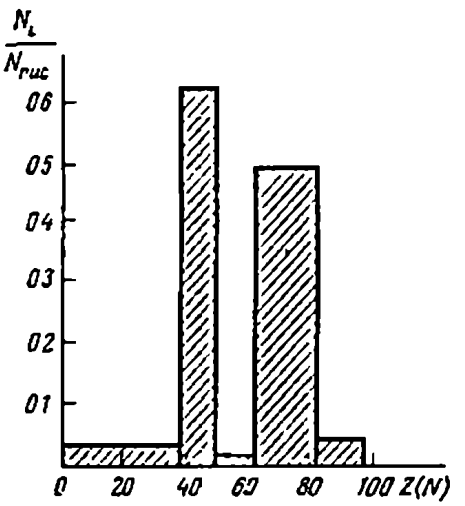

Fig. 127

second) different, but the final states as well. The latter circumstance is apparent from the fact that the initial states have quite different angular momenta and hence beta transitions from these states to the same energy state of the daughter nucleus are not possible.

An example of this type of an isomer is the nucleus $^{60}_{27}$Co, the deexcitation of whose metastable state occurs as a result of direct beta transition from the metastable state in 10% of the cases, while in 90% cases a γ-quantum is emitted.

In some cases, the nucleus may have two metastable states and hence three values of half-life are observed.

One such nucleus is $^{124}_{51}$Sb, which emits electrons with half-lives of 60 days, 21 min and 1.3 min. The transition diagram for this nucleus is shown in Fig. 126.

Isomerism may also be exhibited in the form of several half-lives for the spontaneous fission of the nucleus. The nucleus ^{242}Am is a good example of this type of nucleus. In the isomeric state, this

nucleus undergoes spontaneous disintegration with a half-life $T_{1/2} = 1.4 \times 10^{-3}$ s, while $T_{1/2}$ for the ground state is $\sim 10^8$ years.

Metastable states may also be observed for β-stable nuclei. In this case, the metastable state is de-excited through emission of γ-quanta and conversion electrons. An example of β-stable isomer is the nucleus $^{115}_{49}In$ with a metastable level 0.393 MeV and lifetime 104 min. Thus, in all cases, the essence of isomerism lies in the existence of an excited state of the nucleus with a measurable lifetime.

On account of the comparatively long lifetime, this state in fact exhibits the properties of a new isomeric nucleus with altered values of mass M, spin I, parity P, isospin T, lifetime τ and so on (but with the same values of Z and A).

Nuclear isomerism is by no means a rare phenomenon. About a hundred long-lived isomeric nuclei are known to exist. A statistical analysis of their distribution according to the number of nucleons contained in them leads to the following interesting regularities. Nuclei with odd mass number A have the largest number of isomeric states; isomeric states are encountered quite frequently in odd-odd nuclei, while they are very rare in even-even nuclei. If isomeric nuclei with odd A are distributed in accordance with the number of protons or neutrons contained in them, an extremely sharp dependence (*isomerism islands*) shown in Fig. 127 and Table 21 are observed.

Table 21

Number of nuclei and isomers	Number of neutrons or protons (nucleus with odd A)				
	1-37	39-49	51-81	83-81	83-97
Number of nuclei N_{nuc}	106	58	65	69	56
Number of isomers N_i	3	36	1	34	2
N_i/N_{nuc}	0.028	0.62	0.015	0.49	0.036

These regularities can be explained with the help of the shell model (see Sec. 2.3.3).

It was mentioned above that depending on the multipolarity of the gamma transition, the lifetime of the excited state may vary over a wide interval. Hence in principle there should be isomeric states with quite diverse periods (from very small fractions of a second to several thousand years). It can be expected that the new experimental techniques will lead to the discovery of isomers with

much shorter and much longer periods. For example, it is well known that the isomer ^{236}Np has $T_{1/2} \simeq 5000$ years, while for the isomer ^{135}Cs, $T_{1/2} = 2.8 \times 10^{-10}$ s.

3.4.4. Mössbauer Effect

While considering the energy states of the atomic nucleus, we have so far assigned definite energy values to them. However, this is not quite true.

Let us consider, for example, the nucleus ^{191}Ir, which is in an excited state with energy $E = 129$ keV and from which it can go over to the ground state by emitting a γ-quantum with half-life $T_{1/2} \simeq 10^{-10}$ s (Fig. 128). According to the uncertainty relation, the energy E of the excited state is then known with an error

$$\Delta E \simeq \hbar/\Delta t = \frac{10^{-27}}{10^{-10} \times 1.6 \times 10^{-12}} \simeq 5 \times 10^{-6} \text{ eV}.$$

The quicker the de-excitation of the excited state, the higher the uncertainty in the value of the energy of the excited state. Only the ground state of a stable nucleus has $\Delta E = 0$ and is, therefore, characterized by a definite energy value.

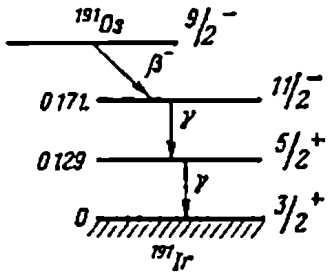

Fig. 128

The uncertainty in the excited state energy leads to nonmonochromatism of the gamma radiation emitted during the transition of the nucleus from the excited state to the ground state. This nonmonochromatism is called the *intrinsic line width* Γ of the gamma radiation. In the example under consideration, $\Gamma \simeq 5 \times 10^{-6}$ eV. This is a very small quantity in comparison with the gamma transition energy $E = 129$ keV. Hence if a change in the energy by an amount of the order of the intrinsic line width of the radiation could be detected, it would become possible to measure energy with a very high relative accuracy which is equal to Γ/E. In the example considered by us, $\Gamma/E \simeq 4 \times 10^{-11}$. For narrower lines, i.e. for gamma transitions with large periods, the value of Γ/E must be even lower.

In principle, it is possible to measure the energy variation equal to the intrinsic line width of the radiation with the help of resonance absorption of gamma radiation. *Resonance absorption* of gamma radiation is a process in which the nucleus is excited under the action of γ-quanta emitted by these nuclei during the inverse transitions from the given excited state to the ground state.

The resonance absorption can be experimentally observed quite easily by studying the passage of resonance gamma radiation through a thin plate of a given substance. When the energy of gamma radiation coincides with the transition energy, the absorption sharply increases, thus making it possible to measure small variations in energy near the resonance value. However, this method could be used up to 1958 only for quite large values of line width.

The transition of a nucleus from an excited state with energy E to the ground state is accompanied by the emission of a γ-quantum which takes away not the entire excitation energy E, but a somewhat lower value $E_{\gamma_{em}}$ because a fraction of the energy T_{nuc} is imparted as recoil energy to the emitting nucleus:

$$E_{\gamma_{em}} = E - T_{nuc} < E \tag{3.4.19}$$

(cf. similar phenomenon in alpha and beta decay). In the same way, the excitation of the nucleus to energy E requires gamma radiation with energy

$$E_{\gamma_a} = E + T_{nuc} > E, \tag{3.4.20}$$

where T_{nuc} is the recoil energy imparted by the γ-quantum to the absorbing nucleus. Thus, the emission and absorption lines for the same state of a given nucleus are displaced with respect to each other by $2T_{nuc}$ (Fig. 129*a*).

The recoil energy can be easily calculated by considering that the law of momentum conservation $p_\gamma = p_{nuc}$ must be obeyed during the emission of a γ-quantum:

$$T_{nuc} = P_{nuc}^2/2M_{nuc} = p_\gamma^2/2M_{nuc} = E_\gamma^2/2M_{nuc}c^2 \simeq E^2/2M_{nuc}c^2. \tag{3.4.21}$$

In the problem under consideration, we get a very small value of the recoil energy:

$$T_{nuc} = (1.29 \times 10^6)^2/2 \times 191 \times 931 \times 10^6 \simeq 0.05 \text{ eV}.$$

However, this value is much larger than the intrinsic line width of the radiation:

$$T_{nuc} \gg \Gamma.$$

It seems that this should indicate the absolute impossibility of a resonance process taking place. However, this is not true since the real width of the emission (absorption) line is determined not by the intrinsic width Γ, but by the Doppler broadening[47]

$$D = 2\sqrt{T_{nuc}kT^\circ}. \tag{3.4.22}$$

[47] Doppler broadening is due to different Doppler shifts of the lines emitted by different atoms on account of the fact that the velocity and direction of their thermal motion are different.

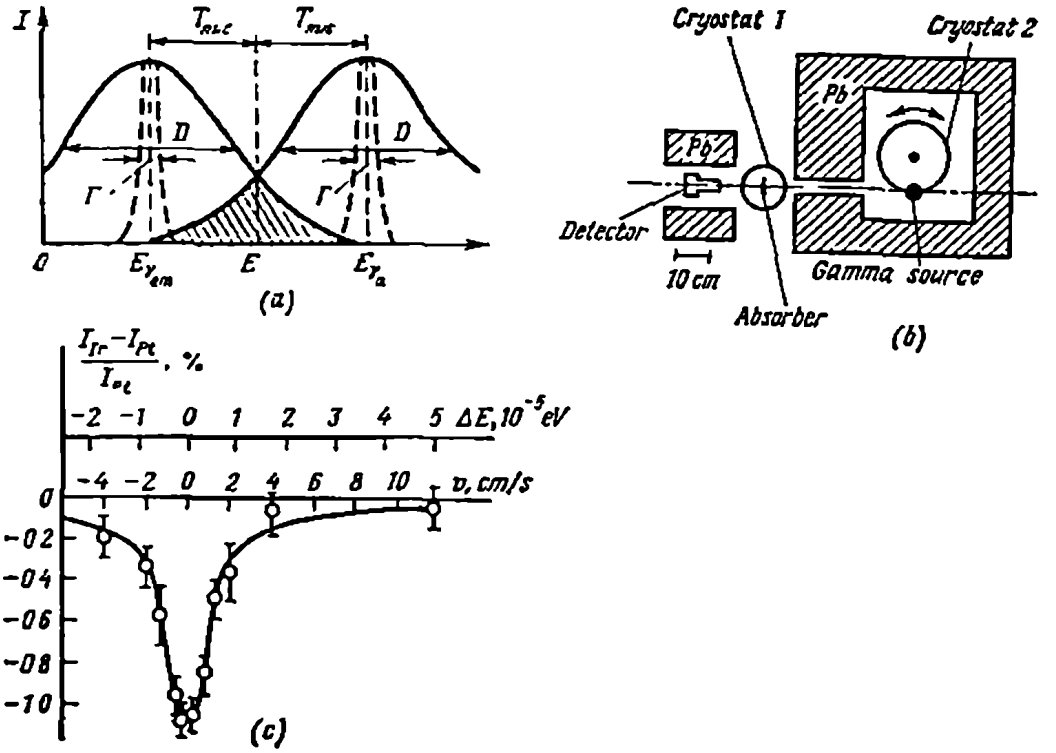

Fig. 129

At room temperature ($T = 300$ K, $kT = 0.025$ eV), this quantity is equal to

$$D\,(300\ K) = 2\sqrt{0.05 \times 0.025} \simeq 0.07 \text{ eV}.$$

Since $D \simeq T_{\text{nuc}}$, the Doppler broadenings of emission and absorption lines partially overlap (hatched region in Fig. 129*a*) and the resonance becomes possible. However, the resonance is not very sharp, since

$$D/E = 0.07/1.3 \times 10^5 \simeq 0.5 \times 10^{-6},$$

and can be observed only for a very small number of γ-quanta belonging to the small region of line overlapping.

3.4.4a. Mössbauer's Experiments

The German physicist Mössbauer, while investigating in 1958 the resonance absorption in the case of a partial overlapping of lines due to Doppler broadening, decided to reduce D by cooling the source and the absorber. Due to a decrease in the overlapping region in this case, one could naturally expect a decrease in the fraction of

absorbed quanta. Instead, the experiment revealed an enhanced effect, pointing towards an increase in the overlapping region.

In order to explain this strange result, Mössbauer assumed that under certain conditions (a very low transition energy and low temperature in comparison with the Debye temperature of the crystal), the recoil momentum and energy during the emission (absorption) of a γ-quantum are used neither for knocking out an atom from a lattice site, nor to change the energy state of the crystal. Instead, these are elastically imparted to the crystal as a whole (more exactly, to a very large group of atoms $N \simeq 10^6$ covered by the travelling acoustic wave during emission). In this case, the correlation between the momentum and energy of the emitting (absorbing) nucleus suffers a discontinuity, since the recoil energy R is practically equal to zero on account of a large mass of the crystal:

$$R = P_{\text{nuc}}^2/2 \times 10^6 M_{\text{nuc}} = T_{\text{nuc}}/10^6 \simeq 5 \times 10^{-10}\ \text{eV} \ll \Gamma.$$

Consequently, a recoilless emission (absorption) of γ-quanta becomes possible or, in other words, the shift between the emission and absorption lines disappears:

$$E_{\gamma_{\text{em}}} = E_{\gamma_a}. \tag{3.4.23}$$

Simultaneously, for these acts of emission and absorption the Doppler broadening D must disappear, since it will be less than the intrinsic line width Γ:

$$D(88\ \text{K}) = 2\sqrt{RkT_{\text{eff}}} = 2\sqrt{5 \times 10^{-10} \times 0.0075} \simeq 4 \times 10^{-6}\ \text{eV} < \Gamma.$$

In other words, under the conditions mentioned above, a sharp recoilless resonance with width equal to the intrinsic line width must be observed. This explanation was brilliantly proved by Mössbauer in his famous second experiment.

Mössbauer's experiment is schematically represented in Fig. 129*b*. Here a ^{191}Ir source emits gamma radiation with energy 129 keV[48], and the absorber is made of iridium. The source and the absorber were placed in cryostats[49] 1 and 2 in which a temperature of 88 K is maintained. Cryostat 2 containing the source is capable of rotation. Upon rotation of the cryostat in one direction, the source moves towards the absorber with a certain velocity while for rotation in the opposite direction, the source moves away from the absorber with the same velocity.

The absorption of γ-quanta was measured in the experiment for different source velocities. The results of the experiment are presented in Fig. 129*c*.

---

[48] As a matter of fact, the source is ^{191}Os, which is transformed into ^{191}Ir in the excited state as a result of beta decay (see Fig. 128).

[49] A cryostat is a thermostat for maintaining temperatures below 0 °C.

The relative velocity of the source and the absorber, and the corresponding change ΔE in the energy of the emitted γ-quanta (due to the Doppler effect) are plotted along the abscissa axis. The relative difference in the intensities of gamma radiation passing through the iridium absorber and a platinum absorber of the same thickness (to estimate the background) are plotted along the ordinate axis. It can be seen from the figure that even at velocities of a few centimetres per second, corresponding to a Doppler shift of less than 10^{-5} eV in the energy of γ-quanta, the resonance is disrupted. This means that a recoilless line with intrinsic width $\Gamma \simeq 5 \times 10^{-6}$ eV of gamma transition was indeed observed in the experiment.

The resonance absorption method can be used for measuring very small energy variations. It was mentioned above that the measure of accuracy of this method is the ratio Γ/E which is equal to 4×10^{-11} for the example considered here. Actually, the relative accuracy of measurements is still higher, since it is possible to observe experimentally a change in absorption when a line shifts by 1/100 of its intrinsic width.

The Mössbauer effect was observed in many materials, and still narrower lines were observed for some of them. The magnitude of this effect is usually about 1% or even less, the working temperature varies from room temperature for some substances to helium temperature (about 4 K) for some others. With increasing temperature, the effect gradually weakens and ultimately disappears.

In the following sections, we shall give an elementary explanation for these features of the Mössbauer effect and also consider some examples involving the application of this effect in nuclear and general physics for detecting and investigating quite fine effects.

Mössbauer was awarded the Nobel Prize in physics in 1961 for the discovery of recoilless radiation, scattering and absorption.

3.4.4b. Physical Nature of the Mössbauer Effect

To explain the Mössbauer effect, we shall use the simplest quantum model of a solid proposed in 1904 by Einstein to explain the temperature variation of specific heat. According to this model, a solid consisting of N atoms is a set of $3N$ harmonic oscillators having the same frequency Ω. This frequency is determined from the condition

$$\hbar\Omega = k\theta_E, \tag{3.4.24}$$

where k is the Boltzmann constant and θ_E is a characteristic constant describing the elastic properties of the solid (this constant was later termed the Einstein temperature).

The energy of an oscillator can assume only quantized values

$$E_n = n\hbar\Omega, \tag{3.4.25}$$

where n is an integer.

The relative probability of an oscillator being in a state with a given n at a given temperature T is

$$P_n = \frac{\exp(-n\hbar\Omega/kT)}{\sum_{m=0}^{\infty} \exp(-m\hbar\Omega/kT)}. \tag{3.4.26}$$

The average energy of an oscillator at a given temperature T is

$$\bar{E} = \frac{\sum_{n=0}^{\infty} n\hbar\Omega \exp(-n\hbar\Omega/kT)}{\sum \exp(-n\hbar\Omega/kT)} = \frac{\hbar\Omega}{\exp(\hbar\Omega/kT)-1} = \bar{n}\hbar\Omega, \tag{3.4.27}$$

where

$$\bar{n} = \frac{1}{\exp(\hbar\Omega/kT)-1}.$$

It can be seen from formulas (3.4.26) and (3.4.27) that at very low temperatures ($kT \leqslant \hbar\Omega$), $P_n \simeq 0$ for all n except $n=0$, for which $P_0 \simeq 1$ (Fig. 130a). In this case, the major part of the oscillators will be in the unexcited state.

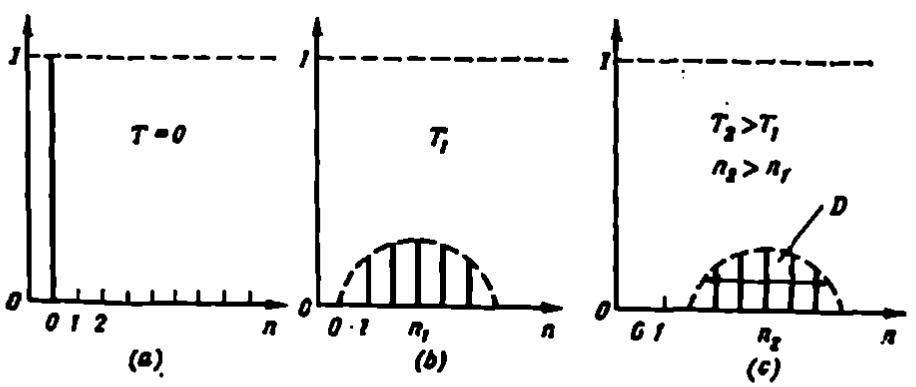

Fig 130

With increasing temperature, the value of n corresponding to the maximum probability, and the average energy $\bar{E}$ of an oscillator increase (see Fig. 130b). For $kT \gg \hbar\Omega$, the average energy of an oscillator is given by

$$\bar{E} \simeq kT \gg \hbar\Omega.$$

i.e. all the oscillators are in the excited state. Due to the thermal motion of atoms, the energy spectrum of the oscillators has a Doppler width (see Fig. 130*c*).

The energy of an oscillator can change only by an amount ΔE, which is an integer multiple of $\hbar\Omega$:

$$\Delta E = \pm m\hbar\Omega$$

(m is a positive integer).

The minimum energy received or given away by an oscillator is

$$\Delta E_{\min} = \hbar\Omega = k\theta_E. \tag{3.4.28}$$

In quantum mechanics, formula (3.4.25) was refined through the introduction of the zero-point vibration energy:

$$E_n = (1/2 + n)\,\hbar\Omega. \tag{3.4.29}$$

In quantum mechanics, the energy of an oscillator at $T = 0$ is not equal to zero, but rather assumes the lowest possible value

$$E_{\min} = (1/2)\,\hbar\Omega. \tag{3.4.30}$$

An oscillator in the state with lowest energy can only receive energy, but cannot relinquish any.

So far, heating or cooling of a solid was considered to be the only means of energy transfer to the oscillators. However, all the properties associated with the excitation of oscillators must remain intact in other methods of energy transfer as well. If we consider recoil as the mechanism of energy transfer, the Einstein model of a solid can be used to explain graphically the physical nature of the Mössbauer effect.

Suppose that a solid (say, a crystal) consists of atoms with excited nuclei. The emission of a γ-quantum by such a nucleus is associated with a recoil energy R which is generally not equal to the recoil energy for a free nucleus (not bound to the crystal lattice), and may be higher or lower than its value:

$$R \neq T_{\text{nuc}}^{\text{free}} = E_\gamma^2/2M_{\text{nuc}}c^2.$$

This difference is due to the fact that the atoms are mutually connected in a lattice and participate in thermal motion. However, it is borne out by special calculations that the average recoil energy $\overline{R}$ for a bound nucleus is equal to the recoil energy for a free nucleus:

$$\overline{R} = T_{\text{nuc}}^{\text{free}} = E_\gamma^2/2M_{\text{nuc}}c^2. \tag{3.4.31}$$

It was mentioned above that the recoil energy can be transmitted in three different ways: to knock out an atom from a lattice site (if the recoil energy is about 10 eV), to excite the phonon spectrum

of the lattice, or to move the "entire" crystal. Let us assume that the recoil energy $\overline{R}$ lies in the interval

$$\hbar\Omega < \overline{R} < 10 \text{ eV}.$$

In this case, all the acts of transmission of recoil energy will be accompanied by an excitation of oscillators whose spectrum will be displaced to the right by $\Delta E = \overline{R}$ (the distance between the peaks in Fig. 130*b* and *c* will be approximately equal to $\overline{R}$). Naturally, the energy spectrum of the emitted γ-quanta will differ from the transition energy E_0 of the nucleus by the same amount $\overline{R}$:

$$E_{\gamma_{em}} = E_0 - \overline{R}. \tag{3.4.32}$$

The width of the energy spectrum of γ-quanta will coincide with the spectral width of the oscillators, i.e. will be equal to the Doppler width.

The situation is quite similar when γ-quanta are absorbed by nuclei in a crystal in their ground state. When a γ-quantum is emitted or absorbed, the nucleus experiences a recoil $\overline{R}$. Hence to transfer a nucleus from the ground state to an excited state with energy E_0, we require γ-quanta with energy

$$E_{\gamma_a} = E_0 + \overline{R}. \tag{3.4.33}$$

The width of the absorption spectrum of γ-quanta is also equal to the Doppler width.

If both the spectra are plotted on the same graph, we obtain the pattern of resonance absorption of γ-quanta observed before the discovery of the Mössbauer effect (see Fig. 129*a*). The centres of gravity of the emission and absorption spectra for γ-quanta are displaced by twice the recoil energy.

Let us now consider the case

$$\overline{R} < \hbar\Omega.$$

On account of the existence of a minimum energy of excitation for the oscillator, viz. $\Delta E_{min} = \hbar\Omega$ [see formula (3.4.28)], some acts of emission of γ-quanta in this case must be recoilless (i.e. without any excitation of oscillators). This is due to the fact that the number of acts of emission will exceed the number of excited oscillators for $\overline{R} < \hbar\Omega$. Figure 131 shows schematically the excitation of oscillators at a low temperature $kT \leqslant \hbar\Omega$. Before the emission, the oscillator spectrum is a discrete line corresponding to $n = 0$ (dashed

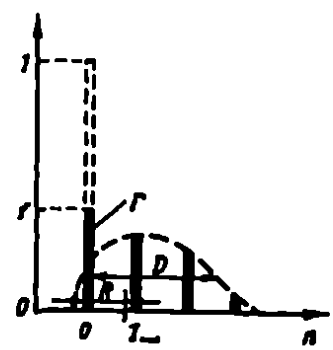

Fig. 131

line at height *1* in the figure). After the emission of γ-quanta, the average energy of the oscillators increases by $\overline{R} < \hbar\Omega$, and the zero-level line must be preserved in the oscillator spectrum (with a reduced height *f*). Besides, a broad (Doppler) region with half-width *D* (shown by the dashed curve in the same figure) must appear to the right.

Accordingly, the emission spectrum of γ*-quanta must have an* undisplaced line $E_{\gamma_{em}} = E_0$ with intrinsic width Γ (determined by

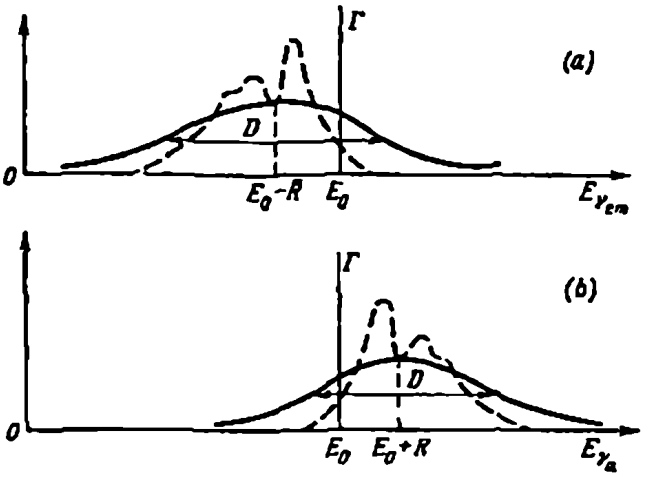

Fig. 132

the zero-point vibrations) and a broad (Doppler) maximum with centre of gravity at the energy $E_{\gamma_{em}} = E_0 - \overline{R}$ displaced to the left (Fig. 132*a*).

The shape of the spectrum of absorber oscillators is identical to that of the emitter oscillators. As regards the spectrum of γ-quanta, it will have a Doppler maximum on the right in the case of the absorber spectrum (Fig. 132*b*)[50]. A comparison of Figs. 132*a* and *b* shows that the spectra of emittep and absorbed γ-quanta contain undisplaced lines with energy E_0 equal to the nuclear transition energy, which make a sharp resonance possible with an intrinsic line width $\Delta E = \Gamma$.

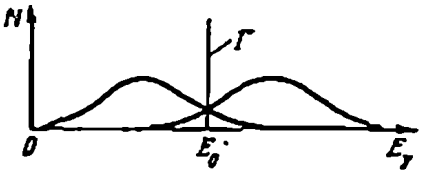

Fig. 133

It can be easily seen that the probability of a Mössbauer-type resonance process must decrease with increasing temperature of the emitter and the absorber. This is due to the fact that at $T \neq 0$ the

[50] The dashed lines show the emission and absorption spectra taking into account the quantum-mechanical effects.

crystal lattice cannot only receive energy from a γ-quantum, but also impart energy to it. Consequently, the spectra of emitted and absorbed γ-quanta have Doppler broadenings from both sides (Fig.133), the amount of the broadening increasing with temperature. Naturally, this effect leads to a relative decrease in the fraction of γ-quanta emitted with the energy corresponding to the undisplaced line. As a result, the share of processes taking place without recoil decreases.

3.4.4c. Simple Formulas

We shall use simple arguments to obtain formulas for estimating the share of recoilless processes.

The condition $\overline{R} < \hbar\Omega$ can be written in the form of equality

$$\overline{R} = (1-f)\,\hbar\Omega, \tag{3.4.34}$$

where $0 \leqslant f \leqslant 1$. Obviously, the coefficient

$$f = 1 - (\overline{R}/\hbar\Omega) \tag{3.4.35}$$

defines the fraction of recoilless processes. This coefficient is called the *Mössbauer coefficient*.

Let us estimate the value of the Mössbauer coefficient at $T = 0$. In this case,

$$E_{osc} = (1/2)\,\hbar\Omega,$$

i.e.

$$\hbar\Omega = 2E_{osc} = 4\overline{T} = 4\,(\overline{p^2}/2M_{nuc}),$$

where T and p are the kinetic energy and momentum of an oscillating nucleus with mass M_{nuc}. On the other hand,

$$\overline{R} = p_\gamma^2/2M_{nuc} = \hbar^2/\lambda_\gamma^2 2M_{nuc}.$$

Whence

$$\overline{R}/\hbar\Omega = \hbar^2/4\overline{p^2}\lambda_\gamma^2 = \overline{x^2}/\lambda_\gamma^2,$$

where $\overline{x^2}$ is the mean square displacement of the oscillator. The last equality follows from the uncertainty relation for the oscillator at $T = 0$ and $n = 0$:[61]

$$\overline{\Delta x^2}\,\overline{\Delta p^2} = \hbar^2/4.$$

Thus, the value of the coefficient at $T = 0$ is

$$f = 1 - (\overline{x^2}/\lambda_\gamma^2). \tag{3.4.36}$$

[61] In an oscillator, $\overline{\Delta x^2} = \overline{x^2}$ and $\overline{\Delta p^2} = \overline{p^2}$.

Because of the imperfection of the employed model and rough interpretation, the above reasoning cannot be considered rigorous. However, it gives a correct qualitative idea about the essence of the effect. A more rigorous analysis leads to the following formula for coefficient f:

$$f = \exp(-\overline{x^2}/\lambda_\gamma^2). \tag{3.4.37}$$

This formula is valid for the general case $T \neq 0$. In the theory of elastic scattering of X-rays and neutrons, this expression is known as the Debye-Waller factor. Since $E_n = (1/2 + n)\hbar\Omega$ and $\Delta x \Delta p = 1/2 + n)\hbar$ at $T \neq 0$, and since $\overline{\Delta x^2} \propto \overline{\Delta p^2}$ in an oscillator, we obtain $\overline{\Delta x^2} \propto n \propto T$, i.e. $\overline{x^2}$ decreases as $T \to 0$. Thus, as $T \to 0$, formula (3.4.37) is transformed into the semiquantitative expression (3.4.36).

An analysis of formula (3.4.37) shows that for $f \simeq 1$, we must have

$$\overline{x^2} < \lambda_\gamma^2. \tag{3.4.38}$$

Thus, quite large values can be expected for the coefficient f if the following conditions are satisfied:

(1) a low absolute temperature T (low energy and small amplitude $\overline{x^2}$ of the oscillators);

(2) a solid emitter, i.e. as before, a small amplitude $\overline{x^2}$ of the oscillators (in liquids and gases, $\overline{x^2}$ is large because of the possibility of free motion of molecules);

(3) a low transition energy E_0 (large λ_γ); and

(4) a high elasticity (rigidity of the crystal), i.e. a high characteristic temperature θ_e (to ensure that the condition $R < \hbar\Omega = k\theta_e$ is satisfied).

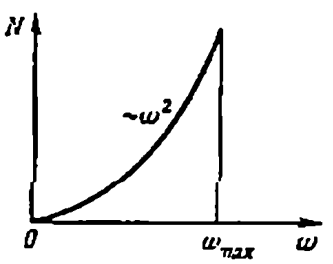

Fig. 134

Formula (3.4.37) is valid for any oscillator spectrum. In the specific heat theory (upon a comparison of the theory and experiment), it was shown that the best results are obtained from the Debye spectrum of oscillators (Fig. 134). According to Debye, the oscillators do not have a single frequency Ω (as in the Einstein theory), but rather a wide spectrum of frequencies which varies according to a quadratic law. The maximum frequency ω_{max} of the spectrum satisfies the condition

$$\hbar\omega_{max} = k\theta_D, \tag{3.4.39}$$

where k is the Boltzmann constant and θ_D is the Debye temperature characterizing the elasticity of the crystal.

It can be easily seen that for the coefficient f in the form (3.4.37) to be nonzero, it is necessary that the same conditions be satisfied as for the coefficient f written in the form (3.4.36). The only difference is that the characteristic temperature will now be θ_D instead of θ_E.

However, substituting the value of $\overline{x^2}$ for the Debye spectrum into (3.4.37), we obtain specific estimates for f in monatomic crystals.[82] The following expression for the coefficient f is obtained as a result of calculations:

$$f = \exp\left\{-\frac{6\bar{R}}{k\theta_D}\left[\frac{1}{4}+\left(\frac{T}{\theta_D}\right)^2\int_0^{\theta_D/T}\frac{x\,dx}{\exp x-1}\right]\right\}. \quad (3.4.40)$$

As $T \to 0$, this formula assumes the form

$$f = \exp\left(-\frac{3}{2}\frac{\bar{R}}{k\theta_D}\right) \to 1-\frac{3}{2}\frac{\bar{R}}{\hbar\omega_{max}}, \quad (3.4.41)$$

which differs from the simple expression of the type (3.4.35) only by the factor 3/2. The appearance of this factor is due to the specific shape of the Debye spectrum.

3.4.4d. Selection of Materials with Good Parameters

The main parameters which are considered while choosing materials for investigations with the help of the Mössbauer effect are the coefficient f, the attainable resolving power $\Delta E/E$, as well as the working temperature.

The coefficient f can be estimated from formula (3.4.40). It follows from this formula that large values of f are possible if the recoil R is small (i.e. the transition energy E_0 is low), temperature T is low and the Debye temperature θ_D is high. Thus, for example, at $\theta_D \simeq 300$ K and $E_0 < 40$ keV, the coefficient f must exceed 0.1 even at room temperature.

These conditions are satisfied for ^{57}Fe, which has $\theta_D \simeq 500$ K and $E_0 = 14.4$ keV. Figure 135 shows the temperature dependence of f for ^{57}Fe. It can be seen that for this isotope $f > 0.6$ right up to room temperature $T \simeq 300$ K. The other characteristics of ^{57}Fe are: $T_{1/2} = 1.0 \times 10^{-7}$ s, $\Gamma = 4.5 \times 10^{-9}$ eV, $\Gamma/E \simeq 3 \times 10^{-13}$. The

[82] Formula (3.4.40) is not applicable for polyatomic crystals and impurity atoms.

transition is schematically shown in Fig. 136. Because of its high-quality parameters, ^{57}Fe is widely used in investigations of the Mössbauer effect. Another substance which can be used at room temperature is ^{119}Sn which has the following parameters: $E_0 = 23.8$ keV, $T_{1/2} = 1.8 \times 10^{-8}$ s, $\Gamma = 2.5 \times 10^{-8}$ eV and $\Gamma/E \simeq 10^{-12}$. The isotope ^{181}Ta is also used, it is characterized by the parameters $E_0 = 6.2$ keV, $T_{1/2} = 6.8 \times 10^{-6}$ s, $\Gamma = 6.7 \times 10^{-11}$ eV, $\Gamma/E \simeq 10^{-14}$. This isotope has a very small value of the ratio Γ/E and a large value of the coefficient $f \simeq 5\%$ at room temperature. In terms of resolving power, ^{67}Zn has unique potentialities. Its parameters are: $E_0 = 93$ keV, $T_{1/2} = 9.4 \times 10^{-6}$ s, $\Gamma \simeq 5 \times 10^{-11}$ eV and $\Gamma/E \simeq 5 \times 10^{-16}$. However, the Debye temperature of ^{67}Zn is so low that $f \simeq 0.3\%$ even at helium temperatures (about 4 K).

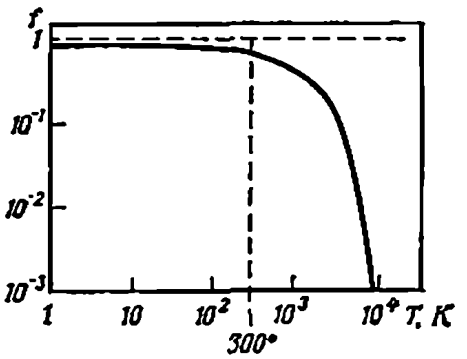

Fig. 135

3.4.4e. Application of the Mössbauer Effect in Nuclear and General Physics

The high accuracy with which energy variations can be measured with the help of the γ-quanta resonance absorption method makes it possible to use this method for detecting and analyzing quite fine effects. Let us consider some examples from nuclear physics and general physics.

Hyperfine splitting of nuclear levels. It is well known (see Sec. 1.5) that the scale of hyperfine splitting is determined by the product of the nuclear magnetic moment ($\mu_{nuc} \simeq \mu_B = 5.05 \times 10^{-21}$ erg/G) and the average magnetic field produced by the atomic electron shells in the region of the nucleus ($\overline{H}_e \simeq 10^5$ G):

$$\Delta E \simeq \mu_B \overline{H}_e \simeq 10^{-7}\text{-}10^{-6} \text{ eV}.$$

The typical value of E_{el}, the energy of transition between electron levels in the optical region, is of the order of 1 eV. Hence the relative value of the hyperfine splitting of electron levels is

$$\Delta E/E_{el} \simeq 10^{-7}\text{-}10^{-6}.$$

The splitting of spectral lines of such magnitude can be easily measured by optical spectroscopy methods.

It is quite obvious that the hyperfine splitting must also be manifested against the background of nuclear transitions. However, on

account of large values of the transition energy in this case ($E_{nuc} \simeq 10^4$-10^5 eV), the hyperfine splitting of nuclear levels is much smaller than for electron levels

$$(10^{-7}\text{-}10^{-6})/(10^4\text{-}10^5) = 10^{-12}\text{-}10^{-10}.$$

Splitting of this order can be measured only with the help of the Mössbauer effect.

Hyperfine splitting of nuclear levels was first discovered in the iron isotope ^{57}Fe. The quantum numbers of the ground and excited states of ^{57}Fe are equal to $1/2^-$ and $3/2^-$ respectively (see Fig. 136).

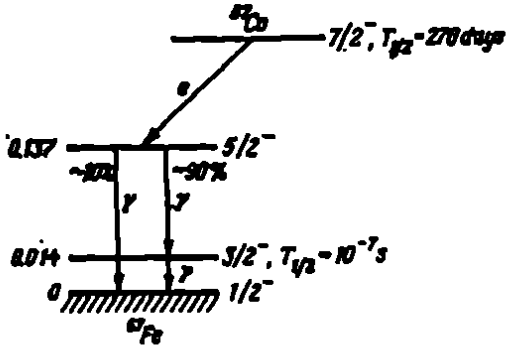

Fig. 136

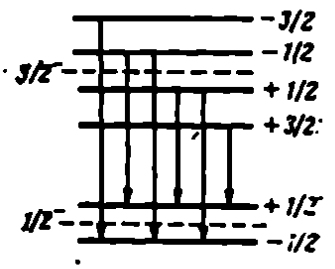

Fig. 137

Consequently, the ground state must split into two sublevels with values $m = +1/2$ and $m = -1/2$, while the excited state must split into four sublevels with values of m equal to $+3/2$, $+1/2$, $-1/2$, $-3/2$. Between these sublevels, six transitions are allowed by the selection rules ($\Delta m = 0, \pm 1$) (Fig. 137). Such a structure of sublevels is possessed by emitter nuclei as well as by absorber nuclei. Hence the dependence of the resonance absorption on the velocity of the source must be quite complicated. To simplify this pattern, the emitter nuclei were placed in a diamagnetic stainless steel grating. In this case, there is no hyperfine splitting for these nuclei and the number of valleys on the experimental Mössbauer spectrum is the same as the number of transitions in the absorber nucleus ^{57}Fe (Fig. 138). The splittings ΔE_{gr} and ΔE_{exc} for the ground and the excited states of ^{57}Fe, as well as the sequential order of the megnetic quantum number m for the excited state sublevels (see Fig. 137), can be calculated by analyzing the experimental curve. This allows us to calculate the average magnetic field due to electrons in the region of the nucleus ^{57}Fe from ΔE_{gr} and known value of the megnetic moment of ^{57}Fe in the ground state ($\mu_{gr} = 0.09\mu_B$):

$$H_e = 3.33 \times 10^5 \text{ G}.$$

In turn, the value of $\overline{H}_e$ obtained in this way can be used to determine the numerical value and sign of the magnetic moment of the excited state of the nucleus ^{57}Fe with the help of the value of ΔE_{exc} and the alternation of the quantum number m:

$$\mu_{exc} = -0.153\mu_B.$$

It should be noted that displacement of the source at the rate of about 1 mm per second is required for carrying out such experiments.

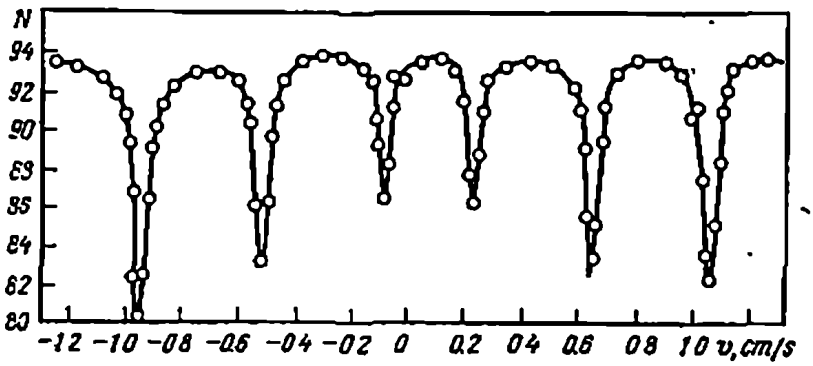

Fig. 138

Estimation of the nuclear radius in the excited state. So far, by the energy of the Mössbauer transition we have meant the difference in the nuclear energies in the excited and ground states. However, experiments are conducted not with bare nuclei but with atoms, i.e. with nuclei surrounded by electrons. The interaction of the nucleus with the electron shell leads to a shift of nuclear and electron levels (in the same way as the hyperfine splitting which is manifested for nuclear as well as electron levels). The magnitude δE of this shift depends on the binding energy of electrons with the nucleus, which is determined by the electron density $e\,|\psi(0)|^2$ in the region of the nucleus, the nuclear radius R and its charge Ze:

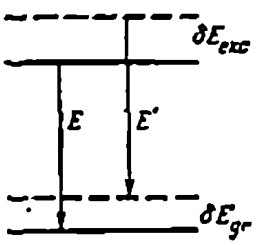

Fig. 139

$$\delta E = (2\pi/5)\, Ze^2\, |\psi(0)|^2\, R^2 \qquad (3\,4\,42)$$

If the dimensions of the nucleus in the ground and excited states are different ($R_{gr} \neq R_{exc}$), the energy shifts for the two states will also be different, i.e. $\delta E_{gr} \neq \delta E_{exc}$ (Fig. 139). The difference ΔE

between these quantities gives the correction to the transition energy E:

$$E' = E + \Delta E, \tag{3.4.43}$$

where

$$\Delta E = \delta E_{exc} - \delta E_{gr} = (2\pi/5)\, Ze^2\, |\psi(0)|^2 \{R^2_{exc} - R^2_{gr}\}.$$

If the emitter and absorber atoms are identical, this correction will also be the same for both atoms ($\Delta E_{em} = \Delta E_a$) and would not detune the resonance. However, if the chemical compositions of the emitter and absorber are different (for identical nuclei), the difference between the binding energies of the electrons with the emitter and absorber nuclei (on account of different electron shells, we have $|\psi(0)|^2_{em} \neq |\psi(0)|^2_a$) will cause different shifts in the nuclear levels of the absorber and the emitter ($\Delta E_{em} \neq \Delta E_a$). This will lead to different corrections to the transition energy E' for the emitter (E'_{em}) and the absorber (E'_a). The difference $E'_a - E'_{em}$ is called the *chemical* or *isomeric shift of nuclear levels*:

$$\Delta E_{chem} = E'_a - E'_{em} = \Delta E_a - \Delta E_{em}.$$

According to formula (3.4.43), the chemical shift is given by

$$\Delta E_{chem} = (2\pi/5)\, Ze^2 \{R^2_{exc} - R^2_{gr}\} [|\psi(0)|^2_a - |\psi(0)|^2_{em}]. \tag{3.4.44}$$

In some cases (under certain assumptions), the expression in the brackets can be calculated. Hence the measurement of ΔE_{chem} can provide an estimate for the radius of the nucleus in excited state.

The chemical shift is very small ($\Delta E_{chem} \simeq 10^{-7}$ eV, $\Delta E/E \simeq 10^{-12}$) but can be certainly measured with the help of the Mössbauer method. Measurements have shown that a nucleus in an excited state can have a larger or a smaller radius in comparison with the radius of the nucleus in the ground state:

$$\begin{aligned} &R_{exc}(^{57}\mathrm{Fe}) < R_{gr}(^{57}\mathrm{Fe}) \quad \text{by } 0.1\%, \\ &R_{exc}(^{119}\mathrm{Sn}) > R_{gr}(^{119}\mathrm{Sn}) \quad \text{by } 0.01\%. \end{aligned} \tag{3.4.45}$$

Doppler velocities of about 0.1 mm/s are required for such measurements.

Measurement of red shift under laboratory conditions. Still lower velocities (about 1 μm/s) were required to verify one of the predictions of Einstein's general theory of relativity (GTR) under laboratory conditions. According to GTR, a γ-quantum with energy E_γ must behave in the gravitational field as a particle with gravitational mass $m = E_\gamma/c^2$. When the γ-quantum moves (falls) along the lines of force of the gravitational field, it must acquire energy $\Delta E = mgH = (E_\gamma/c^2)\, gH$, where g is the acceleration due to gravity

and H is the path traversed by the quantum. Its frequency increases by

$$\Delta\nu = (E_\gamma/hc^2)\, gH \qquad (3.4.46)$$

(blue shift).

Conversely, the γ-quantum must lose energy as it moves against the gravitational field (upwards). Accordingly, its frequency will decrease (red shift). The relative variation of energy is very small, and for $H = 1$ m we have

$$\Delta E/E = gH/c^2 = 9.81/9 \times 10^{16} \simeq 10^{-16}.$$

The experiment was carried out in 1959 by Pound and Rebka in the 22.6-m-high tower of Harvard University. For such a length of the path of a γ-quantum, the relative variation in energy was $\Delta E/E \simeq 2.5 \times 10^{-15}$, which is about 1/150 of the value of $\Gamma/E \simeq 3 \times 10^{-13}$ for the ^{57}Fe isotope used in the experiment. Thus, to observe the effect reliably, we must be able to measure energy with an absolute error of $10^{-3}\Gamma \simeq 5 \times 10^{-12}$ eV and with a relative error $\Delta E/E \simeq 5 \times 10^{-16}$. Such an accuracy could be attained by conducting the experiment under certain special conditions (helium medium between the emitter and the absorber, temperature control, protection from vibration). It can be easily seen that a negligibly small Doppler velocity (about 0.75 μm/s) is required to compensate the displacement being measured. Such values of velocity were attained with the help of a hydraulic unit with two pistons of different diameters, the smaller being set in motion by a clockwork. In a later experiment (1965), Pound and Snyder improved the sensitivity of the method by measuring the absorption at the steepest parts of the resonance curve (Fig. 140). For this purpose, the emitter velocity was periodically modulated within the required limits $v_0 \pm \Delta v$ by a piezoelectric vibrator. The results of measurements are in accord with the predictions of GTR. It is interesting to note that the registered terrestrial effect is 10^9 weaker than the solar effect measured by astrophysical methods.

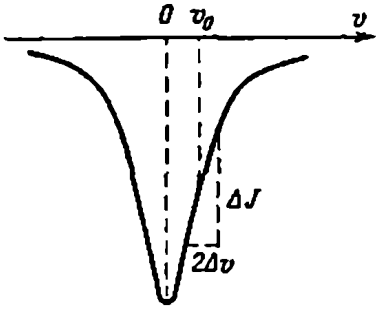

Fig. 140

3.4.5. Parity Violation in Gamma Transitions

Since a nuclear state is characterized in the most general case by a wave-function of the type

$$\psi = \psi_{reg} + F\psi_{irreg},$$

where $F\psi_{irreg}$ is the admixture of the state with opposite parity (see Sec. 1.6), a gamma transition may be accompanied by effects associated with the parity violation. This is so because the γ-quanta corresponding to the main part of the wave-function ψ_{reg} and to the admixture $F\psi_{irreg}$ must be of different types for the same multipolarity (these quanta will be of electric and magnetic type respectively). Interference between them leads to effects that are proportional to F and are manifested as terms with odd Legendre polynomials in the angular distribution of gamma radiation from polarized nuclei. Experimentally this effect is observed as an asymmetry in γ-quantum emission with respect to the direction of polarization of the nuclei. This result is quite natural, since $P\psi \neq \pm\psi$, i.e. parity is not conserved and hence there can be no mirror symmetry in the emission of gamma radiation.

On account of the extremely low value of the effect (it should be recalled that $F \simeq 10^{-7}$), the experiments are very difficult, and almost impossible. However, experimental measurements become possible if we choose a nuclear transition for which the effect is amplified. There are three different mechanisms in which this amplification can occur.

(a) Kinematic amplification due to a proper choice of the main transition (corresponding to the regular part of the wave-function) and the admixture transition. For example, a correct combination will be the less probable $M1$-transition for the main transition and the more probable $E1$-transition for the admixture transition. The kinematic amplification factor R_k can attain values up to 10.

(b) Structural amplification associated with the suppression of the main transition due to the structure of nuclear levels (for example, the prohibition with respect to the additional quantum numbers in the region of deformed nuclei). The structural amplification factor R_s can attain values up to 10^3-10^4.

(c) Dynamic amplification due to mixing of states with opposite parities. This type of amplification takes place in complex nuclei upon a strong excitation. Possible values of the dynamic amplification factor are $R_d \simeq 10^2$.

Of course, one cannot hope to find a nucleus and a level for which all the amplification factors will be favourable. However, by a proper choice of the nucleus and the transition, it is possible to attain $R = R_k R_s R_d \simeq 10^3$. In this case, the measure of parity nonconservation will be the quantity $a = RF \simeq 10^{-4}$, which can be measured in principle.

The asymmetry in γ-quantum emission was first observed in 1964 by the Soviet physicists Abov, Krupchitsky and Oratovsky.[53] The

[53] Yu.G. Abov, P.A. Krupchitsky and Yu.A. Oratovsky. *Phys. Lett.*, 12, 25 (1964).

investigations were carried out on the nucleus ^{113}Cd, which satisfies the following three conditions:

(a) a large capture cross section of thermal neutrons;

(b) the formation of the excited nucleus ^{114}Cd upon neutron capture, with a subsequent $M1$-transition to the ground state (the diagram for the main transitions in this nucleus is shown in Fig. 141);

(c) a large theoretical value of $R \simeq 10^3$.

Measurements were carried out with the help of a set-up shown schematically in Fig. 142. A thermal neutron beam n from a heavy water reactor (Institute of Theoretical and Experimental Physics,

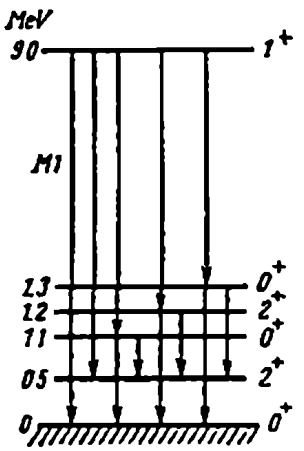

Fig. 141

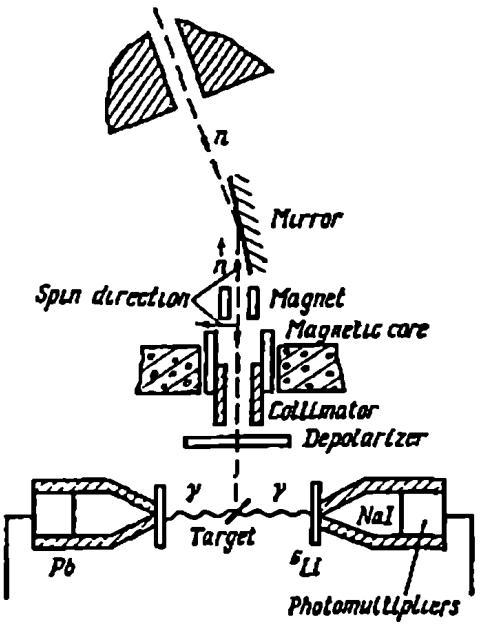

Fig. 142

Moscow) is incident on a cobalt mirror, is polarized by it and passes through a rotating magnet (for changing the direction of polarization of neutrons), a magnetic core, a collimator, a depolarizer (the construction of the depolarizer permitted measurements on polarized and unpolarized beam alternately at the rate of 20 times per second). After this, the beam is incident on the cadmium target whose nuclei are polarized and go into an excited state. The γ-quanta emitted by the target were registered by two scintillation spectrometers with *NaI(Tl) crystal and photomultipliers. To reduce the background,* the spectrometers were shielded by lead Pb (to reduce the γ-quantum background) and lithium (^6Li) carbonate (to reduce background due to scattered neutrons). An electronic unit separated γ-quanta with energy 8.5-9.5 MeV and permitted separate recording of results corresponding to polarized and unpolarized neutrons.

As a result of measurements, the following value was obtaine the asymmetry coefficient:

$$a = -(3.7 \pm 0.9) \times 10^{-4}.$$

This result was confirmed by a series of check experiments in w the direction of polarization of neutrons was varied, the interv γ-quantum energies being measured was shifted, and so on. In anc experiment, the direction of neutron polarization was rapidly ied (10 times per second) and measurements were carried ou unpolarized neutrons. As a result, the following value was obta for a:

$$a = -(3.5 \pm 1.2) \times 10^{-4}.$$

This value is close to the one obtained in the above experin Finally, the third experiment gave

$$a = -(2.5 \pm 0.9) \times 10^{-4}.$$

The mean value of the asymmetry coefficient is found to be

$$a = -(3.3 \pm 0.6) \times 10^{-4}$$

or, if we take into account the contribution from quanta with en 8.5 MeV,

$$a = -(4.1 \pm 0.8) \times 10^{-4}.$$

This result led to the following experimental estimate for rameter F:

$$F_{exp} \simeq 2 \times 10^{-7},$$

which is close to the theoretical value.

Thus, the existence of internucleonic (i.e. nuclear) interactio which parity is not conserved was experimentally proved for first time by Abov *et al.*

In the experiment described above, the mirror asymmetry in emission of γ-quanta is accounted for by the pseudoscalar I_{nuc} where I_{nuc} is the nuclear spin (pseudovector) and p_γ is the mo tum of the γ-quantum (vector). To observe the asymmetry it is essary to fix the direction of I_{nuc}, i.e. to carry out the experi with polarized nuclei. There exists another pseudoscalar which be used to characterize the process of gamma radiation. This i

Obviously, nuclear polarization is not required for experimental determination of P_γ, since both vectors appearing in the pseudoscalar $\mathbf{I}_\gamma \mathbf{p}_\gamma$ are the parameters of γ-quanta only.

The P-odd circular polarization of gamma radiation from the nucleus ^{181}Ta was first observed experimentally by Lobashov *et al.*[54] (Leningrad) in 1966. These experiments, as well as the experiment conducted by Abov *et al.*[55], lead to the value $F_{exp} \simeq 10^{-7}$. The authors of these works were awarded the Lenin Prize in 1974.

3.5. New Types of Radioactivity

3.5.1. Proton Radioactivity

From an analysis of the properties of neutron-deficient nuclei, it was mentioned in Sec. 1.3.4 that a new type of radioactive process, viz. the proton radioactivity, can occur in principle. There can be three types of proton radioactivity: emission of protons from the ground state of the nucleus (proton decay), emission of protons from the excited state of the nucleus formed as a result of beta decay (delayed protons), and emission of protons from the isomeric state of the nucleus (isomeric proton decay).

3.5.1a. Proton Decay

If there is a large excess of protons in a neutron-deficient nucleus, the last proton may have $\varepsilon_p < 0$, i.e. the nuclear forces may not be capable of containing it within the nucleus. The proton, however, remains inside the nucleus for some time due to the existence of a Coulomb barrier. Thus, the situation for this proton is analogous to that for an α-particle in the case of alpha decay. The proton with $\varepsilon_p < 0$ escapes from the ground state of the nucleus as a result of tunnelling. Like alpha decay, this process is termed proton decay.

From the theoretical point of view, proton decay is simpler than the alpha decay, since the problem of the formation of the escaping particle does not arise in this case: protons are present in the nucleus in ready-made form. However, the experimental situation in the case of proton decay is much more complicated than in the case of alpha decay because of a very strong β^+-radioactivity of neutron-deficient nuclei near the proton stability boundary.

Theoretical estimates show that the number of emitted positrons may be millions of times more than the number of protons. To detect the proton decay against the background of positron decay, the

[54] V.M. Lobashov *et al.*, *Pis'ma Zh. Eksp. Teor. Fiz.*, 3, 268 (1966).

[55] For details of P-odd nuclear forces, see Yu.G. Abov and P.A. Krupchitsky, *Uspekhi Fiz. Nauk*, 118, 141 (1976).

lifetime of protons must be less than 0.1 s in any case (the smaller the lifetime, the better). Assuming that the experimental techniques allow measurements of lifetimes up to 10^{-12} s, the following energy intervals are favourable for detection of protons:

$$0.5 < E_p < 1.5 \text{ MeV for nuclei with } Z \simeq 50,$$
$$1.0 < E_p < 2.5 \text{ MeV for nuclei with } Z \simeq 80,$$

where the left bounds of the intervals correspond to $\tau_p = 0.1$ s, and the right bounds to $\tau_p = 10^{-12}$ s. In order to detect proton decay, it is preferable to choose odd elements (because of lower separation energy for an odd proton in comparison with an even proton, see Sec. 1.3).

Proton decay was experimentally observed[66] in 1982 for the neutron-deficient nucleus $^{151}_{71}$Lu (which has 24 neutrons fewer than the β-stable isotope $^{175}_{71}$Lu). The nuclei $^{151}_{71}$Lu were obtained in the nuclear reaction

$$^{58}_{28}\text{Ni} + ^{96}_{44}\text{Ru} \rightarrow ^{154*}_{72}\text{Hf} \rightarrow ^{151}_{71}\text{Lu} + p + 2n \qquad (3.5.1)$$

induced by the ions $^{58}_{28}$Ni accelerated to energies 200-400 MeV in a heavy-ion accelerator in Darmstadt (FRG). Measurements showed that the lifetime of the proton-active nucleus $^{151}_{71}$Lu is about 0.085 s, while the energy of the emitted protons is 1.23 MeV.

Special attention was paid in this work to prove that protons are emitted by the ground state of the nucleus. This is a very important circumstance, since neutron-deficient nuclei have a much higher probability of emitting delayed protons (see Sec. 3.5.1b) and it is extremely difficult to detect proton decay against this background.[67]

The conclusion drawn in the above work that protons are emitted from the ground state is confirmed by the kinematics of the decay, measurement of the nuclear excitation function for $^{151}_{71}$Lu and the proton energy, as well as by the absence of annihilating and characteristic X-ray radiation, which must be generated during the conversion transitions of excited nuclei (see Sec. 3.4.2), i.e. during the emission of delayed protons.

Later, a proton-active isotope of thulium $^{147}_{69}$Tm with a lifetime of 0.42 s was obtained in a similar reaction:

$$^{58}_{28}\text{Ni} + ^{92}_{42}\text{Mo} \rightarrow ^{150*}_{70}\text{Yb} \rightarrow ^{147}_{69}\text{Tm} - p + 2n. \qquad (3.5.2)$$

This nucleus emits protons with energy 1.04 MeV.

---

[66] S. Hofmann *et al.*, *Zeitschrift für Physik, A—Atoms and Nuclei*, B305, 111 (1982).

[67] In this connection, we should note that the proton decay was first reported as early as in 1972 in the nucleus ^{131}Pr ($E_p = 0.9$ MeV, $T_{1/2} = 1.5$ s) (D.D. Bogdanov *et al.*, *Yadernaya Fizika*, 16, 890 (1972). However, the proton decay yield was just about 10^{-9} of the yield of delayed protons.

3.5.1b. Delayed Protons

Delayed protons were first detected by Karnaukhov (Dubna) in 1962 upon irradiation of a nickel foil with ^{20}Ne ions. Figure 143 shows the energy level diagram for the emission of delayed protons. As a result of β^+-decay, the nucleus (A, Z) is transformed into the ground state or an excited state of the nucleus $(A, Z-1)$. The excitation of the nucleus is usually removed through the emission of γ-quanta. However, if the excitation energy W of the nucleus $(A, Z-1)$ exceeds the separation energy ε_p required to remove a proton from this nucleus ($W > \varepsilon_p$), the emission of protons also becomes possible besides the emission of γ-quanta. Since these protons can be emitted only after β^+-decay of the nucleus (A, Z), they are called delayed protons.

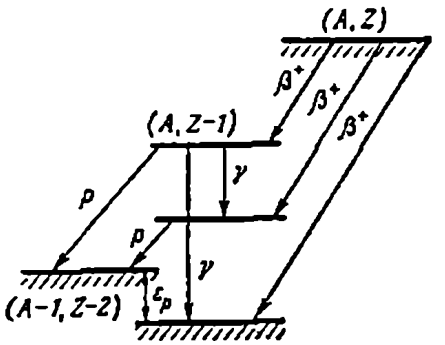

Fig. 143

Delayed protons are monochromatic in nature. Their energy is equal to $T_p = W - \varepsilon_p$. At low proton energies, the probability of their emission is very low (on account of nonpenetrability of the Coulomb barrier) and the decay of the nucleus $(A, Z-1)$ predominantly occurs through gamma radiation ($\Gamma_\gamma > \Gamma_p$). The minimum energy at which a delayed proton can be registered is $T_p^{\min} \simeq 1$ MeV. As the proton energy increases, the barrier penetrability increases and from a certain value T_p of the proton energy, $\Gamma_p > \Gamma_\gamma$.

At present, dozens of delayed proton emitters are known to exist among light as well as heavy nuclei. As an example of a light emitter of delayed protons, we can consider the nucleus $^9_6$C which emits protons with energies 10.92 MeV and 8.24 MeV. The half-life $T_{1/2} = 0.126$ s. This emitter was obtained in the reactions $^{10}_5$B $(p, 2n)$, $^{12}_6$C $(p, p3n)$, and $^7_4$Be $(^3_2$He, $n)$. Another light nucleus $^{14}_8$O is characterized by $T_{1/2} = 0.0089$ s and emits four groups of delayed protons with energies varying between 1.44 MeV and 7.00 MeV. This emitter was obtained in the reaction $^{14}_7$N $(p, 2n)$. We can once again mention the nucleus $^{17}_{10}$Ne (see Sec. 2.3) which has $T_{1/2} = 0.108$ s and emits five groups of delayed protons from 1.68 MeV to 7.04 MeV. The nuclei $^{17}_{10}$Ne can be obtained in the reactions $^{19}_9$F $(p, 3n)$, $^{16}_8$O $(^3_2$He, $2n)$, etc.

The investigation of light proton emitters, which are characterized by sparse energy levels, permits a separate investigation of their characteristics. For example, the enhanced intensity of one of the groups of delayed protons can serve to single out an energy state of the nucleus $(A, Z-1)$ which is analogous to the ground state of the nucleus (A, Z).

For quite heavy proton emitters (starting from $Z > 30$), the level density for the nucleus $(A, Z-1)$ is so high that it becomes difficult to isolate individual transitions. For example, the proton spectrum of the nucleus $^{111}_{52}$Te ($T_{1/2} = 19.3$ s) is characterized by a large number of peaks in the interval of energies between 2 and 5 MeV, while the spectrum of the nucleus $^{161}_{78}$Hg ($T_{1/2} = 3.6$ s) has a broad distribution in the interval between 3 and 6 MeV. However, in this case also the spectrum of protons exhibits a certain fine structure which is due to the fluctuations in the intensities of various transitions. Analyzing the fine structure of a spectrum, we can draw conclusions about the density of levels for different excitation energies of the nucleus.

Another application of delayed protons is associated with the possibility of obtaining information about the difference in masses of the parent and daughter nuclei while measuring the proton spectrum in coincidence with positrons and γ-quanta.[58]

3.5.1c. Isomeric Proton Decay

An excited state with $W > \varepsilon_p$ can appear not only after β^+-decay, but as a result of a nuclear reaction as well. If this state is isomeric, i.e. has a sufficiently long life, a proton decay may be observed in this case also along with the β^+-radioactive decay. The only case involving such a decay was reported[59] for the metastable ($\tau = 0.247$ s) nucleus $^{53m}_{27}$Co obtained in the reaction $^{54}_{26}$Fe $(p, 2n)$ $^{53}_{27}$Co. The proton energy $E_p = 1.6$ MeV, the relative probability $\Gamma_p/\Gamma_{\gamma} = 0.15$.

3.5.2. Double-proton Radioactivity

In 1960, Gol'danskii predicted the existence of another rather exotic type of radioactivity, viz. the simultaneous emission of two protons.[60]

According to (1.3.19), the separation energy of two protons from the nucleus (A, Z) is the quantity

$$\varepsilon_{2p} = \{2m_p + M(A-2, Z-2) - M(A, Z)\}c^2.$$

Comparing this expression with Eqs. (1.3.14) and (1.3.18), we obtain

$$\varepsilon_{2p} = 2\varepsilon_p - P_p, \qquad (3.5.3)$$

where ε_p is the energy of separation of a proton from the nucleus (A, Z), and $P_p = \varepsilon_p(A, Z) - \varepsilon_p(A-1, Z-1)$ is the proton pairing energy.

[58] Detailed information about delayed protons is given in a review by Karnaukhov (V.A. Karnaukhov, *Fiz. Elem. Chast. Atomn. Yadra*, 4, 4, 1018 (1973)).

[59] K.P. Jackson *et al.*, *Phys. Lett.*, 33B, 281 (1970).

[60] V.I. Gol'danskii, *Zh. Eksp. Teor. Fiz.*, 39, 497 (1960).

Since $\varepsilon_p \simeq 0$ near the proton stability boundary, and the pairing energy $P_p > 0$ for nuclei with even Z (see Sec. 1.3.4), the existence of nuclei with $\varepsilon_{2p} < 0$ (and $\varepsilon_p > 0$) is possible in principle. Such nuclei will be unstable with respect to the emission of two protons, but stable with respect to a single proton emission.

Just like the proton radioactivity, the double-proton radioactivity can be observed in principle in three different forms: emission of two protons from the ground state of the nucleus (double-proton decay), emission of two protons from an excited state of the nucleus formed as a result of β^+-decay (delayed double-proton radioactivity), and the emission of two protons from an isomeric excited state (isomeric double-proton radioactivity).

In 1980, Gol'danskii gave a concrete proof to his prediction about delayed double-proton radioactivity[61], indicating two neutron-deficient nuclei $^{22}_{13}$Al and $^{26}_{15}$P which must be transformed after positron emission into highly excited nuclei $^{22*}_{12}$Mg and $^{26*}_{14}$Si capable of emitting proton pairs.

In 1983, delayed double-proton radioactivity was observed[62] in the USA in the following process:

$$^{22}_{13}\mathrm{Al} \xrightarrow{\beta^+} {}^{22*}_{12}\mathrm{Mg} \rightarrow {}^{20}_{10}\mathrm{Ne} + 2p. \qquad (3.5.4)$$

The short-lived ($\tau \simeq 0.07$ s) neutron-deficient nuclei $^{21}_{13}$Al were obtained as a result of irradiation of $^{24}_{12}$Mg by ^{3}He ions with an energy of 110 MeV. Protons escaping from the nuclei $^{22*}_{12}$Mg were registered by a system of three counters connected in the coincidence circuit. Two groups of protons with energies 4.139 and 5.636 MeV were observed as a result of measurements.

Other types of double-proton radioactivity have not been detected so far.

3.5.3. Neutron Radioactivity

Since the neutron does not have an electric charge, there is no Coulomb barrier for it. Hence we can speak of neutron radioactivity with a measurable lifetime only in two cases: when the centrifugal barrier plays any significant role, i.e. when the escaping neutron carries with it a nonzero orbital momentum $l_n \neq 0$, or when the neutron emission follows a β^--decay (delayed neutron radioactivity).

For neutron decay of isomeric nuclear states with excitation energy $W > \varepsilon_n$, the escaping neutron can be expected to have a quite high value of l_n. Estimates for the centrifugal barrier penetrability and

[61] V.I. Gol'danskii, *Pis'ma Zh. Eksp. Teor. Fiz.*, 32, 9, 572 (1980).
[62] M. D. Cable *et al.*, *Phys. Rev. Lett.*, 50, 6, 404 (1983).

a consideration of the structural factor show that the lifetime of neutron isomers may attain values up to 10^2 s.

For $W > \varepsilon_{2n}$, two neutrons can be emitted in principle. Finally, a double-neutron decay of the ground state of a neutron-rich nucleus cannot be ruled out theoretically if $\varepsilon_{2n} < 0$ and $l_n \geqslant 3$. However, the conditions under which this process can be detected are quite hard to realize experimentally. For example, the necessary conditions for the double-neutron decay of a light ($A \simeq 40$) neutron-rich nucleus to occur with a conveniently measurable lifetime ($\tau > 10^{-4}$ s) are $l_n = 3$ and $E_{2n} < 20$ keV. None of the processes mentioned above has so far been observed experimentally.[63]

The delayed neutron radioactivity is much more likely to be observed. We shall consider three different types of this phenomenon: delayed emission of a single neutron, double-neutron delayed emission, and the delayed emission of three neutrons.

3.5.3a. Delayed Neutrons

If the daughter nucleus formed as a result of β^--decay is in an excited state with energy $W > \varepsilon_n$, the excited state can emit a neutron or undergo a gamma transition. Since the neutron is emitted instantaneously, i.e. immediately after the beta decay, it will be characterized by the same half-life as for the beta decay.

The energy T_n of delayed neutrons is determined from the nuclear excitation energy W and the neutron separation energy ε_n:

$$T_n = W - \varepsilon_n. \tag{3.5.5}$$

Delayed neutrons were first discovered during the investigation of fission of heavy nuclei. To date, over 70 nuclei that are sources of delayed neutrons have been discovered and investigated. Delayed neutrons played a very important role in the creation of the first nuclear reactors. Sections 7.4.2 and 7.4.3 describe in detail the properties of delayed neutrons and their applications.

3.5.3b. Delayed Double-neutron Radioactivity

The excitation energy of a nucleus formed as a result of β-decay may exceed the separation energy of not only one neutron, but even two neutrons near the neutron stability boundary:

$$W > \varepsilon_{2n}. \tag{3.5.6}$$

[63] See V.A. Karnaukhov and L.A. Petrov, *Nuclei at Large Distances from the Beta Stability Track*, Energoizdat, Moscow, 1981 (in Russian).

In this case, delayed double-neutron radioactivity must be observed after β^--decay.[64] Since $\varepsilon_{2n} > \varepsilon_n$, this process will occur against the background of a much more intense emission of single delayed neutrons.

Delayed double-neutron radioactivity was discovered[65] in $^{11}_{4}$Be in 1979 at CERN. The isotope $^{11}_{4}$Be is formed as a result of β^--decay of the nuclei $^{11}_{3}$Li ($T_{1/2} \simeq 8.5$ ms) which were obtained during the separation of reaction products in the interaction of high-energy protons (600 MeV) with a boron carbide target.

Spectra of single delayed neutrons were measured with the help of a system of three ionization chambers filled with ^{3}He. As a result of measurements, three monochromatic groups of delayed neutrons and a broad region of continuous spectrum corresponding to the emission of delayed neutron pairs were observed. The simultaneous emission of both neutrons was verified by the neutron-neutron coincidence measurements. The emission probability for a pair of neutrons is about 4%.

The emission of delayed neutron pairs was discovered in 1980 for three more neutron-rich nuclei: ^{30}Na, ^{31}Na and ^{32}Na. The probabilities of neutron-pair emission for these nuclei are respectively equal to 1.2%, 0.7% and 5.1%.

3.5.3c. Delayed Triple-neutron Radioactivity

The group of physicists that discovered the delayed double-neutron radioactivity of the ^{11}Be nucleus at CERN in 1979, reported in 1980 the simultaneuos escape of three delayed neutrons from this nucleus.[66] The experiment was carried out under conditions similar to those described in Sec. 3.5.3b, but with a more perfect neutron detector which reliably separated simultaneous escape of two or three neutrons from the background of events caused by the superposition of pulses of single neutrons or single and paired neutrons. It was shown as a result of measurements that in about 2% cases, the nuclei ^{11}Be disintegrate with a simultaneous emission of three neutrons.

3.5.4. Carbon Radioactivity

A new type of radioactive decay, viz. carbon radioactivity, was reported to have been discovered in the UK in 1984.[67] Operating with the help of the $\Delta T, T$ detector method (see Sec. 11.1), the authors discovered 11 nuclei $^{14}_{6}$C formed during the disintegration of

[64] See Footnote 60.
[65] R.E. Azuma *et al*, *Phys. Rev. Lett.*, 43, 22, 1652 (1979).
[66] R.E. Azuma *et al*, *Phys. Lett.*, 96B, 1-2, 31 (1980).
[67] H.J. Rose and G.A. Jones, *Nature*, 307, 245 (1984).

the α-radioactive radium isotope $^{223}_{88}Ra$ ($T^{(\alpha)}_{1/2} = 11.7$ days, $T_\alpha = 5.7$ MeV):

$$^{223}_{88}Ra \rightarrow {}^{209}_{82}Pb + {}^{14}_{6}C. \qquad (3.5.7)$$

The energy of the nuclei $^{14}_{6}C$ is approximately equal to 30 MeV, which is in good agreement with the theoretical value obtained from the disintegration energy $Q = 31.8$ MeV for the process (3.5.7):

$$T^{\text{theor}} = Q\frac{M_{Pb}}{M_{Ra}} = 31.8 \times \frac{209}{223} = 29.8 \text{ MeV}. \qquad (3.5.8)$$

The yield of the nuclei $^{14}_{6}C$ turns out to be 10^9 times less than the yield of α-particles:

$$\Gamma_{^{14}C}/\Gamma_\alpha = (8.5 \pm 2.5) \times 10^{-10}. \qquad (3.5.9)$$

In view of the extremely low probability of the process under investigation, special attention was paid to the background, both intrinsic and external. For this purpose, the background effect due to cosmic radiation was measured for a long period of time, and the contribution from fourfold pulse coincidences for α-particles, whose total energy is close to the energy of the nuclei $^{14}_{6}C$, was estimated.

The discovery of carbon radioactivity was confirmed in the same year in the USSR[46] and France[46]. Both experiments were carried out with the help of the $\Delta T, T$ technique and gave identical values for $\Gamma_{^{14}C}/\Gamma_\alpha$.

Efforts are being made at present in the Soviet Union and other countries to detect neon radioactivity. According to preliminary experimental estimates, the value of $\Gamma_{^{24}Ne}/\Gamma_\alpha$ must be many orders of magnitude smaller than the corresponding value for carbon radioactivity.

Theoretically, the radioactive processes accompanied by the emission of nuclei heavier than helium are not surprising, since these processes are allowed by all the conservation laws. However, in view of the extremely low probability of these processes, their experimental observation was impossible until recently.

The estimates for the probability of the new radioactive process are based on a nuclear disintegration model similar to the alpha decay model. It should be recalled (see Sec. 3.2.3) that the alpha decay probability is determined by the formation factor for α-particles in the parent nucleus and the barrier penetrability which depends exponentially on the decay energy, barrier height and the reduced mass. It was also mentioned that the alpha decay energy is exceptionally high for alpha transitions resulting in the formation of magic or near-magic nuclei (see Fig. 87).

[46] D.V. Aleksandrov *et al.*, *Pis'ma Zh. Eksp. Teor. Fiz.*, 40, 4, 152 (1984).
[46] S. Gales *et al.*, *Phys. Rev. Lett.*, 53, 8, 759 (1984).

All these parameters and properties can be estimated for the new radioactive process also if we choose a specific version of the decay model (for example, by specifying the nuclear rupture range, effective mass of the collective motion). As in the case of alpha decay, the most serious difficulties encountered here are associated with the estimation of the formation factor. However, in view of the exponential nature of the expression for the barrier penetrability [see formula (3.2.21)], calculations are more sensitive to parameters defining just this coefficient, i.e. to the decay energy Q, and hence to the choice of the daughter nucleus.

In particular, the process (3.5.7) was found to be more probable than the process accompanied by the escape of the nucleus $^{12}_{6}C$, which must have a larger formation factor than the less symmetric nucleus $^{14}_{6}C$. Apparently, this is due to the fact that the daughter nucleus in the process (3.5.7) has not only a magic number of protons, but also a near-magic (127) number of neutrons.

It follows from what has been said above that for the time being the theory of the new radioactive process cannot claim to be very accurate. The difference between $T_{1/2}^{\text{exp}}$ and $T_{1/2}^{\text{theor}}$ may be up to three orders of magnitude.

3.6. A Brief Resumé of Chapter 3

In this chapter, we have considered the basic laws of radioactivity, alpha decay, beta decay and gamma radiation of the nuclei, as well as internal conversion of electrons, nuclear isomerism, Mössbauer effect, various types of proton and neutron radioactivity, and carbon radioactivity.

Alpha decay is the process of spontaneous emission of a helium nucleus $^{4}_{2}He$ (α-particle) from a nucleus (A, Z). This process is accompanied by the release of energy E_α in the form of kinetic energy of the α-particle and the daughter nucleus $(A-4, Z-2)$. From the energy point of view, alpha decay is possible if $E_\alpha = Q > 0$ or if the binding energy of the α-particle in the nucleus is negative:

$$\varepsilon_\alpha = -Q = [M_\alpha + M(A-4, Z-2) - M(A, Z)]c^2 < 0.$$

Alpha radioactivity has been experimentally observed in naturally occurring nuclei starting from $Z = 83$ (as well as in some rare-earth elements). Artificial radioactivity can be observed even in nuclei with $Z \leqslant 82$ if they are highly neutron-deficient. With very few exceptions, the kinetic energy of α-particles does not exceed 4-9 MeV. On the other hand, the half-lives of α-radioactive nuclei vary over a quite wide range: from 10^{-7} s to 5×10^{15} years. This feature of alpha decay was experimentally established in the form of Geiger-Nuttall law and was explained theoretically with the help of the quantum-mechanical process of the passage of microscopic particles through a Coulomb potential barrier.

Alpha spectrum is discrete. A typical feature of alpha spectra is the existence of a fine structure, i.e. closely spaced groups of α-particles. Two isotopes of polonium $^{212}_{84}Po$ and $^{214}_{84}Po$ emit long-range α-particles whose origin is associated with the magic daughter nucleus $_{82}Pb$. An analysis of this phenomenon led to an estimate for the lifetime of one of the excited states of the nucleus ^{212}Po (10^{-13} s).

The emission of *α-particles* takes place for $l = 0$, as well as $l \neq 0$. In the latter case, we must consider the centrifugal barrier $V_c = \hbar^2 l(l+1)/2\mu r^2$ besides the Coulomb barrier. The angular distribution of the emitted α-particles depends on the magnitude of l.

The *theory of alpha decay* connects the kinetic energy T_α of α-particles, the disintegration constant λ, nuclear radius R and charge Z.

Beta decay is the spontaneous emission of an electron (β^--decay) or a positron (β^+-decay) by the nucleus, as well as the capture of an electron from K- or L-orbit of the atom by its nucleus (ε-capture). As a result of beta decay, the nucleus (A, Z) is transformed into the isobar nucleus $(A, Z+1)$ or $(A, Z-1)$. From the energy point of view, the possibility of decay is expressed by the condition $E_{\beta\pm} = [M_{\text{nuc}}(A, Z) - M_{\text{nuc}}(A, Z \mp 1) - m_e]c^2 > 0$, while ε-capture is characterized by the condition $E_\varepsilon = [M_{\text{nuc}}(A, Z) + m_e - M_{\text{nuc}}(A, Z-1)]c^2 > 0$. All these three conditions may be simultaneously satisfied by some nuclei. The energy of beta decay varies from 0.018 MeV to 16.6 MeV, and their half-lives vary between 10^{-3} s and 2×10^{15} years.

Beta decay was also detected in a free neutron, which decays according to the scheme $n \to p + e^- + \tilde{\nu}_e$ with a half-life $T_{1/2} = 10\text{-}11$ min.

Unlike alpha spectra which are discrete, beta spectra are continuous. The energy of electrons (positrons) emitted during beta decay of the same type of nuclei lies in the interval $0 \leqslant T_e \leqslant (T_e)_{\max}$, where $(T_e)_{\max} \simeq E_\beta$. A part of this energy, equal to $E_\beta - T_e = E_\nu$, is carried away by the neutrino (antineutrino) emitted together with the positron (electron). The ε-capture is also accompanied by the emission of a neutrino. The neutrino (antineutrino) has the following properties:

$$s_\nu = 0, \quad m_\nu = 0, \quad \mu_\nu = 0, \quad s_\nu = 1/2. \quad \sigma_{\nu N} \simeq 10^{-43} \text{ cm}^2.^{[1]}$$

Electrones (positrons) and neutrinos (antineutrinos) emitted during beta decay are not contained in the nucleus, but appear just at the moment of beta-decay.

The *theory of beta decay* connects the lifetime τ of a β-radioactive nucleus and the energy of beta decay through a relation of the type $F(\varepsilon_0)\,\tau = \text{const}$, where $F(\varepsilon_0) \propto \varepsilon_0^5$; $\varepsilon_0 = [m_e c^2 + (T_e)_{\max}]/m_e c^2$; $F\tau \simeq 10^3$ for superallowed transitions, $F\tau \simeq 10^6$ for allowed transitions and $F\tau \simeq 10^9$ (10^{13}, 10^{16}) for forbidden transitions (depending on the extent to which the transition is forbidden). Allowed and superallowed transitions satisfy the selection rules for momentum and nuclear parity: $\Delta I = 0, \pm 1$; $P_i/P_f = 1$. Comparing theoretical and experimental results, we obtain the beta interaction constant $g \simeq 10^{-49}$ erg·cm³. The small value of this constant indicates that beta interaction is extremely weak. Investigation of beta decay in polarized nuclei confirmed the conclusion drawn by Li and Yang regarding nonconservation of parity in beta decay.

Gamma radiation is the spontaneous transition of the nucleus from an excited state to the ground state (or to a less excited state), accompanied by the emission of a quantum of short-wave electromagnetic radiation. Depending on its origin, gamma radiation is divided into electric radiation and magnetic radiation, and is characterized by a definite multipolarity or the value of the angular momentum l_E (for electric radiation) or l_M (for magnetic radiation) carried by the γ-quanta.

If I_i, I_f and P_i, P_f are the angular momenta and parities of the initial and final states of the nucleus, possible values of l for allowed gamma transitions satisfy the following selection rules: $|I_i - I_f| \leqslant l \leqslant |I_i + I_f|$; $P_i/P_f = (-1)^{l_E}$, $P_i/P_f = (-1)^{l_M+1}$. Usually, the lowest possible value of l_E or l_M is realized, since an increase in multipolarity by unity decreases the emission probability by a factor of 10^5.

[1] Recently, some preliminary studies have indicated that $m_\nu \neq 0$.

If the lowest value of l is quite high ($l = 4$) and ΔE is small, the excited nuclear state has long lifetime (metastable state). A nucleus in the metastable state is called an isomer of the given nucleus. Isomerism may lead to several half-lives for beta decay or spontaneous fission of the same nucleus. The isomer nuclei are concentrated in certain regions of variation of Z (or N), forming isomeric "islands".

Besides gamma radiation, the nuclear excitation energy can be spent on the emission of internal conversion electrons (usually from the K-shell). This process is accompanied by the emission of characteristic X-rays and Auger electrons.

The gamma transition energy E and the energy E_γ of the emitted γ-quantum are usually connected through the relation $E = E_\gamma + T_{\text{nuc}}$, where $T_{\text{nuc}} = E_\gamma^2/2M_{\text{nuc}}c^2$ is the recoil energy of the nucleus.

The value of T_{nuc} is quite small ($\sim$0.01 eV), but is still much higher than the intrinsic line width Γ of the radiation. Under certain conditions, however (when the nucleus acts as a solid emitter and the temperature is quite low), the recoil energy may become negligibly small, so that $E_\gamma = E$. This may lead to the process of resonant absorption and scattering of γ-quanta (Mössbauer effect), which can be used to measure energy with an accuracy of up to the intrinsic line width Γ

For neutron-deficient nuclei, proton decay of the nucleus in the ground state has been observed, as well as the emission of delayed protons and proton pairs from the excited nuclear states formed as a result of β^+-decay.

For neutron-rich nuclei, delayed emission of one, two or three neutrons has been observed from the excited states of the nuclei formed as a result of β^--decay.

Carbon radioactivity has been observed in the α-radioactive radium isotope $^{223}_{88}$Ra:

$$^{223}_{88}\text{Ra} \rightarrow {}^{209}_{82}\text{Pb} + {}^{14}_{6}\text{C}.$$

Chapter 4

Interaction of Particles and Radiation with Matter

4.1. General Description of the Interaction of Charged Particles, Neutrons and Gamma-quanta with Matter

While passing through matter, particles interact with the atoms constituting the substance, i.e. with electrons and atomic nuclei (or nucleons).

If we neglect the very weak gravitational interaction, there are three types of interaction in which the particles can participate, viz. strong[1], electromagnetic and weak. Among the particles considered by us so far in this book (n, p, e^-, e^+, ν, $\tilde{\nu}$ and γ), the neutron and the proton take part in strong interactions, all particles except ν and $\tilde{\nu}$ participate in electromagnetic interaction, while all particles with the exception of γ-quanta are involved in weak interaction.

The simplest example of strong interaction is the attraction between nucleons located at very small distances from one another (about 10^{-13} cm) inside the atomic nucleus. Later (see Vol. II), we shall show that there are other particles also (π- and K-mesons, hyperons, antinucleons, antihyperons, unstable particles, or resonances, etc.) which take part in strong interactions. Pions serve as the carriers of quanta in strong interactions (see Chap. 6, Vol. II).[2]

Strong interaction is the most intensive interaction existing in nature, and it is termed strong for this very reason. This type of interaction can be manifested in the form of direct interaction (scattering by nuclear forces, nuclear reactions, i.e. the capture of some particles resulting in the formation of other particles), or as disintegration (decay of resonances). Strong processes involving direct interaction are characterized by very large cross sections (10^{-27}-10^{-24} cm^2), while the decay processes have very short periods (10^{-23}-10^{-22} s).

Large cross sections for strong interaction processes mean that when strongly interacting (nuclear-active) particles pass through a medium, they are effectively deflected from a collimated beam due to absorption and scattering processes.

[1] Strong interaction is sometimes termed nuclear interaction.

[2] We shall adhere to the old phenomenology of strong interaction in this volume and assume that this interaction takes place through pions. The concept of quantum chromodynamics, which is associated with the modern model of strong interaction, will be introduced in Vol. II.

Electromagnetic interaction is also treated as intensive interaction in nature, although it is weaker than the nuclear interaction (this follows from the existence of stable nuclei which contain likely charged protons).

The carriers of this interaction are electromagnetic radiation quanta, called *photons*, *X-rays* or *γ-quanta* depending on their origin, as well as *radio waves*. Electromagnetic radiation quanta are produced as a result of interaction of an electric charge with the electromagnetic field surrounding it.

The electromagnetic interaction is manifested in several ways: for charged particles, it may be in the form of Coulomb scattering, ionization losses, radiation losses, Cherenkov radiation, synchrotron and transition radiation; for γ-quanta, it may occur as photoelectric effect, Compton effect, electron-positron pair formation, gamma transitions in nuclei, photonuclear reactions; in the case of neutrons, this interaction can appear in the form of polarization upon passage through a ferromagnetic and reflection by a cobalt mirror, magnetic confinement of ultracold neutrons, etc.

Estimates for the strength of electromagnetic interaction show that it is 10^2-10^3 times weaker than the nuclear interaction (within the range of action of the latter). Accordingly, the electromagnetic disintegration processes occur at least 10^2-10^3 times more slowly than the strong processes and are characterized by half-lives $T_{1/2} \simeq 10^{-19}$ s.

When charged particles and γ-quanta pass through matter, significant energy losses occur due to electromagnetic interaction.

The process of beta decay considered in Chap. 3 is an example of *weak interaction*. Beta decay is a specific interaction between nucleons and the electron-neutron field surrounding them, resulting in the emission or absorption of electrons (positrons) and antineutrinos (neutrinos). It was shown that beta decay is characterized by an extremely small value of the interaction constant g, hence it is called weak interaction.

Besides beta decay, other processes involving weak interaction are also characterized by similarly low values of the interaction constant. These include (π-μ)-decay, (μ-e)-decay, and decay of K-mesons and hyperons (see Chap. 7, Vol. II). Weak interactions have about 10^{13} times lower intensity than strong interactions. Accordingly, the decay processes for weak interactions occur at least 10^{13} times more slowly than for strong interactions, i.e. their characteristic lifetime τ is not less than 10^{-10} s.[3] However, the decay processes associated with the weak interaction have to be considered when particles cover large distances before they reach the detector, since at a velocity $v \simeq c$, a particle having even a lifetime $\tau = 10^{-10}$ s can cover a distance of 10-100 cm without disintegrating.

[3] Recently, the discovery of τ-lepton with a lifetime $\tau_\tau \simeq 5 \times 10^{-13}$ s has been reported (see Sec. 5.8, Vol. II).

Besides the decay processes, the weak interaction may also be manifested in direct interactions, for example, in the process of the capture of a neutrino (antineutrino) by a nucleon. However, the cross sections of such direct processes of weak interaction are so small (about 10^{-43} cm^2 for $E_\nu \simeq 1$ MeV) that they can be generally ignored while considering the passage of particles through matter.

The diversity of the processes listed above makes it impossible to analyze all of them in the same chapter. We shall describe here in detail the main types of interaction with matter for charged particles (ionization losses, elastic scattering, bremsstrahlung, Cherenkov radiation and transition radiation) and γ-quanta (photoelectric effect, Compton effect, and formation of electron-positron pairs), as well as the synchrotron radiation of electrons in vacuum (in a magnetic field). We shall also consider briefly the interaction of neutrons with matter.

A detailed description of interaction of neutrons with matter (including nuclear reactions induced by neutrons) will be considered in Part Two of this book, where we shall also consider nuclear reactions induced by charged particles and γ-quanta. Finally, in Vol. II, we shall discuss some problems concerning the scattering of protons, neutrons and electrons, as well as the characteristic properties of interaction of neutrinos (and antineutrinos), muons, mesons (π and K), hyperons, antinucleons, antihyperons, resonances, etc. with matter.

4.2. Ionization Losses Due to Collisions of Charged Particles

4.2.1. Bohr's Formula for Specific Ionization. Relativistic Effects and the Density Effect

Ionization is the main cause of energy loss as a heavy charged particle passes through matter. In this mechanism, the kinetic energy of the particle is spent in exciting and ionizing the atoms of the substance through which it passes. In order to determine the factors on which ionization losses depend and to find the ionization range of the particle over which it loses all its energy, let us first consider the basic pattern of interaction of the charged particle with one electron and then sum the effect for all electrons with which the particle interacts.

Suppose that a particle with charge ze and velocity v passes at a distance ρ from a free (unbound) electron with mass m_e and charge $-e$ (Fig. 144). Assuming that the mass M of the particle is much larger than the electron mass, we find that its interaction with the

electron imparts to the latter a momentum in a direction perpendicular to the direction of its flight[4]:

$$\Delta p_\perp = \int F_\perp \, dt. \tag{4.2.1}$$

Here, $\int F_\perp \, dt$ is the impulse of force during interaction. Assuming that the interaction is effective over a segment comparable with ρ,

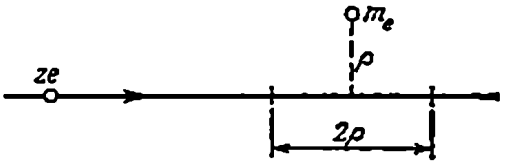

Fig. 144

say over a distance 2ρ which the particle covers in time $\Delta t = 2\rho/v$ and where the Coulomb force is approximately equal to ze^2/ρ^2, we obtain

$$\Delta p_\perp = 2ze^2/\rho v. \tag{4.2.2}$$

The kinetic energy corresponding to this momentum is equal to

$$\Delta T = \Delta p_\perp^2/2m_e = (2z^2e^4/m_e v^2)\,(1/\rho^2). \tag{4.2.3}$$

This is the energy acquired by the electron when a particle with a charge ze passes at a distance ρ from it with a velocity v. This is also the amount of energy lost by the moving particle.

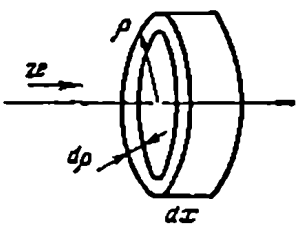

Fig. 145

In order to consider the effect of all electrons with the given impact parameter ρ, we construct around the trajectory of the particle a cylindrical layer with radius ρ, thickness $d\rho$ and height dx (Fig. 145). The volume of this layer will be $V = 2\pi\rho d\rho \, dx$. If n_e is the electron density, the number of electrons in the cylindrical layer will be equal to $Vn_e = 2\pi\rho n_e d\rho \, dx$.

As a result of interaction of the charged particle with all the electrons in the cylindrical layer, it loses the kinetic energy given by

$$dT = \Delta T V n_e = \left(\frac{4\pi n_e z^2 e^4}{m_e v^2}\right) \frac{d\rho}{\rho} dx. \tag{4.2.4}$$

[4] The momentum component in the direction of motion of the particle is equal to zero, since it is composed of two equal terms with opposite signs (corresponding to the situations when the particle approaches the electron and when it moves away from it).

The loss of kinetic energy per unit length will be

$$\frac{dT}{dx}(\rho) = \left(\frac{4\pi n_e z^2 e^4}{m_e v^2}\right)\frac{d\rho}{\rho}. \tag{4.2.5}$$

Obviously, this result is valid if the interaction of the particle with the given electron is independent of the presence of other electrons in the neighbourhood. In actual practice, this is not quite true, and consequently we must introduce a correction for the density effect into the final expression (see below).

The total specific loss is obtained by integrating $\frac{dT}{dx}(\rho)$ over all the possible values of the impact parameter ρ (from 0 to ∞). Difficulties are encountered for $\rho = 0$, since ρ is in the denominator of the expression (4.2.5), and for $\rho = \infty$ since the integral $\int_0^\infty \frac{d\rho}{\rho}$ is divergent.

However, it can be shown that the integration limits are not 0 and ∞ but have some finite values ρ_{min} and ρ_{max}. Consequently,

$$\frac{dT}{dx} = \int_{\rho_{min}}^{\rho_{max}} \frac{dT}{dx}(\rho)\, d\rho = \frac{4\pi n_e z^2 e^4}{m_e v^2} \ln \frac{\rho_{max}}{\rho_{min}}. \tag{4.2.6}$$

Calculation of ρ_{min} and ρ_{max} is a quite complicated problem. We shall not solve this problem here, but only mention some classical arguments which can provide an idea of the effects considered here.

It is well known that the maximum energy that a heavy particle moving with a velocity $v \ll c$ can impart to a fixed electron is

$$\Delta T_{max} = 2m_e v^2. \tag{4.2.7}$$

This result can be easily obtained by considering the momentum diagram for the appropriate case (see Sec. 4.4).

Equating the expression (4.2.3) to the value obtained above, we get the following condition for ρ_{min}:

$$\left.\begin{aligned} &\Delta T_{max} = (2z^2e^4/m_e v^2)\,(1/\rho_{min}^2) = 2m_e v^2; \\ &(\rho_{min})_{class} = ze^2/m_e v^2. \end{aligned}\right\} \tag{4.2.8}$$

The condition for ρ_{max} is obtained from classical considerations by taking into account the fact that electrons are bound in the atom. For large values of the impact parameter ρ, the transmitted energy ΔT becomes comparable with the binding energy of electrons in the atom. Electrons can no longer be treated as free, and for quite large ρ the transmitted energy may not be sufficient to excite the atom. Consequently, ρ_{max} must be associated with the average ionization

potential of the atom. Finally, to calculate $\ln(\rho_{max}/\rho_{min})$, we must take into account the relativistic effects. These include an increase in the maximum transferred energy to $\Delta T_{max} = 2m_e v^2/(1-\beta^2)$, an increase in ρ_{max}, i.e. the role of distant collisions, loss of energy due to Cherenkov radiation[5], etc.

Exact calculations lead to the following formula for specific ionization losses dT/dx (in erg·cm^{-1}) for a heavy charged particle (proton, α-particle, etc.) at energies $T \ll (M/m_e)Mc^2$:

$$\left(-\frac{dT}{dx}\right)_{ion} = \frac{4\pi n_e z^2 e^4}{m_e v^2}\left[\ln\frac{2m_e v^2}{\bar{I}} - \ln(1-\beta^2) - \beta^2 - \delta - U\right], \quad (4.2.9)$$

where $\bar{I} = (13.5Z) \times 1.6 \times 10^{-12}$ is the average ionization potential of the absorber atoms (in ergs), $\beta = v/c$, δ and U are terms tak-

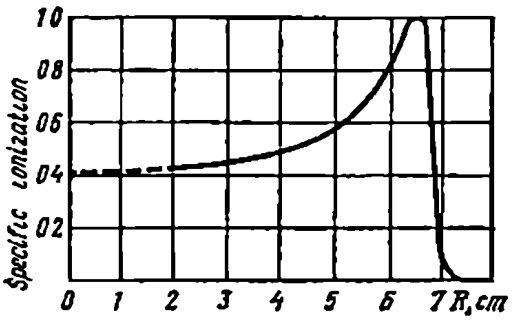

Fig. 146

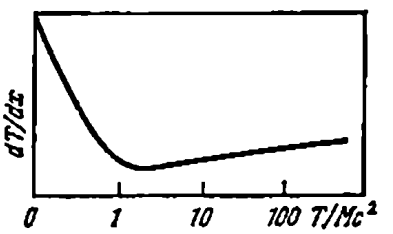

Fig. 147

ing into account the density effect and the fact that K- and L-electrons are bound (see below).

The main result following from formula (4.2.9) is that the specific loss of the particle energy due to ionization is proportional to the square of the particle charge, number density of electrons in the medium, a certain function of velocity $\varphi(v) \propto 1/v^2$, and is independent of the mass M of the particle:

$$dT/dx \propto z^2 n_e \varphi(v). \quad (4.2.10)$$

Such a regularity can be illustrated by considering the Bragg curve for specific ionization of α-particles, which is well known in atomic physics (Fig. 146). An increase in the specific ionization can be seen at the end of the α-particle track, i.e. upon a decrease in its velocity.

Formula (4.2.9) shows that with increasing particle energy, the specific ionization losses first decrease very rapidly (in inverse proportion to energy), but the decrease becomes slower as the particle

[5] This fraction is noticeable only for light gases (about 15% relativistic increase for hydrogen).

velocity approaches the velocity of light. At a certain value of energy, the specific energy loss on ionization attains its lowest value. This means that the denominator in formula (4.2.9) contains a nearly constant quantity $v^2 \simeq c^2$.

However, an examination of terms in the brackets shows that starting from a certain quite high particle energy, the magnitude of dT/dx again starts increasing slowly (logarithmically) and reaches a certain plateau (Fig. 147).

The suppression of the logarithmic growth of dT/dx is associated with the polarization of atoms near the particle trajectory, which leads to a decrease in the electromagnetic field acting on remote electrons. This effect is proportional to the density of the substance (more exactly, to the density of electrons) and is therefore called the density effect. This effect is described in formula (4.2.9) by the δ-term whose structure is such that it compensates the logarithmic increase in ionization losses at very high energies.

The density effect sets in earlier in condensed media than in rarefied ones. Quantitatively, this means that the relativistic increase in ionization losses is different for different media. In condensed media, this effect is measured in percent, while for gases, it is several tens percent. As an example illustrating the role of relativistic increase in ionization losses and the density effect, let us consider the data concerning the motion of charged particles in a photographic emulsion. In this case, the curve for dT/dx attains its minimum value at $T \simeq (2\text{-}3)\, Mc^2$, rises by about 10%, and attains its plateau beginning from $T \simeq (20\text{-}50)\, Mc^2$.

The last term in formula (4.2.9), denoted by U, is the correction factor for relatively low energies of the ionizing particle. If the particle velocity is comparable with the orbital velocity of K- or L-electrons, the latter stop participating in collisions and hence the value of dT/dx decreases. The energy of the particle at which this correction must be introduced increases with the value of Z for the medium. For $Z \simeq 30$, the correction for K-electrons should be introduced at $T_p \simeq 50$ MeV, and for L-electrons at $T_p \simeq 10$ MeV.

The role of M, N and other electrons becomes significant for still lower energies ($T_p \simeq 1$ MeV). Besides, in this energy region we must consider (especially for multiply charged particles) the effect of capture and loss of electrons by slowly moving particles.

The formula for calculating the ionization losses of electrons has a somewhat different form as compared with formula (4.2.9) for heavy particles:

$$\left(-\frac{dT_e}{dx}\right)_{\text{ion}}^{(e)} = \frac{2\pi e^4 n_e}{m_e v^2}\left[\ln \frac{m_e v^2 T_e}{2I^2(1-\beta^2)} - \ln 2\,(2\sqrt{1-\beta^2} - 1 + \beta^2) + 1 - \beta^2 + 1/8\,(1-\sqrt{1-\beta^2})^2 - \delta\right], \quad (4.2.11)$$

where T_e is the relativistic kinetic energy of an electron, n_e is the electron density in the medium, and δ is the correction for the density effect.

This difference is due to the fact that while considering the elementary process of interaction between two electrons, we must take into account the repulsion between them and the quantum-mechanical exchange effect caused by the identity of the two particles. For high-energy electrons, as for heavy charged particles, we must also consider the density effect which leads to a decrease in ionization losses in comparison with formula (4.2.11). However, at very high energies, electrons begin to lose energy effectively due to an ever increasing role of bremsstrahlung. If the electron energy exceeds the critical value, these losses prevail over the ionization losses (see Sec. 4.5).

4.2.2. Dependence of Ionization Losses on the Medium

The simple form of the dependence of dT/dx on the parameters of a moving particle and a medium [see formula (4.2.10)] permits an easy computation of dT/dx for other particles and media. Indeed, let us suppose that two particles with the same charge (say, a proton and a deuteron) move in the same medium ($n_e = \text{const}$). In this case, the value of dT/dx will be the same for both particles in the regions of equal velocities (where $\varphi(v) = \text{const}$):

$$(dT_p/dx)_{v=v_0} = (dT_d/dx)_{v=v_0}. \qquad (4.2.12)$$

However, at identical velocities the particle energies are in the same ratio as their masses. Hence, for the example being considered here, we have

$$(dT_d/dx)_{T=T_0} = (dT_p/dx)_{T=T_0/2}. \qquad (4.2.13)$$

Similarly, we can calculate the value of dT/dx for particles with other values of z ($z \neq 1$). In this case, we must remember that a particle with $z \neq 1$ has z^2 times higher value of dT/dx than a particle with $z = 1$ moving at the same velocity. For example, values of dT/dx for an α-particle and a proton are connected through the relation

$$(dT_\alpha/dx)_{v=v_0} = 4\,(dT_p/dx)_{v=v_0} \qquad (4.2.14)$$

or

$$(dT_\alpha/dx)_{T=T_0} = 4\,(dT_p/dx)_{T=T_0/4}. \qquad (4.2.15)$$

Calculations for another medium can be easily carried out if we remember that dT/dx is a linear function of the electron number density n_e in the medium. It is well known that the electron number density n_e in a medium is equal to $n_{nuc}Z$, where Z is the charge of the nuclei constituting the medium and n_{nuc} is their number density.

However, $n_{nuc} \simeq$ const for all media, and therefore we must introduce for recalculations the factor Z_2/Z_1, where Z_1 and Z_2 are the nuclear charges for the first and the second medium respectively. Thus, for example, for equal velocities (and, consequently, equal energies), the ionization losses for a particle moving in lead will be 14 times higher than the ionization losses for the same particle if it were to move in carbon:

$$Z_{Pb}/Z_C \simeq 82/6 \simeq 14.$$

Thus, dT/dx varies strongly as we go over from one medium to another. Hence we sometimes use the term specific ionization losses $dT/d\xi$, which is calculated not per unit length x (in cm), but per unit "density" ξ, expressing the thickness in g/cm^2.

Obviously, $\xi = x\rho$, where ρ is the density of the medium. This gives

$$dT/d\xi = (dT/dx)\ (dx/d\xi) = (dT/dx)\ (1/\rho). \qquad (4.2.16)$$

Since $\rho \propto Z$ and $dT/dx \propto Z$, we find that $(dT/dx)\ (1/\rho) \simeq$ const. Thus, the quantity $dT/d\xi$ is practically constant for all media and is therefore more convenient that dT/dx for quick rough calculations.

For the sake of comparison, the values of $dT/d\xi$ for protons moving in air and in lead are given in Table 22 for different energies.

Table 22

T, MeV	$(dT/d\xi)_{air}$, MeV/(g·cm^{-2})	$(dT/d\xi)_{Pb}$, MeV/(g·cm^{-2})	T, MeV	$(dT/d\xi)_{air}$, MeV/(g·cm^{-2})	$(dT/d\xi)_{Pb}$, MeV/(g·cm^{-2})
1	300	150	100	7.5	5
10	50	30	$>10^3$	2.3	1.6

4.2.3. Relation Between Range and Energy

For a given medium and a particle with a charge z, the quantity dT/dx is a function of velocity alone and hence, for a particle with a given mass, a function of kinetic energy only:

$$dT/dx = \varphi(T). \qquad (4.2.17)$$

Integrating this expression over all values of T between 0 and T_0, we obtain the entire range X of the particle:

$$X = \int_0^{T_0} \frac{dT}{\varphi(T)}. \qquad (4.2.18)$$

The range of particles is usually denoted by R and is measured in units of length (m, cm, μm) or "density" (g/cm²).

Let us consider certain formulas connecting the ranges and energies of various particles in different media.

1. Calculations and subsequent experimental verification (measurement of the range of monochromatic particles) led to the following formula for protons in photographic emulsion:

$$T_p = \alpha R_p^n, \tag{4.2.19}$$

where $\alpha \simeq 0.25$, $n \simeq 0.58$, T is measured in MeV, and R in micrometres.[6] Formula (4.2.19) can be easily modified for any particles moving in a photographic emulsion. Indeed, for nonrelativistic energies, we have[7]

$$\frac{dT}{dx} = \frac{d}{dx}\left(\frac{mv^2}{2}\right) = mv\frac{dv}{dx}. \tag{4.2.20}$$

Since in accordance with formula (4.2.10) $dT/dx = z^2\varphi(v)$ for a given medium, we get

$$z^2\varphi(v) = mv\frac{dv}{dx} \quad \text{and} \quad dx = \frac{m}{z^2}\frac{v}{\varphi(v)}dv,$$

whence

$$X = \frac{m}{z^2}\int \frac{v}{\varphi(v)}dv = \frac{m}{z^2}\Phi(v). \tag{4.2.21}$$

Thus, the ranges of two particles having equal velocities in a given medium are in the same ratio as the values of m/z^2 for these particles:

$$X_1 : X_2 = \frac{m_1}{z_1^2} : \frac{m_2}{z_2^2}. \tag{4.2.22}$$

But the energies of particles having the same volocity are in the same ratio as their masses. Hence, denoting the masses of a proton and of an unknown particle by m_p and m, their charges by $z = 1$ and z, and their ranges by R_p, and R, respectively, we obtain

$$R_p : R = m_p : \frac{m}{z^2} \quad \text{or} \quad R_p = R\left(\frac{m_p}{m}\right)z^2; \tag{4.2.23}$$

$$T_p : T = m_p : m \quad \text{or} \quad T_p = T\left(\frac{m_p}{m}\right). \tag{4.2.24}$$

Substituting the expression for R_p and T_p into (4.2.19), we get

$$T = \alpha\left(\frac{m}{m_p}\right)^{1-n} z^{2n} R^n. \tag{4.2.25}$$

[6] The values of α and n vary slightly as we go over from one type of photographic emulsion to another.

[7] Obviously, these arguments are also valid for relativistic energies.

This formula is valid for any heavy charged particles moving in a photographic emulsion [the values of α and n, as well as the units of measurement of T and R, are the same as in formula (4.2.19)].

2. The relation between the range and energy of electrons in aluminium is expressed through an empirical formula of the type

$$\left.\begin{aligned} R &= 0.407T_e^{1.38} \text{ g/cm}^2 \text{ for } 0.15 < T_e < 0.8 \text{ MeV}, \\ R &= 0.542T_e - 0.133 \text{ g/cm}^2 \text{ for } T_e > 0.8 \text{ MeV}. \end{aligned}\right\} \quad (4.2.26)$$

This formula can be also used for other materials. Sometimes (for rough estimates), we can use the approximate formula

$$R = 0.5T - 0.1_5$$

where R is expressed in g/cm^2 and T in MeV.

3. The energy and range in air for the α-particles emitted by natural α-particle emitters are connected through the formula

$$R = 0.318T_\alpha^{3/2} \text{ for } 3 < R_\alpha < 7 \text{ cm}, \quad (4.2.27)$$

where R is measured in cm, and T in MeV.

At higher energies (up to 200 MeV), the exponent of energy increases from 3/2 to 1.8 and the formula assumes the form

$$R = (T_\alpha/37.2)^{1.8}.$$

Here R is measured in metres in air, and the energy T_α in MeV. According to the recalculation rules (4.2.23) and (4.2.24), this formula can be written in the following form for protons:

$$R = (T_p/9.3)^{1.8}. \quad (4.2.28)$$

4.3. Dirac Monopole

We have seen that the distinguishing feature of formula (4.2.9) is the inverse proportionality of the specific ionization to the square of the particle velocity and its independence of mass. Let us consider the interesting situation in which the dependence of $(dT/dx)_{\text{ion}}$ on v vanishes. This is the case of ionization loss for a hypothetical particle called the Dirac monopole.

It is well known that the electric charge or the electric pole (monopole) is the elementary carrier of the electrical properties of matter, while the magnetic dipole is the carrier of magnetic properties. As a result, the Maxwell equations are not quite symmetric with respect to the electric and magnetic quantities:

$$\left.\begin{aligned} \operatorname{curl} \mathbf{E} &= -\frac{1}{c}\frac{\partial \mathbf{H}}{\partial t}, & \operatorname{div} \mathbf{E} &= 4\pi\rho_e, \\ \operatorname{curl} \mathbf{H} &= \frac{1}{c}\frac{\partial \mathbf{E}}{\partial t} + \frac{4\pi}{c}\mathbf{j}_e, & \operatorname{div} \mathbf{H} &= 0. \end{aligned}\right\} \quad (4.3.1)$$

In 1931, Dirac observed that Eqs. (4.3.1) can be symmetrized by introducing the magnetic charge μ and the magnetic current j_m:

$$\left.\begin{aligned} \operatorname{curl} \mathbf{E} &= -\frac{1}{c}\frac{\partial \mathbf{H}}{\partial t} + \frac{4\pi}{c}\mathbf{j}_\mu, & \operatorname{div} \mathbf{E} &= 4\pi\rho_e, \\ \operatorname{curl} \mathbf{H} &= \frac{1}{c}\frac{\partial \mathbf{E}}{\partial t} + \frac{4\pi}{c}\mathbf{j}_e, & \operatorname{div} \mathbf{H} &= 4\pi\rho_\mu. \end{aligned}\right\} \quad (4.3.2)$$

Dirac was able to show that there was no inconsistency in the electrodynamics based on Maxwell's symmetric equations. According to Dirac, it would be astonishing if nature were to leave this possibility unexploited. Thus the existence of a particle with the properties of a single magnetic pole, viz. a magnetic monopole, was predicted. This particle must possess quite specific properties. In the first place, it is obvious that it must behave like an electric charge which also possesses the properties of an (electric) monopole. Hence the magnetic monopole must create a Coulomb magnetic field $H \propto \mu/r^2$. Two monopoles must interact in accordance with the Coulomb law: $F_C = \mu_1\mu_2/r^2$. In a magnetic field H, the monopole must be subjected to a force $F = \mu H$. Finally, a moving monopole μ must create an electric field $E = Hv/c$.

Since the magnetic monopole participates in electromagnetic interaction, it must undergo ionization losses. The formula for specific ionization losses $(dT/dx)_{ion}$ can be obtained in the same way as formula (4.2.6):

$$\Delta p_\perp = F\tau, \quad F = eH\frac{v}{c} = \frac{e\mu}{r^2}\frac{v}{c}, \quad \tau = \frac{2r}{v},$$

$$\Delta p_\perp = \frac{2e\mu}{rc}, \quad \Delta T = \frac{\Delta p^2}{2m_e} = \frac{2e^2\mu^2}{m_e r^2 c^2} \quad \text{and} \quad \frac{dT}{dx} \propto e^2\mu^2.$$

Thus, the ionization losses for a monopole are proportional to the square of its charge and are independent of its velocity. The track of a monopole must have a uniform thickness throughout its length.

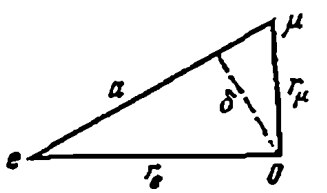

Fig. 148

Quantitatively, the charge of a monopole must be $68.5n$ times higher than a unit electric charge (n is an integer). This can be shown quite simply as follows. Suppose that a charge e and a monopole μ are at a distance a apart (Fig. 148). Then at the point 0 the electric field created by the charge is given by $E = e/r_e^2$, the magnetic field produced by the monopole is $H = \mu/r_\mu^2$, the momentum for a unit volume is $\mathbf{p} = [\mathbf{EH}]/4\pi c \propto e\mu/a^4c$, and the angular momentum is given by

$$\int \mathbf{p}\delta dV = e\mu/c.$$

Since the angular momentum is a quantized quantity, we can write

$$2e\mu/c = n\hbar \tag{4.3.3}$$

(the factor 2 appears as a result of rigorous calculations). This gives

$$\mu = \frac{n}{2}\,\frac{\hbar c}{e^2}\,e = 68.5ne, \tag{4.3.4}$$

where $e^2/\hbar c = \alpha = 1/137$ is the fine-structure constant.

The large value of the monopole charge is responsible for many of its properties. In the first place, it is a strongly ionizing particle. The ionization losses for the monopole are at least $68.5^2 \simeq 4700$ times higher than for a single charged particle, i.e. are of the order of

$$4700 \times 2\,\frac{\text{MeV}}{\text{g/cm}^2} = 9400\,\frac{\text{MeV}}{\text{g/cm}^2} \simeq 10\,\frac{\text{BeV}}{\text{g/cm}^2}. \tag{4.3.5}$$

A monopole with energy 10^{12} eV loses all of its energy in passing just 1 m of water. However, the monopole rapidly acquires an energy in a magnetic field. Indeed, it follows from the relation $F = \mu H$ that over a distance of 1 cm in a field of 1 G, the monopole acquires an energy of $300 \times 68.5 = 2 \times 10^4$ eV. This means that the energy acquired by the monopole in a standard magnetic field of 10^4 G over a distance of 1 m will be 2×10^{10} eV, i.e. 20 BeV. If the monopole really exists and is discovered, it would become possible to create the minutest particle accelerators.

Efforts have been going on for many years to detect a monopole in nature (in cosmic rays, magnetic ores, meteorites, lunar soil) and in accelerators. The latter investigations were carried out in 1975 at Berkeley with the help of a multilayer lexane detector with a total area of 20 m² which was lifted on balloons to an altitude of 40 km. Lexane is sensitive only to nuclei with a high Z and hence to the monopole as well. The particle ruptures the chemical bonds in its track, and this is observed in the form of shallow conical pits after etching. The etching rate depends on Z/β for the passing particle.

After a flight for 2.6 days, one event was registered in which the dependence on Z/β was not observed and which was reminiscent of a monopole because of its characteristics. However, later investigations of this event revealed that the absence of dependence on Z/β was due to an alternative effect, viz. the simultaneous emission of α-particles and protons by a nucleus during deceleration (i.e. a simultaneous decrease in Z and β). The registered particle could have been uniquely identified if it had remained in the detector. However, the thickness of the lexane was not sufficient for this purpose.

4.4. Elastic Scattering of Particles

Elastic scattering is the process of interaction between two particles during which the total kinetic energy of both particles is conserved and is simply redistributed between them, while the particles change the direction of their motion.

In nuclear physics, the Coulomb and nuclear forces (strong interaction)[8] are assumed to be responsible for elastic scattering. Charged particles with low energies are scattered by Coulomb forces, while high-energy charged particles and neutrons are scattered by nuclear forces. The nature of scattering by Coulomb or nuclear forces is determined by the impact parameter ρ (in classical analysis) or by orbital quantum number l (in quantum-mechanical analysis). Apparently, a charged particle ze (Fig. 149) passing at a velocity v near another charged particle Ze (small impact parameter, $\rho = \rho_1$) is scattered at a larger angle φ_1 than a particle passing at a large distance (the impact parameter $\rho = \rho_2$ is large, and hence the angle φ_2 is smaller).

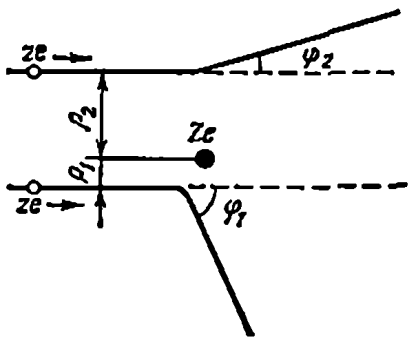

Fig. 149

For long-range (Coulomb or gravitational) forces, the impact parameter ρ may be quite large. In the case of short-range (nuclear) forces, the impact parameter ρ must be smaller than the range a of nuclear forces for an effective interaction (the particle must pass within the effective range of the force). According to quantum mechanics, a particle with a given momentum p will have, instead of the entire continuous range of values of ρ satisfying the inequality

$$\rho < a, \tag{4.4.1}$$

only a certain discrete set of values connected by the condition

$$\rho_l = (\hbar/p)\sqrt{l(l+1)} = \lambda\sqrt{l(l+1)} < a, \tag{4.4.2}$$

where $l = 0, 1, 2, \ldots$ This condition is obtained by comparing the classical and quantum-mechanical expressions for the angular momentum l of the particle:

$$|\mathbf{l}| = p\rho = \hbar\sqrt{l(l+1)}.^9 \tag{4.4.3}$$

[8] Of late, the weak interaction theory also considers the process of elastic scattering by *weak* forces (see Sec. 10.1, Vol. II).

[9] This analysis is not rigorous. In quantum mechanics, the exact values of the momentum p and coordinate ρ of the particle cannot be known simultaneously.

The slower a particle (the smaller its momentum p), the fewer the possible values of the orbital quantum number l and the fewer the possible values ($\rho < a$) of the impact parameter. For example, it can be easily established by calculation that the scattering of a neutron with energy $T < 10$ MeV by a proton can occur only for $l = 0$ and $\rho = 0$ (an analogue of a head-on collision in classical mechanics). On the contrary, p is quite large for fast particles and condition (4.4.2) can be satisfied for different values of l and ρ. In this case, each value of l will dictate its own law of angular distribution for the scattered particle. (The quantum-mechanical scattering problem is considered in detail in Sec. 1.4, Vol. II.)

4.4.1. Momentum Scattering Diagram

If the direction of motion of a scattered particle is known (from experiment or calculations for a given impact parameter ρ and given forces), there is a simple geometrical method for calculating the velocity and direction of the second particle (after scattering) from known values of the velocity and direction of the incident particle. This method is called the *momentum diagram*.[10]

Suppose that a particle with a mass M_1 and a velocity v undergoes an elastic collision with a particle of mass M_2 at rest.[11] The centre of mass of both particles has a velocity $v_{c.m.} = \frac{M_1}{M_1+M_2} v$. The velocity of particle M_2 in the centre-of-mass system will be $v'_{M_2} = -\frac{M_1}{M_1+M_2} v = -v_{c.m.}$. The momentum of the particle in this system will be $p'_{M_2} = \frac{M_2}{M_1+M_2} P_{M_1}$, while the momentum of the particle M_1 will be equal and opposite: $p'_{M_1} = -p'_{M_2} = \frac{M_2}{M_1+M_2} p_{M_1}$ (according to the property of the centre-of-mass system).

Suppose that the segment AB represents on a certain scale the initial momentum of particle M_1 in the laboratory coordinate system before scattering: $p_{M_1} = AB$ (Fig. 150). We divide this segment at point O in the ratio of masses of the particles, i.e. $AO : OB = M_1 : M_2$. In this case,

$$OB = \frac{M_2}{M_1+M_2} p_{M_1} = p'_{M_1}, \quad \text{and} \quad p'_{M_2} = -p'_{M_1} = OC.$$

[10] We shall consider the construction of momentum diagram for the nonrelativistic case. The concept of momentum diagram for elastic scattering in the relativistic case will be introduced in Sec. 2.1.1, Vol. II.

[11] The following arguments are valid for any ratio of masses, but we shall assume for the sake of definiteness that $M_1 < M_2$.

According to the law of conservation of momentum, the momenta of both the particles in the centre-of-mass system must remain equal and opposite after collision. Besides, the absolute value of momentum also cannot change in the case of an elastic collision, when the total kinetic energy of the particles is conserved.

Thus, the description of the scattering process for two particles in the centre-of-mass system is reduced to a rotation of the momentum couple $p'_{M_1} = OB$ and $p'_{M_2} = OC$ through a certain angle θ' so that the momenta of the particles M_1 and M_2 after collision will be represented by the segments $\vec{p}'_{M_1} = OD$ and $\vec{p}'_{M_2} = OE$ (the symbol v has been used to distinguish between the momenta p of the particles before and after collision).

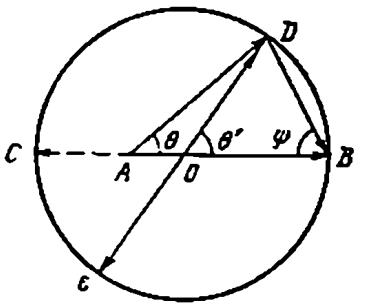

Fig. 150

For a transition back to the laboratory coordinate system, we must take into account the motion of the centre-of-mass system with a velocity $v_{c.m.} = M_1 v/(M_1 + M_2)$ relative to the laboratory coordinate system. Both particles participate in this motion, and hence they will acquire additional momenta due to translation:

$$\left.\begin{aligned}(p_{M_1})_{tr} &= M_1 v_{c.m.} = \frac{M_1^2}{M_1+M_2}\, v = \frac{M_1}{M_1+M_2}\, p_{M_1},\\ (p_{M_2})_{tr} &= M_2 v_{c.m.} = \frac{M_1 M_2}{M_1+M_2}\, v = \frac{M_2}{M_1+M_2}\, p_{M_1}.\end{aligned}\right\} \qquad (4.4.4)$$

In Fig. 150, segments AO and OB correspond to the momenta $(p_{M_1})_{tr}$ and $(p_{M_2})_{tr}$. Thus, in the centre-of-mass system, the momentum of particle M_1 after scattering is measured by segment $\vec{p}'_{M_1} = OD$, while its additional momentum is measured by segment AO. The vector sum of these segments is the vector $AD = OD + AO$, which represents the particle momentum $\vec{p}_{M_1}$ in the laboratory coordinate system after scattering. Similarly, the addition of vectors $\vec{p}'_{M_2} = OE$ and $(p_{M_2})_{tr} = OB$ gives the vector $DB = OB - OD = OB + OE$, representing the momentum of the recoil nucleus in the laboratory coordinate system after scattering. As expected, both vectors AD and DB together with the initial momentum $p_{M_1} = AB$ of particle M_1 form a vector triangle, such that

$$\vec{p}_{M_1} = \vec{p}_{M_1} + \vec{p}_{M_2}.$$

Thus, the following construction is required for obtaining the mo-

menta of the scattered particle and the recoil nucleus:

1. Lay off segment AB equal to the initial momentum of particle M_1: $AB = p_{M_1}$.

2. Divide this segment at point O in the ratio of the particle masses $AO/OB = M_1/M_2$, and draw a circle from point O, passing through point B.

3. From point A, draw a straight line at the scattering angle θ (known, for example, from experiment) until it intersects the circle at point D. Join points D and B.

4. Pass a diameter through point D.

Then, in accordance with the above analysis, segment AD represents the momentum of the scattered particle, $\angle BAD = \theta$ is the scattering angle for particle M_1, segment DB corresponds to the momentum of the recoil nucleus, while $\angle DBA = \psi$ is the scattering angle for recoil nucleus M_2, $\angle DOB = \theta'$ is the scattering angle for particle M_1 in the centre-of-mass system. The momenta of particle M_1 in the centre-of-mass system before and after collision is represented by segments OB and OD, while OC and OE represent the corresponding values for particle M_2.

If the scattering angle θ is unknown and the diagram is constructed with the purpose of finding this angle besides the values of momenta of the scattered particle and the recoil nucleus, items 3 and 4 in the above scheme must be interchanged. In this case, point D is obtained as a result of intersection of the circle with the diameter drawn at an angle θ' which determines the direction of scattering of the particle M_1 in the centre-of-mass system.

We leave it for the reader to derive independently the following obvious relations.

1. The total kinetic energy of both particles in the centre-of-mass system (relative kinetic energy)

$$T' = \frac{M_1 M_2}{M_1 + M_2} \frac{v^2}{2} = \frac{M_2}{M_1 + M_2} T = \frac{\mu v^2}{2}, \qquad (4.4.5)$$

where $\mu = M_1 M_2/(M_1 + M_2)$ is the reduced mass of the particles M_1 and M_2.

2. The kinetic energy of translatory motion of both particles $T_{c.m.} = (M_1 + M_2)\, v_{c.m.}^2/2$ or, since $v_{c.m.} = M_1 v/(M_1 + M_2)$,

$$T_{c.m.} = \frac{M_1^2}{M_1 + M_2} \frac{v^2}{2} = \frac{M_1}{M_1 + M_2} T. \qquad (4.4.6)$$

Comparing relations (4.4.5) and (4.4.6), we get $T' + T_{c.m.} = T$, where T is the initial kinetic energy of particle M_1 in the laboratory coordinate system ($T = M_1 v^2/2$).

3. After collision, the kinetic energies of particles M_1 and M_2 in the laboratory coordinate system are

$$\check{T}_{M_1} = \frac{M_1^2 + M_2^2 - 2M_1M_2\cos 2\psi}{(M_1+M_2)^2}\,T \qquad \begin{matrix}(\check{T}_{M_1})_{\min} = \left(\frac{M_1-M_2}{M_1+M_2}\right)^2 T,\\ (\check{T}_{M_1})_{\max} = T;\end{matrix} \tag{4.4.7}$$

$$\check{T}_{M_2} = \frac{2M_1M_2}{(M_1+M_2)^2}(1+\cos 2\psi)\,T \qquad \begin{matrix}(\check{T}_{M_2})_{\max} = \left(\frac{4M_1M_2}{(M_1+M_2)^2}\right)T,\\ (\check{T}_{M_2})_{\min} = 0.\end{matrix} \tag{4.4.8}$$

In accordance with the law of conservation of energy, we obtain the following relation for the elastic collision:

$$\check{T}_{M_1} + \check{T}_{M_2} = T.$$

4. The scattering angles for particles M_1 and M_2 in the laboratory coordinate system are connected through the relation

$$\tan\theta = \frac{\sin 2\psi}{M_1/M_2 - \cos 2\psi}. \tag{4.4.9}$$

The scattering angle θ for particle M_1 in the laboratory coordinate system is connected with its scattering angle θ' in the centre-of-mass system through the relation

$$\tan\theta = \frac{\sin\theta'}{M_1/M_2 + \cos\theta'}. \tag{4.4.10}$$

5. If $M_1 > M_2$ (Fig. 151), there exists a maximum value for the scattering angle of particle M_1 in the laboratory coordinate system. This value is determined from the condition

$$\sin\theta_{\max} = M_2/M_1. \tag{4.4.11}$$

The momentum diagram can be used for a rapid and convenient solution of various problems of elastic scattering. For known par-

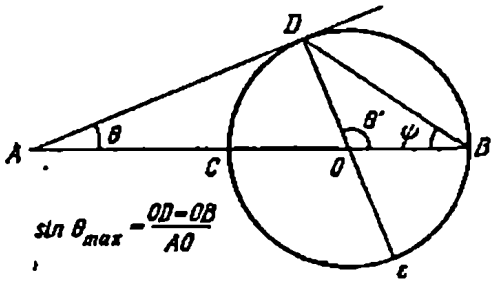

Fig. 151

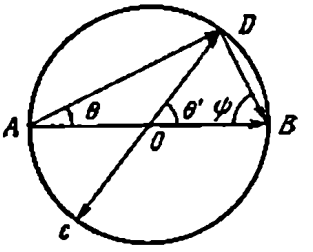

Fig 152

ticle masses, it can be used to determine their momenta and energies after collision for any scattering angle [formulas (4.4.7) and (4.4.8)]. If the scattering angles θ and ψ for both particles are known as well

as the mass of one particle, this diagram can be used to find the mass of the other particle [formula (4.4.9)].

The momentum diagram assumes an especially simple form if the two particles have the same mass $M_1 = M_2$ (Fig. 152). In this case,

$$\left.\begin{aligned}
&p_{M_1} = AB;\ p_{M_2} = 0;\ p'_{M_1} = p_{M_1}/2 = OB;\ p'_{M_2} = OA;\\
&\mu = M_1/2 = M_2/2;\ T'_{M_1} = (p'_{M_1})^2/2M_1 = T/4;\\
&T'_{M_2} = (p'_{M_2})^2/2M_2 = T/4;\ T'_{M_1} + T'_{M_2} = T/2;\\
&\theta' = 2\theta;\ \theta + \psi = \pi/2;\ \cot\theta\cot\psi = 1;\\
&p_{M_1} = AD = AB\cos\psi = p_{M_1}\cos\theta = p_{M_1}\sin\psi;\\
&\check{p}_{M_2} = DB = AB\cos\psi = p_{M_1}\cos\psi = p_{M_1}\sin\theta;\\
&\check{T}_{M_1} = T_{M_1}\cos^2\theta;\ \check{T}_{M_2} = T_{M_1}\cos^2\psi = T_{M_1}\sin^2\theta;\\
&(\check{T}_{M_1})_{max} = T_{M_1};\ (\check{T}_{M_1})_{min} = 0;\ (\check{T}_{M_2})_{max} = T_{M_1};\\
&(\check{T}_{M_2})_{min} = 0.
\end{aligned}\right\} \quad (4.4.12)$$

Later, in Sec. 6.3.1, we shall show that the mean value $\bar{\check{T}}_{M_1} = T_{M_1}/2$. As a result of collision, the particle loses half its energy on the average.

4.4.2. Rutherford's Formula

For $M_1 \ll M_2$ ($m \ll M$), the above momentum diagrams show that

$$\left.\begin{aligned}
&(\check{p}_m)_{min} = -(M-m)\,p_m/(M+m) \simeq -p_m,\\
&(\check{T}_m)_{min} = [(M-m)/(M+m)]^2\,T_m \simeq T_m.
\end{aligned}\right\} \quad (4.4.13)$$

This means that the momentum and energy of the particle practically remain unchanged. The main result of the elastic scattering is a deflection of the particle from its original path. The angle θ at which the particle is deflected can be found from the condition $\tan\theta = \Delta p/p$, where p is the momentum of the particle and Δp is the increment in momentum as a result of interaction with the scattering centre (Fig. 153).

The angle θ is determined by the efficiency of the interaction between the particles, i.e. depends on the law of interaction and the impact parameter ρ.

When two charged particles interact, the law of interaction (the variation of force with distance ρ) is known, and the expression for tan θ can be calculated in the same way as in Sec. 4.2:

$$\tan\theta = \Delta p/p = F\,\Delta t/p \simeq (Zze^2/\rho^2)\,(2\rho/v)\,(1/p) = (2Zze^2/pv)\,(1/\rho). \tag{4.4.14}$$

It can be easily seen that for small angles (and nonrelativistic energies), this formula is the same as the classical formula in atomic physics

$$\tan\frac{\theta}{2} = (Zze^2/mv^2)\,(1/\rho), \tag{4.4.15}$$

where it is obtained from the laws of conservation of energy and angular momentum under the assumption that the Coulomb law is valid at short distances ($\rho < 10^{-8}$ cm).

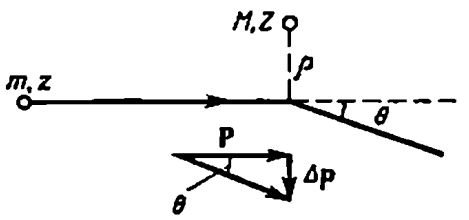

Fig. 153

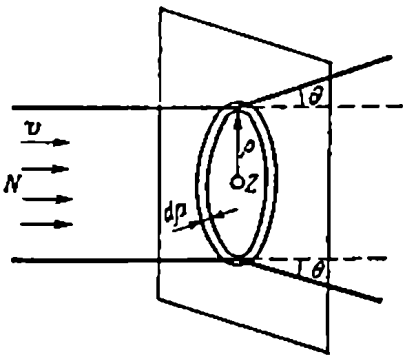

Fig. 154

This formula cannot be verified directly on account of the fact that besides the experimentally measurable quantity θ, it also contains the impact parameter ρ which cannot be measured. However, the formula can be verified statistically by analyzing a large number of cases of scattering for all possible values of the impact parameter ρ.

Let N be the intensity of a beam of particles with a given mass m, charge z and velocity v (the number of particles passing through 1 cm² per second). If a fixed particle with a charge Z lies in the path of this beam (Fig. 154), the number of particles deflected at an angle θ will be $dN = 2\pi\rho d\rho N$, where ρ is computed from formula (4.4.15). The quantity $d\sigma = dN/N = 2\pi\rho d\rho$ is called the *effective differential scattering cross section* (see Sec. 1.4.3). It characterizes the probability of scattering of a particle at a given angle θ by a single nucleus. Since in actual practice the beam encounters not a single particle but a target containing n nuclei per square centimetre of area, we obtain

$$dN = Nn2\pi\rho d\rho = Nnd\sigma. \tag{4.4.16}$$

The quantity $d\Sigma = dN/N$ is called the *macroscopic effective differential scattering cross section*. It characterizes the probability of scattering a particle at an angle θ by all nuclei in 1 cm^3 of the target[12].

Expressing ρ and $d\rho$ in terms of θ and making simple trigonometric transformations, we obtain the following expressions for $d\sigma$ and $d\Sigma$:

$$d\sigma = \left(\frac{Ze^2}{mv^2}\right)^2 \frac{d\Omega}{4\sin^4(\theta/2)}, \quad d\Sigma = n\,d\sigma, \tag{4.4.17}$$

This is the well-known Rutherford formula which was derived in 1911. In the particular case when $s = 2$, this formula becomes

$$d\Sigma = n\,d\sigma = n\left(\frac{Ze^2}{mv^2}\right)^2 \frac{d\Omega}{\sin^4(\theta/2)}. \tag{4.4.18}$$

This formula was obtained by Rutherford within the framework of the classical theory. However, the same result can also be obtained from rigorous quantum-mechanical calculations and in the Born approximation. This is explained by the specific nature of the Coulomb potential.

Formula (4.4.18) was used by Rutherford to explain the scattering of α-particles. It should be recalled that in these experiments, a very strong scattering (up to 180°) was observed for some of α-particles. This cannot be explained on the basis of the model of an atom with a "smeared" positive charge.[13] Rutherford derived formula (4.4.18) on the basis of the nuclear model of the atom, and it is possible to experimentally verify this formula as it contains only experimentally measurable quantities. Thus, when an α-particle beam with a given intensity N and a velocity v is scattered by the nuclei of a certain target (with given n and Z), the Rutherford formula

$$d\Sigma = \frac{dN}{N} = n\left(\frac{Ze^2}{mv^2}\right)^2 \frac{d\Omega}{\sin^4(\theta/2)}$$

---

[12] When the effect of many nuclei is considered, it may appear at first glance that the action of nuclei on different sides of the line of flight of a particle will tend to cancel out. However, this is not true since the values of ρ are bounded from above by the value ρ_{max} at which the nuclear charge is completely screened by the atomic electrons. If a particle flies at a distance $\rho > \rho_{max}$ from the nucleus, it does not interact with it ($\rho_{max} \simeq R_{at}$). While introducing the concept of macroscopic effective cross section for charged particles, it is assumed that the target is so thin that its nuclei do not "overshadow" one another and a particle passing through the target does not change its energy due to ionization losses. For thick targets, the concept of yield is introduced instead of macroscopic cross section (see Sec. 9.1.3). This restriction is not applied when matter interacts with neutrons. The macroscopic cross section then means the quantity $d\Sigma = n\,d\sigma$, where n is the number of nuclei per cubic centimetre of the target.

[13] This is obvious from an analysis of formula (4.4.15) in which $Ze^2/mv^2 \simeq 3 \times 10^{-12}$ cm (for $Z = 50$). If Thomson's model is valid, we get $\rho \gg 10^{-8}$ cm, whence $\theta \simeq 0.03°$.

contains only two variable quantities dN and θ, and hence we get

$$(dN/d\Omega)\sin^4(\theta/2) = \text{const}. \qquad (4.4.19)$$

The experimental verification carried out by Geiger and Marsden fully confirmed the correctness of formula (4.4.19) and hence the validity of the nuclear model of atom underlying the derivation of this formula. The experimental set-up of Geiger and Marsden is schematically shown in Fig. 155. Measurements could be carried out at angles between 15° and 150°, and the number dN of α-particles scattered in this interval during the same time varied from 1.3×10^5

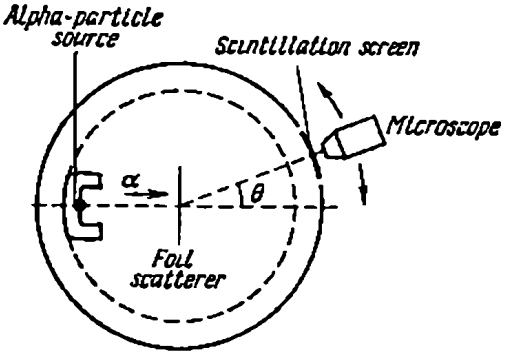

Fig. 155

to 30. As a result of the experiment, the value of $dN/d\Omega\ (\theta)\sin^4\theta/2 =$ 29-38 was obtained for all the angles in the interval between 15° and 150°.

Rutherford's formula can be used for determining the atomic charge Z in a direct experiment. It should be recalled that the nuclear charge was identified with the atomic number of the element in the Periodic Table with the help of Moseley's law. Although this method gives exact results, it is not direct. Rutherford's formula can be used to compare the nuclear charge Z with the deflection θ caused *directly by this charge. From the experimental point of view, it is* more convenient to compare the number N of incident α-particles with the number dN of α-particles scattered at a given angle θ. In this case, $(dN/N)^{r=\text{const}}_{\theta=\text{const}}$ is a function of only the charge Z of the scatterer and hence this charge can be calculated.

This experiment was conducted by many scientists, but did not lead to any reliable results until 1920 since dN and N from different experiments were compared. Chadwick was the first to compare in 1920 dN and N in the same experiment. The experimental set-up used by him is shown schematically in Fig. 156. If the source of α-particles and the detector (scintillating screen) are at the same distance from the scatterer in the form of a ring, the geometry of the experiment turns out to be especially convenient for calculations

and quite useful for measurements since the detector "collects" particles scattered at a certain angle from the whole surface of the annular scatterer. The number dN of the scattered α-particles was measured under conditions when the direct α-particle beam (from the source to the detector) was intercepted by a screen that was opaque to α-particles. Conversely, the scatterer was covered by an opaque screen when N was measured. In this case, to reduce the effect during

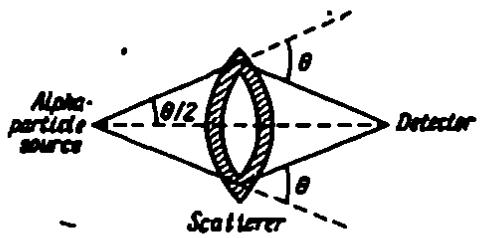

Fig. 156

the measurement of N (this number is several thousand times larger than dN), a rapidly rotating disc with a narrow slit was used. The width of the slit was such that dN and N were comparable.

Different materials were investigated in this kind of an experiment and it was found that within the limits of experimental error, the nuclear charge is equal to the atomic number of the element. For example, the following values were obtained for Z of copper and platinum:

$$Z_{_{29}Cu} = 29.3 \pm 0.45; \quad Z_{_{78}Pt} = 77.4 \pm 0.77.$$

4.4.3. Mott's Formulas (Basic Ideas)

Rutherford's formula was derived under the assumption that $m \ll M$. This considerably simplified the analysis, since the α-particle energy practically does not change as a result of collision ($p = \text{const}$), and the scattering heavy nucleus is not displaced upon collision. In this case, it is convenient to carry out the analysis in laboratory coordinate system.

In the general case of scattering of charged particles with comparable masses, these assumptions are no longer valid and the laboratory coordinate system is not convenient for the analysis. However, the centre-of-mass system can be conveniently used in this case. Obviously, the analysis should again lead to the same result as in the case $m \ll M$, the only difference being that θ, $d\Omega$ and m in (4.4.17) are now replaced by θ', $d\Omega' = 2\pi \sin\theta' d\theta'$ and the reduced mass $\mu = Mm/(M + m)$ respectively (the velocity v remains unchanged,

since the velocity of relative motion of two particles is the same in the centre-of-mass system and the laboratory coordinate system):

$$d\rho = \frac{dN}{Nn} = \left(\frac{Zze^2}{\mu v^2}\right)^2 \frac{d\Omega'}{4\sin^4(\theta'/2)}. \qquad (4.4.20)$$

For a transition to the laboratory coordinate system, we must use a formula connecting the angle θ in the laboratory system to the angle θ' in the centre-of-mass system. We shall not do this for the general case, but shall consider only the particular case of Coulomb scattering of two identical particles. This case is interesting because of two specific features.

According to formulas (4.4.12), we obtain $\theta' = 2\theta$, $\theta + \psi = \pi/2$, $d\Omega' = 2\pi \sin\theta' \, d\theta' = 4\cos\theta \, d\Omega$, $\mu = m/2$ and

$$d\sigma = \left(\frac{z^2e^2}{T}\right)^2 \frac{\cos\theta \, d\Omega}{\sin^4\theta}. \qquad (4.4.21)$$

However, in this form the formula does not lead to a correct value of the effective cross section, since it has been derived without taking into account the following additional effects associated with the identity of both particles.

1. In the first classical effect, the identity of two particles makes it impossible to distinguish experimentally between the scattering at an angle θ and the scattering at an angle $\psi = \pi/2 - \theta$, since the recoil nucleus in the latter case of scattering flies at an angle θ and is registered by the detector as a scattered particle. Consequently, an additional term proportional to $1/\cos^4\theta$ appears in formula (4.4.21). The cross section increases and is given by the formula

$$d\sigma = \left(\frac{z^2e^2}{T}\right)^2 \cos\theta \, d\Omega \left(\frac{1}{\sin^4\theta} + \frac{1}{\cos^4\theta}\right). \qquad (4.4.22)$$

According to this formula, the identical nature of the two particles leads to a doubling of the cross section when the scattering takes place at an angle $\theta = 45°$.

2. An experimental verification of formula (4.4.22) showed that it gives too low results in some cases (scattering of α-particles by helium), while in some cases the results are exaggerated (scattering of protons by hydrogen) in comparison with experimental results. This is explained by the fact, that besides the classical effect of increase in the effective cross section due to additional contribution from the recoil nuclei scattered at the same angle as the incident particles, we must also take into account the quantum-mechanical exchange effect associated with the indistinguishability of both particles. The essence of this effect lies in the interference of waves describing the motion of the scattered particle and the recoil nucleus,

and consequently the square of the amplitude of the resultant wave (which is proportional to the scattering probability or the scattering cross section) is not equal to the sum of the squares of amplitudes of the two waves (which are proportional to the contributions of the scattered particle and the recoil nucleus to the cross section without taking the interference into account). Appropriate corrections to the formula obtained by Mott have the following form (in the nonrelativistic case)[14]:

for particles with zero spin (scattering of α-particles by helium)

$$d\sigma = \left(\frac{z^2e^2}{T}\right)^2 \left\{\frac{1}{\sin^4\theta} + \frac{1}{\cos^4\theta} + \frac{2\cos\left[\frac{(ze)^2}{\hbar v}\ln\tan^2\theta\right]}{\sin^2\theta\cos^2\theta}\right\}\cos\theta\, d\Omega; \quad (4.4.23)$$

for particles with half-integral spin (scattering of protons by hydrogen)

$$d\sigma = \left(\frac{z^2e^2}{T}\right)^2 \left\{\frac{1}{\sin^4\theta} + \frac{1}{\cos^4\theta} - \frac{\cos\left[\frac{(ze)^2}{\hbar v}\ln\tan^2\theta\right]}{\sin^2\theta\cos^2\theta}\right\}\cos\theta\, d\Omega. \quad (4.4.24)$$

Analysis of the argument of cosine in these formulas shows that the last term is always positive in both cases. Hence the consideration of the quantum-mechanical exchange effect increases the cross section in the first case and decreases it in the second case. It can be easily seen that in both cases the cross section changes by a factor of 2 if the scattering takes place at an angle of 45°.

Mott's quantum-mechanical formulas are found to be in good agreement with the results of the experiments on scattering of α-particles by helium and of protons by hydrogen at comparatively low energies. As the energy increases, a disagreement with the experiment due to nuclear attraction is observed (see Sec. 1.5.5, Vol. II).

4.4.4. Delta-electrons

In the process of ionization losses, the kinetic energy of a charged particle is spent to excite and ionize the atoms of the medium through which it passes.

Electrons which are knocked out during ionization of atoms and are themselves capable of ionizing other atoms are called δ-electrons. Since their energy is large in comparison with the ionization energy, the process of formation of δ-electrons can be considered as the scattering of a heavy charged particle by a free electron. This process corresponds to the above-mentioned momentum scattering pattern for the case when the mass of the incident particle is much larger than the mass of the target particle (see Fig. 151). It can be seen from

[14] Mott's formulas for scattering of relativistic electrons by nuclei and protons are derived in Secs. 3.2. and 3.3, Vol. II.

Fig. 151 that the angle ψ of escape of a δ-electron lies between 0° and 90°, while its energy is a function of this angle according to formula (4.4.8):

$$T_e = \frac{4m_eM}{(M+m_e)^2} T\cos^2\psi. \qquad (4.4.25)$$

The lowest energy value $(T_e)_{\min} = 0$ is attained for $\psi = 90°$. The maximum energy is acquired by a δ-electron when it is knocked out in the forward direction ($\psi = 0°$):

$$(T_e)_{\max} = \frac{4m_eM}{(M+m_e)^2} T \simeq \frac{4m_e}{M} T \qquad (4.4.26)$$

(if $M = m_p$, we get $(T_e)_{\max} \simeq T_p/460$).

Formula (4.4.25), which is obtained in the nonrelativistic approximation, provides a rough estimate for the energy of an ionizing particle from the range of the δ-electron and the angle of its escape. Thus, for example, the existence of δ-tracks (δ-rays) with energy T_e along a proton track indicates that the proton energy $T_p \geqslant 460T_e$.

More exact characteristics of an ionizing particle can be obtained by determining the number of δ-electrons. This possibility is due to the fact that the cross section of δ-electron formation is a function of the energy and charge of the ionizing particle.

The formula for calculating the δ-electron formation cross section can be obtained by transforming the Rutherford formula (4.4.20) in the particle-electron centre-of-mass system:

$$d\sigma = \left(\frac{ze^2}{\mu v^2}\right)^2 \frac{2\pi \sin\theta' d\theta'}{4\sin^4(\theta'/2)}. \qquad (4.4.27)$$

This formula gives the cross section for particles scattered in the centre-of-mass system at angles between θ' and $\theta' + d\theta'$, or for electrons knocked out in the opposite directions (according to the properties of the centre-of-mass system). However, it follows from Fig. 151 that $\theta' = \pi - 2\psi$, where ψ is the angle at which a δ-electron escapes in the laboratory coordinate system. Besides,

$$\mu v^2 = \frac{Mm_e}{M+m_e} v^2 \simeq m_e v^2,$$

whence

$$d\sigma_\delta = \left(\frac{ze^2}{m_e v^2}\right)^2 \frac{2\pi \sin\psi d\psi}{\cos^3\psi} = \left(\frac{ze^2}{m_e v^2}\right) \frac{d\Omega}{\cos^3\psi}. \qquad (4.4.28)$$

This result can be easily recalculated from the angle interval between ψ and $\psi + d\psi$ to the energy interval for δ-electrons between T_e and $T_e + dT_e$. Indeed, it follows from (4.4.25) that

$$\frac{\sin\psi d\psi}{\cos^3\psi} = -\frac{2m_eM}{(M+m_e)^2} T \frac{dT_e}{T_e^2}. \qquad (4.4.29)$$

Substituting this expression into (4.4.28) and considering that $T = Mv^2/2$ and $m_e \ll M$, we obtain

$$d\sigma_\delta = \frac{2\pi e^4 z^2}{m_e v^2} \frac{dT_e}{T_e^2}. \qquad (4.4.30)$$

Thus, the cross section of δ-electron formation is proportional to the square of the charge and inversely proportional to the square of the velocity of the ionizing particle. It also depends strongly on the energy of the knocked out δ-electrons (as $1/T_e^2$ approximately).

The majority of the electrons is knocked out with a low energy at an angle ψ close to $\pi/2$.

The dependence of the δ-electron formation cross section on the charge of the ionizing particle can be used to determine the charge by counting the number N_δ of δ-electrons per unit length of the particle track in the material. The number N_δ of δ-electrons with a given energy T_e must obviously be equal to

$$N_\delta (T_e) = d\sigma_\delta n_e, \qquad (4.4.31)$$

where n_e is the number density of electrons in the medium.

The number of δ-electrons having energy between T_e and $(T_e)_{max}$ is given by

$$N_\delta = n_e \sigma_\delta = \frac{2\pi e^4 z^2}{mv^2} n_e \int_{T_{e_1}}^{(T_e)_{max}} \frac{dT_e}{T_e^2} = \frac{2\pi n_e e^4 z^2}{mv^2} \left[\frac{1}{T_{e_1}} - \frac{1}{(T_e)_{max}} \right]. \qquad (4.4.32)$$

4.4.5. Multiple Scattering

It follows from the Rutherford formula (4.4.17) that the probability of Coulomb scattering of a charged particle at a certain angle θ sharply increases with decreasing scattering angle. Hence a charged particle moving in a dense medium must experience along its track a large number of successive scattering acts at very small angles. This process is called *multiple Coulomb scattering*.

Multiple scattering leads to several effects which must be taken into account during an analysis of the experimental data. These include, for example, an increase in the transverse dimensions of a particle beam upon passing through matter, imitation of magnetic bending of particle tracks in tracking instruments (apparent curvature), spreading along the path traversed by electrons in matter, etc.

Since multiple scattering is caused by the Coulomb interaction of a particle with the nuclei of the medium, the experimental characteristics of multiple scattering must be associated with the parameters of the particle as well as the medium. Hence an investigation

of the experimental regularities of multiple scattering of a particle can provide information about the properties of this particle.

All this obviously points towards the importance of theoretical and experimental investigation of the multiple scattering. Naturally, it is impossible to follow experimentally the process of multiple scattering acts experienced by a particle as it passes through matter. However, a track detector (for example, photographic emulsion) can be used for measuring the resultant deviation from the initial direction of motion of the particle (mean multiple scattering angle), i.e. the change in the course of the particle as it covers a certain path x in the medium and undergoes a certain number N of collisions. Let us express this angle as a function of the parameters of the particle and the medium.

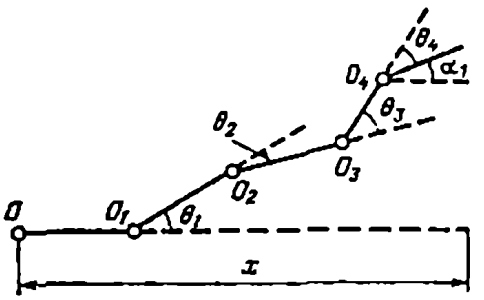

Fig. 157

Let OO_1 be the initial direction of motion of a particle in a medium, and let $O_1, O_2, O_3 \ldots$ be the points of successive elastic collisions of the particle with the first, second, third, etc. nuclei (Fig. 157).

As a result of these collisions, the particle undergoes successive deflections through angles $\theta_1, \theta_2, \theta_3, \ldots$. Each of these angles ($\theta_i$) depends on the specific conditions of the collision (the value of the impact parameter ρ_i) and hence $\theta_1 \neq \theta_2 \neq \theta_3 \ldots$ in general. Moreover, each ith collision may take place in any direction relative to the previous $(i-1)$th collision (the angles θ_i in Fig. 157 do not lie in one plane).

In covering a certain distance x in the medium, the particle undergoes a certain number N of collisions and deviates from its initial direction OO_1 by the resultant angle Θ_1 whose projection on the plane of the figure is α_1. (The angle Θ_1 itself is not shown in the figure.)

If this analysis is repeated for another particle having the same velocity, charge and mass and covering the same path length x, we obtain a somewhat different angle Θ_2 with a projection α_2. For the third particle, we obtain the resulting angle Θ_3 having a projection α_3, and so on. For the kth particle, the corresponding values will be denoted by Θ_k and α_k respectively.

The plane angles $\alpha_1, \alpha_2, \ldots, \alpha_k$ can be easily measured by observing, say, the track of the particle in photographic emulsion under a microscope.

Obviously, on account of the random disposition of different segments of the path of the particle ($OO_1, O_1O_2, O_2O_3, \ldots$) for different particles, the statistical distribution of possible values of α_i will

be described by a Gaussian function, while the average value will be given by

$$\bar{x} = \sum_1^k \alpha_j/k = 0. \tag{4.4.33}$$

This quantity cannot serve as a measure of deviation from the initial direction of motion of the particle as a result of multiple scattering. An estimate of this deviation can be had by calculating the mean square value $\overline{\alpha^2}$ of the projections of angles Θ_j:

$$\overline{\alpha^2} = \sum_1^k \alpha_j^2/k. \tag{4.4.34}$$

This must be an essentially positive quantity.

Apparently, the mean square of the space angles Θ_j themselves is

$$\overline{\theta^2} = 2\overline{\alpha^2}.$$

The quantity $\theta = \sqrt{\overline{\theta^2}}$ is called the *mean multiple scattering angle*. Sometimes, the same term is used for the quantity $\alpha = \sqrt{\overline{\alpha^2}}$ which is usually obtained as a result of measurements.

The angle α can be measured either by the above-mentioned method of averaging $\alpha_1, \alpha_2, \ldots, \alpha_k$ for several (k) identical tracks, or by averaging $\alpha_1, \alpha_2, \ldots, \alpha_k$ measured for k successive segments of the track of a single particle. The segments are chosen to be of the same length x and have the same total length kx for which the particle velocity v practically remains unchanged.

On the other hand, the same value of the mean multiple scattering angle $\alpha = \sqrt{\overline{\alpha^2}}$ can be represented in terms of the parameters of the particle and the medium. To begin with, it can be shown from an analysis of Fig. 157 that

$$\overline{\Theta^2} = 2\overline{\alpha^2} = \sum_1^N \overline{\theta_i^2}, \tag{4.4.35}$$

where each θ_i is averaged over k trajectories[15]. Since scattering is caused by identical nuclei, the value of $\overline{\theta_i^2}$ is the same for any i ($\overline{\theta_i^2} = \overline{\theta^2}$), and

$$\overline{\Theta^2} = N\overline{\theta^2}, \tag{4.4.36}$$

where N is the number of nuclei encountered by the particle over the path x, while $\overline{\theta^2}$ is obtained by averaging θ^2 over all values of

[15] See, for example, E. Fermi, *Nuclear Physics*, University of Chicago Press, Chicago, 1950.

the impact parameter ρ. The value of θ can be calculated from formula (4.4.14):

$$\theta(\rho) \simeq \tan\theta = (2Zze^2/pv)(1/\rho),$$

whence

$$\theta^2(\rho) = (4Z^2z^2e^4/p^2v^2)(1/\rho^2). \qquad (4.4.37)$$

The number of collisions $N(\rho)$ encountered by the particle over a path x and resulting in a deflection of the particle by an angle $\theta(\rho)$ is

$$N(\rho) = 2\pi nx\rho\, d\rho \qquad (4.4.38)$$

(where n is the concentration of nuclei). Averaging of θ^2 is reduced to the computation of the integral

$$\overline{\theta^2} = \frac{\int_{\rho_{min}}^{\rho_{max}} N(\rho)\,\theta^2(\rho)}{\int_{\rho_{min}}^{\rho_{max}} N(\rho)} = \frac{\int_{\rho_{min}}^{\rho_{max}} \frac{8\pi Z^2z^2e^4nx}{p^2v^2}\frac{d\rho}{\rho}}{N}, \qquad (4.4.39)$$

where $\rho_{min} \simeq R_{nuc}$ (more precisely, it is equal to the distance at which the angle of individual deviation would be quite small, say, $\theta_i \ll 1$ rad), and $\rho_{max} \simeq R_{at}$ (more precisely, to the distance from the nucleus at which its charge is completely screened by atomic electrons).

Thus,

$$\overline{\Theta^2} = N\overline{\theta^2} = \int_{\rho_{min}}^{\rho_{max}} \frac{8\pi Z^2z^2e^4nx}{p^2v^2}\frac{d\rho}{\rho} \propto \frac{Z^2z^2xn}{(pv)^2}\ln\frac{\rho_{max}}{\rho_{min}}. \qquad (4.4.40)$$

The estimate for $\ln(\rho_{max}/\rho_{min})$ and consideration of scattering by electrons lead to the following expression for $\overline{\Theta^2}$:

$$\overline{\Theta^2} = 0.157\,\frac{Z(Z+1)}{A}\,\frac{z^2x}{(pv)^2}\ln\left\{1.13\times10^4\,\frac{Z^{1/3}}{A}\,\frac{z^2x}{\beta^2}\right\}, \qquad (4.4.41)$$

where A (atomic mass of the foil) is in grams, pv in MeV and x in g/cm^2.

Thus (neglecting the weak logarithmic dependence), the mean multiple scattering angle for a particle having a charge z and moving in a medium with given p and v (β) can be written in the form

$$\Theta = \sqrt{\overline{\Theta^2}} \propto z\sqrt{x}/pv. \qquad (4.4.42)$$

This relation can be used for determining the value of $p\beta$ (and z) for a charged particle from experimental values of the mean multiple scattering angle Θ (or α).

There are several empirical formulas connecting pv and Θ (or α). Thus, for singly charged particles in photographic emulsions, we have

$$\alpha = 2.5\sqrt{x}/pv. \qquad (4.4.43)$$

where α is measured in degrees, x in micrometres, and pv in MeV. The numerical coefficient in this formula slightly depends on β and the choice of segment x over which α is measured. The coefficient used in formula (4.4.43) corresponds to $x = 100$ μm.

For a very rough estimate of the mean multiple scattering angle, it is convenient to use the following formula:

$$\overline{\Theta^2}_{\text{radian}} = z^2 (21.2/pv)^2 (x/x_0). \qquad (4.4.44)$$

(Θ is in radians and pv in MeV), which is applicable for any medium with a known radiation length x_0 (see Sec. 4.5). In the general case, however, this formula gives an exaggerated value of $\overline{\Theta^2}$, and can be used only for $x \gg x_{\min}$, where $x_{\min} \simeq 20x_0$ for lead and $x_{\min} \simeq 200x_0$ for carbon. This formula is naturally inapplicable for electrons which create photon-electronic showers even at $x \simeq x_0$ (see Sec. 4.10.3).

The experimental estimate for pv (from the value of Θ) and an independent determination of v (from the ionization losses) can be used to calculate the mass of a charged particle (see Sec. 6.1.1. Vol. II).

In the process of multiple scattering, a charged particle is displaced by a certain distance r from its initial path. The law of distribution of spatial displacements is given by the Fermi formula

$$F(r)\,dr = \frac{6r\,dr}{\overline{\Theta^2}\,(x/x_0)^2} \exp\left(-\frac{3r^2}{\overline{\Theta^2}\,(x/x_0)^2}\right), \qquad (4.4.45)$$

which can be used, say, for estimating the transverse dimensions of cosmic showers.

4.5. Radiation Losses for Electrons

The rapid deceleration of a charged particle in the electric field of the atomic nucleus and atomic electrons results in radiation losses (bremsstrahlung). The loss of energy $(dT/dx)_{\text{rad}}$ by radiation is proportional to the square of acceleration $\ddot{x}^2$. Since the force F of Cou-

Comparing formula (4.5.6) with formula (4.2.11) for ionization losses of electrons written in the simplified form

$$-(dT/dx)_{\text{ion}} \propto nZ, \tag{4.5.7}$$

we get

$$\frac{(dT/dx)_{\text{rad}}}{(dT/dx)_{\text{ion}}} \propto T_e Z. \tag{4.5.8}$$

If T_e is measured in MeV, we obtain

$$\frac{(dT_e/dx)_{\text{rad}}}{(dT_e/dx)_{\text{ion}}} \simeq \frac{T_e Z}{800}. \tag{4.5.9}$$

This means that the radiation losses in water ($\overline{Z} = 8$) become comparable with ionization losses at $T_e \simeq 100$ MeV. Such a situation arises in lead at $T_e \simeq 10$ MeV. The energy at which radiation losses become comparable with ionization losses is called the *critical energy*. For electrons whose energy is higher than the critical value, the energy is mainly lost by radiation, the (average) change in the energy as a function of the traversed path being given by the exponential law

$$\overline{E} = E_0 \exp(-x/x_0). \tag{4.5.10}$$

The distance x_0 at which the mean electron energy is reduced to $1/e$ of its value on account of radiation losses is called the *radiation length*. The radiation length for water (and air), aluminium and lead is approximately equal to 36, 24 and 6 g/cm^2 respectively.

Since the energy lost by an electron in a single act of bremsstrahlung is equal to $h\nu$ and the bremsstrahlung spectrum is $N(\nu) \propto d\nu/\nu$, the energy loss due to radiation is independent of ν:

$$(dT/dx)_{\text{rad}} \propto N(\nu)\, h\nu \propto d\nu.$$

In any part of the bremsstrahlung spectrum, the electron loses the same amount of energy by radiation. This energy may be lost through the emission of one hard quantum $h\nu$ carrying away the entire energy $dT_e = h\nu$ lost over the path dx, or several soft quanta having the same total energy.

An electron with $T_e > T_{\text{cr}}$ emits over a path $x = x_0$ one quantum on the average with an energy of the order of T_e.

Fig. 160

Figure 160 schematically shows the elementary act in which a fast electron emits a hard bremsstrahlung quantum which even-

tually forms an electron-positron pair. On account of the considerable loss of energy during the emission of the quantum, the path of the primary electron undergoes a sharp change in its curvature in a magnetic field.

The possibility of a sharp decrease in onergy due to radiation losses complicates the determination of the electron momentum by measuring the curvature of its track in a magnetic field. This method can be used only for the part x of the track, which is small in comparison with the radiation length x_0 (even in this case it is possible to obtain only rough estimates). For the same reason, it is meaningless to speak of the ionization range for a fast electron, since the actual range of a relativistic electron is much smaller than its ionization range. Radiation loss for high-energy electrons is one of the factors responsible for photon-electron showers in cosmic rays (see Sec. 4.10.3).

4.6. Synchrotron Radiation

An electron moving in a curved trajectory, i.e. with an acceleration, must radiate. Indeed, it is shown experimentally that electrons moving in a circular orbit emit electromagnetic radiation over a very wide range frequencies (from radiofrequencies to soft gamma radiation). This radiation was discovered in astronomical observations, and was later detected and thoroughly investigated in a circular electron accelerator (synchrotron). It is therefore called the synchrotron radiation.

Synchrotron radiation is emitted by relativistic electrons in a narrow cone with half-angle

$$\theta = m_e c^2/T_e \simeq 1/\gamma, \tag{4.6.1}$$

where $\gamma = 1/\sqrt{1-\beta^2}$. The cone axis is directed along the tangent to the electron beam. This is true for any point on the electron orbit. Hence synchrotron radiation is concentrated in a thin ring in the plane of the orbit. The radiation is continuous and has its maximum at the frequency

$$\nu_0 = 4.6 \times 10^{-6} H T_e^2 \tag{4.6.2}$$

(H is in gauss, and T_e in electron-volts). For high-energy electrons, this frequency is much higher than the rotational frequency of electrons in the synchrotron (10^7 Hz). For $H = 10^4$ G and $T_e = 100$ MeV, synchrotron radiation is emitted in a cone with $\theta = 17'$ and has $\nu_0 = 4.6 \times 10^{14}$ Hz, corresponding to the red region of the visible spectrum. At $T_e = 20$ BeV, the synchrotron radiation is essentially

hard X-rays in the forward direction with a cone angle $\theta \simeq 5°$.[16]

Synchrotron radiation is polarized, and the strength E is always parallel to the electron orbit plane. The polarization is maximum (about 100%) for radiation in the orbital plane having optimal frequency (from intensity point of view). The energy losses on synchrotron radiation increase with energy roughly as γ^4.

Besides synchrotrons, electron storage rings can also be used for obtaining synchrotron radiation. The latter method is even preferable, *since in this case the synchrotron radiation has* a constant spectrum, geometry and intensity. It should also be noted that the synchrotron radiation emitted by storage rings is of pulse type (on account of the fact that the electron clusters several centimetres long circulate in the ring).

It was mentioned above that the first experiments with synchrotron radiation were carried out with the help of electron accelerators. In 1968, a special storage synchrotron "Tantalus I" was constructed at Wisconsin University (USA). This accelerator was specially designed to match a source of synchrotron radiation with the electron energy 240 MeV. Similar machines (but with higher energy and intensity) will be put in operation shortly in the USSR and elsewhere. At present, the sources of high-energy and high-intensity synchrotron radiation are the storage rings DESY (Deutsches Elektronen-Synchrotron) and SPEAR (Stanford Positron-Electron Asymmetric Rings)[17].

Synchrotron radiation has a continuous spectrum. Hence for practical applications, monochromators consisting of mirrors and diffraction gratings (made of quartz or silicon single crystals for X-ray region) are used in experiments. Crystal monochromators can be used to isolate extremely narrow lines of any frequency with an accuracy of the order of $\Delta E/E \simeq 10^{-6}$ from a continuous spectrum. The intensity left after monochromatization is still 10^2-10^3 times higher than the intensity of most powerful X-ray tubes.

The high intensity, the wide energy range, the possibility of monochromatization and polarization, as well as the pulse nature of synchrotron radiation make it a very useful instrument for investigating the structure of matter and for solving many important practical problems. Let us consider some aspects of these investigations.

[16] For electrons with $\beta \ll 1$, the synchrotron radiation is concentrated in the volume of a torus rotating together with the electron. The axis of the torus is along the orbital radius. The radiation frequency coincides with the rotational frequency *of electrons in the synchrotron orbit. As* β *increases, the torus is* gradually transformed into a narrow cone in the forward direction, while the radiation maximum shifts towards higher harmonics. The order of the highest harmonic at which a significant fraction of energy is emitted is equal to γ^3. Because of closely spaced harmonics and a finite line width, the line spectrum is transformed into a continuous one.

[17] See Sec. 9.2, Vol. II for details.

(1) The investigation of absorption of electromagnetic radiation by gases; including the fine effects like the simultaneous excitation of two electrons in an atom and the interference effects in this process. The investigation of the absorption spectra of molecules and their dissociation fragments for obtaining information about the chemistry of molecules (energy of intraatomic bonds, lifetimes of excited states, reaction rate, etc.).

(2) Fluorescence investigations for determining the lifetimes and decay modes for excited states.

(3) Spectroscopy of solids with a view to investigate their electronic structure, including the absorption spectrum corresponding to the inner electrons (this spectrum is sensitive to a change in the configuration of surrounding atoms). The information is obtained by registering photons reflected by a sample (or transmitted by it), as well as the electrons emitted as a result of the photoemission.

(4) In astronomy and radioastronomy, data on the electron number density and spectrum are obtained by measuring nonthermal radio and optical radiation (in a magnetic field known from other sources). The data concerning the structure of the magnetic field are obtained from the polarization of the registered radiation.

(5) In accelerator techniques, the luminescence of an electron beam is measured with the help of a special stroboscopic equipment for analyzing the beam cross section with a view to adjust the accelerator.

(6) In microelectronics, the lithographic method is used for preparing microcircuits with dimensions of elements ~ 0.1 μm. In this region of wavelengths, optical methods are unsuitable, while X-ray techniques do not have sufficient intensity. A resolving power of about 0.01 μm has been obtained in recent years with the help of hard radiation from DESY.

(7) Synchrotron radiation is used in biology for obtaining the spatial structure of samples.[18]

4.7. Cherenkov Radiation

In 1934 P.A. Cherenkov, a post graduate student of Acad. S. I. Vavilov (at present, Dr. Cherenkov is an academician), investigated the luminescence of uranyl salts under the action of γ-rays from radium and discovered a new type of luminescence which could not be explained by the ordinary fluorescence mechanism.

It is well known that fluorescence is the result of transitions between excited states of atoms or molecules. The duration of fluorescent emission $\tau \geqslant 10^{-10}$ s, and the transition probability is influ-

[18] See E. Rowe and J. Weaver, *Uspekhi Fiz. Nauk*, 126, 2, 269 (1978) for details on the applications of synchrotron radiation.

enced by the addition of quenching agents or by a purification of the material, a change in temperature, etc. However, none of these methods is able to quench the fluorescent emission completely.

Subsequent investigation of the new emission, which was termed Cherenkov radiation, revealed the following properties.

1. The polarization of the luminescence changes sharply when a magnetic field is applied. This means that the luminescence is caused by charged particles rather than by γ-quanta. In Cherenkov's experiment, these particles could be electrons produced by the interaction of γ-quanta with the medium due to the photoelectric effect or the Compton effect (see Sec. 4.10.2).

2. The intensity of the radiation is independent of the charge Z of the medium; hence it cannot be of radiative origin.

3. The radiation is at a certain angle to the direction of motion of charged particles.

The Cherenkov radiation was explained in 1937 by Frank and Tamm on the basis of classical electrodynamics.[19] They observed that the statement of classical electrodynamics concerning the impossibility of energy loss by radiation for a charged particle moving uniformly and rectilinearly in vacuum is no longer valid if we go over from vacuum to a medium with a refractive index $n > 1$.

The conclusion drawn by Frank and Tamm can be illustrated with the help of the following arguments based on the laws of conservation of energy and momentum.

Suppose that a charged particle uniformly moving in a straight line can lose energy and momentum through radiation. In this case, the following equality must be satisfied:

$$(dE/dp)_{\text{part}} = (dE/dp)_{\text{rad}}. \tag{4.7.1}$$

It can be easily seen that this equality cannot be satisfied for vacuum, but may be valid for a medium with $n > 1$.[20]

Indeed, on the one hand, the total energy E of a particle having a mass $m \neq 0$ and moving freely in vacuum with a momentum p (velocity v) is

$$E_{\text{part}} = \sqrt{m^2c^4 + p^2c^2}, \tag{4.7.2}$$

and hence

$$(dE/dp)_{\text{part}} = pc^2/E = \beta c = v. \tag{4.7.3}$$

On the other hand, we have for electromagnetic radiation in vacuum

$$E_{\text{rad}} = pc, \tag{4.7.4}$$

[19] For discovery and explanation of Cherenkov radiation, Cherenkov, Tamm and Frank were awarded the Nobel Prize in 1958.

[20] In this section, it is assumed that $n = \text{const}$ (cf. Sec. 4.8).

i.e.

$$(dE/dp)_{\text{rad}} = c. \tag{4.7.5}$$

Since $v < c$, we get

$$(dE/dp)_{\text{part}} < (dE/dp)_{\text{rad}}. \tag{4.7.6}$$

Thus, the laws of conservation of energy and momentum prevent a charged particle moving uniformly and rectilinearly in vacuum from giving away its energy and momentum in the form of electromagnetic radiation[21].

However, this restriction is removed when the particle moves in a medium with a refractive index $n > 1$. In this case, the velocity of light in the medium is

$$c' = c/n < c, \tag{4.7.7}$$

and the velocity v of the particle may not only become equal to the velocity of light c' in the medium, but even exceed it:

$$v \geqslant c' = c/n. \tag{4.7.8}$$

Obviously, for $v = c'$, the condition (4.7.1) will be satisfied for electromagnetic radiation emitted strictly in the direction of motion of the particle ($\theta = 0°$). For $v > c'$, the condition (4.7.1) will be satisfied for a direction θ along which $v' = c'$, where $v' = v \cos \theta$ is the projection of the particle velocity v on this direction.

Thus, in a medium with $n > 1$, the conservation laws allow a charged particle moving uniformly and rectilinearly with a velocity $v \geqslant c' = c/n$ to lose fractions dE and dp of its energy and momentum, that can be carried away by electromagnetic radiation propagating in this medium at an angle

$$\theta = \arccos (1/n\beta) \tag{4.7.9}$$

to the direction of motion of the particle.

Arguments based on the conservation laws do not provide any idea about the mechanism of the energy and momentum losses. However, it is clear that this mechanism must be associated with certain processes occurring in the medium ($n > 1$), since the losses under consideration cannot occur in vacuum.

The Cherenkov radiation is of the same nature as certain other processes observed in various media when bodies move in these media at a velocity exceeding that of wave propagation. Among well-known examples of such processes are the formation of a V-shaped wave in the wake of a ship, and a conical wave caused by a supersonic plane or missile. In all these cases, the wave field of the superfast object

[21] Electromagnetic radiation cannot accept the entire momentum given away by the particle.

is found to be strongly perturbed (as compared with the field of a slow object), and begins to decelerate it.

In the above-mentioned case of the superfast motion of a charged particle in a medium with a refractive index $n > 1$, the mechanism of the Cherenkov radiation is the coherent emission by the dipoles formed due to the polarization of the medium atoms by the charged moving particle.

Dipoles are formed under the action of the electric field of the particle, which displaces the electrons of the surrounding atoms rela-

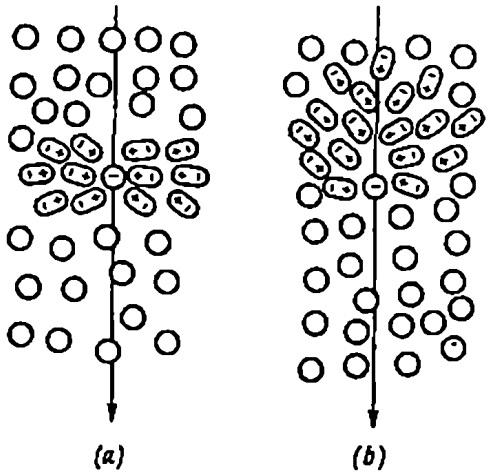

Fig. 161

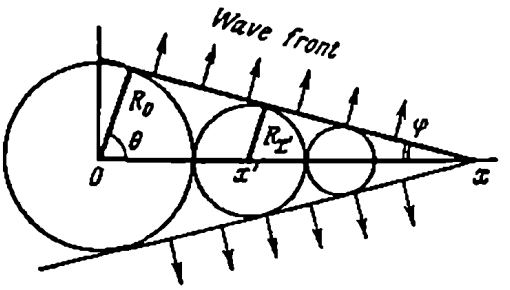

Fig. 162

tive to their nuclei. The return of the dipoles to the normal state (after the particle has left the given region) is accompanied by the emission of an electromagnetic pulse.

If a particle moves rather slowly, the resulting polarization will be distributed symmetrically with respect to the particle position (Fig. 161*a*), since the electric field of the particle "manages" to polarize all the atoms in the neighbourhood, including those lying ahead in its path. In this case, the resultant field of all dipoles away from the particle are equal to zero and their radiations neutralize one another.

If a particle moves in a medium with a velocity exceeding the velocity of propagation of the electromagnetic field ($v > c' = c/n$), a delayed polarization of the medium is observed, and consequently the resulting dipoles will be preferably oriented along the direction of motion of the particle (see Fig. 161*b*). Obviously, in this case, there must be a direction along which a coherent radiation from dipoles emerges, since the waves emitted by the dipoles at different points along the path of the particle may turn out to be in the same phase. This direction can be easily found.

Suppose that a charged particle moves from left to right with a velocity v in a medium with a refractive index $n > 1$, where $v > c' = c/n$ (Fig. 162).

Let us use the Huygens principle to construct the wave front for the emitted wave. Suppose that at instant t, the particle is at the point $x = vt$. We construct the surface enveloping the spherical waves emitted by the particle on its path from the point $x = 0$ to the point x. The radius of the wave at the point $x = 0$ at moment t is equal to $R_0 = c't$. At the same instant, the wave radius at the point x is equal to $R_x = c'[t - (x/v)] = 0$. At any intermediate point x', the wave radius at instant t is equal to $R_{x'} = c'[t - (x'/v)]$, i.e. decreases linearly with increasing x'. Obviously, the enveloping surface is a cone with angle 2φ, where

$$\sin \varphi = R_0/x = c't/vt = c'/v = c/vn = 1/\beta n.$$

The normal to the enveloping surface determines the direction of propagation of the Cherenkov radiation. The angle θ between the normal and the x-axis is equal to $(\pi/2) - \varphi$ and is defined by the condition

$$\cos \theta = 1/\beta n \qquad (4.7.10)$$

Quantum mechanics introduces only a slight correction to this classical result.

It follows from formula (4.7.10) that the Cherenkov radiation propagates along the generators of a cone whose axis coincides with the direction of motion of the particle and the cone angle is equal to 2θ. This radiation can be registered on a colour film placed perpendicular to the direction of motion of the particle (Fig. 163). Radiation emanating from a radiator leaves a blue ring on the photographic film.

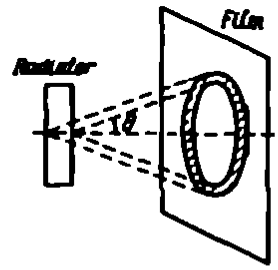

Fig. 163

The sharp directivity of the Cherenkov radiation makes it possible to determine the particle velocity β from the value of angle θ. From formula (4.7.10) it follows that the possible range of measurement o β is equal to

$$1/n \leqslant \beta < 1 \qquad (4.7.11)$$

For $\beta = 1/n$, the radiation is observed at an angle $\theta = 0°$, while for $\beta = 1$, the angle θ has its maximum value

$$\theta_{max} = \arccos (1/n) \qquad (4.7.12)$$

Thus, for example, for water ($n = 1.33$), we have

$$\beta_{min} = 1/1.33 = 0.75.$$

The Cherenkov radiation is observed for $\beta \geqslant 0.75$. For electrons, this condition is satisfied at an energy

$$T_e = m_e c^2 \left(\frac{1}{\sqrt{1-\beta^2}} - 1 \right) = 0.5 \left(\frac{1}{\sqrt{1-0.75^2}} - 1 \right) = 0.26 \text{ MeV}.$$

Thus, the Cherenkov effect should be observed in water even for low-energy electrons (for example, in the case of electrons produced in beta decay, or Compton electrons, or photoelectrons resulting from the interaction between water and γ-quanta from radioactive products). The maximum angle at which the Cherenkov radiation can be observed in water can be obtained from the condition (4.7.12):

$$\cos \theta_{max} = 1/n = 0.75$$

This angle is found to be equal to 41°30′.

In accordance with the Tamm-Frank theory, the number of photons in the frequency interval between ν and $\nu + d\nu$ emitted by a particle with charge z moving with a velocity β in a medium with a refractive index n is given by

$$N(\nu)\, d\nu = 4\pi^2 \frac{(ze)^2}{hc^2} \left(1 - \frac{1}{n^2\beta^2}\right) d\nu. \qquad (4.7.13)$$

It follows from this formula that: (1) the spectrum is identical for particles with $z = \text{const}$, for example, for p, e, π and μ. As z increases, the number of emitted photons increases as z^2; (2) $N(\nu)$ increases with β from zero for $\beta = 1/n$ to $4\pi^2(e^2z^2/hc^2)(1 - 1/n^2)$ for $\beta \simeq 1$; (3) $N(\nu)$ is independent of ν: $dN(\nu) \propto d\nu$.

The spectrum is uniform in frequency. Since $E = h\nu$, this means that the main energy of radiation is concentrated in the extreme short-wave region of the spectrum

$$dE_{Ch} \propto \nu\, d\nu. \qquad (4.7.14)$$

This explains the bluish-violet colour of the Cherenkov radiation. This also indicates the necessity of choosing materials for practical applications that are transparent up to the highest possible frequencies (including the ultraviolet region). As a rule, $n < 1$ in the X-ray region and hence the condition (4.7.1) is not satisfied. However, it was recently shown that in some narrow regions of the X-ray spectrum, $n > 1$ and the Cherenkov radiation can be observed in these regions.[23]

[23] V.A. Bazylev, V.I. Glebov, E.I. Denisov *et al.*, *Zh. Eksp. Teor. Fiz.*, 81, 1664 (1981).

The Cherenkov effect is widely used in designing instruments for determining the velocity of fast charged particles. These instruments are called Cherenkov counters.

The choice of the medium for generating the Cherenkov radiation depends on the range of velocities β over which measurements have to be carried out with the help of a Cherenkov counter. Transparent plastics are a very convenient material for this purpose. Cherenkov counters filled with liquids and gases are also used.

Depending on their design, Cherenkov counters can be classified as threshold counters (registering particles with $\beta > 1/n$) and differential counters (capable of isolating particles with a given velocity β).

Figure 164 shows the schematic diagram of a threshold Cherenkov counter. The charged particle moves along the axis of a radiator.

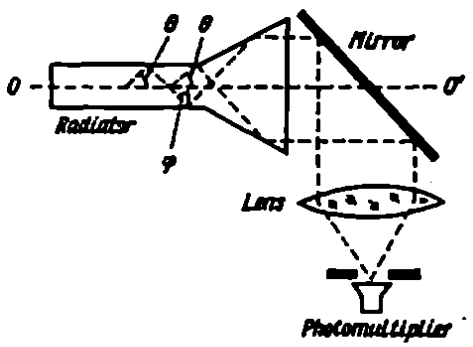

Fig. 164

If the particle velocity $\beta > 1/n$, where n is the refractive index of the material of the radiator, the Cherenkov radiation will be emitted at angle $\theta = \arccos(1/\beta n)$. If the radiator is of cylindrical shape, light is incident on the interface between the medium with $n > 1$ and air at an angle $\varphi = (\pi/2) - \theta$, where $\varphi > \varphi_0 = \arcsin(1/n)$ in view of the fact that $\theta < \arccos(1/n)$. However, the inequality $\varphi > \varphi_0$ is the condition for total internal reflection. Hence the entire light falls on the conical part of the radiator and after reflection from its surface and from a plane mirror is condensed by a lens to a photomultiplier. (The purpose of the plane mirror is to keep the photomultiplier away from the direction of the particle beam.)

The threshold counter can be used to isolate particles of a given type from a beam. If, for example, the beam contains protons and π^+-mesons with identical momenta $p_p = p_{\pi^+} = p$, their velocities will be different in view of the fact that they have different masses: $\beta_\pi > \beta_p$. If the refractive index of the radiator satisfies the condition $\beta_\pi > 1/n > \beta_p$, the photomultiplier will register a light pulse only

when a π-meson passes. Protons will pass through the counter without causing any luminescence.

Figure 165 shows (in two projections) a possible design of a differential Cherenkov counter. It can be seen from the figure that such an instrument can register the Cherenkov radiation only from particles with a definite velocity $\beta \pm \Delta\beta$ corresponding to the angle $\theta \pm \Delta\theta$. The Cherenkov radiation caused by particles with other velocities does not fall into the photomultiplier. This type of instrument was used for the first time to register antiprotons (see Sec. 4.2, Vol. II).

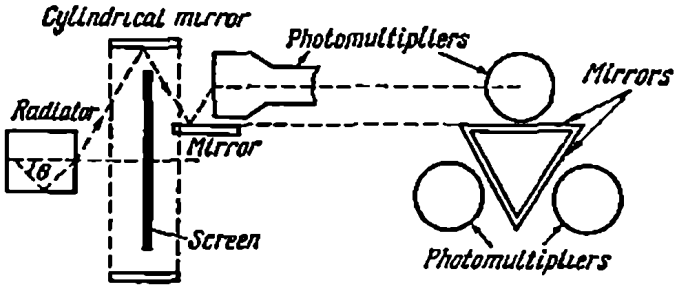

Fig. 165

Velocities of ultrarelativistic particles ($\beta \simeq 1$) are measured with the help of gaseous Cherenkov detectors with a refractive index just slightly higher than unity (its value can be varied by regulating the gas pressure in the counter).

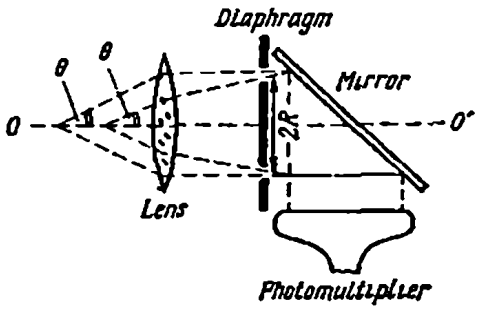

Fig. 166

The schematic diagram of a gaseous differential counter is shown in Fig. 166.

Charged particles move with a velocity β in a gaseous medium along the axis OO' and emit the Cherenkov radiation at any point along their trajectory at the same angle θ (β) to the axis. It is known from optics that such rays must be condensed by a lens in the focal plane in the form of a ring whose radius R depends on the angle θ (and the focal length of the lens). If the focal plane of the lens contains an annular diaphragm with an annular slit of radius R (θ), it will allow only radiation from particles with velocity $\beta \pm \Delta\beta$. These rays, after reflection at a mirror, will be registered by a photomultiplier. Particles with a velocity β' will emit radiation at a different angle θ′ to the axis OO'. After passing through the lens, this

radiation will be condensed into a ring of a different radius $R(\theta')$ and will not pass through the diaphragm.

Gaseous Cherenkov counters are widely used in the high-energy particle physics. Modern counters (for example, in experiments conducted with the Serpukhov accelerator) have dimensions of about 10 m.

4.8. Transition Radiation

The transition radiation is emitted by a charge moving uniformly in a straight line in a medium that is either inhomogeneous or varying in time. The essence of this phenomenon can be easily understood by recalling the conditions for the emergence of other kinds of radiation. It was shown in Sec. 4.7 that the Cherenkov radiation is possible at $v > c/n$, i.e. $vn/c > 1$ or $n > 1$. Here, v is constant. For bremsstrahlung and synchrotron radiation, the condition $n > 1$ is not necessary, and the only requirement for the emission of such radiation is $v \neq \text{const}$ ($dv/dt \neq 0$), which means that the quantity vn/c must be varying. However, a variation of this quantity is possible not only by varying the velocity v, but also by varying the refractive index n. The emergence of transition radiation is associated with the case when n varies but v remains constant. In this case, vn/c can be greater or smaller than unity, i.e. the transition radiation can be accompanied by the Cherenkov radiation, or appear when the latter type of radiation cannot be emitted. The refractive index can vary either in space when a particle moves from one region of an inhomogeneous medium to another, or in time when the refractive index of a homogeneous medium changes abruptly (say, due to a change in the pressure).

The transition radiation was predicted by Ginzburg and Frank in 1944 from an analysis of the problem in which a charge crosses the interface between two media.[23] A graphic interpretation of the Ginzburg and Frank ideas can be reduced to the following. For the sake of simplicity, let us consider the case of normal incidence of a charge at the vacuum-ideal mirror (metal) interface. In this case, the electromagnetic field in vacuum is the sum of two fields, viz. the field of the moving charge and the field of the "image" of this charge (with opposite sign) moving from the opposite direction. Upon crossing the interface, the charged particle continues to move in the medium with a constant (or nearly constant) velocity. However, if this phenomenon is observed from vacuum, it would appear that the charge and its "image" simultaneously move towards the

[23] V.L. Ginzburg and I.M. Frank, *Zh. Eksp. Teor. Fiz.*, 16, 15 (1946).

interface and instantaneously disappear (stop).[24] The radiation emitted by the chargo and its "image" is called the transition radiation. In this particular case, the transition radiation is equivalent to the bremsstrahlung of the charge and its "image" in the mirror.

Naturally, the similarity of the mathematical expressions for energy does not mean that the transition radiation is a particular case of bremsstrahlung. The physical nature of the transition radiation is quite different from that of bremsstrahlung. While the variation in the charge velocity is the primary cause of bremsstrahlung, it is just a mathematical tool in the case of the transition radiation. It should be recalled that in the case considered above, the transition radiation is emitted as a *uniformly* moving charge goes from one medium into another.

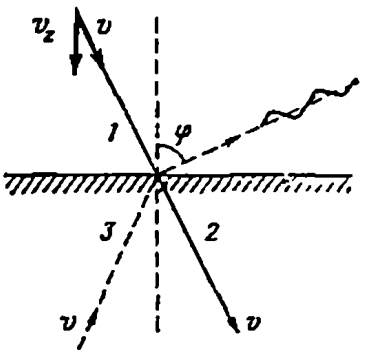

Fig. 167

In the general case of an arbitrary medium, complete screening is impossible and the amplitude of the transition radiation is obtained by calculating three components (Fig. 167), viz. bremsstrahlung of charged particle *1* moving in vacuum and as if arrested at the interface; bremsstrahlung of charged particle *2* which as if starts moving deep inside the medium at the moment of arrest of the first particle; and bremsstrahlung of "image" particle *3* moving towards the first particle and coming to a halt together with this particle at the interface.

Consequently, we obtain the following expression for the spectral density of radiation of a nonrelativistic electron in vacuum:

$$\frac{dW_\omega}{d\Omega} = \frac{e^2 v_z^2}{\pi^2 c^3} \sin^2\varphi \left| \frac{(n_2^2-1)\cos\varphi}{n_2^2\cos\varphi + \sqrt{n_2^2 - 1 + \cos^2\varphi}} \right|^2, \qquad (4.8.1)$$

where v_z is the component of the particle velocity along the normal to the medium surface, φ is the angle at which the radiation is observed in vacuum (measured from the normal), and $n_2 = n + ik$ is the complex refractive index of the medium.

For an ideal conductor, $n_2 \to \infty$ and hence

$$\frac{dW}{d\Omega} = \frac{e^2 v_z^2}{\pi^2 c^3} \sin^2\varphi, \qquad (4.8.2)$$

i.e. has its maximum value at $\varphi = 90°$. For real metals and dielectrics, the radiation maximum is observed at $\varphi = 60\text{-}70°$.

[24] The field of the charge which continues to move in the metal (behind the mirror) is completely screened by conduction electrons.

neutron is equal to 10^{-22} cm^2, which is about a millionth part of the corresponding value for a charged particle.[29]

Although this value is considerably higher than the cross section for the interaction of a fast neutron with nuclei ($\sigma \simeq 10^{-24}$ cm^2), the insignificant role of ionization losses during the motion of a neutron in a medium becomes clear if we consider the fact that while the neutron loses only a negligible fraction of its energy (about 10 eV) upon interaction with electrons, it may lose a considerable part of its energy in nuclear collisions (in the case of a head-on collision with a proton, the neutron may lose all its energy).

The interaction of the magnetic moments of an electron and a neutron becomes noticeable only when the magnetic moments of all the electrons have the same orientation (in ferromagnetics). In this case, the interaction of magnetic moments of the neutron and electrons leads to a macroscopic effect of additional scattering whose investigation can provide an estimate for the magnetic moment of the neutron (see Sec. 1.5.4).

Besides the magnetic interaction between neutrons and electrons, their electric interaction must also be observed. It was mentioned in Sec. 1.5.5 that the existence of a magnetic moment in a neutron can be explained by assuming that during a part of its lifetime the neutron consists of two particles with opposite electric charges. Consequently, the neutron must have a distributed electric charge which will interact with the electron charge. However, this interaction is even weaker than the magnetic interaction.[30]

The main type of interaction of neutrons with matter is their interaction with atomic nuclei. Depending on whether a neutron falls into a nucleus or not, its interaction with nuclei can be divided into two classes:

(1) elastic potential scattering by nuclear forces $(n, n)_{\text{pot.}}$; in this case the neutron does not enter the nucleus;

(2) different types of nuclear reactions, viz. (n, γ), (n, p), (n, α) and fission reactions; inelastic scattering (n, n'); elastic scattering involving the entry of the neutron into the nucleus, i.e. the elastic resonance scattering $(n, n)_{\text{res}}$.

The relative role of each process is defined by the cross section corresponding to it. In some materials, the role of elastic scattering is comparatively significant, and in this case a fast neutron loses its energy in a series of successive elastic collisions with the nuclei of these materials (moderation of neutrons). The process of moderation continues until the kinetic energy of the neutron becomes comparable with the thermal energy of the atoms of the moderating

[29] The value $\sigma \simeq 10^{-22}$ cm^2 corresponds to a single electron. However, calculations for an atom do not significantly change this value because there are not many weakly bound electrons ($E_e \simeq 10$ eV) in an atom.

[30] See Sec. 3.1, Vol. II for details.

The first results on the experimental observation of transition radiation caused by protons with energy 1-5 MeV were obtained in 1959 by Goldsmith and Jelley. Electrons were employed in later experiments. In experiments involving many metals and dielectrics, the yield and polarization of radiation were measured. These measurements confirmed the theoretical predictions. In the optical region of the spectrum emitted by metals, the transition radiation was found to dominate over bremsstrahlung and luminescence. This follows from an increase in the radiation yield as the square of velocity[27] and the existence of polarization which means that the electric vector lies in the plane passing through the normal and the direction of observation. For metals, polarization increases with increasing electron energy and reaches the value 100% at $E \simeq 50$-100 keV. The first counter for the transition radiation was constructed in 1963 by Arutyunyan and coworkers (Yerevan). Modern transition counters use stacks of Mylar films whose transition radiation is registered (in the X-ray region) by scintillators and proportional chambers. The efficiency of these counters can be as high as 90%, and they can compete with Cherenkov counters in the energy region corresponding to $v \simeq c$. It has been shown experimentally that a transition counter can distinguish π-mesons and electrons at an energy of 10 BeV.

To investigate the electron component of cosmic radiation with the help of balloons, a large hybrid detector was used in 1977. The transition radiation detector consisted of six thick (about 15 cm) layers of porous polyethylene separated by 2-cm wire proportional chambers. Orientation of wires in neighbouring chambers differed by 90°. The chambers were filled by Xe (+20% CO_2).[28] In view of the linear dependence of the transition radiation yield on E/mc^2 of the particle, the detector practically does not respond to protons with energy between 3 and 3000 BeV, while the transition radiation caused by electrons attains saturation values.

4.9. Interaction of Neutrons with Matter

The electromagnetic interaction between neutrons and electrons is determined by the interaction between their magnetic moments. The latter interaction, however, is so weak that its energy reaches the atomic ionization potential (about 10 eV) only at distances of about 10^{-11} cm. Thus, the cross section of ionization losses for a

[27] The yield of bremsstrahlung and luminescence in the optical spectral region must decrease due to a decrease in scattering and ionization losses of electrons with increasing velocity. Scattering losses cause bremsstrahlung, while ionization losses cause the excitation of luminescence.

[28] G. Gurtmann *et al.*, *Phys. Rev. Lett.*, 38, 23, 1368 (1977).

neutron is equal to 10^{-22} cm^2, which is about a millionth part of the corresponding value for a charged particle.[29]

Although this value is considerably higher than the cross section for the interaction of a fast neutron with nuclei ($\sigma \simeq 10^{-24}$ cm^2), the insignificant role of ionization losses during the motion of a neutron in a medium becomes clear if we consider the fact that while the neutron loses only a negligible fraction of its energy (about 10 eV) upon interaction with electrons, it may lose a considerable part of its energy in nuclear collisions (in the case of a head-on collision with a proton, the neutron may lose all its energy).

The interaction of the magnetic moments of an electron and a neutron becomes noticeable only when the magnetic moments of all the electrons have the same orientation (in ferromagnetics). In this case, the interaction of magnetic moments of the neutron and electrons leads to a macroscopic effect of additional scattering whose investigation can provide an estimate for the magnetic moment of the neutron (see Sec. 1.5.4).

Besides the magnetic interaction between neutrons and electrons, their electric interaction must also be observed. It was mentioned in Sec. 1.5.5 that the existence of a magnetic moment in a neutron can be explained by assuming that during a part of its lifetime the neutron consists of two particles with opposite electric charges. Consequently, the neutron must have a distributed electric charge which will interact with the electron charge. However, this interaction is even weaker than the magnetic interaction.[30]

The main type of interaction of neutrons with matter is their interaction with atomic nuclei. Depending on whether a neutron falls into a nucleus or not, its interaction with nuclei can be divided into two classes:

(1) elastic potential scattering by nuclear forces $(n, n)_{pot.}$; in this case the neutron does not enter the nucleus;

(2) different types of nuclear reactions, viz. (n, γ), (n, p), (n, α) and fission reactions; inelastic scattering (n, n'); elastic scattering involving the entry of the neutron into the nucleus, i.e. the elastic resonance scattering $(n, n)_{res}$.

The relative role of each process is defined by the cross section corresponding to it. In some materials, the role of elastic scattering is comparatively significant, and in this case a fast neutron loses its energy in a series of successive elastic collisions with the nuclei of these materials (moderation of neutrons). The process of moderation continues until the kinetic energy of the neutron becomes comparable with the thermal energy of the atoms of the moderating

[29] The value $\sigma \simeq 10^{-22}$ cm^2 corresponds to a single electron. However, calculations for an atom do not significantly change this value because there are not many weakly bound electrons ($E_e \simeq 10$ eV) in an atom.

[30] See Sec. 3.1, Vol. II for details.

material (moderator). Such neutrons are called thermal neutrons. Subsequent collisions of thermal neutrons with the moderator atoms practically do not change the energy of the neutrons and result only in their displacement in the material (diffusion of thermal neutrons) which continues until the neutron is absorbed by the nucleus.

The interaction of fast and slow neutrons with matter is of utmost importance in various problems of neutron physics, and in particular in the design of nuclear reactors. Some of these problems, for example, the moderation of fast neutrons, should have been considered in this chapter on the basis of the momentum diagram. However, a close relation between all the above-mentioned processes involving the interaction of neutrons with matter make it expedient to consider these questions together (see Chap. 6).

4.10. Interaction of Gamma Radiation with Matter

Besides the nuclear reactions induced by gamma radiation (nuclear photoeffect), which we shall consider in Chap. 11, there exist the following main types of interaction of gamma radiation with matter: photoeffect, Compton effect, and the formation of electron-positron pairs.

4.10.1. Photoeffect

Photoeffect is the process of interaction of a γ-quantum with an electron attached to an atom, during which the entire energy of the γ-quantum is transferred to the electron. As a result of this interaction, the electron is ejected from the atom with a kinetic energy

$$T_e = E_\gamma - I_i, \tag{4.10.1}$$

where E_γ is the energy of the γ-quantum and I_i is the ionization potential of the ith atomic shell.[31]

Obviously, for $E_\gamma < I_K$, photoeffect is possible only on the L-, M-, . . . shells and not on the K-shell. Similarly, for $E_\gamma < I_L$, photoeffect is possible only on the M-, N-, . . . shells and not on K- and L-shells, and so on.

The vacancy created in an electron shell as a result of the photoeffect is filled by electrons from higher orbits. This process is accompanied by the emission of X-rays or Auger electrons (when an excited atom directly transfers its excitation energy to one of its

[31] We neglect the recoil energy T_{at} of the atom, since it can be easily shown that it is much smaller than T_e (and even I_i). However, the same conclusion cannot be drawn about the momentum of the recoil atom, which plays a quite significant role in photoeffect (see below).

electrons; this process is analogous to the internal conversion effect considered in Sec. 3.4).

Photoeffect cannot take place for a free electron (not associated with an atom). This follows from the incompatibility of the laws of conservation of energy and momentum with the converse assumption. Indeed, if photoeffect were possible for a free electron, the energy and momentum conservation laws would lead to the following relations:

$$E_\gamma = m_e c^2 \left(\frac{1}{\sqrt{1-\beta^2}} - 1 \right), \tag{4.10.2}$$

$$E_\gamma / c = m_e \beta c / \sqrt{1-\beta^2}. \tag{4.10.3}$$

Whence

$$E_\gamma / m_e c^2 = (1/\sqrt{1-\beta^2}) - 1 = \beta/\sqrt{1-\beta^2} \quad \text{or} \quad (1-\beta)/\sqrt{1-\beta^2} = 1$$

and

$$(1-\beta)^2 = 1 - \beta^2.$$

This equation is satisfied for two values of β:

$$\beta = 0 \quad \text{and} \quad \beta = 1.$$

The first of these values corresponds to the trivial solution $E_\gamma = T_e = 0$, while the second is devoid of a physical meaning for particles with $m \neq 0$. Thus, in the case of photoeffect, it is very important that the electron be associated with an atom to which a part of the photon energy is transferred. Photoeffect is therefore possible only for bound electrons. The weaker the bond between an electron and an atom in comparison with the photon energy, the less probable is the photoeffect. This circumstance determines all the main properties of the photoeffect, viz. the dependence of cross section on energy, the ratio of probabilities of photoeffect on different electron shells, and the dependence of the cross section on the charge of the medium.

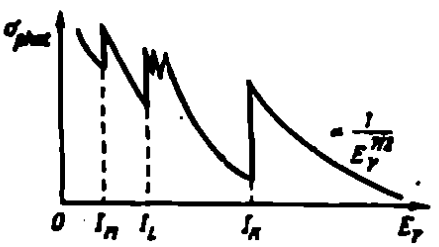

Fig. 168

Figure 168 shows the dependence of the photoeffect cross section on the photon energy. It can be seen from the figure that for large values of the γ-quantum energy (at which all electrons are weakly coupled to the atom), the cross section is quite small.

With decreasing E_γ (increasing ratio of the electron binding to the photon energy I_K/E_γ), the cross section increases first as $1/E_\gamma$, and later (as E_γ approaches I_K) more rapidly as $1/E_\gamma^{7/2}$. The increase

in the cross section continues until E_γ becomes equal to the ionization potential for the K-shell ($E_\gamma = I_K$). Beyond $E_\gamma < I_K$, photoeffect is impossible for K-shell electrons and its cross section is determined only by the interaction of γ-quanta with electrons of L-, M-, . . . shells. But the binding of these electrons with the atom is weaker than for K-electrons. Hence for equal energies of γ-quanta, the probability of photoelectric effect for an electron from the L-shell is much lower than for a K-electron (the probability of photoeffect for an M-electron is even lower). As a result, a sharp discontinuity is observed in the cross section curve at $E_\gamma = I_K$.

For $E_\gamma < I_K$, the photoeffect cross section begins to increase once again, since the relative electron binding I_L/E_γ increases. This increase continues up to $E_\gamma = I_L$, where another discontinuity is observed in the cross section, and so on.

The probability of photoeffect depends very strongly on the charge Z of the atom in which the effect is observed: $\sigma_{\text{phot}} \propto Z^5$. This is again due to the difference in bindings of electrons. In light elements (small Z), the electrons are bound more weakly by Coulomb forces of the nucleus than in heavy atoms.

Thus, for the photoeffect cross section we obtain the following dependence on the gamma radiation energy and nuclear charge of the medium:

$$\sigma_{\text{phot}} \propto Z^5/E_\gamma \quad \text{for} \quad E_\gamma \gg I_K,$$

and (4.10.4)

$$\sigma_{\text{phot}} \propto Z^5/E_\gamma^{7/2} \quad \text{for} \quad E_\gamma > I_K.$$

Photoeffect is especially significant for heavy materials where the probability is considerable even for high energies of γ-quanta. In light materials, this effect becomes significant only for relatively low energies of γ-quanta (see Sec. 4.10.4).

Expressions for the photoeffect cross section are obtained with the help of quantum electrodynamics and have the following form:

$$\left.\begin{aligned} (\sigma_{\text{phot}})_K &= 1.09 \times 10^{-18} Z^5 [13.61/h\nu]^{7/2} \quad \text{for small} \quad h\nu, \\ (\sigma_{\text{phot}})_K &= 1.34 \times 10^{-33} [Z^5/h\nu] \quad \text{for} \quad h\nu \gg m_e c^2. \end{aligned}\right\} \quad (4.10.5)$$

where σ is in cm^2, while $h\nu$ is in eV for the first formula and in MeV for the second one.

Formulas (4.10.5) can be used to calculate the cross section of the photoeffect for K-electrons. It was mentioned above that the relative contribution to the cross section from the effect for L-, M-, . . . shells is quite small. The following values were obtained theoretically for the ratio of photoeffect cross sections for different shells:

$$\sigma_L/\sigma_K \simeq 1/5 \quad \text{and} \quad \sigma_M/\sigma_L \simeq 1/4 \quad (\text{i.e. } \sigma_M/\sigma_K \simeq 1/20). \quad (4.10.6)$$

The first of these ratios has been experimentally confirmed. Hence a coefficient equal to 5/4 is introduced in formula (4.10.5) in order to calculate the total cross section of the photoeffect.

For the differential cross section of the photoeffect for $E_\gamma \ll m_e c^2$, the formula has the following form:

$$d\sigma_{\text{phot}} = 4\sqrt{2}\,\frac{Z^5}{137^4}\,r_e^2\,(m_e c^2/E_\gamma)^{7/2}\sin^2\theta\cos^2\varphi \times (1+4\beta\cos\theta)\,d\Omega, \qquad (4.10.7)$$

where Z is the atomic charge, $r_e = e^2/m_e c^2 = 2.8 \times 10^{-13}$ cm is the classical radius of the electron, θ is the angle between the momentum p_γ of the γ-quantum and the electron momentum p_e, φ is the angle between planes (p_e, p_γ) and (E, p_γ), and $\beta = v/c$.

It follows from formula (4.10.7) that photoelectrons obtained from very soft (long-wave) γ-quanta are emitted predominantly in the direction of the electric vector E. As the energy E_γ increases, the electron distribution is stretched forward (Figs. 169*a* and *b* respectively).

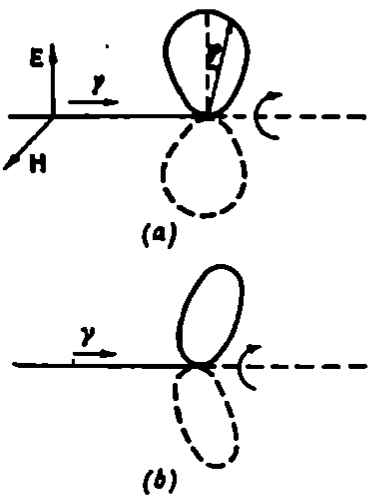

Fig. 169

The specific nature of photoelectric absorption (existence of sharp selective bands) is employed for measuring the energy of gamma radiation. In this method, the energy of gamma radiation is determined by comparing its photoelectric absorption in various absorbers having different values of absorption boundaries. The absorption

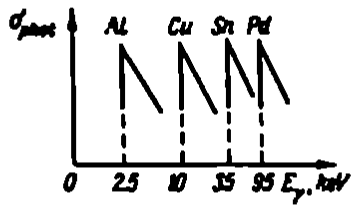

Fig. 170

boundaries for gamma radiation in some materials are shown in Fig. 170.

Photoeffect is the principal mechanism of absorption of soft gamma radiation in heavy materials.

4.10.2. Scattering of Gamma Radiation

Besides photoeffect, in which the entire energy of a γ-quantum is transferred to an atomic electron, the interaction of gamma radiation with matter may result in its scattering, i.e. the deviation from its initial direction of propagation by a certain angle θ. It will be shown at a later stage [see formula (4.10.17)] that the wavelength λ of the scattered radiation increases by an amount $\Delta\lambda$ (θ) proportional to $\sin^2(\theta/2)$. It is remarkable that the value of $\Delta\lambda$ (θ) depends only on the scattering angle θ and is independent of λ. The highest value of $\Delta\lambda$ is observed for $\theta = \pi$. For all λ, this is equal to

$$(\Delta\lambda)_{max} = 4.84 \times 10^{-10} \text{ cm}. \qquad (4.10.8)$$

It can be easily seen that $(\Delta\lambda)_{max}$ is comparable with the wavelength for gamma radiation of medium energy ($E_\gamma \simeq 1$ MeV, $\lambda = 10^{-10}$ cm) and short-wave X-rays ($E_X \simeq 100$ keV, $\lambda \simeq 10^{-9}$ cm), is small in comparison with the wavelength of soft gamma radiation and X-rays ($E \simeq 1$-10 keV, $\lambda \simeq 10^{-8}$-10^{-7} cm), and is quite insignificant for visible light ($E \simeq 1$ eV, $\lambda \simeq 10^{-4}$ cm).

4.10.2a. Thomson Scattering

The scattering of relatively soft electromagnetic radiation (long-wave X-ray radiation) was first studied experimentally followed by hard radiation (short-wave X-rays and gamma radiation). Hence the first experiments showed that the wavelength practically does not change as a result of scattering. These results were explained with the help of the classical theory of scattering of electromagnetic radiation, which was developed earlier to explain the scattering of light.

According to this theory, an electron under the action of an electromagnetic wave $E = E_0 \exp(-i\nu t)$ is set into forced oscillations with the same frequency ν and thus itself becomes a source of electromagnetic radiation of this frequency. This is called the scattered wave.

In the simplest case of scattering of a nonpolarized primary wave by a free electron, the differential cross section is given by

$$d\sigma = (r_e^2/2)(1 + \cos^2\theta)\, d\Omega, \qquad (4.10.9)$$

while the total scattering cross section is

$$\sigma = \frac{8\pi}{3} r_e^2 = 0.66 \times 10^{-24} \text{ cm}^2. \qquad (4.10.10)$$

These formulas were first derived by J.J. Thomson. The Thomson scattering is independent of the wavelength of the incident radiation and is symmetric about the plane $\theta = 90°$ (Fig. 171).

It should be recalled that when a long-wave gamma radiation is incident on a crystal whose lattice constant d is comparable with the wavelength λ ($\lambda \simeq d$), the scattered radiation becomes coherent and hence an interference pattern is observed. The direction of the scattered radiation is determined with the help of the well-known Bragg relation which can be derived from Fig. 172. It can be seen from this figure that the path difference for the rays *1* and *2* is equal

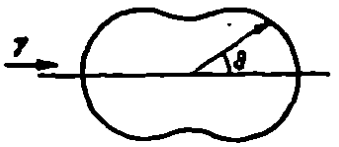

Fig. 171

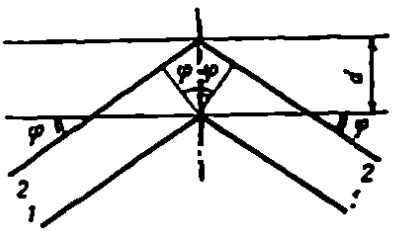

Fig. 172

to $2d \sin \varphi$. Equating this quantity to an integral number $n\lambda$ of the wavelengths, we obtain the condition under which the waves scattered by different crystal planes augment each other[23]:

$$2d \sin \varphi = n\lambda. \qquad (4.10.11)$$

The most conveniently observable values of the angle φ are obtained for $\lambda \simeq d$. For $\lambda \ll d$, the angles are very small, while for $\lambda > 2d$ coherent scattering is impossible since $\sin \varphi = (n\lambda/2d) > 1$.

4.10.2b. Compton Effect

The classical theory of scattering is valid for $h\nu \ll m_e c^2$. If this condition is not satisfied, scattering is accompanied by a change in wavelength. Such scattering was first observed in experiments on investigation of the properties of short-wave X-rays. These experiments showed that the penetrating power of X-rays is reduced upon scattering, *i.e.* their wavelength increases.

Detailed investigations of the scattering of electromagnetic waves accompanied by a change in the wavelength were made in 1923 by Compton. The experimental set-up used by Compton (Fig. 173) consisted of an X-ray tube with a molybdenum anticathode, a scatterer, a collimator, a crystal and an ionization chamber. Graphite was used as the scatterer.

[23] It can be easily shown that the existence of a third, fourth, and other planes does not alter this condition, but only contracts the attainable scattering angles and increases the contrast between maxima and minima.

The scattering angle θ was fixed by rotating the X-ray tube about a vertical axis. The wavelength of the scattered radiation was measured with the help of a calcite crystal $CaCO_3$ with a lattice constant $d = 3 \times 10^{-8}$ cm. The wavelength was calculated by using the Bragg relation (4.10.11) from the value of angle φ corresponding to the maximum current in the ionization chamber.

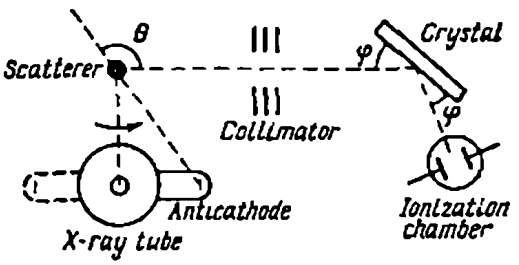

Fig. 173

As a result of his experiments, Compton observed that

(1) besides the initial wavelength λ_0, the scattered radiation spectrum also contains a displaced line with a wavelength $\lambda' > \lambda_0$;

(2) $\Delta\lambda = \lambda' - \lambda_0$ increases with increasing scattering angle;

(3) $(\Delta\lambda)_\theta$ is independent of λ_0 for a given angle of scattering; and

(4) $(\Delta\lambda)_\theta$ is constant for all scattering materials.

These irregularities cannot be explained by the classical wave theory according to which the wavelength of the scattered radiation must be the same as that of the incident radiation. Compton and Debye were able to explain the observed effect with the help of the quantum theory.

Compton noted that the first two regularities were quite similar to the pattern of elastic scattering of particles, where the energy of the scattered particle is different from its initial value and depends on the scattering angle (see Sec. 4.4.1). Therefore he proposed a quantum-mechanical interpretation of the phenomenon of scattering, according to which the X-rays must be treated as a particle flux of photons which undergo elastic scattering upon colliding with other particles, viz. electrons. Since electrons are present in all atoms and the condition $E_\gamma > \varepsilon_e$ is always satisfied for them (the binding of electrons with atoms is not very strong), the process can be described as scattering of a photon by a free electron in any medium. Consequently, the nature of scattering (at a given angle) is independent of the material of the scatterer.

In order to obtain a relation connecting the wavelength of the scattered radiation with the scattering angle, we write the laws of conservation of energy and momentum under the assumption

that the electron is free. The law of energy conservation is written as follows:

$$h\nu = h\nu' + T_e = h\nu' + m_e c^2 \left(\frac{1}{\sqrt{1-\beta^2}} - 1\right). \qquad (4.10.12)$$

After obvious transformations, we obtain

$$m_e^2 c^4/(1-\beta^2) = m_e^2 c^4 + (h\nu)^2 + (h\nu')^2 + 2m_e c^2 h(\nu - \nu') - 2h\nu h\nu'. \qquad (4.10.13)$$

The law of momentum conservation is written in the form $\mathbf{p}_\gamma = \mathbf{p}'_\gamma + \mathbf{p}_e$ (Fig. 174), i.e.

$$\overrightarrow{h\nu/c} = \overrightarrow{h\nu'/c} + \overrightarrow{m_e \beta c}/\sqrt{1-\beta^2}, \qquad (4.10.14)$$

or, in scalar form

$$m_e^2 \beta^2 c^4/(1-\beta^2) = (h\nu)^2 + (h\nu')^2 - 2h\nu h\nu' \cos\theta. \qquad (4.10.15)$$

Simultaneously solving Eqs. (4.10.13) and (4.10.15), we obtain

$$(c/\nu') - (c/\nu) = (h/m_e c)(1 - \cos\theta) \qquad (4.10.16)$$

or

$$\Delta\lambda = \lambda' - \lambda = \Lambda(1 - \cos\theta) = 2\Lambda \sin^2(\theta/2), \qquad (4.10.17)$$

where $\Lambda = h/m_e c = 2.42 \times 10^{-10}$ cm is the Compton wavelength of the electron. It follows from Eq. (4.10.17) that the wavelength λ' of the displaced line increases with the scattering angle θ in such a way that

$\Delta\lambda = 0$ for $\theta = 0$,

$\Delta\lambda = \Lambda$ for $\theta = \pi/2$, and

$\Delta\lambda = 2\Lambda$ for $\theta = \pi$.

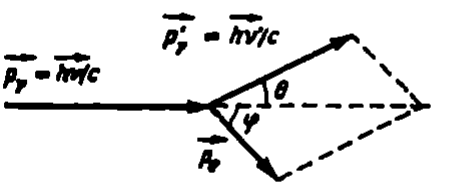

Fig. 174

However, for scattering at a given angle θ, the quantity $\Delta\lambda$ is independent of λ. Hence the Compton effect is insignificant for long-wave radiation, when $\Delta\lambda \ll \lambda$ (for example, for visible light or even for long-wave X-rays). Conversely, this effect plays a very important role for short-wave gamma radiation, when $\Delta\lambda \simeq \lambda$. Solving Eq. (4.10.16) for ν', we obtain the following formula for the energy of a quantum scattered at an angle θ:

$$h\nu' = h\nu \Big/ \left[1 + \frac{h\nu}{m_e c^2}(1 - \cos\theta)\right]. \qquad (4.10.18)$$

It can be seen from this formula that $h\nu(1 - \cos\theta)/m_e c^2 \ll 1$ and $h\nu' \simeq h\nu$ for quite small scattering angles in the case when $h\nu >$

mc^2, and for all angles when $h\nu \ll m_e c^2$. For $h\nu \gg m_e c^2$ and large scattering angles, $h\nu\,(1 - \cos\theta)/m_e c^2 \gg 1$ and

$$h\nu' \simeq m_e c^2/(1 - \cos\theta). \qquad (4.10.19)$$

Hence $h\nu' \simeq m_e c^2$ for $\theta = \pi/2$ and $h\nu' \simeq m_e c^2/2$ for $\theta = \pi$. A decrease in the energy $h\nu'$ and hence the momentum $h\nu'/c$ of the scattered quantum with increasing scattering angle corresponds to an increase in the energy and momentum of the recoil electron. Figure 175

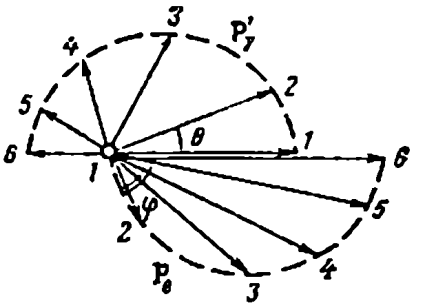

Fig. 175

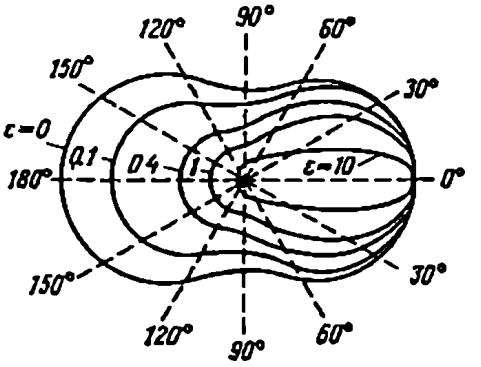

Fig. 176

shows the momentum distribution curves for the scattered photon and the recoil electron in the laboratory system of coordinates. Identical digits have been used to denote the corresponding momenta of the scattered γ-quantum and the recoil electron. It can be seen from Fig. 175 and formula (4.10.18) that $\varphi_e \leqslant \pi/2$ and $0 \leqslant T_e \leqslant (T_e)_{max}$, where

$$(T_e)_{max} = 2h\nu\varepsilon/(1 + 2\varepsilon), \quad \varepsilon = h\nu/m_e c^2.$$

The formula for calculating the differential Compton scattering cross section was obtained by Klein and Nishina, and independently by Tamm. This expression has the following form:

$$d\sigma(\theta) = r_e^2 \frac{1+\cos^2\theta}{2} \frac{d\Omega}{[1+\varepsilon(1-\cos\theta)]^2} \times \left\{1 + \frac{\varepsilon^2(1-\cos\theta)^2}{(1+\cos^2\theta)[1+\varepsilon(1-\cos\theta)]}\right\}. \qquad (4.10.20)$$

where $r_e = e^2/m_e c^2$, $\varepsilon = h\nu/m_e c^2$, and θ is the scattering angle. The dependence of $d\sigma(\theta)$ on scattering angle for different ε is shown in Fig. 176. For $\varepsilon \simeq 0$, this figure becomes identical to Fig. 171. With increasing ε, the scattering diagram is stretched forward.

The formula for the total Compton scattering cross section is obtained by integrating Eq. (4.10.20) over all angles:

$$\sigma_{\text{Com}} = 2\pi r_e^2 \left\{ \frac{1+\varepsilon}{\varepsilon^3} \left[\frac{2(1+\varepsilon)}{1+2\varepsilon} - \frac{1}{\varepsilon} \ln(1+2\varepsilon) \right] + \frac{1}{2\varepsilon} \ln(1+2\varepsilon) - \frac{1+3\varepsilon}{(1+2\varepsilon)^2} \right\}. \quad (4.10.21)$$

Let us consider two particular cases.

1. For $\varepsilon \ll 1$, this formula is transformed into

$$\sigma_{\text{Com}} = \sigma_{\text{Th}} \left(1 - 2\varepsilon + \frac{26}{5}\varepsilon^2 + \ldots \right), \quad (4.10.22)$$

where in accordance with (4.10.10), we have

$$\sigma_{\text{Th}} = (8\pi/3)(e^4/m_e^2 c^4)$$

For low energies ($\varepsilon \ll 0.05$), the Compton scattering cross section increases linearly with decreasing energy and tends to the value σ_{Th} in the limit.

2. For $\varepsilon \gg 1$, the formula assumes the form

$$\sigma_{\text{Com}} = \pi r_e^2 \frac{1}{\varepsilon} \left(\frac{1}{2} + \ln 2\varepsilon \right). \quad (4.10.23)$$

where r_e and ε have the same values as before. Thus, the cross section of Compton scattering by an electron for $E_\gamma \gg m_e c^2$ ($\varepsilon \gg 1$) varies in inverse proportion to the energy of the γ-quantum. Since there are Z electrons in an atom, the cross section for an atom is Z times larger, and hence for $\varepsilon \gg 1$ varies as Z/E_γ:

$$\sigma_{\text{Com}} \propto Z/E_\gamma. \quad (4.10.24)$$

The Compton effect can be observed not only for a fixed electron, but for a moving electron as well. Formulas for the energy E_γ of a photon scattered by a moving electron can be obtained by transforming formula (4.10.18) from a system of coordinates attached to the electron to the laboratory system of coordinates:

$$E'_\gamma = E_\gamma \frac{1 - \beta\cos\theta_1}{1 - \beta\cos\theta_2 + [E_\gamma(1-\cos\theta)/E_e]}, \quad (4.10.25)$$

where E_γ is the initial energy of the photon, β is the electron velocity, θ_1 is the angle between the direction of motion of the electron and the incident photon, θ_2 is the angle between the direction of motion of the electron and the scattered photon, E_e is the electron energy and θ is the angle between the incident and scattered quanta.

Electron-positron pairs can also be formed under the action of two photons with total energy $E_{\gamma_1} + E_{\gamma_2} > 2m_e c^2$, or as a result of collision of two electrons if the total energy of the moving electron $E_e \geqslant 7m_e c^2$.

We recommend it to the reader to derive independently these results by using the invariance of the relation $E^2 - P^2c^2 = \text{inv}$ (having written it for the threshold energy value in the laboratory system of coordinates and in tho centre-of-mass system). It should

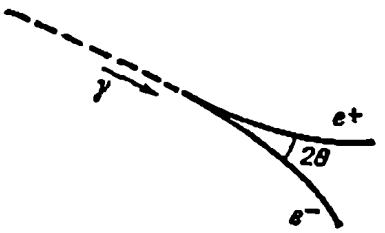

Fig. 177

Fig. 178

be recalled that E and P in the invariance relation denote the total energy and the resultant momentum of the interacting particles (see Sec. 6.1.4, Vol. II).

The expression for the cross section of the electron-positron pair formation in the field of a nucleus is quite complicated. In analytic form, it can be written only for a limited interval of variation of energy E_γ:

$$\sigma_{\text{pair}} = \frac{Z^2}{137} r_e^2 \left(\frac{28}{9} \ln \frac{2E_\gamma}{m_e c^2} - \frac{218}{27} \right) \qquad (4.10.31)$$

for $m_e c^2 \ll E_\gamma \ll 137 m_e c^2 Z^{-1/3}$ (without taking into account the screening), and

$$\sigma_{\text{pair}} = \frac{Z^2}{137} r_e^2 \left[\frac{28}{9} \ln (183Z^{-1/3}) - \frac{2}{27} \right] \qquad (4.10.32)$$

for $E_\gamma \gg 137 m_e c^2 Z^{-1/3}$ (complete screening), where $137 m_e c^2 Z^{-1/3}$ is equal to 30 MeV for aluminium and about 15 MeV for lead.

For other energy values, the cross section is calculated by numerical integration of the expression for differential cross section. The general form of the dependence of σ_{pair} on E_γ is shown in Fig. 179.

The cross section of the electron-positron pair formation in the Coulomb field of an electron is much (about 1000 times) smaller than the cross section of their formation in the field of a nucleus, especially if the comparison is made at low energies and for large Z. However, for $E_\gamma > 10$ MeV, the pair formation on electrons may constitute

about 1% of the total cross section in heavy elements and about 10% in light elements.

Besides the radiation losses for electrons, the process of electron-positron pair formation is responsible for electron-photon showers in cosmic rays. If a γ-quantum created as a result of radiation losses by an electron has an energy $E_\gamma > 2m_e c^2$, it can create a pair whose

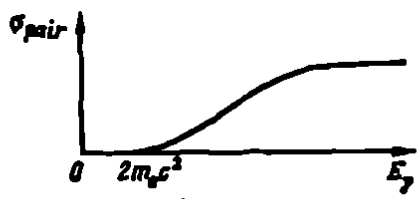

Fig. 179

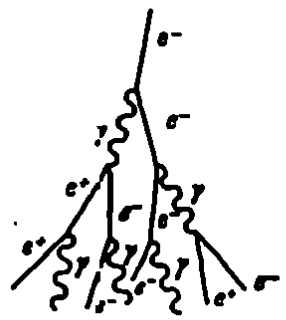

Fig. 180

electron and positron again give rise to γ-quanta as a result of radiation losses, and so on (see Fig. 180). The process is intensified in an avalanche-like manner until the energy attains its critical value (see Sec. 4.5).

4.10.4. General Nature of Interaction of Gamma Radiation with Matter

While considering the interaction of γ-quanta with matter, we must take into account all the possible processes, viz. the photoeffect, the Compton effect and the electron-positron pair formation.

The total cross section for these processes is given by

$$\sigma = \sigma_{phot} + \sigma_{Com} + \sigma_{pair}. \qquad (4.10.33)$$

where $\sigma_{phot} \propto Z^5/E_\gamma^{7/2}$ (E_γ) is the cross section for the photoeffect, $\sigma_{Com} \propto Z/E_\gamma$ is the Compton effect cross section and $\sigma_{pair} \propto Z^2 \ln (2E_\gamma)$ is the cross section for pair formation.

It follows from the nature of dependence of cross sections on energy E_γ of gamma radiation and the charge Z of the medium that the photoeffect is the principal mechanism of interaction of gamma radiation with matter for low energies $(E_\gamma < E_1)$, the Compton effect is mainly responsible for interaction in the intermediate energy range $(E_1 < E_\gamma < E_2)$, while the electron-positron pair formation

dominates in the high-energy region ($E_\gamma > E_2$). The boundary values of energy demarcating the regions of predominance of each of these effects are different for different media. For aluminium, these values are $E_1 = 0.05$ MeV and $E_2 = 15$ MeV, while the corresponding

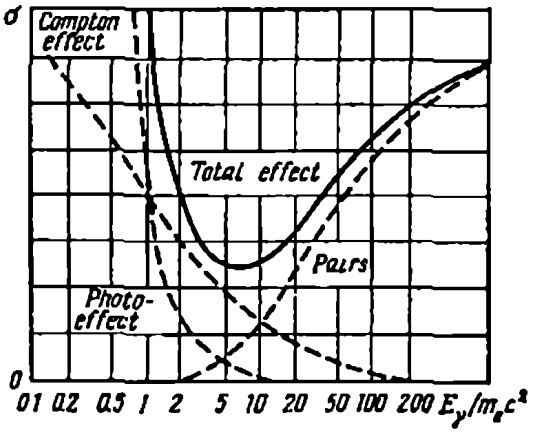

Fig. 181

values for lead are $E_1 = 0.5$ MeV and $E_2 = 5$ MeV. Figure 181 shows the energy dependence of the absorption cross section for γ-quanta in lead for each of the three interaction mechanisms, as well as for the total cross section $\sigma_{phot} + \sigma_{Com} + \sigma_{pair}$.

4.11. A Brief Resumé of Chapter 4

This chapter is devoted to the interaction of charged particles, neutrons and γ-quanta with electrons and atomic nuclei.

Three types of interaction are considered in nuclear physics, viz. strong (nuclear), electromagnetic, and weak. Nuclear interaction has the highest strength and the largest effective cross section ($\sigma \simeq 10^{-27}$-10^{-24} cm^2), and takes place in the shortest time ($\tau_{nuc} \simeq 10^{-23}$-$10^{-22}$ s). The carriers of nuclear interaction are the nuclear quanta, viz. π-mesons. The simplest examples of nuclear interactions are the mutual attraction between nucleons inside the nucleus, and the nucleon-nucleon scattering.

Electromagnetic interaction is 10^2-10^3 times weaker than nuclear interaction and occurs over periods $\tau_{e\,m} \geqslant 10^{-19}$ s. Electromagnetic interaction takes place through electromagnetic radiation quanta, i.e. photons. Examples of electromagnetic processes are the ionization losses, the Coulomb scattering, and the photoelectric effect.

Weak interaction is about 10^{13} times less intensive than strong interaction, is the slowest of all interactions (as a rule, $\tau_w \geqslant 10^{-10}$ s) and has the smallest cross section ($\sigma \simeq 10^{-43}$ cm^2). The beta decay of nuclei is an example of weak interaction.

All types of interaction, be it strong, electromagnetic or weak, can be divided into elastic and inelastic, depending on the way in which they occur. Elastic interaction, i.e. the elastic scattering of one particle by another, is characterized by the conservation of the total kinetic energy of both particles and can be described (for all types of interaction) with the help of a simple geometric

diagram called the *momentum diagram* (relativistic version of the diagram should be used for high energies). Inelastic processes are characterized by a (partial or complete) conversion of kinetic energy of the moving particle into other forms, for example, the excitation energy of the atom or nucleus, emission energy, or the rest energy of the particles formed in these processes.

In this chapter, we have mainly considered elastic and inelastic processes associated with electromagnetic interaction. A particular case of elastic electromagnetic interaction is the Coulomb scattering of α-particles by atomic nuclei, which is described by the Rutherford formula: $d\sigma = (Ze^2/mv^2)^2 \times [d\Omega/4 \sin^4(\theta/2)]$. The experimental verification of the Rutherford formula led to the nuclear model of the atom. Elastic scattering of two identical charged particles (proton-proton scattering, scattering of an α-particle by the helium nucleus $^4_2$He) is described with the help of Mott's quantum-mechanical formulas.

A charged particle moving in a dense medium experiences a series of successive elastic scatterings by nuclei encountered by it on its trajectory (multiple Coulomb scattering). As a result of this process, the particle suffers a mean deviation by a certain resulting angle α relative to its original direction of motion (mean multiple scattering angle), whose value is given by the formula $\alpha \propto Zz\sqrt{x}\sqrt{n}/p\beta$, where Z is the nuclear charge of the medium; x is the path traversed by the particle; n is the number density of nuclei in the medium; p, β and z are the momentum, velocity and charge of the particle respectively. By measuring the value of α, we can use this formula to determine $p\beta$ for the particle.

An interesting process of elastic scattering of γ-quanta by electrons is the Compton effect in which the quantity $\Delta\lambda = \lambda' - \lambda_0$ is independent of the nature of the scattering material (for a given scattering angle θ):

$$\Delta\lambda = 2\Lambda \sin^2(\theta/2) = 2(\hbar/m_e c)\sin^2(\theta/2)$$

The differential cross section of Compton scattering is determined with the help of the Klein-Nishina-Tamm formula. For $E_\gamma \gg m_e c^2$, the Compton scattering cross section per atom σ_{Com} is proportional to Z/E_γ.

One form of inelastic electromagnetic interaction of charged particles with matter is the *ionization losses*, when the kinetic energy of the particle is spent on exciting and ionizing the atoms of the medium. The specific loss of energy on ionization is independent of the mass of the particle, is proportional to the square of its charge and the electron number density in the medium, and is inversely proportional (in the first approximation) to the square of the particle velocity: $dT/dx \propto z^2 n_e/v^2$. This relation can be used to obtain formulas connecting the energy and the ionization range for any charged particle in various media. Electrons knocked out of atoms during the ionization losses by a charged particle are δ-electrons. From the direction of motion, energy and the number of δ-electrons per unit length, it is possible to estimate the energy and charge of the particle responsible for their formation.

Another inelastic process, viz. *bremsstrahlung*, occurs when a charged particle is suddenly stopped in the electric field of the atomic nucleus. The loss of energy due to bremsstrahlung by particles with the same charge is in inverse proportion to the square of their masses. Hence bremsstrahlung is significant only for the lightest charged particles, viz. electrons, for which the following formula is valid in the first approximation:

$$(dT_e/dx)_{rad} \propto nT_e Z^2$$

Here n is the number density of nuclei in the medium, T_e is the kinetic energy of electrons, and Z is the nuclear charge of the medium. The energy at which ionization and radiation losses are comparable in magnitude is called *critical* energy. Beyond the critical energy, the average energy of electrons decreases exponentially with the distance x traversed by them, i.e. according to the law $\exp(-x/x_0)$, where x_0 is called the *radiation length*.

A very peculiar inelastic electromagnetic process was discovered in 1934 by Cherenkov at the laboratory of Acad. S.I. Vavilov. When charged particles move with a velocity exceeding the phase velocity c/n of light (n is the refractive index in a given medium), a sharply directional glow ($\cos\theta = 1/n\beta$), which was later termed the Cherenkov radiation, is observed. This glow is due to the coherent radiation of oriented dipoles created along the charged particle trajectory under the action of its electric field. The theory of the Cherenkov radiation was constructed in 1937 by Tamm and Frank. The Cherenkov effect is widely used for determining the velocity of fast charged particles.

Ginzburg and Frank predicted in 1944 the transition radiation caused by uniform motion of charged particles in a straight line in an inhomogeneous medium or in a medium varying in time.

When relativistic charged particles move in a magnetic field (in vacuum), synchrotron radiation is observed. This radiation, which is most significant for light charged particles like electrons and positrons, has wide practical applications.

Among the inelastic electromagnetic processes for γ-quanta, we have considered in this chapter the photoeffect and the electron-positron pair formation.

In the photoeffect, the entire energy of the γ-quantum is imparted to one of the electrons constituting an atom. This effect cannot occur for a free electron. For $E_\gamma \gg I_K$ (I_K is the ionization potential for the K-shell), the cross section of the photoeffect per atom varies according to the law $\sigma \propto Z^5/E_\gamma$. This effect is the principal mechanism of absorption of long-wave gamma radiation in heavy materials.

For sufficiently high gamma radiation energies ($E_\gamma > E_0$), the process of electron-positron pair formation (in the Coulomb field of the nucleus or electron) becomes possible. The threshold energy for this process in the nuclear field is $E_0 = 2m_e c^2$, and its cross section (for energies $5m_e c^2 < E_\gamma < 50m_e c^2$) is given by the law $\sigma_{pair} \propto Z^2 \ln(2E_\gamma)$.

For $E_\gamma > 50\ m_e c^2$, the increase in the cross section slows down and is independent of energy in the limit. The threshold energy of the $(e^+\text{-}e^-)$-pair formation process in the field of an electron is given by $E_0 = 4m_e c^2$. The formation of an electron-positron pair by a γ-quantum in vacuum is impossible.

In order to describe correctly the interaction with a medium, we must take into account all three processes, viz. the Compton effect, the photoeffect and the electron-positron pair formation (as well as nuclear reactions induced by γ-quanta).

Part Two

Nuclear Interactions

Chapter 5

General Laws Governing Nuclear Reactions

5.1. Classification of Nuclear Reactions

Owing to nuclear forces, two particles (two nuclei or a nucleus and an elementary particle, say, a nucleon) enter into a strong nuclear interaction upon coming close to distances of about 10^{-13} cm. This results in a nuclear transformation and the process is called a *nuclear reaction*. A nuclear reaction is accompanied by a redistribution of the energies and momenta of both particles, and this may lead to the creation of several other particles escaping from the region of interaction.

There are many different types of nuclear reactions. Depending on the particles responsible for these reactions, we can classify them as neutron-induced reactions, reactions induced by charged particles or by γ-quanta. The last type of reactions is associated with the electromagnetic interaction rather than the nuclear interaction, but it is appropriate to label these reactions as nuclear reactions as well, since the interaction takes place in the vicinity of the nucleus and results in its transformation.

Nuclear reactions may also include *Coulomb excitation of the nucleus*, i.e. a change in its intrinsic state as a result of electromagnetic interaction with a charged particle which does not hit the nucleus.

Each of the three main classes of reactions has its own specific features which will be considered in detail in the appropriate chapters of this book. Besides, we shall also consider separately the reactions involving the fission of heavy nuclei, fusion reactions, and reactions involving the creation of transuranic elements.

Depending on the mechanism of interaction nuclear reactions will be divided into two classes, viz. reactions involving an intermediate stage of a compound nucleus, and direct interactions. The first class of interactions will be considered mainly in Chaps. 6 and 7, while the second type will be described in Chap. 10. It should

be noted at the very outset that this division is quite arbitrary, since there are reactions which can proceed simultaneously in both ways. In this introductory chapter, we shall consider the basic laws governing nuclear reactions.

A nuclear interaction can be written in the general form as follows:

$$a_1 + a_2 \to b_1 + b_2 + \ldots, \tag{5.1.1}$$

where a_1 and a_2 are the reacting particles and b_1, b_2, . . . are particles formed as a result of the reaction (reaction products).

The most commonly encountered type of nuclear reaction involves a light particle a and a nucleus A, resulting in the formation of a light particle b and a nucleus B:

$$a + A \to b + B, \tag{5.1.2}$$

or, in short,

$$A\ (a, b)\ B. \tag{5.1.3}$$

The particles a and b may be chosen from neutron (n), proton (p), α-particle (α), deuteron (d), γ-quantum (γ), π-meson (π), etc.

The process described by (5.1.2) usually takes place not uniquely, since the reaction may occur in several competing ways:

$$\begin{array}{l} \to B + b \\ \nearrow \\ a + A \to \ldots \\ \searrow \\ \to A^* + a \\ \to A + a \end{array} \tag{5.1.4}$$

The initial stage is called the *entrance channel* while the different possible ways in which a nuclear reaction may proceed in the second stage are called the *exit channels* of the reaction. Various reaction channels differ in the type of the particles, their intrinsic state, spin orientation and the orientation of their orbital angular momenta.

The last two reaction channels in (5.1.4) correspond to the case f inelastic ($A^* + a$) and elastic ($A + a$) nuclear scattering. These re special cases of nuclear reactions and differ from other cases in hat the reaction products are the same as the particles entering nto the reaction. In elastic scattering, the type and the intrinsic tate of the nucleus are preserved, while upon inelastic scattering the

intrinsic state of the nucleus changes (the nucleus passes into an excited state).

Elastic scattering of particles with nonzero spins may proceed via different spin channels. A specific spin channel is characterized by a definite spin orientation of the particles, which can be preset with the help of polarizers and analyzers.

The investigation of a nuclear reaction is aimed at identifying reaction channels, determining the relative probability of its occurrence through different channels for different energies of the incident particles, finding the energy and angular distribution of the reaction products, as well as their intrinsic parameters (excitation energy, spin, parity, isotopic spin). A great deal of information concerning nuclear reactions can be obtained by applying the conservation laws which impose certain restrictions on the course of nuclear reactions. We shall consider the following conservation laws: the conservation of electric charge, number of nucleons, energy, momentum, angular momentum, parity and isotopic spin.

5.2. Laws of Conservation of Electric Charge and Baryon Number

Experimental investigation of nuclear interactions has shown that the total electric charge of the particles entering into a reaction is equal to the total electric charge of the reaction products in all cases. Besides, in ordinary nuclear reactions (not involving the creation of antiparticles), the total number of nucleons is also conserved.

Both these conservation laws are valid for nuclear transformations of the radioactive disintegration type, e.g. beta decay, alpha decay, e-capture, spontaneous fission, as well as for any other type of interaction (see Vol. II).

Obviously, the nucleon number conservation law indicates that processes of the type

$$p + e^- \nrightarrow 2\gamma$$

("annihilation" of a hydrogen atom) cannot occur in nature or, in other words, the world surrounding us is stable.

When applied to simplest nuclear reactions, the nucleon number conservation law indicates that the mass number A is conserved in these reactions. Hence we can introduce the concept of nucleon (nuclear) charge, which is equal to unity for proton and neutron, and to the mass number A for atomic nuclei. However, it will be shown in Sec. 7.2, Vol. II that the nucleon charge of all heavy particles, i.e. baryons, is also equal to unity. Hence it is customary to use the term *baryon charge* instead of the nucleon charge and denote it by B ($B_n = B_p = 1$).

5.3. Energy and Momentum Conservation Laws

In view of the large distance (about 10^{-8} cm) by which nuclei having small dimensions (about 10^{-12} cm) are separated in a condensed medium, the small range of nuclear forces and the small value of the chemical binding, we can consider a system of two interacting nuclear particles to be closed (isolated). The total energy and total momentum in isolated system are conserved.

5.3.1. Reaction Energy

For process (5.1.2), the law of energy conservation can be written in the form

$$E_1 = E_2$$

or

$$E_{01} + T_1 = E_{02} + T_2, \tag{5.3.1}$$

where E_{01} and E_{02} denote the rest energy of the initial and final particles, while T_1 and T_2 represent their respective kinetic energies[1]: $E_{01} = M_A c^2 + m_a c^2$, $E_{02} = M_B c^2 + m_b c^2$, $T_1 = T_A + T_a$, $T_2 = T_B + T_b$. In the general case, $E_{01} \neq E_{02}$. The difference $E_{01} - E_{02}$ is called the *reaction energy* and is denoted by Q:

$$Q = E_{01} - E_{02} = T_2 - T_1. \tag{5.3.2}$$

If $Q > 0$, the reaction is accompanied by a liberation of kinetic energy at the expense of the rest energy and is called *exoergic*. Exoergic reactions can occur at any kinetic energy of the incident particle (if the energy is sufficient to overcome the Coulomb barrier of the nucleus in the case of a charged particle).

If $Q < 0$, the reaction involves an increase in the rest energy at the expense of the kinetic energy and is called *endoergic*. Endoergic reactions can take place only when the incident particle has a sufficiently high kinetic energy, since it follows from (5.3.2) for $Q < 0$ that $T_1 = |Q| + T_2 > |Q|$ [see formula (5.3.21) for details].

Finally, the case $Q = 0$ corresponds to elastic scattering, when $T_1 = T_2$ and $E_{01} = E_{02}$, i.e. the total energy is conserved as well as the kinetic energy, and hence the rest energy (or the mass of the particles) also remains unchanged. Elastic collisions result only in a redistribution of kinetic energy (in the laboratory system of coordinates) between the colliding particles. (It was mentioned in Sec. 4.4.1 that the kinetic energy of each particle is conserved during elastic collisions in the centre-of-mass system.)

[1] If the target nucleus is at rest, $T_A = 0$ and $T_1 = T_a$

An example of exoergic reaction is the reaction ${}_1^2H + {}_1^3H \rightarrow {}_2^4He + n$ in which the reaction energy $Q = 3.25$ MeV is released in the form of kinetic energy of the reaction products. An even higher amount of energy is liberated in the analogous reaction of a deuteron with tritium: ${}_1^2H + {}_1^3H \rightarrow {}_2^4He + n$; here, $Q = 17.6$ MeV, which is about 0.5% of the rest energy of the particles. It should be noted that this value is about 10^6 times higher than the energy of a chemical reaction.

Both these reactions belong to the fusion reactions for light elements, which must be accompanied by the liberation of energy (see Sec. 1.3). Such reactions will be considered in greater detail in Chap. 13.

Highly exoergic reactions also include the fission of heavy nuclei, where about 200 MeV of energy is released per nucleus. These reactions will be described in Chap. 7.

We shall consider some examples of endoergic reactions in the following subsection.

5.3.2. Energy Diagram for Nuclear Reactions. Endoergic Reaction Threshold

For reactions of type (5.1.2), the law of momentum conservation is written in the form

$$\mathbf{p}_c + \mathbf{p}_A = \mathbf{p}_B + \mathbf{p}_b. \qquad (5.3.3)$$

The target nucleus A is usually assumed to be at rest, and hence

$$\mathbf{p}_A = 0, \qquad \mathbf{p}_a = \mathbf{p}_B + \mathbf{p}_b. \qquad (5.3.4)$$

It was shown by Bohr (see Sec. 6.4) that a nuclear reaction can be assumed to proceed in two stages in many cases.[2] In the first stage, a compound (intermediate) nucleus O is formed from the two initial particles a and A:

$$a + A \rightarrow O. \qquad (5.3.5)$$

This nucleus has quite definite parameters (charge, mass, system of energy levels, spin and other quantum numbers) and exists for quite a long time τ (in comparison with the nuclear time τ_{nuc})[3] which is of the order of 10^{-14} s.

At the second stage of the nuclear reaction, the compound nucleus disintegrates into reaction products according to the scheme

$$O \rightarrow B + b. \qquad (5.3.6)$$

[2] It was mentioned earlier that there exists, besides Bohr's mechanism, another mechanism of direct transfer which we shall discuss in Chap. 10.

[3] The nuclear time τ_{nuc} characterizes the time during which a particle crosses the nucleus: $\tau_{nuc} = R/v = (10^{-13}\text{-}10^{-12})/(10^9\text{-}10^{10}) \simeq 10^{-22}\text{-}10^{-21}$ s.

We shall use the concept of compound nucleus to describe a nuclear reaction in greater detail from the energy point of view. Let us consider the first stage of a nuclear reaction, viz. the formation of compound nucleus O. The laws of energy and momentum conservation can be written in this case as follows:

$$\mathbf{p}_A = \mathbf{p}_O, \tag{5.3.7}$$
$$(M_A + m_a)\,c^2 + T_a = M_O^* c^2 + T_O,$$

where $\mathbf{p}_O$ is the momentum of the compound nucleus, T_O is its kinetic energy, and $M_O^* c^2$ is the rest energy.

The asterisk over M_O indicates that the compound nucleus may be formed in an excited state, in which case $M_O^* c^2$ denotes its rest energy in the excited state. The value of T_O can be easily calculated:[4]

$$T_O = \frac{p_O^2}{2M_O^*} = \frac{m_a}{M_O^*}\frac{p_a^2}{2m_a} = \frac{m_a}{M_O^*}T_a. \tag{5.3.8}$$

Substituting the value of T_O thus obtained into (5.3.7) we get the relation

$$M_O^* c^2 = (M_A + m_a)\,c^2 + T_a\,(1 - m_a/M_O^*). \tag{5.3.9}$$

The second term in this expression is a negligible fraction of the first term since it is less than the kinetic energy of the incident particle $T_a \leqslant 10$ MeV, while the first term $(M_A + m_a)\,c^2 \simeq 931 A_{M+m}$, where A_{M+m} is the overall mass number of particles A and a. Hence we can write in the first approximation

$$M_O^* c^2 \simeq (M_A + m_a)\,c^2. \tag{5.3.10}$$

Substituting this expression into the right-hand side of Eq. (5.3.9), we obtain a fairly accurate second approximation for $M_O^* c^2$:

$$M_O^* c^2 = (M_A + m_a)\,c^2 + T_a\,[1 - m_a/(M_A + m_a)]$$

or

$$M_O^* c^2 = (M_A + m_a)\,c^2 + M_A T_a/(M_A + m_a). \tag{5.3.11}$$

Similarly, substituting (5.3.10) into (5.3.8), we obtain

$$T_O = m_a T_a/(M_A + m_a). \tag{5.3.12}$$

Knowing the mass of the excited compound nucleus, we can easily determine its excitation energy:

$$W = M_O^* c^2 - M_O c^2 = (M_A + m_a - M_O)\,c^2 + M_A T_a/(M_A + m_a). \tag{5.3.13}$$

In accordance with Sec. 1.3, the first term in this expression represents the binding energy $\varepsilon_a\,(O)$ of particle a relative to the compound

[4] We are considering nonrelativistic particles with low kinetic energies ($T_a \simeq 10$ MeV).

nucleus O. As regards the second term (see Sec. 4.4), it is equal to the kinetic energy T_1' of particles A and a in the centre-of-mass system (relative kinetic energy):

$$\frac{M_A}{M_A+m_a}T_a=\frac{m_a v^2}{2}\frac{M_A}{M_A+m_a}=\frac{\mu v^2}{2}=T_1' \qquad (5.3.14)$$

(v is the relative velocity of the particles).

Thus, the excitation energy of the compound nucleus O is the sum of the binding energy of the incident particle and the kinetic energy of particles A and a in the centre-of-mass system:

$$W=\varepsilon_a(O)+T_1'. \qquad (5.3.15)$$

Note that $W\neq 0$ even for $T_1'=0$ (i.e. for $T_a=0$). If, however, $T_a\neq 0$, a part of this energy, equal to $T_1'=M_AT_a/(M_A+m_a)$,

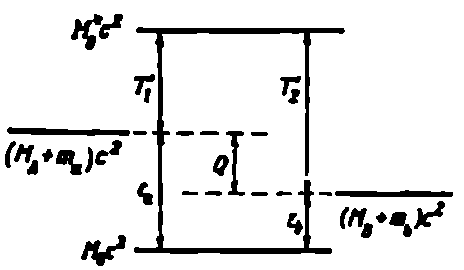

Fig. 182

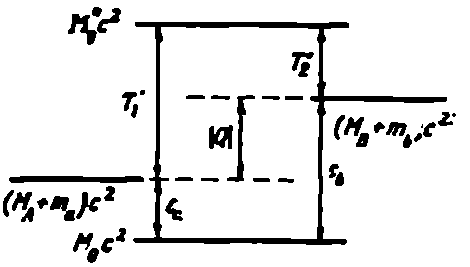

Fig. 183

is spent in exciting the compound nucleus, while the remaining energy $T_O=m_aT_a/(M_A+m_a)$ is spent in moving the compound nucleus (to satisfy the law of momentum conservation):

$$T_1'+T_O=M_AT_a/(M_A+m_a)+m_aT_a/(M_A+m_a)=T_a. \qquad (5.3.16)$$

Let us represent the process of the formation of the compound nucleus with the help of the energy diagram (Fig. 182, left side). The process of disintegration of the compound nucleus into particles B and b can be obviously represented in an analogous manner (Fig. 182, right side), the only difference being that the middle line defines the rest energy of particles B and b, while its distance from the lower and upper lines respectively represents the binding energy of particle b in the compound nucleus and the relative kinetic energy of particles B and b (in the centre-of-mass system.)[b]. Figure 182 shows

[b] Note that the compound nucleus O is the common centre-of-mass system for particles A, a, and B, b.

the diagram for an exoergic reaction ($Q > O$). It can be seen from the figure that

$$Q = T_2' - T_1' = \varepsilon_a - \varepsilon_b. \tag{5.3.17}$$

The energy diagram for an endoergic reaction is shown in Fig. 183. It differs from the diagram shown in Fig. 182 in that $(M_B + m_b)\,c^2 > (M_A + m_a)\,c^2$. Consequently,

$$T_2' - T_1' = Q < O \text{ and } T_1' = T_2' + |Q|. \tag{5.3.18}$$

Thus, $T_1' \geqslant |Q|$ for all endoergic reactions. The sign of equality corresponds to the minimum value of the kinetic energy of particles A and a

$$(T_1')_{\min} = |Q| \tag{5.3.19}$$

for which the reaction is still possible.

Using the relation $T_1' = M_A T_a/(M_A + m_a)$, we obtain the condition for the minimum (threshold) energy in the laboratory system of coordinates:

$$M_A\,(T_a)_{\min}/(M_A + m_a) = |Q|.$$

This gives

$$(T_a)_{\min} = \frac{M_A + m_a}{M_A}\,|Q|. \tag{5.3.20}$$

Writing this relation in the form

$$\begin{aligned}(T_a)_{\min} &= |Q| + \frac{m_a}{M_A}\,|Q| = |Q| + \frac{m_a}{M_A + m_a}\,(T_a)_{\min} \\ &= |Q| + (T_0)_{\min},\end{aligned} \tag{5.3.21}$$

we find that $(T_a)_{\min}$ is higher than $|Q|$ by exactly the kinetic energy of the compound nucleus (which cannot be used in the reaction).

Let us now consider some examples involving calculations for reactions with $Q > 0$ and $Q < 0$.

1. $$^{32}_{16}\mathrm{S} + n \rightarrow {}^{32}_{15}\mathrm{P} + p,$$

$$Q = -0.92 \text{ MeV}, \quad T_{\min} = \frac{32+1}{32}\,0.92 = 0.95 \text{ MeV}, \tag{5.3.22}$$

If the reaction takes place at the threshold value $T_{\min}$ of the energy, then according to formulas (5.3.18) and (5.3.19) $T_2' = 0$, i.e. the reaction products are at rest in the centre-of-mass system, and hence they move in the laboratory system of coordinates with the same velocity which is equal to the velocity of the centre-of-mass system. As a result, the kinetic energy of the compound nucleus

$$T_0 = \frac{m_a}{M_A + m_a}\,T_{\min} = 0.95/33 \simeq 0.03 \text{ MeV}$$

is distributed between reaction products in proportion to their masses $T_n : T_{^{32}P} = 1 : 32$ and $T_n = T_{min}/33^2 \simeq 1$ keV. It should be observed that the kinetic energy of the neutrons formed is nonzero (in the laboratory system of coordinates) and cannot be less than the value obtained above.

2. The above results are not valid for endoergic reactions induced by γ-quanta. For example, let us consider the reaction involving photodissociation of deuteron

$$\gamma + {}_1^2H \to p + n \qquad (5.3.23)$$

($Q = -2.22$ MeV), which was first observed upon irradiation of deuteron by ThC'' γ-quanta ($E_\gamma = 2.62$ MeV). According to (5.3.21), we have

$$(E_\gamma)_{min} = |Q| + (T_0)_{min},$$

$$(T_0)_{min} = \frac{(p_0^2)_{min}}{2M_C} = \frac{(p_\gamma^2)_{min}}{2M_0} = \frac{(E_\gamma^2)_{min}}{2M_0c^2} < \frac{E_\gamma^2}{2M_0c^2},$$

$$(T_0)_{min} < \frac{2.62^2 \text{ MeV}}{4 \times 931 \text{ MeV}} \simeq 1.5 \text{ keV}.$$

We have considered the lightest nucleus, viz. the deuteron. The value of $(T_0)_{min}$ is even lower for heavier nuclei. Thus, it can be

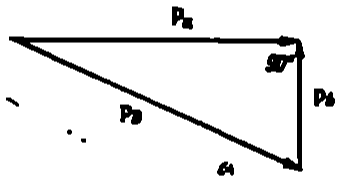

Fig. 184

assumed that the threshold of endoergic photonuclear reactions practically coincides with the modulus of the reaction energy:

$$(T_0)_{min} \simeq 0 \text{ and } (E_\gamma)_{min} \simeq |Q|.$$

3. The following two fusion reactions considered in Sec. 5.3.1 and resulting in the formation of neutrons are widely used in practice:

$${}_1^2H + {}_1^2H \to {}_2^3He + n, \quad Q = 3.25 \text{ MeV}, \qquad (5.3.24)$$

$${}_1^2H + {}_1^3H \to {}_2^4He + n, \quad Q = 17.6 \text{ MeV}. \qquad (5.3.25)$$

This is so because these reactions lead to the creation of fast monoenergetic neutrons.

Let us write these two reactions in the general form ($a + A \to B + b$) and consider the particular case (Fig. 184) when the resulting neutron (particle b) is emitted at an angle 90° to the incident

deuteron (particle a). Then in accordance with the laws of conservation of energy and momentum, we obtain

$$T_a + Q = T_B + T_b, \tag{5.3.26}$$

$$p_a^2 + p_b^2 = p_B^2. \tag{5.3.27}$$

Dividing the last equation by $2M_B$ and replacing p_a^2 by $2m_aT_a$, we can write

$$m_aT_a/M_B + m_bT_b/M_B = T_B. \tag{5.3.28}$$

Solving Eqs. (5.3.26) and (5.3.28) simultaneously, we obtain

$$T_b = \frac{M_B}{M_B+m_b}Q + \frac{M_B-m_a}{M_B+m_b}T_a. \tag{5.3.29}$$

On account of the small height of the Coulomb barrier and the large cross sections of reactions (5.3.24) and (5.3.25), the reactions proceed effectively at comparatively low kinetic energies of incident deuterons ($T_a \simeq 0.2$ MeV). In this case, the energy of the neutrons formed in the reactions (5.3.24), (5.3.25) and escaping at an angle 90° to the incident deuteron are given respectively by

$$T_n = \frac{3}{4}\,3.25 + \frac{1}{4}\,0.2 \simeq 2.49 \simeq 2.5 \text{ MeV},$$

$$T_n = \frac{4}{5}\,17.6 + \frac{2}{5}\,0.2 \simeq 14 \text{ MeV}.$$

5.3.3. Momentum Diagram for Nuclear Reactions

The kinematic pattern of a nuclear reaction can be easily analyzed graphically with the help of the momentum diagram. For the sake of definiteness, let us consider an exoergic reaction of the type

$$a + A \to O \to B + b \tag{5.3.30}$$

under the assumption that the target nucleus A is at rest and the momentum of the bombarding particle a is equal to p_a.

The construction of the diagram is similar to the one described in Sec. 4.4 for the case of elastic scattering. As before, the momentum of the product particle is obtained as a result of adding the momentum $\mathbf{p}_{tr}$ of translatory motion (with velocity $v_{c.m.}$) and the momentum $\mathbf{p}'$ in the centre-of-mass system:

$$\mathbf{p} = \mathbf{p}_{tr} + \mathbf{p}'. \tag{5.3.31}$$

Since $\mathbf{p}_a = \mathbf{p}_O$, i.e. $m_av_a = M_Ov_O$ (we are considering the nonrelativistic case), we obtain

$$v_{c.m.} = v_O = m_av_a/M_O = p_a/M_O. \tag{5.3.32}$$

Hence we obtain the momentum of the translatory motion of particles b and B:

$$(p_b)_{tr} = m_b v_{c.m.} = m_b p_a / M_0 \simeq m_b p_a / (M_B + m_b), \tag{5.3.33}$$

$$(p_B)_{tr} = M_B v_{c.m.} = M_B p_a / M_0 \simeq M_B p_a / (M_B + m_b). \tag{5.3.34}$$

These values can be obtained geometrically by dividing the initial momentum p_a in the same ratio as the masses of the reaction products.

As regards the momentum of the particles in the centre-of-mass system, its value

$$p_1' = p_B' = p_b' = p_a \sqrt{\frac{\mu_{Bb}}{m_a}\left(\frac{Q}{T_a} + \frac{M_A}{M_A + m_a}\right)} \tag{5.3.35}$$

is obtained from the following obvious relations:

$$T_2' = T_1' + Q = M_A T_a / (M_A + m_a) + Q, \tag{5.3.36}$$

$$p_2' = \sqrt{2\mu_{Bb} T_2'}, \tag{5.3.37}$$

where $\mu_{Bb} = M_B m_b / (M_B + m_b)$ is the reduced mass of particles B and b. Unlike the case of elastic scattering, we have $p_2' \neq p_1'$ here.

Thus, the momentum diagram for interpretation of nuclear reactions is constructed as follows (Fig. 185). The segment AB, representing the momentum p_a of the bombarding particle on a certain scale, must be divided at point O in the same ratio as the masses of the product particles:

$$AO/OB = m_b / M_B. \tag{5.3.38}$$

With point O as the centre, we draw a circle having the radius

$$R = p_2' = p_a \sqrt{\frac{\mu_{Bb}}{m_a}\left(\frac{M_A}{M_A + m_a} + \frac{Q}{T_a}\right)}. \tag{5.3.39}$$

Then the radii forming a diameter of this circle (say, OC and OD) will represent the momenta of both the product particles in the centre-of-mass system, the segments $AO = m_b p_a / (M_B + m_b)$ and $OB = M_B p_a / (M_B + m_b)$ represent the momentum of the translatory motion of these particles, and hence the segments $AC = OC + AO$ and $CB = OB + OD = OB - OC$ represent the momenta of the particles in the laboratory system of coordinates. The angles at which the particles b and B escape in the laboratory system are equal to θ and ψ respectively, while the angle at which the particle b is ejected in the centre-of-mass system is θ'.

The momentum diagram was constructed for the case $Q > 0$, but the reasoning is valid for $Q < 0$ as well. Such a diagram can be used

to determine graphically the possible values of energies and the angles at which the products of a nuclear reaction escape.

The momentum diagram of reactions (5.3.24) and (5.3.25) was constructed in Fig. 186 for the case when the neutrons formed in these reactions escape at an angle of 90° to the incident deuterons.

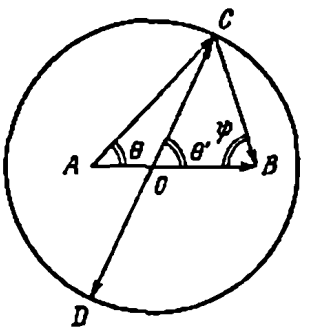

Fig. 185

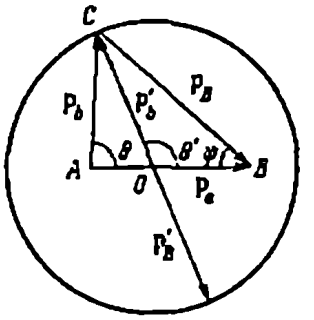

Fig. 186

It can be seen from the figure that the momentum p_b of the neutron can be obtained from the right-angled triangle AOC in which AO is defined by formula (5.3.33) and OC by formula (5.3.35). The computed values of p_b and $T_b = p_b^2/2m_b$ coincide with expression (5.3.29). If the momentum diagram is constructed to scale, the value of p_b, as well as the momentum p_B of the other product particle, can be determined with the help of a ruler.

5.4. Law of Conservation of Angular Momentum

5.4.1. General Remarks

The total angular momentum of the interacting particles in a nuclear reaction is conserved as well as its projection on a chosen direction.

Let us consider a reaction of the type

$$a + A \to O \to B + b.$$

In this case,

$$\mathbf{I}_1 = \mathbf{I}_O = \mathbf{I}_2, \tag{5.4.1}$$

where

$$\mathbf{I}_1 = \mathbf{I}_A + \mathbf{i}_a + \mathbf{l}_{Aa} \text{ and } \mathbf{I}_2 = \mathbf{I}_B + \mathbf{i}_b + \mathbf{l}_{Bb}. \tag{5.4.2}$$

Here, $\mathbf{I}_A$, $\mathbf{i}_a$, $\mathbf{I}_O$, $\mathbf{I}_B$ and $\mathbf{i}_b$ are the spins of the corresponding particles and can be either determined experimentally or calculated (for example, with the help of the shell model). It is well known that the proton spin is equal to 1/2, the spins of all even-even nuclei are

equal to zero, nuclei with an even mass number have integral spins and those with an odd mass number have half-integral spins. Since the angular momentum of a nucleus depends on the spins as well as the intrinsic motions (orbital angular momentum) of the nucleons, it has different values for different states. The *spin of a nucleus* is its angular momentum for the ground state.

The quantities l_{Aa} and l_{Bb} define the orbital angular momenta of the corresponding pairs of particles and characterize their relative motion. Orbital angular momentum can assume only integral values (0, 1, 2, . . .) and its specific value is determined by the nature of motion of the particles.

In considering a nuclear reaction of the type

$$a + A \to B + b,$$

one is usually interested in the initial and final states of the system, when the interacting particles are separated by such large distances that their motion can be considered to be free (independent). In this case, the initial and final states of the system can be described by wave-functions ψ_i and ψ_f which are products of three wave-functions:

$$\psi_i = \psi_A \psi_a \psi_{l_{Aa}}. \tag{5.4.3}$$

$$\psi_f = \psi_B \psi_b \psi_{l_{Bb}}. \tag{5.4.4}$$

The first two functions describe the intrinsic motion of particles A and a (B and b), while the third describes their relative motion (and spin orientation). If the motion of the particles is considered in a spherical system of coordinates, $\psi_{l_{Aa}}$ can be represented in the form

$$\psi_{l_{Aa}} = R(r)\, P_l^m(\cos\theta) \exp(im\varphi), \tag{5.4.5}$$

where $R(r)$ is a function of the distance between the particles, and $P_l^m(\cos\theta)$ is the associated Legendre function which has different forms for different values of the orbital angular momentum l_{Aa} and its projection m on the polar axis. A spherically symmetric function corresponds to the case $l_{Aa} = 0$ (motion with an impact parameter $\rho_0 = 0$), a linear function of $\cos\theta$ to the case $l_{Aa} = 1$ ($\rho_1 \simeq \lambda$), a linear function of $\cos^2\theta$ to the case $l_{Aa} = 2$ ($\rho_2 \simeq 2\lambda$), and so on. The function $\psi_{l_{Bb}}$ has a similar form.

It should be recalled that all vectors appearing in the expression (5.4.2) are quantum-mechanical, i.e. possess the following properties:

1. It is impossible to measure all the three components of a vector simultaneously. For the quantum-mechanical vector I, we can si-

multaneously measure only the square of its modulus $|\mathbf{I}|^2 = I(I+1)\hbar^2$ and one projection I_z on some direction z.

The projection may assume $2I+1$ values $I\hbar$, $(I-1)\hbar$, ..., $-(I-1)\hbar$, $-I\hbar$, corresponding to $2I+1$ different orientations of vector $\mathbf{I}$ in space.

2. The sum of two quantum-mechanical vectors $\mathbf{I}_1$ and $\mathbf{I}_2$ is not single-valued. The quantum number for the vector sum $\mathbf{I}_1 + \mathbf{I}_2$ can assume $2I_{\min}+1$ values:

$$I_1 + I_2,\ I_1 + I_2 - 1,\ \ldots,\ |I_1 - I_2|, \tag{5.4.6}$$

where $I_{\min}$ is the smaller of the two quantum numbers I_1 and I_2.

Application of the conservation law for angular momentum taking into account these properties results in certain selection rules which were encountered in the case of alpha and beta decays and gamma radiation. For example, the emission processes are not possible when nuclei undergo transitions between states with zero momenta, since a γ-quantum carries away an integral momentum ($l \neq 0$). Other cases involving the application of the law of angular momentum conservation will be encountered in the analysis of specific nuclear reactions (see Secs. 9.3 and 10.4).

Calculations are considerably simplified when one of the components (or the entire sum) in (5.4.2) is equal to zero. Of particular interest are the cases when $\mathbf{I}_O = 0$, $\mathbf{l}_{Aa} = 0$ and $\mathbf{l}_{Bb} = 0$. It can be easily seen that all these cases correspond to a spherically symmetric distribution of the nuclear products in the centre-of-mass system. Indeed, for $\mathbf{I}_O = 0$, there is no preferred direction in space relative to which anisotropic scattering can take place. If $\mathbf{I}_O \neq 0$ but $l_{Aa} = 0$, there is a preferred direction for the reaction products, but there is no such direction for the vector $\mathbf{I}_O$ in view of the spherical symmetry of the wave-function $\psi_{l_{Aa}}$ ($l_{Aa} = 0$). Finally, the case $l_{Bb} = 0$ corresponds to the spherically symmetric function $\psi_{l_{Bb}}$ characterizing the angular distribution of the reaction products.

5.4.2. The Role of Orbital Angular Momentum

The role of $l_{Aa} \neq 0$ is quite different when neutrons or charged particles interact with nuclei. It was shown in Sec. 3.2.4 by considering the example of alpha decay that in the interaction of particles with $l \neq 0$ we must take into account the centrifugal potential

$$V_c = \hbar^2 l(l+1)/2\mu r^2, \tag{5.4.7}$$

whose value is independent of the particle charge, increases as the square of l, and decreases as the square of r. The value of V_c for a

nucleon at the boundary of a nucleus ($r = R$) is called the *height* B_c *of the centrifugal barrier*:

$$B_c = V_c(R) = \frac{\hbar^2 l(l+1)}{2\mu R^2}$$

$$= \frac{10^{-54} l(l+1)}{2 \times 1.66 \times 10^{-24} \times (1.4 \times 10^{-13} A^{1/3})^2 \times 1.6 \times 10^{-6}} \approx \frac{10 l(l+1)}{A^{2/3}}, \quad (5.4.8)$$

where B_c is measured in megaelectron-volts.

The centrifugal potential is responsible for different interactions of neutral and charged particles having low energy with nuclei.

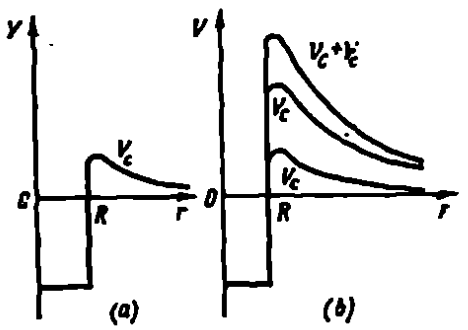

Fig. 187

In the interaction of neutrons with nuclei, there is no Coulomb barrier, but for $l \neq 0$ a centrifugal barrier of height $B_c = \hbar^2 l(l+1)/2\mu R^2$ appears (Fig. 187*a*). Hence neutrons with energy $T < B_c$ cannot effectively interact with the nucleus on account of a low penetrability D_c of the centrifugal barrier.

For an effective (above-barrier) interaction with nuclei at $l \neq 0$, the kinetic energy of the neutrons must satisfy the condition

$$T > \hbar^2 l(l+1)/2\mu R^2. \quad (5.4.9)$$

If the energy T of the neutrons is specified, condition (5.4.9) means that neutrons with a given energy effectively interact with a nucleus only when $l < l_T$, where

$$l_T(l_T+1) < 2\mu T R^2/\hbar^2 = p^2 R^2/\hbar^2 = (R/\lambda\!\!\!^{-})^2,$$

i.e.

$$l_T < R/\lambda\!\!\!^{-}_T. \quad (5.4.10)$$

For a given energy T, neutrons with $l > l_T$ practically do not interact with the nucleus since they cannot overcome the centrifugal barrier. It can be seen from formula (5.4.10) that l_T increases with the energy of the incident neutrons. At quite low neutron energies

$T < (B_c)_{min}$, the interaction of neutrons with $l \neq 0$ becomes practically impossible. Slow neutrons interact with nuclei only at $l \simeq 0$.

Table 23

Nucleus	$(B_c)_{min}$, MeV	B_C, MeV	Nucleus	$(B_c)_{min}$, MeV	B_C, MeV
$^{1}_{1}H$	20	1	$^{118}_{50}Sn$	0.8	10
$^{7}_{3}Li$	5.5	1.5	$^{238}_{92}U$	0.4	15
$^{16}_{8}O$	3.2	3.5			

Table 23 shows the minimum value of the centrifugal barrier[6] $(B_c)_{min}$ in MeV for $l = 1$:

$$(B_c)_{min} = 20/A^{2/3}. \quad (5.4.11)$$

It can be seen from Table 23 that right up to $T \simeq 20$ MeV, neutrons must interact with protons only for $l = 0$. This conclusion is experimentally confirmed by the isotropy of the angular distribution of $(n\text{-}p)$-scattering.

For heavy nuclei, the limiting energy is much lower, but even in this case quite slow neutrons interact with nuclei only for $l = 0$.

The situation is quite different for the charged particles, where the the Coulomb potential $V_C = Zze^2/r$ (see Fig. 187*b*) must be taken into consideration besides the centrifugal potential V_c. It was shown in Sec. 3.2.3 that the height $B_C = V_C(R)$ of the Coulomb barrier can be calculated from the simple formula (B_C is in MeV)

$$B_C = Zz/A^{1/3}. \quad (5.4.12)$$

The results of computation for $z = 1$ are given in Table 23. A comparison of the Coulomb barrier height with the minimum height of the centrifugal barrier shows that $(B_c)_{min}$ is higher than B_C only for the lightest nuclei ($Z < 8$), and for all other nuclei $B_C > (B_c)_{min}$. Beginning from the middle of the Periodic Table, $B_C \gg (B_c)_{min}$ and hence $B_C + (B_c)_{min} \simeq B_C$. Consequently, the interaction of slow ($T < B_C$) charged particles with quite heavy nuclei takes place with about the same probability for $l = 0$ and for $l = 1$. As l increases, the centrifugal barrier increases quadratically and the interaction probability decreases. However, for small l ($l \leqslant l_0$), the condition $B_C > B_c$ continues to hold and the interaction prob-

[6] Calculation of $(B_c)_{min}$ and B_C for light nuclei, and especially for a nucleon, with the help of formulas (5.4.11) and (5.4.12) gives quite rough results because of a fairly high uncertainty in the value of radius R (see Sec. 1.4 of this volume and Sec. 3.2, Vol. II. for a detailed account of radius R).

ability does not depend significantly on l as before. Only for quite large values of $l > l_0$ does the role of the centrifugal barrier become so significant that the interaction probability is considerably reduced. The limiting value l_0 can be roughly estimated by assuming that the Coulomb barrier and centrifugal barrier have the same order of magnitude at $l = l_0$:

$$B_c = \hbar^2 l_0 (l_0 + 1)/2\mu R^2 \simeq Zze^2/R = B_C.$$

This gives

$$l_0 (l_0 + 1) \simeq 2\mu B_C R^2/\hbar^2 = R^2/\lambda\!\!\!^{-2}_{B_C}, \quad \text{or} \quad l_0 \simeq R/\lambda\!\!\!^{-}_{B_C},$$

where $\lambda\!\!\!^{-}_{B_C} = \hbar/p_{B_C} = \hbar/\sqrt{2\mu B_C}$ is the de Broglie wave corresponding to the energy $T = B_C$.

The following value of l_0 is obtained as a result of more precise calculations:

$$l_0 = \sqrt{R/2\lambda\!\!\!^{-}_{B_C}}. \tag{5.4.13}$$

It is worth noting that the quantity l_0 does not depend on the energy of the incident particles. Thus, unlike neutrons, slow charged particles (with $T < B_C$) have comparable interaction probabilities at $l = 0$ and at $l = 1, 2, \ldots$ right up to $l_0 = \sqrt{R/2\lambda\!\!\!^{-}_{B_C}}$. Consequently, their angular distribution may be anisotropic in the centre-of-mass system.

In the above discussion, it was assumed that $T < B_C$. If $T > B_C$, the interaction of charged particles with nuclei becomes analogous to the interaction of neutrons. The interaction will be effective for $l \neq 0$ if

$$\Delta T = T - B_C > B_0 = \hbar^2 l (l + 1)/2\mu R^2. \tag{5.4.14}$$

If the energy T of the particle is specified, effective interaction should be observed for $l < l_{\Delta T}$, where $l_{\Delta T}$ satisfies the condition

$$l_{\Delta T} (l_{\Delta T} + 1) = 2\mu \Delta T R^2/\hbar^2 = p^2_{\Delta T} R^2/\hbar^2 = (R/\lambda\!\!\!^{-}_{\Delta T})^2.$$

Hence

$$l_{\Delta T} \simeq R/\lambda\!\!\!^{-}_{\Delta T}. \tag{5.4.15}$$

5.5. Law of Parity Conservation

It is well known that parity is conserved in strong and electromagnetic interactions (see Sec. 1.6). Nuclear transformations which we shall discuss here belong just to this type of interactions. Hence the law of parity conservation is valid for nuclear reactions. When applied to a nuclear reaction of the type

$$a + A \to B + b,$$

Chapter 6

Interaction of Neutrons with Nuclei

Interaction of neutrons with nuclei forms one of the most extensive and diverse classes of nuclear interactions. This is due to the fact that, together with protons, neutrons are essential constituents of every nucleus, where they are strongly bound by nuclear forces. Hence neutrons must effectively interact with a nucleus at short range. Unlike protons which cannot effectively interact with a nucleus at low energies on account of the Coulomb barrier, neutrons (being neutral particles) can interact with nuclei even at low energies.

6.1. Properties of Neutrons and Methods of Their Production

Neutron is a neutral particle ($z = 0$) with a spin $s_n = 1/2$ and a negative magnetic moment $\mu_n \simeq -1.9\mu_B$, which essentially determines the electromagnetic interaction of the neutron. Like protons, neutrons are assigned a unit baryon charge $B_n = +1$, isotopic spin $T = 1/2$ (with projection $T_\zeta = -1/2$) and a positive intrinsic parity $P_n = +1$. The mass of the neutron is $m_n = 1.00867$ amu $= 939.6$ MeV $= 1838.6m_e$, which is 1.3 MeV (or $2.5m_e$) larger than the proton mass. Consequently, neutron is a β-radioactive particle. It decays with a half-life $T_{1/2} \simeq 11$ min according to the scheme

$$n \to p + e^- + \tilde{\nu}_e. \qquad (6.1.1)$$

Investigation of the neutron structure carried out in the 1960s (see Sec. 3.3, Vol. II) led to the assumption that the neutron has a mutually compensated charge distribution, which is responsible for its magnetic moment.

It is well known (see Sec. 1.2.3) that neutrons were first obtained in the reaction involving the interaction of radium α-particles with beryllium nuclei:

$$^{9}_{4}\mathrm{Be}\,(\alpha, n)^{12}_{6}\mathrm{C}, \qquad Q = 5.5 \text{ MeV}. \qquad (6.1.2)$$

This reaction is used even today for obtaining neutrons with a wide energy spectrum. The (Ra-Be)-source has a very high neutron yield (about 2×10^7 neutrons per gram of Ra). A significant drawback of this source is that besides neutrons it also emits gamma radiation which frequently obscures the results of experiments.

The (Po-Be)-source does not suffer from this drawback, since alpha decay of Po is practically free from gamma radiation. This source also has a high neutron yield (about 3×10^6 neutrons per curie of Po).

A common drawback of both these neutron sources is that they have a wide energy spectrum.

Monoenergetic neutrons are obtained with the help of various reactions, some of which were described above [reactions (4.9.24) and (4.9.25)].

Besides these reactions, the following reactions are also widely employed for this purpose:

$$p + {}^{3}_{1}\mathrm{H} \rightarrow {}^{3}_{2}\mathrm{He} + n, \quad Q = -0.82 \text{ MeV}, \tag{6.1.3}$$

$$p + {}^{7}_{3}\mathrm{Li} \rightarrow {}^{7}_{4}\mathrm{Be} + n, \quad Q = -1.65 \text{ MeV}. \tag{6.1.4}$$

In these reactions, neutrons with energies $T_n = 60$ keV and 30 keV respectively are produced when the reactions proceed at the threshold value of the energy of protons $T_p = T_{\min}$. For $T_p > T_{\min}$, these reactions can be used to obtain monoenergetic neutrons with a higher energy, if the neutrons are registered at a definite angle to the incident protons.

Monoenergetic neutrons can also be obtained in the reaction of photodisintegration of deuterons:

$$\gamma + {}^{2}_{1}\mathrm{H} \rightarrow p + n, \quad Q = -2.22 \text{ MeV} \tag{6.1.5}$$

induced by γ-quanta from ThC'' ($^{208}_{81}$Tl, $E_\gamma = 2.62$ MeV). An analysis of this reaction shows (see Sec. 1.2.3) that it can serve as a source of neutrons with energy $T_n = 200$ keV.

Similarly, γ-quanta from RaC ($^{214}_{83}$Bi) with an energy $E_\gamma \simeq 1.78$ MeV induce photodisintegration of $^{9}_{4}$Be:

$$\gamma_{\mathrm{RaC}} + {}^{9}_{4}\mathrm{Be} \rightarrow 2{}^{4}_{2}\mathrm{He} + n, \quad Q = -1.65 \text{ MeV}, \tag{6.1.6}$$

leading to the emission of monoenergetic neutrons with an energy $T_n \simeq 110$ keV.

Photoneutron sources must be prepared in such a way that only gamma radiation can lead to the emission of neutrons. For this purpose, the radioactive specimen is isolated in an ampoule whose walls are impervious to α-particles. Naturally, such precautionary measures need not be taken if the radioactive specimen emits only gamma radiation. One such source is (^{124}Sb + Be) which emits monoenergetic neutrons with an energy of about 30 keV. For this source, radio-

active antimony is obtained by preliminary irradiation in a nuclear reactor.

Still slower neutrons are obtained as a result of moderation of fast neutrons. This process consists of successive elastic collisions of neutrons with nuclei of the moderator (see Sec. 6.3.1). The spectrum of neutrons emitted by the moderator has a maximum at the neutron energy equal to the thermal energy of the moderator atoms (thermal neutrons) and smoothly drops towards higher energies (see Sec. 6.3.2). Neutron spectroscopic methods are used for isolating neutrons with a definite energy from this spectrum (see Sec. 6.5).

New prospects of obtaining high-intensity beams of fast and slow neutrons appeared after the invention of nuclear reactors and cyclotron-like accelerators of charged particles. In accelerators, fast neutrons are produced as a result of (α, n)-, (p, n)- or (d, n)- reactions in which accelerated α-particles, protons or deuterons collide with the target. In most commonly used nuclear reactors, slow (mainly thermal) neutrons are obtained as a result of moderation of neutrons emitted in the nuclear fission reactions involving uranium or any other nuclear fuel. In both cases, the neutron beams have a by far higher intensity than from neutron sources. Especially high intensity of neutron beams [about 10^{18} neutrons/(cm^2·s)] is obtained in pulsed nuclear reactors.

Neutrons can also be obtained through the (γ, n)- reaction induced by γ-quanta formed in electron accelerators.

Certain transuranic elements having a high probability of spontaneous fission with the emission of fission neutrons (see Secs. 7.5.6 and 8.3.2) are sources of neutrons. Plutonium and americium are also used as sources of α-particles for preparing neutron sources of the type (Po-Be).

Finally, very fast neutrons (with energies of several hundred megaelectron-volts) are obtained during proton charge exchange and in deuteron stripping reactions (see Sec. 9.1 in this volume and Sec. 2.1.1, Vol. II).

6.2. Types of Interaction of Neutrons with Nuclei

6.2.1. Radiative Capture of Neutrons

One of the most prevalent types of neutron-induced nuclear reactions is the (n, γ)-reaction

$$(A, Z) + n \rightarrow (A + 1, Z) + \gamma, \qquad (6.2.1)$$

resulting in the formation of the nucleus $(A + 1, Z)$ which is usually β^--radioactive, i.e. disintegrates as follows:

$$(A+1, Z) \rightarrow (A+1, Z+1) + e^- + \tilde{\nu}. \qquad (6.2.2)$$

Since reactions of the type (n, γ) involve the capture of a neutron followed by the emission of a γ-quantum, they are called the *reactions of radiative capture of neutrons*.

Radiative capture reactions have a high probability of being induced by slow neutrons with an energy between 0 and 500 keV, and are widely used for detection of such neutrons.

An example of the (n, γ)-reaction is the capture by indium of neutrons with an energy of 1.46 eV:

$$^{115}_{49}\mathrm{In} + n \rightarrow {}^{116}_{49}\mathrm{In} + \gamma, \tag{6.2.3}$$

The radioactive isotope $^{116}_{49}\mathrm{In}$ formed in this process disintegrates with a half-life $T_{1/2} = 54$ min:

$$^{116}_{49}\mathrm{In} \rightarrow {}^{116}_{50}\mathrm{Sn} + e^- + \tilde{\nu}. \tag{6.2.4}$$

6.2.2. Reactions Involving the Formation of Protons

Reactions of the type (n, p) are frequently induced by neutrons with an energy $T_n \simeq 0.5$-10 MeV

$$(A, Z) + n \rightarrow (A, Z-1) + p. \tag{6.2.5}$$

Usually, $Q > 0$ for (n, p)-reactions (since $m_n > m_p$); if $Q < 0$, then $|Q| \simeq 1$ MeV. However, the neutron must have a quite high energy in order that the proton escaping from the nucleus is able to overcome the Coulomb barrier.

Examples of the (n, p)-reaction are the threshold reaction

$$^{32}_{16}\mathrm{S} + n \rightarrow {}^{32}_{15}\mathrm{P} + p, \tag{6.2.6}$$

having $Q \simeq -0.92$ MeV, and the reaction

$$^{14}_{7}\mathrm{N} + n \rightarrow {}^{14}_{6}\mathrm{C} + p, \tag{6.2.7}$$

which has $Q \simeq 0.6$ MeV and can be induced even by thermal neutrons (since light nuclei have a comparatively low barrier for the protons formed in such reactions). Reaction (6.2.6) was used for detecting fission neutrons in the first experiments on the investigation of fission of heavy nuclei, while reaction (6.2.7) is used for registering thermal neutrons by the photoemulsion method in which proton tracks of several microns are formed.

6.2.3. Reactions Involving the Formation of Alpha-particles

Reactions of the type (n, α) are quite widely used in nuclear physics:

$$(A, Z) + n \rightarrow (A-3, Z-2) + {}^{3}_{2}\mathrm{He}. \tag{6.2.8}$$

Such reactions also require neutrons with an energy between 0.5 and 10 MeV. In some cases, however, the reaction energy is so high (and the Coulomb barrier is so low) that the reaction has a high probability of being induced by thermal neutrons.

Examples of such reactions are

$$^{6}_{3}\mathrm{Li} + n \rightarrow {}^{3}_{1}\mathrm{H} + {}^{4}_{2}\mathrm{He}, \quad Q = 4.5 \text{ MeV}, \tag{6.2.9}$$

$$^{10}_{5}\mathrm{B} + n \rightarrow {}^{7}_{3}\mathrm{Li} + {}^{4}_{2}\mathrm{He}, \quad Q = 2.8 \text{ MeV}, \tag{6.2.10}$$

which are used for registering thermal neutrons (for this purpose, ionization chambers with a lithium coating, counters filled with the gaseous compound BF_3, boron glass counters, etc. are used). The cross sections of reactions (6.2.9) and (6.2.10) are so large (900×10^{-24} and 4000×10^{-24} cm^2 respectively) that both lithium and boron can be used in the form of naturally occurring isotopic mixtures (containing 7.5% $^{6}_{3}$Li and 19% $^{10}_{5}$B).

As an example of an endoergic reaction of the type (n, α), we can consider the interaction of neutrons with nitrogen:

$$^{14}_{7}\mathrm{N} + n \rightarrow {}^{11}_{5}\mathrm{B} + {}^{4}_{2}\mathrm{He}, \quad Q = -0.28 \text{ MeV}. \tag{6.2.11}$$

6.2.4. Fission Reactions

When heavy nuclei ($_{90}$Th, $_{91}$Pa, $_{92}$U and transuranic elements) are irradiated by neutrons with an energy $T_n > 1$ MeV (even thermal neutrons can be used for some isotopes of uranium and transuranic elements), a heavy nucleus disintegrates into two fission fragments with their average masses in the ratio 2 : 3,

$$(A, Z) + n \rightarrow (A_1, Z_1) + (A_2, Z_2), \tag{6.2.12}$$

where

$$A_1 + A_2 = A + 1, \quad Z_1 + Z_2 = Z,$$
$$\overline{A}_1 : \overline{A}_2 \simeq 2 : 3.$$

This type of reactions are called *fission reactions* and are usually denoted by (n, f).

Fission reactions are widely used for generating atomic (to be more precise, nuclear) energy (see Sec. 7.4).

6.2.5. Reactions Involving the Formation of Two or More Nucleons

For $T_n > 10$ MeV, reactions of the type $(n, 2n)$, (n, np), $(n, 3n)$, etc. become possible. These reactions are widely used for detecting fast neutrons (see Sec. 2.1.1, Vol. II). Some examples of such reactions are

$$^{12}_{6}\mathrm{C} + n \rightarrow {}^{11}_{6}\mathrm{C} + 2n, \tag{6.2.13}$$

$$^{63}_{29}\mathrm{Cu} + n \rightarrow {}^{62}_{29}\mathrm{Cu} + 2n. \tag{6.2.14}$$

The threshold energy values for these reactions are 20 and 10 MeV respectively.

The high threshold values for reactions of the type $(n, 2n)$ and other similar reactions is apparently due to the fact that, as a rule, the separation energy of two nucleons is higher than the corresponding value for one nucleon (see Sec. 1.3.4).

An interesting exception is the $(n, 2n)$-reaction for beryllium:

$$^{9}\mathrm{Be} - n \rightarrow 2^{4}\mathrm{He} + 2n \qquad (6.2.15)$$

having a threshold of just 2 MeV.

6.2.6. Inelastic Scattering of Neutrons

A neutron having an energy of a few hundred kiloelectron-volts can excite a nucleus upon entering it, and then leave it (the nucleus may not necessarily emit the same neutron that entered it), albeit with a reduced energy. This process is called *inelastic scattering of a neutron*. Of course, the limiting energy $T_n > 0.5$ MeV (as well as the energy values in other cases) is a quite rough estimate, since its position for each specific nucleus depends on the distribution of excited state levels.

6.2.7. Elastic Scattering of Neutrons

Finally, let us consider the process of *elastic scattering* of neutrons. As a result of the elastic scattering, the nucleus remains in the same state and the neutron retains its initial kinetic energy in the centre-of-mass system (in the laboratory system of coordinates, the total kinetic energy of the neutron and the nucleus is conserved).

Elastic scattering of neutrons is used quite extensively for registering fast neutrons by observing the tracks of the recoil nuclei (mostly recoil protons) in various tracking instruments (Wilson's cloud chamber, nuclear emulsion, bubble chamber, etc.). This type of scattering is also used for registering recoil nuclei by ionization methods (ionization chambers, counters).

We mentioned earlier the role of elastic scattering in the moderation of fast neutrons, which is one of the most important processes taking place in a nuclear reactor. The diffusion of thermal neutrons is also a typical form of elastic scattering.

In view of the limited scope of this book, we shall confine ourselves to just a few phenomena that are directly associated with nuclear physics. These include the theory of moderation of fast neutrons and diffusion of thermal neutrons, interaction of slow neutrons with nuclei and Bohr's theory of nuclear reactions, methods of neutron spectroscopy, scattering of fast neutrons (applied for determining nuclear radii), and the physics of nuclear fission.

of the recoil energy of protons, carried out with the help of an ionization chamber, as well as other experiments (see Sec. 1.5.1, Vol. II), showed that all the values of the proton energy (and hence the neutron energy as well) are equally probable (Fig. 189). Consequently, the spectrum of the scattered neutrons after the first collision has the form

$$f_1(T)\,dT = dT/T_0 \tag{6.3.3}$$

(the spectrum is normalized to unity). Obviously, the average energy of neutrons after the first collision is

$$\overline{T_1} = T_0/2. \tag{6.3.4}$$

In this uniform spectrum, we isolate a portion of width dT' in the region of a certain energy T' of neutrons. The number of such neutrons is $dN = dT'/T_0$. In analogy with the above considerations, these neutrons after collision with protons (second collision of neutrons) will have all possible energy values from 0 to T' with the same probability (small horizontal rectangle in Fig. 189). Consequently, their contribution to the interval dT of the neutron spectrum for an energy $T < T'$ after the second collision is given by

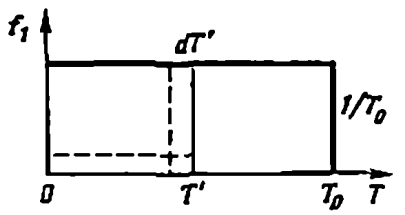

Fig. 189

$$\Delta N = (1/T_0)\,(dT'/T')\,dT. \tag{6.3.5}$$

The total contribution to the interval dT from all neutrons with energy $T' > T$ is

$$\frac{dT}{T_0}\int_T^{T_0}\frac{dT'}{T'} = \frac{dT}{T_0}\ln\frac{T_0}{T} \tag{6.3.6}$$

Hence the neutron spectrum acquires the following form after the second collision:

$$f_2(T) = (1/T_0)\ln(T_0/T). \tag{6.3.7}$$

This spectrum can be obtained graphically by dividing the rectangle in Fig. 189 into a series of narrow vertical columns having a width ΔT each (Fig. 190*a*). For a quite small ΔT, neutrons in each column can be treated as monoenergetic. Hence in accordance with the above arguments, each vertical column will be transformed after the second collision into a rectangle of equal area whose length will

depend on the position of the column (Fig. 190b). The enveloping curve gives the approximate shape of the spectrum $f_2(T)$, i.e. corresponds to formula (6.3.7) as $\Delta T \to 0$. It follows from Fig. 190b and formula (6.3.7) that after two collisions with protons, the neutron spectrum is no longer uniform (unlike after one collision), but decreases monotonically according to a logarithmic law.

In the above discussion, we have not taken into account the thermal motion of the atoms of the medium in which the neutrons are slowed down. On account of this thermal motion, the neutrons are

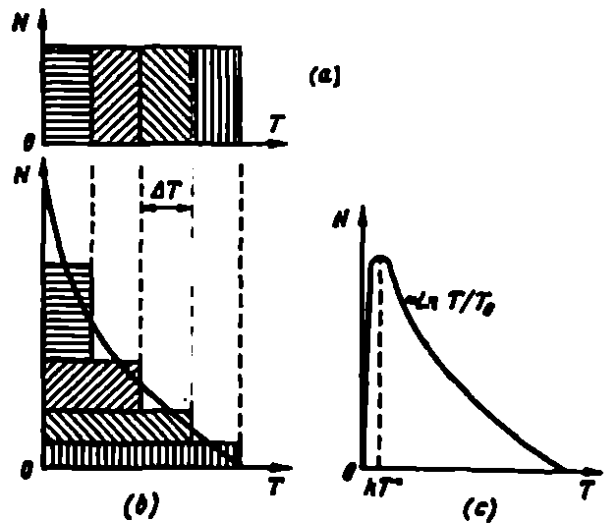

Fig. 190

practically slowed down only to the thermal energy kT° at which the monotonic nature of the spectral curve is violated (see Fig. 190c)[2]. The average energy of the neutrons after the second collision is given by

$$\bar{T}_2 = \frac{\int_0^{T_0} T f_2(T)\,dT}{\int_0^{T_0} f_2(T)\,dT} = \frac{\int_0^{T_0} T \ln \frac{T_0}{T}\,dT}{\int_0^{T_0} \ln \frac{T_0}{T}\,dT} = \frac{T_0}{2^2}. \qquad (6.3.8)$$

It can be easily seen that the majority of neutrons (about 60%) has an energy

$$T < \bar{T}_2 = T_0/2^2. \qquad (6.3.9)$$

[2] The absolute temperature is denoted by T° in order to distinguish it from the kinetic energy T. See Sec. 6.3.2 for a detailed description of the thermal energy.

A similar analysis shows that after the third collision the neutron spectrum has the form

$$f_3(T)=\frac{1}{2T_0}\left(\ln\frac{T_0}{T}\right)^2, \tag{6.3.10}$$

while after the nth collision the shape of the spectrum is given by

$$f_n(T)=\frac{1}{(n-1)!T_0}\left(\ln\frac{T_0}{T}\right)^{n-1}. \tag{6.3.11}$$

The average energy of neutrons after the nth collision is[3]

$$\overline{T}_n=\frac{\int_0^{T_0} Tf_n(T)\,dT}{\int_0^{T_0} f_n(T)\,dT}=\frac{T_0}{2^n}. \tag{6.3.12}$$

It would appear that this formula can be used for determining the number n of collisions required to slow down a neutron to a given energy T, by using the relation

$$n=\log_2\frac{T_0}{T}=\frac{\ln\frac{T_0}{T}}{\ln 2}=1.4\ln\frac{T_0}{T}. \tag{6.3.13}$$

This, however, is not true.

It can be easily seen that the average energy $\overline{T}_n$ of neutrons is not a very reliable characteristic for their moderation since most neutrons have an energy $T<\overline{T}_n$ for a logarithmically decreasing spectrum.

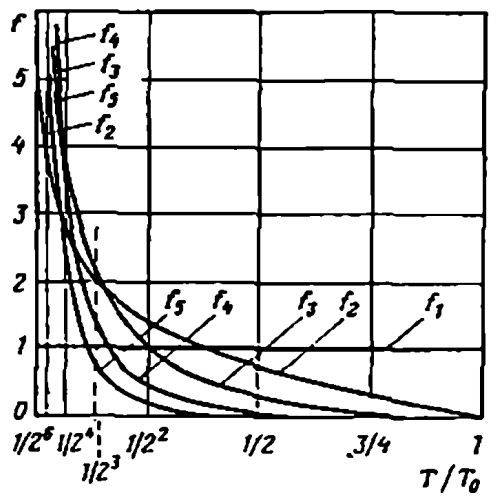

Fig. 191

Figure 191 shows the deformation of the neutron energy spectrum after first, second, and subsequent collisions.

It can be seen from the figure that as the number n of collisions increases, the fraction of slow neutrons increases rapidly. For each specific value T of the final energy of the moderated neutrons, there exists an optimal number n_{opt} of collisions beyond which the spectrum will contain the maximum number of neutrons with this energy. Subsequent collisions lead to a decrease in this number. Thus,

[3] Formula (6.3.11) was first obtained in 1935 by Kurchatov, Artsimovich *et al.* [*Zh. Eksp. Teor. Fiz.*, 5, 659 (1935)].

for example, the highest number of neutrons with energy $T = \overline{T}_3 = T_0/2^3$ is practically attained at $n = 2$ (curve f_2), remains unchanged for $n = 3$ (curve f_3), and decreases for $n \geqslant 4$ (curves f_4 and f_5).

The correct value of the average number $\bar{n}$ of collisions needed to slow down the maximum number of neutrons to a certain energy T can be obtained with the help of formula (6.3.11) by averaging[4] over all values of n, assuming that the energy T remains *constant*:

$$\bar{n} = \frac{\sum_1^\infty n f_n(T)}{\sum_1^\infty f_n(T)} = \frac{\sum \frac{n}{(n-1)!}\left(\ln\frac{T_0}{T}\right)^{n-1}}{\sum \frac{1}{(n-1)!}\left(\ln\frac{T_0}{T}\right)^{n-1}} = \ln\frac{T_0}{T} + 1 \quad (6.3.14)$$

or, for large values of $\ln(T_0/T)$,

$$\bar{n} \simeq \ln(T_0/T). \quad (6.3.15)$$

Thus, for example, the average number of collisions required to slow down neutrons from energy $T = 5$ MeV to thermal energy $kT^\circ = 0.025$ eV is

$$\bar{n} = \ln(5 \times 10^6/0.025) = \ln(2 \times 10^8) \simeq 18$$

as against the value 27 obtained from formula (6.3.13).

The quantity $\ln(T_0/T)$ is called the *lethargy of neutrons*. It is extensively used in the theory of moderation of neutrons.

We have considered above the case of hydrogen as a moderator ($A = 1$). If we use a moderator with $A \neq 1$, the elastic scattering of neutrons by these nuclei is described by the momentum diagram shown in Fig. 150. It can be seen from this figure that

$$AC = p_n^{\min} = \frac{A-1}{A+1}\, p_0, \qquad AB = p_n^{\max} = p_0. \quad (6.3.16)$$

Thus, unlike hydrogen, moderators with $A \neq 1$ cannot make a neutron lose all its energy in a single collision. The energy spectrum of neutrons after the first collision lies between

$$T_n^{\min} = \left(\frac{A-1}{A+1}\right)^2 T_0 \quad \text{and} \quad T_n^{\max} = T^0. \quad (6.3.17)$$

We shall show that the spectrum is uniform within these limits.

Suppose that a neutron flies past a nucleus at a distance ρ (Fig. 192). The angular momentum of the neutron with respect to the nucleus is equal to $p\rho \approx \hbar l$, where l is the orbital angular momentum. Hence

[4] Since n is a discrete quantity, averaging is done by summation and not by integration.

$\rho \simeq \lambda l$. For the scattering to be caused by the nuclear forces, the condition $\rho = \lambda l < a$ or $l < a/\lambda$ must be satisfied a being the range of nuclear forces. Assuming that a is equal to the mean separation between nucleons in the nucleus, $\delta = 2 \times 10^{-13}$ cm (see Sec. 2.1),

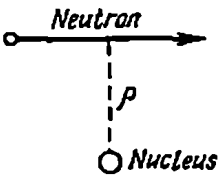

Fig. 192

and using formula (3.2.24), we obtain $\lambda > 2 \times 10^{-13}$ cm, i.e. $l < 1$ if $T < 5$ MeV.

Thus, scattering of neutrons with a not very high value of energy can take place only with $l = 0$, i.e. the scattering is spherically symmetric in the centre-of-mass system:

$$\frac{dN}{d\Omega'}(\theta') = \text{const}, \qquad dN \propto d\Omega'. \tag{6.3.18}$$

However, we can see from the triangle ADO in Fig. 150 that

$$AD^2 = AO^2 + OD^2 + 2AO\,OD\cos\theta', \quad \text{i.e.} \quad p_n^2 = \frac{A^2+1+2A\cos\theta'}{(A+1)^2}\,p_0^2$$

or

$$T_n/T_0 = p_n^2/p_0^2 = [A^2 + 1 + 2A\cos\theta']/(A+1)^2.$$

This gives

$$\frac{dT_n}{T_0} = -\frac{2A\sin\theta'\,d\theta'}{(A+1)^2} \propto d\Omega'. \tag{6.3.19}$$

Comparing (6.3.19) with (6.3.18), we find that $dN \propto dT_n$, which means that the spectrum is uniform (Fig. 193).

The width of the rectangular spectrum thus obtained is given by

$$\Delta T = T_n^{\max} - T_n^{\min} = 4AT_0/(A+1)^2.$$

Consequently, the normalized height is equal to $(A+1)^2/(4AT_0)$.

Naturally, since $T_n^{\min} \neq 0$ in a heavy moderator, the slowing-down process is not so rapid as in hydrogen. Thus, for example, the minimum energy of neutrons after the ith collision in carbon ($A = 12$) is equal to $(11/13)^{2i}$; this value is equal to $0.72T_0$ after the first collision, $0.52T_0$ after the second collision, and so on. It can be easily seen that $T_n^{\min}$ attains a value of 1 eV only after the seventieth collision.

Exact calculations lead to the following formula for the average number of collisions:

$$\bar{n} = (1/\xi) \ln (T_0/T), \qquad (6.3.20)$$

where ξ is the average logarithmic loss of energy per collision,

$$\xi = \overline{\ln (T'/T'')} = 1 + [(A-1)^2/2A] \ln [(A-1)/(A+1)] \qquad (6.3.21)$$

(T' and T'' are the neutron energies before and after the collision).

It follows from formula (6.3.20) that the quantity ξ is one of the most important characteristics of a moderator. [8] The higher the value

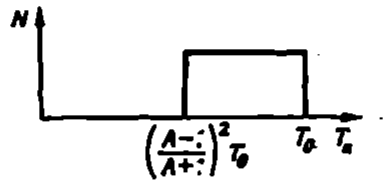

Fig. 193

of ξ, the better the moderator (other conditions remaining the same; see Table 24 in Sec. 6.3.5). It should be noted that $\xi \simeq 2/(A + 2/3) \simeq 2/A$ for quite large A ($A \geqslant 12$), so that we can use the approximate formula

$$\bar{n} = \left(\frac{A}{2} + \frac{1}{3}\right) \ln \left(\frac{T_0}{T}\right) \simeq \left(\frac{A}{2}\right) \ln \left(\frac{T_0}{T}\right). \qquad (6.3.22)$$

It follows from this formula that n is very large for heavy nuclei. For example, in the case of uranium ($A = 238$), neutrons with energy 5 MeV can be slowed down to thermal energy only after $\bar{n} \simeq (A/2) \ln (T_0/T) = 119 \ln (5 \times 10^6/0.025) \simeq 2200$ elastic collisions.

A more correct approximation of formula (6.3.20) should be used for light nuclei:

$$\bar{n} = \left(\frac{A}{2} + \frac{1}{3} + \frac{1}{18A}\right) \ln \frac{T_0}{T}. \qquad (6.3.23)$$

This gives a 90% accuracy even in the case of a deuteron moderator ($A = 2$).

Finally, we shall make two remarks concerning the moderation in the region of high and low neutron energies.

1. In the above discussion, it was assumed that neutrons are slowed down only as a result of elastic collisions with nuclei. In the general case, neutrons can also be slowed down by inelastic collisions if their kinetic energy exceeds the excitation energy for the first excited level

[8] Other important characteristics of a moderator are the scattering cross section σ_s and the absorption cross section σ_a for thermal neutrons (see Secs. 6.3.4 and 6.3.5).

of the scattering nuclei. For light nuclei (which are considered to be the best moderators if we take into account the parameter ξ), however, the first excited level is usually several megaelectron-volts higher than the ground level. Hence in most of the practical problems in which the moderation of neutrons with a relatively low initial energy by light nuclei is considered (the average energy of the fission spectrum neutrons is about 2 MeV), the effect of inelastic scattering need not be taken into consideration.

In heavy nuclei, the first excited level is closer to the ground level than in light nuclei (the mean separation between these levels is several hundred kiloelectron-volts). Hence neutrons are slowed down quite effectively as a result of inelastic collisions with heavy nuclei. But even in this case the role of inelastic collisions is confined to just a few first collisions. On account of significant loss of kinetic energy in these collisions, the residual energy of neutrons is not sufficient to excite the nucleus, and the process then takes place only through elastic collisions.

2. If the energy of the neutrons being moderated becomes comparable with the chemical binding energy of the moderator atoms ($T \simeq 1$ eV), the nature of moderation of neutrons (the rate of moderation and the angular distribution) changes. This is mainly due to an increase in the effective mass of the particles with which a neutron collides.

While hydrogen atoms in the molecules of a moderator (say, water) can be considered to be free at energies $T_n > 1$ eV, this cannot be done at $T_n \simeq 1$ eV. A neutron with such an energy does not knock out a proton from a molecule, but only excites vibrational or rotational levels in it, and for $T_n < 1$ eV, the neutron is scattered elastically by the molecule which behaves as a single heavy particle. Thus the reduced mass of the neutron and proton is doubled. This leads to a change in the scattering cross section, mean energy loss per collision and the mean value of the cosine of the scattering angle.

Besides the chemical bond, the thermal motion of the moderator atoms also influences the process of slowing down of neutrons with energy below $\sim$1 eV (see Sec. 6.3.2). The process of slowing down of neutrons with such values of energy is called *thermalization* (in the case of water, $T_n < 0.3$ eV). The main characteristic feature of thermalization is a decrease in the moderation rate. The final stage of thermalization is the onset of thermal equilibrium between neutrons and the moderator atoms.

6.3.2. Thermal Neutrons

It was mentioned above that a considerable increase in the neutron scattering cross section by the moderator nuclei to values exceeding the capture cross section is the necessary condition for an effective

slowing down of neutrons. In this case, the neutron energy will fall during moderation until it becomes equal to the thermal energy of the moderator atoms, viz.

$$T_{\text{therm}} = kT^{\circ}, \tag{6.3.24}$$

where k is the Boltzmann constant and T° is the absolute temperature.

Neutrons having such energies are called *thermal* neutrons.

It can be easily calculated that at room temperature ($T^{\circ} \simeq 300$ K), the most probable velocity of thermal neutrons is 2.2×10^{5} cm/s and the thermal energy corresponding to this velocity is

$$kT^{\circ} \simeq 0.025 \text{ eV} \tag{6.3.25}$$

[the average thermal energy of a particle is equal to (3/2) kT°].

Subsequent collisions of thermal neutrons with the moderator nuclei do not slow down the neutrons any further, since the latter have equal probabilities of losing or gaining energy equal to about kT° (all nuclei of the moderator have an energy of this order). Hence thermal neutrons only move, or diffuse, in the material upon subsequent collisions (their average energy still remains equal to the thermal energy) until they are absorbed by a nucleus or leave the moderator. As a result, thermal neutrons are accumulated inside the moderator. The neutron spectrum in the moderator should be close to Maxwellian distribution curve with a raised right wing (due to a continuous arrival of fast neutrons in the moderator). Calculations show that the decrease in the number of neutrons at high energies must be governed by the law $T^{-3/2}$ (Fig. 194). These neutrons (whose energy is higher than that of the neutrons in the Maxwellian spectrum) are called *epithermal* neutrons. Neutrons whose energy is lower than that of thermal neutrons (left part of the curve) are called *cold* neutrons (see Sec. 6.5.4 for details). All neutrons with $T_n > 0$, including cold, thermal and epithermal neutrons, are called *slow* neutrons. The upper boundary of the slow neutron spectrum is quite arbitrary. Sometimes, it is "stretched" to 10^{4}-10^{6} eV and sometimes even neutrons with energy $T_n > 10^{4}$ eV are called fast neutrons (see, for example, Sec. 7.4.3).

The correctness of these arguments concerning the properties of thermal neutrons can be verified experimentally. The idea of the experiment to prove the existence of thermal neutrons lies in an attempt to observe a change in the energy of thermal neutrons upon a change in the temperature of the moderator. The experimental set-up is schematically shown in Fig. 195. A vessel containing paraffin oil into which a neutron source is immersed is placed between a heater and an absorber. The detector is a BF_3-filled counter. The aim of the experiment is to measure the fraction of neutrons passing through the absorber for various thickness (the so-called transmission

of the absorber), viz.

$$P = N/N_0 = \exp(-n\sigma x) \qquad (6.3.26)$$

and to plot the dependence of ln P on thickness x (Fig. 196).

This dependence must be linear:

$$\ln P = -n\sigma x. \qquad (6.3.27)$$

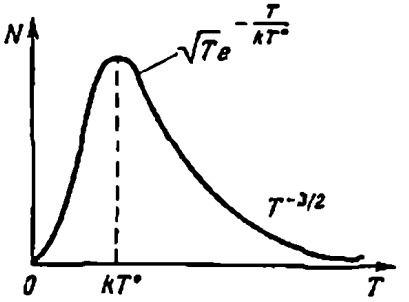

Fig. 194

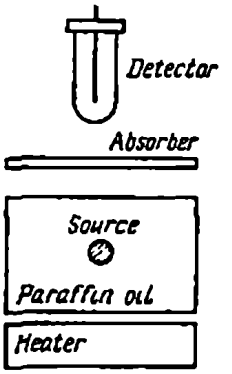

Fig. 195

The slope of this straight line determines the interaction cross section of neutrons at the given temperature

$$\tan\alpha = n\sigma. \qquad (6.3.28)$$

Measurements of the cross section carried out with a boron absorber at different temperatures of the paraffin oil led to the following dependence of cross section on temperature:

$$\sigma \propto 1/\sqrt{T^\circ}. \qquad (6.3.29)$$

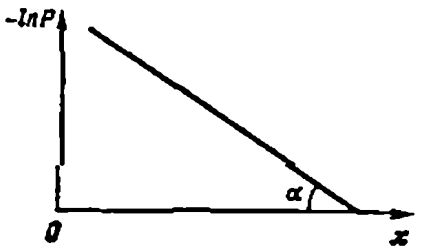

Fig. 196

The results of this experiment can be explained as follows. Slowing down of fast neutrons indeed leads to the formation of thermal neutrons whose energy is determined by the temperature of the moderator:

$$T_{\text{therm}} = kT^\circ.$$

Thermal neutrons constitute a considerable part of neutrons leaving the moderator and being registered by the detector. The cross section of neutron capture by boron depends on the neutron energy and varies according to the law

$$\sigma \propto 1/\sqrt{T} \propto 1/v \qquad (6.3.30)$$

called the $1/v$-law.

In the same experiment, it was shown that if a cadmium sheet of about 1 mm thickness is placed between the moderator and the absorber (or between the absorber and the detector), the observed temperature dependence completely disappears. Consequently, it can be stated that Cd is a very strong absorber of thermal neutrons.

Later, the existence of thermal neutrons was confirmed by the neutron spectroscopy methods (see Sec. 6.5.4).

6.3.3. Resonance Neutrons

It can be seen from Fig. 194 that the spectrum of neutrons in a moderator contains, besides thermal neutrons, many neutrons with a higher energy. In order to detect these neutrons, Fermi measured the transmission through cadmium with the help of detectors made of silver and rhodium (Fig. 197).

In these materials, neutrons emitted by a moderator induce the following radiative-capture reactions:

$$^{109}_{47}\mathrm{Ag}\,(n,\,\gamma)\,^{110}_{47}\mathrm{Ag}, \qquad (6.3.31)$$

$$^{103}_{45}\mathrm{Rh}\,(n,\,\gamma)\,^{104}_{45}\mathrm{Rh}. \qquad (6.3.32)$$

This is followed by a disintegration of the β-radioactive isotopes formed in these reactions:

$$^{110}_{47}\mathrm{Ag} \xrightarrow[24\ \mathrm{s}]{\beta^-} {}^{110}_{48}\mathrm{Cd}, \qquad (6.3.33)$$

$$^{104}_{45}\mathrm{Rh} \xrightarrow[44\ \mathrm{s}]{\beta^-} {}^{104}_{46}\mathrm{Pd}. \qquad (6.3.34)$$

By measuring the beta radioactivity with the help of beta counters, we can determine the number of neutrons passing through the absorber and registered by the detector.

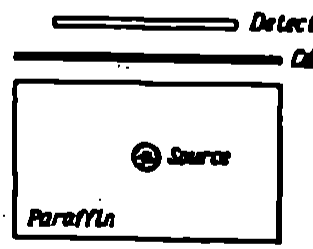

Fig. 197

The results of the experiment are shown in Fig. 198 in which the transmission of cadmium (measured by silver and rhodium detectors) is plotted as a function of its thickness. It can be seen from the figure that as the thickness of the absorber increases, the transmission of cadmium decreases very rapidly at first, and then attains a practically constant value of about 0.5 for silver and 0.3 for rhodium. Obviously, the steep fall in the curves at the initial stage corresponds to the absorption of thermal neutrons by cadmium. Estimation of the absorption cross section carried out by the above-men-

tioned method of determining the slope of the straight line $\ln P = -\sigma n x$ gives the following value:

$$\sigma_{kT^\circ}(\mathrm{Cd}) \simeq 2500 \times 10^{-24}\ \mathrm{cm}^2. \qquad (6.3.35)$$

It can be easily calculated that for such a cross section, a cadmium foil of 1 mm thickness allows about one-thousandth part of thermal neutrons incident on it to pass through. Hence cadmium is a very good absorber of thermal neutrons.

The right-hand parts of the curves correspond to the effect induced in the detectors by neutrons transmitted through cadmium, i.e.

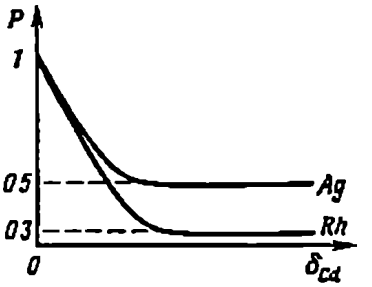

Fig. 198

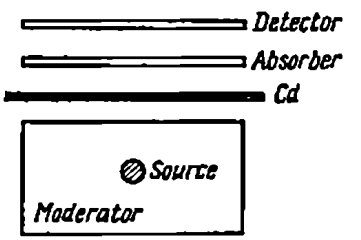

Fig. 199

not by thermal neutrons but by neutrons that have not attained thermal equilibrium and whose energy is higher than thermal energy ($T > kT^\circ$). These neutrons in the spectrum of neutrons being slowed down were called *epicadmium* neutrons. It can be seen from Fig. 198 that epicadmium neutrons are responsible for a considerable part of the activity of detectors (30% in Rh and 50% in Ag), i.e. react strongly with the nuclei of these materials.

This result is in contradiction with the $1/v$-law of variation of cross section, which was established for the capture of thermal neutrons by boron. Indeed, if this law were valid for Ag and Rh, the capture cross section of epicadmium neutrons ($v_{\mathrm{epiCd}} > v_{kT^\circ}$) would have to be less than the capture cross section of thermal neutrons and the effect of epicadmium neutrons would not be so strong.

A detailed investigation of the properties of epicadmium neutrons was carried out in a series of experiments whose set-up is shown schematically in Fig. 199. Here, a source surrounded by a moderator is under a 1-mm thick cadmium sheet, above which an absorber whose thickness can be varied and a detector are arranged. The activity A of the detector is measured in four different versions (at different thickness of the absorber): (1) with cadmium and the absorber ($A_{\mathrm{Cd\,abs}}$), (2) with cadmium but without the absorber (A_{Cd}), (3) without Cd but with the absorber (A_{abs}), and (4) without Cd and without the absorber (A_0).

The obtained data were used to plot the transmission as a function of the absorber thickness separately for thermal and epicadmium neutrons:

$$P_{epiCd}(\delta) = A_{Cd\ abs}/A_{Cd},\ P_{kT^\circ}(\delta) = (A_{abs} - A_{Cd\ abs})/(A_0 - A_{Cd}). \quad (6.3.36)$$

Two series of measurements were made. In one series, the absorber and the detector were prepared from different materials (abs ≠ det), while the same material was used for them in the second series (abs = det).

The results of measurements are shown in Fig. 200*a* and *b*. A comparison of these figures shows that for abs = det the absorption of epicadmium neutrons is much stronger than that of thermal neutrons, while the reverse situation prevails for abs ≠ det.[6]

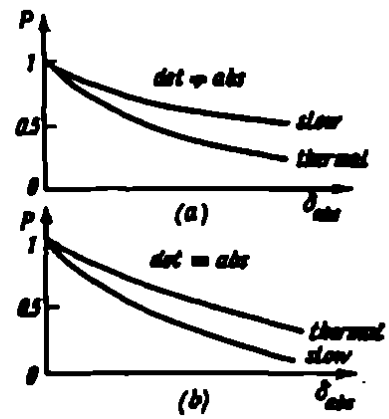

Fig. 200

These results can be explained by assuming that each material is characterized by a sharp selectivity in its ability to capture neutrons of a certain (resonance) energy, and that the resonance regions for different materials do not overlap. In this case, the absorption of resonance neutrons in the absorber for abs ≠ det cannot affect the activity of the detector, since the latter is not activated by these neutrons. Conversely, for abs = det, resonance energy of neutrons is the same for the absorber and the detector ($T_{abs} = T_{det}$) and hence the detector must sharply perceive the absorption of its resonance neutrons in the absorber.[7]

The resonance energies for various materials were initially determined by the boron method which involves the application of the well-known law ($\sigma \propto 1/v$) for absorption of neutrons by boron.

Since $\sigma \propto 1/\sqrt{T}$ for boron, we can write

$$\sigma_{kT^\circ}/\sigma_{res} = \sqrt{T_{res}/kT^\circ}. \quad (6.3.37)$$

The values of σ_{kT° and σ_{res} are determined with the help of the experiments described above, taking boron as the absorber and the material whose resonance energy T_{res} is to be found as the detector.

---

[6] In Fig. 200, epicadmium neutrons are termed slow neutrons (Fermi's terminology).

[7] The resonant absorption of neutrons of a definite energy was explained by I.V. Kurchatov and G.Ya. Shchepkin [*Phys. Z. Sow.*, 9, 1, 102 (1936)].

As a result, the following quite rough values of T_{res} were obtained for various materials that were employed as detectors:

Material	In	Rh	Ag	Au
T_{res}, eV	1	1	3	4

Naturally, the accuracy of the boron method is not sufficient for determining the width of the resonance capture range for In and Rh. However, it is clear that this quantity is not large since In and Rh, for which identical values of the resonance energy are obtained, behave as different materials in the above experiments (abs $\neq$ det). It can be assumed that the level width Γ is at least an order of magnitude lower than the value of the resonance energy, i.e. does not exceed 0.1 eV.

Finally, let us summarize the results obtained in the above experiments. The cross section of interaction of epicadmium neutrons with matter can obey the $1/v$-law (as in the case of boron) only if there are no resonance levels. As the energy approaches the resonance level ($\sigma = \sigma_{res}$), the cross section increases abruptly and then falls once again.

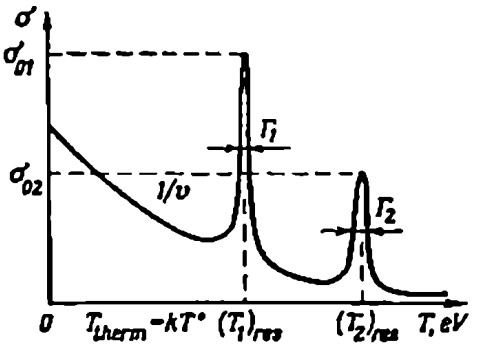

Fig. 201

An analysis of many heavy nuclei shows that their resonance levels are situated at an energy of several electron-volts. Apparently, this indicates that the separation between levels in this energy range is also of the same order (1-10 eV). Thus, the possibility of the same nucleus having several levels cannot be ruled out. In this case, as the energy approaches the second level, the cross section increases once again, and so on (Fig. 201).

Since the width Γ of levels is very small while the effect due to resonance neutrons is very strong, the resonance cross section has usually a very large value.

We shall see at a later stage that the entire body of facts described here led to the theory of nuclear reactions (Sec. 6.4), which was confirmed by experiments on neutron spectroscopy (Sec. 6.5).

For about two decades, the Bohr theory played a decisive role in explaining various nuclear processes. At present, nuclear reactions are interpreted by this theory, as well as by the direct interaction mechanism (see Chap. 10).

6.3.4. Basic Principles of the Slowing-down Theory

During the slowing-down process, a neutron follows a complex trajectory, moving from one moderator nucleus to another. The mean path traversed by a neutron between two successive collisions is called the mean free path λ_s. Obviously,

$$\lambda_s = 1/n\sigma_s, \tag{6.3.38}$$

where n is the number density of nuclei in the medium and σ_s is the effective scattering cross section.

It can be seen from formula (6.3.38) that the quantity λ_s is different for different media and is a function of the neutron energy for a given medium.[8] Like ξ, the quantity λ_s is one of the most important characteristics of a moderator, since the slowing down occurs more rapidly for materials with low λ_s. The coefficient ξ/λ_s is called the *moderating power of a moderator*.

During each act of scattering, a neutron deviates from its initial direction of motion, and hence it follows a zigzag path in the moderator. The total length of the path traversed by a neutron during the slowing down from its initial energy T_0 to a given energy T is

$$\Lambda = \sum_{1}^{\bar{n}} \lambda_s(T_l), \tag{6.3.39}$$

where $\bar{n} = (1/\xi) \ln (T_0/T)$ is the average number of collisions required to slow down neutrons from energy T_0 to energy T [see formula (6.3.20)], and $\lambda_s(T_l)$ is the mean free path at an energy corresponding to the lth act of scattering.

Neglecting the dependence of λ_s on energy, we can obtain a rough estimate for Λ by multiplying $\bar{n}$ by $\bar{\lambda}_s$:

$$\Lambda = \bar{n}\bar{\lambda}_s, \tag{6.3.40}$$

where $\bar{\lambda}_s$ is the mean free path averaged over the energy interval in which the slowing down is considered. When fast neutrons ($T_n > 50$ keV) are slowed down in hydrogen, λ_s can be assumed to be proportional to v, while $\lambda_s \simeq$ const for neutrons with energy 1 eV $< T_n <$ 50 keV. For other light elements, $\lambda_s \simeq$ const.

In order to solve certain problems (for example, to calculate the shielding design), it is very important to know the distance r to which neutrons are displaced from their initial position during slow-

[8] The values of λ_s and other characteristics of moderators are given in Tables 24 and 25 at the end of Sec. 6.3.

ing down. Obviously, the quantity Λ cannot serve as a measure of this displacement, since on account of the statistical nature of the process the neutron may be displaced almost by Λ in one case (Fig. 202*a*), while in another case the process may terminate in the vicinity of the initial point (Fig. 202*b*).

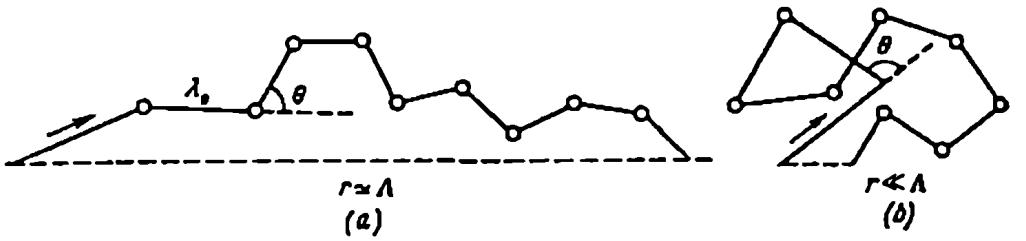

Fig. 202

It can be shown that the mean square displacement is given by

$$\overline{r^2} = 2\bar{n}\,(\bar{\lambda}_s)^2/[1 - 2/3A] \qquad (6.3.41)$$

where $\bar{n} = (1/\xi)\ln(T_0/T)$, and A is the mass number of the moderator.

The numerator of formula (6.3.41) coincides with the well-known expression for the mean square Brownian displacement of particles. The denominator takes into account the anisotropy of neutron scattering.

It was shown in Sec. 4.4 that elastic scattering of a neutron by a heavy nucleus can take place at any angle θ, while the angle at which a neutron is scattered by a proton cannot exceed 90°. Consequently, the trajectory of motion of neutrons in a hydrogen moderator is stretched forward in comparison to that in a heavy moderator. Quantitatively, this difference can be characterized by the mean value of cosine of the scattering angle, i.e. $\overline{\cos\theta}$, which is equal to zero for isotropic scattering and increases with increasing anisotropy. With the help of the momentum diagram (see Sec. 4.4), it can be easily shown that for a moderator whose nuclei have a mass number A,

$$\overline{\cos\theta} = 2/3A. \qquad (6.3.42)$$

This quantity appears in the denominator of formula (6.3.41).[9] The quantity $\lambda_s/(1 - \overline{\cos\theta}) = \lambda_s\,[1 - 2/3A]$ is often called the *transport length*[10] and is denoted by λ_t:

$$\lambda_t = \lambda_s/(1 - \overline{\cos\theta}) = \lambda_s/[1 - 2/3A]. \qquad (6.3.43)$$

[9] While considering the Brownian movement, the number A can be assumed to be so large that $\overline{\cos\theta} = 0$ and $\overline{r^2} = 2n\lambda^2$.

[10] The physical meaning of the transport length is the mean distance covered by a neutron in the initial direction (before rotation by 90°). Obviously, $\lambda_t = \lambda_s + \lambda_s\overline{\cos\theta} + \lambda\,\overline{(\cos\theta)^2} + \ldots = \lambda_s/(1 - \overline{\cos\theta})$.

Consequently, the approximate formula (6.3.41) can be written in the form

$$\overline{r^2} = 2\bar{n}\bar{\lambda}_s\bar{\lambda}_t. \tag{6.3.44}$$

In the particular case of a hydrogen moderator, we have

$$\lambda_t = \lambda_s/(1 - 2/3) = 3\lambda_s \tag{6.3.45}$$

and

$$\overline{r^2} = 6\bar{n}(\bar{\lambda}_s)^2. \tag{6.3.46}$$

At a distance $r = \sqrt{\overline{r^2}}$ from the source, most neutrons have an energy lower than the final moderation energy.

Formulas (6.3.41), (6.3.44) and (6.3.46) are rough approximations, since it was assumed during their derivation that λ_s, ξ and $\cos\theta$ do not change during the slowing down of neutrons. A more exact formula for $\overline{r^2}$ has the following form:

$$\overline{r^2} = \int_T^{T_0} \frac{2\lambda_s\lambda_t}{\xi}\frac{dT}{T}. \tag{6.3.47}$$

This formula can be easily obtained by using the expressions (6.3.41) and (6.3.44) for a small interval of energy between T and $T + dT$ (the value of $\lambda_s(T)$ can be treated as constant in this interval), and integrating these expressions with respect to energy. Indeed, let us suppose that neutrons are slowed down in the energy interval between $T + dT$ and T, and that Δn collisions are required for this purpose. Then, in accordance with formulas (6.3.41) and (6.3.44), the mean square displacement is given by

$$\overline{\Delta r^2} = 2\lambda_s^2\Delta n/[1 - 2/3A] = 2\lambda_s\lambda_t\Delta n, \tag{6.3.48}$$

where Δn is calculated from formula (6.3.20):

$$\begin{aligned}\Delta n &= (1/\xi)\ln[(T + dT)/T] \\ &= (1/\xi)[\ln(T + dT) - \ln T] \simeq dT/\xi T.\end{aligned} \tag{6.3.49}$$

Substituting this expression into (6.3.48) and integrating with respect to T, we obtain (6.3.47).

While deriving formula (6.3.49), we assumed that the energy loss due to one collision is small, i.e. the slowing down of neutrons is a *continuous* process. Under the assumption, it is possible to develop a theory of moderation for media with small ξ and a weak dependence of λ_s on energy. This theory is called the *age theory*. In the age approximation, the slowing-down process is described by a diffusion-type equation similar to the equation for thermal conductivity:

$$\Delta q(\mathbf{r}, \tau) = (\partial q/\partial\tau)(\mathbf{r}, \tau), \tag{6.3.50}$$

where $\tau = \int_T^{T_0} \frac{\lambda_s \lambda_t}{3\xi} \frac{dT}{T}$ is the *age of the neutrons*, and $q(r, \tau)$ is their flux density along the τ-axis. The term for τ is associated with the fact that when a small amount of energy is lost in a single collision, the magnitude of τ is uniquely connected with the neutron energy and the time during which it is slowed down.

The age theory can be used to obtain a number of results that are quite important for solving practical problems in the physics of neutron moderation. Thus, the solution of the age equation for a point source gives

$$q(r, \tau) = (4\pi\tau)^{-3/2} \exp(r^2/4\tau). \quad (6.3.51)$$

In this case, $\overline{r^2} = 6\tau$ [cf. (6.3.47)].

The age τ and the *slowing-down length*[11] $L_s = \sqrt{\tau}$ are frequently used as moderation characteristics (see Table 25).

The age theory is applicable for the slowing-down process in quite heavy moderators, for example, graphite. The basic criterion for the applicability of this theory, viz. a continuous slowing down of neutrons, is not satisfied in hydrogenous media in which a neutron may lose all its energy in a single collision. Hence it is not applicable for such media and in such cases we have to resort to a complex kinetic equation (or some other approximation of this equation) to describe theoretically the process of slowing down of neutrons.

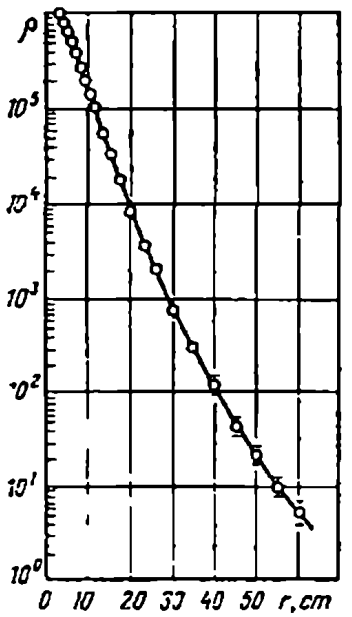

Fig. 203

In view of the difficulties in the description of the process of slowing down, the above formulas (as well as other formulas) usually give only a rough estimate of the quantity $\overline{r^2}$ (and an estimate of the influence of various parameters of the moderator, say, density, on the value of $\overline{r^2}$). The exact value of $\overline{r^2}$ is usually obtained experimentally.

The value of $\overline{r^2}$ for neutrons from a point source can be determined experimentally by measuring, for example, the distribution of the

[11] Sometimes, the quantity $\sqrt{\overline{r^2}} = \sqrt{6\tau}$ is called the slowing-down length.

neutron density $\rho(r)$ in the moderator with the help of a resonance detector whose resonance energy is close to therma. energy. The quantity $r^2\rho(r)\,dr$ will then be proportional to the number of neutrons having resonance energy in a spherical layer of radius r and thickness dr, and $\overline{r^2}$ can be calculated from the relation

$$\overline{r^2} = \frac{\int \rho(r)\, r^4\, dr}{\int \rho(r)\, r^2\, dr}. \qquad (6.3.52)$$

The experimental investigation of the slowing down of neutrons formed during the fission of uranium or other fissionable nuclei is very important from a practical point of view (see Chap. 7). Figure 203 shows the distribution of the density of neutrons with an

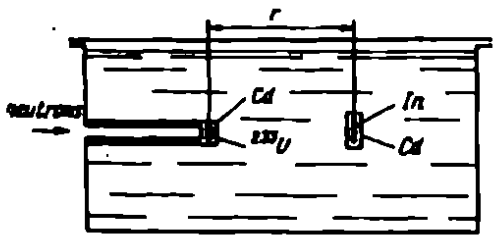

Fig. 204a

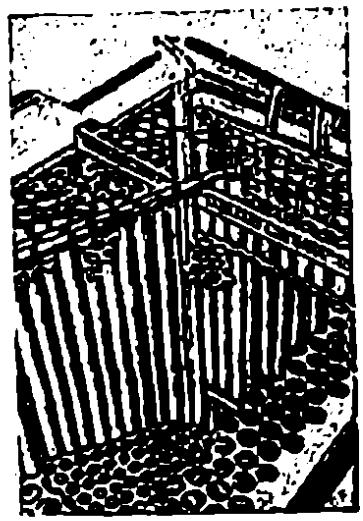

Fig. 204b

energy of 1.46 eV formed by slowing down the neutrons obtained from fission of ^{235}U in water. Measurements were carried out in a large tank (140 × 100 × 105 cm³) into which a beam of thermal neutrons from the reactor was introduced with the help of a 50-cm long steel tube soldered to the tank (Fig. 204*a*)[12]. A target made of ^{235}U served as the source of fission neutrons, which was placed at the soldered end of the tube and was covered with a cadmium jacket.

[12] For the sake of clarity, it is shown in Fig. 204*a* that neutrons are introduced into the tank through its end face. Actually, to reduce the background, neutrons were introduced through the lateral face, i.e. at an angle of 90° to the direction of measurement [L.M. Barkov and K.N. Mukhin, *Atomnaya Energiya*, 3, 31 (1956)].

An indium foil in cadmium holders, in which artificial beta radioactivity was induced by neutrons with an energy of 1.46 eV, was used as a detector.

The curve shown in Fig. 203 gives the following value of $\overline{r^2}$:

$$\tau = \overline{r^2}_{1.46\ \text{eV}}/6 = 29.4 \pm 1.5\ \text{cm}^2, \qquad (6.3.53)$$

or, taking into account the correction for the size of the source,

$$\tau = 28 \pm 1.5\ \text{cm}^2.$$

The age of neutrons for more complex media, for example, the uranium-water lattice (Fig. 204*b*) can be measured in a similar manner.

It was mentioned above that this method allows us to determine not the total age τ_{kT} of neutrons (up to the thermal energy), but a somewhat smaller quantity τ_{res}, i.e. the age of neutrons slowed down to the resonance energy of the detector being employed for measurements. However, if the resonance energy of the detector is about 1 eV, the correction is found to be quite small (about 1 cm²). It can be calculated with the help of formula (6.3.47) or measured experimentally (see Sec. 6.3.5).

6.3.5. Diffusion of Thermal Neutrons

After the neutrons have been slowed down to thermal energies their energy does not decrease any further and they move in the moderator retaining their thermal energy on the average. It can be easily seen that this process can be approximately described by the simple diffusion equation from the kinetic theory of gases. This becomes possible because in a good moderator (in which the scattering cross section σ_s considerably exceeds the absorption cross section σ_a[13]), a thermal neutron may undergo a very large number of collisions with nuclei before being captured:

$$N = \sigma_s/\sigma_a = \lambda_a/\lambda_s. \qquad (6.3.54)$$

Due to a small mean free path λ_s for thermal neutrons, the condition for the applicability of the diffusion approximation is satisfied, i.e.

---

[13] The absorption cross section σ_a is the third important characteristic of a moderator (the first two being ξ and σ_s or λ_s). The smaller the value of σ_a, the better the moderator. The final index of the quality of a moderator is the quantity $\xi\sigma_s/\sigma_a$, called the *moderating ratio*. This ratio can be used to compare the slowing-down time t_{sl} for a neutron and the lifetime of a thermal neutron $t_{cap.}$ before it is captured (not to be confused with the lifetime for the decay $n \to p + e^- + \tilde{\nu}$, which is considerably longer). Thus, it can be shown that if $\xi\sigma_s$ is independent of energy, then $t_{cap.}/t_{sl} = \frac{1}{2}(\xi\sigma_s/\sigma_a)$. Water, heavy water, beryllium and carbon have the highest moderating ratios.

the neutron density changes insignificantly over λ_s. Finally, the velocity of thermal neutrons can be treated as constant:

$$v_{kT^\circ} \simeq 2.2 \times 10^5 \text{ cm/s}. \quad (6.3.55)$$

The diffusion equation has the following form:

$$\frac{\partial \rho}{\partial t} = D\Delta\rho - \frac{\rho}{t_{cap.}} + q, \quad (6.3.56)$$

where ρ (r, t) is the density of thermal neutrons at point r at instant t, Δ is the Laplacian, D is the diffusion coefficient, $t_{cap.}$ is the mean lifetime of thermal neutrons, and q is the density of the thermal neutron sources.

Equation (6.3.56) is the balance equation describing the change in the density of neutrons with time, i.e. $(\partial\rho/\partial t)$, due to three processes, viz. the influx of neutrons from neighbouring regions $(D\Delta\rho)$, absorption of neutrons $(-\rho/t_{cap.})$, and the formation of neutrons (q).

In the general case (taking into account the anisotropy of scattering), the diffusion coefficient can be written in the form

$$D = \lambda_t v/3 \quad (6.3.57)$$

For thermal neutrons, this coefficient can be written to a fairly high degree of accuracy in the following simple form:

$$D = \lambda_s v/3. \quad (6.3.58)$$

This is because of the fact that the energy of thermal neutrons is lower than the chemical binding energy of atoms in a molecule. As a result, the scattering of thermal neutrons takes place not by free atoms, but by heavy bound molecules (or even by the crystal grains of the medium). According to the momentum diagram, such a scattering must be isotropic ($\overline{\cos\theta} = 0$ and $\lambda_t = \lambda_s$).

As an example of the solution of Eq. (6.3.56), let us consider the problem of the distribution of thermal neutrons in a moderator having a point source of fast neutrons at the centre. We shall confine ourselves to only such distances r from the source, at which the slowing-down process has already terminated, i.e. where no new thermal neutrons are formed. In this case, we can consider the equation for a steady-state diffusion $(d\rho/dt = 0)$ without any source $(q = 0)$:

$$D\Delta\rho - \rho/t_{cap.} = 0. \quad (6.3.59)$$

This equation can be written in the form

$$L^2\Delta\rho - \rho = 0, \quad (6.3.60)$$

where $L^2 = Dt_{cap.}$.

The quantity $L = \sqrt{Dt_{cap.}}$ is called the *diffusion length* of thermal neutrons. This quantity is a measure of the displacement of thermal neutrons in the process of their diffusion (in the same way

as the slowing-down length L_s is a measure of the displacement of neutrons in the process of slowing down). Since $D = \lambda_s v/3$ and $t_{cap.} = \lambda_a/v = N\lambda_s/v$, we get

$$L = \sqrt{Dt_{cap.}} = \sqrt{\frac{1}{3}\lambda_s\lambda_a} = \lambda_s\sqrt{\frac{N}{3}}. \quad (6.3.61)$$

The solution of this equation is the function

$$\rho(r) \propto \exp(-r/L)/r. \quad (6.3.62)$$

It follows from this relation that $\ln[r\rho(r)]$ is a linear function of r:

$$\ln[r\rho(r)] = -r/L. \quad (6.3.63)$$

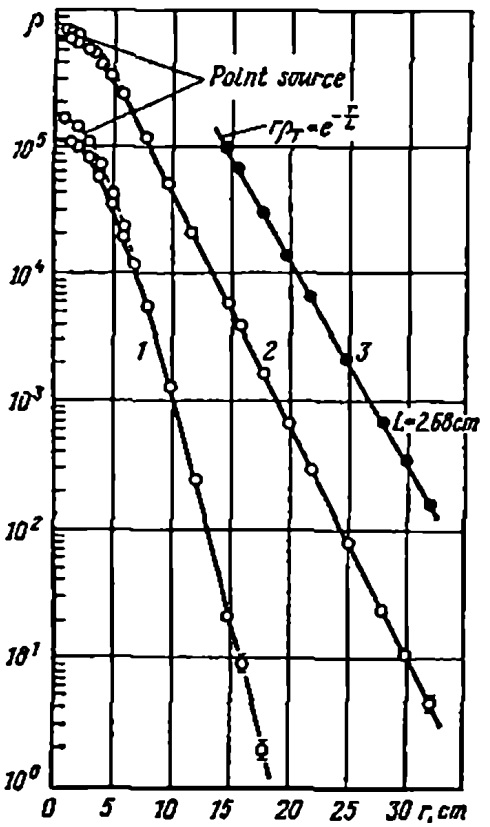

Fig. 205

Hence, plotting this function on a semilogarithmic scale, we can determine the diffusion length L from the slope of the straight line.

Figure 205 shows the experimental distribution curves for resonance (curve *1*) and thermal (curve *2*) neutrons obtained by slowing down in water the photoneutrons from a small (Sb + Be)-source with an energy of ~30 keV. Measurements were carried out in a large water-filled tank by the method of indium detector ($T_{res} = 1.46$ eV). Additional measurements were made with a point source in the region of small values of r (dashed parts of the curves). A comparison of curves *1* and *2* shows that for $r > 15$ cm, the moderator contains only thermal neutrons arriving from the region of the source (since the density of the resonance neutrons which are responsible for the creation of thermal neutrons is very low for $r > 15$ cm). Hence the dependence given by (6.3.63) (curve *3*) must be satisfied for $r > 15$ cm. It follows from the slope of this curve that

$$L = 2.68 \pm 0.02 \text{ cm}. \quad (6.3.64)$$

In the same experiment, an estimate was obtained for the age $\Delta\tau$ of neutrons slowed down in water from the resonance energy of indium (1.46 eV) to thermal energy (0.025 eV)

$$\Delta\tau = M^2 - \tau_{1.46\text{ eV}} - L^2, \quad (6.3.65)$$

where $M^2 = \tau_{kT^\circ} + L^2$ is the *migration area*, $\tau_{1.46\,eV}$ is the age of neutrons up to the resonance energy 1.46 eV, and $\tau_{kT^\circ} = \tau_{1.46\,eV} + \Delta\tau$ is the age of neutrons up to thermal energy. The migration area M^2 is determined by computing the ratio $\overline{r^2}/6$ for curve *2* and $\tau_{1.46\,eV}$ for curve *1*.

As a result of calculations, we obtain

$$M^2 = 13.64 \pm 0.25 \text{ cm}^2, \qquad \tau_{1.46\,eV} = 5.48 \pm 0.15 \text{ cm}^2,$$
$$L^2 = 7.18 \pm 0.11 \text{ cm}^2,$$

whence

$$\Delta\tau = 1.0 \pm 0.5 \text{ cm}^2. \tag{6.3.66}$$

The quantity $\Delta\tau$ can be used to determine the age of fission neutrons in water up to thermal energy:

$$\tau_{kT^\circ} = \tau_{1.46\,eV} + \Delta\tau. \tag{6.3.67}$$

Using the value of $\tau_{1.46\,eV}$ obtained above [see formula (6.3.53)], we get

$$\tau_{kT^\circ} = 28 + 1 = 29 \pm 2 \text{ cm}^2. \tag{6.3.68}$$

This quantity is very important in calculations concerning nuclear reactors in which water is used as a moderator.

The characteristics of basic moderators are listed in Tables 24 and 25.

Table 24

Nucleus	Mass number A	ξ	$\overline{\cos\theta}$	$\bar{n}$ (from 2 MeV to kT°)
H	1	1	0.667	18
D	2	0.725	0.333	25
Be	9	0.206	0.074	85
C	12	0.159	0.056	115

Table 25

Moderator	L_0, cm (2 MeV–kT°)	Slowing-down time t_{sl}, s	Age τ, cm²	Slowing-down length L_0, cm	$(\sigma_a)_{kT^\circ}$, 10^{-24} cm²	$(\sigma_s)_{kT^\circ}$, 10^{-24} cm²	$(L_a)_{kT^\circ}$, cm	$(L_s)_{kT^\circ}$, cm	Diffusion time, t_{diff}, s	Diffusion length L, cm
H_2O	1.1	10^{-6}	29	5.4	103.0	0.66	0.29	45	2.1×10^{-4}	2.7
D_2O	2.6	4.6×10^{-6}	125	11.0	13.6	0.001	2.23	3×10^4	0.15	120
Be	1.6	6.7×10^{-6}	85	9.3	7.0	0.01	1.16	805	4.3×10^{-3}	22
C (graphite)	2.6	1.5×10^{-5}	315	17.7	4.8	0.003	2.6	3845	1.2×10^{-2}	54

6.4. Bohr's Theory of Nuclear Reactions

6.4.1. Compound Nucleus

The existence of narrow levels ($\Gamma \simeq 0.1$ eV) in a nucleus at an excitation energy exceeding the binding energy of a nucleon seems to be incomprehensible at first sight. Indeed, according to the quantum-mechanical uncertainty relation

$$\Delta E \Delta t \simeq \hbar, \tag{6.4.1}$$

where $\hbar = 6.6 \times 10^{-16}$ eV·s, a small level width indicates a long lifetime for the nucleus in the given state:

$$\tau = \hbar/\Gamma \simeq 6.6 \times 10^{-16}/0.1 \simeq 10^{-14} \text{ s}. \tag{6.4.2}$$

This time is much longer than the time taken by a neutron to cross an atomic nucleus, viz.

$$\Delta t = R_{\text{nuc}}/v_n \simeq 10^{-12}/10^9 = 10^{-21} \text{ s}, \tag{6.4.3}$$

which should apparently characterize the duration of nuclear interaction and which corresponds to $\Gamma \simeq 1$ MeV.

This difficulty as well as some other difficulties (large cross sections and high level density) in the interpretation of experimental results on the resonant capture of slow neutrons by nuclei was overcome in 1936 by Bohr who proposed the theory of nuclear reactions based on the liquid drop model of the nucleus.

According to Bohr, a nuclear reaction proceeds in two stages. In the first (fast) stage, the neutron enters the nucleus and is captured by it, thus forming a compound system (compound nucleus) with an excitation energy

$$W = \varepsilon_n + AT_n/(A + 1) \tag{6.4.4}$$

and certain definite values of angular momentum, parity, etc.

On account of a strong interaction, the excitation energy is rapidly distributed among all the nucleons of the nucleus, and hence each one of them has an energy much smaller than the binding energy and thus cannot leave the nucleus until a nucleon near the boundary of the nucleus acquires an energy exceeding the binding energy. Another possible way of decay of a compound nucleus, i.e. the emission of a γ-quantum, is also known to be a slow process. This is the reason behind a long lifetime of the compound nucleus, and this time period is so long that the compound system even "forgets" the mechanism of its formation. The parameters of the compound nucleus (energy, angular momentum and parity) are independent of the type of the reaction in which this nucleus was formed (see Sec. 9.3.3).

After the passage of a sufficiently long time τ (lifetime of the compound nucleus), the second stage of the nuclear reaction sets in, viz.

the decay of the compound nucleus accompanied by the escape of a nucleon or the emission of a γ-quantum (or some other process in general).

The disintegration probability for the compound nucleus is $\omega = 1/\tau = \Gamma/\hbar$. A nucleus can disintegrate in different ways: by gamma radiation, neutron emission, proton emission, etc. Hence the disintegration probability can be expressed as the sum of the partial probabilities, each of which characterizes a disintegration channel:

$$\omega = \omega_\gamma + \omega_n + \omega_p + \ldots = \Gamma_\gamma/\hbar + \Gamma_n/\hbar + \Gamma_p/\hbar + \ldots \quad (6.4.5)$$

The relative disintegration probability of the compound nucleus for a given channel is given by

$$\eta_i = \omega_i/\omega = \Gamma_i/\Gamma, \quad (6.4.6)$$

where Γ_i is the partial width (Γ_γ is the radiation width, Γ_n the neutron width, and so on). According to Bohr's theory, the relative disintegration probabilities of a compound nucleus are independent of the way in which it was formed. This conclusion is confirmed experimentally from a comparison of the decay patterns of identical compound nuclei (with the same values of A, Z, E, I, T and P) obtained in different nuclear reactions.

6.4.2. Compound Nuclear Levels

According to the liquid drop model, a strong interaction between many nucleons must result in their collective motion (for example, to the rotation of the nucleus or to surface oscillations of the nuclear drop, as mentioned in Sec. 2.4).

The collective nature of the interaction of nucleons during the excitation of a nucleus determines the nature of the distribution of its levels which condense very rapidly with increasing excitation energy. The higher the excitation energy of a nucleus, the higher the probability that a given complex motion results from the simplest types of motion.

This conclusion is fully confirmed by the data on the structure of nuclear levels obtained from different experiments. An analysis of alpha and beta decays and the gamma radiation accompanying them (Chap. 3) showed that for comparatively low excitation energies (1-3 MeV) of a heavy ($A > 100$) nucleus, its levels are spaced rather far apart ($\Delta E \simeq 100$ keV). Experiments on the resonance capture of slow neutrons show that at excitation energies slightly exceeding the adhesion energy of a nucleon (about 8 MeV), the separation between levels becomes much smaller ($\Delta E \simeq$ 1-10 eV) but the level spectrum remains discrete. Finally, at still higher excitation energies ($W \gg \varepsilon_n$), the levels come so close that they begin to overlap, and the spectrum becomes continuous.

Thus, the neutron width Γ_n is determined not by the quantity $\hbar/T$ but by a p-times smaller quantity:

$$\Gamma_n = p\frac{\hbar}{T} = 4\frac{k}{k_0}\frac{\Delta}{2\pi}. \qquad (6.4.17)$$

It follows from this expression that $\Gamma_n \ll \Delta$. Taking into consideration the remark made above concerning formula (6.4.8), we can state that for the compound nuclear levels in the region of excitation energies $W \geqslant \varepsilon_n$, the condition (6.4.7) concerning the possibility of the existence of discrete level spectrum is satisfied.

The existence of discrete energy states with a finite lifetime $\tau \neq \infty$ ($\tau \simeq 10^{-14}$ s) for a compound nucleus makes these states considerably different from the stable ground state of the nucleus with $\tau = \infty$.

From the uncertainty relation

$$\Gamma\tau = \hbar,$$

it follows that the energy of a nucleus in the ground state is strictly defined, and hence the energy state of the nucleus in this case can be characterized by a δ-function (Fig. 207*a*) with $\Gamma = 0$. Such a state of the nucleus is called a *stationary* state. The wave-function of the stationary state with the energy $W = W_0$ is written in the form

$$\psi \propto \exp(-iW_0 t/\hbar)$$

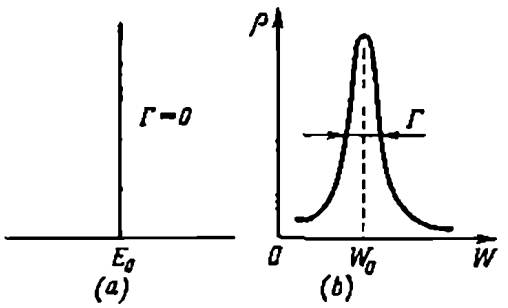

Fig. 207

Similar properties are possessed by the excited states of the nucleus for which the excitation energy is lower than the minimum energy of separation for a particle (n, p, α), while the gamma radiation is strongly forbidden. Such long-lived states are called *metastable* states. They are also characterized by a very small level width Γ and hence the energy of such states can also be represented by a δ-function to a good approximation (for example, for an isomer with lifetime $\tau \simeq 1$ min, $\Gamma \simeq \hbar/\tau = 6.6 \times 10^{-16}/60 \simeq 10^{-17}$ eV).

States with a small lifetime $\tau \simeq 10^{-14}$ s differ considerably from the long-lived stationary and metastable states in that they have a much larger level width Γ. Such states are called quasistationary states and are characterized by $\Gamma \simeq \hbar/\tau = 0.1$ eV $\gg 0$. Hence the probability of the system being in an energy state W is characterized not by a δ-function, but by a function $\rho(W)$ which differs from zero not only at a certain value of the excitation energy $W = W_0$, but also in the vicinity of this value (Fig 207*b*).

The size of the region, where $\rho(W) \neq 0$, is determined by the maximum width Γ. Hence the condition $\rho(W) \propto \Gamma$ must be satisfied. Besides, it is intuitively clear that the curve $\rho(W)$ must be smooth (with a continuous derivative) with wings extending to $\pm\infty$. All these requirements are met by a dispersive distribution of the type

$$\rho(W) = \alpha \frac{\Gamma}{(W-W_0)^2+(\Gamma/2)^2},$$

where α is a multiplication factor. Indeed, in this case,

$$\rho(W_0) = 4\alpha/\Gamma \propto \tau \text{ and } \rho(W_0 \pm \Gamma/2) = 2\alpha/\Gamma = (1/2)\,\rho(W_0).$$

6.4.3. Dispersive Nature of the Energy Distribution for a Compound Nucleus

A more rigorous[15] dispersion relation for the function $\rho(W)$ can be obtained by assuming that the disintegration of the compound nucleus takes place according to the law of radioactive decay, i.e. by assuming that the disintegration probability is independent of time. This assumption seems quite natural since the nature of disintegration of the compound nucleus does not depend on the past history of its emergence.

Under this assumption, the probability that the compound nucleus is still in a given energy state at the instant t is proportional to

$$|\psi|^2 \propto \exp(-\omega t) = \exp(-t/\tau) = \exp\left(-\frac{\Gamma}{\hbar}t\right). \quad (6.4.18)$$

As regards the wave-function itself (to be more precise, its time component), it can be written for $\Gamma \ll W_0$ in the form

$$\psi(t) = a \exp\left(-\frac{iW_0 t}{\hbar} - \frac{\Gamma t}{2\hbar}\right), \quad (6.4.19)$$

which satisfies the requirement of the existence of a quasistationary level at $W = W_0$, as well as the condition (6.4.18).

We expand $\psi(t)$ in eigenfunctions $\varphi(W)$ of the energy operator:

$$\psi(t) = \int_0^\infty C(W) \exp\left(-\frac{iWt}{\hbar}\right) dW,$$

where $C(W)$ are the Fourier coefficients.

[15] An absolutely rigorous derivation of the dispersion relation is beyond the scope of the book.

Consequently, the geometrical cross section is given by

$$S = \sum_{l=0}^{R/\lambda} (2l+1)\,\pi\lambda^2 = \pi\,(R+\lambda)^2. \qquad (6.4.29)$$

The geometrical cross section determines the upper limit of the cross section of the formation of a compound nucleus:

$$\sigma^*_{max} = S, \qquad \sigma^* \leqslant S \qquad (6.4.30)$$

In order to determine the cross section of the formation of a compound nucleus, viz.

$$\sigma^* = \sum_{l=0}^{R/\lambda} (2l+1)\,\pi\lambda^2\xi_l \qquad (6.4.31)$$

we must find the adhesion coefficient ξ_l, whose value for a neutron is determined by the penetrability D_c of the centrifugal barrier (for charged particles, we must also take into account the penetrability D_C of the Coulomb barrier), the coefficient p of transmission through the surface of the nucleus, and the probability of a neutron getting "stuck" inside the nucleus. The latter quantity can be put equal to unity, since the computation of σ^* involves only the first stage of the nuclear reaction (preceding the emission of a particle or a γ quantum from the nucleus).

If the energy of the incident neutrons is not very high ($T_n < 10$ keV), then $\lambda \gg R$ and $l_{max} = 0$. As a result, the geometrical cross section becomes

$$S = S_0 = \pi\lambda^2, \qquad (6.4.32)$$

and the centrifugal potential $V_c = 0$. Thus, for slow neutrons, we must consider only the effect of reflection at the boundary of the nucleus. The coefficient p of transmission through the surface of the nucleus is given, in accordance with (6.4.15), by

$$p = 4kk_0/(k + k_0)^2$$

and, according to the relation (6.4.17), $p \propto \Gamma_n$. Hence, for slow neutrons, ξ must be proportional to Γ_n:

$$\xi_0 \propto \Gamma_n. \qquad (6.4.33)$$

Besides, it is obvious that the capture of slow neutrons must have a selective resonance nature, since the compound nucleus in this range of excitation energies has discrete levels.

In accordance with (6.4.22), the probability of finding a nucleus in the energy state W in the vicinity of a quasistationary level W_0 is proportional to the quantity

$$\rho(W) \propto \frac{\Gamma}{(W-W_0)^2+(\Gamma/2)^2}, \qquad (6.4.34)$$

i.e. the probability increases as the excitation energy W approaches the resonance value $W = W_0$. However, the energy T of a neutron is connected with the excitation energy of the nucleus through the relation[17]

$$W = \varepsilon_n + T, \tag{6.4.35}$$

whence $(W - W_0)^2 = (T - T_0)^2$. This means that the probability of formation of a compound nucleus dispersively depends on the energy of the incident neutron:

$$\xi_{e0} \propto \frac{\Gamma}{(T-T_0)^2+(\Gamma/2)^2}. \tag{6.4.36}$$

Combining the relations (6.4.32), (6.4.33) and (6.4.36), we get

$$\sigma^* = S_{e0}\xi_{e0} \propto \pi\lambda^2 \frac{\Gamma\Gamma_n}{(T-T_0)^2+(\Gamma/2)^2}. \tag{6.4.37}$$

But for a coefficient of the order of unity, this expression is identical to the well-known one-level Breit-Wigner formula. In order to obtain the coefficient in formula (6.4.37), we must carry out a more detailed analysis which requires a brief digression to introduce a new concept.

Detailed balancing principle. It is known from classical and quantum mechanics that the equations of motion for many systems are invariant to a change in the direction in which time is measured (a change from t to $-t$). This invariance can be used to establish a very important relation between the probabilities of direct and inverse course of processes.

Let 1 and 2 be two simple quantum states of a system with a discrete energy spectrum. We denote by ω_{12} the probability of transition of the system from state 1 to state 2, and by ω_{21} the probability of the reverse transition from state 2 to state 1. From the invariance of the equations of motion with respect to time reversal, it follows that

$$\omega_{12} = \omega_{21}. \tag{6.4.38}$$

If state 2 consists of a group of close states numbering g_2 (the statistical weight of states 2), the probability P_{12} of transition from a single state 1 to all the states 2 will be g_2 times higher than ω_{12}, i.e.

$$P_{12} = g_2\omega_{12}. \tag{6.4.39}$$

Similarly, if g_1 is the statistical weight of all states 1, the probability P_{21} of transition from state 2 to all states 1 is

$$P_{21} = g_1\omega_{21}. \tag{6.4.40}$$

[17] Here, by T we mean the relative kinetic energy (i.e. the kinetic energy of the neutron and the nucleus in the centre-of-mass system).

From the equality $\omega_{12} = \omega_{21}$, we get $P_{12}/g_2 = P_{21}/g_1$, or

$$g_1 P_{12} = g_2 P_{21}. \tag{6.4.41}$$

This relation is called the *detailed balancing principle* and establishes a connection between a direct and a reverse process, and also allows us to determine the missing characteristics of one of these processes.

Let us consider the reaction

$$a + A \to B + b \tag{6.4.42}$$

with a cross section σ_{ab}, and the reverse reaction

$$b + B \to A + a \tag{6.4.43}$$

with a cross section σ_{ba}. Both these cross sections must be averaged over spins[18]. We assign the first state to nucleus A and to particle a interacting with it, and the second state to the reaction products B and b.

Assuming that the system is contained in a certain arbitrarily large volume V, we can write the statistical weight of the first state and the transition probability P_{12} as follows:

$$g_1 = (2I_A + 1)\,(2s_a + 1)\,4\pi V p_a^2 dp_a/(2\pi\hbar)^3, \tag{6.4.44}$$

$$P_{12} = \sigma_{ab} v_a / V, \tag{6.4.45}$$

where I_A is the spin of nucleus A, s_a is the spin of the particle interacting with it, p_a is the relative momentum of the system $A + a$, and v_a is the relative velocity of particle a and nucleus A.

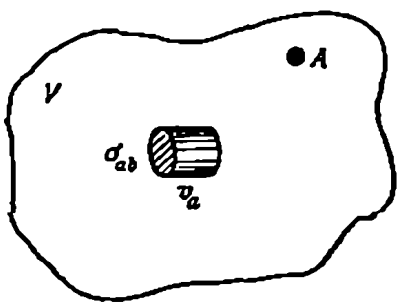

Fig. 209

The meaning of these expressions is quite obvious. The first two parentheses in (6.4.44) take into account all possible spin orientations of nucleus A and particle a, while the factor $4\pi V p_a^2 dp_a/(2\pi\hbar)^3$ gives the number of states of the system with momentum values between p_a and $p_a + dp_a$ (see Footnote 25 in Chap. 3). Formula (6.4.45) is the ratio of the volume of a cylinder of length v_a and the cross-sectional area σ_{ab}, i.e. the volume covered by particle a in a unit time ("interaction volume" $\sigma_{ab} v_a$), to the entire volume V in which the system is enclosed (*Fig.* 209). *Similarly, we can write*

$$g_2 = (2I_B + 1)\,(2s_b + 1)\,4\pi V p_b^2 dp_b/(2\pi\hbar)^3, \tag{6.4.46}$$

$$P_{21} = \sigma_{ba} v_b / V, \tag{6.4.47}$$

[18] The spin is flipped upon a replacement of t by $-t$

where I_B is the spin of nucleus B, s_b is the spin of particle b, p_b is the relative momentum of the system $B + b$, and v_b is the relative velocity of particle b and nucleus B.

Substituting expressions (6.4.44)-(6.4.47) into (6.4.41) and cancelling out the coefficients and factors[19] $v_a dp_a$ and $v_b dp_b$, which are equal, we obtain

$$(2I_A + 1)(2s_a + 1) p_a^2 \sigma_{ab} = (2I_B + 1)(2s_b + 1) p_b^2 \sigma_{ba}. \tag{6.4.48}$$

This formula can be used to determine the spin of one of the four particles a, A, b or B participating in the reaction. The spin of π^+-meson, for example, was determined in this way (see Sec. 6.1.5, Vol. II).

Breit-Wigner formulas. Let us apply the detailed balancing principle for determining the cross section σ^* of the formation of a compound nucleus.

We assign the first state to nucleus A and the neutron n interacting with it, and the second state to the excited compound nucleus with a quasistationary level $\rho(W)$ defined in the form (6.4.22). Then, in analogy with the above discussion, we can write

$$g_1 = (2I + 1)(2s + 1)\, 4\pi V p^2 dp/(2\pi\hbar)^3, \tag{6.4.49}$$

$$P_{12} = \sigma^* v/V, \tag{6.4.50}$$

where I is the spin of nucleus A, s is the spin of the neutron, p is the relative momentum of the system, and v is the relative velocity of the neutron and nucleus A.

For the inverse process of emission of a neutron from the compound nucleus A, we have

$$g_2 = 2J + 1, \tag{6.4.51}$$

where J is the angular momentum of the compound nucleus, and

$$P_{21} = \Gamma_n \rho(W)\, dW/\hbar, \tag{6.4.52}$$

where Γ_n is the neutron width and $\rho(W)$ is determined by formula (6.4.22). The meaning of formula (6.4.52) is obvious: $\Gamma_n/\hbar$ gives the probability of escape of a neutron in accordance with (6.4.6), and $\rho(W) = \rho(T + \varepsilon_n)$ defines the probability that its energy will be between T and $T + dT$ (corresponding to the variation of the momentum between p and $p + dp$).

---

[19] These factors are equal because $v_a dp_a = d(\mu_{Aa} v_a^2/2) = dT'_{Aa}$, $v_b dp_b = d(\mu_{Bb} v_b^2/2) = dT'_{Bb} = d(T'_{Aa} + Q) = dT'_{Aa}$, where T'_{Aa} is the relative kinetic energy of particles a and A, T'_{Bb} is the relative kinetic energy of particles B and b, and Q is the reaction energy.

Substituting (6.4.49)-(6.4.52) into (6.4.41), we obtain

$$(2I+1)(2s+1)\frac{4\pi V p^2 dp}{(2\pi\hbar)^3}\frac{\sigma^* v}{V} = (2J+1)\frac{\Gamma_n}{\hbar}\rho(W)\,dW. \quad (6.4.53)$$

Cancelling out $dW = dT = vdp$ and replacing p by $\hbar/\lambda$, we can transform this equation as follows:

$$\sigma^* = \frac{2J+1}{(2I+1)(2s+1)} 2\pi^2\lambda^2\Gamma_n\rho(W). \quad (6.4.54)$$

Substituting here the value of $\rho(W)$ from (6.4.22) in which $(W - W_0)^2$ has been replaced by $(T - T_0)^2$, we obtain

$$\sigma^* = \frac{2J+1}{(2I+1)(2s+1)}\pi\lambda^2\frac{\Gamma_n\Gamma}{(T-T_0)^2+(\Gamma/2)^2}. \quad (6.4.55)$$

A comparison of (6.4.55) and (6.4.37) shows that they differ only in the numerical factor $(2J + 1)/[(2I + 1)(2s + 1)]$, which is usually of the order of unity.

Substituting formula (6.4.55) into (6.4.23) and using the value of η_i from (6.4.6), we obtain the Breit-Wigner formula for reactions of radiative capture ($\eta_\gamma = \Gamma_\gamma/\Gamma$) and the resonance scattering of a neutron ($\eta_n = \Gamma_n/\Gamma$):

$$\sigma(n, \gamma) = \sigma^*\frac{\Gamma_\gamma}{\Gamma} = \frac{2J+1}{(2I+1)(2s+1)}\pi\lambda^2\frac{\Gamma_n\Gamma_\gamma}{(T-T_0)^2+(\Gamma/2)^2}, \quad (6.4.56)$$

$$\sigma(n, n) = \sigma^*\frac{\Gamma_n}{\Gamma} = \frac{2J+1}{(2I+1)(2s+1)}\pi\lambda^2\frac{\Gamma_n^2}{(T-T_0)^2+(\Gamma/2)^2}. \quad (6.4.57)$$

Let us analyze the Breit-Wigner formula for radiative capture in different intervals of energy of the incident neutrons. We assume that $T \ll T_0$. In this case,

$$\lambda^2 \propto 1/v^2, \quad \Gamma_n \propto p \simeq 4k/k_0 \propto 1/\lambda \propto v, \text{ while } \Gamma_\gamma = \text{const},$$

since the probability of emission of a γ-quantum is determined by the excitation energy $W = \varepsilon_n + T$ of the excited nucleus, which changes insignificantly with a variation of the kinetic energy of neutrons ($T \ll \varepsilon_n$). Since $\Gamma \propto v$ and $\Gamma_\gamma \simeq$ const, $\Gamma_n \ll \Gamma_\gamma$ and

$$\Gamma = \Gamma_n + \Gamma_\gamma \simeq \Gamma_\gamma \quad (6.4.58)$$

for very low energies T of the neutrons.

Thus, for $T_n \ll T_0$,

$$\sigma(n, \gamma) \propto 1/v, \quad (6.4.59)$$

i.e. away from resonance, the radiative capture cross section increases according to the $1/v$-law with decreasing neutron energy. This is the reason why a large number of materials have large capture cross sections for thermal neutrons.

As the neutron energy approaches the resonance value T_0, the cross section begins to increase and for $T = T_0$, it becomes equal to

$$\sigma_0 = \sigma(T_0) = \pi\lambda_0^2 \frac{\Gamma_n(T_0)\Gamma_\gamma}{(\Gamma/2)^2}, \qquad (6.4.60)$$

(the spin factor has been omitted) or, considering that $\Gamma_\gamma \simeq \Gamma$,

$$\sigma_0 = 4\pi\lambda_0^2\Gamma_n(T_0)/\Gamma. \qquad (6.4.61)$$

The large value of λ at low neutron energies ($\lambda = 4.5 \times 10^{-10}/\sqrt{T}$, where T is in eV) results in huge resonance capture cross sections. For $T > T_0$, the cross section again decreases.

If a level lies close to the thermal energy ($T_0 \simeq 1/40$ eV), the capture cross section of thermal neutrons becomes exceptionally large. An example of such a material is cadmium, which has an energy level at $T_0 = 0.176$ eV (see Sec. 6.5.5 and Fig. 222).

Substituting the relation (6.4.61) into (6.4.56), we obtain the cross section for the (n, γ)-reaction in terms of its resonance value with a well-defined $1/v$-law (the spin factor has been omitted):

$$\sigma = \sigma_0 \frac{(\Gamma/2)^2}{(T-T_0)^2+(\Gamma/2)^2}\sqrt{\frac{T_0}{T}}. \qquad (6.4.62)$$

This formula is obtained under the assumption that a compound nucleus has only one level. However, it can be used in all cases where the level separation is much larger than the level width. If this condition is not satisfied, the dispersion relation cannot be used in this form, since we must take into account the interference effects.

It was mentioned above that the cross section for a second possible resonance process, i.e. for elastic resonance scattering[20], is given by formula (6.4.57). This process is usually improbable for slow neutrons on account of a strong competition from radiative capture. However, as the neutron energy increases, the relative role of elastic resonance scattering becomes more significant since the neutron width Γ_n increases with the neutron energy ($\Gamma_n \propto v$). One such example is the resonance of the scattering cross section of $^{59}_{27}$Co at energy $T_0 = 115$ eV (see Sec. 6.5.5).

Besides, the scattering of slow neutrons takes place due to potential scattering (the neutron does not enter the nucleus in this case)[21], whose cross section is equal to $4\pi R^2$ (1-10 b). Hence while considering scattering, we must take into account the possibility of interference between the resonance and potential scatterings.

[20] In principle, the resonance (n, p)-interaction is also possible, but the Coulomb barrier of the protons formed in such interactions hinders the realization of such a resonance.

[21] See Sec. 1.4, Vol. II.

6.5. Neutron Spectroscopy

Bohr's theory of nuclear reactions and the Breit-Wigner formulas were brilliantly confirmed during a detailed investigation of the variation of reaction cross sections with the energy of incident neutrons. A detailed study of cross sections became possible owing to the development of neutron spectroscopic methods, which allow us to single out the effect caused by neutrons of a certain energy whose value can be varied.

Neutron spectroscopy makes it possible to determine the distribution of nuclear levels and their width, as well as the angular momentum corresponding to them (if beams of polarized neutrons and polarized target nuclei are used).

The idea underlying the most widely used methods of neutron spectroscopy is to single out neutrons with a certain energy from the continuous spectrum. This can be done either in space when monoenergetic neutrons fly in a given direction (mechanical monochromator method, or neutron diffraction by the crystal), or in time when neutrons of all energies fly simultaneously in a given direction but pass a certain point at different instants depending on their energy (faster neutrons, i.e. neutrons with higher energies pass this point sooner than slower neutrons). This type of a selection in time is called the *time-of-flight method*. At low neutron energies (up to about 10-100 keV), there are two versions of this method, viz. the mechanical selector method, in which the simultaneous flight of neutrons is ensured by using a mechanical neutron-beam chopper or a shutter, and the time-of-flight method in which short neutron pulses are obtained by a pulsed bombardment of the target by charged particles or (in the secondary process) by γ-quanta.

Obviously, there are no theoretical restrictions on the application of the time-of-flight method to high-energy neutrons as well. The only problem that arises in this case is that it becomes necessary to register very short times of flight (less than 10^{-10} s) for fast neutrons. However, this difficulty has been overcome in recent years owing to the development of millinanosecond pulse electronics and the use of scintillators with high-speed photomultipliers as detectors. The time-of-flight method is now used extensively for determining the velocities (energies) of very fast (including relativistic) particles. We describe some applications of this method in Vol. II.

Besides these four methods (discussed in detail below), other neutron spectroscopy methods are used in nuclear physics. One of them uses nuclear reactions and photoneutron sources to obtain monoenergetic neutrons (see Sec. 6.1). In other methods, neutron energy is determined from the energy of recoil nuclei (see Secs. 7.4.1 and 7.5.3). Note that the latter methods do not require any (space or time) monochromatization of a neutron beam.

Helium counters, distinguishing between neutrons with energies from 0.1 to 2 MeV due to a small value of Q (0.765 MeV) for the reaction $^3He(n, p)^3H$, are very convenient for neutron spectroscopy.

6.5.1. Mechanical Monochromator Method

The first instrument to isolate neutrons of a certain energy from the moderation spectrum by the method of mechanical chopping of a neutron beam was constructed by Dunning in 1935. It consists of two cadmium discs[23] mounted on an axle (Fig. 210) a certain distance δ ($\delta \simeq 50$ cm) apart. Radial slits at an angle φ are cut in these discs. If the axle with such discs is placed in the path of a neutron beam and is rotated at a high speed, the slit in the second disc will allow only such neutrons to pass through it which satisfy the condition

$$v = 6n\delta/\varphi, \qquad (6.5.1)$$

where n is the number of revolutions per minute, δ is the separation of discs, cm, and φ is the angle between the slits (in degrees). By varying φ (or n), we can single out neutrons with different velocities v.

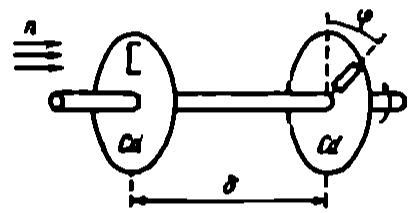

Fig. 210

Thus, Dunning's apparatus serves as a *mechanical monochromator for neutrons.*

Naturally, condition (6.5.1) is satisfied not only by monoenergetic neutrons, but also by neutrons in a certain interval of velocities between v and $v + \Delta v$ (or energies between T and $T + \Delta T$). The interval Δv (or ΔT) determines the resolving power of the instrument. If the instrument has a high resolution (i.e. $\Delta T < \Gamma$, where Γ is the width of the level under investigation), the experimental curve correctly describes the variation of cross section in the resonance energy region (i.e. the dependence is described by the Breit-Wigner formula). If the resolving power of the instrument is not high, i.e. if $\Delta T > \Gamma$, the experimental curve only approximately describes the variation of the cross section (the height of the resonance peak decreases while its width increases). If $\Delta T > \Delta$, where Δ is the separation between levels, resonance peaks do not appear on the experimental curve which gives only a roughly averaged result.

The resolving power of the Dunning monochromator, i.e. the precision with which neutrons of a given velocity can be isolated from a neutron beam, can be naturally increased by increasing the distance δ between the discs and the rotational velocity n, or by

[23] Several discs are used in the refined version of this instrument.

decreasing the slit width $d\varphi$. The resolving power was limited in the earlier experiments by the intensity of the primary neutron beam, which was not high in those years (a (Rn + Be)-source was used in the experiment). Besides, the applicability of Dunning's instrument was restricted to $T_n < 0.3$ eV, since cadmium is practically transparent to neutrons with a higher energy. Nevertheless, the first measurements of the spectrum of thermal neutrons were made with the help of this method.

Following the advent of nuclear reactors capable of providing high-intensity beams of slow (mainly thermal) neutrons, it became possible to improve this technique.

The main unit of a modern mechanical neutron monochromator is a steel cylinder (rotor) with curvilinear slits of specially computed shape drilled parallel or perpendicular to the axis of this cylinder.

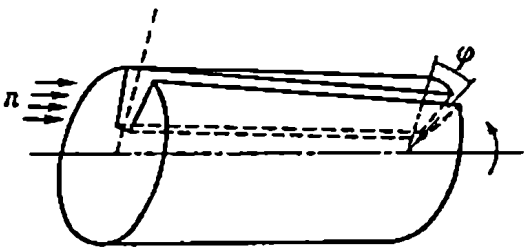

Fig. 211

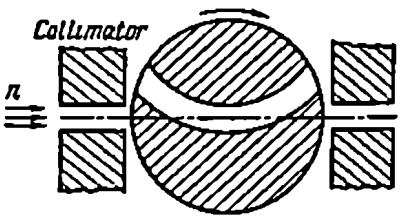

Fig. 212

In the construction employing longitudinal cuts, the slits are of nearly helical shape (Fig. 211). As the rotor turns with a certain velocity, neutrons with a definite energy between T and $T + \Delta T$ will pass through these slits. As in the case of Dunning's instrument, the velocity of these neutrons can be determined by using formula (6.5.1). Thus, the energy of the neutrons being monochromatized can be varied by varying the rotational speed of the rotor.

If slits are made on the entire surface of the cylinder, a practically *uninterrupted beam of monoenergetic neutrons* will emerge from the other side of the cylinder. Such a mechanical monochromator has a high transmission and a high resolving power. It can be used for measurements in the neutron energy interval from 10^{-3} to 1 eV. By constructing rotors of materials preventing total internal reflection of very slow neutrons from the slit surface, we can reduce the lower limit to 10^{-4} eV.

When transverse slits are drilled in the rotor, their shape is usually parabolic (Fig. 212). In this case, a *pulsed beam of monoenergetic neutrons* is obtained by irradiating the moving rotor by neutrons emerging from a collimator placed in front of it.

The resolving power of a mechanical monochromator can be increased by narrowing the slit, increasing the diameter of the cylinder (or its length in the case of longitudinal slits) or the rotational

speed. Sometimes, the resolving power is increased by placing in the path of the neutrons several rotors in sequence, their rotational speeds being in phase.

As was mentioned above, a mechanical neutron monochromator actually separates monoenergetic neutrons from a continuous spectrum. Hence this instrument can be used for various specific applications requiring irradiation by neutrons of a certain energy.

6.5.2. Mechanical Selector Method

A different principle is employed for the operation of mechanical neutron selector which isolates monoenergetic neutrons by the time-of-flight method. The first such instrument was constructed by Fermi and his coworkers in 1947 for thermal neutrons. This instrument is schematically shown in Fig. 213. Here, a steel cylinder of diameter $d = 4$ cm, has a hollow part filled with alternate layers of aluminium and cadmium of thickness 0.75 and 0.15 mm respectively. Obviously,

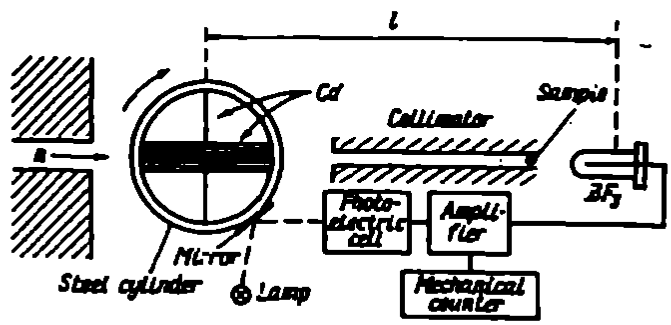

Fig. 213

if these layers are parallel to the neutron beam, the cylinder will allow up to $0.75/(0.75 + 0.15) = 5/6$ of the initial beam of thermal neutrons to pass through it. A well-collimated neutron beam, however, will be completely blocked if the cylinder is slightly rotated ($\Delta_\varphi \simeq 3°$). Thus, a rotating cylinder acts like a shutter.

When a cylinder is rotated at a high speed (about 15000 rpm), a pulsed beam of thermal neutrons is obtained. These neutrons emerge from the cylinder in short pulses in packets with a pulse-repetition frequency of 500 pulses/s (two pulses per revolution) and duration $\Delta\tau = (1/500) \times (3/180) = 3.3 \times 10^{-5}$ s. Unlike in a mechanical monochromator, the neutrons in each packet have a continuous spectrum with a fairly wide range of neutron energy from T_{min} to T_{max} (the values of these quantities will be determined later).

In Fermi's instrument, neutrons of a certain velocity are isolated with the help of a detector whose sensitivity can be controlled. This detector is an ionization chamber filled with BF_3. The chamber is

connected to a mechanical counter through an amplifier which is rendered conducting for a short time $\Delta\tau$ by the signals from a photocell, generated by it in a certain time τ after each neutron pulse (Fig. 214). This is attained with the help of a mirror which reflects the light from a lamp to the photocell when the cylinder is in a certain position. (Alternatively, the light beam is made to pass through a slit in the cylinder axle.) The sample under investigation is placed in the collimator.

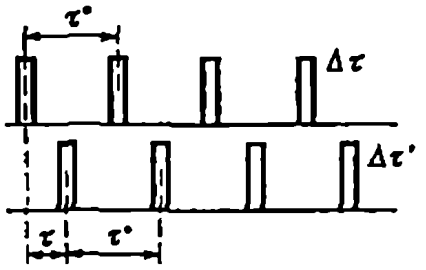

Fig. 214

The required time shift τ is determined from the condition

$$\tau = l/v, \qquad (6.5.2)$$

where v is the neutron velocity in which we are interested and l is the flight length (between the cylinder and the detector). The requisite time shift is attained in practice by appropriately positioning the mirror. Results can be obtained more quickly by employing multichannel registration, i.e. by simultaneously using several (in the present case, six) photocells turned at a small angle relative to each other. Each photocell opens its channel at a different time τ and thus singles out neutrons with different velocities from the beam

$$v_l = l/\tau_l. \qquad (6.5.3)$$

The shutter described here is a good chopper of neutron beams only in the region of thermal and epithermal energies, since cadmium

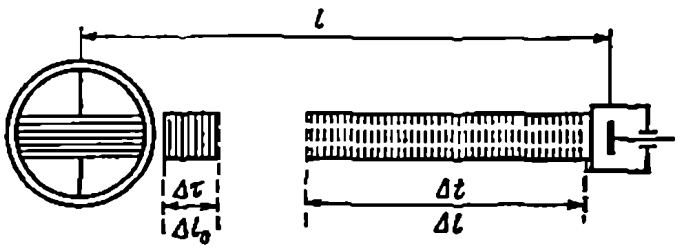

Fig. 215

freely allows the passage of neutrons with energy exceeding 0.3 eV (see Fig. 222). Thus, $T_{max} = 0.3$ eV ($v_{max} = 7.5 \times 10^5$ cm/s). Besides, there exists a natural lower bound for energy, given by $T_{min} = 7.5 \times 10^{-3}$ eV ($v_{min} = d/\Delta\tau = 4/3.3 \times 10^{-5} = 1.2 \times 10^5$ cm/s), since slower neutrons do not manage to cross the cylinder core during the time of favourable positioning of cadmium.

Neutrons with energies between T_{min} and T_{max} form packets of duration $\Delta\tau = 3.3 \times 10^{-5}$ s which appear behind the rotating cylinder (Fig. 215). As these neutron packets, which are initially short-

duration narrow pulses [$\Delta l_0 = \Delta\tau\,(v_{max} - v_{min}) \simeq 20$ cm], advance towards the detector, they expand due to the fact that the leading pulse edges move faster than the trailing edges. It can be easily shown that when the leading edge of a pulse packet reaches the detector, the length of the packet is $\Delta l \simeq 20\Delta l_0$, while the entire packet takes a time $\Delta t \simeq 100\Delta\tau$ to pass through the detector. Obviously, such a packet can be decomposed into segments with different values of neutron velocity (energy) by switching on the detector for a short time[28] $\Delta\tau'$ during which the section of the pulse packet passing through it has the velocity (energy) in which we are interested.

Since

$$v = l/\tau \text{ and } T = mv^2/2 = (ml^2/2)\,(1/\tau^2), \qquad (6.5.4)$$

where τ is determined with an accuracy $d\tau = \Delta\tau + \Delta\tau'$, the energy of the isolated neutrons will have an uncertainty given by

$$dT = (ml^2/2)\,(2d\tau/\tau^3) = -2Td\tau/\tau. \qquad (6.5.5)$$

The ratio of the uncertainty in energy to the energy itself (i.e. the relative error in the determination of energy) is a measure of the resolving power of the instrument. It follows from (6.5.4) and (6.5.5) that

$$dT/T = -2d\tau/\tau = -2vd\tau/l. \qquad (6.5.6)$$

This formula shows that the resolving power of the instrument depends on the velocity of the neutrons being investigated. The interaction of the slowest neutrons ($v \simeq v_{min}$) with nuclei can be investigated with the highest degree of accuracy. For a fixed velocity of neutrons, the resolving power is higher for a smaller $d\tau$ and a larger l. Hence the resolving power of an instrument is often given as the ratio of these quantities, viz. $d\tau/l$, expressed in microseconds per metre.

The set-up described above was a significant advance in comparison with the Dunning monochromator. However, it suffers from some serious drawbacks. In the first place, this instrument can be used only for the investigation of thermal and epithermal neutrons, and even in this energy range the results are not very reliable due to a poor resolving power ($dT/T = 0.03$ at $T = T_{min}$, and $dT/T = 0.2$ at $T = T_{max}$).

Further development of the mechanical selector method was directed at eliminating these drawbacks. To extend the range of neutron energy under investigation, cadmium was replaced by other materials (nickel, steel, chromium) which have a smoother dependence of the neutron cross section on energy and can be used to ab-

[28] The quantity $\Delta\tau'$ includes the time during which neutrons pass through the detector (the ionization chamber) and the time for which the amplifying unit is rendered conducting.

sorb neutrons with relatively high energies if the thickness of these absorbers is quite large. The range of this method was increased up to about 10^4 eV using solid cylinders of these materials as shutters (Fig. 216). A combination of metallic cylinders and hydrogenous slabs allowed an extension of this range to 10^2 keV. Since the resolving power deteriorates with increasing energy of neutrons, this new opportunity could not be used without a significant improvement in the resolving power. This, in turn, was made possible by increasing the rotational speed (up to 40000 rpm) a better collimation of the beam, decreasing the channel width (to 0.5 μs) and increasing the flight length (to 100-200 m).[24] Naturally, each new step in this direction required an increase in the intensity of the primary neutron beam.

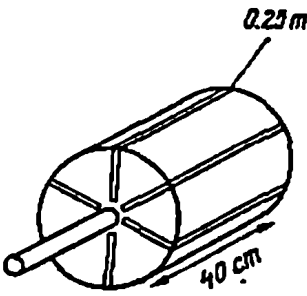

Fig. 216

On the low-energy side, measurements are usually made up to 10^{-3} eV. For lower values of energy, measurements are hampered due to the fact that the spectrum of thermal neutrons contains an extremely small number of such neutrons.

To increase the efficiency of measurements, modern instruments have shutters with many (several dozens) slits instead of just one. Detection is carried out with the help of a time analyzer which provides results for many (up to 2000) values of neutron energy simultaneously.

The background is lowered and pulse duration is decreased by using multirotor mechanical selectors whose rotors are successively arranged in the beam at a certain distance from one another. Considerable attention is paid to the beam formation (collimation, suppression of scattering by passing the beam through vacuum or helium-filled tubes) and to the design of detectors (increase in the registration efficiency).

6.5.3. Pulsed Accelerator Method

Another version of the time-of-flight method, viz. the pulsed accelerator method, was proposed in 1938 by the American physicist Alvarez. The basic idea behind this method is to obtain a pulsed beam of slow neutrons with the help of a pulsed accelerator (a cyclotron was used in the earlier experiments). If an arc source of ions,

[24] Flight distances up to 10^3 m can be used in the pulsed reactor created in the USSR (Dubna).

say, deuterons in a cyclotron, is periodically switched on for a short period $\Delta\tau_0$, accelerated deuterons are produced in the cyclotron with the same time period. By placing a beryllium target in the path of the deuterons, we can obtain a pulsed beam of fast neutrons which, after being slowed down in paraffin, are transformed into narrow pulses of slow neutrons. The detection process is practically the same as in the mechanical selector method, the only exception being that the detection is synchronized with the instant at which the voltage is supplied to the ion source, and not with the instant at

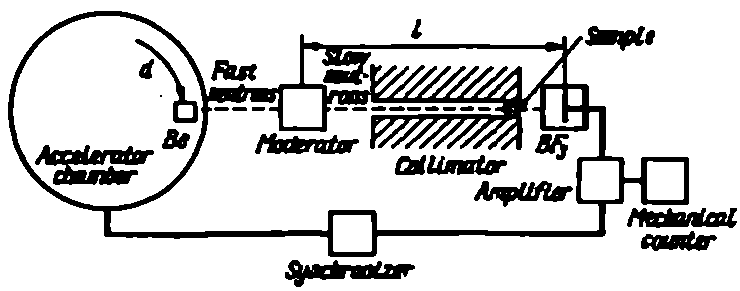

Fig. 217

which a neutron packet is released. Hence the delay between the application of voltage to the ion source and the emergence of the neutron beam must be taken into consideration. This delay consists of the deuteron acceleration period (about 5 μs) and the slowing-down time for fast neutrons in paraffin (about 10-15 μs).

The experimental set-up for investigation of cross section of interaction of neutrons with nuclei with the help of pulsed cyclotron method is shown in Fig. 217. The ionization chamber is filled with gaseous BF_3; the detection is carried out by using a mechanical counter or any other pulse recorder.

The resolving power of the pulsed cyclotron method is defined in the same way as in the mechanical selector method:

$$dT/T = -2d\tau/\tau,$$

where $\tau = l/v$ is the time of flight and $d\tau$ is its uncertainty. It was mentioned above (see Sec. 6.5.2) that

$$d\tau = \Delta\tau + \Delta\tau',$$

where $\Delta\tau$ is the duration of the neutron packet and $\Delta\tau'$ is the recording time.

The quantity $\Delta\tau$ is determined by the duration $\Delta\tau_1$ of the pulse controlling the ion source and by the time-spread $\Delta\tau_2$ in the slowing down of neutrons of various energies. Since the spread in the slowing-down time for low-energy neutrons may be as high as 1 μs, or even

several microseconds, there is no point in making $\Delta\tau_1$ less than 10^{-6} s.

Owing to the application of vertical beam deflection to the target and a small-size moderator, it became possible to subsequently reduce $\Delta\tau$ to 0.05 μs. For l varying between 100 and 200 m, this gives $d\tau/l \simeq 0.0005$ μs/m.

The pulsed accelerator method has the advantage that there is practically no upper limit of the energy that can be measured by this method (in the mechanical selector method, the upper limit is set by the speed of rotation, i.e. by the strength of the cylinder). Thus, for example, there are instruments operating in the energy range between 1 and 30 MeV with a quite satisfactory resolving power which lies between 0.7×10^{-2} and 4×10^{-2}. Besides, this method has an advantage over the mechanical selector method in that it has a lower background and can be used for wider beams, i.e. larger samples.[25]

6.5.4. Diffraction of Slow Neutrons by a Crystal, or the Crystal Monochromator Method

The de Broglie wavelength λ for neutrons is given by the formula

$$\lambda = \frac{4.5 \times 10^{-10}}{\sqrt{T}}, \tag{6.5.7}$$

where T is in eV and λ is in cm.

For slow neutrons having energy between 0.01 and 100 eV, we have

$$\lambda = 0.45 \times 10^{-10}\text{-}0.45 \times 10^{-8} \text{ cm},$$
$$\lambda = 2\pi\lambda = 3 \times 10^{-10}\text{-}3 \times 10^{-8} \text{ cm} = 0.03\text{-}3 \text{ Å}.$$

But these values are of the same order as the separation between planes in crystals. For example, the lattice constant d for LiF crystal is equal to 2.32 Å. Hence it can be expected that when slow neutrons are incident at a small angle θ on a crystallographic plane, monochromatic neutrons are reflected at an angle equal to the angle of incidence. The angle θ, the wavelength λ of the reflected neutrons and the lattice constant d are connected through the well-known Bragg relation (see Sec. 4.10.2)

$$2d \sin\theta = n\lambda = 2\pi n\lambda, \tag{6.5.8}$$

where n is the reflection order.

[25] On the contrary, when rare isotopes are investigated, we must be able to use small samples. Such a possibility is provided by the mechanical selector method.

Since $\lambda = h/p = h/\sqrt{2mT}$, this equation provides a relation between the neutron energy T and the angle of reflection θ:

$$T = (h^2/8md^2)\ (n^2/\sin^2\theta). \qquad (6.5.9)$$

By changing the angle θ, we can change the energy of the reflected neutrons.

It follows from formula (6.5.9) that neutrons with various values of energy can be reflected at a given angle θ:

$$T_n = n^2 T_0, \qquad (6.5.10)$$

where

$$T_0 = h^2/8md^2 \sin^2\theta, \qquad n = 1, 2, 3, \ldots .$$

However, the intensity of the reflected neutrons decreases with increasing n in view of the fact that for neutrons with a high energy, i.e. with a small wavelength, the thermal motion of the lattice atoms causes a stronger violation of the coherence of waves scattered by different atoms.

Differentiating formula (6.5.9) with respect to θ, we can find the resolving power of the method:

$$dT/T = -2\cot\theta d\theta. \qquad (6.5.11)$$

The resolving power of the latest available instruments is about 10^{-3}, a value close to the lower limit of the energy interval.

It can be easily seen that the angle θ in formulas (6.5.9)-(6.5.11) is quite small. Thus, for example, $\theta = 3.5°$ for 1-eV neutrons when $d = 2.32$ Å and $n = 1$; for 100-eV neutrons, the corresponding value of θ is just 0.35°. Consequently, the above-mentioned formulas can be replaced by the following approximations:

$$T_n \simeq n^2 T_0, \qquad (6.5.12)$$

where

$$T_0 \simeq h^2/8md^2\theta^2$$

and

$$dT/T \simeq -2d\theta/\theta. \qquad (6.5.13)$$

It is obvious from formulas (6.5.12) and (6.5.13) that as in the first two methods the resolving power decreases with increasing neutron energy.

A deterioration in the resolving power and a decrease in the angle of reflection with increasing neutron energy restrict the range of applicability of the crystal monochromator method to energies $T_{max} \simeq 5$-100 eV. The lower limit of energy is $T_{min} \simeq 0.01$ eV, since neutrons having e lower energy (i.e. lying to the left of the peak on

the Maxwellian distribution curve) are difficult to investigate due to the large impurity effect from the second-order reflection [$n = 2$ in formula (6.5.9)]. This circumstance is explained by the increasing intensity of the spectrum to the left of the peak.[26]

Figure 218 shows schematically the measuring technique employing the diffraction of slow neutrons by a crystal.

As was mentioned above, the diffraction technique has the advantage that it is actually possible to isolate neutrons of a particular energy from a beam. This allows an irradiation of samples by monoenergetic neutrons. Obviously, such experiments cannot be carried

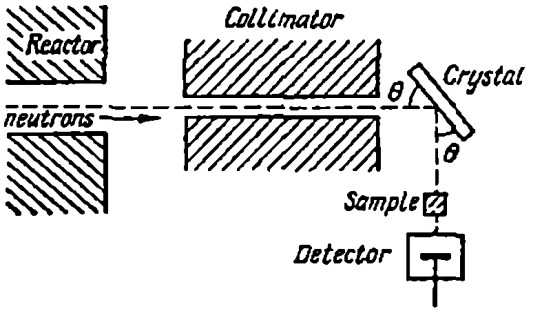

Fig 218

out by using the time-of-flight methods, since the neutron beam in such methods contains neutrons with all values of the moderation spectrum energies. This feature, however, makes these methods quite useful, since it enables a simultaneous detection of the effect due to monoenergetic neutrons of several energy values.

Finally, let us consider the cold neutrons mentioned in Sec. 6.3.2. It can be seen from formula (6.5.8) that reflection is not possible for $\lambda > 2d$ ($\sin\theta = n\lambda/2d > 1$). According to formula (6.5.9), such values of λ correspond to neutron energies $T_n < 5 \times 10^{-3}$ eV, i.e. to cold neutrons. This means that cold neutrons can be isolated from the spectrum of slow neutrons by passing them through a very thick slab of a polycrystalline material (say, graphite). In accordance with formula (6.5.8), all neutrons with $\lambda < 2d$ are reflected and do not pass through the slab. However, cold neutrons will be able to pass through (since they cannot undergo reflection).

Neutrons with a still lower energy ($T_n < 10^{-4}$ eV) are called *ultracold* neutrons. Ultracold neutrons with energy $T_n \simeq 10^{-7}$ eV have such a large wavelength λ that they undergo total internal reflection at the vacuum(air)-material interface for any angle of incidence (see Sec. 6.8).

[26] Sometimes, a mechanical monochromator is used to remove the reflection for $n \geqslant 2$.

6.5.5. Results of Measurements

The advancement of neutron spectroscopy made it possible to verify and confirm Bohr's and Fermi's views on the interaction of neutrons with nuclei, as well as the correctness of the Breit-Wigner formulas, described in Secs. 6.3 and 6.4. We shall describe some of the most significant results of measurements made by neutron spectroscopy techniques.

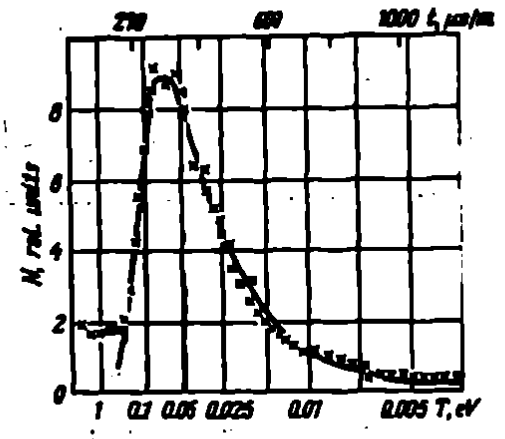

Fig. 219

Figure 219 shows the spectrum of neutrons emerging from paraffin. It was found that this spectrum can indeed be described by the Maxwellian curve $N \propto \sqrt{T_{kin}} \exp(-T_{kin}/kT^\circ)$ with an elevated right branch[27] ($N \propto T_{kin}^{-3/2}$). The peak of the curve lies at an energy corresponding to a neutron temperature of 390 K, which is about 100° higher than the moderator temperature. This is due to the fact that neutrons in paraffin do not attain a complete thermal equilibrium with the medium as their lifetime is comparatively short (about 200 μs). The latter fact is accounted for by an increase in the absorption with a decrease in the neutron energy (1/v-law).

Figure 220 depicts the variation of absorption cross section of slow neutrons in boron. The validity of 1/v-law was experimentally confirmed in the energy interval of 10^{-3}-10^{3} eV. The numerical value of the cross section for boron can be approximately given by the expression

$$\sigma_B \simeq (120/\sqrt{T}) \times 10^{-24}, \qquad (6.5.14)$$

[27] In Fig. 219, the curve has been plotted as a function of the time of flight t. Hence the energy scale is not uniform and the energy increases from right to left. Consequently, the left part of the figure corresponds to the right branch of the Maxwellian curve (see Fig. 194).

where T is in eV and σ is in cm². At high energies (right up to 0.5 MeV) the cross section continues to decrease monotonically. Such a character of the curve for boron is explained by a large level separation for this nucleus.

A typical curve showing the resonance variation of the absorption cross section of slow neutrons can be seen in Fig. 221, where the de-

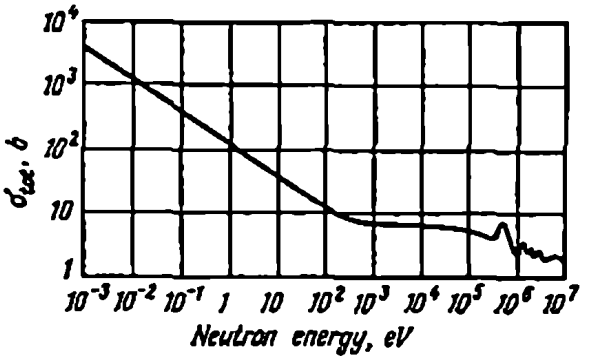

Fig. 220

pendence of the (n, γ)-reaction cross section has been plotted for indium. The figure clearly shows the region where the cross section varies according to the $1/v$-law, three sharp resonances at energies 1.46, 3.8 and 8.5 eV, as well as several resonances at higher energies (12.7, 14.5, 22.6 eV, etc.).

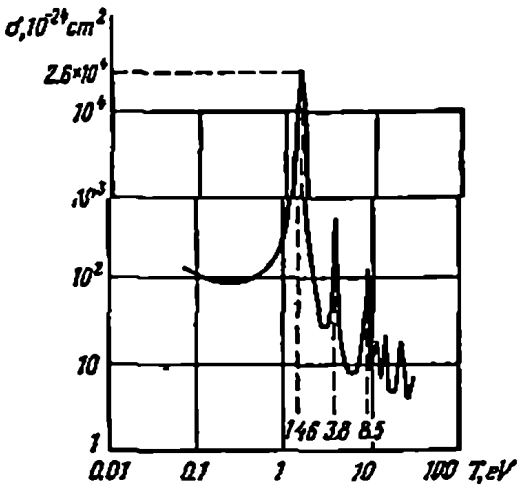

Fig. 221

In all the cases, the cross section in the region of a resonance is described by the Breit-Wigner formulas. Similar results were also obtained for other materials used by Fermi in his experiments on selective capture of slow neutrons. Thus, in the case of silver, the

existence of a level around 5.2 eV was confirmed as well as of levels at energies 16.6 and 31 eV; a level at energy 4.9 eV was discovered for gold.

Thus, the method of boron absorber described in Sec. 6.3 gives a correct qualitative idea of the position of resonance levels in various materials used by Fermi in his experiments.

The estimates concerning the level separation (from 1 to 10 eV) and the values of radiative (Γ_γ) and neutron (Γ_n) level widths were also confirmed. Measurements showed that for energies between 0.1 and 1 eV, $\Gamma_\gamma \simeq 0.1$ eV and $\Gamma_n \simeq 0.001$ eV.[28]

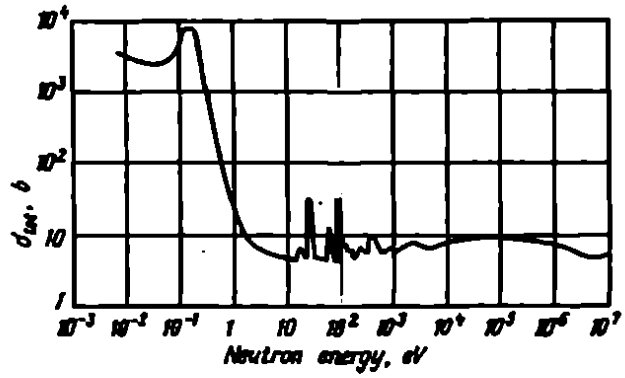

Fig. 222

Finally, Fig. 221 confirms that the resonance neutrons are indeed absorbed more strongly than thermal neutrons. It can be seen from the figure that the resonance cross section for $^{115}_{49}$In is 26400 b, while the cross section of thermal neutrons for the same isotope is just 140 b.

However, even in the thermal energy range, the cross section may be exceptionally large if a resonance level lies in this range. This is the case with cadmium, whose cross section is plotted in Fig. 222.

It can be seen from the figure that cadmium (isotope $^{113}_{48}$Cd) has a resonance level at energy $T_{res} = 0.176$ eV. It should be noted that the peculiar shape of the curve for cadmium (a broad resonance peak) is due to a superposition of the effect of $1/v$-law which is quite significant at low energies. The joint action of the $1/v$-law and selective capture makes cadmium a very effective absorber of all neutrons with energies less than 0.3 eV, including thermal neutrons.

The measured absorption cross section for cadmium (natural isotope mixture) is equal to 7000 b at resonance and 2500 b for thermal neutrons.

---

[28] The value of Γ_n is obtained from formula (6.4.61) for resonance energy and can be calculated for any other energy according to the law $\Gamma_n \propto v$.

The resonance absorption cross section for the isotope $^{113}_{48}$Cd is equal to 60000 b. However, even this is not a record-high value. The cross section of $^{157}_{64}$Gd for thermal neutrons is 190000 b, while for $^{135}_{54}$Xe it is as high as 3.5×10^6 b.

The large value of the thermal neutron capture cross section in xenon is responsible for *xenon poisoning* of nuclear reactors. One of the fission products in a nuclear reactor is $^{135}_{54}$Xe which strongly captures thermal neutrons and leads to an extinction of the chain reaction, thus deteriorating the operation of the nuclear reactor.

For illustration, the parameters of some levels measured by the neutron spectroscopy methods are compiled in Table 26.

Table 26

Isotope	T_{res}, eV	σ, b	Γ, eV	$\Gamma_n(T_{res})$, eV	$\Gamma_n(1\text{ eV})$, eV
^{113}Cd	0.176	60000	0.115	1.56×10^{-4}	3.7×10^{-4}
^{115}In	1.46	26400	0.085	25×10^{-4}	21×10^{-4}
^{157}Gd	0.044	190000	0.05	3.2×10^{-4}	15.2×10^{-4}

Selective capture is not always the dominant process in the interaction of neutrons with nuclei. A number of elements (for example, Ag, Au) with large (n, γ)-reaction cross sections have also appreciable resonance scattering cross sections (tens of barns), while some elements have very large scattering cross sections ($\sigma_{Co} \simeq 1200$ b for $T_{res} = 115$ eV, and $\sigma_{Mn} \simeq 50$ b for $T_{res} = 300$ eV). Figure 223 shows two resonance peaks in the scattering cross section for Co.

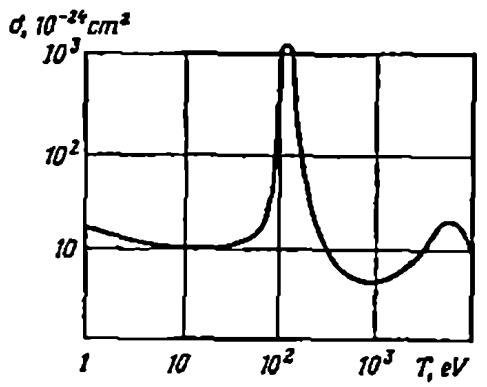

Fig 223

As a rule, scattering resonances are observed for light nuclei which are characterized by a large level separation, and hence [see formula (6.4.17)] a large neutron width Γ_n. For example, the scattering resonance mentioned above for Mn has $\Gamma_n = 20$ eV which is several times larger than the radiation width Γ_γ. In heavy nuclei, sharp scattering resonances are observed when these nuclei contain a magic number of neutrons (in such cases, it is difficult to accomodate an additional neutron, i.e. the value of Γ_γ is relatively small).

Resonance scattering cross section can be measured either by the method of radioactive indicators prepared from the material under

investigation and irradiated by neutrons scattered by the same material, or by neutron spectroscopy employing a special detector, viz. a counter in the form of two coaxial cylinders. The working volume of the counter lies between the walls of these two cylinders. Hence when a neutron beam passes through the inner cylinder, the counter registers only the scattered neutrons.

It is evident from Figs. 222 and 223 that resonance processes can be observed right up to energies 10^3-10^4 eV.

6.6. Scattering of Fast Neutrons

The above arguments concerning the resonance nature of variation of compound nucleus formation cross section with a change in neutron energy are valid for comparatively low energies. As the neutron energy increases, the density and width of levels increase to such an extent that levels begin to overlap. Obviously, in this energy range the cross section will be described by a smoother function. In the first approximation, such a function can be obtained by writing the compound nucleus formation cross section in the form

$$\sigma^* = \sum_{l=0}^{R/\lambda} S_l \xi_l, \qquad (6.6.1)$$

where S_l is the geometrical cross section and ξ_l is the adhesion coefficient for neutrons with orbital angular momentum l.

According to formula (6.4.26), we have

$$S_l = (2l + 1)\,\pi\lambda^2.$$

The quantity ξ_l is determined by the penetrability of the centrifugal barrier, by the coefficient p of transmission through the nuclear boundary and by the probability of neutron capture by the nucleus. For neutrons with $l < R/\lambda$, the penetrability of the centrifugal barrier is almost equal to unity since the condition $l < R/\lambda$ is equivalent to the condition $T > B_0$ (l) (see Sec. 5.4.2). The capture probability for a neutron is also equal to unity (first stage of the reaction). Hence the adhesion coefficient ξ_l is equal to the transmission coefficient p which is defined by the formula (6.4.15):

$$p = 4kk_0/(k + k_0)^2.$$

Thus, the cross section for the formation of a compound nucleus in the interval of merging levels must be given approximately by the expression

$$\sigma^* = \sum_{l=0}^{R/\lambda} \frac{4kk_0}{(k+k_0)^2}(2l+1)\,\pi\lambda^2 \simeq \pi(R+\lambda)^2 \frac{4kk_0}{(k+k_0)^2}. \qquad (6.6.2)$$

It can be easily seen that this is a monotonically decreasing function and tends to its limiting value πR^2 with increasing energy.

Indeed, for fast neutrons $\lambda \ll R$ and $k \simeq k_0$, whence $\pi (R + \lambda)^2 \simeq \pi R^2$ and $\xi = 4k_0k/(k + k_0)^2 \simeq 1$.

The equality $\xi = 1$ means that a neutron flying towards a nucleus definitely enters it and gets stuck there for a long time (the lifetime of the compound nucleus). The possibility of such a capture is associated with a high density of nucleons in the nucleus and with a strong nuclear interaction between them. The mean free path of a neutron having energy 1-10 MeV inside the nucleus is less than the nuclear radius. Hence once a neutron enters a nucleus, it inevitably collides with other nucleons and transfers its energy to them.

In order to obtain the cross section of the process taking into account the second stage of the reaction, it is usually necessary to determine the relative disintegration probability $\eta_l = \Gamma_l/\Gamma$ of the compound nucleus via a particular channel.

Of all the Γ_l in the energy range considered here, Γ_n has the highest value. This means that scattering is the main process through which a compound nucleus disintegrates. Indeed, it was shown above that $\Gamma_\gamma \simeq 0.1$ eV and is practically independent of the neutron energy, $\Gamma_n \simeq 10^{-3}$ eV at neutron energies of about 1 eV, and increases as the square root of energy. Thus, for neutrons with energy $T_n > 1$ MeV, the neutron width $\Gamma_n > 1$ eV, i.e. $\Gamma_n \gg \Gamma_\gamma$ or,

$$\Gamma = \Gamma_n + \Gamma_\gamma + \Gamma_p + \Gamma_\alpha + \ldots \simeq \Gamma_n \tag{6.6.3}$$

(Γ_p, Γ_α, etc. are small on account of the Coulomb barrier). Hence

$$\eta_n = \Gamma_n/\Gamma \simeq 1, \tag{6.6.4}$$

while the scattering cross section is given by

$$\sigma_n = \sigma^* \eta_n = \pi (R + \lambda)^2 \tag{6.6.5}$$

or

$$\sigma \simeq \pi R^2. \tag{6.6.6}$$

Let us now consider the basic characteristics of this process. Obviously, the inverse process involving the escape of a neutron from a nucleus (not necessarily the same neutron) is possible not only when the entire initial energy is concentrated on the neutron near the boundary of the nucleus. All that is required is that this energy exceed the separation (binding) energy of the neutron. Since the probability of concentration of a lower energy is comparatively higher, neutrons with lower energies should escape more frequently from a nucleus. In other words, scattering must be inelastic.

When fast neutrons enter a nucleus, their interaction with the latter is not confined just to inelastic scattering. The wave nature of particles means that elastic potential scattering, which must be of

diffraction type, is also possible. The possibility of such a process is due to the fact that for $\xi = 1$, the nucleus can be treated as a black ball on which a neutron wave of wavelength $\lambda\!\!\!^{-}$ must undergo diffraction scattering.

The theory of optical diffraction by an opaque circular screen predicts that the diffraction scattering must be highly anisotropic. The differential cross section of diffraction scattering at an angle θ is determined from the formula (for $\theta \ll 1$ and $\lambda\!\!\!^{-} \ll R$):

$$d\sigma(\theta) = R^2 \left| \frac{J_1(R\theta/\lambda\!\!\!^{-})}{\theta} \right|^2 d\Omega, \qquad (6.6.7)$$

where J_1 is the first Bessel function having roots at $\alpha = R\theta/\lambda\!\!\!^{-} = 0$, 3.8, 7.0, and a maximum at $\alpha = 5.2$.

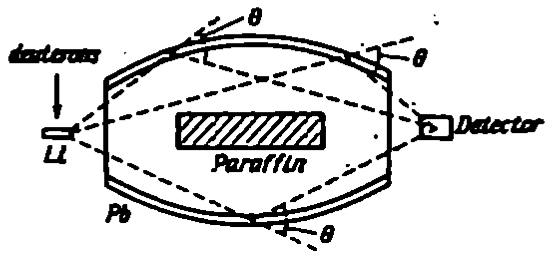

Fig. 224

According to this formula, the diffraction scattering cross section must have a maximum at $\alpha = 0$ (because of the presence of angle θ in the denominator) and at $\alpha = 5.2$, while it should be equal to zero at $\alpha = 3.8$ and $\alpha = 7.0$.

According to the diffraction theory, the total diffraction scattering cross section must be

$$\sigma \simeq \pi (R + \lambda\!\!\!^{-})^2 \qquad (6.6.8)$$

or, for $\lambda\!\!\!^{-} \ll R$,

$$\sigma = \pi R^2. \qquad (6.6.9)$$

These conclusions were confirmed in 1946 in experiments on elastic scattering of neutrons with an energy of about 14 MeV. The experimental set-up is schematically shown in Fig. 224. A lithium target is bombarded with a beam of deuterons with energy 0.9 MeV. A paraffin screen is used to prevent a direct entry of neutrons from the target to the detector. The reaction

$$^{7}_{3}\mathrm{Li} + {}^{2}_{1}\mathrm{H} \rightarrow 2{}^{4}_{2}\mathrm{He} + n\,(Q \simeq 13\ \mathrm{MeV}) \qquad (6.6.10)$$

results in the formation of neutrons with an energy of about 14 MeV, incident on the inner surface of a barrel-shaped lead scatterer at all possible angles. If the lateral surface of the barrel is generated by the

revolution of an arc of a circle while the source of neutrons (Li) and the detector lie on the intersection of this circle with the axis of the barrel, the scattering angle θ for all the incident neutrons is the same.

Such an experimental set-up is a modification of the annular scatterer method used by Chadwick (see Sec. 4.4.2) and sharply enhances the effect.

The elastically scattered neutrons were registered by a copper detector surrounded by cadmium. It was mentioned in Sec. 6.2.5 that neutrons with energy $T_n > 11.2$ MeV are responsible for the reaction

$$^{63}\mathrm{Cu}\,(n,\ 2n)^{62}\mathrm{Cu}, \qquad (6.6.11)$$

which leads to the formation of a positron-active isotope ^{62}Cu with a half-life of about 10 min.

In order to measure the angular dependence of the scattering cross section, several barrels were used in the experiment, each for a particular angle of scattering (θ = 20°, 30°, 35°, 40°, 50°, 60°, 70° and 80°). The results of measurements are shown in Fig. 225 which also shows, for the sake of comparison, theoretical curves plotted under the assumption that the radius R of the black ball is equal to 6×10^{-13} cm (curve *1*), 7.5×10^{-13} cm (curve *2*) and 9×10^{-13} cm (curve *3*). It is clearly seen from the figure that the experimental points are in best agreement with the theoretical diffraction scattering curve plotted under the assumption that $R = 7.5 \times 10^{-13}$ cm. The radius of the lead nucleus is just close to this value. Thus, it was proved that fast neutrons undergo diffraction scattering at lead nuclei.

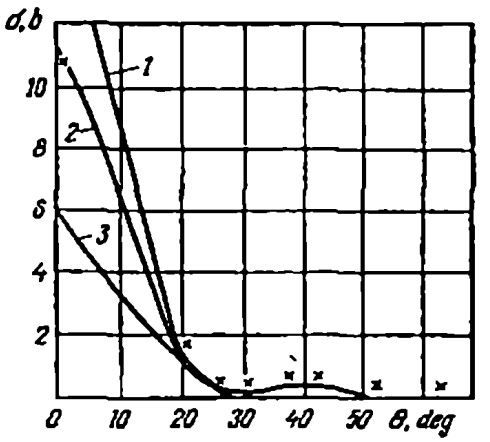

Fig. 225

The diffraction scattering was subsequently investigated experimentally for various atomic nuclei over a wide energy interval with the help of different methods. The experimental results (in particular, the displacement of peaks depending on the neutron energy) invariably confirmed the diffraction nature of this phenomenon. It should be noted that the diffraction scattering must be observed (and is indeed observed) for charged particles also if steps are taken to eliminate the masking effect due to Rutherford scattering.

According to formulas (6.6.5) and (6.6.8), the overall cross section of inelastic and diffraction scattering is given by

$$\sigma_s = \sigma_{i.s.} + \sigma_{d.s.} = \pi (R + \lambda\!\!\!^{-})^2 + \pi (R + \lambda\!\!\!^{-})^2 = 2\pi (R + \lambda\!\!\!^{-})^2. \qquad (6.6.12)$$

For the energy range considered in the present case, the scattering cross section considerably exceeds the capture cross section. Hence we can assume that the total cross section of interaction of neutrons with nuclei is

$$\sigma_{tot} \simeq \sigma_s = 2\pi (R + \lambda)^2 \simeq 2\pi R^2. \qquad (6.6.13)$$

To a first approximation, this conclusion must be valid for higher-energy neutrons, where processes other than scattering also occur with an appreciable cross section [for example, the reactions (n, p), $(n, 2n)$], since the cross section of the formation of the compound nucleus remains equal to πR^2, while the total disintegration coefficient η is always equal to unity:

$$\eta = \sum \eta_i = \Gamma_\gamma/\Gamma + \Gamma_n/\Gamma + \ldots = \Gamma_i/\Gamma = 1. \qquad (6.6.14)$$

This circumstance made it possible to carry out very important experiments on the determination of nuclear radii by a method based

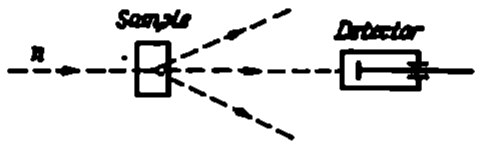

Fig. 226

on the attenuation of a neutron beam upon passing through matter. The schematic of such an experiment is shown in Fig. 226. Neutrons from the primary beam fall on the sample and are scattered by it (or undergo some other type of interaction). Consequently, some of these neutrons leave the beam, and the beam is attenuated by a factor of $\exp(n\sigma_{tot}\delta)$, n being the number density of the sample nuclei, σ_{tot} the total cross section and δ the thickness of the sample.

By measuring the beam attenuation

$$N/N_0 = \exp(-n\sigma_{tot}\delta), \qquad (6.6.15)$$

with the help of a detector, we can find the experimental value for the total cross section σ_{tot} which in accordance with the above considerations, must be

$$\sigma_{tot} = 2\pi R^2.$$

Hence the nuclear radius is given by

$$R = \sqrt{\sigma_{tot}/2\pi}. \qquad (6.6.16)$$

First measurements of nuclear radii with the help of this method were made in 1945-46 for neutrons with energies 14 and 25 MeV. It was borne out by measurements that the dependence of the nuclear

radius (in cm) on the mass number A can be expressed in the following form:

$$R = (1.37A^{1/3} + 1.7) \times 10^{-13}. \quad (6.6.17)$$

A similar result was obtained in more accurate experiments carried out in 1952:

$$R = (1.37A^{1/3} + 1.3) \times 10^{-13}, \quad (6.6.18)$$

where R is in cm.

These results confirm the correctness of the assumption made in the liquid drop model (see Sec. 2.1), according to which the nucleus can be considered, to a first approximation, as a spherical drop of an incompressible nuclear fluid whose radius varies as $A^{1/3}$:

$$R = r_0 A^{1/3}. \quad (6.6.19)$$

However, difficulties were encountered in the interpretation of results when experiments were carried out with higher-energy neutrons (90 MeV) obtained by deuteron stripping (see Sec. 10.3). It was found that the nuclear radius (in cm) calculated from the values of the total cross section does not vary linearly with $A^{1/3}$ but assumes lower values for light nuclei:

$$R = (1.37A^{1/3} + 0.5)\,(1 - e^{-0.49\sqrt{A}}) \times 10^{-13}. \quad (6.6.20)$$

Since there are no grounds to question the validity of the law $R \propto A^{1/3}$, the results indicate the erroneous nature of the assumption that the total cross section is equal to $2\pi R^2$.

The results of experiments with neutrons having an energy equal to 90 MeV show that the assumption about the nucleus being an opaque black ball ($\xi = 1$) is inexact. For such energy values, the nucleus becomes translucent, and the cross section of interaction of neutrons with the nuclei differs from $2\pi R^2$. Nevertheless, the investigation of scattering of fast neutrons by nuclei is one of the most accurate methods of determining the radius of atomic nuclei [to be more precise, the range of interaction of a neutron with the nucleus, which is somewhat larger than the nuclear radius (see Sec. 1.4.6)].

6.7. On the Optical Model of Nuclear Interactions [29]

The results of the experiment described at the end of Sec. 6.6 show that the concept of the nucleus as a black sphere is incorrect for neutrons with an energy $T \simeq 100$ MeV. This conclusion seems quite natural, since the interaction cross section of a neutron decreases with its energy, and hence its mean free path in the nucleus $l = 1/n\sigma$

[29] The model considered here is frequently called the optical model of the nucleus.

(n is the number density of the nucleons in the nucleus) increases and becomes comparable with the nuclear radius.

However, a detailed investigation of the variation of cross section with energy for many nuclei points towards a deviation from the Bohr model for other (much lower) energy values as well.

It should be recalled that according to the Bohr model, which is based on the assumption that $\xi = 1$, i.e. $l \ll R$, the total cross section of interaction of fast neutrons with a nucleus must be $\sigma_{tot} \simeq 2\pi (R + \lambda\!\!\!^{-})^2$ [see formula (6.6.13)], i.e. must decrease monotonically with increasing energy and approach the value of $2\pi R^2$ for

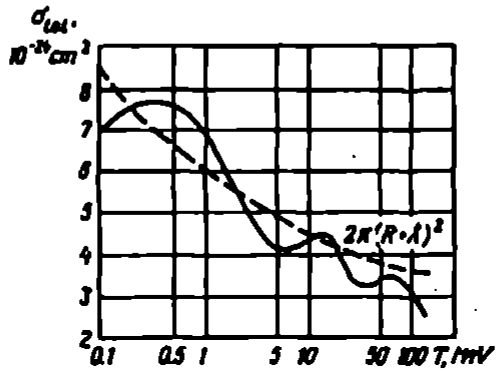

Fig. 227

$\lambda\!\!\!^{-} \ll R$ ($T_n > 50$ MeV). It follows from the same formula that the cross section must increase smoothly with increasing nuclear radius $R = r_0 A^{1/3}$, i.e. increasing mass number, according to the law $\sigma \propto A^{2/3}$.

Figure 227 compares the experimental values of total cross section σ_{tot}^{exp} and the theoretical value $\sigma_{tot}^{theor} = 2\pi(R + \lambda\!\!\!^{-})^2$ for cadmium over a wide energy interval from 0.1 to 100 MeV.[30] It is obvious from the figure that instead of the monotonically decreasing dependence of σ_{tot}^{theor} (dashed curve), several peaks are observed in the experimental dependance (solid curve). The dependence of the cross section on the mass number also differs appreciably from the law $\sigma \propto A^{2/3}$.

If σ_{tot}^{exp} is plotted as a function of T_n and A, we obtain a complex surface of the type shown in Fig. 228.

The discrepancy between σ_{tot}^{exp} and $\sigma_{tot}^{theor} = 2\pi (R + \lambda\!\!\!^{-})^2$, which is predicted by the Bohr model, is explained in the *optical model of the nucleus* constructed in analogy with the wave optics. The first

[30] In the range of $T < 1$ MeV, the cross section σ_{tot}^{exp} was obtained by averaging over close resonances.

neutrons will become ultracold. This idea was put into practice by using an aluminium disc of diameter 1.7 m with bent copper foils (mirrors) arranged on its rim at an interval of 7 mm (neutron turbine). A linear velocity $v_m = 25$ m/s of the mirrors, equal to half the velocity of cold neutrons ($v_0 = 50$ m/s) used in the experiment, can be ensured by rotating the disc. Neutrons are incident on the mirrors at grazing angles and leave from the other side of the disc after about 10 reflections (approximately at right angles to the

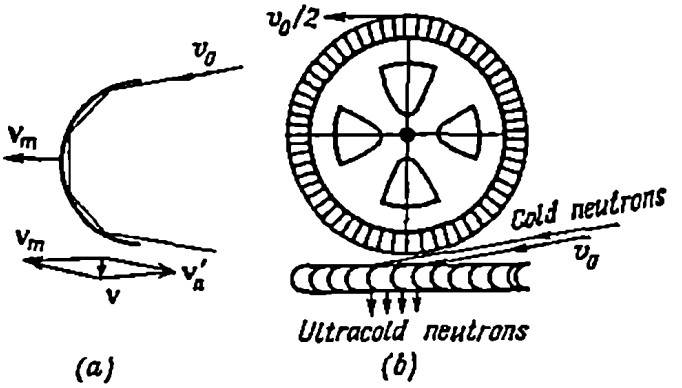

Fig. 230

plane of the disc) with a residual velocity $v \leqslant 10$ m/s (Fig. 230*b*). The entire set-up is enclosed in a steel jacket in which a vacuum of 10^{-4} mm Hg is maintained.

Ultracold neutrons can be obtained by slowing down faster neutrons in the gravitational field of the Earth, i.e. by directing them upwards along the neutron guide. It is interesting to note that the change in the gravitational energy of a neutron over a length of 1 m is equal to 10^{-7} eV with a fairly high degree of accuracy.

Finally, another method of controlling the behaviour of ultracold neutrons was proposed by Vladimirskii in 1960. It turns out that the kinetic energy of such neutrons ($\sim 10^{-7}$ eV) is comparable with the energy $\mu_n H$ of interaction of the neutron magnetic moment μ_n with a magnetic field of strength 20 kG. Hence ultracold neutrons can be kept away from the walls of a vessel with the help of a nonuniform magnetic field with a strength of the same order. Such a field can be created, for example, by arranging several current-carrying conductors along the generatrices of a torus in such a way that the directions of the current in adjacent conductors are opposite.

In view of the above, it is obvious that for ferromagnetics with a saturation induction B, the limiting energy E_{11m} can have two values:

$$E_{11m} = \frac{h^2 N b}{2\pi m_n} \pm \mu_n B. \qquad (6.8.10)$$

Thus, for iron $(E|\|^{p}_{m})_{Fe} = 3.4 \times 10^{-7}$ eV and $(E|\|^{p}_{m})_{Fe} = 0.8 \times 10^{-7}$ eV, while for cobalt the values of $E_{\|m}$ have even opposite signs: $(E|\|^{p}_{m})_{Co} = 1.66 \times 10^{-7}$ eV and $(E|\|^{p}_{m})_{Co} = -0.488 \times 10^{-7}$ eV.

The first experimental investigations of the properties of ultracold neutrons were carried out by Shapiro *et al.* (USSR) in 1968. A flux of ultracold neutrons equal to 3×10^{-4} neutrons/(cm^2·s) was used in these experiments. The storage effect was confirmed and storage times of up to 70 s were attained. However, these values were found to be smaller than the theoretical results in all cases.

At present, it has become possible to increase the flux of ultracold neutrons by a factor of 10^6 and storage times of about 600 s have been attained in large vessels, but the above-mentioned discrepancy between theory and experiment persists and no explanation has been found so far. Most probably, this discrepancy is associated with the hydrogenous contamination on the vessel walls, which is hard to get rid of.[38]

The possibility of magnetic confinement of ultracold neutrons was experimentally demonstrated in 1976 in Dmitrovgrad (USSR) with the help of a closed system of plane magnetic mirrors. Each mirror is a system of conductors with alternating directions of the current flowing through them.

6.8.3. Application of Ultracold Neutrons

A magnetic storage ring based on the principle of magnetic confinement of neutrons was constructed in 1977 at Bonn University. The ring was a torus of diameter 1.2 m. Superconducting magnets were used for producing a nonuniform magnetic field whose maximum strength was 3.5 kG. The field strength increased from the axis to the edges, and hence neutrons with a certain direction of polarization were confined to the toral axis.

At the end of 1977, the storage ring was transferred to France and was installed in the reactor in Grenoble. Neutrons from the reactor are injected into the storage ring with the help of a system of curved nickel-coated mirrors. The injector is equipped with a high-speed pneumatic unit for its rapid removal from the ring (over a period shorter than the time taken by the neutrons to complete one revolution in the ring). In order to ensure a large number of accumulated neutrons, the ring is designed to operate over a wide range of momenta, viz. $\Delta p/p \simeq 3$.

The accumulated neutrons are detected by a ^{3}He-counter which is introduced into the ring at the required instant. Measurements showed that intensity of neutrons accumulated in the ring increases

[38] Ultracold neutrons are heated up as a result of collisions with hydrogen.

potential barrier inside which there must exist quasistationary states of ultracold neutrons. The quantum-mechanical characteristics of these states can be determined by considering the one-dimensional Schrödinger equation. If the energy of ultracold neutrons is equal to the energy of one of such states, the probability of their passing through the potential barrier sharply increases, and the probability of reflection decreases. Figure 233*a* shows the characteristics of the targets and the results of experiments on resonance reflection. The solid curve shows the exact solution of the one-dimensional Schrödinger equation for a multistep potential shown on the right side of Fig. 233*a*. It can be seen from the figure that the experimental points are in quite good agreement with the theoretical curve with the minimum at a height of 108.5 cm of neutron incidence. The width of the minimum corresponds to the lifetime 2×10^{-7} s of the bound state of ultracold neutrons. Similar results were also obtained by using another target, in which a resonance in the transmission of ultracold neutrons was observed when their energy was equal to the energy of the quasistationary levels (Fig. 233*b*).

6.9. A Brief Resumé of Chapter 6

In this chapter, we have considered the properties, methods of production and nuclear interactions of neutrons.

The neutron possesses the following properties: $z_n = 0$; $m_n = 1.00866$ amu $=$ 939.6 MeV $= 1838.6 m_e$; $B_n = +1$; $P = +1$; $s_n = 1/2$; $\mu_n = -1.91 \mu_B$; $T_{1/2} \simeq 10$ min (according to the decay scheme $n \to p + e^- + \tilde{\nu}$); $T = 1/2$ and $T_z = -1/2$.

Neutrons are obtained from neutron sources [(α, n)- and (γ, n)-reactions, spontaneous fission], in accelerators [(α, n)-, (d, n)-, (γ, n)- and (p, n)-reactions], and in nuclear reactors.

The main types of nuclear interactions induced by neutrons with energy $T_n < 10$ MeV are reactions of the type (n, γ), (n, α), (n, p), and fission reactions, as well as processes of elastic and inelastic scattering. For $T_n > 10$ MeV, neutrons induce reactions involving the escape of two or more particles [$(n, 2n)$, (n, pn), $(n, 3n)$, etc.]

Upon elastic (or inelastic) collisions with nuclei, neutrons rapidly lose their kinetic energy and are slowed down. The most rapid loss of energy during slowing down is observed in elastic collisions of neutrons with hydrogen. The average energy of neutrons after n collisions with hydrogen nuclei is $\bar{T}_n = T_0/2^n$ (T_0 is the initial energy), and the average number of collisions required to slow down neutrons with energy T_0 to energy T is $\bar{n} = \ln (T_0/T)$. For a heavy moderator ($A \geqslant 12$) $\bar{n} \simeq (A/2) \ln (T_0/T)$ or, to be more precise (for $A \geqslant 2$),

$$\bar{n} = (A/2 + 1/3 + 1/18A) \ln (T_0/T).$$

In heavy moderators, where the loss of energy by a neutron upon one collision is small, the process of slowing down can be treated as a continuous drop in neutron energy. In this case, the neutron energy is a function of the slowing-down time, and the process of slowing down can be described by a diffusion-type equation (age theory).

The process of slowing down of neutrons in a medium continues until a neutron is captured (when $\sigma_s \gg \sigma_a$) or until the neutrons attain a thermal equilibrium with the moderator atoms (thermal neutrons). The energy of thermal neutrons is $T_{therm} = kT^\circ$, where k is the Boltzmann constant and T° is the absolute temperature of the moderator. At room temperature ($T^\circ \simeq 300$ K), $kT \simeq 0.025$ eV. When neutrons attain thermal energy, they diffuse into the moderator without any subsequent loss of energy, i.e. continue to be thermal neutrons. The neutron spectrum in a moderator is described by a Maxwellian curve with an elevated right branch (epithermal neutrons). The existence of thermal neutrons was proved in experiments involving the heating of the moderator. Cadmium is a good absorber of thermal neutrons.

Neutrons passing through cadmium are called *epicadmium* neutrons. Neutrons whose energy is less than the thermal energy are called *cold* neutrons, while those having an energy $0 < T_n < 10^4$-10^5 eV are called *slow* neutrons. Among these are neutrons which have a very high probability of capture or scattering by nuclei (*resonance* neutrons).

The properties of slow neutrons were investigated by Fermi and coworkers, who showed that the cross section of their interaction with nuclei in the low-energy region follows the $1/v$-law, increases sharply when neutrons have resonance energy T_0, and then decreases once again. The formulas describing the change in the cross section of interaction of resonance neutrons with nuclei were obtained by Breit and Wigner on the basis of Bohr's idea that a nuclear reaction proceeds through an intermediate stage involving the formation of a compound nucleus:

$$\sigma(n, \gamma) \simeq \pi\lambda^2 \frac{\Gamma_n \Gamma_\gamma}{(T - T_0)^2 + (\Gamma/2)^2},$$

$$\sigma(n, n) \simeq \pi\lambda^2 \frac{\Gamma_n^2}{(T - T_0)^2 + (\Gamma/2)^2}$$

(the spin factors are omitted in these formulas).

A detailed investigation of the interaction between resonance neutrons and thermal neutrons was carried out with the help of neutron spectroscopy which allows neutrons of a given energy to be separated from the continuous spectrum. Among neutron spectroscopy methods, four methods have been used most extensively. Two of these methods (the mechanical monochromator method and the diffraction of neutrons by a crystal) actually isolate monoenergetic neutrons in a given direction, the other two methods (the pulsed accelerator method and the mechanical selector method) isolate neutrons with a given energy according to time of flight. Neutron spectroscopy confirmed the correctness of Bohr's prediction about the formation of a compound nucleus, and also the Breit-Wigner formulas.

Fast neutrons ($T_n = 10$-20 MeV) have a high probability of undergoing inelastic scattering whose cross section according to Bohr's model of nucleus as a black sphere is equal to $\sigma_{i.s.} = \pi(R + \lambda)^2 \simeq \pi R^2$, as well as elastic diffraction scattering whose cross section according to the same model is equal to $\sigma_{d.s.} = \pi(R + \lambda)^2 = \pi R^2$. The diffraction nature of the latter process is confirmed by the specific dependence of cross section on the scattering angle. The total scattering cross section, which is equal to $\sigma_s = 2\pi(R + \lambda)^2 \simeq 2\pi R^2$, constitutes an overwhelming part of the cross section of interaction of neutrons with nuclei: $\sigma_s \simeq \sigma_{tot}$. Measurements of σ_{tot} provide a value of the range of interaction R_{int} between a neutron and a nucleus (this range is slightly larger than the nuclear radius R): $R_{int} = 1.4 \times 10^{-13} A^{1/3}$ cm.

A more detailed investigation of the experimental cross section σ_{tot}^{exp} over a wide range of energies (0.1-100 MeV) and mass numbers (1-240) showed that

σ_{tot}^{exp} is a much more complex function of T_n and A (having maxima and minima) than $\sigma_{tot}^{theor} = 2\pi (R + \lambda)^2$. This discrepancy in the cross section in comparison to that given by Bohr's model is explained with the help of the optical model of the nucleus, which is constructed under the assumption of a partial transparency of the nuclear matter to neutrons. According to this model, the maxima and minima in the cross section of interaction of neutrons with a nucleus are due to the interference of the incident neutron wave with a wave transmitted through the translucent nucleus and undergoing a phase shift $\delta = \delta (A, T_n)$.

The properties of ultracold neutrons having an energy of about 10^{-7} eV have been the subject of extensive research during the last few years. Ultracold neutrons with an energy $T_n < E_{lim}$, where E_{lim} is determined by the properties of the medium, undergo total internal reflection at the vacuum-medium interface at all angles of incidence. As a result, ultracold neutrons entering a closed volume must be accumulated in it. The possibility of accumulation and storage of ultracold neutrons in a closed volume has been confirmed experimentally. The kinetic energy of ultracold neutrons is comparable with the energy of interaction of the magnetic moment of a neutron with a magnetic field of strength 17 kG (1.03×10^{-7} eV), or with a change in the gravitational energy of a neutron over 1 m (1.02×10^{-7} eV). The first property is used for the magnetic confinement of ultracold neutrons, while the second one is employed in spectrometry. Experiments involving gravitational spectrometers have shown that ultracold neutrons have wave properties during interaction with an object having optical parameters (a glass mirror, diffraction grating with 1000 slits per mm, etc.). This raises hopes about the construction of a neutron microscope in future.

Chapter 7

Nuclear Fission

7.1. Discovery and Basic Properties of Fission

The history of nuclear fission dates back to 1934 when Fermi carried out investigations of artificial radioactivity induced by neutrons. Irradiating uranium among other elements, Fermi discovered that the radioactive products formed in the process had several half-lives. A detailed analysis of this phenomenon revealed several chains of successive transformations of radioactive elements.

The following interpretation of the observed phenomena seemed to be quite natural: the capture of a neutron by uranium nucleus leads to the formation of a heavier uranium isotope which is β-radioactive because of an excess of neutrons and is transformed into ${}_{93}\mathrm{R}$ by emitting an electron. In turn, the 93rd element can emit an electron and be transformed into ${}_{94}\mathrm{R}$, and so on.

Since the elements ${}_{92}\mathrm{U}$, ${}_{93}\mathrm{R}$, ${}_{94}\mathrm{R}$, . . . lie below the elements ${}_{74}\mathrm{W}$, ${}_{75}\mathrm{Re}$, ${}_{76}\mathrm{Os}$, . . . in the Periodic Table, the new elements were termed Ekarhenium (*Eka* Re), Ekaosmium (*Eka* Os), and so on (the prefix *eka* indicates "behind" or "under").

The existence of several radioactive chains is explained by the fact that uranium has several isotopes, each of which serves as the starting point of a chain upon being irradiated by neutrons.

However, studies of the chemical properties of the products formed as a result of irradiation revealed that they are similar not to the transuranic elements in the Periodic Table, but to those in front of uranium (${}_{88}\mathrm{Ra}$ and ${}_{89}\mathrm{Ac}$). Subsequent experiments by Joliot-Curie and Savič, and also by Hahn and Strassmann, confirmed that the investigated products could be chemical analogues of Ra and Ac rather than being these elements themselves. Finally, Hahn and Strassmann (1938) proved from exact radiochemical analysis that the irradiation of uranium by neutrons leads to the formation of the element ${}_{56}\mathrm{Ba}$ from the middle of the Periodic Table, which is a chemical analogue of ${}_{88}\mathrm{Ra}$.

This astonishing result was explained by Frisch and Meitner who put forth the hypothesis that heavy nuclei are unstable to variations in their shape, and hence a uranium nucleus excited upon capturing a neutron may split into two nearly equal parts (*fission fragments*) containing the nucleons of the parent nucleus, i.e.

$$Z_1 + Z_2 = Z_U,\ A_1 + A_2 = A_U + 1 \simeq A_U. \qquad (7.1.1)$$

The basic properties of fission can be easily predicted.

The fission of a heavy nucleus must be accompanied by the release of a large amount of energy Q. This conclusion is based on a comparison of the mass of the parent nucleus undergoing fission (M_U) and the masses M_1 and M_2 of the fission fragments:

$$Q = \{M_U - (M_1 + M_2)\} c^2. \tag{7.1.2}$$

Indeed, as was mentioned in Sec. 1.3, the mass of any nucleus is given by

$$M = Zm_p + (A - Z)m_n - \varepsilon A/c^2. \tag{7.1.3}$$

Substituting this expression into (7.1.2) and taking into account Eq. (7.1.1), we obtain

$$Q = \varepsilon_1 A_1 + \varepsilon_2 A_2 - \varepsilon A = A(\bar{\varepsilon} - \varepsilon), \tag{7.1.4}$$

where $\bar{\varepsilon} = (\varepsilon_1 A_1 + \varepsilon_2 A_2)/A$ is the average binding energy per nucleon for the fission fragments. Since ε is about 0.8 MeV higher for nuclei from the middle of the Periodic Table than for the uranium nucleus, we get

$$Q = A(\bar{\varepsilon} - \varepsilon) \simeq 238 \times 0.8 \simeq 200 \text{ MeV} \tag{7.1.5}$$

The main part of fission energy must be released in the form of kinetic energy Q_{fis} of the fission fragments. This conclusion follows from the fact that the fragments formed by the fission of a nucleus into two parts must inevitably fly apart due to the large forces of Coulomb repulsion between their charges. The Coulomb energy of two fragments separated by a distance δ is given by

$$V_C = Z_1 Z_2 e^2/\delta, \tag{7.1.6}$$

where Z_1 and Z_2 are the charges of the fragments, $\delta = R_1 + R_2$, R_1 and R_2 being the radii of the nuclear fragments (in cm), which can be calculated with the help of the following formula (see Sec. 1.4):

$$R = r_0 A^{1/3} = 1.4 \times 10^{-13} A^{1/3} \tag{7.1.7}$$

Assuming that $Z_1 = Z_2 = 92/2 = 46$ and $R_1 = R_2$ ($A_1 = A_2 = 238/2 = 119$), we obtain

$$V_C = \frac{46^2 (4.8 \times 10^{-10})^2}{2 \times 1.4 \times 10^{-13} \sqrt[3]{119} \times 1.6 \times 10^{-6}} \simeq 220 \text{ MeV} \simeq 200 \text{ MeV}. \tag{7.1.8}$$

which is of the same order as Q.

The fission fragments must be β-radioactive and may emit neutrons. This result is obvious from a consideration of the ratio of the neutrons and protons in various stable nuclei in the Periodic Table:

Nucleus	$^{16}_{8}O$	$^{109}_{47}Ag$	$^{137}_{56}Ba$	$^{238}_{92}U$
$\frac{N}{Z}$	1.0	1.3	1.45	1.6

It follows from the above data that at the instant of their formation, the fission fragments must have an excess of neutrons since they are formed from uranium, for which $N/Z = 1.6$. It is well known that such nuclei must exhibit β^--radioactivity, and owing to a large excess of neutrons the radioactive decay products themselves will be β^--radioactive, and so on. Hence the fission fragments must serve as the starting point of quite long chains of radioactive nuclei (as was indeed observed by Fermi in his experiments).

Thus, a part of the fission energy is released in the form of beta decay energy Q_β.

Besides, it can be assumed that some of the excess neutrons will be directly emitted by the fission fragments as *fission neutrons*, or *secondary neutrons*, which also take away a part Q_n of the fission energy.

The fission fragments must have a high ionizing power and a small range. Indeed, it can be easily shown that at the moment of their formation, the fission fragments have a velocity higher than the velocity of electrons in their outer Bohr orbits. As a result, the fragments "shake off" some of the electrons and thus acquire a considerable effective positive charge ($Z_{\text{eff}} \simeq 20$). According to (4.2.9), however, the ionization losses of a charged particle are proportional to the square of its charge. This is the reason behind the high ionizing power and short range of the fragments.

All the fission properties mentioned above were actually observed in the very first experiments carried out in the beginning of 1939 in various laboratories. We shall describe some of these experiments.

7.2. First Experiments on Nuclear Fission

7.2.1. Measurement of the Kinetic Energy of Fission Fragments

Fission can be observed in the most natural form by measuring the large kinetic energy of the fission fragments. For this purpose, an ionization fission chamber was constructed, which differs from ordinary ionization chamber in that a thin layer of a uranium

salt was coated on its electrode (Fig. 234*a*). The chamber was connected to a linear amplifier and an oscillograph.

Experiments showed that in the absence of neutrons, small ionization pulses (current bursts) were produced in the ionization chamber only by the uranium α-particles with an energy of 4.5 MeV. When the ionization chamber was irradiated by the source neutrons, powerful ionization pulses caused by the fission fragments were observed.

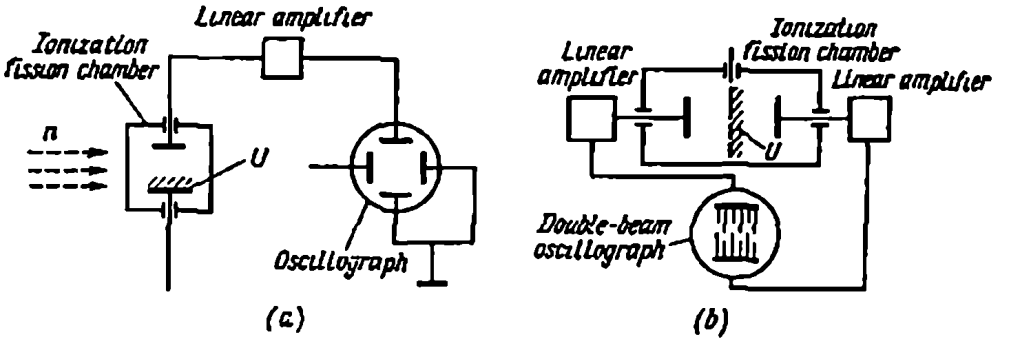

Fig. 234

Later (in 1940), it became possible to simultaneously measure the ionization pulses from both the fission fragments in more refined experiments involving a double ionization chamber (Fig. 234*b*). This allowed the ionization pulse distribution to be plotted for the fragments. (The ionization pulses are shown on the screen of the double-beam oscillograph as pairs of lines of different length

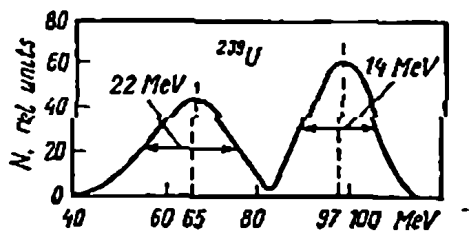

Fig. 235

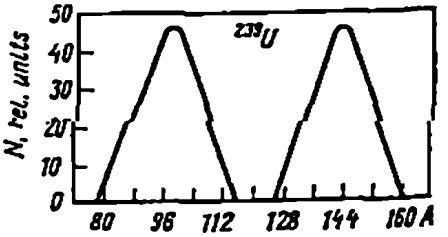

Fig. 236

emanating from opposite direction.) The distribution was found to have two peaks at energies 65 MeV and 97 MeV (Fig. 235).

Knowing the kinetic energy of the fragments, we can easily determine their mass. This is obvious from the fact that according to the (angular) momentum conservation law, the momenta of fragments should be nearly equal in magnitude and opposite in direction (since the momentum of the primary neutron is small):

$$p_1 \simeq -p_2,$$

whence

$$M_1/M_2 \simeq A_1/A_2 = T_2/T_1. \qquad (7.2.1)$$

Using this expression and the known sum of masses

$$M_1 + M_2 \simeq M_U + m_n, \quad A_1 + A_2 = A_U + 1, \quad (7.2.2)$$

we can obtain a plot for the mass distribution of fragments (Fig. 236)[1]. It can be seen from the figure that the peaks are quite broad (ΔA is equal to about 20 at half the height). This indicates the diverse nature of fission processes.

Comparing the average values of the masses and energies of fission fragments, we obtain the average kinetic energy per nucleon of the fission fragments:

$$\overline{T}_l/\overline{M}_l = 97/95 \simeq 1 \text{ MeV for light fragment,}$$

$$\overline{T}_h/\overline{M}_h = 65/140 \simeq 0.5 \text{ MeV for heavy fragment.}$$

Besides uranium, fission for thorium and protactinium was also observed with the help of ionization chamber. It was also found that if the neutron source and the ionization chamber are covered by parafin, the effect is intensified for uranium but remains unchanged for thorium and protactinium. This leads to the conclusion that fission of uranium can be caused by fast as well as thermal neutrons, while for thorium and protactinium, fission is possible only due to fast neutrons. Later (in 1940), when small amounts of uranium isotopes (^{235}U and ^{238}U) were obtained with the help of a mass spectrometer, it was shown that thermal neutrons cause the fission of ^{235}U, while the fission reaction threshold for $^{238}_{92}$U and the naturally occurring isotopes $_{90}$Th and $_{91}$Pa is roughly equal to 1 MeV. The isotope $^{232}_{90}$Th splits under the action of thermal neutrons, but it is not encountered in nature.

7.2.2. Observation of Fragment Tracks

In another experiment involving a thin layer of uranium in a Wilson cloud chamber, tracks of fission fragments flying in opposite directions from the place of their origin were registered.

The characteristics of the observed tracks (high ionizing power, short range) confirmed that they are produced by fission fragments with a high effective charge and a high kinetic energy (see Sec. 7.5 for details).

[1] Figures 235 and 236 are not obtained from each other by simple inversion, since the fission probability strongly depends on the ratio of masses of fragments and their kinetic energy (see Sec. 7.5.1 for details).

7.2.3. Registration of Beta Radioactivity of Fragments

In the third experiment conducted by F. Joliot-Curie, the beta radioactivity of the fission fragments was registered. The experimental set-up is shown in Fig. 237. The outer surface of the brass cylinder is coated with the fissile material (uranium), and the bakelite cylinder has a larger diameter.

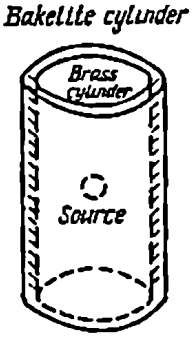

Fig. 237

The experiment involved the beta radioactivity testing of the outer bakelite cylinder after the entire instrument had been irradiated by source neutrons for some time. The testing was carried out with the help of a beta counter which showed beta radioactivity when the bakelite cylinder was mounted on it. Since bakelite is not activated by neutrons, the results of the experiment could be explained only by assuming that radioactive fragments flying from the fissile material (with which the outer surface of the brass cylinder was coated) are deposited on the inner surface of the bakelite cylinder.

7.2.4. Detection of Fission Neutrons

Finally, in the fourth experiment which was also made by F. Joliot-Curie (1939), secondary neutrons formed during fission were detected.

The experimental set-up is shown in Fig. 238. A photoneutron (γ-Ra + Be)-source emitting monochromatic neutrons with an energy of 0.11 MeV was placed in the aqueous solution of a uranium salt. Neutrons which were slowed down in water to thermal energy caused the fission of uranium nuclei. If the secondary neutrons produced in this process have sufficient energies[2], they can be registered by using a threshold reaction whose threshold is higher than 0.11 MeV.

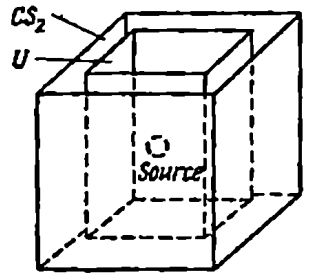

Fig. 238

In this experiment, carbon disulphide, which was used as detector, surrounded a vessel containing a uranium salt solution. Carbon

[2] This idea seems to be quite natural, since neutrons must be emitted very rapidly by the fragments overloaded by them. The period of their emission must be much smaller than the time during which ionization losses occur in the fragment. Hence the neutrons will be emitted by moving fragments, i.e. in any case their average energy will not be less than the average kinetic energy of the fragments, whose value is about (0.5-1) MeV per nucleon.

disulphide was chosen as a detector because neutrons with energies $T_n > 0.95$ MeV cause the reaction

$$^{32}_{16}S + n \rightarrow ^{32}_{15}P + p. \qquad (7.2.3)$$

resulting in the production of radioactive phosphorus. Radioactive phosphorus can be chemically isolated from carbon disulphide and subjected to beta radioactivity test with the help of a beta counter.

Measurements showed that radioactive phosphorus is indeed formed in the experiment, and this could happen only as a result of interaction of neutrons of energy $T_n > 0.95$ MeV with sulphur. Since the maximum energy of primary source neutrons is just 0.11 MeV, the observed effect could be caused only by the fission neutrons of uranium. This conclusion was confirmed in the test experiments carried out without uranium. Thus, secondary (fission) neutrons are formed during fission of uranium. Some of these neutrons have an energy $T_n > 0.95$ MeV.

7.3. Elementary Theory of Fission

The first version of the fission theory was put forth in 1939 by Bohr, Wheeler and Frenkel, who used the liquid drop model of the nucleus to analyze the hypothesis of Frisch and Meitner on the instability of heavy nuclei relative to a change in their shape. We shall describe the basic concepts, achievements and drawbacks of this theory, and also indicate the possible ways of its modification.

7.3.1. Fission Energy

It was mentioned above that the energy Q released during fission is mainly liberated in two forms, viz. the kinetic energy Q_{fis} of fission fragments and the energy Q_β of radioactive transformation of fragments (the value of Q_n is small and will not be taken into consideration):

$$Q \simeq Q_{fis} + Q_\beta \qquad (7.3.1)$$

The values of Q_{fis} and Q_β can be calculated.

In order to calculate Q_{fis}, we assume that the mass number A and atomic number Z are conserved in the process of fission:

$$A_1 + A_2 = A + 1 \simeq A, \quad Z_1 + Z_2 = Z. \qquad (7.3.2)$$

This assumption is equivalent to confining the fission process to just the first stage in which high-energy fission fragments are formed. The condition (7.3.2) is not satisfied in radioactive transformations of fission fragments (β^--decay, neutron emission), since β^--decay

involves an increase in the charge, while neutron emission results in a decrease in the mass number of the fragments:

$$Z_l + Z_h > Z, \quad A_l + A_h < A. \tag{7.3.3}$$

If the condition (7.3.2) is satisfied, the value of Q_{fis} will be the same as the reaction energy Q which, by definition, is equal to the difference between the masses of the parent (fissile) nucleus and the daughter nuclei (fission fragments), i.e.

$$Q_{fis} = M_{nuc} - (M_l + M_h), \tag{7.3.4}$$

which is the same as [see Eq. (1.3.1)]

$$Q_{fis} = \Delta W_l + \Delta W_h - \Delta W_{nuc}, \tag{7.3.5}$$

where ΔW is the total binding energy of the nucleus for all the nucleons constituting it. According to the semiempirical formula (2.1.10), we have

$$\Delta W = \alpha A - \beta A^{2/3} - \gamma \frac{Z^2}{A^{1/3}} - \zeta \frac{(A/2-Z)^2}{A} + \delta A^{-3/4}, \tag{7.3.6}$$

where $\alpha = 15.4$ MeV, $\beta = 17$ MeV, $\gamma = 0.69$ MeV, $\zeta = 96$ MeV, $|\delta| = 34$ MeV.

In view of the experimentally established fact of asymmetry of fission, we further assume that $\overline{A}_h/\overline{A}_l = \overline{Z}_h/\overline{Z}_l = 3/2$, i.e.

$$\begin{aligned} &\overline{A}_h = 3A/5, \ \overline{A}_l = 2A/5, \\ &\overline{Z}_h = 3Z/5, \ \overline{Z}_l = 2Z/5. \end{aligned} \tag{7.3.7}$$

In this case, it can be easily seen that substitution of the expressions for ΔW, ΔW_l and ΔW_h calculated by using formula (7.3.6) (except the last term which is negligibly small) and the conditions (7.3.7) into (7.3.5), the first and the fourth terms in the expression for ΔW cancel out with the corresponding terms in the expressions for ΔW_l and ΔW_h. Thus, the expression for Q_{fis} assumes the form

$$Q_{fis} = W_s + W_C - W_{s\,fr.} - W_{C.fr.}. \tag{7.3.8}$$

where $W_s = \beta A^{2/3}$ is the energy of surface tension of the nucleus, $W_C = \gamma Z^2/A^{1/3}$ is the Coulomb energy of the nucleus and $W_{s.fr.}$ and $W_{C\,fr.}$ are the corresponding values for the fragments. Note that

$$W_{s.fr.} = \beta\,(3A/5)^{2/3} + \beta\,(2A/5)^{2/3} = 1.25W_s \tag{7.3.9}$$

(the surface energy increases upon fission); and

$$W_{C.\,fr.} = \gamma \frac{(3Z/5)^2}{(3A/5)^{1/3}} + \gamma \frac{(2Z/5)^2}{(2A/5)^{1/3}} = 0.64W_C \tag{7.3.10}$$

(the Coulomb energy decreases upon fission).

Finally, we get

$$Q_{fis} = 0.36W_C - 0.25\ W_s. \qquad (7.3.11)$$

The change in the surface and Coulomb energies of the nucleus serves as a measure of the energy liberated as kinetic energy of the fission fragments during fission.

For example, if we consider the fission of the nucleus $^{236}_{92}U$, the calculation of W_s and W_C by taking into account the coefficients (7.3.6) gives (Fig. 239)

$$W_s = 650 \text{ MeV},$$
$$W_{s.fr.} = 1.25W_s = 813 \text{ MeV},$$
$$\Delta W_s = -163 \text{ MeV},$$
$$W_C = 950 \text{ MeV}, \quad W_{C.fr.} = 0.64W_C = 607 \text{ MeV}, \quad \Delta W_C = 343 \text{ MeV},$$
$$\Delta W = W_s + W_C - W_{s.fr.} - W_{C.fr.} = \Delta W_C + \Delta W_s,$$
$$Q_{fis} = \Delta W = 343 - 163 = 180 \text{ MeV}. \qquad (7.3.12)$$

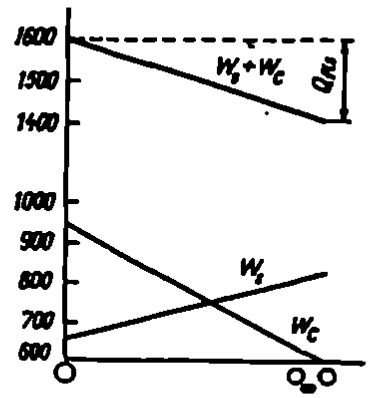

Fig. 239

Thus, the liberation of energy during fission of $^{236}_{92}U$ is explained by the fact that a decrease in W_C by 180 MeV exceeds the increase in W_s.

The energy Q_β of beta decay, released during radioactive transformation of fragments, can also be calculated with the help of the semiempirical formula if we impose the condition (7.3.3) on the variation of A and Z. Such a computation leads to the value $Q_\beta \simeq 20$ MeV. Out of this, 5 MeV each are carried away by the electrons and γ-quanta, while 10 MeV are carried away by the antineutrinos:

$$Q_\beta = E_e + E_\gamma + E_{\tilde{\nu}} = 5 + 5 + 10 = 20 \text{ MeV}.$$

The total energy liberated during fission is

$$Q = Q_{fis} + Q_\beta = 180 + 20 = 200 \text{ MeV}.$$

The result is in good agreement with the average results of measurements (see Sec. 7.5.11).

7.3.2. Fission Mechanism

It follows from (7.3.11) that $Q_{fis} > 0$ for

$$\frac{W_C}{W_s} = \frac{\gamma Z^2/A^{1/3}}{\beta A^{2/3}} = \frac{\gamma}{\beta}\frac{Z^2}{A} > \frac{0.25}{0.36} = 0.7 \qquad (7.3.13)$$

or, if we take into account the values of β and γ,

$$Z^2/A > 17 \qquad (7.3.14)$$

Moreover, Q increases with increasing Z^2/A (fission parameter). This condition is satisfied for all sufficiently heavy nuclei starting from silver:

$$Z^2/A\ (^{108}_{47}\mathrm{Ag}) = 47^2/108 = 20 > 17. \qquad (7.3.15)$$

Thus, fission is advantageous from the energy point of view for all nuclei in the second half of the Periodic Table of elements. However, fission was experimentally detected only for three heaviest elements in the Periodic Table, viz. $_{90}$Th, $_{91}$Pa and $_{92}$U. For other nuclei

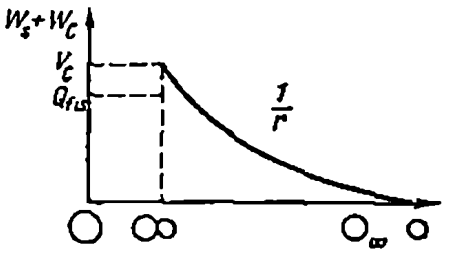

Fig. 240

the process of fission under the experimental conditions described in Sec. 7.2 is not possible in spite of the fact that it is advantageous from the energy point of view.

In order to clarify this situation, let us consider the process inverse to fission. We shall assume that the energy of the fragments formed as a result of fission is equal to zero, i.e. $W_s + W_C = 0$. As the fragments get closer and ultimately come in contact with each other, their energy will be $V_C \simeq 220$ MeV in accordance with (7.1.8), while according to (7.1.5), the energy Q_{fis} of the nucleus before fission is $\simeq$190 MeV (Fig. 240). It can be assumed that this barrier at the nuclear boundary makes the fission of nuclei with $Z < 90$ impossible.

Of course, in view of the rough nature of these arguments, we cannot attribute any great importance to them. However, the obtained experimental results show that an increase in the nuclear energy in the initial stage of fission cannot be ruled out, thus indicating that the problem requires a more thorough analysis.

Let us assume that as a result of neutron capture, the excited nucleus starts oscillating. Depending on the excitation energy, two situations are possible in this case. At low excitation energies, the nucleus will perform oscillations in which its shape changes from spherical to ellipsoidal and back. The role of elastic forces which return the ellipsoid to its original spherical shape is played by the forces of surface tension in the nucleus [see Sec. 2.1].

If, however, the excitation energy is quite large, the oscillating nucleus may pass through the critical point corresponding to the elastic limit deformation, after which the original shape of the nucleus cannot be restored. Under the action of large Coulomb repulsion forces between the poles of the stretched nucleus, the latter becomes more and more stretched, passing successively through the following stages of deformation: sphere, ellipsoid, dumb-bell, two pear-shaped fragments, and two spheres (Fig. 241). The action of the

Fig. 241

Coulomb forces is found to be so strong that it cannot be counterbalanced by the surface tension forces. In the second stage of the process (beginning from the dumb-bell shape) the surface forces even facilitate splitting by "helping" both halves of the dumb-bell to assume spherical shape.

Assuming that the ellipsoid formed in the first stage of deformation is an ellipsoid of revolution, we can easily calculate the change in the Coulomb and surface energies of the nucleus.

Suppose that the ellipsoid of revolution is characterized by a major axis $a = R(1 + \varepsilon)$ and a minor axis $b = R/\sqrt{1 + \varepsilon}$, where ε is a small parameter. Such a choice of axes satisfies the condition of incompressibility of the nuclear fluid since the volume of the nucleus does not change during its ellipsoidal deformation:

$$V_{ell} = 4\pi ab^2/3 = 4\pi R^3/3. \qquad (7.3.16)$$

The surface area of the ellipsoid of revolution with axes a and b is

$$S_{ell} = 2\pi ab\left(\sqrt{1-\gamma^2} + \frac{\arcsin\gamma}{\gamma}\right), \qquad (7.3.17)$$

where $\gamma = \sqrt{a^2 - b^2}/a$. Substituting into the above expression the values of a and b, and expanding into a series in ε, we get

$$S_{ell} = 4\pi R^2(1 + 2\varepsilon^2/5 + \ldots). \qquad (7.3.18)$$

Since the surface energy W_s' of the nucleus is proportional to its surface area, we can write

$$W_s' = W_s(1 + 2\varepsilon^2/5 + \ldots), \qquad (7.3.19)$$

where W_s is the surface energy of a sphere. The surface energy increases with ε.

The Coulomb energy of an ellipsoidally-shaped nucleus can be determined by solving Poisson's equation for an ellipsoid of revolution with a uniform charge distribution over its volume. This gives

$$W'_C = W_C (1 - \varepsilon^2/5), \qquad (7.3.20)$$

where W_C is the Coulomb energy of a sphere. The Coulomb energy decreases with increasing ε.

A comparison of Eqs. (7.3.19) and (7.3.20) shows that for small ε the increase in W'_s is more rapid (with a coefficient 2/5) than the decrease in W'_C (coefficient 1/5). The sum of the surface energy and

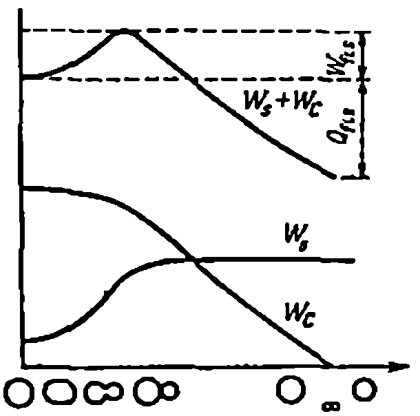

Fig. 242

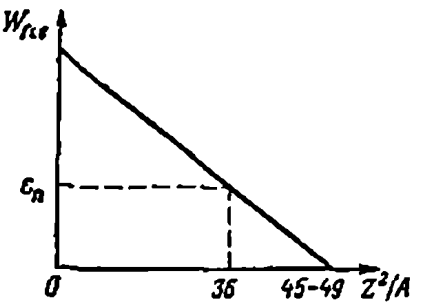

Fig. 243

Coulomb energy, i.e. $W'_s + W'_C$, which is a measure of the energy of the fissile nucleus, varies with ε as follows:

$$W'_s + W'_C = W_s + W_C + \varepsilon^2 (2W_s - W_C)/5. \qquad (7.3.21)$$

The nature of variation of $W'_s + W'_C$ depends on the sign of the quantity $(2W_s - W_C)$. According to (7.3.12), this quantity is positive for the uranium nucleus, while $W'_s + W'_C$ increases for small ε and the curve showing the change in the energy of the nucleus during fission assumes the form shown in Fig. 242.

Thus, upon small ellipsoidal deformations the energy of the nucleus first increases, thus leading to the formation of an energy barrier W_{fis} similar to the one considered in Sec. 3.2 for describing alpha decay. From the energy point of view, this barrier renders the fission process impossible (in classical physics) or, to be more exact, improbable (in quantum mechanics) even though it is more advantageous from this view point ($Q_{fis} > 0$).

The barrier height W_{fis} will be smaller for smaller value of $(2W_s - W_C)$, i.e. for smaller ratio

$$\frac{2W_s}{W_C} = \frac{2\beta A^{2/3}}{\gamma Z^2/A^{1/3}} = 2\frac{\beta}{\gamma}\frac{A}{Z^2} \qquad (7.3.22)$$

or for higher value of the fission parameter Z^2/A (Fig. 243).

For $Z^2/A = 49$, the quantity $(2W_s - W_C)$ vanishes and $W_{fis} = 0$. The fission of such a nucleus ($Z \simeq 125$) must take place spontaneously and instantaneously (during nuclear time). In other words, Mendeleev's Periodic Table must terminate in the region of $Z = 125$.[3]

For $Z^2/A < 49$, $W_{fis} \neq 0$ and *spontaneous fission* is possible only through the quantum-mechanical effect of barrier penetration in a manner similar to the one described for the alpha decay (see Sec. 7.5).

The probability of spontaneous fission is determined by the ratio Z^2/A. The smaller this ratio, the lower the probability of spontaneous fission. Spontaneous fission of uranium ($Z^2/A = 36$) has a very low probability, i.e. takes place very slowly.

A nucleus with fission parameter $Z^2/A < 49$ can fission faster if an excitation energy W exceeding the fission barrier is first imparted to it,

$$W > W_{fis} \qquad (7.3.23)$$

This energy can be supplied to the nucleus, say, by irradiating it with γ-quanta. Fission becomes possible for

$$E_\gamma > W_{fis}. \qquad (7.3.24)$$

This provides an experimental method for determining W_{fis}.

If the nuclear fission is induced by neutrons, the condition (7.3.23) can be written in the form

$$W = \varepsilon_n + T'_n > W_{fis}, \qquad (7.3.25)$$

where ε_n is the binding energy of a neutron in the nucleus and T'_n is the relative kinetic energy of the neutron and the nucleus. Two cases are possible here:

(1) $\varepsilon_n > W_{fis}$. The fission can be caused by thermal neutrons.

(2) $\varepsilon_n < W_{fis}$. Fission is possible only if neutrons have a kinetic energy T_n satisfying the condition

$$AT_n/(A+1) = T'_n > W_{fis} - \varepsilon_n. \qquad (7.3.26)$$

[3] Naturally, the value $Z^2/A = 49$ is a rough guide. It is found to be different in different methods of calculation (between 45 and 49), thus leading to the value $Z = 116$-126 for the atomic number of the last element in the Periodic Table (for A/Z, the value corresponding to uranium is used). Besides, the elementary theory considered here does not take into account the shell corrections which may make the lifetime of nuclei with large Z quite long (see Sec. 8.4).

It is known from experiment that $^{238}_{92}U$ and naturally-occurring isotopes of $_{91}Pa$ and $_{90}Th$ undergo fission by neutrons with energy $T_n \simeq 1$ MeV, while the uranium isotope $^{235}_{92}U$ can disintegrate under the action of thermal neutrons. Here the fission barrier for $^{238}_{92}U$, $_{91}Pa$ and $_{90}Th$ is

$$W_{fis} = \varepsilon_n + T_{thres} \simeq (\varepsilon_n + 1)\ \text{MeV}, \tag{7.3.27}$$

while for $^{235}_{92}U$

$$W_{fis} < \varepsilon_n. \tag{7.3.28}$$

Different fission mechanisms for two isotopes of the same nucleus ($^{235}_{92}U$ and $^{236}_{92}U$) are due to two reasons. Firstly, in accordance with the fission theory considered above the nucleus $^{236}_{92}U$ has a lower barrier height W_{fis} because its fission parameter Z^2/A is larger than that of nucleus $^{235}_{92}U$. Secondly, the binding energy of a neutron to the nucleus $^{235}_{92}U$ is higher than the corresponding value for the nucleus $^{234}_{92}U$. This is due to the fact that the addition of a neutron to the nucleus $^{235}_{92}U$ leads to the formation of an even-even nucleus $^{236}_{92}U$, while in the case of $^{234}_{92}U$ an even-odd nucleus $^{235}_{92}U$ is formed (see Sec. 1.3).

It has been shown experimentally and theoretically that the fission barriers for $^{236}_{92}U$ and $^{239}_{92}U$ are equal to 6 MeV and 7 MeV respectively. Accordingly, the binding energy of a neutron for the nucleus $^{235}_{92}U$ is 6.5 MeV which exceeds the fission barrier, while for the nucleus $^{238}_{92}U$, the neutron binding energy is about 5 MeV which is smaller than the barrier height.

By estimating the fission barrier for uranium, we can plot on the W_{fis} vs. Z^2/A curve another point $W_{fis} \simeq \varepsilon_n$ for $Z^2/A = 36$ besides the point $W_{fis} = 0$ for $Z^2/A = 49$ (see Fig. 243).

For lighter nuclei ($Z^2/A < 36$), the value of W_{fis} can be estimated from the formula

$$W_{fis} \propto \left[1 - \frac{Z^2/A}{(Z^2/A)_{cr}}\right]^3. \tag{7.3.29}$$

The fission barrier W_{fis} for these nuclei is much higher than the neutron binding energy. Hence the fission of nuclei with $Z^2/A < 36$ can be caused only by quite fast particles (and spontaneous fission will occur with a very long half-life).

Figure 244 schematically shows the variation of the fission barrier and fission energy upon a decrease in the fission parameter. The ideas developed here on the fission of nuclei with $Z < 90$ will be experimentally confirmed in Sec. 7.5.5.

We can see that even the simplified version of the fission theory correctly describes the general pattern of fission for the heaviest nuclei ($_{92}U$, $_{91}Pa$, $_{90}Th$) and is capable of explaining a whole lot of regularities already observed, as well as predicting new phenomena

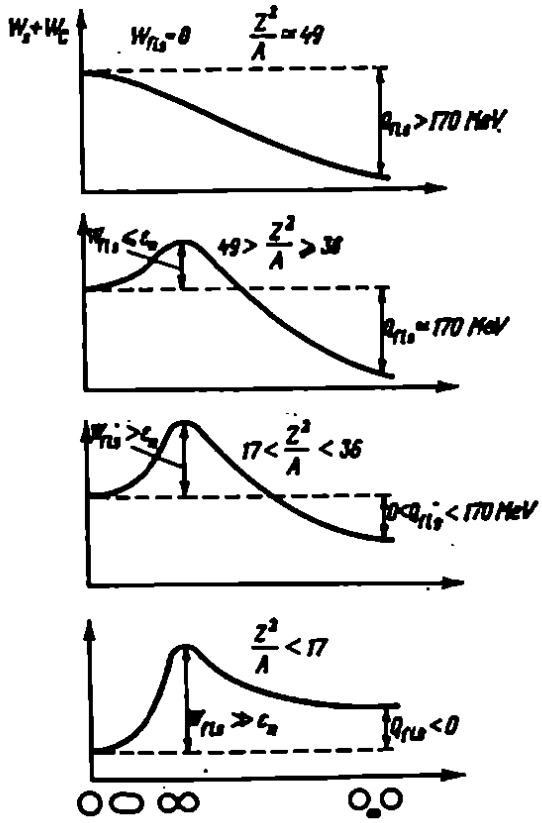

Fig. 244

like spontaneous fission, properties of fission of moderately heavy nuclei by fast particles.

However, there are serious drawbacks in this theory. For example, it cannot explain one of the principal regularities of fission, viz. a distinct mass asymmetry of fission fragments. According to the theory described above, disintegration into two equal parts must have a higher probability than into unequal parts.

The liquid drop fission theory was modified in 1966 by Strutinsky who proposed the introduction of shell corrections to the energy values given by the liquid drop theory. The new theory provides a satisfactory explanation for many regularities in the properties of known elements, including the variation of half-lives, fission asymmetry, shape isomerism (see Sec. 7.5.5), etc. Application of this theory to unexplored nuclei makes it possible to predict the existence of new magic numbers ($Z = 114$ and $N = 184$), i.e. an islet of quite stable nuclei in which the number of protons and neutrons is close to these values.

7.4. Utilization of Fission Energy

Experimental verification of basic properties of fission reactions, especially the liberation of large amounts of energy and the emission of secondary neutrons, is significant not only from the scientific *point of view, but also has an enormous practical significance.*

Indeed, it can be expected that the formation of neutrons during fission will make it possible to use them for fission of neighbouring nuclei, accompanied by the liberation of more energy and creation of new neutrons which in turn will cause the fission of more uranium nuclei, and so on.

If more than one neutron can be obtained in an act of fission, it becomes possible to obtain a cascade chain reaction for nuclear fission. Thus, if each act of fission gives rise to two neutrons, they can split two more nuclei in the ideal case, thus leading to the creation of four neutrons which in turn can split four uranium nuclei and produce eight neutrons, and so on *(neutron multiplication).*

In view of the high speed of this reaction, the number of fission nuclei can increase to enormous proportions in a short period of time, resulting in the liberation of a huge amount of intranuclear energy which is termed *atomic energy.*

Thus, in order to determine the possibility of obtaining a nuclear chain reaction, it is extremely important to know the number ν of *secondary neutrons formed in a single act of fission.*

For practical realization of a chain reaction, however, it is not sufficient to know just the quantity ν, since the fate of the resulting fission neutrons may not be the same on account of the numerous types of interaction of neutrons with matter. Even if a nuclear reactor consists only of the fissionable material, or fuel (which is not possible in actual practice), secondary neutrons reacting with the fuel nuclei will not necessarily cause their fission: neutrons may undergo inelastic *scattering, radiative capture, or simply leave the reactor.* These harmful side effects may seriously hamper neutron multiplication or even render a chain reaction impossible.

The theory of chain reactions was developed by the Soviet physicists Zel'dovich and Khariton, who showed that a self-sustained chain reaction is possible only if the *neutron-multiplication factor* k is more than or equal to unity, i.e.

$$k \geqslant 1 \qquad (7.4.1)$$

(k is the ratio of neutrons causing fission in the given and the previous generation). If $k = 1$, the chain reaction has a constant power, while for $k > 1$ the power of the reaction increases.

The multiplication factor is determined by the quantity ν, the probabilities of various types of interaction (leading or not leading to fission) of neutrons with uranium and impurities, and also by

the design and size of the installation. Hence it is very important to know the cross sections of fission processes, inelastic scattering and capture of neutrons by uranium at energies with which they are created. In other words, we must know the energy spectrum of secondary neutrons.

The role of the reactor size is obvious. The number of escaping neutrons is proportional to the surface S of the reactor, while the number of neutrons formed is proportional to its volume V. With decreasing size of the reactor ratio S/V increases as well as the percentage of neutrons escaping from its surface, so that a nuclear chain reaction is impossible in a small-size reactor even for a favourable relation between the neutron absorption and creation processes. The smallest size of the nuclear reactor for which a chain reaction is still possible is called the *critical size*. Similarly, the smallest mass of the fissionable material in which a chain reaction can take place is called the *critical mass*. The critical size can be reduced by surrounding the installation by a *reflector* in the form of a layer of a non-fissile material with a low capture cross section and a high scattering cross section. The reflector returns a considerable part of neutrons escaping from the reactor surface. Other conditions being equal, spherical reactors must obviously have the smallest critical size. The role of design and arrangement of various materials in a reactor will be discussed in Sec. 7.4.3.

One of the most important characteristics of a chain reaction is its growth rate which is determined by the neutron-multiplication factor k and the time that elapses between two successive acts of fission, or the average lifetime τ of one generation of neutrons. Indeed, the increase in the number of neutrons over one generation is given by

$$dn = n(k-1). \tag{7.4.2}$$

The increase per unit time will then be

$$dn/dt = n(k-1)/\tau. \tag{7.4.3}$$

The average lifetime of one generation or the average time interval between two successive acts of fission is the sum of the fission time, the delay in the escape of a neutron from the fissile nucleus relative to the instant of fission, and the time taken by the escaping neutron to reach the next fissionable nucleus.

To decrease τ, i.e. to obtain an explosive chain reaction, the neutron-multiplication process must be realized for instantaneously escaping and rapidly moving neutrons. For a controlled chain reaction, on the other hand, the delay time for escape and the time of flight of neutrons should be as large as possible. The first quantity is determined by the mechanism of formation of secondary neutrons, and the second one depends on the nature of their interaction with

the surrounding nuclei after escaping from the disintegrating nucleus, i.e. on the processes of slowing down, diffusion and capture.

Consequently, it is extremely important to know the mechanism of formation of secondary neutrons and the cross sections of their interaction with various materials used in nuclear reactors (nuclear fuel, moderator, reflector and construction materials). Cross-sectional data are required over a very wide range of energies, starting from energies with which secondary neutrons are released at the instant of fission, down to thermal energies.

Thus, the problem of accomplishing a nuclear chain reaction is indeed quite complicated. A detailed description of this problem is beyond the scope of this book, nor is it necessary to include these details in a course on nuclear physics. We shall confine ourselves to description of the most important experiments from the point of view of nuclear physics, which facilitated the harnessing of nuclear energy.

7.4.1. Average Number ν of Secondary Neutrons Emitted During One Act of Fission

The quantity ν was measured in the USSR (by Flyorov) and abroad (by Zinn and Szilard, and others). We shall describe the experiment of Zinn and Szilard in which the energy spectrum of fission neutrons of uranium was observed for the first time (1939) and a value of ν which is quite close to the existing estimate was obtained.

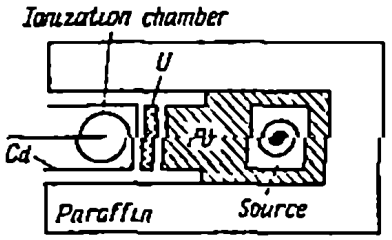

Fig. 245

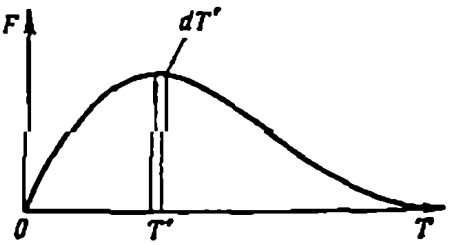

Fig. 246

The main part of the set-up (Fig. 245) was a spherical ionization chamber filled with a mixture of argon (at a pressure of 8 atm) and hydrogen (at a pressure of 10 atm), capable of registering recoil protons with energy $T_p > 0.6$ MeV. Recoil protons were produced as a result of elastic scattering of uranium fission neutrons from hydrogen nuclei.

Fission neutrons were emitted by a uranium plate placed near the ionization chamber. The fission of uranium nuclei was induced by neutrons from a (γ-Ra + Be)-source prepared from 1 g of radium.

To protect the chamber from gamma radiation, the source was shielded by a lead screen. The instrument was immersed in paraffin to protect the chamber from stray neutrons, while a cadmium covering shielded it from thermal neutrons.

It can be easily shown that such an apparatus can be used to determine the energy spectrum of secondary neutrons by measuring the energy spectrum of recoil protons (in all possible directions) registered by the ionization chamber.

Let $F(T)$ be the required neutron spectrum. We select neutrons with energy $T' \pm dT'$, equalling $F(T')\,dT'$ in number (Fig. 246). After colliding with protons, these neutrons will have any energy between 0 and T' with the same probability $F(T')/T'$ (see Sec. 6.3.1).

The number of recoil protons with energy $T \pm dT$ is

$$dN_p(T) = F(T')\,\sigma(T')\,dT'dT/T', \tag{7.4.4}$$

where $\sigma(T')$ is the $(n\text{-}p)$-scattering cross section and $T \leqslant T'$ [$dN_p(T) = 0$ for $T > T'$].

The total number of recoil protons with energy $T \pm dT$ is obtained by integrating the expression

$$dN_p/dT = F(T')\sigma(T')\,dT'/T' \tag{7.4.5}$$

with respect to T' over the entire neutron spectrum $F(T')$ for $T' \geqslant T$:

$$N(T)\,dT = \int_T^\infty \frac{F(T')}{T'}\,\sigma(T')\,dT'\,dT. \tag{7.4.6}$$

It can be seen from this expression that the spectrum of recoil protons in all possible directions is represented by a monotonically decreasing function of energy T.

Differentiation of this expression gives

$$dN/dT = -F(T)\,\sigma(T)/T$$

and

$$F(T) = (-T/\sigma(T))dN(T)/dT. \tag{7.4.7}$$

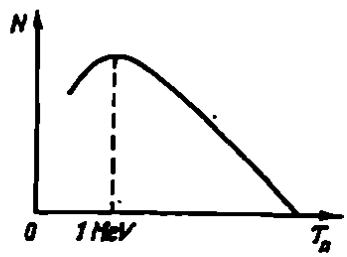

Fig. 247

Figure 247 shows the graph of spectrum of secondary neutrons obtained with the help of this method. It is clear from this figure that the spectrum of secondary neutrons has a peak around 1 MeV and drops smoothly on either side of the peak.

Of course, the method described here gives only a rough shape of the fission neutron spectrum since it involves differentiation of the experimental curve, which leads to considerable errors. But even in

this form, this result is quite significant in that it provides in the same experiment an idea on the number ν of secondary neutrons emitted during one act of fission.

To determine ν in two independent measurements, the number N_n of the neutrons emitted by a uranium plate and the number N_{fis} of the fission acts occurring in the plate during this time were determined. Obviously

$$\nu = N_n/N_{fis}. \tag{7.4.8}$$

The number of neutrons was counted in terms of the number of registered recoil protons by taking into account the $(n\text{-}p)$-scattering cross section for the fission spectrum neutrons, as well as the geometry of the experiment.

The number N_{fis} of fission acts was determined with the help of a small auxiliary ionization fission chamber which was installed instead of the uranium plate. Since the fissile material was in the form of a thin film (with a thickness smaller than the mean free path of the fragment), the fission chamber registered all the acts of fission occurring in it. The value of N_{fis} could be calculated by comparing the mass of uranium in the fission chamber and in the plate.

As a result of measurements, Zinn and Szilard obtained the following value of ν:

$$\nu = \frac{N_n}{N_{fis}} = 2.3 \pm 0.3, \tag{7.4.9}$$

and thus proved for the first time the possibility of a nuclear chain reaction. More accurate results on the secondary neutron spectrum and the value of ν were obtained in subsequent experiments which will be described in Secs. 7.5.3 and 7.5.8.

7.4.2. Delayed Neutrons

In one of the experiments involving the registration of secondary neutrons formed during fission of uranium by neutrons from the $(d + d)$-reaction, it was found that the emission of secondary neutrons continues for some time after the instant t_0 when the accelerator producing deuterons is switched off. Analysis of this phenomenon showed that about 1% of the secondary neutrons are emitted not at the instant of fission, but some time after the fission has terminated and the flying fragments have come to a halt. These neutrons were called *delayed* neutrons (Fig. 248*a* and *b*).

Measurements of the change in the number of delayed neutrons with time showed that their decrease is described by a curve which can be decomposed into several exponential curves with different half-lives (these curves are tentatively shown by dashed lines in Fig. 248*c*).

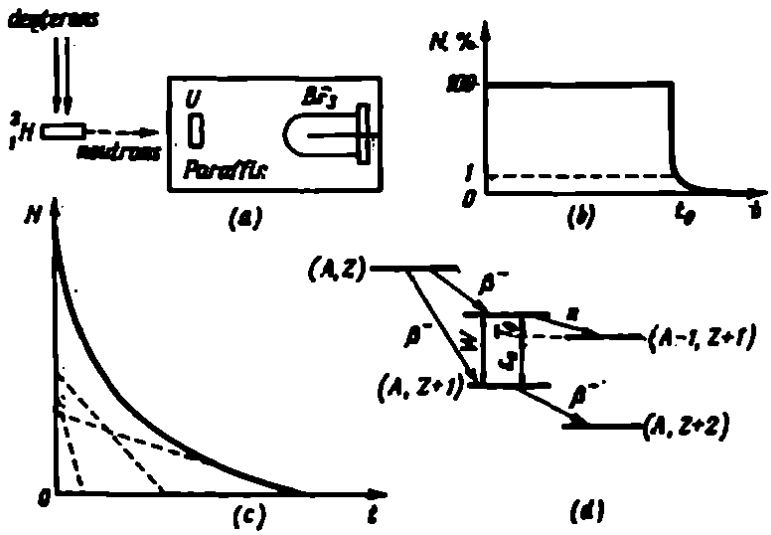

Fig. 248

Table 27 gives the values of these half-lives and the fraction of the delayed neutrons corresponding to a given half-life.

Radiochemical analysis of fission fragments revealed that all the half-lives of delayed neutrons mentioned in Table 27 are encountered among the half-lives characterizing the β^--transformations of the fission fragments.

Table 27

Half-life, s	Yield, % (fraction of the total number of secondary neutrons)	Kinetic energy of delayed neutrons, MeV
55.7	0.021	0.25
22.7	0.140	0.56
6.2	0.125	0.43
2.3	0.253	0.62
0.6	0.074	0.42
0.2	0.027	—
	0.640	

For the longest half-lives in Table 27 (55.7 s and 22.7 s), the corresponding fission products ($^{87}_{35}$Br and $^{137}_{53}$I) were isolated and their properties were studied. It was found that the isolated products do emit delayed neutrons whose half-lives coincide with the half-life of

The possibility of using uranium for obtaining energy appeared only when it was discovered that ^{235}U undergoes fission by thermal neutrons. The absence of a fission reaction threshold for $^{235}_{92}U$ renders the process of inelastic scattering of neutrons harmless for a chain reaction which thus becomes feasible in pure ^{235}U. Moreover, it is found that a chain reaction in pure ^{235}U can be sustained by fast neutrons as well as by neutrons that have been slowed down (this is so because the role of the other disturbing factor, viz. the resonance capture of slow neutrons, is comparatively small). Thus a sufficient amount of pure ^{235}U isotope can help solve both problems, viz. the realization of an explosive chain reaction or the creation of an atomic bomb, the weapon that can cause havoc, and the attainment of a controlled chain reaction which can be used for peaceful purposes as a source of energy.

Such a solution of these problems, however, was found to be impossible at the initial stage of investigations because it is extremely difficult to obtain the isotope $^{235}_{92}U$ in pure form. An atomic bomb was produced only in 1945 after the difficulties associated with the separation of heavy elements with close values of masses had been overcome, and sufficient quantities of another nuclear fuel, viz. $^{239}_{94}Pu$, had been obtained. As regards the controlled nuclear chain reaction, the problem was solved much earlier (by the end of 1942) by using the natural mixture of uranium isotopes.

It is well known that the isotope $^{235}_{92}U$ constitutes only 1/140 of naturally occurring uranium. The first measurements of the cross section of uranium fission by thermal neutrons were carried out by using natural uranium and gave the following order of magnitude for the cross section

$$\sigma_{hT}(_{92}U^{nat}) = (2\text{-}4) \times 10^{-24}\ cm^2. \qquad (7.4.12)$$

When recalculated for the isotope $^{235}_{92}U$, this leads to an encouraging result for the cross section:

$$\sigma_{hT}(^{235}_{92}U) = 140\sigma_{hT}(_{92}U^{nat}) = (280\text{-}560) \times 10^{-24}\ cm^2. \qquad (7.4.13)$$

This result was later confirmed in measurements of the fission cross section as a function of neutron energy for the isotope $^{235}_{92}U$ (Fig. 250). The latest value of the cross section of fission of $^{235}_{92}U$ by thermal neutrons is approximately equal to $580 \times 10^{-24}\ cm^2$.

Such a large value of the fission cross section for $^{235}_{92}U$ makes the fission probability for uranium in the thermal region comparable with the probability of *resonance capture* (i.e. the radiative capture of neutrons by uranium nuclei during the process of slowing down) in spite of the fact that all uranium nuclei participate in the resonance capture process while fission involves only 1/140 of these nuclei.

This generated the idea of obtaining a controlled chain reaction based on the $^{238}_{92}U$ isotope without isolating it from the naturally occurring isotope mixture.

The schematic for obtaining a chain reaction is quite simple. The secondary neutrons from the fission of uranium nuclei (spontaneous or caused, say, by cosmic rays) are slowed down to thermal energies and are captured by the nuclei of the isotope $^{238}_{92}U$, causing their fission with the emission of new secondary neutrons which in turn are slowed down, and so on.

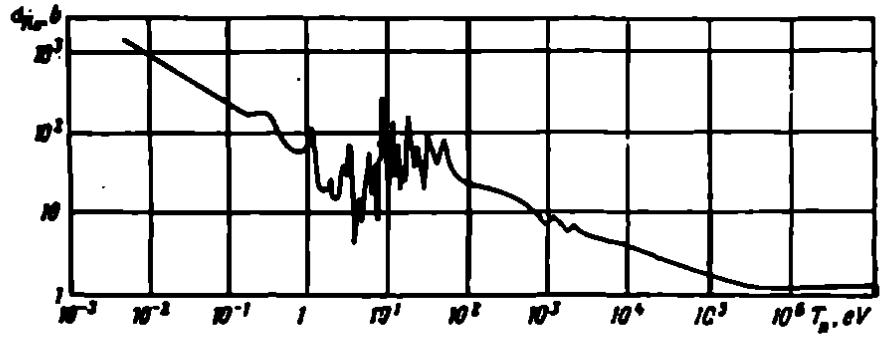

Fig. 250

It would appear that the simplest way to accomplish a chain reaction in this way involves the moderating properties of uranium itself, i.e. slowing down of secondary neutrons due to inelastic and elastic scattering by uranium nuclei. In actual practice, however, this is not true, since with decreasing neutron energy the role of radiative capture increases and its probability (considering that this process can also be accomplished by $^{238}_{92}U$ nuclei) becomes much higher than the fission probability at all neutron energies (except thermal).

In order to eliminate the harmful effect of resonance capture, moderation can be carried out with the help of another material whose nuclei have a smaller mass, a very small radiative capture cross section and a large scattering cross section. "Dilution" of uranium by such a moderator must weaken the effect of resonance capture (since a neutron colliding with light moderator nuclei loses energy in larger portions than upon collision with heavy uranium nuclei). Thus, a much larger fraction of neutrons is successfully slowed down to thermal energies. However, the role of resonance capture remains quite significant if uranium and the moderator are in the form of a homogeneous mixture. In this case, a neutron of any intermediate energy (including resonance energy) can always come across a $^{238}_{92}U$ nucleus in its path and get absorbed without causing fission.

This difficulty is overcome by replacing the homogeneous mixture of uranium and a moderator with a *lattice* in which uranium blocks and the moderator are periodically arranged. If the separation between the blocks is quite large, a secondary neutron from one block can fall into another block after traversing a quite long path over which it is slowed down by the moderator, as a result of which its energy drops below the resonance value. Besides, the block arrangement of uranium leads to a very important effect called screening, according to which the resonance neutrons are absorbed practically by a very thin layer of the block surface. Thus, the block (heterogeneous) system is equivalent in its resonance absorption effect to a homogeneous system with a considerably lower percentage of uranium.[6]

A combination of all these factors leads to a decrease in the probability of radiative (resonance) capture of neutrons in uranium, thus making a chain reaction possible in naturally occurring uranium. The theory of resonance absorption in heterogeneous systems with small blocks was developed in 1943 by Gurevich and Pomeranchuk.[7]

A system consisting of natural uranium and a moderator can be quantitatively characterized by the multiplication factor

$$k = k_\infty \varkappa, \tag{7.4.14}$$

where k_∞ is the multiplication factor for an infinite medium, i.e. for a reactor of infinite size and $\varkappa$ is the probability of avoiding a leak, i.e. the probability that a neutron does not escape from a finite-size reactor. In turn, k_∞ is defined by the *four-factor formula*

$$k_\infty = \eta \varepsilon p f, \tag{7.4.15}$$

where $\eta = \nu\sigma_{f_{1s}}/\Sigma$ is the number of fast neutrons produced as a result of capture of one thermal neutron by uranium [$\sigma_{f_{1s}}$ and Σ are the fission cross section and the sum of fission and radiative capture cross sections in ^{235}U and ^{238}U in accordance with the percentage composition of natural uranium, i.e. $\Sigma = \sigma_{f_{1s}} + \sigma(n, \gamma)_{235} + 140\sigma(n, \gamma)_{23}$], ε is the *multiplication factor for fast neutrons*, i.e. the increase in the number of neutrons due to fission by fast neutrons, p is the *probability of avoiding resonance capture during moderation*, $f = \varphi_U N_U/(\sigma_U N_U + \sigma_m N_m)$ is the *thermal utilization factor*, i.e. the probability that the slowed-down neutrons will be absorbed by

[6] Obviously, the probability of resonance absorption in an infinitely diluted system is equal to zero.

[7] References to the work mentioned in this section are given in the book *Construction and Commissioning of the First Atomic Reactor in the Soviet Union* by I.F. Zhezherun (Atomizdat, Moscow, 1978, in Russian). Detailed analysis of the problems discussed in this section can also be found in the same book.

uranium nuclei and not by the moderator[8] (σ_U and σ_m are the cross sections of absorption of the thermal neutrons by uranium and moderator nuclei, and N_U and N_m are the number densities of uranium and moderator nuclei respectively). Typical values of these coefficients for a real system composed of natural uranium and graphite are as follows: $\eta = 1.35$, $\varepsilon \simeq 1.03$, $\varepsilon pf \simeq 0.8$ (for an optimal lattice). It follows from these values that $k_\infty = 1.08$, i.e. for $k \geqslant 1$ we must have $\varkappa \geqslant 0.93$. This corresponds to a reactor size of 5-10 m. This was the size of the first nuclear reactor built by Fermi in Chicago in December 1942.

The first Soviet reactor, built under the supervision of I.V. Kurchatov and commissioned in December 1946 in Moscow, was also of the same size. In both these reactors, graphite in a highly purified form (free from cadmium and boron impurities which strongly absorb thermal neutrons) was used as a moderator. Graphite was prepared in the form of slugs with holes to accomodate uranium blocks, and was tightly stacked in a pile having a nearly spherical shape (to decrease the relative probability of a neutron escaping from the reactor, i.e. to reduce its critical size).

Fermi's reactor contained 45 t uranium and 450 t graphite. It did not have any ventillation or shielding, and initially had a power of 200 W ($k = 1.0006$). The reactor was later dismantled and reassembled (with ventillation and shielding) at the Argonne Laboratory in Chicago. The modified reactor had a power of 100 kW.

Kurchatov's reactor was built from 50 t uranium and 500 t graphite. It had a rated power of 10 kW which could be spiked to 4000 kW during the "big" start-up.

The first reactors were controlled with the help of special rods made of materials that strongly absorb thermal neutrons (Cd, B). When a rod was introduced into the area of the lattice (*active zone*), the chain reaction terminated due to a strong absorption of thermal neutrons by cadmium or boron.

It should be noted that a control of the chain reaction occurring in a reactor operating on thermal neutrons was a comparatively simple problem on account of the fact that some of the fission neutrons are delayed neutrons.

Indeed, let us suppose that the multiplication factor k does not exceed 1.0064. For example, let

$$k = 1.005.$$

Considering that about 0.64% secondary neutrons are delayed neutrons, it can be easily seen that multiplication of neutrons cannot

[8] In this case, "moderator" means all materials except uranium (for example, construction materials).

occur through instantaneous neutrons only (for which $k < 1$), and delayed neutrons also must take part in the process.

Hence to determine the average lifetime $\bar{\tau}$ of one generation of neutrons, we must take into account the emission time for the delayed neutrons. Calculation of $\bar{\tau}$, taking into account the fraction of the delayed neutrons, gives the value

$$\bar{\tau} \simeq 0.1 \text{ s}$$

(instead of the value $\bar{\tau} \simeq 10^{-3}$ s obtained without taking into account the delayed neutrons).

Solving Eq. (7.4.3) for $\tau = 0.1$ s, we get

$$n = n_0 \exp(0.05t), \tag{7.4.16}$$

which means that the number of neutrons increases in 1 s by a factor of 1.05 only (for $\bar{\tau} \simeq 10^{-3}$ s, the number of neutrons increases by a factor of 150 in 1 s). It is the slow rise in the intensity of the chain reaction that makes it possible to easily control its course. The effect of the delayed neutrons is also manifested in that the chain reaction does not terminate abruptly upon the introduction of cadmium absorber, but dies down slowly.

Soon after the commissioning of the first nuclear reactors, extremely powerful reactors were built and used for obtaining the transuranic element plutonium, one of whose isotopes ($^{239}_{94}$Pu) has properties similar to those of $^{235}_{92}$U and can therefore be used as nuclear fuel (even in explosion reactions).

Plutonium is formed in a reactor as a result of the radiative capture of resonance neutrons by ^{238}U and two subsequent beta decays:

$$^{238}_{92}\text{U}\,(n, \gamma)\,^{239}_{92}\text{U} \xrightarrow[23\text{ min}]{\beta^-} {}^{239}_{93}\text{Np} \xrightarrow[2.35\text{ day}]{\beta^-} {}^{239}_{94}\text{Pu} \tag{7.4.17}$$

(see Sec. 8.2 for details). The production of $^{239}_{94}$Pu and the isolation of $^{235}_{92}$U from the natural uranium paved the way for realizing explosion chain reaction, i.e. to the creation of an atomic bomb.

At present, a very large number of nuclear reactors of different designs are operating on thermal, intermediate and fast neutrons.

In thermal reactors, fission is mainly caused by thermal neutrons, the intermediate reactors operate on neutrons with moderate energy (1-10^3 eV), while fast reactors employ fast neutrons for fission ($T_n > 10^4$ eV).

The active zone of thermal and intermediate reactors consists of a fuel and a moderator. Besides graphite, heavy water and ordinary water (if natural uranium is used as a fuel, ordinary water is unsuitable as a moderator), beryllium and beryllium oxide, as well as certain organic materials can be used as moderators.

Nuclear reactors operating on fast neutrons do not contain any moderator.

The nuclear fuel employed in a reactor can be $^{235}_{92}U$, $^{233}_{92}U$, $^{239}_{94}Pu$, natural uranium containing 99.3% $^{238}_{92}U$ and 0.7% $^{235}_{92}U$, as well as natural uranium enriched in $^{235}_{92}U$. It was mentioned above that $^{239}_{94}Pu$ is produced in nuclear reactors, $^{235}_{92}U$ and enriched uranium are obtained during isotopic separation of uranium, while $^{233}_{92}U$ is obtained through the reaction

$$^{232}_{90}Th\ (n, \gamma)\ ^{233}_{90}Th \xrightarrow{\beta^-} {}^{233}_{91}Pa \xrightarrow{\beta^-} {}^{233}_{92}U. \qquad (7.4.\ 8)$$

Nuclear fuel can be in solid, liquid or ceramic (oxides, carbides) form.

Depending on their design, nuclear reactors are called heterogeneous, in which fuel is distributed discretely over the active zone (in the form of a lattice), or homogeneous (when fuel and moderator are used in the form of a homogeneous mixture, say, a solution or a suspension).

According to their duty, reactors are called power reactors (used for obtaining power), research reactors (for research in nuclear and neutron physics and for testing materials) or regenerative reactors (for obtaining nuclear fuel). Regenerative reactors are of two types: converters and breeders. Converters produce about the same quantity of fuel as they consume. Breeders produce more fuel than what they expend. New fissile nuclei are formed either by converting ^{238}U present in natural uranium [reaction (7.4.17)] or from ^{232}Th introduced specially into the reactor [reaction (7.4.18)].

Usually, the same reactor can be used to perform different functions. The applications of atomic energy are discussed in Sec. 7.6.

7.4.4. Natural Nuclear Reactor

It has been mentioned above that quite specific conditions must be created for realizing a controlled fission chain reaction in natural uranium. These include the use of ultrapure graphite, beryllium or heavy water, an optimal relative content of uranium and a moderator, block arrangement, large-size systems, and the presence of regulators. Heavy water and pure beryllium or graphite are not available in nature, while a chain reaction with natural uranium containing 0.72% ^{235}U is not possible with ordinary water as a moderator. Hence it would appear that a fission chain reaction cannot occur in nature. However, this statement, although perfectly true today, is not valid for distant past.

It is well known that the half-lives of ^{238}U and ^{235}U are respectively equal to $T^{238}_{1/2} = 4.51 \times 10^9$ years and $T^{235}_{1/2} = 7.13 \times 10^8$ years. Hence the ^{235}U content in natural uranium was a lot higher about

2 billion years ago as compared to our time, and was about 3%. For such an "enrichment" of natural uranium with the isotope ^{235}U, a chain reaction is possible in a mixture of natural uranium and ordinary water. The power of such a natural reactor can be stabilized only through the temperature effect.

The assumption that a real nuclear reactor existed in nature was first put forth after the analysis of a uranium ore sample in France, which revealed that the ^{235}U content in the ore was 0.717% and not 0.72%. This seemingly insignificant discrepancy alerted the scientists who traced the batch of the ore right back to its origin. The fact is that 0.72% is a sort of absolute constant which is characteristic not only of all uranium mines on the Earth, but also of the lunar soil and meteorites.

Analysis of the ore in the immediate vicinity of the deposits in Western Africa showed a further depletion of the ^{235}U content (up to 0.64%) in uranium-rich ore (over 20% U). Besides, an excess of rare-earth elements which are the products of fission reactions were found in the composition of the ore.

A thorough survey of the region around the natural reactor showed that the huge uranium vein of (600-900)-m width and (4-10)-m thickness with ground waters contained large-size clay lenses [(10-20) × 1 m] with a high uranium content (20-40%). These are the sites where the fission chain reaction occurred.

From the amount of the burnt-up uranium, the age of the reactor was estimated at 1.8×10^9 years. The amount of ^{239}Pu formed indicated the duration of the process (about 600 000 years) and the power of the reactor (about 25 kW). All calculations were made by using the latest available data on cross sections, positions and widths of resonances, and were found to be in perfect mutual agreement. This leads to the conclusion that the strong (and electromagnetic) interaction constant has remained practically unchanged during this period (about 2 billion years).[9]

7.5. Supplementary Problems in Fission Physics

7.5.1. Properties of Fission Fragments

The main properties of fission fragments are a large kinetic energy, beta radioactivity and the ability to emit instantaneous and delayed neutrons.

We shall consider some of these properties in detail.

A nucleus may disintegrate in several ways. During fission of ^{235}U by thermal neutrons, more than 80 different fragment nuclei were detected. As a result of beta decay, these nuclei are transformed into

[9] See Yu.V. Petrov, *Uspekhi Fiz. Nauk*, 123, 3, 473 (1977) for details.

fission products. In all about 300 different isotopes were identified in these radioactive chains. Thus, the average length of a chain is 3-4 links. Three examples of long chains of radioactive transformations of fission fragments are given below:

$$\left.\begin{aligned} &{}^{135}_{52}\mathrm{Te} \xrightarrow{\beta^-} {}^{135}_{53}\mathrm{I} \xrightarrow{\beta^-} {}^{135}_{54}\mathrm{Xe} \xrightarrow{\beta^-} {}^{135}_{55}\mathrm{Cs} \xrightarrow{\beta^-} {}^{135}_{56}\mathrm{Ba},\\ &{}^{140}_{53}\mathrm{Xe} \xrightarrow{\beta^-} {}^{140}_{54}\mathrm{Cs} \xrightarrow{\beta^-} {}^{140}_{55}\mathrm{Ba} \xrightarrow{\beta^-} {}^{140}_{57}\mathrm{La} \xrightarrow{\beta^-} {}^{140}_{58}\mathrm{Ce},\\ &{}^{97}_{36}\mathrm{Kr} \xrightarrow{\beta^-} {}^{97}_{37}\mathrm{Rb} \xrightarrow{\beta^-} {}^{97}_{38}\mathrm{Sr} \xrightarrow{\beta^-} {}^{97}_{39}\mathrm{Y} \xrightarrow{\beta^-} {}^{97}_{40}\mathrm{Zr} \xrightarrow{\beta^-} {}^{97}_{41}\mathrm{Nb} \xrightarrow{\beta^-} {}^{97}_{42}\mathrm{Mo}. \end{aligned}\right\} \quad (7.5.1)$$

It can be seen from these examples that during successive beta transitions, the charge of the initial fragment may change by 4-6 units (possibly even more, since the initial parts of the chain are not easily detectable on account of their very short lengths).

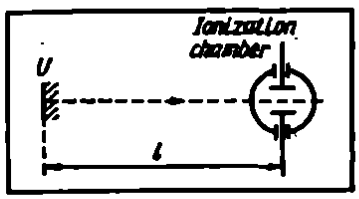

Fig. 251

Considering that the transformation chains have different lengths in different cases, and that two fragments are formed in an act of fission, we can estimate the average number of electrons and antineutrinos per act. This number is approximately equal to six. Besides, beta transitions of fission fragments and products involve the emission of γ-quanta which accompany beta decay.

It is well known that the main part of fission energy is released in the form of the kinetic energy of fragments. Calculations carried out in Sec. 7.3.1 give the value $Q_{fis} = 180$ MeV for this quantity. The experimental value of the kinetic energy of fission products is somewhat lower, viz. about 170 MeV.

The kinetic energy of fragments is spent on ionizing the atoms of the medium. The ionization range and specific ionization of the fragments at various points of their path in air were determined experimentally with the help of a small-sized ionization chamber placed in a vessel in which the air pressure could be varied (Fig. 251).

If the source of fission fragments (say, a uranium target) is placed at a certain distance l from the ionization chamber, the range R of the fission fragments will be longer or shorter than l, depending on the air pressure. By determining the pressure at which $R = l$ and recalculating for normal pressure, we can find the range R_0 of the fragments in air at normal pressure. This gives the value of 25 mm for the range of the light fission fragment, and 19 mm for the range of the heavy fission fragment.

There are other methods of measuring the ionization range. For example, the range of fission fragments can be easily measured in

a photographic emulsion by introducing particles of a fissile material in the latter. After the development, such emulsions reveal short thick tracks of the fragments with an average length 13.4 μm for light fragments and 10.4 μm for heavy fragments.

The tracks of fragments in a Wilson cloud chamber have very interesting shapes (Fig. 252). The fragment track is thick at the beginning, thins out gradually and terminates in one or several V-shaped forks similar to those observed for elastic scattering. The abrupt narrowing

Fig. 252

of the track near the end of the range indicates a sharp fall in the ionizing power with decreasing velocity of the fragment, which seems to contradict Bohr's formula for specific ionization.

This result is explained by the fact that a fragment formed during fission is deprived of a considerable part of its electrons, i.e. the charge of its nucleus is heavily uncompensated. As a result, the fragment ionizes as a multiply charged particle at the beginning of its path ($Z \simeq 20$). During deceleration, the fragment gradually "accumulates" electrons which find it possible to "perch" on Bohr orbits if the velocity of the fragment is comparable with the velocity of an electron on the appropriate orbit.

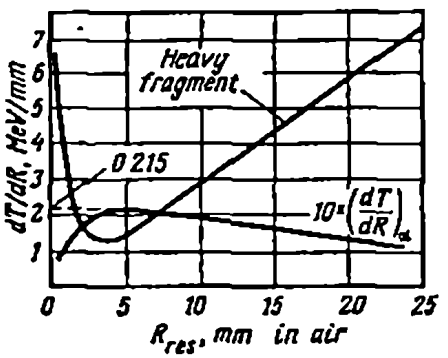

Fig. 253

The dependence of the specific ionization dT/dR of a fragment on the residual range R_{res} was measured with the help of the small-sized ionization chamber described above, in which a small part of the range is accommodated. The specific ionization at any part of the path can be measured by varying l. The dependence thus obtained is shown in Fig. 253. It can be seen from the figure that the specific ionization for the fragments is considerably higher than for α-particles (lower curve), and sharply decreases with residual range at the beginning of the path of the fragment. This result is explained by the above-mentioned process of "accumulation" of electrons in the fragments. At the end of the path (small residual ranges), the specific ionization increases once again since the fragments start losing energy rapidly due to nuclear interaction.

Measurement of angular distribution of fission fragments showed that the distribution is anisotropic with respect to the direction

of the beam of particles responsible for fission. If this anisotropy α is defined as the ratio of the fission cross sections at 0 and 90° to the beam direction, then fission by fast particles usually leads to $\alpha > 1$ while fission caused by γ-quanta gives $\alpha < 1$. Qualitatively, this result follows from the law of conservation of angular momentum. Indeed, a fast particle introduces an angular momentum l to the nucleus in a direction perpendicuar to its motion. Hence the resultant angular momentum of the disintegrating nucleus and the orbital angular momentum of the fission fragments must also have the same

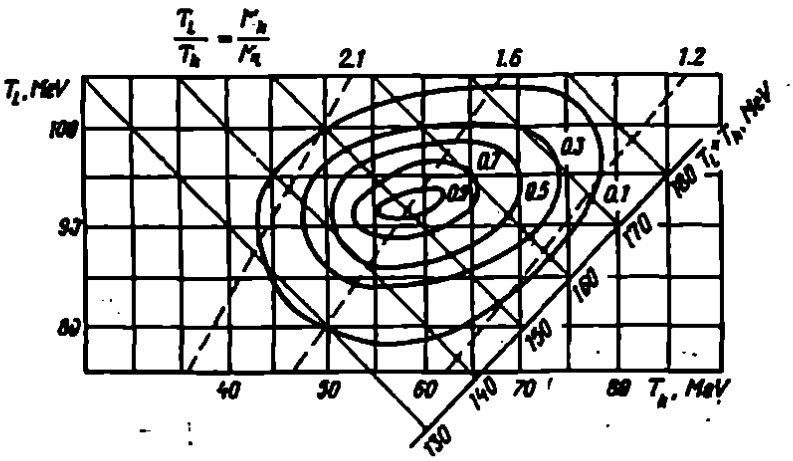

Fig. 254

preferential orientation on the average. For a dipole γ-quantum whose angular momentum is collinear with the beam direction, the orbital angular momentum L of the fragments also must be collinear with the beam and hence the fragments fly mainly in a direction perpendicular to the beam.

It was mentioned in Sec. 7.2.1 that the kinetic energy and mass distributions of the fragments obey relation (7.2.1) only to a first approximation, since the fission probability strongly (and ambiguously) depends on the ratio of the masses and kinetic energies of the fragments. A detailed experimental investigation of this problem was carried out with the help of a single-channel analyzer whose window can be fixed relative to a certain energy of one of the fragments. The results of measurements are shown in Fig. 254, where T_l, T_h and $T_l + T_h$ denote the kinetic energy of the light, heavy and both fragments respectively, M_h/M_l is the ratio of their masses, and the numbers on the closed curves indicate the relative fission probabilities. It is clear from the figure that for a fixed fission probability, different values of $T_l + T_h$ correspond to the same value of M_h/M_l, and vice versa. This means, in particular, that $T_l > \bar{T}_l$ and $T_h > \bar{T}_h$ are simultaneously possible.

7.5.2. Mechanism of Formation and Emission Time of Fission Neutrons

It seems obvious that secondary neutrons are emitted by neutron-rich fragments. However, another mechanism is also possible, according to which fission neutrons are released by the disintegrating nucleus at the moment of fission.

The choice between these two mechanisms can be made by experimentally measuring the angular correlation between the preferential direction of motion of secondary neutrons and the direction in which the fission fragments fly. When neutrons are emitted by the fission

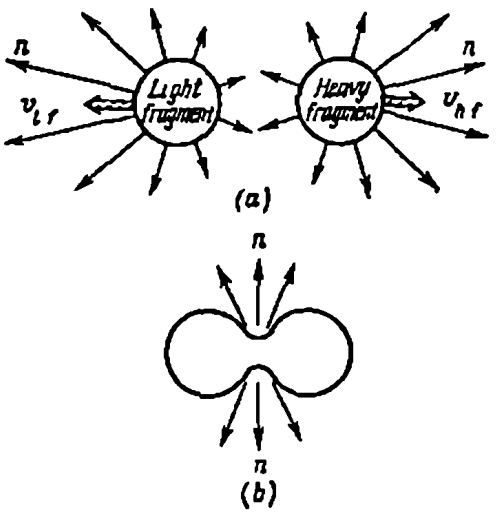

Fig. 255

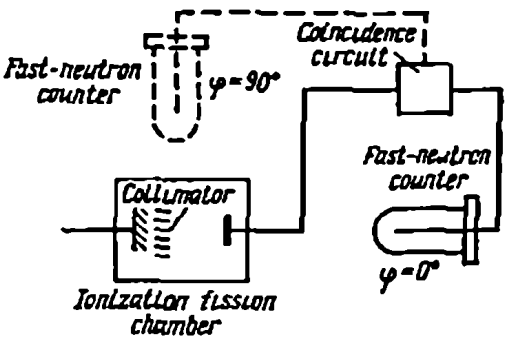

Fig. 256

fragments, the neutrons (n) will predominantly fly in the direction of motion of the light fragment and the heavy fragment (since the time of emission of instantaneous neutrons must be less than the time of ionization losses by the fragments and so the neutrons are emitted by the moving fragments). However, if neutrons are emitted by the disintegrating nucleus, their direction is perpendicular to the direction of motion of the fragments, since the most likely place from where the neutrons escape is the neck of the disintegrating nucleus, where the nuclear excitation has the highest value (Fig. 255*a* and *b*).

The first experiment on determining the angular correlation between the direction of emission of secondary neutrons and the direction of motion of the fission fragments was carried out in 1947 with the help of the apparatus shown in Fig. 256. The set-up included an ionization fission chamber with a collimator to single out fragments in a particular direction. A fast-neutron counter was connected in a coincidence circuit to the ionization chamber and could be turned

at different angles φ to the direction of motion of the fragments. Measurements revealed that the number of coincidences at an angle $\varphi = 0$ or $\varphi = \pi$ was about five times larger than the corresponding value at $\varphi = \pi/2$. This leads to the conclusion that the secondary neutrons move mainly in the direction of motion of the fragments, i.e. are emitted by the moving fragments (at any rate, most of them).

The results of this experiments were used in 1948 to determine the fragments (light, heavy or both) emitting secondary neutrons. For this purpose, an experiment was made (Fig. 257) to detect fission

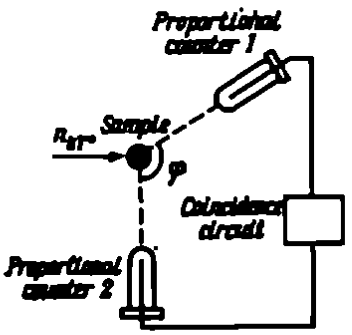

Fig. 257

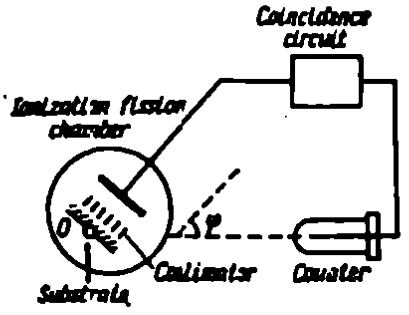

Fig. 258

neutrons emitted simultaneously by the disintegrating (under the action of thermal neutrons n_{th}) sample at various angles. Neutrons were registered by proportional counters with polyethylene films (for the formation of recoil protons) connected in a coincidence circuit.

Experiment showed that the number of neutron pairs emitted in opposite directions (i.e. by different fragments) is about twice the number of neutron pairs emitted in the same direction (i.e. by the same fragment).

Angle between the counters, deg	30	60	90	135	180
Number of coincidences per minute	1.2	1.3	1.2	1.8	2.4

Thus, secondary neutrons are emitted by light as well as heavy fission fragments.

The third experiment in this series was carried out in 1949. It allowed a comparison of the relative numbers of fission neutrons emitted by light and heavy fragments, as well as an estimation of the time of emission of secondary neutrons.

The schematic of this experiment (Fig. 258) is similar to that of the first experiment. It includes an ionization fission chamber with a collimator capable of rotation about the axis O. This makes it possible to change the angle φ between the directions of motion of fragments and secondary neutrons which are registered by a counter connected in a coincidence circuit with the chamber. The distinguishing feature of this experiment was the possibility of isolating the effect due to light fragments (which have a higher kinetic energy than heavy fragments and hence cause a larger pulse in the ionization chamber).

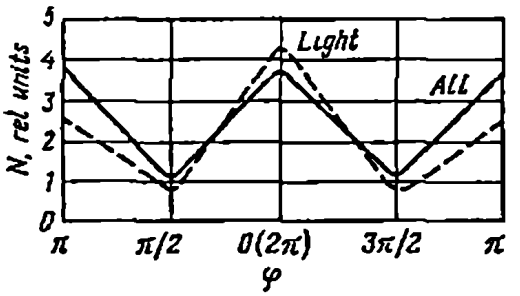

Fig. 259

The experimental results (for $^{239}_{94}$Pu) are shown in Fig. 259. It is clear from the figure that the number of coincidences at angles $\varphi = 0$ and $\varphi = \pi$ is the same for all fragments, but differs [$N(0)/N(\pi) = 1.72$] for light fragments. Hence we can easily conclude that light fragments emit more neutrons than heavy fragments. A quantitative analysis of the experimental results indicates an increase of about 30%.

Similar results were also obtained for other nuclei which undergo fission by thermal neutrons [the ratio $N(0)/N(\pi) = 2.05$ for $^{233}_{92}$U, and 1.85 for $^{235}_{92}$U].

This experiment makes it possible to draw conclusions about the time that elapses between the instant of fission and the moment of emission of secondary neutrons. Indeed, it follows from the mechanism of emission of neutrons that for $\varphi = 0$ and $\varphi = \pi$, the neutron counter essentially registers neutrons emitted by the fragments moving towards the counter. Moreover, the number of coincidences is found to be the same (with an error of about 2%) in both cases. However, these cases differ from each other in that for $\varphi = 0$ the fragments moving towards the counter escape from the layer of the fissile material directly into the ionization chamber, while for $\varphi = \pi$ they must first pass through a 0.5 μm-thick substrate coated with a layer of the fissile material (see Fig. 258). Since the initial velocity of the fragments is 1.2×10^9 cm/s, the time spent by them in passing through the substrate is given by

$$\tau_0 = 5 \times 10^{-5}/1.2 \times 10^9 = 4 \times 10^{-14} \text{ s}. \qquad (7.5.2)$$

In doing so, the fragments lose about 5 MeV of their kinetic energy, which causes a decrease in their velocity. However, the nature of emission of secondary neutrons depends on the velocity of the fragments emitting them. As the velocity of the fragments decreases, the

angular distribution of the neutrons must become more isotropic, which means that fewer neutrons will move in the direction of motion of the fragments. Hence the number of counts in the counter for $\varphi = \pi$ must depend on whether the neutrons are emitted by the fragments before or after passing through the substrate. In the first case, the number of counts for $\varphi = \pi$ will be the same as for $\varphi = 0$, while in the second case the number of counts must be lower for $\varphi = \pi$. Since the number of counts for $\varphi = 0$ is equal to that for $\varphi = \pi$, we can conclude that neutrons are emitted before the fragments pass through the substrate. This gives the following estimate for the emission time of secondary neutrons:

$$\tau < \tau_0 = 4 \times 10^{-14} \text{ s}. \tag{7.5.3}$$

7.5.3. Spectrum of Fission Neutrons

The spectrum of fission neutrons was studied by measuring the energy distribution of head-on recoil protons produced in a nuclear emulsion as a result of irradiation by secondary neutrons.

The experimental set-up is shown in Fig. 260. Thermal neutrons n_{th} emerging from the channel of a nuclear reactor fall on a small sample made of a fissile material and cause its fission accompanied by the formation of fission neutrons which fly out in all possible directions. The photographic plate registering these neutrons was placed away from the beam of thermal neutrons at a certain distance from the sample.

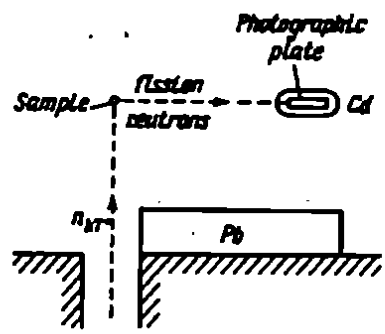

Fig. 260

To shield the photographic film from thermal neutrons (which interact with nitrogen in the emulsion and produce protons with an energy of about 0.6 MeV), it was placed in a cadmium cassette. Besides, the effect of the background was taken into account by carrying out a blank experiment in which the photographic plate was irradiated by using a mock-up nonfissile material (instead of the sample) which, however, was capable of scattering the neutrons in the beam.

In order to obtain the neutron spectrum, recoil proton tracks corresponding to head-on or nearly head-on collisions (with a recoil angle not exceeding 10°) were chosen. In accordance with Sec. 4.4, the energy of the recoil proton in this case was practically the same as the energy of the neutron that produced this proton:

$$T_p = T_0 \cos^2 \psi \simeq T_0, \tag{7.5.4}$$

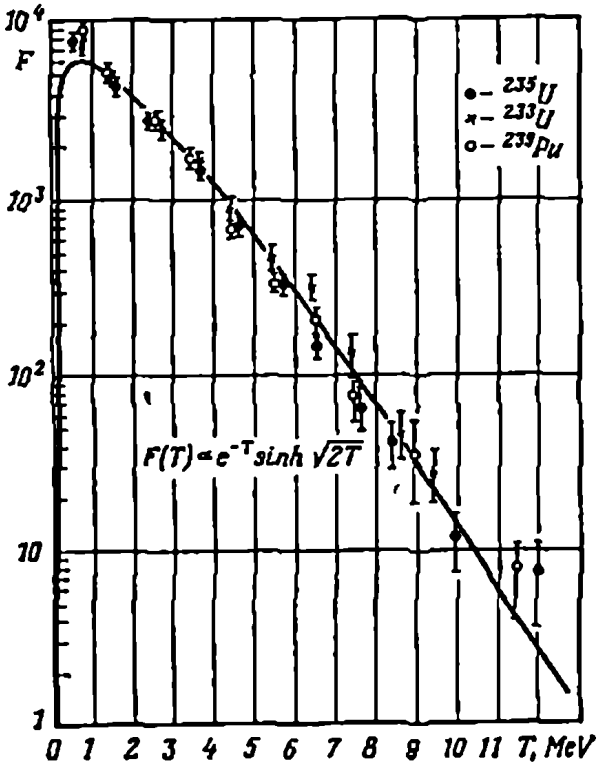

Fig. 261

and the neutron spectrum $F(T_n)$ is obtained from the spectrum of head-on recoil protons $\Phi(T_p)$ by dividing the latter with the $(n\text{-}p)$-scattering cross section at the appropriate energy:

$$F(T_n) \simeq \Phi(T_p)/\sigma_{np}. \tag{7.5.5}$$

Several thousand tracks were analyzed in order to obtain reliable results and in view of the strongly diminishing neutron spectrum, the entire spectrum was divided into several intervals. Each of these intervals was analyzed separately and the results for overlapping segments were matched.

Estimation of resolving power and energy calibration of the method were carried out in special experiments in which photographic plates were irradiated with 2.5 and 14 MeV neutrons from the reactions

$$^3_1H + ^3_1H \rightarrow n + ^3_2He, \quad ^2_1H + ^3_1H \rightarrow n + ^4_2He. \tag{7.5.6}$$

The results of measurements of the spectrum of secondary neutrons are shown in Fig. 261. The spectral form is given to a fairly high degree of accuracy by the formula

$$F(T) \propto e^{-T} \sinh \sqrt{2T}, \tag{7.5.7}$$

where T is the neutron energy in MeV. This formula can be obtained theoretically by assuming that neutrons are "vaporized" by the moving fragment.[10]

A certain increase in the experimental values in comparison with the theoretical curve at low energies probably indicates that the spectrum contains a small amount (10-20%) of neutrons that are emitted not by the fission fragments but directly by the disintegrating nucleus.

It can be seen from Fig. 261 and formula (7.5.7) that the spectrum of secondary neutrons contains neutrons with quite high energies (at present, neutrons with energies up to 17 MeV have been detected). In view of the steep fall of the curve towards higher energies, the average energy of the fission neutrons is

$$\bar{T} \simeq 2 \text{ MeV}. \qquad (7.5.8)$$

7.5.4. Emission of Instantaneous Gamma-quanta in Fission

Besides γ-quanta which accompany the beta decay of fission fragments and other fission products and are consequently emitted over a length of time, instantaneous γ-quanta emitted by the primary fission fragments during their transition to the ground state after the emission of instantaneous fission neutrons were also observed in investigations of the fission processes.

In the first experiments, instantaneous γ-quanta were detected by a Geiger-Muller counter with a thick cathode and an ionization chamber operating in coincidence circuit. The efficiency of a thick-walled counter is approximately proportional to the energy of the γ-quanta being registered. Hence the ratio of the number of coincidences to the number of fragments must be proportional to the energy of gamma radiation emitted during one act of fission.

After calibration of the counter with γ-quanta from ThC'' and ^{60}Co, it was found that about 5 MeV of energy are released in the form of instantaneous γ-quanta. In subsequent experiments, this value was modified (7 MeV), and it was also shown that about 8 quanta with an average energy of nearly 1 MeV are emitted in an act of

[10] Formula (7.5.7) was first published in *Nucleonics*, 8, 9, 78 (1951) as a semi-empirical expression approximating the observed spectrum of fission neutrons. In the Soviet Union, the spectrum of fission neutrons satisfying formula (7.5.7), as well as the formula itself, was obtained independently in the same year by I.I. Gurevich and K.N. Mukhin. Spectra of fission neutrons for ^{235}U, ^{233}U and ^{239}Pu over a wide range of energies (see Fig. 261) were first obtained in 1950-51 by K.N. Mukhin, L.M. Barkov and R.I. Gerasimova [see the review article by B.G. Erozolimskii in *Nuclear Fission Physics*, Atomizdat, Moscow, 1957 (in Russian), as well as Terrell James, *Phys. Rev.*, 113, 2, 527 (1959)].

fission. The spectrum of the emitted gamma radiation is continuous and diminishes with increasing energy. The maximum energy of γ-quanta is approximately 7 MeV. An estimation of the emission time for instantaneous γ-quanta showed that it does not exceed a few nanoseconds for most of them.

7.5.5. Fast Particle Fission and Its Properties. Fission Asymmetry

Quite interesting results were obtained in a comparison of the shapes of mass distribution curves for fission fragments at different excitation energies of the disintegrating nucleus.

It was shown in Sec. 7.2 that the yield of fission fragments during uranium fission by thermal neutrons is highly asymmetric with respect to the mass of the fragments. The average ratio of the masses of light and heavy fragments is 2 : 3. A detailed analysis of the

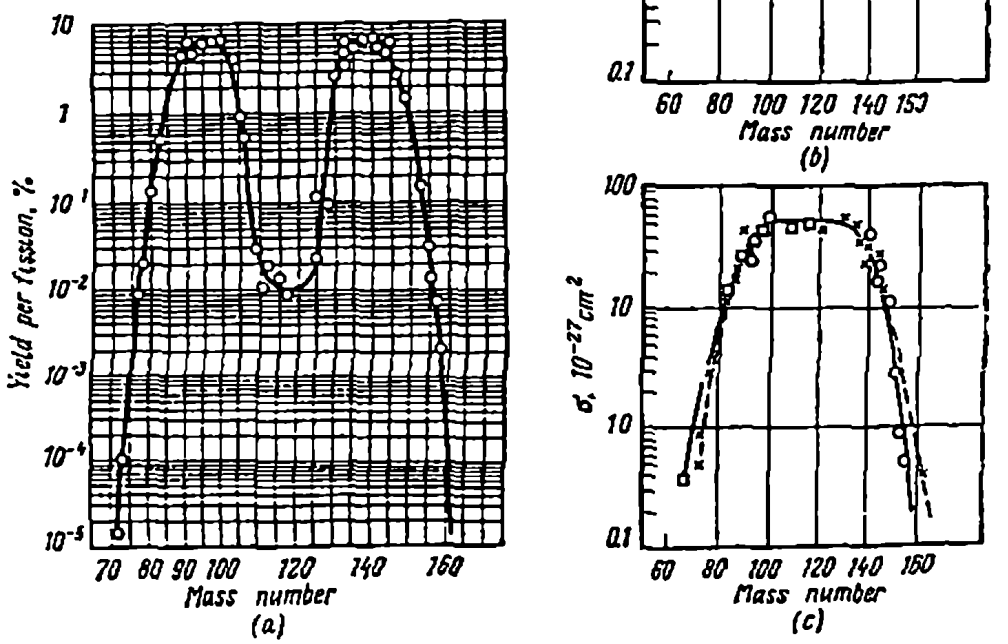

Fig. 622

fission of ^{235}U showed that the probability of asymmetric fission is 3×10^2 *times higher than for symmetric fission (Fig. 262a).* Similar results were also obtained for other nuclei undergoing fission by thermal neutrons ($^{233}_{92}U$, $^{239}_{94}Pu$).

Besides, asymmetric fission is observed in induced fission of all elements beyond Th if it is caused by particles of not very high energies, as well as during spontaneous fission of heavy nuclei. Thus, in all the cases of nuclear fission at moderate excitation energies, the mass curve for the fragments has two humps.

As the nuclear excitation energy increases, the fission becomes more symmetric. For example, for the fission of a uranium nucleus by 32-MeV protons, the probability of symmetric fission increases by a factor of about 300 (see Fig. 262*b*), and the mass curve has only one hump at an excitation energy of about 150 MeV (see Fig. 262*c*).

The problem of asymmetric fission is one of the most complicated problems in fission physics. Calculations of the fission barrier height W_{fis} as a function of the nuclear deformation show that W_{fis}^{min} corresponds to symmetric fission, i.e. the energy surface $W_C + W_s$ has a saddle point for symmetric deformation. Hence from the point of view of the liquid drop model of fission (which has been experimentally verified in many respects), symmetric fission must have the highest probability.

The discrepancy between theory and experiment has been attributed by many authors to the appearance of shell effects during the formation of fission fragments. This explanation can be summarized as follows. The initial deformation of the nucleus is symmetric. After the attainment of the saddle point, however, the actual disintegration of the nucleus into fragments does not occur instantaneously, but takes place only after the nucleon shells of the would-be fission fragments have been formed. The number of nucleons in these shells turns out to be different, hence the asymmetry of fission. This hypothesis is in agreement with the rough estimates for the time τ_{sh} of the formation of shells and the fission time τ_{fis}:[11]

$$\tau_{sh} \simeq \hbar/\overline{\Delta E}_{sh} \simeq 10^{-21}\ \text{s} < \tau_{fis} = \delta/v \simeq 10^{-20}\ \text{s},$$

where $\overline{\Delta E}_{sh} \simeq 1$ MeV is the average separation between one-particle levels in the shell model, δ is the distance between the flying fragments (about 10^{-11} cm), and v is the fragment velocity (about 10^9 cm/s). In order to illustrate the mechanism of asymmetry emergence, let us consider as an example the fission of the nucleus $^{236}_{92}U$ by thermal neutrons. The fissile nucleus $^{236}_{92}U$ contains 144 neutrons, which is a sufficient quantity for the formation of two different shells, one with 82 neutrons (for the heavy fragment) and the other with 50 neutrons (for the light fragment). Suppose that the remaining 12 neutrons are divided equally between the two fragments. Thus the light and heavy fragments then contain 56 and 88 neutrons respectively.

[11] Experimentally estimated values of τ_{fis}, obtained from the shadow method (see Sec. 10.2), lie around $\tau_{fis}^{exp} \leqslant 10^{-17}$ s.

Considering that the neutron to proton ratio in these fragments must be the same as for $^{236}_{92}U$, we find that the light fragment must contain 36-38 protons and thus have a mass number $A_l \simeq 92\text{-}94$, while the heavy fragment must have 54-56 protons and a mass number $A_h \simeq 142\text{-}144$.

These characteristics of the fragments are in good agreement with the experiment both with respect to the average mass numbers for the light and heavy fragments, viz. $A_l : A_h = (92\text{-}94) : (142\text{-}144) = 2 : 3$, and with respect to the charge of most of the primary fission fragments. Radiochemical analysis of the yield of various fragments shows that there are eight radioactive chains starting from $Z = 36$ and seven chains starting from $Z = 54$, with a total yield of 75%. Each of these chains has a yield of not less than 4.6%.

This point of view is also confirmed by the position and shape of the right hump on the mass curve which practically coincide for all the investigated fissionable nuclei (from $^{234}_{92}U$ to $^{252}_{98}Cf$), while the left hump is displaced to the right for heavy nuclei. Probably, this means that in the heavy fragment a neutron shell with 82 neutrons is formed as well as a proton shell with 50 protons, and hence the heavy fragment has a double-magic core to which nucleons cannot be added easily.

Finally, the above-mentioned symmetrization of fission with increasing excitation energy of the fissile nuclei also supports the shell mechanism of the emergence of asymmetry, since it is well known that shell effects appear only at low excitation energies.

Note that all the above considerations are qualitative in nature. Another possible explanation of fission asymmetry is given in Sec. 7.5.6.

7.5.6. Spontaneous Fission. Shape Isomers

It was shown in Sec. 7.3 that a tunnel transition may cause instantaneous fission of a nucleus without any preliminary excitation. This process, called *spontaneous fission*, is similar to alpha decay. The fission fragments "leak" through the potential barrier formed during the initial deformation of the fissile nucleus (see Fig. 242).

The probability of spontaneous fission is determined by the penetrability of the potential barrier for the fragments. It can be estimated by a formula similar to (3.2.17) used for alpha decay:

$$D \simeq \exp\left(-\frac{2}{\hbar}\sqrt{2MW_{fis}}\,d\right), \qquad (7.5.9)$$

where M is the reduced mass of the fragment, W_{fis} is the height of the fission barrier and d is its width (radius of the fragment).

Estimates made by using formula (7.5.9) lead to very large values of half-life for spontaneous fission ($\tau \simeq 10^{20}$ years), which makes an experimental observation of this phenomenon extremely difficult.

The first experiment aimed at detecting spontaneous fission was carried out in 1940 by the Soviet physicists G.N. Flyorov and K.A. Petrzhak under the supervision of I.V. Kurchatov. A special multilayer fission chamber (Fig. 263) was constructed for registering spontaneous fission. The plates of this chamber were coated by a thin layer of uranium oxide (10-20 mg/cm^2). The chamber contained a total of 15 plates with an overall area of 10^3 cm^2 (it was subsequently increased to 6×10^3 cm^2). The fragments formed as a result of fission created ionization pulses in the chamber, which were supplied to an amplifier and registered by a mechanical counter.

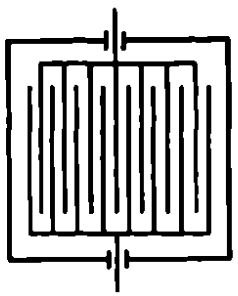

Fig. 263

Special measures were taken while designing the amplifier to increase its resolving power in order to exclude the registration of false "fragment"-type pulses which may arise as a result of superposition of a large number of pulses from α-particles emitted by uranium.

The instrument was first tested by registering induced fission caused by a very weak neutron source. The instrument was found to be highly sensitive and was used for studying the shape of ionization pulses caused by the fragments, and for measuring the distribution of pulses with respect to the pulse height.

In the first experiments which were carried out without a neutron source, a small number of ionization pulses (on the average, six pulses per hour) whose size and shape were found to be similar to those of pulses caused by induced fission fragments. These pulses were naturally attributed to spontaneous fission.

In order to rule out any other possible explanation for these pulses, a series of blank experiments were performed. It was shown that the registered pulses could not be caused by stray currents in the amplifier, by a superposition of a large number of α-particle pulses, or by the fission of uranium induced by cosmic radiation.

The emergence of pulses due to stray currents was ruled out since no such pulses were observed in the experiment when the chamber did not contain uranium. To exclude the second possibility, the background of α-particles in the chamber was doubled by filling it with radioactive thoron gas. This did not result in any enhancement of the effect. Finally, to rule out the possibility of induced uranium fission by cosmic radiation, the experiment was repeated in a Moscow metro station at a depth of 50 m. The effect was not diminished in this experiment.

Thus, as a result of a series of blank experiments, the existence of spontaneous fission in uranium was finally established.

The half-life of the process was estimated at $(4\pm1) \times 10^{16}$ years (the latest available value is $T_{1/2} = 0.8 \times 10^{16}$ years).

At present, spontaneous fission has been observed and studied for a large number of heavy nuclei from thorium to the element with $Z = 107$. The regularities established as a result of these investigations are found to be very helpful in identification of new isotopes of transuranic elements (see Sec. 8.4).

The characteristics of spontaneous fission are very similar to those of induced fission at low excitation energies. For example, both types of fission are characterized by a sharp two-hump curve for the yield of fragments, and the emission of fission neutrons and spontaneous γ-quanta is observed in both cases (with similar energy spectra).

Neutrons emitted during spontaneous fission were first detected in 1941 by Fermi during the construction of the first nuclear reactor. Measurements revealed that during spontaneous fission of uranium, $\nu = 2.2\pm0.3$ neutrons are emitted in each act of fission. A detailed account of the value of ν for spontaneous fission of various nuclei is given is Sec. 7.5.8.

In 1961, S.M. Polikanov and coworkers at Flyorov's laboratory in Dubna discovered a new nuclear phenomenon, viz. spontaneous fission in the isomeric state (i.e. an excited state with a quite long lifetime). This discovery was made accidentally during the first experiments on the synthesis of the 104th element (see Sec. 8.3.7).

The experiments involved an investigation of the reaction

$$^{22}_{10}\mathrm{Ne} + {}^{242}_{94}\mathrm{Pu} \rightarrow {}^{260}104 + 4n \qquad (7.5.10)$$

induced by $^{22}_{10}$Ne ions having an energy of 115 MeV, and the monitoring reaction

$$^{16}_{8}\mathrm{O} + {}^{238}_{92}\mathrm{U} \rightarrow {}^{254*}_{100}\mathrm{Fm} \begin{cases} \nearrow {}^{250}_{100}\mathrm{Fm} + 4n \\ \searrow {}^{248}_{100}\mathrm{Fm} + 5n \end{cases} \qquad (7.5.11)$$

induced by $^{16}_{8}$O ions and resulting in the formation of a fermium isotope with known properties.

The experiment was carried out by using the set-up shown in Fig. 264. After passing through a thin aluminium plate, ions were made to interact with the target nuclei. The product nuclei thus formed flew from the target and were deposited on a rapidly rotating aluminium disc. When the disc was turned at a certain angle, the reaction products face two detectors of spontaneous fission fragments. The difference in the counts of these detectors can be used to determine the half-life. Ionization chambers or photographic plates were used as detectors. Since ejected ion beams were not available at that time, the entire set-up was placed inside an accelerator.

The experiment gave $T_{1/2}^{\text{sp.fis.}} = 0.014$ s, whose exceptionally small value rules out the possibility of its belonging to one of the product nuclei formed by the interaction of $^{16}_{8}$O with $^{238}_{92}$U (in princi-

ple, the product nucleus could be an isotope of one of the eight transuranic elements from $_{93}$Np to $_{100}$Fm). The only explanation for the observed result was that the period $T_{1/2}^{sp.fs.} = 0.014$ s belongs to the isomeric state of one of these isotopes.

Later experiments with particles lighter than $^{16}_{8}$O showed that the spontaneously fissioning isomer is the americium isotope $^{242m}_{95}$Am whose ground state has a spontaneous fission half-life $T_{1/2}^{sp.fs.} = 10^{14}$ years.

Two astonishing results were obtained in this experiment. Firstly, the ratio of half-lives for the ground and isomeric states was found to be 10^{23}, which is 10^7 times higher than the maximum possible value corresponding to the interpretation of the isomeric state as

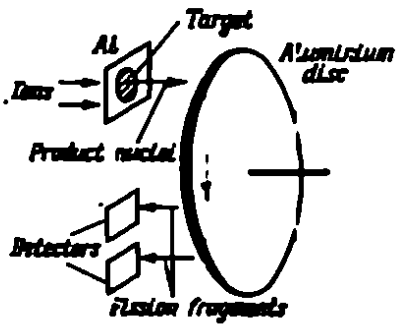

Fig. 264

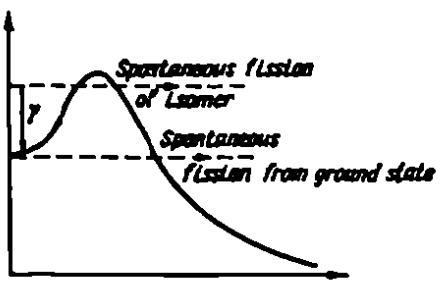

Fig. 265

a level in the potential well formed by the fission barrier (Fig. 265). Secondly, it is not clear why there are no gamma transitions from the excited state to the ground state at such high excitations.

Soon after the discovery of the first spontaneously fissioning isomer, isomers for other isotopes of this element were discovered. This was followed by the discovery of many other isomers of heavy nuclei. By 1976, over thirty spontaneously fissioning isomers had been discovered for elements from $_{92}$U to $_{97}$Bk with half-lives varying between 2×10^{-9} s and 1.4×10^{-3} s. In all these cases, the same astonishing result was observed, viz. an exceptionally high probability of spontaneous fission (about 10^{24} times higher than the probability of spontaneous fission from the ground state) and a very strong inhibition to gamma transitions. A systematic analysis of the properties of the new type of isomers was required to explain these results.

It is well known (see Sec. 3.4) that ordinary nuclear isomerism is observed for excited states that are close to the ground state and differ strongly from it in its angular momentum. Hence an important aspect of the investigation of the observed effect was to determine the energy and spin of the isomeric states. At the early stages of

investigation, the energy of isomeric states was obtained from a comparison of the thresholds of formation of a given isotope in the ground and isomeric states. For most isomers, this difference lies between 2 and 4 MeV, forming a group around 2.5-3 MeV. The spontaneously fissioning isomers must have small spins. This follows from the fact that the cross section of isomer formation in a neutron radiative capture reaction (which cannot lead to a sharp increase in spin) is larger than the cross section of their formation in reactions induced by heavy ions (which can introduce large angular momenta into the product nucleus).

Thus, spontaneously fissioning isomers are characterized by a large excitation energy and a small spin, which distinguishes them from ordinary isomeric nuclei. Besides, the new isomers have an anomalously large ratio of the half-lives for ground and excited states, which is also in contradiction with the ordinary isomerism. A possible explanation of the nature of the new class of isomers (known as shape isomers) was proposed in 1966 by Flyorov[12] and substantiated in 1967 by Strutinsky[13].

It is well known that while calculations based on the liquid drop model give a qualitative or a rough quantitative agreement with the experiment, they cannot lead to exact results which can, however, be obtained by introducing appropriate corrections based on the single-particle models. This is the case with the semiempirical formula for binding energy which involves correction terms taken from single-particle models. It should be recalled that in order to obtain the best agreement between theory and experiment, shell corrections were introduced into this formula. Hence the attempt to introduce single-particle (shell) corrections for the fission barrier obtained by using the liquid drop model seems quite natural.

In keeping with this idea, it is assumed that the nuclear potential energy is composed of two terms

$$V = V_{ldm} + \delta, \tag{7.5.12}$$

where V_{ldm} is the part of the potential energy described by the liquid drop model, and δ is the shell correction to this energy. The value of V_{ldm} varies smoothly from nucleus to nucleus, while the value of δ depends strongly on the number of nucleons in the nucleus and is comparable in order of magnitude to the height of the fission barrier.

Quite interesting results were obtained upon a detailed analysis for different nuclei. It was found that the fission barrier has the form of two humps instead of one at the saddle point. This results in the appearance of a second potential energy minimum for large nuclear deformations (Fig. 266). This minimum corresponds to a fairly long-

[12] G.N. Flyorov and V.A. Druin, *Structure of Complex Nuclei*, Atomizdat, Moscow, 1966 (in Russian).
[13] V.M. Strutinsky, *Nucl. Phys.*, A95, 420 (1967).

lived excited state (i.e. isomeric state) of the nucleus. However, this isomerism is of a different nature in comparison with the ordinary isomerism described earlier. In the present case, the low probability of gamma transitions is due not to a large difference in the angular momenta of the excited and ground states of the nucleus, but to the large potential barrier separating two potential wells. The wave-function characterizing the isomeric nuclear state has a low penetrability for the first minimum. However, it is clear that there is a very high probability of spontaneous fission in the isomeric state due to a low height and a small width $W_{fis}^{(2)}$ of the second barrier.

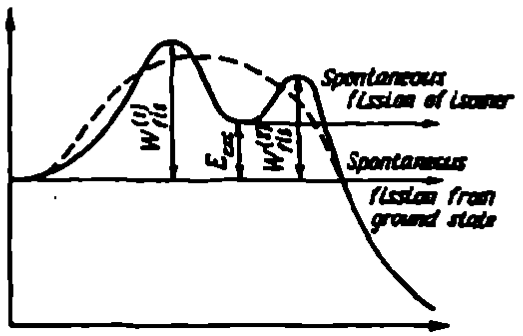

Fig. 266

The spontaneous fission from the ground state is determined by the parameters of both barriers, i.e. in fact by the parameters of the old one-humped barrier defined by the liquid drop model (dashed curve in Fig. 266). Thus, the two-humped fission barrier naturally explains not only the enormous difference in the half-lives of spontaneous fission for ground and excited states, but also the strong inhibition of gamma transitions. It is also interesting to note that a consideration of shell effects lowers the height of the second barrier for $_{92}$U, $_{91}$Pa and $_{90}$Th by 2 MeV in the case of octupole (pear-shaped) deformation. In other words, the fission asymmetry is naturally explained by an easier transition through the second barrier in the case of an asymmetric deformation.

If the model described above is correct, the observed isomers of spontaneous fission should be classified as shape isomers. To verify this model, many experiments are being made to determine the parameters of the model: the heights $W_{fis}^{(1)}$ and $W_{fis}^{(2)}$ of the first and second barriers, the energy E_{exc} of the nucleus (in ground and excited states) at the second minimum, nuclear deformation, etc. Preliminary results show that

$$\begin{cases} W_{fis}^{(1)} > W_{fis}^{(2)} & \text{for Pu, Am and Cf,} \\ W_{fis}^{(1)} < W_{fis}^{(2)} & \text{for Th and U,} \end{cases} \qquad E_{exc} = 2\text{-}3 \text{ MeV}.$$

An interesting confirmation of the nuclear model with two potential wells is the experimental observation of conversion electrons in $^{240}_{94}$Pu, which are emitted prior to the spontaneous fission of the isomer of this nucleus. From the energies of the electrons, we can reconstruct the spectrum of the excited states of the isomer. This spectrum can be interpreted as a rotational spectrum (Fig. 267). Its structure (the energy of the first level is half that of ordinary rotational spectra of heavy nuclei, see Sec. 2.4.2) shows that the spontaneously fissioning isomer $^{240}_{94}$*Pu has the shape of a prolate ellipsoid of revolution with 2 : 1 ratio of the semi-axes, which considerably exceeds the corresponding ratio for the ground state of this nucleus. Thus, the observation of the conversion electrons is naturally attributed to the rotational spectrum for the isomeric state of the strongly deformed nucleus. Spontaneously fissioning isomers were called shape isomers.

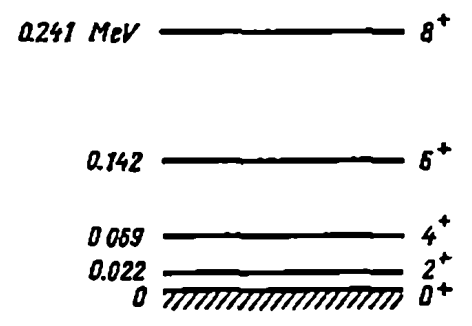

Fig. 267

If the results of the experiment of Bemis *et al.*[14] are confirmed subsequently, it can be considered as the first direct experimental evidence that spontaneously disintegrating isomer-nuclei have a large deformation. In Bemis' experiment, which was carried out on the isochronous cyclotron at Oak Ridge (USA), the optical isomeric shift was measured for the $(^8S_{7/2}$-$^{10}P_{7/2})$-atomic transition in neutral americium for the spontaneously fissioning isomer ^{240}Am^m with a half-life of 1 ms. The isomeric nuclei ^{240}Am^m were obtained by bombarding a uranium target by doubly charged lithium ions ^{7}Li^{+2} having an energy of 49 MeV:

$$^{238}\mathrm{U} + {}^{7}\mathrm{Li} \rightarrow {}^{240}\mathrm{Am}^{m} + 5n. \qquad (7.5.13)$$

The optical transition was excited with the help of a special laser-pumping technique which was applied to the beam particles. The experiment was made in the beam traverse geometry (at right angles) for the ^{240}Am^m nuclei by using a circularly polarized laser beam whose frequency could be varied. At the resonance frequency corresponding to the transition energy, a dynamic nuclear orientation must take place, leading to an anisotropic emission of the spontaneous fission fragments of ^{240}Am^m (see Sec. 7.5.1).

In this experiment, the number of coincidences from spontaneous fission fragments were registered for varying laser frequencies. The smallest number of fission fragments was registered at resonance

[14] C.E. Bemis *et al.*, *Phys. Rev. Lett.*, 43, 25, 1854 (1979).

frequency. The transition wavelength was found to be 6407±0.2 Å, which is 2.6±0.2 Å longer than the corresponding wavelength for the ground state of the $^{240}Am^{95}$ atom. This difference $\Delta\lambda$ in wavelength was used to compute the difference in the mean square radii of the isomer and ground states of the ^{240}Am nucleus:

$$\delta\langle r^2\rangle = \langle r^2\rangle_i - \langle r^2\rangle_{gr} = 5.1 \pm 0.2\ \text{fm}^2. \qquad (7.5.14)$$

Such a large value of $\delta\langle r^2\rangle$ indicates a strong increase in nuclear deformation upon a transition from the ground state to the state of spontaneously fissioning isomer. The value of $\delta\langle r^2\rangle$ obtained above leads to the following value of the intrinsic quadrupole electric moment of the isomer:

$$Q_0 = 32.7 \pm 2.0\ e\cdot\text{b}. \qquad (7.5.15)$$

This value corresponds to the ratio 2 : 1 of the axes of a prolate ellipsoid and is in good agreement with the values expected for fissioning isomers in the vicinity of $A = 240$.

In a review article on the properties of strongly deformed nuclei[15], Metag has mentioned that such a correspondence has already been observed for five different nuclides with Q_0 between 30 and 35 $e\cdot$b in the isomeric state and 10 $e\cdot$b in the ground state.

At present, more than 40 fission isomers are known to exist, their spontaneous fission half-lives varying between 5 ps and 14 ms. Many nuclei have two isomers, and in some cases the half-lives of these isomers differ enormously (up to a factor of 10^4 for $^{244}_{96}Cm$ isomers, for which $T^{1)}_{1/2} \leqslant 5$ ps end $T^{2)}_{1/2} > 100$ ns). The longest half-life is enjoyed by $^{242}_{95}Am$ ($T_{1/2} = 14$ ms).

7.5.7. Delayed Fission

Continuing their quest for spontaneously fissioning isomeric nuclei, Flyorov and his coworkers discovered in 1966–67 that some nuclei have a fission-fragment activity with periods as long as several minutes. This could be interpreted in two ways. The effect could be explained as a spontaneous fission from the isomeric state of nuclei formed directly in the reaction under investigation, or as a delayed fission of the daughter nucleus formed as a result of e-capture. The first explanation was found to be improbable, since the isomeric nuclei have a much shorter half-life $T_{1/2}$ of spontaneous fission in the region under investigation. The second explanation involves the assumption that new nuclei (A, Z), which are formed in these reactions and which have not been investigated earlier, are e-active and form daughter nuclei $(A, Z-1)$ in the excited state after capturing an electron. These nuclei subsequently undergo fission.

[15] V. Metag, *Comments Nuc. Part. Phys.*, 10, 2, 79 (1981).

In principle, delayed fission can be observed not only after e-capture, but also after $\beta^{\mp}$-decay. Figure 268 is a schematic of the possible versions of delayed fission. Here, the energy of the nucleus is plotted as a function of its deformation in a two-humped barrier model. The parent nucleus (A, Z) here is β-radioactive, and arrows with indices $\beta^{\mp}$ indicate $\beta^{\mp}$-transitions to the excited states of the daughter nucleus $(A, Z\pm1)$. The excitation energy of this state is W_i, the arrows with index γ show the possible gamma transitions, while different versions of delayed fission are shown by the index f.

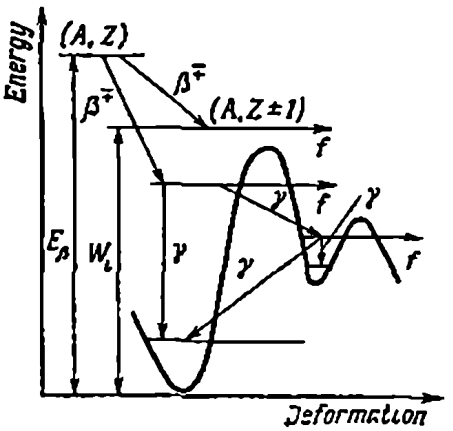

Fig. 268

The following three conditions must be satisfied for the delayed fission registration:

1. The probability of occupation of levels of the fissionable (daughter) nucleus at excitation energies comparable with the fission barrier height must be quite high.

2. The probability of competing de-excitation processes for the daughter nucleus (gamma decay or emission of delayed nucleons) must be lower than the fission probability (or of the same order in the worst case).

3. The probabilities of other channels of disintegration of the parent nucleus (alpha decay, spontaneous fission) must be low in comparison with the beta decay probability.

The first exploratory experiments were made by using the multiply charged ion cyclotron U-300, in which ^{233}U and later ^{230}Th were irradiated by ^{10}B and ^{11}B ions. Irradiation was carried out on the inner cyclotron beam, and the energy of boron ions was between 50 and 90 MeV. As a result of irradiation of ^{233}U by boron ions with energy $T_{ion} > 75$ MeV, fission fragments with half-life $T_{1/2} = 2.6$ min were registered. Solid-state track detectors, which are insensitive to α-particles, were used for registering fission fragments. Reactions were identified from the form of the excitation function corresponding to the emission of an α-particle and several neutrons in the final state:

$$\left.\begin{array}{l} {}^{233}_{92}\mathrm{U}\,({}^{11}_{5}\mathrm{B},\ \alpha xn)\,{}_{95}\mathrm{Am}, \\ {}^{233}_{92}\mathrm{U}\,({}^{10}_{5}\mathrm{B},\ \alpha yn)\,{}_{95}\mathrm{Am}, \end{array}\right\} \qquad (7.5.16)$$

i.e. to the formation of the americium nuclei $_{95}$Am.

Irradiation of a $^{230}_{90}$Th target by boron ions with energy 50-90 MeV also led to the formation of fission fragments with $T_{1/2} = 2.6$ min. The excitation function was of vaporization type, which means that the reactions must lead to the formation of americium. The

number of evaporating neutrons could be determined, and hence the resulting isotope could be identified, by comparing the theoretical and experimental positions of the maxima of excitation functions:

$$\left.\begin{array}{l} {}^{230}_{90}\mathrm{Th}\,({}^{11}_{5}\mathrm{B},\ 7n)\,{}^{234}_{95}\mathrm{Am}, \\ {}^{232}_{90}\mathrm{Th}\,({}^{11}_{5}\mathrm{B},\ 6n)\,{}^{237}_{95}\mathrm{Am}. \end{array}\right\} \qquad (7.5.17)$$

According to the hypothesis put forth earlier, this neutron-deficient isotope is transformed as a result of e-capture into the nucleus ${}^{234}_{94}\mathrm{Pu}$ in an excited state, which subsequently undergoes fission. This hypothesis is based on the calculation of relative probabilities of alpha decay and e-capture for the nucleus ${}^{234}_{95}\mathrm{Am}$, which gives $\lambda_e \gg \lambda_\alpha$. Since fission takes place after e-capture, i.e. is delayed by its half-life, it was termed delayed fission.

Similarly, irradiation of ${}^{232}_{90}\mathrm{Th}$ by ${}^{11}_{5}\mathrm{B}$ ions with energy $T_{\mathrm{ion}} > 82$ MeV led to the registration of half-life $T_{1/2} = 1.4$ min for the fission fragment. This period was associated with the reaction

$${}^{232}_{90}\mathrm{Th}\,({}^{11}_{5}\mathrm{B},\ 8n)\,{}^{235}_{95}\mathrm{Am}. \qquad (7.5.18)$$

In this case, estimates show that $\lambda_e < \lambda_\alpha$. However, the fraction of electron capture is quite significant. Hence it can be stated that ${}^{235}_{95}\mathrm{Am}$ is transformed into an excited state of ${}^{235}_{94}\mathrm{Pu}$, which subsequently undergoes fission. Similarly, the reaction

$${}^{209}_{83}\mathrm{Bi}\,({}^{22}_{10}\mathrm{Ne},\ 3n)\,{}^{228}_{93}\mathrm{Np} \qquad (7.5.19)$$

led to the formation of the isotope ${}^{228}_{93}\mathrm{Np}$, which is transformed as a result of e-capture into an excited state of ${}^{228}_{92}\mathrm{U}$, and subsequently undergoes fission. The half-life in this case was found to be $T_{1/2} = 1$ min.

Subsequent investigations of delayed fission in neutron-deficient nuclei were directed at the analysis of reactions involving the interaction of ${}^{14}_{7}\mathrm{N}$ ions with ${}^{238}_{92}\mathrm{U}$ und ${}^{232}_{90}\mathrm{Th}$ and leading to the formation of isotopes of einsteinium and berkelium. The mass numbers of these isotopes were determined from the position of the maximum of the excitation function on the ion energy scale:

$$\left.\begin{array}{l} {}^{238}_{92}\mathrm{U}\,({}^{14}_{7}\mathrm{N},\ 6n)\,{}^{246}_{99}\mathrm{Es}, \\ {}^{232}_{90}\mathrm{Th}\,({}^{14}_{7}\mathrm{N},\ 6n)\,{}^{240}_{97}\mathrm{Bk}. \end{array}\right\} \qquad (7.5.20)$$

The half-life $T_{1/2}$ for the fission fragment ${}^{246}_{99}\mathrm{Es}$ (${}^{246}_{98}\mathrm{Cf}$) was found to be 8 ± 2 min, while the corresponding value for the isotope ${}^{240}_{97}\mathrm{Bk}$ (${}^{240}_{96}\mathrm{Cm}$) was 5 ± 2 min. These values are close to the values of $T^{(e)}_{1/2}$ for the e-capture of these nuclei: $T^{(e)}_{1/2}$ (${}^{246}_{99}\mathrm{Es}$) = 7.7 min (obtained experimentally) and $T^{(e)}_{1/2}$ (${}^{240}_{97}\mathrm{Bk}$) = 4.0 min (obtained theoretically)[16]. Other neutron-deficient nuclei were also investigated later.

[16] Direct experiments on the measurements of coincidences between beta decay processes (or the registration of X-rays after e-capture) and fission have not been carried out so far on account of the extremely small magnitude of the effect.

Besides neutron-deficient nuclei, certain neutron-rich nuclei ($^{238}_{91}$Pa, $^{236}_{91}$Pa, $^{234}_{91}$Pa) were also found to exhibit delayed fission.

Investigation of delayed fission provides the values of the barrier parameters for fission of nuclei that are remote from the beta stability track[17].

7.5.8. Refined Data on Value of ν

We have described in Secs. 7.4.1 and 7.5.6 the first experiments on the determination of the number of secondary neutrons emitted during induced and spontaneous fission. These experiments, which were conducted in 1940-41, gave only an approximate value of ν; it was found that $\nu = 2.2 \pm 0.3$ in both these cases.

More accurate methods of determining ν are based on a direct count of the number of secondary neutrons emitted in a single act of fission followed by an averaging of the obtained values over a large number of fission processes.

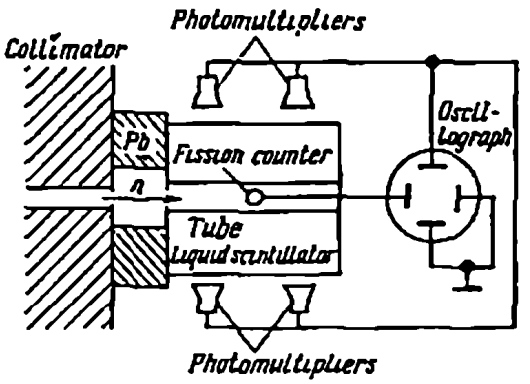

Fig. 269

Figure 269 shows one of the instruments used for this purpose. The instrument consists of a tank with a liquid scintillator into which neutrons are introduced through a tube. A fission counter with a foil of the fissile material is placed at the centre of the tube.

Neutrons are introduced into the tube through a collimator prepared from paraffin containing boric acid as an impurity. The tank is shielded from gamma radiation by placing a lead plate between the source and the tank. (The neutron source and the collimator are omitted when the instrument is used for studying spontaneous fission.)

The instrument operates in the following manner. The pulse appearing in the counter at the instant of fission starts a triggered sweep

[17] For a detailed account of delayed fission, see V.I. Kuznetsov, *Fiz. Elem. Chast. Atom. Yadra*, 12, 6, 1285 (1981).

of duration 30 μs in the oscillograph. Neutrons formed as a result of fission enter the scintillator and create recoil protons in their first collisions. Together with the instantaneous γ-quanta, these protons cause a fast scintillation pulse *1* to appear (Fig. 270*a*), which is registered by the photomultipliers and falls on the oscillograph screen.

After tens of collisions, the fission neutrons are slowed down to thermal energy and are captured by cadmium which has been dissolved as a salt in the liquid scintillator. The neutron capture involves

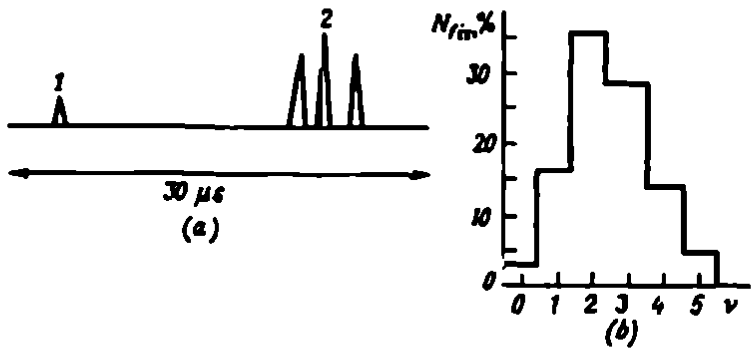

Fig. 270

a (n, γ)-reaction accompanied by the emission of γ-quanta which also create pulses *2* in the scintillator. These pulses are displaced with respect to the first pulse along the horizontal sweep of the oscillograph by the duration for which the neutrons are slowed down. The number of pulses is equal to the number of fission neutrons emitted in the process.

As a result of measurements, curves are obtained showing the distribution of the number of fission acts over the number of emitted fission neutrons (Fig. 270*b*). This can be used to obtain the average value of ν.

Table 28 shows the values of ν obtained in this experiment as well as in other similar experiments.

It can be seen from the table that the value of ν increases with Z and A of the fissile nucleus. For uranium, $\nu = 2.4$. Taking into account formula (7.5.8), we obtain the average energy carried away by secondary neutrons:

$$\nu\bar{T}_n = 2.4 \times 2 \simeq 5 \text{ MeV}. \qquad (7.5.21)$$

A comparison of the values of ν for induced fission of ^{239}Pu, ^{241}Pu, ^{242}Cm with the corresponding values of spontaneous fission of ^{240}Pu, ^{242}Pu, ^{244}Cm (the same nucleus undergoes fission in both cases) shows that ν increases with the excitation energy of the nucleus.

Table 28

Fission by thermal neutrons		Spontaneous fission		Fission by thermal neutrons		Spontaneous fission	
Nucleus	ν	Nucleus	ν	Nucleus	ν	Nucleus	ν
^{229}Th	2.08±0.03	^{232}Th	2.13±0.14	^{241}Am	3.07±0.04	^{242}Cm	2.51
^{233}U	2.480±0.007	^{238}U	1.99±0.07	^{242}Am	3.25±0.10	^{244}Cm	2.691±0.032
^{235}U	2.407±0.007	^{240}Pu	2.150±0.015	^{243}Cm	3 430±0.047	^{252}Cf	3.756±0.010
^{239}Pu	2.874±0.009	^{242}Pu	2.141±0.011	^{249}Cf	4.56±0.21	^{254}Fm	3.98±0.14
^{241}Pu	2.874±0.015						

Table 29 contains the values of $\Delta\nu$ for these nuclei, as well as the neutron binding energy ε_n and the value of $\Delta\nu/\varepsilon_n$.

Table 29

Nuclei	$\Delta\nu$	ε_n, MeV	$\Delta\nu/\varepsilon_n$, MeV^{-1}
^{239}Pu-^{240}Pu	0.724	6.83	0.106
^{241}Pu-^{242}Pu	0.733	6.54	0.112
^{243}Cm-^{244}Cm	0.739	6.97	0.106

It can be seen from the table that at low nuclear excitations (spontaneous and thermal fission), an increase in ν by unity requires an increase in the nuclear excitation energy by $\Delta E \simeq 9$ MeV. Similar results were obtained for large excitation energies. A comparison of the values of ν for the fission of ^{235}U and ^{239}Pu by thermal and fast (14 MeV) neutrons gave $(\Delta\nu/\Delta E)_{235} = 0.128$ MeV^{-1} and $(\Delta\nu/\Delta E)_{239} = 0.12$ MeV^{-1}. It can be inferred from these results that the value of $(\Delta\nu/\Delta E)$ varies insignificantly with the excitation energy and is roughly the same for different nuclei:

$$\overline{\Delta\nu/\Delta E} \simeq 0.11\text{-}0.13\ \text{MeV}^{-1}. \qquad (7.5.22)$$

This corresponds to an increase in the value of ν *by* $\Delta\nu = 1$ *upon* an increase in the excitation energy of the nucleus by $\Delta E = 8$-9 MeV.

Since $\varepsilon_n = 6$-7 MeV *and* $\bar{T}_n = 2$ MeV, *we get*

$$\Delta E = \varepsilon_n + T_n. \qquad (7.5.23)$$

In other words, practically the entire excitation energy of the nucleus is transformed into the excitation energy of the fragments and is then realized as the energy of secondary neutrons.

7.5.9. Dependence of ν on the Mass and the Kinetic Energy of the Fission Fragment

If the fission counter in the set-up shown in Fig. 269 is replaced by a double ionization fission chamber displaced towards one side, the instrument will register only fission neutrons emitted by fragments

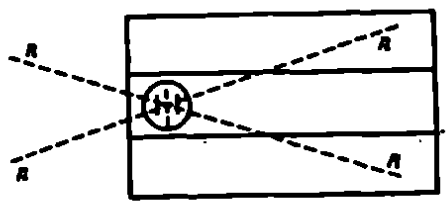

Fig. 271

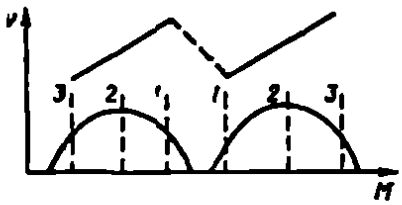

Fig. 272

moving to the right (Fig. 271). As before, the triggered sweep system described above can be used to associate the registered neutrons with a particular act of fission. In this case, however, the double ionization fission chamber can also give the mass of the fragment emitting the registered neutrons. As a result, we can obtain the dependence of ν on

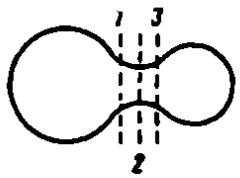

Fig. 273

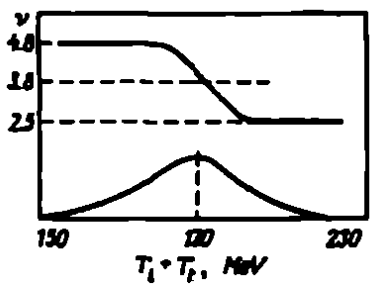

Fig. 274

the mass of the fission fragment. The experiment showed that the neutrons are mainly emitted by the heaviest fragments, i.e. by the heaviest among heavy fragments and the heaviest among light fragments (Fig. 272). A graphic interpretation of this result is given in Fig. 273 which shows three possible methods of division of a deformed nucleus. In the first case, the nucleus disintegrates into the lightest among heavy fragments and a nearly unexcited (close to spherical) fragment which should emit few neutrons according to Sec. 7.5.8. This is accompanied by the formation of the heaviest among light fragments in a highly excited state, which must emit a large number of neutrons. In the second case corresponding to the most probable fission scheme, both fragments are excited to nearly

the same extent and emit nearly equal numbers of neutrons. In the third case, the lightest among light fragments is in a weakly excited state and emits a small number of neutrons, while the heaviest among heavy fragments is in a highly excited state and must emit a large number of neutrons.

The distribution of ν as a function of the kinetic energy of the fission fragments is also in accord with this scheme. By way of an example, Fig. 274 shows the distribution of $\nu(T_l + T_h)$ for the spontaneous fission of ^{252}Cf. It can be seen that the higher (lower) kinetic energy of the fission fragments corresponds to the smaller (larger) value of ν. Qualitatively, this can be explained by the fact that the total fission energy is realized partly as the kinetic energy of the fragments and partly as their excitation energy. The higher the kinetic energy, the lower the excitation energy and hence the smaller the value of ν, and vice versa.

7.5.10. Parity Violation in Fission. Asymmetry of Fission Fragment Escape

The discovery of the violation of spatial parity in strong and electromagnetic interactions (see Secs. 3.2.6 and 3.4.5) brings to mind the possibility of new manifestations of this phenomenon. In particular, an interesting object for investigation is the fission of polarized heavy nuclei. If parity is violated in this case, an asymmetry must be observed in the escaping light (heavy) fission fragments.

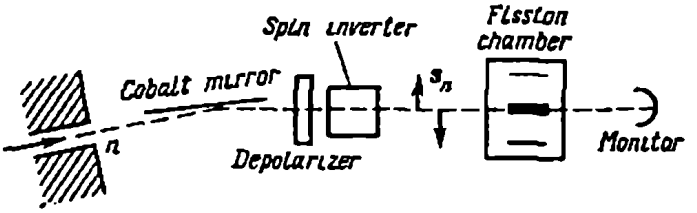

Fig. 275

The asymmetry of escaping fragments was first observed in 1978 by G.V. Danilyan and coworkers in Moscow. The experimental set-up used is shown in Fig. 275. The cobalt mirror placed in the path of a thermal neutron beam ensures an 84%-polarization of neutrons. After passing through a depolarizer, the neutrons enter a unit in which their spin s_n is inverted. The fission chamber is equipped with a discriminator for isolating light fragments from heavy ones. Finally, the neutron beams is made to enter a neutron beam monitor.

The fission chamber consists of an aluminium substrate coated on both sides with a thin layer (100 $\mu g/cm^2$) of uranium oxide or plutonium oxide. The fission fragments were registered by silicon surface-

Table 30

Fissile nucleus	^{236}U	^{234}U	^{240}Pu
$a_{fis} \times 10^4$	1.37±0.35	2.8±0.3	−4.8±0.8

barrier detectors for two orientations of the neutron spin (along the direction of motion of the fragment and against it). Each detector could alternately register light or heavy fragments. The spin reorientation and the polarity reversal of the detectors were carried out in accordance with the law of chance. Measurements were made for the depolarized beam in the blank experiment.

Table 30 lists the values of asymmetry coefficients which were obtained as a result of measurements: $a_{fis} = (\dot{N}_l - \downarrow N_l)/(\uparrow N_l + \downarrow N_l)$. The plus (minus) sign corresponds to an excess (deficiency) of light fragments in the direction of neutron spin. It is worth noting that for all the investigated nuclei, the magnitude of the effect is of the same order (about 10^{-4}).

The fission asymmetry can be detected in yet another way. It was shown in Sec. 7.5.2 that light fragments emit more neutrons than heavy fragments. Hence the neutron emission must be asymmetric in the case of an asymmetry in the escape of light fragments. Naturally, this effect is of a secondary nature and must be weaker. However, we can choose a thick target of the fissile material for these investigations, thus ensuring a much larger number of fission acts for the same flux of incident neutrons.

The experiment was carried out by V.A. Andreev and coworkers who used the same three fissile isotopes ^{236}U, ^{234}U and ^{240}Pu. The

Table 31

Fissile nucleus	^{236}U	^{234}U	^{240}Pu
$a_n \times 10^4$	0.7±0.4	4±0.6	−6.7±0.7

fission neutrons were detected by scintillators placed in such a way that they could register fission neutrons escaping in the direction of the spin and against it. Table 31 shows the values of the asymmetry coefficients obtained in this experiment for the fission neutrons with respect to the direction of the spin of polarized neutrons respon-

sible for fission. Recalculation of the results for a_{fis} leads to a value close to that obtained in the direct experiment described above.

The effect was subsequently confirmed in other experiments as well, and its existence can be treated as irrefutably proved .[18] However, it continues to baffle physicists even today, since its existence seems to be less natural than its absence. Indeed, unlike the processes of alpha decay and gamma radiation involving parity violation, fission process is characterized by an enormous number of final states (10^7-10^{10}). This is due to a diversity of masses, kinetic energies, spins, etc. of the fission fragments. It would appear that any asymmetry should be averaged out and completely vanish for such a large number of final states. However, the observed effect (about 10^{-4}) indicates that either such an averaging out does not occur, or the effect of parity violation during fission is so large that it remains significant even after averaging (for 10^8 final states, the attenuation factor associated with averaging is equal to $(10^8)^{-1/2} = 10^{-4}$).

At present, there is still no comprehensive theoretical interpretation of the asymmetry of escaping fission fragments. The existing theoretical models are based on the concept of a two-humped fission barrier. According to this concept, a nucleus in the region of the second potential energy minimum finds it more favourable from the energy point of view to be in a strongly deformed asymmetric (pear-shaped) state. Since the entire excitation energy is spent on deforming the nucleus upon passing through the saddle point[19], this deformation must be "optimal", i.o. unique. In any case, if there are several close collective levels, there will only be a small number of such highly deformed states characterizing the "cold" pear-shaped stage of the fissile nucleus. Thus, in spite of the large number of channels in the initial (hot compound nucleus) and final (multitude of fragments and their properties) stages, fission takes place through a small number of channels determined by the cold intermediate stage.

On the whole, the mechanism of parity violation during fission can be interpreted as follows.[20] On account of weak interaction, mixed states with opposite parities are formed at the compound-nucleus stage. Moreover, the high level density may cause a significant dynamic amplification. On account of a small uncertainty in the excitation energy of the nucleus ($\Delta E = \Gamma \simeq kT$), this P-odd mixing is "memorized for life" by the nucleus ($\Delta t > \hbar/\Gamma = \tau$), i.e. right up to the cold stage. At the final stage of fission, the P-odd effect is manifested as asymmetry of escaping light (heavy) fragments relative to the direction of spin of the neutron captured by the nucleus.

---

[18] For details see G.V. Danilyan, *Uspekhi Fiz. Nauk*, 131, 3, 329 (1980).

[19] We are considering the case of fission of a nucleus by thermal neutrons when the excitation energy is practically equal to the height of the fission barrier

[20] See O.P. Sushkov and V.V. Flambaum, *Uspekhi Fiz. Nauk*, 136, 1, 3 (1982)

It should be noted that unlike the gamma transitions involving parity violation and considered earlier, asymmetry in the present case is observed in the direction of motion of the material flux consisting of tens of nucleons.

7.5.11. Distribution of Fission Energy

Finally, the fission energy is distributed among various modes of its release upon fission of ^{235}U by thermal neutrons as follows:

Kinetic energy of fragments	166.2±1.3 MeV
Energy of fission neutrons	4.8±0.1 MeV
Energy of instantaneous γ-quanta	8.0±0.8 MeV
Energy of β-particles from the fission products	7.0±0.3 MeV
Energy of gamma radiation from the fission products	7.2±1.1 MeV
Energy of antineutrinos from the fission products	9.6±0.5 MeV
Total energy	202.8±0.4 MeV

7.6. Basic Trends in Modern Atomic Power Engineering

The first fission chain reaction was obtained in the USA about forty five years ago (1942), and the first industrial nuclear power station with a power of 5000 kW was built in the USSR a little more than thirty years ago (1954). At present, atomic energy is being used in practically all spheres of science and engineering, and is making a significant contribution to the power resources of many countries in the world. In the long run, atomic energy will replace organic fuels in almost every conceivable sphere of life.

For the time being, nuclear power plants are more expensive than the conventional ones, but the cost of electric power obtained from these plants is already lower than that obtained from thermal power plants. The nuclear power plants must have a high power output in order to be economically viable. Hence the construction of very powerful plants is the prime concern of present-day atomic power engineers. For example, the Leningrad nuclear power station, which is one of the most powerful nuclear plants in the world, produces 4 million kW (about 800 times more than the power of the first nuclear power plant).

While comparing the economic indices of different types of power plants, we must take into account a large number of factors including the geography of the region (the existence of fuel deposits and

the fuel reserves in these deposits, powerful water resources, special working conditions in some, for example uninhabited, regions, etc.).

Simple calculations have shown that the fuel consumption in a reactor capable of producing 1 million kW electric power is about 1 kg of ^{235}U per day[21], while an equivalent thermal power plant would require about 10000 tons of coal per day. The following conclusions can be easily drawn from this comparison. If a power plant is built in the immediate neighbourhood of the main consumers of electricity, it would involve enormous expenditure on transportation of coal over large distances. If, on the other hand, the power plant is built near the fuel deposits, serious problems arise on transmission of electric power over large distances. Moreover, the situation will be further aggravated overy year since the problems will become more serious as the capacity of the power plants increases.

Besides, it must not be forgotten that we are living under conditions of an imminent power crisis, since the reserves of organic fuel on the Earth are rapidly dwindling. Estimates show that in view of the rising fuel consumption, coal reserves may last for some 200-500 years, while oil and natural gas may run out in just 20-50 years. Hence a replacement of thermal power plants by nuclear ones will help to preserve organic fuels for chemical purposes. Finally, another important circumstance is that there are practically no limitations on the construction of nuclear power plants of any capacity, and the size of nuclear plants is much smaller than that of other types of power plants of equivalent power output.

Most of the nuclear power plants, which are either in operation or in the design stage, employ thermal neutrons. This trend in the construction of nuclear power plants is likely to continue for another decade or so. However, naturally occurring uranium contains just 0.7% of the isotope ^{235}U, whose separation (or enrichment of natural uranium in ^{235}U) is a very complicated and laborous process. Besides, the energy reserves in terms of easily extractable ^{235}U isotope in the Earth crust are roughly equal to the reserves of organic fuel, i.e. are rather limited. Hence it is expedient to create new powerful reactors (capable of generating about one million kilowatt of electric power) based on fast neutrons. These reactors can employ the more abundant nuclear fuels, viz. ^{238}U and thorium. In this case, each kilogram of naturally occurring uranium is capable of giving 20-30 times higher power than in the case when thermal neutron reactors are employed. Thus, uranium sort of becomes cheaper, and hence its extraction from poor ores becomes economically viable. The same criterion will hold in future for extraction of uranium from sea water and granite (which contain inexhaustible supplies of uranium).

[21] In actual practice, the fuel used in nuclear power plants is enriched uranium containing about 3% ^{235}U.

The operation of fast neutron reactors can be explained as follows. Nuclear energy is released as a result of fission of the isotope ^{239}Pu (a small amount of this isotope is placed in the reactor together with uranium). The process is accompanied by the generation of fission neutrons, a part of which is captured by ^{238}U nuclei. The following reaction takes place:

$$^{238}U(n, \gamma) \rightarrow {}^{239}U \xrightarrow{\beta^-} {}^{239}Np \xrightarrow{\beta^-} {}^{239}Pu. \qquad (7.6.1)$$

As a result, ^{238}U nuclei are transformed into ^{239}Pu nuclei. Thus, the expensive ^{239}Pu consumed in a fast neutron reactor is reproduced from the cheap ^{238}U during the operation of the reactor. It was shown by calculations and numerous experiments that extensive reproduction of ^{239}Pu is possible under certain conditions, when the reactor produces more ^{239}Pu than the amount consumed by it during fission. The excess ^{239}Pu thus formed can be used for commissioning new reactors based on fast as well as thermal neutrons, and so on. Reactors of this type are called breeders. At present, fast neutron reactors have already been designed and commissioned.

For a quick and successful solution of the problem of using nuclear reactors for generating an overwhelming fraction of electric power, it is essential to design fast neutron reactors in such a way that the amount of fuel generated in the reactor is doubled in a very short time. The electric energy consumption in the world is doubled every 10 years. Hence the advanced development of atomic power engineering is possible only by doubling the amount of reactor fuel in a much shorter period (preferably not more than 6-7 years). There are reasons to believe that this problem will be solved in the near future.

Thus, it should be possible to produce all the electric energy required with the help of fission reactions. In view of what has been stated above, the nuclear fuel on the Earth should suffice for several thousand years. However, even a changeover to 100% atomic power generation does not rid mankind of the risk of a power crisis because only 20% of natural resources (petroleum, natural gas, coal) are used for production of electric power. Hence such a changeover will result in saving only these 20% resources (while the economy of the especially precious fuel, viz. petroleum, will be just about 10%). About 80% of the organic fuel is spent on industrial (30%) and domestic (30%) heating, and on transport needs (20%). Hence the main problem is to replace the energy obtained from organic fuel by atomic energy in these fields. It remains for us to find the ways of solving this problem.

In many advanced countries, including the USSR, reactors are being designed at present, in which the temperature of the waste

gases reaches 1000 °C. These gases can be used as the source of heat in metallurgy and chemical industry. By way of an example, we would like to mention the nuclear-metallurgic complex designed in Japan for direct reduction of the iron ore. The nuclear reactor is cooled by helium which is heated to a temperature of 1000 °C at the outlet. The feasibility of such a project is confirmed by the fact that a similar (but smaller) unit is already in operation for several years in the FRG.

Projects are being developed all over the world to utilize the heat released by high-temperature reactors for the production of zinc and aluminium, in powder metallurgy, in chemical industry (especially for manufacturing fertilizers), etc. Another important application of heat from high-temperature reactors involves the production of hydrogen by cracking methane or decomposing water. Mass production of such "nuclear" hydrogen is necessary not only in metallurgy (for reduction and energy transport) and chemical industry (for production of ammonium fertilizers), but also for solving the vital problem of replacing petroleum products in transport. Apparently, the simplest albeit indirect method of using atomic energy for transport is to create hydrogen engines. In principle, hydrogen engines should be more effective than petrol engines, since hydrogen has a higher calorific value, its combustion product is water and not harmful exhaust gases, and it does not upset the oxygen balance in the atmosphere.[22]

The problem of replacing the energy of organic fuel by atomic energy for the purpose of domestic (and small-scale industrial) heating can be solved by creating nuclear heating plants (NHP) and nuclear power-and-heating plants (NPHP). Every NHP consists of two reactors of 500-MW power each. In order to preclude the possibility of activation of water supply to the consumers, a three-loop heat-removal system is employed in NHP and NPHP. The total safety of NHP's makes it possible to station them in close proximity of the consumers (about 1.5-2 km from residential areas). A wide application of NHP's should lead to a considerable saving of petroleum and to a decrease in the cost of thermal energy (by a factor of two).

Besides the solution of global problems with the help of large-scale reactors, the construction and design of small nuclear power plants and NPHP's are also given serious consideration. Units of this kind are convenient and useful for operation under certain conditions (for example, in remote areas), desalination of water, creation of atomic transport facilities, and for special scientific projects. Stationary and mobile nuclear power plants of moderate power have been constructed and are in operation. The latter type of sys-

[22] The amount of oxygen consumed in the combustion of hydrogen is the same as that realeased during the decomposition of water.

tems are self-propelled and can be driven to regions that are not easily accessible.

The conversion of nuclear energy into electrical energy in nuclear power plants is achieved through the intermediate stage of high-temperature steam generation. This steam is used for setting into motion steam turbines and electric generators. In this respect, a nuclear power plant differs from a thermal power station only in the type of block in which the thermal energy is obtained. However, the specific nature of nuclear heat sources permits the construction of convenient electric power sources in which thermal energy is converted directly into electric energy (without boilers, turbines and generators). The operation of such installations involves the production of thermoelectricity from heat released during radioactive decay or in a fission chain reaction. The first type of units are called isotopic power sources, while units of the second type are called thermal converter reactors.

In an isotopic power source, artificially prepared α- and β-active preparations are used as heat sources for thermoelements. The duration of operation and the power of source depend on the half-life and the quantity of the radioactive isotope used. For example, American meteorological satellites employ an isotopic source based on the α-active isotope ^{238}Pu ($T_{1/2} = 86.4$ years). It has a power of 25 W and can work uninterrupted for 5-10 years. Short-lived isotopes (for example, ^{242}Cm with $T_{1/2} = 162.7$ days) are used for constructing isotopic power sources having a relatively short operating life, but a large power (up to 100 W).

For many years, the isotopic power supply "Beta", based on the β-active isotope ^{144}Ce ($T_{1/2} = 290$ days), is being used in the Soviet Union for supplying power to automatic meteorological stations. This unit is equipped with a special accumulator which can produce power up to 200 W for a long-range radio transmitter (with a range of 600 km). Other isotopic power supplies have been constructed on the basis of ^{90}Sr ($T_{1/2} = 28$ years). They have a long service life (up to 10 years), and this makes them exceptionally suitable for use in remote and not-easily-accessible areas (mountainous regions, Siberian forests, deserts, etc.). Another type of isotopic power supply, based on ^{210}Po, was used in Soviet moon rovers.

Thermal converters employ high-temperature reactors ($t_{max} = 1800$ °C) whose core consists of refractory materials, uranium dicarbide enriched in ^{235}U isotope up to 90%, and graphite. The reactor core (of cylindrical form) is surrounded from all sides by a beryllium reflector. The outer surface of the reflector carries a thermoelectric converter consisting of a large number of germanium-silicon plates. The inner side of these plates is heated by the reactor, while the outer side is cooled. Another method of transforming thermal energy into electrical energy is based on the use of thermionic transducer

reactors. The operation of such a transducer involves the excitation of electron emission from a cathode which is strongly heated by the heat supplied by a reactor.

One of the most promising fields of application of atomic energy is the desalination of sea and ground waters. The consumption of fresh water is ever increasing for industry and for irrigation as more areas are brought under cultivation. Hence the problem of fresh water is at present as serious as that of organic fuels. Although water resources on our planet are inexhaustible, only 3% of all the water is fresh, and even this small fraction is distributed highly nonuniformly: about 60% of the Earth surface suffers from a deficiency of water. However, these regions often have a lot of sea and mine water which can be desalinated.

Desalination is a very expensive process. For example, 80 kg of coal is required to distil 1 m^3 of water. A medium-sized industrial town with a population of a few tens of thousands, requires about 200000 m^3 of water per day. To provide the town with fresh water, some 15000 tons of coal have to be burnt everyday. Obviously, this is not expedient from economical point of view, especially under the present conditions of rapidly dwindling resources of organic fuel. However, the problem of desalination of sea or ground water can be tackled successfully with the help of atomic energy.

Preliminary estimates made by specialists show that the problem of supplying fresh water to a medium-sized industrial town can be solved by using a fast neutron reactor with a thermal power of 2-2.5 million kW, which will simultaneously generate about 500 megawatts of electric power and transform ^{238}U into ^{239}Pu. Estimates show that by using a reactor of this type, we can reduce the cost of desalinated water to a value below that of the water brought by a canal from a distant place. If a reactor having 5-10 times higher output is used, the cost of desalinated water will become so low that it can be used for irrigating fertile land in arid areas. The nuclear desalination plant of this type, based on a fast neutron reactor and commissioned in Shevchenko (USSR) in 1974, is a good illustration of the correctness of these estimates. This plant produces 80000 m^3 fresh water per day and supplies electricity to the town.

The achievements of the Soviet Union in construction of ice-breaker ships are known all over the world. The first nuclear-powered ice-breaker "Lenin" with unprecedented parameters was commissioned in 1959. Its engine has a power of 44000 hp. In principle, this ice-breaker can cover a distance of 300000-400000 km without refuelling and practically without a change in the displacement. It can stand up to two-metre thick ice.

Two nuclear-powered ice-breakers of higher power (75000 hp), called "Arktika"[23] and "Sibir", were commissioned in 1975-77.

[23] This ice-breaker is now called "Leonid Brezhnev".

They are operating successfully in the Northeast passage to prolong the navigation period. For the first time in the history of navigation, "Arktika" reached the North Pole in 1977 by sea. Another powerful atomic ice-breaker "Rossia" was commissioned in 1985.

Nuclear energy was found to be very convenient for constructing nuclear-powered submarines, which have several advantages over the conventional submarines. The specific properties of nuclear fuel (a high power intonsity in a small volume and "combustion" without oxygen) permit the construction of high-speed submarines which can remain under water for long periods. The exceptionally high quality of Soviet nuclear submarines was demonstrated in their voyages to the North Pole and around the Earth.

Finally, let us briefly mention some other fields in which nuclear energy is utilized. Special nuclear reactors with very high densities of neutron fluxes have been designed and commissioned for fundamental investigations and for obtaining transuranic elements. The pulse reactor ИБР-2 for large-flight-path neutron spectroscopy has already been put into operation. Large materials-science laboratories have been constructed for studying the behaviour of fissile and construction materials at high temperatures, under conditions of radiation and in corrosive media. Plants have been set up for the manufacture of stable isotopes. Ionizing radiation is being put to use on a large scale. Radioactive isotopes and nuclear radiation are being used in industry (flaw detection, automation, etc.), medicine (diagnostics and cure), biology (genetics), agriculture (increased crop production) and chemistry (organic synthesis).

The development of the nuclear power engineering in the USSR and the entire Soviet nuclear physics research is being led by A.P. Alexandrov.

7.7. A Brief Resumé of Chapter 7

This chapter is devoted to the fission of atomic nuclei and the application of atomic energy.

Fission is a reaction involving the splitting of a nucleus (usually a heavy one) into two parts with nearly equal masses (called fission fragments). Heavy nuclei ($Z \geqslant 90$) undergo fission as a result of a weak excitation of the atomic nucleus, say, by irradiating it with neutrons having an energy $T_n \simeq 1$ MeV or even with thermal neutrons for some nuclei (induced fission), or without any preliminary excitation (spontaneous fission).

Induced fission was discovered in 1938 by Hahn and Strassmann, while spontaneous fission was first observed by Petrzhak and Flyorov in 1940.

In 1961, Polikanov and coworkers at Flyorov's laboratory discovered spontaneous fission in isomeric state.

Nuclei with $Z < 90$ can only undergo induced fission [21], and the energy of excitation required for fission increases with decreasing fission parameter

[21] Strictly speaking they have an unobservably long half-life of spontaneous fission.

Z^2/A. Induced fission takes place almost instantaneously ($\tau < 10^{-14}$ s). The half-life for spontaneous fission varies for different nuclei over a very wide range (from 10^{21} years for ^{232}Th to a few tenths of a second for heavier transuranic elements). The half-life decreases with increasing fission parameter.

The fission of a nucleus is accompanied by the liberation of energy $Q \simeq 200$ MeV. Most of this energy (about 170 MeV) is imparted as kinetic energy to the fission fragments. The fission fragments have a large excess of neutrons and hence serve as the starting points for β-radioactive chains of fission products, and emit instantaneous neutrons (1-4 neutrons per act of fission of $^{235}_{92}U$ by thermal neutrons), delayed neutrons (about 0.6% of the number of instantaneous neutrons), as well as instantaneous γ-quanta. Fission neutrons (having an average energy of 2 MeV) carry away about 5 MeV of energy, while instantaneous γ-quanta carry some 7 MeV. Subsequent beta transformations of the fission products involve the liberation of further energy to the tune of 25 MeV. Of this, about 8 MeV is taken away by β-particles, about 7 MeV by γ-quanta, and the rest is carried away by antineutrinos.

Instantaneous neutrons are emitted by moving fission fragments, while delayed neutrons are emitted by stationary fission products after a preliminary β^--decay. The spectrum of instantaneous fission neutrons is described by the semiempirical formula

$$I(T) \simeq [\exp(-T)] \sinh \sqrt{2T}.$$

Delayed neutrons form several monoenergetic groups. These properties of neutrons are valid for induced fission as well as spontaneous fission.

The induced fission of weakly excited nuclei and spontaneous fission take place nonsymmetrically: the ratio of the masses of light and heavy fragments is approximately 2 : 3 (two-humped mass curve). As the excitation energy increases, fission gradually becomes symmetric and the curve showing the mass distribution of fission fragments becomes one-humped.

The basic properties of fission can be explained with the help of an elementary theory developed by Bohr, Wheeler and Frenkel on the basis of the liquid drop model of the nucleus. This theory can be used to compute the value of Q, and to understand the role of the fission parameter Z^2/A as well as the nature of spontaneous fission.

The quantity Q is calculated as the difference in the masses (energies) of the parent nucleus and the fragments, expressed through Weizsacker's semiempirical formula. These calculations show that fission is favourable from the energy point of view ($Q > 0$) for $Z^2/A > 17$ (i.e. for $Z > 47$), and that Q increases with Z^2/A. More detailed calculations reveal that during the deformation preceding fission, the energy of the nucleus must increase at first and only then decrease (energy barrier of fission). The height of the fission barrier decreases with increasing Z^2/A and becomes equal to zero for $Z^2/A = 45$-49, i.e. for $Z \simeq 120$. Induced fission is possible only if the nucleus is first excited by an amount of energy exceeding the height of the fission barrier. Spontaneous fission takes place as a tunnelling transition. For $Z \simeq 120$, spontaneous fission must take place instantaneously, i.e. over nuclear time. This prediction of the liquid drop model is a rough approximation, since the model does not take into account the shell effects. The liquid drop theory of fission does not explain the asymmetry in the mass distribution of fission fragments.

In 1966, Strutinsky perfected the liquid drop theory of fission by introducing the shell correction to the energy. The most distinguishing feature of the perfected theory is a two-humped fission barrier which can quite naturally explain the asymmetry of fission and the properties of spontaneously fissioning isomers (shape isomerism).

The release of a large amount of energy, emission of several neutrons and the possibility of fission at relatively low excitation energies help solve the prob-

lem of liberation of nuclear energy (also called *atomic* energy) for peaceful and military purposes through fission chain reactions.

The idea behind a fission chain reaction is to use the fission neutrons released during fission to cause the fission of new nuclei with the formation of more neutrons, and so on. If in such a successive process the creation of neutrons exceeds their loss, the number of neutrons will increase and an avalanche-like chain reaction will be observed.

The theory of fission chain reactions was formulated by Zel'dovich and Khariton in 1939. According to this theory, a fission chain reaction is possible if the neutron multiplication factor k, i.e. the ratio of the numbers of neutrons in two successive generations of a chain process, is greater than (or equal to) unity. The multiplication factor is determined by the number of neutrons emitted in a single act of fission, the cross sections of interaction of neutrons with uranium and other nuclei (construction materials, impurities in uranium, etc.), the design and dimensions of the reactor (its size must be larger than the critical value).

The first nuclear reactor was made of uranium and graphite. It was constructed by Fermi and coworkers, and commissioned in Chicago (USA) in the end of 1942. The first Soviet reactor was constructed by Kurchatov and coworkers, and commissioned in the end of 1946 in Moscow. The first source of atomic electric power was the nuclear power plant constructed in Obninsk in 1954. The first nuclear-powered ice-breaker "Lenin" was put out to sea in 1959. At present, fission energy is widely used in science, industry, agriculture, medicine, etc.

The most promising direction of application of atomic energy in the next 10-15 years is the creation of powerful nuclear power plants based on thermal neutron reactors. In the future, fast reactors will be given preference. Investigations are being carried out and some practical advances have already been made towards using atomic energy for desalinating sea water, production of high-potential industrial heating and low-potential domestic heating, as well as mass production of hydrogen to replace petroleum products in engines.

The Soviet atomic energy programme is being carried out under the overall supervision of A.P. Alexandrov.

Chapter 8

Reactions of Formation of Transuranic Elements

8.1. Neptunium, the First Transuranic Element. Methods of Its Investigation

The Periodic Table of elements occurring in nature terminates at the 92nd element, viz. uranium. This circumstance by no means indicates that *transuranic elements*, i.e. elements with $Z > 92$, cannot exist in principle, but is due to a decrease in the periods of alpha decay and spontaneous fission with increasing Z.

A systematic analysis of the properties of radioactive nuclei shows that the periods of alpha decay and spontaneous fission for elements with $Z > 92$ must be much shorter than the age of the Earth. As a result, the transuranic elements which were originally formed gradually "perished" and are thus not available in nature.[1]

Elements with $Z > 92$ can be formed artificially with the help of nuclear transformations leading to an increase in the charge of the product nucleus in comparison to the charge of the target nucleus. If the heaviest of the naturally occurring elements, viz. uranium, is taken as the target nucleus, this will result in the formation of transuranic elements.

The simplest nuclear transformation of this type is the reaction of radiative neutron capture by the $^{238}_{92}U$ nucleus followed by the beta decay of the resulting heavier isotope $^{239}_{92}U$:

$$^{238}_{92}U \rightarrow (n, \gamma)\, ^{239}_{92}U \xrightarrow[23\ \text{min}]{\beta^-} {}^{239}_{93}Np \xrightarrow[2.35\ \text{day}]{\beta^-} \qquad (8.1.1)$$

It was in this process that the first transuranic element neptunium $_{93}Np$ was discovered in 1940 by McMillan and Abelson.

McMillan's first experiment (1939) was similar to the one performed by F. Joliot-Curie to register the activity of fragments formed during fission of a uranium target. McMillan compared the properties of escaping fragments with those of the uranium target after irradiation and discovered that besides the half-lives characteristic of ^{239}U and the fission fragments (which are formed during fission but have not escaped from the target), the uranium target had

[1] Negligible traces of the 93rd and 94th elements have been discovered in uranium ores. These elements are formed as a result of the $(n, 2n)$ process as well as reaction (8.1.1) (see below), induced by spontaneous fission neutrons, or as a result of (α, n)-reactions.

another half-life $T_{1/2} = 2.35$ days that does not correspond to any of the fragments escaping from it.

It was naturally assumed that the value $T_{1/2} = 2.35$ days corresponds to $^{239}_{93}$Np. Chemical identification of this isotope of neptunium was jointly carried out by McMillan and Abelson (1940). It was shown that the activity with $T_{1/2} = 2.35$ days results from beta decay of ^{239}U with a half-life of 23 min.

Another isotope $^{238}_{93}$Np was obtained by irradiating $^{238}_{92}$U with 16-MeV deuterons:

$$^{238}_{92}\mathrm{U}\,(d,\ 2n)^{238}_{93}\mathrm{Np}\xrightarrow[2.1\ \mathrm{day}]{\beta^-}. \qquad (8.1.2)$$

In all, eleven isotopes of neptunium have been discovered so far, their mass numbers ranging from 231 to 241. The element Np is a heavy ($\rho = 19.5$ g/cm^3) metal with a silver glance which gets slowly oxidized upon exposure to air. The melting point of neptunium is 640 °C.

The investigation of transuranic elements involves three main problems, viz. the production of a particular isotope, its separation from the mixture or compounds with other elements, and the identification of its mass and atomic number.

The possibility of obtaining an isotope depends on the choice of a suitable nuclear reaction. For example, it is obvious that if reaction (8.1.1) is carried out in a nuclear reactor for a long time, it will lead to a secondary effect, viz. the adhesion of a neutron to the isotope $^{239}_{93}$Np and hence the creation of the isotope $^{240}_{93}$Np. Similarly, reactions induced by fast α-particles may involve the emission of different numbers of neutrons $(\alpha, 2n)$, $(\alpha, 3n)$, and hence the formation of different isotopes of transuranic elements. The same also applies to other nuclear reactions.

It is very difficult to separate a new element from the parent material or other substances formed together with the element in which we are interested. The difficulty lies in that we have to separate microscopic amounts of substances which are quite similar in their chemical properties (like the formation of rare-earth elements, the formation of transuranic elements involves the filling of an inner electron shell). Transuranic elements are separated by using radiochemical methods. We described in Sec. 6.3 some of these methods based on the use of carriers whose chemical properties are similar to those of the substance being investigated. A similar method is used for transuranic elements.

Transuranic elements are separated with the help of *ion-exchange chromatography*. This method is based on the property of some resins to exchange ions with the corresponding ions of a salt whose solution washes the resin. The efficiency of interaction of an ion with the resin

depends on its charge and size, and hence has different values for different ions.

If a solution containing various ions is passed through an ion-exchange column containing a resin, the most effectively interacting ions get absorbed at the very beginning, i.e. at the column inlet, while the remaining ions are distributed over the column in accordance with the efficiency of their interaction.

To extract various ions separately from the column, a solvent is passed through it, washing away the ions most loosely connected with the resin in the beginning, and the most tightly bound ions at the end. The separation effect can be enhanced by using special solvents, whose efficiency of interaction with the ions being separated varies inversely relative to the efficiency of interaction of the resin with them. This method is widely used for separating transuranic elements right up to mendelevium with $Z = 101$.

The third problem in the investigation of transuranic elements, viz. the identification of an isotope, is solved by comparing its properties with the corresponding empirical regularities of their variation with Z and A. Such properties include energy and half-life of alpha and beta decays, half-life of spontaneous fission, etc. (see Sec. 8.4). For the same purpose, we can also use the data on the accumulation of isotopes in reactions of the type (8.1.1) as a function of time, or the data on the yield of a given isotope as a function of the energy of the bombarding particles. Direct mass spectroscopic analysis can also be used.

8.2. Plutonium. Properties and Applications

The second transuranic element was discovered in 1940 by Seaborg *et al.* together with $^{239}_{93}$Np in reaction (8.1.2). Taking into account the beta decay of $^{239}_{93}$Np, we obtain from this reaction an isotope of the 94th element, viz. plutonium:

$$^{239}_{93}\mathrm{Np} \xrightarrow[2.1\ \mathrm{day}]{\beta^-} {}^{239}_{94}\mathrm{Pu}. \qquad (8.2.1)$$

Neptunium and plutonium were named after the planets Neptune and Pluto which lie behind the planet Uranus in the Solar system.

The isotope $^{239}_{94}$Pu discovered by Seaborg *et al.* is α-active and has a half-life $T_{1/2} = 86.4$ years. At present, this isotope is used for preparing isotopic current sources (see Sec. 7.6).

The next plutonium isotope $^{239}_{94}$Pu was discovered in 1941 by Seaborg *et al.* as a reaction product in the beta transformation of another isotope of neptunium:

$$^{239}_{93}\mathrm{Np} \xrightarrow[2.35\ \mathrm{day}]{\beta^-} {}^{239}_{94}\mathrm{Pu}. \qquad (8.2.2)$$

This isotope is also α-active with a half-life of 2.44×10^4 years. As a result of alpha decay, this isotope is transformed into $^{234}_{92}U$. It can be easily surmised that both these nuclei ($^{239}_{94}Pu$ and $^{235}_{92}U$) must undergo fission in identical processes. Indeed, both $^{239}_{94}Pu$ and $^{235}_{92}U$ contain an even number of protons and an odd number of neutrons and are thus strongly excited when a neutron is attached to them. Besides, the fission parameter Z^2/A for $^{239}_{94}Pu$ is even larger than for $^{235}_{92}U$. Hence it can be expected that $^{239}_{94}Pu$ also satisfies the condition for fission by thermal neutrons:

$$\varepsilon_n > W_{fis}.$$

An analysis of the properties of $^{239}_{94}Pu$ confirmed this assumption and showed that this isotope of plutonium has a very large cross section of fission by thermal neutrons (738 b), emitting on the average 3 neutrons in every act of fission. This opened the possibility of using $^{239}_{94}Pu$ as a nuclear fuel besides $^{235}_{92}U$. Thus the problem of obtaining large amounts of $^{239}_{94}Pu$ with the help of reaction (8.1.1) becomes extremely important. It was proposed to solve this problem in practice by separating plutonium from uranium extracted from a nuclear reactor after a prolonged operation.

In order to design plants for processing irradiated uranium, it was necessary to know the chemical properties of plutonium. This could be possible only by separating this element in sufficient quantities. The only method available at that time (1941-42) for obtaining plutonium was the neutron irradiation of uranium in cyclotrons. After a prolonged irradiation (over several months) of several hundred kilograms of uranium in a number of cyclotrons, about 500 μg of plutonium salts were obtained by the end of 1942. This quantity was found to be sufficient for investigating the properties of plutonium by the methods of ultramicrochemistry.

To get an idea of the scale of ultramicrochemical investigations, it should be noted that the error in the balance used is 10^{-5} g, the "test-tubes" in which the reactions take place have a diameter of 0.1-1 mm, all operations are carried out with the help of micromanipulators and observed under microscopes. By the time of commissioning of the first reactor (December 1942), the ultramicrochemical investigations provided a complete picture (to the scale $1:10^{10}$) of the industrial methods of separating plutonium from uranium irradiated in the reactors.

Plutonium has now been studied most thoroughly. Fifteen of its isotopes with mass numbers between 232 and 246 are already known. The element plutonium is a lustrous metal with a bluish tint. Its density in different modifications varies from 15.9 to 19.8 g/cm^3, and its melting point is 640 °C. Plutonium has a negative coefficient of linear expansion.

8.3. Transuranic Elements with $Z > 94$

8.3.1. Americium and Curium

The next two transuranic elements, americium (named in honour of America) and curium (named after Marie and Pierre Curie), were discovered in 1944.[2] Both these elements have a silver glance, and their densities are $\rho_{Am} = 11.7$ g/cm^3 and $\rho_{Cm} = 7$ g/cm^3.

Americium was first detected in the reaction

$$^{239}_{94}\mathrm{Pu}\,(n,\,\gamma)\,^{240}_{94}\mathrm{Pu}\,(n,\,\gamma)\,^{241}_{94}\mathrm{Pu} \xrightarrow{\beta^-} {}^{241}_{95}\mathrm{Am}, \qquad (8.3.1)$$

which occurs in a nuclear reactor. The same isotope of americium was also obtained by irradiating uranium with 40-MeV alpha particles:

$$^{238}_{92}\mathrm{U}\,(\alpha,\,n)\,^{241}_{94}\mathrm{Pu} \xrightarrow{\beta^-} {}^{241}_{95}\mathrm{Am}. \qquad (8.3.2)$$

At present, 11 isotopes of americium with mass numbers between 237 and 247 have been discovered. Notable among these is $^{242}_{95}$Am which has a very large cross section of capture by thermal neutrons (about 8000 b) and an isomeric state with a very small half-life relative to spontaneous fission:

$$T^{\mathrm{sp.\,fis.}}_{1/2}\,(^{242m}_{95}\mathrm{Am}) = 14 \times 10^{-3}\ \mathrm{s}.$$

The discovery of this isomer in Dubna in 1961 served as the starting point of the investigation of a very interesting nuclear phenomenon, viz. the shape isomerism (see Sec. 7.5.5). At present, spontaneous fission from the isomeric state has been observed in many transuranic elements, from neptunium to berkelium (as well as for uranium).

Curium, the 96th element, was first discovered in the reaction

$$^{239}_{94}\mathrm{Pu}\,(\alpha,\,n)^{242}\mathrm{Cm}. \qquad (8.3.3)$$

Later, the same isotope was obtained as the product of beta decay of americium formed in the subsequent chain of the reaction (8.3.1),

$$^{241}_{95}\mathrm{Am}\,(n,\,\gamma)\,^{242}_{95}\mathrm{Am} \xrightarrow{\beta^-} {}^{242}_{96}\mathrm{Cm}. \qquad (8.3.4)$$

Besides, $^{242}_{96}$Cm can be obtained by irradiating Pu with α-particles:

$$^{239}_{94}\mathrm{Pu}\,(\alpha,\,n)\,^{242}_{96}\mathrm{Cm}. \qquad (8.3.5)$$

The isotope $^{242}_{96}$Cm emits α-particles with half-life 162.7 days. Its alpha activity is so high (10^{13} α-particles are emitted per minute by 1 mg of this isotope) that it leads to heating, splashing, and even the decomposition of water in aqueous solutions of curium salts, as well as to their luminescence in dark. Such strong α-radioactive pre-

[2] It is interesting to note that curium was the first to be discovered. This was followed by the discovery of americium.

parations are handled in hermetically sealed chambers made of transparent plastic and equipped with built-in rubber gloves. The isotope $^{242}_{96}Cm$ is used for preparing isotopic current sources having a power up to 100 W.

Other isotopes of curium can be obtained by attaching a neutron to $^{239}_{96}Cm$ in successive (n, γ)-reactions upon a prolonged irradiation in a reactor. Since the isotopes of curium with $A > 242$ have long half-lives, a long chain of successive (n, γ)-reactions is obtained:

$$^{242}_{96}Cm\,(n,\ \gamma)\ ^{243}_{96}Cm\,(n,\ \gamma)\ ^{244}_{96}Cm\,(n,\ \gamma)\ ^{245}_{96}Cm\,(n,\ \gamma)$$
$$\rightarrow\ ^{246}_{96}Cm\,(n,\ \gamma)\ ^{247}_{96}Cm\,(n,\ \gamma)\ ^{248}_{96}Cm\,(n,\ \gamma)\ ^{249}_{96}Cm. \qquad (8.3.6)$$

In all, thirteen isotopes of curium with mass numbers between 238 and 250 are known to exist.

8.3.2. Berkelium and Californium

The first isotope of the 97th element berkelium, viz. $^{243}_{97}Bk$, named after the city Berkeley (USA), was obtained in 1949 by irradiating $^{241}_{95}Am$ with 35-MeV α-particles:

$$^{241}_{95}Am\,(\alpha,\ 2n)\ ^{243}_{97}Bk \xrightarrow[4.5\ h]{\varepsilon,\ \alpha}. \qquad (8.3.7)$$

Other isotopes of this element were obtained by irradiating americium and curium targets in a cyclotron, and by prolonged irradiation of plutonium and americium targets with neutrons in reactors.

For example, the isotope $^{249}_{97}Bk$ was obtained after a prolonged irradiation of $^{239}_{94}Pu$ in a reactor:

$$^{239}_{94}Pu\,(n,\ \gamma)\ ^{240}_{94}Pu\,(n,\ \gamma)\ \ldots\ ^{243}_{94}Pu \xrightarrow{\beta^-}\ ^{243}_{95}Am\,(n,\ \gamma)$$
$$\rightarrow\ ^{244}_{95}Am \xrightarrow{\beta^-}\ ^{244}_{96}Cm\,(n,\ \gamma)\ ^{245}_{96}Cm\,(n,\ \gamma)\ \ldots\ ^{249}_{96}Cm \xrightarrow{\beta^-}\ ^{249}_{97}Bk. \qquad (8.3.8)$$

In all, nine isotopes of berkelium with mass numbers between 243 and 251 are known to exist.

The 98th element, californium, was discovered in 1950 (two months after the discovery of berkelium) at the University of California in Berkeley. The first isotope of this element to be discovered was $^{245}_{98}Cf$, which was obtained as a result of irradiation of $^{242}_{96}Cm$ by 35-MeV α-particles:

$$^{242}_{96}Cm\,(\alpha,\ n)\ ^{245}_{98}Cf \xrightarrow[44\ min]{\varepsilon,\ \alpha}. \qquad (8.3.9)$$

Other isotopes of californium were obtained in similar reactions involving the emission of different numbers of neutrons. This element is obtained in large quantities by irradiation of $^{239}_{94}Pu$ in reac-

tors. The processes first occur in accordance with the scheme (8.3.8), after which they follow the chain

$$^{249}_{97}\mathrm{Bk}\,(n,\ \gamma)^{250}_{97}\mathrm{Bk}$$

$$\xrightarrow{\beta^-} {}^{250}_{98}\mathrm{Cf}\,(n,\ \gamma)^{251}_{98}\mathrm{Cf}\,(n,\ \gamma)\ {}^{252}_{98}\mathrm{Cf}\,(n,\ \gamma)\ {}^{253}_{98}\mathrm{Cf}\,(n,\ \gamma)^{254}_{98}\mathrm{Cf}. \qquad (8\ 3\ 10)$$

A new nuclear reaction involving the irradiation of target nuclei with accelerated carbon ions $^{12}_{6}\mathrm{C}$ was first used for obtaining certain isotopes of californium:

$$\left.\begin{aligned} {}^{238}_{92}\mathrm{U} + {}^{17}_{6}\mathrm{C} &\rightarrow {}^{244}_{98}\mathrm{Cf} + 4n, \\ {}^{238}_{92}\mathrm{U} + {}^{12}_{6}\mathrm{C} &\rightarrow {}^{244}_{98}\mathrm{Cf} + 6n \end{aligned}\right\} \qquad (8.3.11)$$

The ions are accelerated in a cyclotron. To obtain the highest possible energy [required for overcoming the high Coulomb barrier $B_C = Zz/A^{1/3}$ MeV $\simeq (92 \times 6)/6 = 92$ MeV], multiply ionized atoms (C^{6+}) are accelerated. Such ions are produced (in small quantities of the order of 0.1%) as a result of collisions of doubly ionized atoms (obtained in the source) with the residual gas in a cyclotron chamber. Calculations show that a cyclotron intended for accelerating doubly ionized atoms also accelerates sixfold ionized atoms (C^{6+}). The $^{12}_{6}\mathrm{C}$ ions accelerated to energies of about 120 MeV were used in reactions (8.3.11).

Isotopes of californium have short half-lives of spontaneous fission. Thus, ^{252}Cf has $T^{sp.\,fiss.}_{1/2} = 82$ years, while the corresponding value for ^{254}Cf is 60.5 days. It can be easily seen that such short half-lives correspond to a large number of acts of spontaneous fission per unit time and to a high flux density of the fission neutrons released in these acts.

As a result, the isotope $^{252}_{98}\mathrm{Cf}$ (which can be obtained in large quantities) is used for studying fission and also as a source of neutrons (1 g of this isotope must emit 3×10^{12} neutrons per second).

Sixteen isotopes of californium with mass numbers between 240 and 255 have been discovered so far.

8.3.3. Einsteinium and Fermium

The elements $_{99}\mathrm{Es}$ and $_{100}\mathrm{Fm}$ were obtained in the following processes:

(1) as a result of a prolonged irradiation of $^{239}_{94}\mathrm{Pu}$ by an intense neutron flux (accompanied by separation of intermediate products);

(2) in reactions involving multiply charged ions:

$$\left.\begin{aligned} {}^{238}_{92}\mathrm{U} + {}^{14}_{7}\mathrm{N} &\rightarrow {}^{246}_{99}\mathrm{Es} + 6n\,(T_{^{14}\mathrm{N}} \simeq 100\ \mathrm{MeV}), \\ {}^{238}_{92}\mathrm{U} + {}^{16}_{8}\mathrm{O} &\rightarrow {}^{250}_{100}\mathrm{Fm} + 4n\,(T_{^{16}\mathrm{O}} \simeq 180\ \mathrm{MeV}), \end{aligned}\right\} \qquad (8.3.12)$$

(3) by irradiating a californium target with α-particles.

Both the elements were first discovered during an analysis of the products formed in a thermonuclear explosion. The intense irradiation of uranium (a part of the thermonuclear device) with neutrons at the moment of explosion leads to the formation of very heavy isotopes $^{253}_{92}U$ and $^{255}_{92}U$. After several beta transitions, these isotopes are transformed into $^{253}_{99}Es$ and $^{255}_{100}Fm$ respectively.

Einsteinium and fermium have even shorter half-lives of spontaneous fission and α-particle emission.

The longest-lived isotope $^{254}_{99}Es$ of einsteinium has an alpha decay half-life of about 480 days, while the longest-lived fermium isotope $^{257}_{100}Fm$ has a corresponding half-life of just 79 days. It is interesting to note that the fermium isotope $^{256}_{100}Fm$ has a very short spontaneous fission half-life ($T_{1/2}^{sp.fis.} \simeq 160$ min).

A total of fourteen einsteinium isotopes having mass numbers between 243 and 256, and fifteen fermium isotopes with mass numbers from 244 to 258 are known to exist at present.

8.3.4. Mendelevium

In 1965, the 101st element was identified by Ghiorso's group and named mendelevium in honour of the great Russian scientist Dmitri Mendeleev.

Mendelevium was obtained by irradiating an einsteinium target with 41-MeV α-particles:

$$^{253}_{99}Es + {}^{4}_{2}He \rightarrow {}^{256}_{101}Md + n. \qquad (8.3.13)$$

The target was a gold foil coated electrically with a thin layer of einsteinium containing about 10^9 atoms. The target was bombarded from the rear with an intense beam of α-particles [about 1.2×10^{13} particles/(cm^2·s)]. The emitted (recoil) atoms of mendelevium were deposited on a thin gold-foil detector placed in the vicinity. At the end of irradiation, the detector foil was dissolved and the solution thus obtained (after removal of nonactinide impurities) was passed through an ion-exchange column to separate the mendelevium fraction.

The physical properties of the formed mendelevium isotope (mass number, type of radioactivity, half-life) were determined from the spontaneous fission half-life ($T_{1/2}^{sp.fis.} = 160$ min) registered for the separated fraction. Since this value corresponds to the fermium isotope $^{256}_{100}Fm$, the mendelevium isotope could only be $^{256}_{101}Md$ which is transformed into $^{256}_{100}Fm$ as a result of e-capture:

$$^{256}_{101}Md \xrightarrow[77\,min]{e} {}^{256}_{100}Fm. \qquad (8.3.14)$$

It is interesting to note that only 17 atoms of mendelevium were detected in the first experiments, but even this minute quantity was found to be sufficient for the identification of the new element.

Besides $^{256}_{101}$Md, four other isotopes of mendelevium (^{252}Md, ^{255}Md, ^{257}Md and ^{258}Md) have been identified. Their types of radioactivity (alpha decay and e-capture) and half-lives (from 8 to 290 min) have been determined. Two other isotopes (^{250}Md and ^{253}Md) have been found to undergo electron capture. In all, eleven isotopes of mendelevium with $A = 248$-258 have been discovered.

8.3.5. Nobelium, the 102nd Element

A lot of difficulties had to be overcome during attempts to synthesize the 102nd element. The first report on its synthesis (in the Stockholm cyclotron by bombarding $^{244}_{96}$Cm with $^{13}_{6}$C ions) was published in 1957. It was proposed that the new element be called nobelium in honour of Alfred Nobel, the founder of the Nobel Prize. The results of this work, however, cannot be considered reliable in view of their inherent contradictions. For example, there is no correspondence between the energy (8.5 MeV) of the α-particles attributed to the 102nd element and the half-life (10 min instead of the expected 10 s). Experiments performed in the USA to verify these results failed.

The failure of the first attempt to separate the 102nd element can be ascribed to the fact that the experiment made use of the above-mentioned method of chromatographic analysis which was earlier applied successfully to separate transuranic elements right up to mendelevium ($Z = 101$). Although this method yields quick results, its use is absolutely not justified for elements whose half-lives are of the order of a few seconds or less. Hence subsequent experiments aimed at discovering the 102nd element employed physical methods for separation and identification of this element.

Forestalling the events, we should mention that even the physical technique did not immediately lead to correct results. In fact, the first correct result concerning the 102nd element was obtained only in 1963 in Dubna, while a satisfactory agreement between the results obtained in two large laboratories (Dubna and Berkeley) on all the investigated isotopes of the 102nd element was reached only in 1966-67. Nevertheless, we shall also describe the earlier works which paved the way for identification of the 102nd and subsequent elements with the help of quite intricate experimental techniques.

These investigations were started at the end of 1957 in the USSR and USA. Flyorov's group in Moscow, and the group led by Seaborg and Ghiorso at Berkeley were engaged in attempts to synthesize the 102nd element.

The schematic of Flyorov's experiment is shown in Fig. 276. The 100-MeV ions of $^{16}_{8}O$ were used to irradiate a target made of $^{239}_{94}Pu$ and $^{241}_{94}Pu$. The nuclei formed as a result of capture of $^{16}_{8}O$ acquire recoil energy, leave the target and fall on an aluminium receiver. The receiver can be moved in about 2 seconds by up to 2 metres and placed in the vicinity of a photographic plate which registers α-particles emitted by the nuclei incident on the receiver.

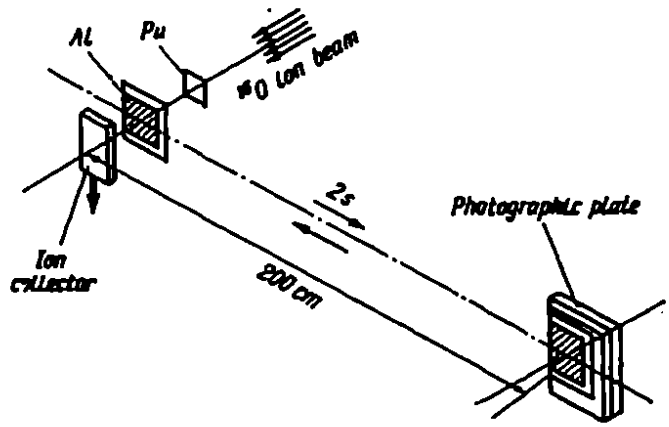

Fig. 276

Measurement of the tracks of the registered α-particles showed that they include particles with an energy of 8.8 MeV. According to the scheme of alpha decay, these particles must come from the 102nd element. Experiments were carried out for different velocities of displacement of the receiver and gave the following estimate for the half-life of this element: $3\ s < T_{1/2} < 40\ s$.[3] Blank experiments showed that α-particles having such energies can also be formed due to the presence of traces of Bi, Pb, Tl and Hg in the plutonium target. This, however, could not explain the observed effect in its entirety. Investigations of the yield of the 102nd element for different energies of the bombarding ions revealed that the mass number of the discovered isotope of the 102nd element is 253.

Ghiorso's experiment is schematically shown in Fig. 277. The bombardment of $^{246}_{96}Cm$ with $^{12}_{6}C$ ions leads to the formation of (ionized) atoms of the 102nd element. On account of their recoil energy, these atoms leave the target and impinge on a negatively charged metallic conveyer belt. The subsequent alpha decay of the atoms of the 102nd element result in the formation of fermium atoms ($Z = 100$) which also leave the belt due to recoil energy and are deposited on a receiver foil which is charged negatively relative to the belt.

[3] The accepted value of the half-life is $T_{1/2}(^{253}102) = 95\text{-}105$ s.

An analysis of the daughter nuclei showed that they have the alpha activity of $^{250}_{100}$Fm (T_α = 7.7 MeV, $T_{1/2}$ = 30 min). This means that the parent nucleus is the isotope ^{254}102.

To determine the half-life of this isotope, the distribution of the number of $^{250}_{100}$Fm nuclei deposited on the foil in the direction of motion of the belt was studied. This was made possible by comparing the alpha activity of different segments of the foil. Comparison of these results with the rate of displacement of the belt provided an estimate for the half-life of the isotope ^{254}102. This value was found to be about 3 s.[4]

It was reported in May 1963 that the isotope ^{256}102 had been synthesized in Flyorov's laboratory at the Joint Institute for Nuclear Re-

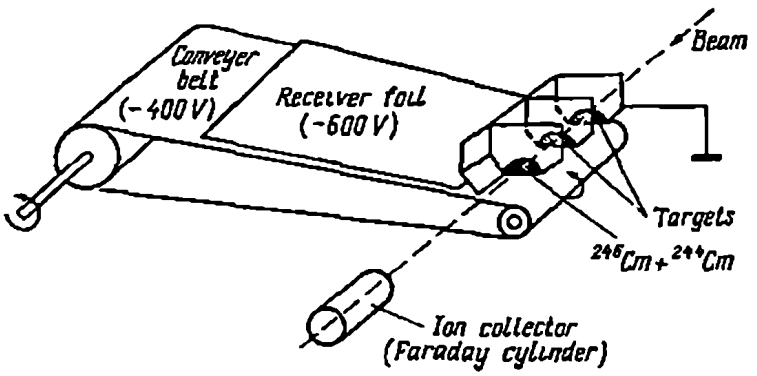

Fig. 277

search (Dubna). This isotope was obtained by bombarding a $^{238}_{92}U$ target with $^{22}_{10}$Ne ions.

The experimental technique employed by Flyorov *et al.* was basically the same as in the previous experiment (a rotating drum for collecting ^{256}102 nuclei and a stationary receiver of the products of alpha decay of these nuclei, i.e. $^{252}_{100}$Fm nuclei). There was, however, a significant modification in one respect. The receiver of daughter nuclei was reliably insulated against the products of the primary reaction with the help of special electric and mechanical plugs.[5] The isotope ^{256}102 was identified from the properties of $^{252}_{100}$Fm, and its half-life was determined by comparing the distribution of Fm nuclei on the receiver as a function of the speed of rotation of the drum. The value of $T_{1/2}^{exp}$ was estimated at about 8 s.[6]

[4] The accepted value of $T_{1/2}$ for this isotope is 75±15 s.

[5] The interaction of neon ions with uranium may lead to processes other than the reaction ^{22}Ne + ^{238}U → ^{256}102 + 4*n*. These processes include the reaction ^{22}Ne + ^{238}U → ^{252}Fm + 4*n* + α. If there are no plugs, the nuclei formed in this primary process may fall on the stationary receiver and distort the true distribution of the recoil nuclei.

[6] The accepted value of this half-life is $T_{1/2}$ = 3-8 s.

This was in fact the first result which was not refuted later. This started a new era in the investigations of this element, which ultimately led to universally accepted results.

The necessity of performing new experiments became apparent when the half-lives of the newly discovered isotope $^{256}102$ and the isotope $^{254}102$ discovered earlier at Berkeley were compared:

$$T_{1/2}^{exp}(256) > T_{1/2}^{exp}(254).$$

However, the opposite result should be expected from theoretical considerations (the existence of a subshell consisting of 152 neutrons):

$$T_{1/2}^{theor}(256) < T_{1/2}^{theor}(254).$$

In this connection, systematic investigations of the properties of all isotopes of the 102nd element discovered up to that time (A = 251-257) were carried out by Flyorov's group at Dubna in 1966 and by Ghiorso's group at Berkeley in 1967. As a result of these investigations, it was revealed that inaccurate values of half-lives were obtained by both groups in their earlier works.

The universally accepted values of half-lives of the isotopes of the 102nd element are compiled in Table 32.

Table 32

A	$T_{1/2}$, s (Dubna)	$T_{1/2}$, s (Berkeley)	A	$T_{1/2}$, s (Dubna)	$T_{1/2}$, s (Berkeley)
251	0.8±0.1	0.8±0.8	255	180±10	180±20
252	4.5±1.5	2.3±0.3	256	6±2	3.2±0.2
253	95±10	105±20	257	Not investigated	23
254	75±15	75±5			

All the isotopes listed in Table 32 are α-active. The energy of α-particles lies between 8.01 and 8.66 MeV (for all isotopes, practically identical values of energy were obtained in both laboratories). Two isotopes (A = 254 and A = 256) with a low probability (10^{-4} and about 0.007) undergo spontaneous fission.

Thus, after these experiments, seven isotopes of nobelium were known (two more isotopes with A = 258 and A = 259 were discovered later).

8.3.6. Lawrencium, the 103rd Element

The discovery of the 103rd element was reported in 1961. It was named lawrencium ($_{103}$Lw) in honour of the American physicist and the inventor of cyclotron, E.O. Lawrence. This element was synthesized by bombarding a californium target ($Z=98$, $A = 250$-252) with boron ions ($Z = 5$, $A = 10$-11). The identification of the new element was carried out from the energy of its α-particles ($T_\alpha = 8.6$ MeV). The isotope obtained in this work was assigned a mass number $A = 257$ and a half-life $T_{1/2} = 8$ s.

Another α-active isotope of lawrencium with the mass number $A = 256$ and half-life $T_{1/2} = 35 \pm 10$ s was discovered at Dubna in 1965 in the reaction

$$^{10}_{5}O + ^{243}_{95}Am \rightarrow ^{256}103 + 5n. \qquad (8.3.15)$$

In 1967, it was shown at the same laboratory that the half-life of $^{257}_{103}$Lw is much longer than 8 s, and is approximately equal to 35 s. Thus, difficulties were encountered in the identification of this element also. The authors of the first report explained the discrepancy in the values of $T_{1/2}$ ($^{257}_{103}$Lw) by the fact that they synthesized ^{258}Lw or ^{259}Lw instead of ^{257}Lw (which could be formed in reactions involving the interaction of boron ions with the californium target which contains several isotopes: ^{250}Cf, ^{251}Cf and ^{252}Cf).

Eight isotopes of lawrencium with mass numbers between 253 and 260 are known to exist at present.

8.3.7. Kurchatovium, the 104th Element

The first isotope of the 104th element with the mass number $A = 260$ was obtained in 1964 by Flyorov at the 310-cm cyclotron for accelerating multiply charged ions at Dubna. The new element was obtained by bombarding a plutonium target (97% ^{242}Pu + 1.5% ^{240}Pu + 1.5% ^{238}Pu) by an internal beam of ^{22}Ne ions accelerated to 115 MeV:

$$^{22}_{10}Ne + ^{242}_{94}Pu \rightarrow ^{264}104 \rightarrow ^{260}104 + 4n. \qquad (8.3.16)$$

As a rule, the compound nucleus ^{264}104 formed in this reaction disintegrates instantaneously into two fragments, and the probability of this reaction proceeding according to scheme (8.3.16) is just 10^{-10}.

The experimental set-up for obtaining the new element is schematically shown in Fig. 278. Absorbers are placed between the neon beam and the target to change the energy of the neon ions.

The principle of registration and identification of the nuclei of the 104th element is as follows. The nuclei escaping from the target due to recoil fall on a moving endless nickel belt and move together with

it towards the detectors which register the spontaneous fission fragments.

The detectors were made from special phosphate and silicate glasses on which the fission fragments leave tracks. On account of their extremely small size, these tracks cannot be seen under an ordinary microscope. However, when the glass is treated with hydrofluoric acid, these tracks become visible. Glasses containing the smallest contamination of thorium and uranium were used, since the fission fragments formed as a result of their interaction with fission neutrons from $^{242}_{94}Pu$ may imitate the required effect.

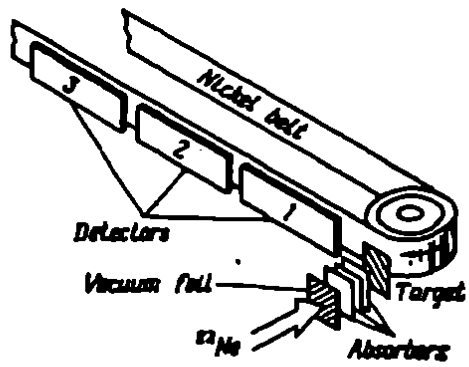

Fig. 278

The half-life of the isotope of this element was estimated by comparing the rate of displacement of the belt with the number of fission fragments registered by different detectors. Its value was found to be $T_{1/2}^{sp.fis.} \simeq 0.3$ s.[7]

Even if this half-life is determined correctly, it is obvious that doubts may arise that it pertains to some other nucleus. Thus, for example, the following reactions are possible in the interaction of ^{22}Ne with ^{242}Pu:

$$\left.\begin{aligned} &^{22}_{10}Ne + {}^{242}_{94}Pu \rightarrow {}^{260}102 + \alpha + 2n, \\ &^{22}_{10}Ne + {}^{242}_{94}Pu \rightarrow {}^{260}103 + p + 3n, \\ &{}^{260}103 \xrightarrow{\beta^-} {}^{260}102. \end{aligned}\right\} \qquad (8.3.17)$$

These reactions involve the formation of new isotopes of the 102nd and 103rd elements which may have the same half-lives as $^{260}104$. Moreover, the nuclei of some lighter transuranic elements, for example, americium, undergo spontaneous fission in the isomeric state with a very short half-life (see Sec. 8.3.1). This half-life may also coincide with that of $^{260}104$.

[7] More precise measurements made later showed that $T_{1/2}^{sp.fis.} = 0.1 \pm 0.05$ s.

To rule out these undesirable possibilities, ^{238}U nuclei were used to carry out a thorough comparative analysis of the reaction of the type (^{22}Ne, $4n$), which is analogous to the reaction (8.3.16), and of the reactions of the type (^{22}Ne, α, $2n$) and (^{22}Ne, p, $3n$), which are analogous to the reaction (8.3.17). It was found that a reaction of type (8.3.16) can be reliably isolated through the cross section and the nature of excitation function.

Finally, the conclusive evidence of the discovery of the 104th element was obtained from an investigation of its chemical properties. The extremely small half-life warranted the creation of a special gaseous technique for a rapid continuous chemical separation of nuclear reaction products near the place of their origin. Such a technique was worked out by a group of Czechoslovakian and Soviet chemists under the supervision of the Czechoslovakian chemist Zvara.

The technique used by Zvara and coworkers employs the difference in the adsorption of the chlorides of elements from the III and IV groups of the Periodic Table by solid surfaces. It was but natural to make use of this difference, since in accordance with the actinide hypothesis (see Sec. 8.4), lawrencium is the last element in the III group of the Periodic Table. The next element ($Z = 104$) must belong to the IV group, i.e. it should be an analogue of hafnium and not actinium.

The experiment was set up in such a way that, on account of the above-mentioned difference in the properties of chlorides of elements from different groups of the Periodic Table, chlorides of only IV-group elements could appear in the vicinity of the detector. After prolonged experiments for selecting proper operating conditions (composition of the gaseous mixture, temperature, pressure, filters) and the type of detector[8], Zvara and coworkers were able to register 12 cases of spontaneous fission which could correspond only to a transuranic element from the IV group, i.e. to the 104th element.

In July 1966, the academic council of the Joint Institute for Nuclear Research decided to name this element kurchatovium (Ku) in honour of Academician Igor Kurchatov, the founder of the Soviet atomic energy programme. Three more isotopes of this element with mass numbers 257, 259 and 261 were discovered in the USA in 1969. All these isotopes are α-radioactive with half-lives of 4.5, 3 and 60 s respectively.

The next step in this direction was taken in 1973 at Dubna, where three isotopes of kurchatovium with even mass numbers (254, 256 and 258) were obtained by bombarding lead nuclei with titanium ions ($Z = 22$). The half-lives of these nuclei vary between 1 and 10 ms.

---

[8] Due to very high temperature (300-350 °C), a special sort of mica was used instead of glass.

8.3.8. Elements with $Z = 105$-107 and 109

The discovery of the 105th element was reported from both Dubna and Berkeley in several publications between 1968 and 1970. In Dubna, this element was discovered in the reaction

$$^{22}_{10}\mathrm{Ne} + {}^{243}_{95}\mathrm{Am} \rightarrow {}^{261}105 + 4n. \qquad (8.3.18)$$

It was shown by using the method of rapid chemical gas analysis that the 105th element is a chemical analogue of tantalum.

In 1974, Flyorov reported the discovery of the 106th element in the reaction

$$^{54}_{24}\mathrm{Cr} + {}^{207}_{82}\mathrm{Pb} \rightarrow {}^{259}106 + 2n. \qquad (8.3.19)$$

This nucleus has a spontaneous fission half-life of about 10^{-3} s. In this case, tightly bound magic nuclei ^{207}Pb were deliberately chosen as target nuclei, since their union with the bombarding ions leads to the formation of less excited composite nuclei than those obtained by using ordinary nonmagic target nuclei. The lower excitation energy is manifested in the emission of a smaller number of neutrons (two instead of four in the previous reaction) and ultimately leads to a significant increase (about 100 times) in the probability of the formation of heavy nuclei.

A similar reaction was carried out in the same laboratory in 1976 by using $^{209}_{83}$Bi magic nuclei as targets. It indicated the formation of the 107th element:

$$^{54}_{24}\mathrm{Cr} + {}^{209}_{83}\mathrm{Bi} \rightarrow {}^{261}107 + 2n. \qquad (8.3.20)$$

This isotope of the 107th element disintegrates with a half-life $T_{1/2} = 2$ ms according to the following two channels:

$$^{261}107 \xrightarrow[80\%]{\alpha} {}^{257}105 \xrightarrow[80\%]{\alpha} \qquad (8.3.21)$$

$$\swarrow\ (\sim 2\ \text{ms})\qquad (\sim 5\ \text{s})\ \searrow$$

Sp. fs. 20% Sp. fs. 20%

Finally, the discovery of the 109th element at Darmstadt (FRG) was reported in the autumn of 1982 at the Conference on Nuclear Interaction:

$$^{58}_{26}\mathrm{Fe} + {}^{209}_{83}\mathrm{Bi} \rightarrow {}^{267}109 \rightarrow {}^{266}109 + n. \qquad (8.3.22)$$

The isotope of the 109th element obtained in this reaction decays according to the scheme

$$^{266}109 \xrightarrow[5\ \text{ms}]{\alpha} {}^{262}107 \xrightarrow[22.3\ \text{s}]{\alpha} {}^{258}105 \xrightarrow{\beta^+} {}^{258}104 \xrightarrow[12.4\ \text{s}]{\text{sp. fs.}}. \qquad (8.3.23)$$

8.4. General Remarks About Transuranic Elements

It was mentioned above that transuranic elements form a group of elements with similar chemical properties.

Another well-known example of a group of elements with similar properties are the rare-earth elements. The properties of the rare-earth elements are analogous to the properties of lanthanum, hence they are called lanthanide elements. Since the properties of transuranic elements are similar to those of actinium, these elements (as well as $_{90}$Th, $_{91}$Pa and $_{92}$U) are termed *actinide* elements.

The specific properties of the lanthanide elements are due to the fact that their formation takes place through a gradual filling of the $4f$ inner electron subshell and not of the outer subshell which determines the chemical properties of the elements (for rare-earth elements, the $5d$ subshell is the outermost). Similarly, the formation of the actinide elements takes place through a gradual filling of the $5f$ inner subshell.

The maximum number of electrons in the f state is equal to $2(2l + 1) = 2(2 \times 3 + 1) = 14$. Hence there are 14 rare-earth elements analogous to lanthanum. Similarly, there must be 14 actinide elements similar to actinium in their chemical properties.

It can be easily seen that the last position in the $5f$ subgroup corresponds to the 103rd element $_{103}$Lw which marks the termination of the actinide group formation. The next element with $Z = 104$ must be an analogue of hafnium.

The similarity of the chemical properties of transuranic elements lends a special importance to the physical methods of identification based on the regularities in the variation of properties of nuclei with the number of nucleons contained in them. Among the most important regularities are the alpha and beta decay and spontaneous fission schemes as well as a very interesting property called the *energy cycle*. We shall briefly describe these properties.

Two experimental regularities concerning alpha decay were described in Sec. 3.2. The first regularity connects the energy of alpha decay with the mass number A and atomic number Z of radioactive nuclei. This dependence is represented by a family of (nearly straight) lines, each of which corresponds to different isotopes of the same element (see Fig. 83).

The second regularity establishes a relation between the alpha decay constant λ, the kinetic energy T_α of an α-particle, and the atomic number Z of an α-active nucleus (see Fig. 96).

It can be seen from Figs. 83 and 96 that both these regularities are also applicable to transuranic elements. Hence they can be used to predict the alpha decay properties of such isotopes of transuranic elements that have not been discovered so far, or have not been investigated properly.

A comparison of β-radioactive isotopes of transuranic elements involves the use of relations connecting the beta decay energy E, the mass number A, and the atomic number Z of β-active nuclei. Like the analogous dependence for alpha decay, this dependence is also represented by a family of nearly straight lines.

A very important law was established in the investigation of the spontaneous fission of transuranic elements. A comparison of spontaneous fission half-lives $T_{1/2}^{sp.fis.}$ for even-even nuclei showed that to a first approximation $\ln T_{1/2}^{sp.fis.}$ varies linearly with the fission parameter Z^2/A:

$$\ln (T_{1/2}^{sp.fis.}) = a - bZ^2/A. \qquad (8.4.1)$$

This relation was established at the earliest stage of investigation of transuranic elements and could be used to roughly predict the spontaneous fission half-lives for as yet undiscovered elements. It is interesting to note that an approximation of *(8.4.1) to the region* of shortest possible fission times $T^{min} = 10^{-20}$ s (the ratio of the nuclear radius to the velocity of the fission fragment) gives the value $Z^2/A = 47$-50, which is close to the value obtained from the elementary theory of fission (see Sec. 7.3). It should be recalled that this result led to the prediction that the Periodic Table must terminate at an element with $Z = 120$-125. However, in spite of the fact that these two predictions based on theory and experiment coincide, they must be considered cautiously, since the theory has not been perfected, and the experimental results are used in the form of a distant extrapolation.

A more detailed investigation of the spontaneous fission of transuranic elements showed that the linear dependence between $\ln T_{1/2}^{sp.fis.}$ and Z^2/A is valid only to a first approximation. Measurements of the half-lives of even-even isotopes of the same element showed that they lie on dome-shaped curves or "caps", two of which (for Cf and Fm) are especially sharp (see Fig. 279). Apparently, the origin of these curves is closely related to the dependence of the stability of nuclei on the ratio of the numbers of protons and neutrons constituting them, which was described in Chap. 2. The sharp curves for Cf and Fm can be attributed to the influence of subshells with $N = 152$ neutrons (the effect of this subshell was earlier noted in the specific properties of alpha decay, see Fig. 83).

It should be recalled that we have considered only even-even nuclei so far. The spontaneous fission half-lives of nuclei with odd mass numbers are a few orders of magnitude longer than for the spontaneous fission of the adjoining even-even nuclei.

It was shown in 1955 by Svyatetskii that the spontaneous fission half-life is very sensitive to the deviation δm of nuclear mass from the smooth value corresponding to the semiempirical formula.

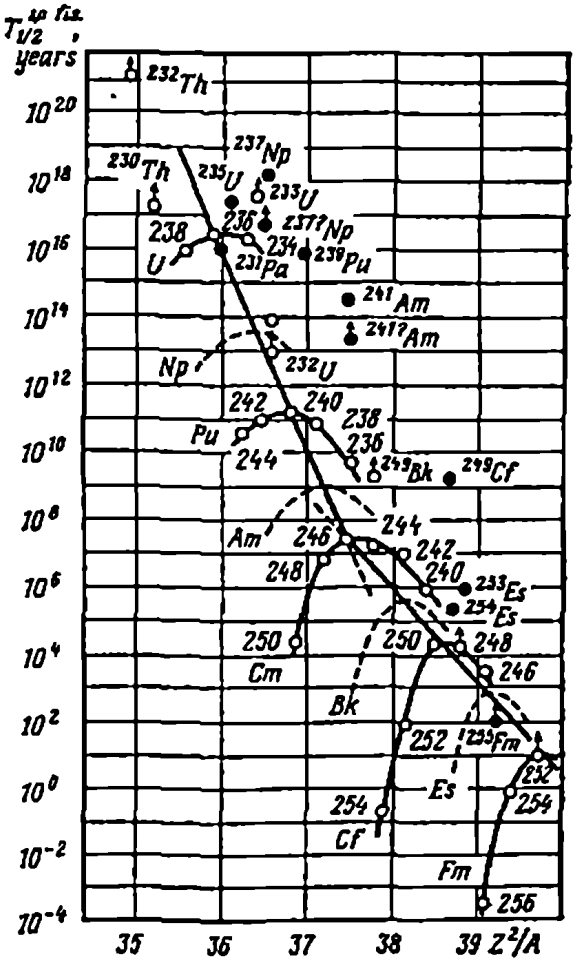

Fig. 279

It was found that $T_{1/2}^{sp.fis.}$ varies by a factor of 10^5 for $\delta m = 1$ MeV. If a correction of the type $k\delta m$ is introduced, where k is an empirically selected factor, the results shown in Fig. 279 are transformed into three straight lines corresponding to even-even, odd, and odd-odd nuclei (Fig. 280).

The heaviest among the discovered transuranic elements ($Z =$ 101-109) deserve a special consideration. For known reasons, information about the spontaneous fission half-lives of these elements is quite sparse and less conclusive (Fig. 281). However, an important and seemingly reliable conclusion can be drawn from this information. The spontaneous fission half-lives of these elements decrease much more slowly than what is expected from formula (8.4.1). Thus, the measured value of $T_{1/2}^{sp.fis.}$ for the nucleus $^{261}107$ was found to be 10^{10} times higher than the value predicted by formula (8.4.1). This allows us to hope that still heavier transuranic elements will be dis-

covered in the near future, which may turn out to be even more stable than the 107th element. In any case, modern theory predicts magic numbers $Z = 114$ and $N = 184$. Nuclei with such numbers of

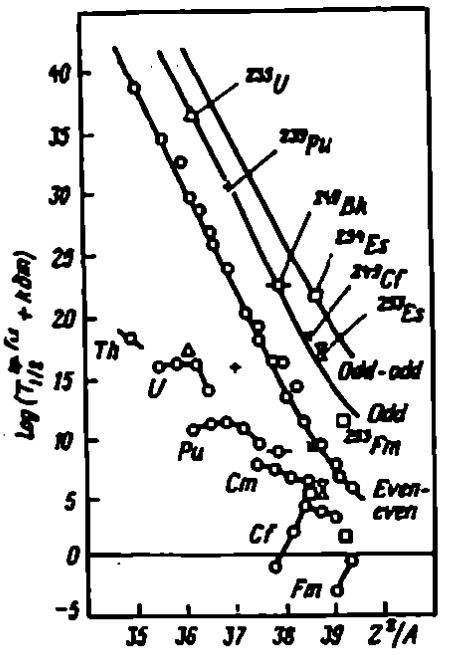

Fig. 280

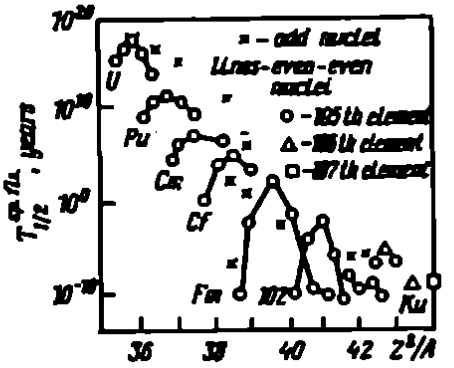

Fig. 281

protons and neutrons are being looked for in nature as well as in accelerators. For example, the reaction

$$^{70}_{32}\mathrm{Ge} + {}^{238}_{90}\mathrm{Th} \rightarrow {}^{308}122 \qquad (8.4.2)$$

was investigated with the hope that after a series of alpha decays, the nucleus $^{308}122$ will be transformed into a stable element with $Z = 114$:

$$122 \xrightarrow{\alpha} 120 \xrightarrow{\alpha} 118 \xrightarrow{\alpha} 116 \xrightarrow{\alpha} 114. \qquad (8.4.3)$$

Reactions involving the formation of other superheavy elements were also investigated in the USA, UK and France. However, no conclusive results have been obtained so far.

A systematic analysis of the properties of transuranic elements not only helps in the identification of new elements, but also facilitates the establishment of new laws for elements discovered earlier. Thus, a detailed analysis of transuranic elements led to the formation of the

missing fourth radioactive family whose members have mass numbers satisfying the law

$$A = 4n + 1, \tag{8.4.4}$$

where n is an integer. (Members of the remaining three well-known radioactive families obey the laws $A = 4n$, $A = 4n + 2$, and $A = 4n + 3$.)

This family is called the *neptunium family* although its first member is the isotope $^{241}_{94}$Pu. By emitting a β-particle, in a short time this nucleus is transformed into $^{241}_{95}$Am which in turn emits an α-particle and is quickly transformed into the long-lived ($T_{1/2} = 2.25 \times 10^6$ years) α-active $^{237}_{93}$Np, after which the series is named. Alpha decay of $^{237}_{93}$Np leads to the formation of β-active $^{233}_{91}$Pa, which is transformed into a long-lived ($T_{1/2} = 1.62 \times 10^5$ years) α-active uranium isotope $^{233}_{92}$U.

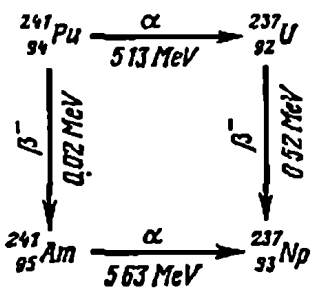

Fig. 282

It was mentioned earlier that $^{233}_{92}$U *has properties similar to* $^{235}_{92}$U, and hence it can be used as a nuclear fuel. This isotope is obtained in large quantities in breeders loaded with thorium.

Notable among other nuclei belonging to the neptunium family are the isotopes $^{221}_{87}$Fr and $^{217}_{85}$At. These two elements, francium and astatine, were among the last elements in the Periodic Table to be discovered (1939-40) (not taking into account the transuranic elements). The last element of this family is the stable bismuth isotope $^{209}_{83}$Bi containing a magic number of neutrons (126).

It should be noted that the existence of short-lived nuclei at the beginning of the neptunium family is not a property confined just to this family. A detailed study of transuranic elements revealed the existence of short-lived "ancestors" for other radioactive families encountered in nature (uranium, thorium and actinouranium families). Besides, isotopes not belonging to any of the four radioactive families were also discovered during investigations of transuranic elements. These nuclei form side families which merge at some link into one of the four main families.

The energy-cycles law mentioned above is a more general law covering the main as well as side families together with their short-lived "ancestors".

The basic idea behind this law can be easily understood from Fig. 282 which shows two different chains of radioactive transformations of $^{241}_{94}$Pu terminating at the same nucleus $^{237}_{93}$Np. Naturally, the total

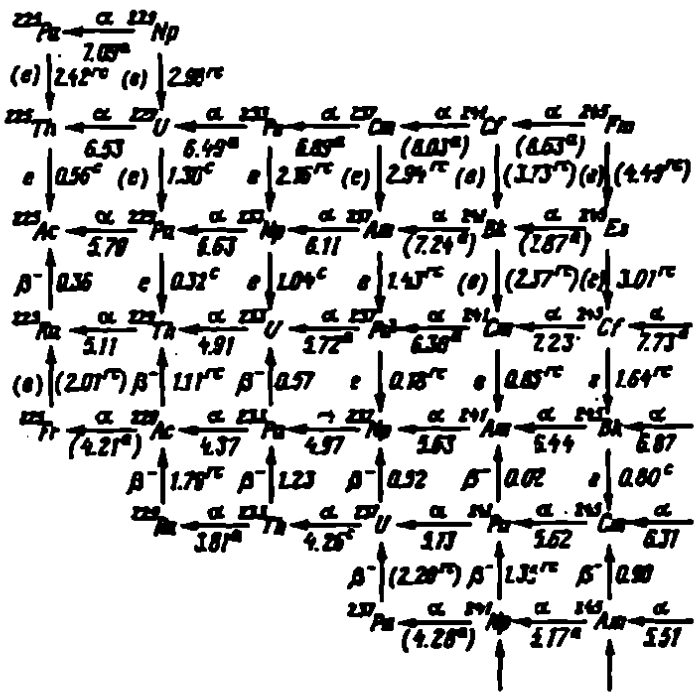

Fig. 283

energy for alpha and beta transitions in each chain must be the same, a fact which is verified experimentally in the present case.

Closed cycles for decay energy can be used to determine the value of the fourth unknown value of energy in a cycle if the other three values are known. A remarkable feature of this process is that the same nucleus may participate in several (up to four) cycles, thus providing an additional method of checking.

Figure 283 depicts a small part of the groups of energy cycles containing nuclei with mass numbers $A = 4n + 1$, where n is an integer. The arrows and letters indicate the direction and nature of the process (alpha decay, beta decay, or e-capture). Numerals indicate the values of the transition energy: the numbers without superscripts indicate the results of measurements, superscript "a" indicates approximate values obtained from the laws of alpha and beta decays, while "c" and "rc" stand for results obtained in closed cycles using experimental (c) and roughly calculated (rc) values. The approximate values of transition energy and the possible nature of the transition are given in parentheses.

Similar groups exist for nuclei whose mass numbers satisfy the laws

$$A = 4n, \quad A = 4n + 2 \quad \text{and} \quad A = 4n + 3.$$

Obviously, closed cycles represent a further development of the concept of radioactive families and seem to indicate the main trends in the transformation of heavy nuclei of a given group ($4n + i$) *into lighter nuclei.*

8.5. A Brief Resumé of Chapter 8

In this chapter, we have described the properties of transuranic elements with atomic number $Z > 92$.

The following transuranic elements have been discovered so far: neptunium $_{93}$Np, plutonium $_{94}$Pu, americium $_{95}$Am, curium $_{96}$Cm, berkelium $_{97}$Bk, californium $_{98}$Cf, einsteinium $_{99}$Es, fermium $_{100}$Fm, mendelevium $_{101}$Md, nobelium $_{102}$Nb, lawrencium $_{103}$Lw, kurchatovium $_{104}$Ku. Besides, tentative evidence has been obtained indicating the existence of the 105th, 106th, 107th and 109th elements.

Transuranic elements are obtained in accelerators and nuclear reactors with the help of reactions which increase the charge of the parent nucleus [bombardment with ions of $_5$B, $_6$C, $_7$N, $_8$O, $_{10}$Ne, $_{24}$Cr, etc., (d, n)-, (α, n)-, $(\alpha, 2n)$-reactions, (n, γ)-reaction followed by a β^--decay, and so on]. Separation of transuranic elements after irradiation is carried out with the help of radiochemical and radiophysical methods (carrier technique, ion-exchange chromatography, rapid gaseous chemistry, and physical methods of separation and identification).

Transuranic elements have many similar properties. Elements from neptunium to lawrencium (both inclusive), as well as thorium, protactinium and uranium, have identical chemical properties and are therefore called actinides.

All transuranic elements are radioactive (they undergo alpha decay, beta decay, ε-capture, or spontaneous fission). Radioactive properties of these elements vary regularly with the variation of A and Z. These regularities include the dependence of alpha decay energy on A and Z, dependence of half-life on the α-particle energy for different Z and A, relation between the beta decay energy, mass number A and atomic number Z for β-active nuclei, closed energy cycles connecting the alpha and beta decay energies of nuclei having the same type of mass numbers ($A = 4n$, $A = 4n + 1$, $A = 4n + 2$ and $A = 4n + 3$), and the relation between $\ln T_{1/2}$ and Z^2/A for spontaneous fission of even-even nuclei.

The probability of spontaneous fission for transuranic elements increases rapidly with Z^2/A, and spontaneous fission may become the dominant decay process for $Z > 105$. It can be assumed that for $Z^2/A = 45$-49 ($Z = 120$-125) the half-life for spontaneous fission will become equal to nuclear time (complete filling of the Periodic Table of elements), although the existence of islets of fairly long-lived nuclei in the region of magic numbers $Z = 114$ and $Z = 126$ cannot be ruled out.

The half-lives of all transuranic elements are shorter than the age of the Earth. Hence transuranic elements are not encountered in nature [with the exception of traces of neptunium and plutonium, which are continuously formed in $(n, 2n)$- and (n, γ)-reactions taking place in uranium].

From the point of view of practical applications, the most important transuranic element is the plutonium isotope ^{239}Pu which is used as a nuclear fuel. Many transuranic elements are used for studying the physics of fission. Some isotopes of transuranic elements, for example ^{238}Pu and ^{242}Cm, are used for preparing isotopic current sources.

Isotopes with short half-lives of spontaneous fission are used for preparing neutron sources having a fission spectrum. Other transuranic elements (for example, Pu) are used for preparing neutron sources in which the (α, n)-reaction in beryllium is used.

Chapter 9

Nuclear Reactions Induced by Light Charged Particles

In this chapter we shall consider the general laws governing the nuclear reactions induced by charged particles with relatively low energies, viz. the α-particle-induced reactions and the reactions induced by protons. Other reactions involving charged particles will be considered in Chap. 10 (reactions induced by deuterons and lithium ions) and Chap. 11 (reactions caused by heavy ions). The interaction of fast protons, electrons, muons, pions and other charged particles with nucleons and nuclei will be considered in Vol. II.

9.1. Some Features of Interaction of Charged Particles with Matter

It is well known (see Secs. 4.1 and 4.2) that one of the main mechanisms of interaction of charged particles with nuclei and electrons of matter is the electromagnetic interaction (to be more specific, ionization losses and Coulomb interaction). To a significant degree, these processes govern nuclear reactions induced by charged particles.

9.1.1. Coulomb Interaction of Charged Particles with Nuclei

It was shown in Sec. 2.2 that the parameters of a potential well for neutrons are characterized by the nuclear radius $R = r_0 A^{1/3} \simeq 10^{-12}$ cm, and the depth of the well, which is about 30-40 MeV (Fig. 284*a*). Such a nature of the potential shows that a neutron will experience a strong attraction upon coming quite close to the atomic nucleus.

For the interaction of charged particles with a nucleus, the potential energy curve has the form shown in Fig. 284*b*, which is similar to Fig. 92. Let us recall the main results corresponding to this curve (see Sec. 3.2.3).

The upper part of the curve is due to the mutual Coulomb repulsion experienced by the nucleus and the charged particle. The decrease in potential energy in this region is described by the law

$$V(r) = Zze^2/r, \qquad (9.1.1)$$

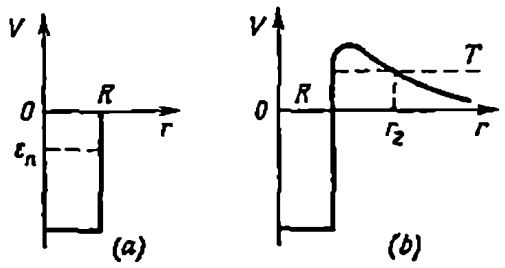

Fig. 284

where Z is the nuclear charge, z is the charge of the particle and r is the distance separating them. At $r = R$ (nuclear radius) the curve sharply falls. This part of the curve is explained by the strong nuclear attraction in the region $r < R$.

The Coulomb interaction of the charged particle with the nucleus is characterized by the height of the Coulomb barrier

$$B_C = Zze^2/R, \qquad (9.1.2)$$

which is numerically equal to (in MeV)

$$B_C \simeq ZzA^{-1/3}. \qquad (9.1.3)$$

Let us consider the nuclear interaction of a charged particle with kinetic energy

$$T < B_C. \qquad (9.1.4)$$

According to classical mechanics, the particle cannot enter the atomic nucleus in this case. According to quantum mechanics, however, a particle with $T < B_C$ has a finite probability of tunnelling through the potential barrier.

The tunnelling probability, or the *penetrability of the potential barrier*, is given by the formula

$$D \simeq \exp\left(-\frac{2}{\hbar}\int_{r_1}^{r_2}\sqrt{2\mu(V_C - T)}\,dr\right), \qquad (9.1.5)$$

where $\mu = Mm/(M + m)$ is the reduced mass and T is the kinetic energy in the centre-of-mass system.

The lower limit of integration coincides with the nuclear radius R, while the upper limit is obtained from the condition $T = Zze^2/r_2$.

Integration of this formula leads to the relation

$$D = \exp(-2g\gamma), \qquad (9.1.6)$$

where $g = R/\lambda\!\!\!^{-}_{B_C}$; $\gamma = \sqrt{B_C/T}\arccos\sqrt{T/B_C} - \sqrt{1 - T/B_C}$; $\lambda\!\!\!^{-}_{B_C} = \hbar/\sqrt{2mB_C}$ is the de Broglie wavelength corresponding to the kinetic energy of the particle, which is equal to the barrier height ($T = B_C$).

It can be easily shown that for $T \ll B_C$, formu a (9.1.6) assumes a simpler form

$$D = \exp\left(-\frac{2\pi R B_C}{\hbar v}\right) = \exp\left(-\frac{2\pi Z e^2}{\hbar v}\right), \qquad (9.1.7)$$

where v is the velocity.

It should be recalled that for nucleons

$$(\lambda_T)_{l.s.c.} = \hbar/\sqrt{2m_N T} = 4.5 \times 10^{-13}/\sqrt{T}, \qquad (9.1.8)$$

where T is in MeV and λ is in cm.

$$(\lambda_T)_{c.m.s.} = \hbar/p' = \hbar\Big/\frac{\mu}{m} p = n\lambda_{l.s.c.}/\mu. \qquad (9.1.9)$$

To determine the function γ, it is convenient to use the plot shown in Fig. 93.

Let us use formula (9.1.6) to calculate the penetrability of the Coulomb barrier of the $^{27}_{13}$Al nucleus for a proton having a kinetic energy $T_p = 1$ MeV:

$$R = 4.2 \times 10^{-13} \text{ cm}, \quad B_C = 4.3 \text{ MeV},$$
$$\lambda_{B_C} \simeq 2.2 \times 10^{-13} \text{ cm}, \quad g = 1.9, \quad \gamma = 1.4,$$
$$D = \exp(-2g\gamma) = \exp(-5.3) \simeq 0.005.$$

Similar calculations for other nuclei and particles of different energies show that the penetrability of the potential barrier sharply increases with the kinetic energy of the particles. Other conditions remaining the same, the penetrability of the barrier for α-particles is a few orders of magnitude lower than for protons.

9.1.2 The Role of Centrifugal Barrier

So far, it was implicitly assumed that the interaction of particles with a nucleus is considered for head-on collisions only. In classical mechanics, such a motion is characterized by a zero impact parameter. In quantum mechanics, such a motion of particles is described by a wave-function characterized by an orbital quantum number $l = 0$.

In the general case, the interaction of a particle with a nucleus may have a nonzero impact parameter corresponding to it. In this case, the wave-function describing the motion of the particle in quantum mechanics is defined by an orbital quantum number $l \neq 0$. It was mentioned in Sec. 5.4.2 that in this case we must take into consideration the centrifugal potential

$$V_c = \hbar^2 l(l+1)/2mr^2. \qquad (9.1.10)$$

For a charged particle, this potential together with the Coulomb potential describes the interaction of the particle with the nucleus. When a neutron interacts with the nucleus, this potential reduces the interaction probability just as the Coulomb barrier reduces the interaction probability for charged particles.

On account of the centrifugal barrier, neutrons can effectively interact with the nucleus only at energies

$$T > \hbar^2 l(l+1)/2\mu R^2, \qquad (9.1.11)$$

i.e. for $l_T < R/\lambda\!\!\!^{-}_T$. Thus, slow neutrons ($\lambda\!\!\!^{-}_T > R$) can interact with the nucleus only if $l = 0$. This conclusion is experimentally confirmed by the spherical symmetry of the angular distribution of interaction products in the centre-of-mass system.

The situation is quite different for charged particles on account of the existence of a Coulomb barrier whose height B_C for fairly heavy nuclei usually exceeds the height B_c of the centrifugal barrier for small l. Consequently, the probability of interaction of charged particles with the nucleus for $l = 0$ does not differ significantly from the interaction probability for

$$l = 1, 2, \ldots, l_0, \quad \text{where} \quad l_0 = \sqrt{R/2\lambda\!\!\!^{-}_{B_C}},$$

which means that the angular distribution of the interaction products may not be spherically symmetric in this case.

As an example, let us consider the nucleus $^{118}_{50}$Sn for which $B_C \simeq 10$ MeV, while in accordance with formula (5.4.8) the height of the centrifugal barrier (in MeV) will be

$$B_c \simeq 10l(l+1)A^{-2/3}.$$

This means that for $l = 1$, $(B_c)_1 = (B_c)_{min} \simeq 0.8$ MeV, for $l = 2$, $(B_c)_2 \simeq 2.5$ MeV, and

$$l_0 = \sqrt{\frac{R}{2\lambda\!\!\!^{-}_{B_C}}} = \sqrt{\frac{1.4\times10^{-13}A^{1/3}}{2\dfrac{4.5\times10^{-13}}{\sqrt{B_C}}}} \simeq 2,$$

where B_C is in MeV. A comparison of these results shows that neutrons having an energy $T < (B_c)_{min} \simeq 0.8$ MeV can effectively interact with a $^{118}_{50}$Sn nucleus only when $l = 0$. Conversely, charged particles with energy $T < B_C \simeq 10$ MeV will have comparable interaction probabilities for $l = 0$, $l = 1$ and $l = 2$.

9.1.3. Ionization Losses for Charged Particles. Yield of a Nuclear Reaction

It is well known that the main mechanism due to which charged particles lose energy in a given energy range is the mechanism of ionization losses involving the expenditure of the kinetic energy of a

particle in ionizing and exciting the atoms of the medium. In each act of ionization, a charged particle loses about 35 eV of its energy.

The cross section of single acts of ionization interaction can be estimated from the distance ρ between two charged particles, at which the Coulomb potential is equal to the ionization potential. From the expression $e^2/\rho = 35$ eV, we get

$$\rho = \frac{(4.8\times10^{-10})^2}{35\times1.6\times10^{-12}} = 0.4\times10^{-8}\ \text{cm}, \qquad (9.1.12)$$

which gives the ionization cross section

$$\sigma_{ion} = \pi\rho^2 = 0.5\times10^{-16}\ \text{cm}^2. \qquad (9.1.13)$$

If a charged particle has an initial kinetic energy of 1 MeV, it loses all its energy, i.e. comes to a halt, after $10^6/35 \simeq 3\times10^4$ acts of ionization. The cross section of this process is

$$\Sigma_{ion} = 0.5\times10^{-16}/3\times10^4 \simeq 2\cdot10^{-21}\ \text{cm}^2, \qquad (9.1.14)$$

which is about 10^3 times larger than the cross section of nuclear interaction ($\sigma_{nuc} \simeq 10^{-24}$ cm^2). Thus, when charged particles having energies of a few megaelectron-volts move in a medium, most of them lose all their energy by ionization and only about a thousandth part undergo nuclear interaction.

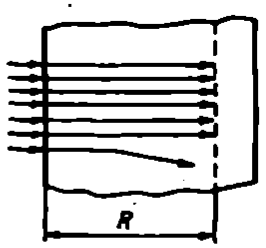

Fig. 285

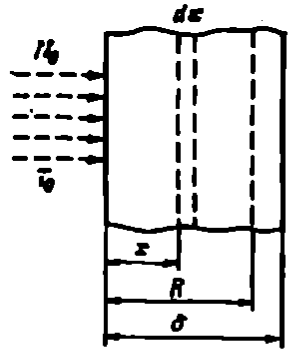

Fig. 286

The process of motion and interaction of charged particles in a medium (say, a photographic emulsion in which they leave a track) is schematically shown in Fig. 285. It is clear from this figure that most of the particles traverse their range R without undergoing nuclear interactions and their tracks are practically straight lines. Only in rare cases does a nuclear interaction take place, when the direction of motion and the energy of the particles change sharply (scattering) or a new particle appears in place of the original one (nuclear reaction).

When a charged particle is moving in a thick target ($\delta > R$), nuclear interaction may take place at any point x on its path, where its kinetic energy is equal to $T(x)$. The longer the path traversed by the particle before interaction, the lower the energy to which it has been decelerated. However, the probability of nuclear interaction is a complex function of energy, and includes the $1/v$-law, possible resonance processes and an increase in the barrier penetrability with energy. Hence, in order to determine the probability of nuclear interaction of charged particles, we must know the energy to which a particle has been decelerated up to the moment of nuclear interaction. In other words, we must take into account the rate with which the energy of a particle decreases as it traverses a path x.

The number of nuclear interactions dv occurring in a thin layer dx at a depth x is obviously given by (Fig. 286)

$$dv = N(x)\, n\sigma(x)\, dx \simeq N_0 n\sigma(x)\, dx, \tag{9.1.15}$$

where $N(x) \simeq N_0$ is the particle flux which practically remains unchanged right down to zero energy since the fraction of nuclear interactions is negligibly small, n is the number density of nuclei, and $\sigma(x)$ is the interaction cross section at the depth x. The total number of interactions in a thick layer of matter ($\delta > R$) is given by

$$v = N_0 n \int_0^R \sigma(x)\, dx = N_0 n \int_0^{T_0} \sigma(T)\, dT \Big/ \left|\frac{dT}{dx}\right|. \tag{9.1.16}$$

The fraction of particles undergoing nuclear interaction is called the *yield Y of a nuclear reaction*:

$$Y(T) = \frac{v}{N_0} = n \int_0^T \sigma(T)\, dT \Big/ \left|\frac{dT}{dx}\right|. \tag{9.1.17}$$

It is clear from this formula that for a given energy T, the yield of a nuclear reaction is a function not only of the cross section $\sigma(T)$, but also of the rate of loss of kinetic energy, i.e. the specific ionization dT/dx of the particle.

The yield Y of a reaction as a function of the kinetic energy T is called the *excitation function of the reaction*. A knowledge of the excitation function allows us to find the reaction cross section. Since in accordance with Eq. (9.1.17)

$$\frac{dY}{dT} = n\sigma(T) \Big/ \left|\frac{dT}{dx}\right|, \tag{9.1.18}$$

we get

$$\sigma(T) = \frac{1}{n} \frac{dY}{dT} \left|\frac{dT}{dx}\right|. \tag{9.1.19}$$

9.2. Reactions Induced by Alpha-particles

The first nuclear reaction was brought about in 1919 by Rutherford who used α-particles emitted by heavy α-active nuclei for the bombardment of target nuclei. For a long time, reactions induced by α-particles remained the only known type of nuclear reactions. The possibility of studying reactions induced by neutrons and protons appeared only after Chadwick discovered the neutron in 1932 and Cockroft and Walton proposed a method for artificial acceleration of protons.

Naturally, α-particles emitted by α-active nuclei can be used to study nuclear reactions involving light nuclei since heavy nuclei have a high Coulomb barrier [$(B_C)_\alpha \simeq 25$ MeV] which is considerably higher than the kinetic energy of even the fastest α-particles [T_α (ThC') = 8.95 MeV].

The main types of nuclear reactions induced by α-particles are the (α, p)-reactions (including the first nuclear reaction) and (α, n)-reactions (one such reaction led to the discovery of the neutron).

The nature of nuclear reactions induced by α-particles is determined to a considerable extent by two factors: the height of the Coulomb barrier and the binding energy of an α-particle in the nucleus. Table 33 shows the average height of the Coulomb barrier $(B_C)_\alpha$

Table 33

Average values of quantities	Z		
	< 20	60	80
$(B_C)_\alpha$, MeV	10	20	25
ε_α, MeV	8	0	−5
$W = (B_C)_\alpha + \varepsilon_\alpha$, MeV	18	20	20

and the binding energy ε_α of α-particles in nuclei with different Z.

The excitation energy of a nucleus capturing an α-particle consists of the kinetic energy (in the centre-of-mass system) of the α-particle and its binding energy. For a nuclear reaction to proceed effectively, the kinetic energy of the α-particle must be comparable with the height of the Coulomb barrier [$T_\alpha \simeq (B_C)_\alpha$]. Hence the excitation energy of the nucleus is given by

$$W = \varepsilon_\alpha + T_\alpha \simeq \varepsilon_\alpha + (B_C)_\alpha. \qquad (9.2.1)$$

It can be seen from Table 33 that in the entire range of variation of Z, the nuclear excitation energy W is practically constant and has a value of about 20 MeV.

Such a high excitation energy of the compound nucleus is quite enough for compensating the binding energy ε_N of an escaping nucleon, as well as for neutralizing the Coulomb barrier $(B_C)_p$ in case the escaping particle is a proton.

Indeed, since $\varepsilon_N \simeq 8$ MeV, $T_N = W - \varepsilon_N = 20 - 8 = 12$ MeV, and $T_N > (B_C)_p \simeq (B_C)_\alpha/2 \simeq 10$ MeV. Hence reactions of the types (α, n) and (α, p) must occur with the same probability when nuclei are bombarded with α-paticles having $T_\alpha = (B_C)_\alpha$.

We shall consider these reactions in greater detail.

9.2.1. Reactions of the (α, p) Type

Reactions of this type were the first nuclear reactions to be studied. The first reaction in which the proton was discovered also belongs to this type of reactions:

$$^{14}_{7}\mathrm{N} + {}^{4}_{2}\mathrm{He} \rightarrow {}^{17}_{8}\mathrm{O} + p. \qquad (9.2.2)$$

This reaction was studied by Rutherford in 1919 with the help of an instrument used for investigating recoil nuclei obtained by bombarding various nuclei with α-particles (Fig. 287).

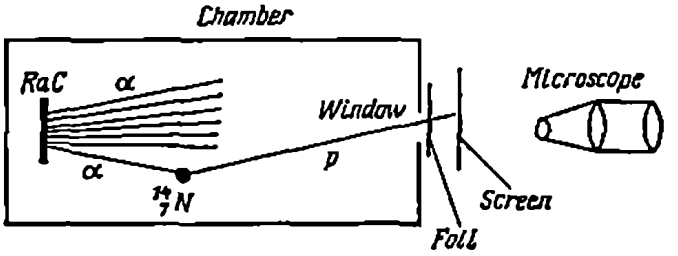

Fig. 287

The window of the hermetic chamber was covered with a thin foil, and a scintillating screen was placed behind it. The luminescence caused by a particle impinging on the screen can be clearly observed under the microscope. The RaC preparation placed at the other end of the chamber emitted α-particles with energy 7.7 MeV, and a range of about 7 cm in air (at normal pressure).

The chamber was filled with the gas under investigation. By suitably adjusting the gas pressure, the range of the particles having a certain energy could be made exactly equal to the distance between the source and the screen. From a simple relation connecting the pressure with the range of a particle, the range of the particle at normal pressure could be determined by measuring the gas pressure in the chamber. The energy of the particle could then be found from the formula connecting the range and the energy of the particle.

By studying the recoil nuclei obtained by bombarding hydrogen, nitrogen and oxygen with α-particles, Rutherford noticed in the case of nitrogen a deviation from the course predicted by the momentum diagram of elastic scattering. It was found that besides the scattered α-particles having a comparatively short range, some other particles with a range about four times longer than that of the bombarding α-particles were also observed.

This phenomenon could not be attributed to the presence of hydrogen as an impurity in the gas, although the maximum range $(R_p)_{max}$ of the recoil nuclei of hydrogen is just four times the range R_α of α-particles. This is so because: (1) the effect was enhanced when air was replaced by pure nitrogen gas; (2) the effect vanished if nitrogen was replaced by oxygen or carbon monoxide; (3) the range of protons in some cases was found to be as large as 40 cm, which is considerably longer than the maximum possible range of recoil protons [$(R_p)_{max}$ = 28 cm]; and (4) the angular distribution of the emerging protons was more uniform than what could be expected for recoil protons (which predominantly move in the forward direction).

Rutherford suggested that the emergence of protons with anomalously large range is associated not with the elastic scattering of α-particles at hydrogen nuclei, but with a new phenomenon, viz. a nuclear reaction in which the original $^{14}_{7}N$ and $^{4}_{2}He$ nuclei are transformed into other nuclei ($^{17}_{8}O$ and $^{1}_{1}H$). This provides a natural explanation for all the above-mentioned properties of long-range protons observed by Rutherford.

The most clear and convincing evidence of the occurrence of the above-mentioned nuclear reaction during interaction of α-particles with nitrogen nuclei was provided by Blackett in 1923. He was able to obtain the photograph of the splitting of a nitrogen nucleus by an α-particle by using a Wilson cloud chamber. This photograph clearly showed the tracks of the primary α-particle, the escaping proton and the resulting nucleus. Calculations of the mass of this nucleus by taking into account the laws of momentum and energy conservation gave a value of 16.72 ± 0.42 amu.

Subsequent investigations revealed that this nuclear reaction is endoergic ($Q = -1.06$ MeV) and has a yield $Y = 2 \times 10^{-4}$ (for $T_\alpha = 7.8$ MeV). It is interesting to note that in spite of the endoergic nature of this nuclear reaction, the maximum energy of the resulting protons is higher than the maximum energy of the recoil protons formed as a result of elastic scattering of α-particles of the same energy by hydrogen nuclei. We leave it to the reader as an exercise to solve this problem by using the laws of energy and momentum conservation and explain why $(T_p)_{reac} > (T_p)_{rec}$.

The splitting of nitrogen by α-particles was followed by the splitting of other nuclei, viz. $_5B$, $_9F$, $_{11}Na$, $_{13}Al$ and $_{15}P$ which also emit protons having ranges of over 28 cm. The interaction of α-particles

with the nuclei $_{12}$Mg, $_{16}$S, $_{17}$Cl, $_{18}$Ar, etc. leads to the emission of protons with $R < 28$ cm. Hence, in order to distinguish these protons from the recoil protons, measurements were carried out in a direction perpendicular to that of the incident α-particles. It follows from the momentum diagram of scattering that the recoil protons in this direction must have the lowest energy and thus cannot cause any spurious effects.

Let us analyze in detail the reaction involving the splitting of aluminium nuclei by α-particles:

$$^{27}_{13}\mathrm{Al} + ^{4}_{2}\mathrm{He} \rightarrow ^{30}_{14}\mathrm{Si} + p. \qquad (9.2.3)$$

This reaction was studied in an instrument similar to the one used by Rutherford, the only difference being that the target was an aluminium foil and the protons were registered in a counter (Fig. 288).

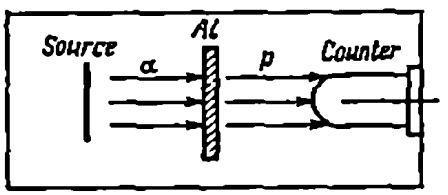

Fig. 288

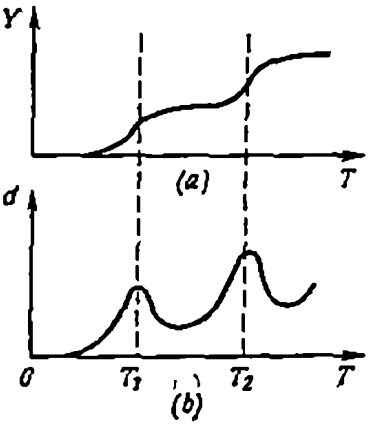

Fig. 289

The thickness of the target (10 μm) was more than the total range of α-particles of the given energy in this material.

In this experiment, protons with a range of 90 cm were detected. Such a long range is explained by the fact that this reaction is exoergic and has $Q = 2.26$ MeV.

Analysis of the yield of the reaction $^{27}_{13}$Al (α, p) $^{30}_{14}$Si showed that depending on the energy of the α-particles, the yield varies as a step function (Fig. 289*a*). According to formula (9.1.19), this means that the reaction cross section (which is proportional to dY/dT) must have the form shown in Fig. 289*b*. The step function indicates that the reaction cross section has a resonance-like dependence on energy.

The origin of resonances in this case is the same as in the above-mentioned reactions involving the interaction of slow neutrons with nuclei (see Sec. 6.4). The existence of a maximum in the cross section means that an α-particle of this energy is captured by one of the quasistationary levels of the compound nucleus.

The resonance nature of variation of cross section of a nuclear reaction upon a change in the kinetic energy of the bombarding particles was first established in (α, p)-reactions involving light nuclei. However, a correct explanation for the mechanism of the emergence of resonances was provided much later (in 1936) by Bohr. This is due to the fact that the level width and level separation for the compound nucleus formed in these reactions differ considerably from the corresponding values for reactions induced by slow neutrons in heavy nuclei ($\Gamma \simeq 1$ keV, $\Delta \simeq 0.1$-1 MeV).

9.2.2. Reactions of the $(\alpha\ n)$ Type

Reactions of this type were discovered in 1932 by Chadwick in an experiment aimed at detecting the neutron. A well-known reaction of this type is the reaction involving the interaction of α-particles with beryllium:

$$^{9}_{4}\mathrm{Be} + {}^{4}_{2}\mathrm{He} \rightarrow {}^{12}_{6}\mathrm{C} + n, \qquad Q = 5.5\ \mathrm{MeV}. \tag{9.2.4}$$

This reaction has an extremely high yield $Y = 2.5 \times 10^{-4}$ for $T_\alpha = 5.44$ MeV, and is used even today as the simplest source of neutrons (see Sec. 6.1).

Unlike reactions of the (α, p) type which, as a rule, give stable products, the (α, n)-reactions are often used for obtaining radioactive isotopes. Irene and Frédérick Joliot-Curie were the first to show (in 1934) that artificial radioactive nuclei can be produced with the help of (α, n)-reactions.

Examples of such reactions are

$$^{4}_{2}\mathrm{He} + {}^{10}_{5}\mathrm{B} \rightarrow {}^{13}_{7}\mathrm{N} + n, \qquad {}^{13}_{7}\mathrm{N} \xrightarrow[10.1\ \mathrm{min}]{\beta^+} {}^{13}_{6}\mathrm{C}, \tag{9.2.5}$$

$$^{4}_{2}\mathrm{He} + {}^{27}_{13}\mathrm{Al} \rightarrow {}^{30}_{15}\mathrm{P} + n, \qquad {}^{30}_{15}\mathrm{P} \xrightarrow[2.55\ \mathrm{min}]{\beta^+} {}^{30}_{14}\mathrm{Si}. \tag{9.2.6}$$

However, a stable nucleus can also be obtained sometimes in an (α, n)-reaction. Such cases are especially important in that these reactions can be easily made to proceed in the reverse direction by using nuclei formed in the forward reaction as targets for the back reaction.

An example of such a reaction is

$$^{4}_{2}\mathrm{He} + {}^{11}_{5}\mathrm{B} \rightarrow {}^{15}_{7}\mathrm{N} \rightarrow {}^{14}_{7}\mathrm{N} + n. \tag{9.2.7}$$

This reaction gives a stable isotope $^{14}_{7}\mathrm{N}$, and has $Q = 0.28$ MeV. The back reaction,

$$n + {}^{14}_{7}\mathrm{N} \rightarrow {}^{15}_{7}\mathrm{N} \rightarrow {}^{11}_{5}\mathrm{B} + {}^{4}_{2}\mathrm{He}, \tag{9.2.8}$$

has $Q = -0.28$ MeV.

Both these reactions involve the same compound nucleus $^{15}_{7}N$ and can be used to determine its energy levels. Moreover, in accordance with *the detailed balancing principle, the position of the energy* levels must be independent of the process direction (forward or backward).

In accordance with formula (5.3.15), the excitation energy of a compound nucleus is given by

$$W = \varepsilon + T',$$

where ε is the binding energy and T' is the relative kinetic energy, i.e. the total kinetic energy of the bombarding particle and the nucleus in the centre-of-mass system. In order to calculate the energy of a level, we must take for T' the resonance energy value corresponding to the highest reaction yield. If the particle energy is taken in the laboratory system of coordinates, formulas for the calculation of energies of the levels of $^{15}_{7}N$ will have the following form for the forward and back reactions:

$$W = \varepsilon_\alpha + 11\ (T_\alpha)_{res}/15, \tag{9.2.9}$$

$$W = \varepsilon_n + 14\ (T_n)_{res}/15. \tag{9.2.10}$$

It was shown both experimentally and theoretically that the value of W_i^{res} calculated by using both these formulas are in the excitation energy range of 12-14 MeV and practically coincide for each level i. The separation between the levels of the compound nucleus is of the order 0.1-1 MeV.

9.3. Reactions Induced by Protons

9.3.1. Types of Proton-induced Reactions

Protons can induce the following nuclear reactions: (p, α), (p, n), (p, p), (p, γ) and, very rarely, (p, d). We shall systematically consider the main characteristics of these reactions.

Reactions of the (p, α) type. These reactions are usually exoergic. Indeed, according to the scheme of a nuclear reaction shown in Fig. 182, the reaction energy $Q = \varepsilon_a - \varepsilon_b$, where ε_a is the binding energy of the incident particle and ε_b is the binding energy of the escaping particle relative to the compound nucleus.

When applied to a reaction of the type (p, α), $Q = \varepsilon_p - \varepsilon_\alpha$. However, $\varepsilon_p \simeq$ const for all β-stable nuclei in the Periodic Table and is equal to about 8 MeV. As regards the binding energy of the α-particle, it can be seen from Table 33 (Sec. 9.2) that it varies from its highest value $\varepsilon_\alpha = 8$ MeV for $Z = 8$ to $\varepsilon_\alpha = 0$ for $Z = 60$, after

which it becomes negative ($\varepsilon_\alpha < 0$) for $Z > 60$ (for α-radioactive nuclei). Hence

$$Q = \varepsilon_p - \varepsilon_\alpha > 0. \tag{9.3.1}$$

The second remark concerning reactions of the type (p, α) pertains to the probability of such reactions. Apparently, it cannot be high for heavy nuclei, since the escape of an α-particle from the nucleus is strongly inhibited by the high Coulomb barrier whose value is 25 MeV for $Z = 80$. This barrier permits only the fastest α-particles to leave the nucleus, and their emission involves a transition of the nucleus to lower (and hence more sparsely arranged) levels. Since the statistical weight of a state is defined by the density of levels, it follows that the probability of reactions of the (p, α) type is quite low.

This condition is not applicable to light nuclei which have a low Coulomb barrier. As examples, we can consider the reactions

$$^{7}_{3}\mathrm{Li}\,(p, \alpha)\,^{4}_{2}\mathrm{He}, \tag{9.3.2}$$

$$^{6}_{3}\mathrm{Li}\,(p, \alpha)\,^{3}_{2}\mathrm{He}. \tag{9.3.3}$$

Reactions of the type (p, α) in light nuclei ($_3$Li, $_5$B and $_9$F) were the first nuclear reactions carried out by Cockroft and Walton in 1932 with the help of protons accelerated artificially to energies of several hundred kiloelectron-volts.

Reactions of the (p, n) type. Such reactions involving stable nuclei are always endoergic with a threshold higher than 0.8 MeV.

In order to prove this, let us represent a (p, n)-reaction in the form

$$p + A \to B + n \tag{9.3.4}$$

and write the following obvious relations:

$$m_n - m_p = 1.3\ \text{MeV}, \tag{9.3.5}$$

$$M_B - M_A > -0.5\ \text{MeV}. \tag{9.3.6}$$

(If the last condition is not satisfied, nucleus A would be transformed into nucleus B through beta decay.) A comparison of these two relations gives

$$|Q| = (M_B + m_n) - (M_A + m_p) > 1.3 - 0.5 = 0.8\ \text{MeV}, \tag{9.3.7}$$

whence, taking into account Eq. (5.3.20), we get

$$T_p^{\min} = \frac{M_A + m_p}{M_A}\,|Q| > 0.8\ \text{MeV}.$$

The threshold of a (p, n)-type reaction is usually 1-3 MeV. A typical example of such a process is the reaction $^{7}_{3}\mathrm{Li}\,(p, n)\,^{7}_{4}\mathrm{Be}$, for which $Q = -1.65$ MeV and $T_{\min} = 1.88$ MeV.

Since the product nucleus in a (p, n)-reaction acquires an additional positive charge, it usually exhibits β^+-radioactivity (or an ability for ε-capture).

Thus, in the example considered above, the radioactive product nucleus ${}^{7}_{4}\mathrm{Be}$ is transformed into ${}^{7}_{3}\mathrm{Li}$ as a result of e-capture with half-life 53.6 days. Another example of this type is the reaction

$$ {}^{11}_{5}\mathrm{B}\ (p, n)\ {}^{11}_{6}\mathrm{C}, \quad Q = -2.76\ \mathrm{MeV}, \tag{9.3.8} $$

resulting in the formation of a positron-active isotope ${}^{11}_{6}\mathrm{C}$ with a half-life of about 20 min.

Reactions of the (p, p) type.[1] The probability of these reactions is comparable with the probability of (p, n)-type reactions if the kinetic energy of the incident protons exceeds the Coulomb barrier height. In the region of low energies, (p, p)-reactions are often used in those cases where a (p, n)-reaction cannot take place, i.e. when the kinetic energy of the incident protons is lower than the threshold value for (p, n)-reaction.

Reactions of the (p, γ) type. Since the probability of emission of particles by a compound nucleus is usually much higher than the probability of emission of a γ-quantum, the reactions of the (p, γ) type have normally very low yields. However, if for some reasons the emission of a particle is not possible or is severely impeded, (p, γ)-type reactions acquire a special significance. For example, if $T_p < T_{\min}$ for a (p, n)-reaction, a (p, γ)-reaction may be observed besides the (p, p)-reaction.

One interesting example of a (p, γ)-reaction with a high yield is the reaction ${}^{7}_{3}\mathrm{Li}\ (p, \gamma)\ {}^{8}_{4}\mathrm{Be}$ (see Sec. 9.3.2). Other examples of reactions accompanied by the emission of γ-quanta were encountered while considering the processes of radiative capture of slow neutrons, where $\Gamma_\gamma \gg \Gamma_n$ (Γ_p, Γ_α).

Reactions of the (p, d) type. These reactions are observed very rarely in comparison to the other reactions, since a deuteron is a weakly bound nucleus ($\varepsilon_d = 2.22$ MeV), and a large amount of energy is required for its formation. Hence, as a rule, a (p, d)-reaction must be endoergic or must have a small positive value of Q. One such reaction is ${}^{9}_{4}\mathrm{Be}\ (p, d)\ {}^{8}_{4}\mathrm{Be}$, for which $Q = 0.56$ MeV.

9.3.2. Reactions of Protons with Lithium

All the above-mentioned reactions are encountered when protons interact with lithium:

$$
\begin{aligned}
&1.\ p + {}^{7}_{3}\mathrm{Li} \to {}^{8*}_{4}\mathrm{Be} \to {}^{4}_{2}\mathrm{He} + {}^{4}_{2}\mathrm{He}, && Q = 17.35\ \mathrm{MeV},\\
&2.\ p + {}^{7}_{3}\mathrm{Li} \to {}^{8*}_{4}\mathrm{Be} \to {}^{8}_{4}\mathrm{Be} + \gamma. && Q = 17.25\ \mathrm{MeV},\\
&3.\ p + {}^{7}_{3}\mathrm{Li} \to {}^{8*}_{4}\mathrm{Be} \to {}^{7}_{4}\mathrm{Be} + n, && Q = -1.65\ \mathrm{MeV},\\
&4.\ p + {}^{7}_{3}\mathrm{Li} \to {}^{8*}_{4}\mathrm{Be} \to {}^{6}_{3}\mathrm{Li} + d, && Q = -5.05\ \mathrm{MeV},\\
&5.\ p + {}^{7}_{3}\mathrm{Li} \to {}^{8*}_{4}\mathrm{Be} \to {}^{7}_{3}\mathrm{Li} + p.
\end{aligned}
\tag{9.3.9}
$$

[1] Elastic and inelastic scattering.

In order to simplify the investigation of these nuclear reactions, we can choose a proton energy $T_p < T_{min}$ for which reactions 3 and 4 cannot occur. This leaves us with reactions 1, 2 and 5 only. Further isolation of reactions is made possible by appropriately choosing the method of detecting the reaction products.

Reaction 1 was studied with the help of two ionization chambers which could register the two α-particles formed as a result of disintegration of the excited nucleus ${}^{8*}_{4}Be$. The thickness of the lithium target was selected in such a way that it was large enough for completely stopping the incident protons and at the same time allowed α-particles to escape from the depth of the target.

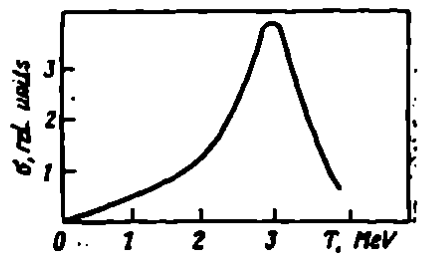

Fig. 290

The measurement of the excitation function for the reaction ${}^{7}_{3}Li(p, \alpha){}^{4}_{2}He$ showed that the cross section of this reaction increases rapidly and monotonically with energy, having a wide maximum (of about 1 MeV thickness) at the kinetic energy $T_p = 3$ MeV of the incident protons (Fig. 290).

The same result is obtained by comparing the kinetic energy of α-particles formed in the reaction ($T_\alpha > 8.65$ MeV) with the height of the Coulomb barrier for an α-particle in the field of the other α-particle (4 MeV). The fact that the energy of the α-particle is more than twice the height of the Coulomb barrier indicates an extremely high probability of decay of the excited compound nucleus ${}^{8*}_{4}Be$ into two α-particles ($\tau \simeq 10^{-21}$ s) and hence a very large level width of the corresponding energy state (several hundred kiloelectron-volts).[1]

It was mentioned above that under normal conditions, a nucleus has a much higher probability of emitting particles than γ-quanta. Hence it would appear that the high yield of a reaction of the (p, α) type should point towards an extremely low probability of a reaction of the type (p, γ). However, it was shown experimentally that the reaction (p, α) is accompanied by a (p, γ)-reaction with a high yield. Moreover, another astonishing fact is that the excitation function for the latter reaction has a strongly resonant nature. The cross section of the (p, γ)-reaction has a very narrow resonance at an energy of 440 keV (Fig. 291).

It would appear that a comparison of the results of investigation of the reactions 1 and 2 should lead to a contradiction: the same

[1] The process ${}^{8}_{4}Be \rightarrow {}^{4}_{2}He + {}^{4}_{2}He$ is possible not only for the excited state, but also for the ground state of the nucleus ${}^{8}_{4}Be$ whose mass exceeds the mass of two α-particles by 0.095 MeV. This process also occurs very quickly ($\tau \simeq 10^{-16}$ s) on account of a low height of the Coulomb barrier.

compound nucleus $^{8}_{4}$*Be behaves in the same excitation energy region as a system with a very broad level and as a system with a sharp resonance.

This seeming discrepancy is explained by the fact that actually different states $(^{8}_{4}\text{*Be})_{I}$ and $(^{8}_{4}\text{*Be})_{II}$ of the compound nucleus are formed in reactions 1 and 2. These states differ in their angular momenta and probably in the signs of the parities of their wave-functions. For even values of the angular momentum I and a positive parity ($P > 0$), the excited state $^{8}_{4}$*Be may disintegrate into two α-particles. This decay is forbidden for other values of I and P, although the corresponding state may turn out to be sufficiently short-lived for a gamma transition into the ground state:

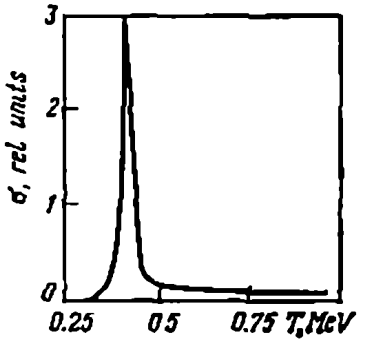

Fig. 291

$$p + {}^{7}_{3}\text{Li} \rightarrow \begin{cases} (^{8}_{4}\text{*Be})_{I} \rightarrow 2\alpha, \\ (^{8}_{4}\text{*Be})_{II} \rightarrow {}^{8}_{4}\text{Be} + \gamma. \end{cases} \quad (9.3.10)$$

Let us consider this question in detail. For the sake of simplicity of presentation, we shall make some most plausible assumptions.

While considering the law of parity conservation (see Sec. 5.5), we have shown that the parity of a system $A + a$ is defined by the product of the intrinsic parities of particles A and a, and the orbital quantum number l characterizing the relative motion of these particles:

$$P_{A+a} = P_A P_a (-1)^l. \quad (9.3.11)$$

The intrinsic parity of the proton is positive ($P_a = 1$). We shall assume the intrinsic parity of the $^{7}_{3}$Li nucleus to be negative ($P_A = -1$), since in accordance with the nuclear shell model, three nucleons of this nucleus are in the p-state. Thus, when a proton with an even l is captured by the $^{7}_{3}$Li nucleus, the compound nucleus $^{8}_{4}$*Be will be in an odd state, while the capture of a proton with an odd l will leave the compound nucleus in an even state. For each state, several values of the angular momentum are possible. These values can be obtained by adding three quantum-mechanical vectors, viz. the nuclear spin (3/2), the proton spin (1/2), and the orbital angular momentum l. The results of addition under two simplest assumption concerning the possible values of l for the proton ($l = 0$ and $l = 1$) are presented in Table 34.

It is not difficult to find the states responsible for the (p, α)-reaction and the states responsible for the (p, γ)-reaction. According to the law of parity conservation, the parity of the compound nucleus $^{8}_{4}$*Be before its disintegration into two α-particles must be the same

Table 34

l	I	$P = P_A P_a (-1)^l$
0	$3/2+1,2+0 = \begin{cases} 2 \\ 1 \end{cases}$	$-1\times1\times(-1)^0 = -1$
1	$3/2+1,2+1 = \begin{cases} 3 \\ 2 \\ 1 \\ 0 \end{cases}$	$-1\times1\times(-1)^1 = +1$

as the parity of the final state (two α-particles). However, the parity of a system consisting of two α-particles is positive, since the operation of reflection for them is equivalent to transposition, which does not change the sign of the wave-function for bosons.

Since $P_{2\alpha} = P_\alpha^2 (-1)^l = +1$, l is even, and since the spin of α-particles is equal to zero, l coincides with the spin of the disintegrating nucleus ${}^{8}_{4}$Be. Thus, α-particles can be emitted from the states 2^+ and 0^+.

Similarly, by using the laws of conservation of angular momentum and parity, we can show that out of the six states of ${}^{8}_{4}$Be mentioned above (0^+, 1^+, 2^+, 3^+, 1^-, 2^-), only two states, viz. 1^- and 1^+, are probably responsible for the gamma transition to the ground state. This follows from the characteristics of the ground state (0^+), as well as a high yield of γ-quanta which, in accordance with Sec. 3.4.1, probably points towards dipole gamma transitions ($E1$ and $M1$).

Thus, a decay into two α-particles can occur from the excited state ${}^{8}_{4}$Be with some values of angular momentum and parity (0^+ and 2^+), while the gamma transition takes place with other values (1^- or 1^+). Hence the above-mentioned difference in the behaviour of the excitation functions for reactions 1 and 2 is a natural consequence of the validity of the law of parity and angular momentum conservation in strong and electromagnetic interactions.

We would like to draw the reader's attention to the fact that the results obtained above are ambiguous and depend on the assumptions on which the presentation is based [$P({}^{7}_{3}\mathrm{Li}) = -1$, $l_p = 0$ or 1, dipole radiation, gamma transition to the ground state]. If even one of these assumptions is not valid, the results change. It is obvious that additional information is necessary for obtaining unambiguous and correct results. This information can be obtained by considering the angular distribution of α-particles and gamma radiation, a comparison of the parameters of all known levels of ${}^{8}_{4}$Be, etc. Apparently, it can be assumed at present that the decay into two α-particles takes place from the broad 2^+ level at an excitation energy $E^* =$

19.9 MeV, while gamma radiation is caused by the narrow 1^+ level at $E^* = 17.64$ MeV. Both these states are formed as a result of the capture of a proton with $l = 1$ by the nucleus. Besides these levels, more than ten other levels have been identified in the nucleus ${}^{8}_{4}\mathrm{Be}$.

9.3.3. The Reaction ${}^{14}_{6}\mathrm{C}(p, n){}^{14}_{7}\mathrm{N}$ and the Proof of Formation of a Compound Nucleus

Another important example of proton-induced reactions is the (p, n)-reaction in carbon isotope ${}^{14}_{6}\mathrm{C}$, i.e.

$$p + {}^{14}_{6}\mathrm{C} \rightarrow {}^{14}_{7}\mathrm{N} + n, \qquad Q = -0.62 \text{ MeV}. \qquad (9.3.12)$$

This isotope of carbon is β^--active. However, in view of a long half-life, which is equal to about 5.73×10^3 years, it can be used as a target.

This reaction is remarkable in that it leads to the formation of the same compound nucleus (${}^{15}_{7}\mathrm{N}$) which, as was shown in Sec. 9.2.2, is formed in the reaction ${}^{11}_{5}\mathrm{B}(\alpha, n){}^{14}_{7}\mathrm{N}$. We can thus compare the energy levels of the nucleus ${}^{15}_{7}\mathrm{N}$ formed in different reactions. If such a comparison shows that the level structure of the compound nucleus *is independent of the method of its formation, i.e. if the compound* nucleus ${}^{15}_{7}\mathrm{N}$ formed in *different* reactions is found to have the same energy levels, it will be proved that the compound nucleus is a physical reality.

The (p, n)-reaction for ${}^{14}_{6}\mathrm{C}$ was studied with the help of a Van de Graaff generator capable of producing monoenergetic protons. These protons were used to irradiate a thin carbon target, and the neutrons formed as a result of this reaction were registered by BF_3 counters. For certain energies $(T_p)_{\mathrm{res}}$ of the incident protons, an increase in the yield of neutrons was observed, indicating the resonance nature of the variation of the reaction cross section. Using the resonance values of the proton energy and the relation

$$W = \varepsilon_p + 14\,(T_p)_{\mathrm{res}}/15, \qquad (9.3.13)$$

we can calculate the energy $W_i^{\mathrm{res}}(p, n)$ of the corresponding level of the excited compound nucleus ${}^{15}_{7}\mathrm{N}$.

Similar investigations were carried out for the back reaction

$${}^{14}_{7}\mathrm{N} + n \rightarrow {}^{15}_{7}\mathrm{N} \rightarrow {}^{14}_{6}\mathrm{C} + p. \qquad (9.3.14)$$

In this case, the energy of the compound nucleus level is calculated from the formula[3]

$$W_i^{\mathrm{res}}(n, p) = \varepsilon_n + 14\,(T_n^{\mathrm{res}})_i/15. \qquad (9.3.15)$$

[3] T_n^{res} was *determined from an increase in the yield of protons. Monoenergetic* neutrons with variable energy were obtained from the reaction $p + {}^{7}_{3}\mathrm{Li} \rightarrow n + {}^{7}_{4}\mathrm{Be}$, for which the protons were accelerated in a Van de Graaff generator.

Moreover, it was found that $W_i^{res}(p, n) \simeq W_i^{res}(n, p)$ and that their average values coincide with the average values of W_i^{res} for (α, n)- and (n, α)-reactions considered in Sec. 9.2.2. It follows from here that the levels of the compound nucleus $^{15}_{7}N$ calculated from *different* reactions coincide. This confirms Bohr's concept that a nuclear reaction occurs in two stages.

It should be observed that we can assume only the coincidence of levels obtained in different reactions (9.2.7) and (9.3.12) as proved. The coincidence of levels in forward and back reactions is a consequence of the detailed balancing principle, and should be valid even in the cases where no compound nucleus is formed.

Bohr's concept of a nuclear reaction is also confirmed by an analogy between the excitation functions and the spectra of particles emitted by the same compound nucleus formed in different reactions, the Maxwellian energy spectrum of the escaping particles (spectrum of "evaporation" of particles from the excited compound nucleus), the symmetry of the angular distribution of reaction products relative to a plane perpendicular to the momentum of the incident particle in the centre-of-mass system.

9.3.4. Formation and Decay of the Compound Nucleus $^{64}_{30}Zn$ in Reactions $p + ^{63}_{29}Cu$ and $\alpha + ^{60}_{28}Ni$

The most convincing evidence of the correctness of Bohr's concept concerning the compound nucleus was obtained in 1950 in experiments conducted by Ghoshal.[4] In these experiments, the excitation functions of three pairs of reactions which can occur through the formation of the same compound nucleus were compared:

$$\alpha + {}^{60}Ni \to {}^{64}Zn \to \begin{cases} {}^{63}Zn + n \\ {}^{62}Zn + 2n \\ {}^{62}Cu + p + n, \end{cases} \tag{9.3.16}$$

$$p + {}^{63}Cu \to {}^{64}Zn \to \begin{cases} {}^{63}Zn + n \\ {}^{62}Zn + 2n \\ {}^{62}Cu + p + n. \end{cases} \tag{9.3.17}$$

If all these reactions occur with the formation of the same compound nucleus, then in accordance with formula (6.4.23) the cross section of each reaction in (9.3.16) must be

$$\sigma_i = \sigma_i^* \frac{\Gamma_i}{\Gamma}, \tag{9.3.18}$$

[4] S.N. Ghoshal, *Phys. Rev.*, 80, 930 (1950).

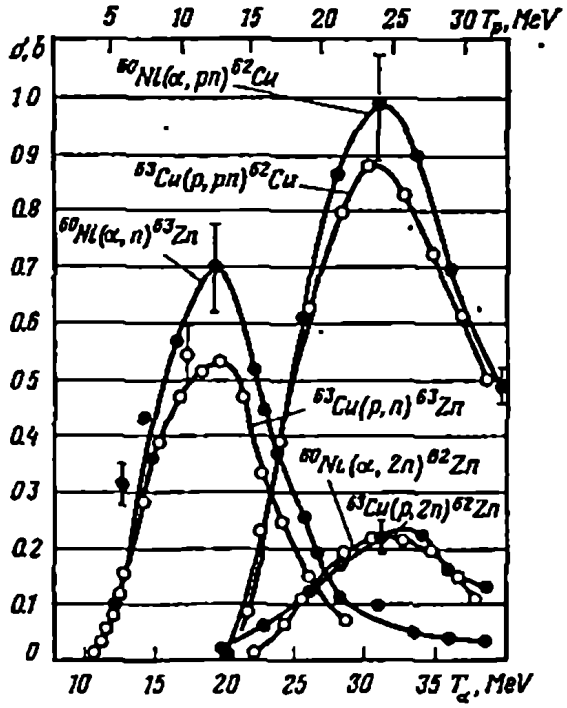

Fig. 292

while for reactions in (9.3.17), the cross section must be

$$\sigma_i' = \sigma_2^* \frac{\Gamma_i}{\Gamma}. \tag{9.3.19}$$

Here, σ_1^* and σ_2^* are the cross sections of formation of the compound nucleus ^{64}Zn in the processes involving the capture of an α-particle by the nucleus ^{60}Ni and of a proton by the nucleus ^{63}Cu respectively, Γ_i is the partial width of decay of the compound nucleus through *the ith channel, and* $\Gamma = \sum \Gamma_i$ *is the total width.*

Comparing (9.3.18) and (9.3.19) for identical excitation energies of the compound nucleus, we obtain $\sigma_i/\sigma_i' = \sigma_1^*/\sigma_2^*$, i.e.

$$\frac{\sigma(\alpha + {}^{60}\mathrm{Ni} \to {}^{63}\mathrm{Zn} + n)}{\sigma(p + {}^{63}\mathrm{Cu} \to {}^{63}\mathrm{Zn} + n)} = \frac{\sigma(\alpha + {}^{60}\mathrm{Ni} \to {}^{62}\mathrm{Zn} + 2n)}{\sigma(p + {}^{63}\mathrm{Cu} \to {}^{62}\mathrm{Zn} + 2n)}$$
$$= \frac{\sigma(\alpha + {}^{60}\mathrm{Ni} \to {}^{62}\mathrm{Cu} + p + n)}{\sigma(p + {}^{63}\mathrm{Cu} \to {}^{62}\mathrm{Cu} + p + n)}. \tag{9.3.20}$$

The results of Ghoshal's experiments are shown in Fig. 292. It can be seen that within the limits of experimental errors, these results correspond to relation (9.3.20).

The general form of the excitation function for a reaction involving the formation of a compound nucleus is shown in Fig. 293. The increase in the cross section sets in at $T = 0$ for $Q > 0$ (Fig. 293*a*) or at $T = T_{min}$ for $Q < 0$ (Fig. 293*b*), and continues up to $T \approx B_C$. This increase can be monotonic or of the resonance type. At $T \simeq B_C$ (if we consider an interaction with $l = 0$), the cross section stops increasing and attains a maximum value. Upon a further increase in the kinetic energy, the cross section of a particular reaction starts to decrease. This happens because at large excitation energies of the compound nucleus, new competitive modes of decay come into play and decrease the relative probability of decay through a particular channel (since the overall cross section for all channels remains equal to about πR^2 as before).

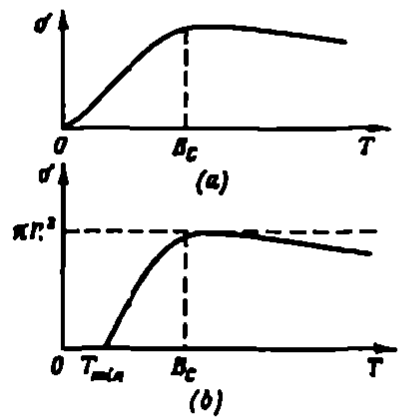

Fig. 293

9.4. A Brief Resumé of Chapter 9

In this chapter, we have considered nuclear reactions induced by light charged particles. The specific features of these reactions are associated with the presence of an electric charge.

One of these features involves the Coulomb interactions of charged particles with the nucleus. The strength of the Coulomb interaction for a given energy T is determined by the height of the Coulomb barrier (in MeV):

$$B_C = Zze^2/R \simeq ZzA^{-1/3},$$

where R, Z and A are the radius, atomic number and mass number of the nucleus respectively, and z is the charge of the particle.

For $T < B_C$, the charged particle enters the nucleus as a result of tunneling, whose probability for $l = 0$ is determined by the penetrability of the Coulomb potential barrier

$$D \simeq \exp\left(-\frac{2}{\hbar}\int_R^{r_T} \sqrt{2\mu(V_C - T)}\, dr\right).$$

where μ is the reduced mass, T is the kinetic energy, and $r_T = Zze^2/T$.

For $l \neq 0$, we must take into account the centrifugal barrier

$$V_c = \hbar^2 l(l+1)/2mr^2,$$

whose height is equal to

$$B_c = \hbar^2 l(l+1)/2mR^2.$$

Usually, $B_c \ll B_C$. Hence for $T < B_c + B_C$, the probabilities of interaction of a charged particle with the nucleus for $l=0, 1, 2, \ldots, l_0$ ($l_0 = \sqrt{R/2\lambda_{B_C}}$) are found to be comparable.

The second feature of nuclear reactions induced by charged particles (having an energy of about 10 MeV) is associated with strong ionization losses suffered by these particles, as a result of which most of these particles lose their kinetic energy without undergoing any nuclear interaction.

A small fraction ν/N_0 of particles undergoing a nuclear interaction is called the yield of a nuclear reaction:

$$Y(T) = \frac{\nu}{N_0} = n \int_0^T \frac{\sigma(T)\, dT}{\left| \frac{dT}{dx} \right|},$$

where $\sigma(T)$ is the reaction cross section, and dT/dx is the rate of the ionization loss of kinetic energy of the particle in a given medium (specific ionization). Charged particles are responsible for the reactions (α, p), (α, n), (p, α), (p, n), (p, p), (p, γ), (p, d), and some other reactions The most interesting among these reactions are the (α, p)-, (α, n)-, (p, α)- and (p, n)-reactions.

Historically, the reaction (α, p) for nitrogen,

$$^4_2\mathrm{He} + {}^{14}_7\mathrm{N} \rightarrow {}^{17}_8\mathrm{O} + p,$$

was the first nuclear reaction observed (Rutherford, 1919). In this reaction as well as in similar (α, p)-reactions, it was shown for the first time that protons are the constituents of all nuclei Besides, the resonance nature of the variation of cross section of nuclear reactions was first observed in an (α, p)-reaction.

Reactions of the (α, n) type were first observed by Chadwick (discovery of the neutron, 1932). Such reactions are used for obtaining neutrons and radioactive isotopes.

Cockroft and Walton (1932) were the first to observe a (p, α)-type reaction induced by artificially accelerated protons

The (p, n)-type reactions involving stable nuclei have $Q < 0$. Another feature of these reactions is that, as a rule, they lead to the formation of radioactive (β^+-decay or e-capture) nuclei.

An analysis of (p, α)- and (p, γ)-reactions between protons and lithium nuclei demonstrates the role of parity and angular momentum conservation laws in nuclear reactions. Depending on the orbital angular momentum for the interaction of a proton with lithium, the compound nuclei have different parities and angular momenta and decay according to different schemes.

A comparison of the levels of the compound nucleus $^{15}_7N$ formed in different reactions [$^{14}_6C(p, n)^{14}_7N$ and $^{11}_5B(\alpha, n)^{14}_7N$] proves the correctness of Bohr's concept about nuclear reactions taking place through an intermediate stage in which a compound nucleus is formed. The most convincing evidence of the correctness of Bohr's concept was obtained in experiments on the comparison of excitation functions for three pairs of reactions involving $^{64}_{30}Zn$ as the compound nucleus.

Chapter 10

Direct Interaction Reactions

10.1. General Properties of Direct Interaction Processes

It is well known that not all experimentally observed reactions can be explained with the help of Bohr's mechanism of the formation and decay of a compound nucleus.

Investigations of the yield, energy spectrum and angular distribution of the products of certain nuclear reactions led to results which are in contradiction to Bohr's concept. For example, the angular distribution corresponding to the inelastic scattering of fast neutrons by lead reveals an asymmetry in the forward direction (in the centre-of-mass system), which cannot be explained by the formation of a compound nucleus. Similar results were also obtained for reactions involving heavy ions. In these cases, the energy spectrum of the emitted particles is not Maxwellian (as it should be if Bohr's concept were true) and contains an excess of fast particles.

From the point of view of Bohr's mechanism, many deuteron-induced reactions proceed in a very unusual way, and this mechanism fails to explain the form of the excitation function or angular distribution of the escaping particles.

Quite interesting results were obtained from a comparison of the reactions $^{14}_{7}N(n, \alpha)^{11}_{5}B$ and $^{14}_{7}N(n, p)^{14}_{6}C$. It was shown in Sec. 9.3 that both these reactions involve the formation of the same compound nucleus $^{15}_{7}N$, i.e. proceed in accordance with Bohr's mechanism. However, a detailed analysis of these reactions at neutron energies of 2-4 MeV showed that the yield of the first reaction is 30 times higher than that of the second reaction. This result is in contradiction to Bohr's mechanism according to which nucleons should have the highest probability of being emitted from an excited nucleus. This means that the reactions considered above can proceed not only through the formation of a compound nucleus, but also in some other way.

To explain all these features of nuclear reactions, another mechanism called *direct nuclear interaction* was proposed. The process is termed direct because in these reactions a transition from the initial to the final state of the nucleus occurs *directly*, without the formation of any compound nucleus in the intermediate stage.

According to this mechanism, the interaction of a fast nucleon with a nucleus should be treated as a fast ($\tau_{int} \simeq 10^{-22}$ s) two-

Usually, $B_c \ll B_C$. Hence for $T < B_c + B_C$, the probabilities of interaction of a charged particle with the nucleus for $l=0, 1, 2, \ldots, l_0$ ($l_0 = \sqrt{R/2\lambda_{B_C}}$) are found to be comparable.

The second feature of nuclear reactions induced by charged particles (having an energy of about 10 MeV) is associated with strong ionization losses suffered by these particles, as a result of which most of these particles lose their kinetic energy without undergoing any nuclear interaction.

A small fraction ν/N_0 of particles undergoing a nuclear interaction is called the yield of a nuclear reaction:

$$Y(T) = \frac{\nu}{N_0} = n \int_0^T \frac{\sigma(T)\, dT}{\left| \frac{dT}{dx} \right|},$$

where $\sigma(T)$ is the reaction cross section, and dT/dx is the rate of the ionization loss of kinetic energy of the particle in a given medium (specific ionization). Charged particles are responsible for the reactions (α, p), (α, n), (p, α), (p, n), (p, p), (p, γ), (p, d), and some other reactions The most interesting among these reactions are the (α, p)-, (α, n)-, (p, α)- and (p, n)-reactions.

Historically, the reaction (α, p) for nitrogen,

$$^4_2\mathrm{He} + {}^{14}_7\mathrm{N} \rightarrow {}^{17}_8\mathrm{O} + p,$$

was the first nuclear reaction observed (Rutherford, 1919). In this reaction as well as in similar (α, p)-reactions, it was shown for the first time that protons are the constituents of all nuclei Besides, the resonance nature of the variation of cross section of nuclear reactions was first observed in an (α, p)-reaction.

Reactions of the (α, n) type were first observed by Chadwick (discovery of the neutron, 1932) Such reactions are used for obtaining neutrons and radioactive isotopes

Cockroft and Walton (1932) were the first to observe a (p, α)-type reaction induced by artificially accelerated protons.

The (p, n)-type reactions involving stable nuclei have $Q < 0$. Another feature of these reactions is that, as a rule, they lead to the formation of radioactive (β^+-decay or e-capture) nuclei.

An analysis of (p, α)- and (p, γ)-reactions between protons and lithium nuclei demonstrates the role of parity and angular momentum conservation laws in nuclear reactions. Depending on the orbital angular momentum for the interaction of a proton with lithium, the compound nuclei have different parities and angular momenta and decay according to different schemes.

A comparison of the levels of the compound nucleus $^{14}_7$N formed in different reactions [$^{13}_6$C$(p, n)^{13}_7$N and $^{11}_5$B$(\alpha, n)^{14}_7$N] proves the correctness of Bohr's concept about nuclear reactions taking place through an intermediate stage in which a compound nucleus is formed. The most convincing evidence of the correctness of Bohr's concept was obtained in experiments on the comparison of excitation functions for three pairs of reactions involving $^{64}_{30}$Zn as the compound nucleus

strips. In recent years, the two-dimensional (dE-E) analysis has been used for identifying the product nuclei.

A comparison of transfer reactions occurring at various energies shows that the complexity of transfer reactions increases with energy, i.e. the cross section of reactions involving the transfer of 3-5 nucleons increases (for example, the bombardment by $^{16}_{8}O$ ions leads to the formation of $^{13}_{7}N$ and $^{11}_{6}C$).

This is probably due to the fact that at high energies, interactions involving large[3] angular momenta l associated with strong centrifugal forces start playing a significant role. These forces impede a combining of both nuclei into a single system, but allow boundary collisions.

Investigation of direct interaction reactions is very important from the point of view of nuclear spectroscopy, since a direct transition from the initial to the final state of a nucleus (without the formation of a compound nucleus) simplifies the problem of determining the parameters of one of these from known parameters of the other (there is no need to take into account the characteristics of the excited compound nucleus).

A detailed description of this interesting field of investigation is beyond the scope of this book. We shall confine ourselves to an analysis of simple but quite instructive transfer processes like the partial penetration of a deuteron into a nucleus and the reactions involving the stripping of nucleons (from deuteron), deuterons, tritons and α-particles (from ^{6}Li and ^{7}Li nuclei). Besides, we shall consider in the next chapter some direct processes induced by heavy ions. The direct process induced by γ-quanta (direct proton emission) will be considered in Sec. 12.2.

10.2. Process of Partial Penetration of a Deuteron into a Nucleus

The diverse mechanisms of nuclear reactions (the formation of a compound nucleus or a direct interaction) can be clearly illustrated by considering deuteron-induced nuclear reactions.

The nature of deuteron-induced nuclear reactions depends to a considerable extent on the properties of the deuteron. The deuteron is a very weakly bound nucleus [$\Delta W(d) = 2.22$ MeV] consisting of a proton and a neutron separated by a fairly large distance (about 4×10^{-13} cm). The low binding energy of the deuteron leads to a high excitation energy of the compound nucleus formed as a result of deuteron capture. Indeed, the binding energy ε_d of the deuteron

[3] It can be easily seen that for heavy ions with an energy of about 100 MeV, the orbital quantum number may be several tens of units.

relative to the compound nucleus is given by

$$\varepsilon_d = \{M_d + M(A-2, Z-1) - M(A, Z)\}c^2 = \Delta W(A, Z) - \Delta W(A-2, Z-1) - \Delta W_d \quad (10.2.1)$$

or

$$\varepsilon_d \simeq [8A - (A-2)\,8 - 2.22] \simeq 14 \text{ MeV}.$$

The excitation energy of the compound nucleus is $W = \varepsilon_d + T'_d = 14 + T'_d$, i.e. considerably exceeds the average separation energy of a nucleon ($\bar{\varepsilon}_p \simeq \bar{\varepsilon}_n \simeq 8$ MeV for all nuclei), as well as the separation energy of an α-particle ($\bar{\varepsilon}_\alpha \simeq 8$ MeV for light nuclei and $\varepsilon_\alpha < 0$ for heavy nuclei). Consequently, all deuteron-induced reactions (d, p), (d, n), (d, α) have $Q > 0$ and a high yield if they involve the capture of the deuteron at the first stage of the reaction.

The most familiar examples of deuteron-induced reactions are

$${}^2_1\mathrm{H} + {}^2_1\mathrm{H} \rightarrow \begin{cases} {}^3_2\mathrm{He} + n, & Q = 3.25 \text{ MeV}, \\ {}^3_1\mathrm{H} + p, & Q = 4.03 \text{ MeV}, \end{cases} \quad (10.2.2)$$

and

$${}^2_1\mathrm{H} + {}^3_1\mathrm{H} \rightarrow {}^4_2\mathrm{He} + n, \qquad Q = 17.6 \text{ MeV}. \quad (10.2.3)$$

Deuteron-induced reactions can be used for obtaining artificial radioactive isotopes. Examples of such reactions are

$${}^{10}_5\mathrm{B}(d, n){}^{11}_6\mathrm{C}, \quad {}^{11}_6\mathrm{C} \xrightarrow[20.4\,\mathrm{min}]{\beta^+} {}^{11}_5\mathrm{B}, \quad (10.2.4)$$

$${}^{31}_{15}\mathrm{P}(d, p){}^{32}_{15}\mathrm{P}, \quad {}^{32}_{15}\mathrm{P} \xrightarrow[14.3\,\mathrm{days}]{\beta^-} {}^{32}_{16}\mathrm{S}. \quad (10.2.5)$$

A thorough investigation of the deuteron-induced reactions showed that, as expected, all the reactions [(d, p), (d, n) and (d, α)] involving nuclei with $Z < 60$ have indeed high yields. However, a detailed analysis of the reaction yields for (d, p)- and (d, n)-reactions led to an unexpected result. It was found that the ratio of the reaction yields $Y(d, p)/Y(d, n)$ for nuclei with $Z < 60$ is roughly equal to unity if the kinetic energy of the incident deuterons is less than the barrier height, while for nuclei with $Z > 60$, this ratio becomes equal to 4-5. This ratio decreases with increasing deuteron energy. Another astonishing effect is the anisotropy of products in (d, n)- and (d, p)-reactions, which predominantly fly in the forward direction.

These results are in contradiction with the concept of a nuclear reaction occurring through a compound nucleus. Indeed, if the reactions (d, p) and (d, n) involve the formation of a compound nucleus, the yield of the (d, p)-reaction must be less than the yield of the (d, n)-reaction under identical conditions on account of the

existence of a Coulomb barrier which hinders the escape of a proton from the nucleus. As the energy increases, the yield of the (d, p)-reaction, and hence the ratio $Y(d, p)/Y(d, n)$, must increase. The angular distribution of the reaction products must be symmetric relative to the angle $\theta = 90°$, i.e. must have a forward-backward symmetry (in the centre-of-mass system).

To explain these peculiarities, Oppenheimer and Phillips proposed in 1935 the mechanism of *partial penetration of a deuteron into a nucleus*.

Unlike the above-mentioned mechanism in which a nuclear reaction proceeds through the formation of a compound nucleus, a deuteron in an Oppenheimer-Phillips process does not enter an atomic

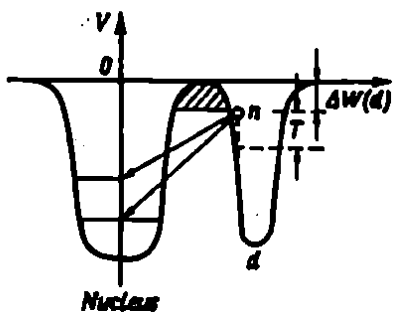

Fig. 295

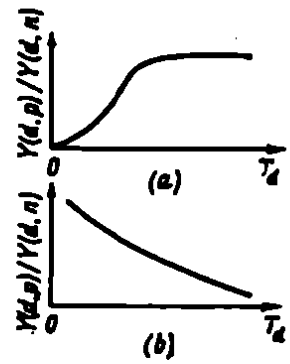

Fig. 296

nucleus, but is rather polarized on approaching it by strong electric forces acting between the nucleus and the proton which is a constituent of the deuteron. If the height of the Coulomb barrier of the nucleus considerably exceeds the binding energy of the deuteron $[B_C > \Delta W(^2_1\mathrm{H})]$, the polarization can be so strong that it leads to the rupture of the deuteron into a neutron and a proton. As a result, one of the nucleons (usually the neutron) is captured by the nucleus while the other flies past the nucleus. Thus, in this mechanism, a reaction of the type (d, p) proceeds in such a way that the proton *does not enter the nucleus at all*. As regards the neutron, it can enter the atomic nucleus only after overcoming a low potential barrier equal to the binding energy $\Delta W(d)$ of the deuteron. In view of the low barrier height, the neutron may enter the nucleus by tunneling (Fig. 295). This results in a high yield of the (d, p)-reaction if it proceeds according to the mechanism of partial penetration of the nucleus by a deuteron.

The anisotropy in the angular distribution of the reaction products is also explained by this mechanism. Since one of the products does not enter the nucleus at all, it naturally flies predominantly in the direction of the incident deuteron.

A deuteron-induced reaction can generally proceed either through the formation of a compound nucleus, or according to the partial penetration mechanism. In some cases it is unknown beforehand as to which of the two courses is followed by a given reaction, or which of the two mechanisms is predominant for it.

A reliable way to determine the predominant mechanism of a reaction is the analysis of the yield curves for the (d, p)- and (d, n)-reactions as functions of the kinetic energy of incident deuterons. If the ratio of the yields of (d, p)- and (d, n)-reactions increases with the kinetic energy (Fig. 296*a*), the nuclear reaction proceeds through the formation of a compound nucleus. If this ratio decreases with increasing kinetic energy of the incident deuterons, the reaction follows the partial penetration mechanism (Fig. 296*b*).

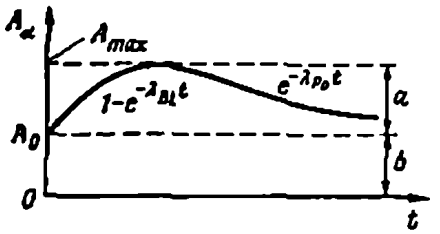

Fig. 297

A classical example is the reaction

$$^{209}_{83}\mathrm{Bi} + {}^{2}_{1}\mathrm{H} \rightarrow \begin{cases} {}^{210}_{84}\mathrm{Po} + n, \\ {}^{210}_{83}\mathrm{Bi} + p, \end{cases} \qquad (10.2.6)$$

which proceeds in two channels. In the first channel, the α-active isotope $^{210}_{84}$Po ($T_{1/2} = 138.4$ days) is formed, while the second channel involves the formation of the β-active $^{210}_{83}$Bi ($T_{1/2} = 5$ days) which is also transformed into $^{210}_{84}$Po after beta decay. Thus, a bismuth target irradiated by deuterons must exhibit alpha and beta radioactivities. Moreover, the alpha activity will first increase from a certain initial value to its maximum value with a half-life of five days, and then decrease with a half-life of 138.4 days (Fig. 297). It can be easily seen that the reaction yields in the two channels are characterized by the segments a and b:

$$Y(d, p)/Y(d, n) = a/b = (A_{max} - A_0)/A_0. \qquad (10.2.7)$$

The experiment was carried out in the following manner. A deuteron beam was used to irradiate a pile of thin bismuth foils, each of which was later tested for alpha activity. Upon successively passing through the foils, the deuterons gradually lost their energy. Hence, the measurement of alpha activity of different foils led to the values of $Y(d, p)/Y(d, n)$ for different kinetic energies of the incident deuterons. The experiment showed that such a curve falls off with the deuteron energy, thereby indicating that the reaction proceeds according to the mechanism of partial penetration.

The shadow effect, discovered simultaneously in 1965 in the USSR (by Tulinov)[3] and abroad, is an original method for determining the mechanism of a nuclear reaction. According to the shadow

[3] A.F. Tulinov, *Uspekhi Fiz. Nauk*, 87, 585 (1965).

effect certain directions are forbidden for the reaction products flying from the lattice sites of a crystal lattice in the direction of its axes (Fig. 298). By placing a photographic plate behind a crystal being irradiated, we can obtain a pattern of shadows characterizing this crystal.

It can be easily seen that the intensity of a shadow pattern depends on the reaction mechanism. Indeed, the formation of shadow according to the above is valid only when the nucleus cannot leave the

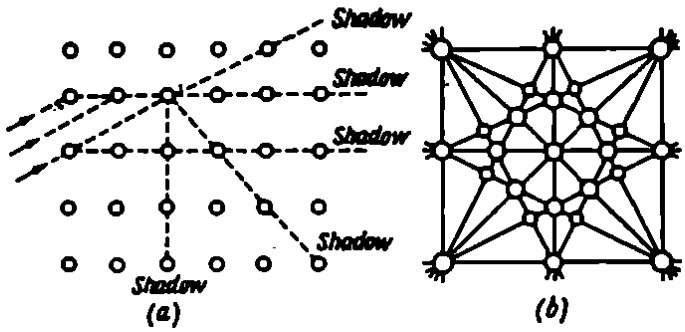

Fig. 298

lattice site (on account of recoil) during the reaction time. This condition is satisfied for fast direct reactions but is invalid if the reaction proceeds according to the mechanism involving the formation of a long-lived compound nucleus. During its lifetime ($\tau \simeq 10^{-15}$-10^{-14} s), the compound nucleus traverses a path $\delta = v\tau$ which considerably exceeds the size of a lattice site (even if we take into account the thermal vibrations). Hence there are no forbidden directions for the reaction products formed as a result of the disintegration of the compound nucleus and no shadows will be formed in this case.

With the help of an appropriate calibration, the shadow effect can be employed for measuring the short lifetimes of nuclei formed in reactions induced by heavy ions (see Chap. 11), as well as for determining the fission time (see Sec. 7.5.5).

10.3. Deuteron Stripping Reactions for $T_d \gg B_C$

The low binding energy and large size of the deuteron also tell on the interaction of deuterons with nuclei at high energies. The calculations are simplified for $T_d \gg B_C$ since the Coulomb interaction of the proton (which is a part of the deuteron) can be neglected.

In 1947, Helmholtz irradiated a Be target with deuterons accelerated in a phasotron to an energy of 190 MeV. He observed beam of neutrons with energy $T_n \simeq T_d/2$ in the direction of motion of

nucleus and as the kinetic energy of the reaction products $[W(^{17}_{8}O) + T'_p]$. If the $^{17}_{8}O$ nucleus is formed in the ground state, $W = 0$, $T'_p = (T'_p)_{max}$ and

$$\varepsilon_n = \Delta W(^{2}_{1}H) - T'_d + (T'_p)_{max}. \qquad (10.4.7)$$

This formula can be used to determine the neutron binding energy from the maximum value of the kinetic energy of protons:

$$\varepsilon_n = 2.2 - 4.0 + 5.9 = 4.1 \text{ MeV}.$$

The latest available value of the neutron binding energy in the ^{17}O nucleus $\varepsilon_n = 4.142$ MeV.

It follows from (10.4.6) that $W + T'_p = \text{const}$, i.e. $dW = -\Delta T'_p$ for a given energy of the deuterons. Hence by measuring the difference in the kinetic energies of the emitted protons, we can determine the difference in the nuclear energy states for the ground state and the first excited state. It follows from the difference $(T'_p)_{max} - T'_p = 0.9$ MeV that the first level of the $^{17}_{8}O$ nucleus is higher than the ground state by 0.9 MeV (see Fig. 301*b*).

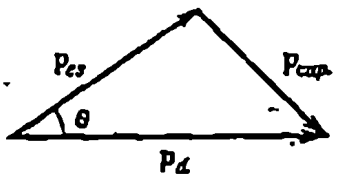

Fig. 302

Similar arguments show that the first level of the $^{17}_{9}F$ nucleus is 0.5 MeV above the ground state of the nucleus since the kinetic energy of the corresponding neutrons in reaction (10.4.2) differs by 0.5 MeV.

Let us now determine the angular momenta and parities of the levels for the formed nucleus $^{17}_{8}O$.

It was shown in 1951 by Butler that for a deuteron with energy $T_d \geqslant B$, where B is the height of the Coulomb barrier, we can use the angular distribution of the escaping (more precisely, passing) protons in the (d, p)-reaction to determine the orbital quantum number l_n of the captured neutron and hence the parity and angular momentum of the corresponding nuclear level (the latter is not always determined uniquely).

Butler's results can be explained qualitatively with the help of the following semiclassical arguments based on the conservation laws and the specific properties of the deuteron.

According to the momentum conservation law, the momentum p_d of the deuteron, the momentum $p_{cap.}$ of the nucleon captured by the nucleus (i.e. the momentum of the neutron in the present case), and the momentum p_{es} of the escaping nucleon (proton in our case) form a momentum triangle (Fig. 302).

In this triangle, the magnitude and direction of p_d are given, while in accordance with (10.4.6), the length of the vector p_{es} (in the centre-of-mass system) is determined from the energy conserv-

ation law (see Sec. 5.3.3 for details). Hence the length of the vector $p_{cap.}$ is determined by the scattering angle θ: the larger the angle, the longer the vector $p_{cap.}$. Angle $\theta = 0$ corresponds to the minimum value

$$p_{cap.}^{min} = |p_d - p_{as}| \neq 0. \quad (10.4.8)$$

The possible scattering angles θ, i.e. the possible values of $p_{cap.}$ are determined from the following two conditions.

1. The value of the transferred momentum $p_{cap.}$ must satisfy the relation

$$p_{cap.}\rho \simeq \hbar l_{cap.} \quad (10.4.9)$$

or

$$p_{cap.} = \hbar l_{cap.}/\rho \geqslant \hbar l_{cap.}/R, \quad (10.4.10)$$

where ρ is the impact parameter ($\rho \leqslant R$), $l_{cap.}$ are the possible values of the orbital quantum number for the captured nucleon defined by the angular momentum and parity conservation laws [see formula (10.4.12)].

2. On account of the specific properties of the deuteron (small intrinsic momentum), its decay usually occurs in such a way that the scattered nucleon flies off at the smallest possible angle θ [see Eq. (10.3.5)] and the captured nucleon imparts the minimum momentum $p_{cap.}$ to the nucleus.

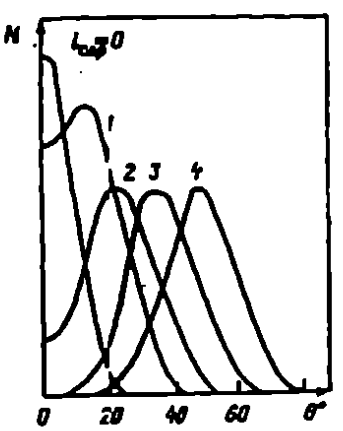

Fig. 303

Normally, both these conditions are satisfied in all cases, except $l_{cap.} = 0$, for $\rho = R$, i.e. for

$$p_{cap.} = \hbar l_{cap.}/R, \quad (10.4.11)$$

and the scattering angle θ is uniquely determined from the value of $p_{cap.}$ i.e. eventually from the value of $l_{cap.}$. When $l_{cap.} = 0$, relation (10.4.9) is satisfied only for $\rho = 0$, i.e. for all possible values of $p_{cap.}$ and θ. However, according to the second condition, the scattering probability for $\theta = 0$ is the highest. Thus, in this case also, $l_{cap.} = 0$ uniquely determines the scattering angle $\theta = 0$.

Summing up, we can state that for $l_{cap.} = 0$ the scattered nucleon predominantly flies off at an angle $\theta = 0$. For $l_{cap.} = 1, 2, 3, \ldots$, the scattering angles will be $\theta_1, \theta_2, \theta_3, \ldots$, where $\theta_1 \neq 0$ and $\theta_1 < \theta_2 < \theta_3 \ldots$ (Fig. 303). If several values of $l_{cap.}$ are possible, the angular distribution of the escaping nucleons will contain several maxima, the highest of these corresponding to the smallest value of θ.

It was mentioned above that the possible values of $l_{cap.}$ are determined by the laws of angular momentum and parity conservation. According to the law of conservation of angular momentum, $l_{cap.}$ must satisfy the condition

$$|I_i + I_f + s_{cap.}|_{max} \geqslant l_{cap} \geqslant |I_i + I_f + s_{cap.}|_{min}, \quad (10.4.12)$$

where I_i and I_f are the spins of the nucleus in the initial and final states, and $s_{cap.}$ is the spin of the captured nucleon. According to the law of parity conservation, all possible values of $l_{cap.}$ must be either odd or even. It can be easily seen that the combined operation of both the conservation laws imposes such stringent restrictions on the choice of $l_{cap.}$ that only a single value of $l_{cap.}$ is often found to be possible.

Let us return to determining the angular momentum and parity of the levels of the $^{17}_{8}O$ nucleus. Measurement of the angular distribution of the protons in reaction (10.4.2) showed that the distribution for protons with the highest energy coincides with the theoretical curve corresponding to the capture of a neutron with $l_{cap.} = l_n = 2$. For protons with a kinetic energy (MeV) $T'_{p1} = (T'_p)_{max} - 0.9$, the experimental angular distribution coincides with the most anisotropic theoretical curve ($l_{cap.} = l_n = 0$). The first case corresponds to the formation of the $^{17}_{8}O$ nucleus in the ground state, while the second case indicates that the nucleus is formed in the first excited state. (The latest available value of $W_1(^{17}_{8}O)$ is 0.871 MeV.)

The total angular momentum I characterizing the ground state can be easily calculated:

$$I(^{17}_{8}O)_{gr} = I(^{16}_{8}O) + s_n + l_n = 0 + 1/2 + 2 = 5/2,\ 3/2.$$

Of the two possible values obtained here for the angular momentum we must choose the value 5/2 for the ground state, since the nucleus $^{17}_{8}O$ lies at the beginning of the shell 1f7/2 (see Sec. 2.3) whose fifteen nucleons are in the state $d_{5/2}$.

The value of the angular momentum for the first excited state of the $^{17}_{8}O$ nucleus is found uniquely. Its value turns out to be

$$I(^{17}_{8}{}^{*}O) = I(^{16}_{8}O) + s_n + l_n = 0 + 1/2 + 0 = 1/2.$$

Both the states have even parity, since all the terms in the expression

$$P(^{17}_{8}O) = P(^{16}_{8}O)P_n(-1)^l = +1\ (+1)\ (-1)^l = +1$$

are even.

Similar results are also obtained for the second reaction which leads to the formation of $^{17}_{9}F$. This should not appear surprising since both the reactions are the result of interaction of particles with similar properties, i.e. a proton and a neutron, with the same nucleus $^{16}_{8}O$.

The example considered here clearly illustrates the possibility of using the stripping reaction for determining the level characteristics for the residual nucleus. It should be emphasized once again that this method can be used for determining the characteristics of energy states of the nucleus below the nucleon binding energy.

Interestingly, such a reaction was used to determine the threshold for the fission of the $^{234}_{92}U$ nucleus by neutrons. We know that $^{238}_{92}U$ undergoes fission only by interacting with fast neutrons and that the fission threshold is about 1 MeV. Fission of $^{235}_{92}U$ is caused by thermal neutrons. From the general consideration of the liquid drop model, it follows that the excitation function for the $^{234}_{92}U$ nucleus must be similar to the function for the $^{238}_{92}U$ nucleus, but its fission threshold should be displaced to the left by a few megaelectron-volts. This is due to a lower height of the fission barrier for the $^{236}_{92}U$ nucleus and a higher neutron binding energy for this nucleus as compared to the corresponding parameters for the $^{238}_{92}U$ nucleus. Thus, it should be expected that the fission threshold for $^{233}_{92}U$ lies in the region of "negative" kinetic energies of the incident neutrons. Deuteron stripping reactions make it possible to irradiate nuclei with such neutrons with "negative" kinetic energies. Experiments on the fission of $^{236}_{92}U$ showed that the threshold of this reaction actually lies in the region of "negative" kinetic energies of neutrons, viz. at an energy of −1.5 MeV.

investigated so far. Reactions involving the transfer of a deuteron, triton or ^{3}He have not been investigated in great details because the cluster nature of these nuclei is not manifested clearly on account of their low binding energy. Hence these reactions cannot be easily identified among other reactions involving the transfer of two or three nucleons. We shall briefly review the experimental results below to reveal the mechanism of α-particle transfer in reactions (^{6}Li, d) and (^{7}Li, t) for lithium ions having an energy higher than 15 MeV.

(a) Correlation of excitation spectra in (^{6}Li, d)- and (^{7}Li, t)-reactions, for example, a similarity between the excitation spectra in the reactions ^{16}O(^{6}Li, d)^{20}Ne and ^{16}O(^{7}Li, t)^{20}Ne for lithium ions having an initial energy of 25-30 MeV. In both reactions, the same levels *corresponding to the following excitation energies were identified:* 0, 1.6, 4.3, 5.8, 7.2, 8.8, 10.3, 12.7 and 15.6 MeV.

(b) Correspondence between the level structures of residual nuclei formed in reactions of the type (^{6}Li, d) and (^{7}Li, t), and the level structure of identical compound nuclei formed during scattering of α-particles. For example, a correspondence was observed between the level structure of the residual nucleus ^{16}O formed in the reaction ^{12}C(^{6}Li, d)^{16}O and of the compound nucleus ^{16}O formed in the scattering process $\alpha + {}^{12}\mathrm{C} \rightarrow {}^{16}\mathrm{O} \rightarrow \alpha + {}^{12}\mathrm{C}$. Such a correspondence points towards a high excitation selectivity of the α-cluster states.

(c) Observance of angular momentum, parity and isospin selection rules for reactions involving the transfer of α-particles. Experimentally, it is manifested in a low excitation probability for levels having quantum numbers that are forbidden by these selection rules (a weak manifestation of these levels is explained by their excitation through the other reaction mechanism).

(d) Specific nature of the angular distribution for direct processes: forward emission and the absence of symmetry about 90°. Significantly, the form of the angular distribution depends on the transferred angular momentum. The general trend is reminiscent of the situation described in Sec. 9.2 for a (d, p) stripping reaction, where the principal maximum is displaced to the right as the transferred angular momentum increases.

It follows from all the experimental facts mentioned above that reactions involving lithium ions having energies higher than 15 MeV have indeed a high probability of direct transfer of an α-particle. Hence these reactions can be used in principle for studying the α-particle excitations in nuclei. However, a quantitative information can be obtained only with the help of the theory of the reaction [1] ...owing a computation of the angular distribution as a function of transferred angular momentum (in the same way as in Butler's theory for the stripping of a nucleon from deuteron). From the clearly manifested effect of the four-nucleon cluster transfer it follows that

four-particle correlations must be taken into account in this theory. For the time being, such a theory has not been developed in its final form. Hence the available experimental data are used for the verification of the α-particle models.

The α-particle model of the nucleus was proposed quite a long time ago in view of the high stability observed for nuclei in which the number of nucleons can be represented by the formula $k(2p+2n)$, where k is an integer. A well-developed α-particle structure was theoretically predicted for the nuclei ^{8}Bo, ^{12}C and ^{16}O. A clear experimental verification of this prediction, however, became possible only by studying reactions involving lithium ions.

A high excitation of several rotational levels of the "molecular" system $^{8}\text{Be} = {}^{4}\text{He} + {}^{4}\text{He}$ was observed in the reaction $^{7}\text{Li}(\alpha, t)^{8}\text{Be}$: 0^+ (ground state), 2^+ (2.9 MeV), and 4^+ (11.3 MeV). A high excitation of several levels of ^{13}C was proved in the reactions $^{9}\text{Be}(^{6}\text{Li}, d)^{13}\text{C}$ and $^{9}\text{Be}(^{7}\text{Li}, t)^{13}\text{C}$. These levels can be attributed to the α-particle levels of ^{12}C.[5] A strongly excited rotational band in the ^{16}O nucleus [0^+ (6.05 MeV), 2^+ (6.52 MeV), 4^+ (10.35 MeV), 6^+ (16.2 MeV)] was observed in the reactions $^{12}\text{C}(^{6}\text{Li}, d)^{16}\text{O}$ and $^{12}\text{C}(^{7}\text{Li}, t)^{16}\text{O}$. A rotational band for the nucleus ^{20}Ne was observed in similar reactions involving ^{16}O.

Rotational levels with quantum numbers 0^+, 2^+, 4^+ and 6^+ were also observed in the next two "α-particle" nuclei ^{24}Mg and ^{28}Si. However, they are not α-particle levels, as can be seen from the low excitation cross section and angular distribution. For nuclei with a mass number $A > 20$, states with excitation energy lower than 10 MeV are not of cluster type but have a shell-type or collective nature. At energies higher than 10 MeV, strong transitions are observed for these nuclei. These transitions may correspond to α-particle states of different types, including rotational states. In heavier nuclei ($A > 40$), formation of α-particle clusters at low excitation energies was not observed.[6]

10.6. A Brief Resumé of Chapter 10

Processes of direct nuclear interaction have been considered in this chapter. The mechanism of direct interaction between two nuclei involves the transfer of one or more nucleons from one interacting nucleus to the other (without a preliminary merging of nuclei, i.e. without the formation of a compound nucleus). In the simplest cases, only one nucleon is transferred (stripping reaction, reaction of partial penetration of the nucleus by a deuteron, pick-up reaction). More complicated reactions involve the transfer of more than one nucleon from one nucleus to the other, as well as a mutual exchange of nucleons between nuclei.

[5] Direct measurements on the ^{12}C nucleus cannot be made due to instability of the ^{8}Be nucleus.

[6] For details of transfer reactions involving lithium ions, see A.A. Ogloblin, *Fiz. Elem. Chast. Atom. Yadra*, 3, 4, 936 (1972).

In the particular case of scattering in the direct interaction mechanism, the bombarding nucleon interacts not with the entire nucleus, but with one or a few nucleons of the target nucleus.

The characteristics of the direct interaction processes (yield, energy spectrum, and angular distribution of products) differ sharply from those of the reactions taking place according to Bohr's mechanism.

One of typical direct interaction processes, viz. a partial penetration of the nucleus by a deuteron, involves the polarization of the deuteron by the Coulomb forces. This is followed by a rupture of the deuteron into a proton and a neutron and a capture of the neutron by the nucleus. Reactions involving a partial penetration of the nucleus by a deuteron are characterized by a decrease in the ratio of the reaction yields $Y(d, p)/Y(d, n)$ with increasing energy, as well as by an angular anisotropy of the reaction products. This feature is associated with the fact that the proton does not enter the nucleus at all, but simply flies past it. The mechanism of partial penetration of the nucleus is usually manifested in interactions of deuterons with heavy nuclei for which a high Coulomb barrier impedes the reaction from proceeding according to Bohr's mechanism.

Another typical reaction involving direct interaction is the stripping reaction which is observed during a noncentral collision of a deuteron with a nucleus. On account of a large separation between the nucleons in the deuteron, they may appear under different conditions: one of them may fall in the range of nuclear forces and get captured by the nucleus, while the other may be out of the range of nuclear forces and hence fly past the nucleus without interacting with it.

Stripping reactions at high deuteron energies are used for producing fast neutrons. It has been shown experimentally and theoretically that this reaction provides a beam of neutrons with energy $T_n \simeq T_d/2$ and a small angle of spread about the direction of initial deuteron beam.

Theoretical analysis of the stripping reaction at an energy $T_d \geqslant B_C$ provides a relation between the experimental characteristics (energy and angular distributions) of the passing nucleons and the energy level parameters of the residual nucleus (energy, angular momentum, parity). Moreover, it is also possible to obtain the characteristics of levels at excitation energies lower than the binding energy of the captured particle.

Specific direct reactions are observed in the interaction of ^{6}Li and ^{7}Li ions with nuclei. Each of these lithium nuclei consists of two weakly bound lighter nuclei or clusters ($^6\text{Li} = {}^4\text{He} + d$ or $^6\text{Li} = {}^3\text{He} + t$, $^7\text{Li} = {}^4\text{He} + t$). In direct interactions, the clusters may be transferred as a whole from one interacting nucleus to the other. The most extensively investigated reactions are the (^{7}Li, t)- and (^{6}Li, d)-reactions involving the transfer of an α-particle. An analysis of these reactions helps investigate many-particle excitation in nuclei of the type "unexcited core + α-particle". These states appear in nuclei at very high excitation energies. Thus, while studying the interaction of nucleons in a nucleus, we must take into account not only pair interaction (and mean field), but also the four-particle correlation.

Chapter II

Nuclear Reactions Induced by Heavy Ions

The development of the techniques for accelerating particles led to the creation of new accelerators and modification of the existing linear accelerators, cyclotrons, phasotrons and synchrophasotrons with a view to accelerate ions of heavy atoms to energies ranging from a few megaelectron-volts to several gigaelectron-volts per nucleon. The first heavy-ion accelerator was developed in the early 1950s in the USA for accelerating nitrogen nuclei. An accelerator of heavy ions (right up to argon) was built in 1960 at Dubna. Another instrument, capable of accelerating xenon ions to energies of about 1 BeV, was constructed at the same institute in 1972. The linear accelerator Superhilac which was reconstructed at Berkeley (USA) in 1973, also had similar properties. The Unilac accelerator in the FRG is intended for accelerating ions of all elements right up to uranium.

Heavy ions were accelerated to relativistic energies for the first time in 1970 at Dubna. The 10-BeV proton accelerator built there in 1967 was modified for accelerating deuteron, and later for helium, carbon, oxygen and neon nuclei as well. Since the limiting energy depends on the charge of the ions, its value for $^{4}_{2}$He is 20 BeV, while the corresponding value for $^{20}_{10}$Ne is 100 BeV, which is the same as for protons, i.e. 10 BeV/Z (but 5 BeV/nucleon). On the basis of the Superhilac and the proton accelerator Bevatron, a heavy-ion accelerator Bevalac was built at Berkeley. This accelerator was capable of accelerating oxygen ions to energies of 2 BeV/nucleon, iron ions to 1.8 BeV/nucleon, and later uranium ions to about 1.1 BeV/nucleon. The rated values of energy are somewhat lower for the accelerator Numatron in Japan (0.67 BeV/nucleon for uranium) and Unilac + synchrotron in the FRG (0.8 BeV/nucleon for uranium).

Further developments of relativistic nuclear physics in the USSR are associated with the creation of a heavy-ion accelerator complex (HIAC) at Dubna, designed to accelerate ions of all elements from He to U in the energy range from several hundred MeV/nucleon to several BeV/nucleon. The complex includes an accelerator of heavy ions of all masses to energies $E \geqslant 300$ MeV/nucleon (heavy-ion synchrotron HIS).[1] The HIS is installed in the magnetic ring of a

[1] For details on the HIAC project and other heavy-ion accelerators, see *Heavy-Ion Accelerator Complex* by A.M. Baldin *et al.*, Joint Institute for Nuclear Research, Dubna, 9-11796, 1978.

synchrophasotron. Fully ionized and accelerated nuclei from HIS enter the synchrophasotron which further accelerates them to energies of $E = 10Z/A$ BeV/nucleon. A new accelerator with superconducting magnets (nucleotron) is expected to be installed in the same complex around the magnetic ring of the synchrophasotron. This will allow uranium ions to be accelerated to energies of about 10 BeV/nucleon.

The interaction of multiply charged ions with nuclei has a number of specific features associated with the large values of Z and M of the ions. These include:

(1) transfer of large momenta;
(2) transfer of large angular momenta;
(3) exchange of a large number of nucleons; and
(4) some specific features of electromagnetic interactions (a high and multiple Coulomb excitation, a strong ionization, short ranges, etc.).

All these features make it possible to investigate the properties of nuclei under unusual extremal conditions: superdense nuclei (with an anomalously high density of the nuclear matter), ultrahigh speed rotation (i.e. nuclei with a very large angular momentum), ultraradioactive nuclei (which lie away from the β-stability line) ultraheavy nuclei (far transuranic elements), supercharged nuclei (i.e. quasiatoms consisting of two nuclei).

11.1. Techniques of Operation with Heavy Ions

As in the case of ordinary nuclear reactions, the analysis of processes induced by heavy ions involves the identification of reaction products, i.e. the determination of their charge Z and mass number A, measurement of their cross section, angular and energy distribution, measurement of lifetime, etc. However, measuring techniques for heavy ions are of a specific nature on account of a large variety of the reaction products, large values of Z, short ranges and lifetimes. Hence new procedures were worked out for reactions induced by heavy ions. We shall now consider some of these techniques.

11.1.1. The T, ΔT Method and Its Applications

The ionization losses in a heavy nonrelativistic particle having a charge Z and velocity v are given by

$$(dT/dx)_{\text{ion}} \propto Z^2/v^2 \propto Z^2M/T, \qquad (11.1.1)$$

where $T = Mv^2/2$ is the kinetic energy of the particle. This gives $T\,\Delta T \propto Z^2M$, which means that by simultaneously measuring T and ΔT we can determine the parameter Z^2A. In view of the fact

that different particles have different values of Z and A, this identification parameter is unique for each nucleus. Thus, for two neighbouring elements $^{23}_{10}$Ne and $^{23}_{11}$Na, the values of Z^2A are equal to 2000 and 2783 respectively, i.e. differ by about 40%. Hence clearly distinguishable regions corresponding to a given value of Z^2A are obtained on the two-dimensional T, ΔT spectrum.

The resolving power of this method decreases with increasing Z and A. Thus, the values of Z^2A for $^{39}_{19}$K and $^{40}_{20}$Ca differ only by 14%, while for $^{115}_{49}$In and $^{119}_{50}$Sn this difference is reduced to just 7%. Since the charge appears in the second power in the identification parameter, identification by charge is easier than by the mass number. The former method has been extended to $Z \simeq 50$, while the latter has been found to be applicable up to $A \simeq 20$ (oxygen isotopes with $15 \leqslant A \leqslant 21$ have been clearly resolved). The resolving power of the T, ΔT method can be increased with the help of a telescope consisting of two or three ΔT-detectors and a special mathematical analysis of the primary data. The ΔT-detectors are chosen in the form of thin (10-100 μm) plane-parallel silicon surface-barrier detectors[2] or gas ionization detectors.

To increase the resolving power of the T, ΔT method, two ΔT-detectors are connected in such a way that the time of flight t between them can be measured. If d is the distance between the two detectors, then $M = 2Tt^2/d^2$ and $\Delta M/M = 2\,\Delta t/t$.

It can be easily calculated that for $d \simeq 100$ cm, a time resolution $\Delta t \simeq 0.3$-0.2 ns is required for resolving masses with $A \simeq 50$-70. Such a high time resolution can be ensured, say, by using thin films (of thickness < 1 μm) of a scintillator as time detectors.

A combination of a T, ΔT telescope and a magnetic spectrometer opens new possibilities for identification of products in reactions induced by heavy ions. In this case, the two-dimensional spectrum contains well-defined regions corresponding to a particular isotope with a definite effective charge (of the ion).

11.1.2. Other Methods of Identification of Nuclei and Determination of Their Lifetimes

Of special importance is the case when the compound nucleus acquires the entire momentum of a primary ion and hence flies in the same direction. In this case, the reaction products are isolated from the

[2] The operating principle of a semiconducting detector is similar to that of an ionization chamber with a solid dielectric between the electrodes. The ionizing radiation falling on the dielectric creates electrons and holes in it, which move towards the electrodes. The amplitude of the registered pulses is a linear function of the energy of the ionizing particle. Semiconducting detectors have a high efficiency and a high resolution, and are used for registering γ-quanta, neutrons and charged particles.

shortest distance from the nucleus does not become equal to zero, but is given by the condition

$$\frac{p'^2}{2M} = \frac{p^2}{2M} - \frac{Z_1 Z_2 e^2}{\rho'}, \qquad (11.2.1)$$

where $p'\rho' \simeq \hbar l$. Thus, $T' = p'^2/2M = \hbar^2 l^2/2M\rho'^2 = V_c(\rho')$ and $T = B_C(\rho') + V_c(\rho')$.

Only electromagnetic processes are possible in both cases: elastic Coulomb scattering, inelastic Coulomb excitation of collective nuclear levels, electrofission, creation of quasiatoms with double nuclei, etc. Some of these processes will be considered in Sec. 11.3.

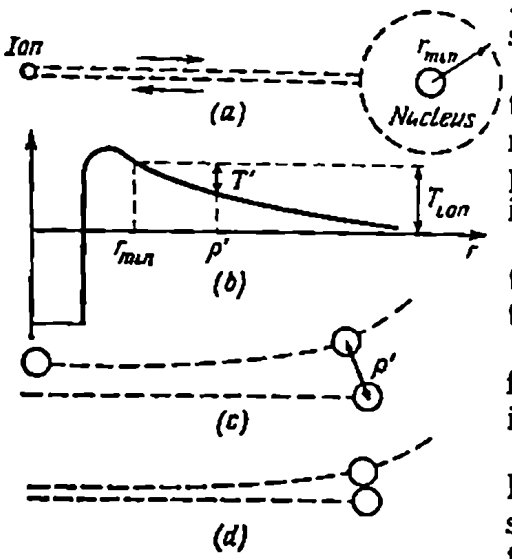

Fig. 308

If the energy of an ion exceeds the Coulomb barrier ($T_{ion} \geqslant B_C$), nuclear interaction also becomes possible besides electromagnetic interaction.

In this case, if $T_{ion} = \text{const}$, then everything is determined by the impact parameter ρ', i.e. by l.

(a) For $\rho' > R_{ion} + R_{nuc}$, i.e. for larger l, only electromagnetic interaction will be observed.

(b) For $\rho' = R_{ion} + R_{nuc}$, nuclear interactions also become possible besides electromagnetic interactions (upon grazing contact).

The condition for grazing contact between the two nuclei can be easily determined by putting $\rho' = R_{nuc} + R_{ion}$ and $B_C(\rho') = Z_{nuc}Z_{ion}e^2/(R_{nuc} + R_{ion})$ (Fig. 308*d*). Calculations lead to the following value for l_{gr} separating purely electromagnetic interaction from electromagnetic and nuclear ones

$$l_{gr} = \frac{R_{nuc}+R_{ion}}{\hbar}\sqrt{2M\left(T - \frac{Z_{nuc}Z_{ion}e^2}{R_{nuc}+R_{ion}}\right)}. \qquad (11.2.2)$$

The value of l_{gr} is uniquely determined by the quantity T_{ion} and can become very large ($l_{gr} \gg 1$) for $T_{ion} \gg B_C$. For $T_{ion} = B_C$, $l_{gr} = 0$ (head-on grazing collision). Grazing (peripheral) collisions are accompanied by inelastic processes with excitation of giant resonances, reactions involving the transfer of one nucleon, and other direct processes with characteristic times of 10^{-23}-10^{-22} s.

For $l < l_{gr}$, the extent of nuclear contact increases, and highly inelastic processes accompanied by the transfer of several nucleons between nuclei are observed. The interacting nuclei form a non-

equilibrium double system with typical lifetimes of 10^{-21} s. A specific double system can also be formed by two nuclei in the ground state, i.e. by nuclei which completely preserve their initial properties. As an example, we can consider the formation of the quasimolecular system $^{12}C+^{12}C$, which is characterized by narrow rotational levels at excitation energy of 20–40 MeV, i.e. higher than principal rotational band of ^{24}Mg. This interesting phenomenon is apparently explained by the formation of a dumb-bell shaped system by two interacting ^{12}C nuclei, rotating around its centre of gravity.

Finally, when l attains its critical value l_{cr}, the ion and the nucleus merge to form a compound system which gradually achieves a state of statistical equilibrium with a subsequent fission or emission of several nucleons. The characteristic lifetime of the system in this case is 10^{-20}–10^{-18} s.

11.3. Interaction of Heavy Ions with Nuclei at $T_{ion} < B_C$

11.3.1. Rotational Spectra for Large Angular Momenta

If $T_{ion} < B_C$ (or if the ion flies beyond the range of nuclear forces), the Coulomb excitation of collective nuclear levels becomes one of the typical processes in this case. Heavy ions are characterized by the excitation of rotational levels with large angular momenta. The process of excitation is found to be multiple, i.e. the same ion flying past nuclei excites them by successive quadrupole jumps.

Figure 309 shows the dependence of the excitation probability of rotational states of the nucleus $^{166}_{68}Er$ by ions of ^{16}O, ^{81}Br and ^{127}I with $T_{ion}/A = 4$ MeV/nucleon. It can be seen that as the mass and charge of the ion increase, levels with higher I are excited. Such a selective nature of excitation can be used to identify excited states with a definite I and to investigate their properties (τ, μ, Q).

Investigation of rotational levels with large angular momenta led to the discovery of a very interesting effect called backbending.

It is well known (see Sec. 2.4.2) that the structure of the rotational levels for the ground state of an even-even nucleus is described by the formula

$$E(I) = \frac{\hbar^2}{2J} I(I+1), \qquad (11.3.1)$$

where E and I are the energy and angular momentum of the level and J is the moment of inertia of the nucleus. It was shown in Sec. 2.4 that right up to $I \simeq 10$, the formula is confirmed experimentally under the assumption that $J = \text{const}$. The E vs. I dependence for larger values of I can be determined by using reactions induced by

heavy ions and the method of (γ-γ) coincidences. It turned out that as I varies from 0 to 10, the moment of inertia smoothly increases (by about 5% for $\Delta I = 2$), while a sharp deviation from the formula is observed for $I = 12$-16, indicating an increase of about 1.5 times in the value of J for $\Delta I = 2$. This effect was first observed in 1971 in the band of the ground state of the nucleus ^{160}Dy. Later, it was observed in many other rare-earth elements as well as for some other nuclei.

Since $E(I)$ increases rapidly with I, formula (11.3.1) is weakly sensitive to variation of J. Hence the anomalous behaviour of the

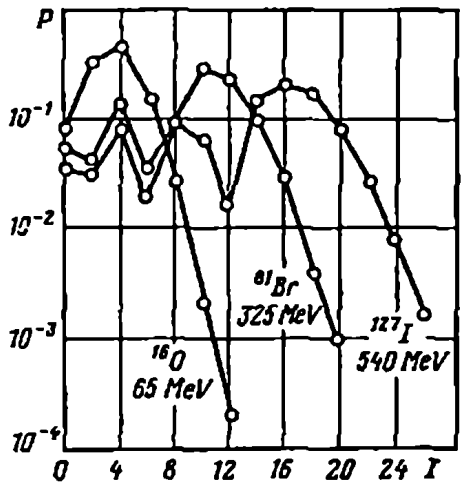

Fig. 309

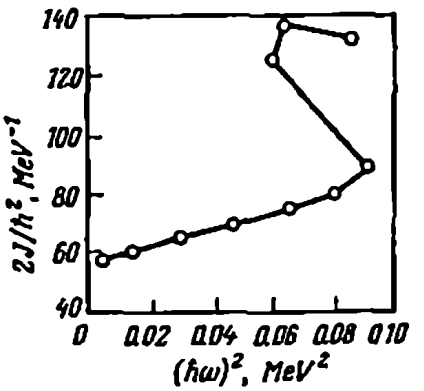

Fig. 310

moment of inertia can be seen much more clearly by considering the dependence of J on the energy increment ΔE for $\Delta I = 2$:

$$\Delta E = \{E(I) - E(I-2)\} = (4I-2)\frac{\hbar^2}{2J} \qquad (11.3.2)$$

Figure 310 shows the dependence of $2J/\hbar^2 = (4I - 2)/\Delta E$ as a function of $(\Delta E/2)^2 = (\hbar\omega)^2$ for the rare-earth element ^{166}Y. The first point in the figure corresponds to the variation of I from 0 to 2, the second from 2 to 4, and so on. It can be seen from the figure that right up to $I = 14$ ($\Delta I = 14$-12), a monotonic increase in the value of $(\hbar\omega)^2$ is observed, corresponding to a slow and smooth increase of J. For the next stage of increment of I, however ($\Delta I =$ 16-14), the value of $(\hbar\omega)^2$ decreases sharply and becomes equal to its value for $\Delta I = 10$-8. This decrease in $(\hbar\omega)^2$ is accompanied by a sharp increase in J, which is shown in the figure by a bending of the J (ΔE) curve in the backward direction (hence the name of the effect).

The anomalous behaviour of rotational spectra is explained by an intersection of the rotational band of the ground state of the

nucleus with some other band (say, with a band corresponding to an excited state) and a predominant occupation of the lower levels.[4] The formation of the anomalous dependences $E(I)$ and $J(\omega)$ is shown in Fig. 311. For small values of I, the levels of the principal band, which lie below the levels of the excited band in this region, are populated. When the bands intersect at the critical value of the angular momentum $I = I_0$, the lower levels of the excited state band are populated. The dashed parts of the curves in the region of intersection correspond to the absence of interaction between the

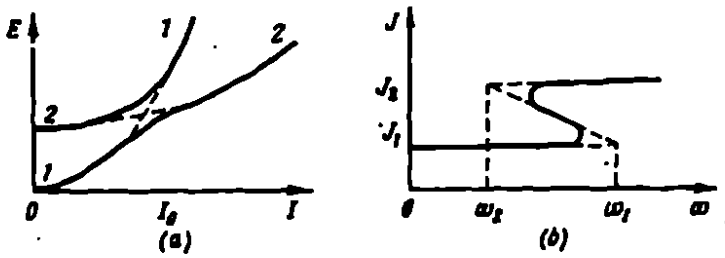

Fig. 311

bands, while the solid lines in this region correspond to weak intersections. The lower curve corresponding to the lowest energy for a given I and consisting of segments *1* and *2* is called the Yrast-line.

A unified microscopic theory of backbending has not been developed so far. The existence of the second band for different types of nuclei is attributed to different reasons. For one type of nuclei, it is associated with the shape isomerism (see Sec. 6.8.6), while for another type of nuclei it is due to a specific two-quasiparticle excitation with an angular momentum directed along the rotational axis of the nucleus. A clear graphic picture of the phenomenon was presented theoretically soon after its experimental discovery. According to this theory, the sharp increase in the moment of inertia of the nucleus for large values of I is explained by a phase transition of the nucleus from superfluid to normal state. Such a transition can be caused by a rupture of nucleonic pairs (which are typical for the superfluid state of the nucleus) due to Coriolis forces. However, this interpretation failed to provide correct values of the critical angular momentum I_0. Current attempts to construct a quantitative theory of rotational anomaly are based on analysis of the solution of the Hartree-Fock-Bogolyubov equations for a rotating nucleus.

[4] The predominant occupation of the lower levels is explained by the fact that the probability of the $E2$-transition is proportional to the fifth power of the transition energy. For a detailed description of anomalies in rotational spectra, see I.M. Pavlichenko, *Uspekhi Fiz. Nauk*, 133, 2, 193 (1981).

11.3.2. Quasiatoms with Double Nuclei

In the Coulomb field of a proton, the electron level lies at $E = -13.6$ eV. An analysis of Dirac's equation shows that with increasing point charge the level becomes lower and corresponds to $E = -m_e c^2$ for $Z_{cr} = 137$. For a real (finite-sized) nucleus, the critical charge Z_{cr} is equal to 170 for $1S_{1/2}$ level (185 for $1P_{1/2}$, and so on). As the charge reaches its critical value, vacuum becomes unstable with respect to the creation of electron-positron pairs. In this case, positrons are emitted while electrons take their place in $1S_{1/2}$ level and form an electron shell.

According to Pauli's exclusion principle, only two electrons can occupy this level, after which the vacuum becomes stable once again. At $Z = 185$, the next level $1P_{1/2}$ drops to the boundary $E = -m_e c^2$ and is also filled by electrons from the vacuum. Thus, an interesting process of electron condensation, leading to a partial neutralization of the nuclear charge, must be observed for $Z \gg Z_{cr}$.

There are no nuclei with $Z > Z_{cr}$. However, the predictions of quantum electrodynamics in this interval of charges can be verified by investigating the reactions induced by heavy ions. Indeed, if two ions with charges Z_1 and Z_2 are brought close to a distance δ satisfying the condition $R_{nuc} \ll \delta \ll R_{at}$, such a system of two nuclei will appear as a single nucleus with charge $Z = Z_1 + Z_2$ as far as the electron shell is concerned. Thus, during the short period in which two nuclei come close, a quasiatom may exist in principle, and its electron shell and radiation will correspond to a nucleus with charge $Z_1 + Z_2$.

The quasiatom formed by two approaching uranium ions will have a charge $Z = 184 > Z_{cr}$. Calculations show that the critical distance to which the two nuclei approach corresponding to $E = -m_e c^2$, is equal to $R_{cr} = 35$ fm. The ion energy required in this case will be $T_{ion} \geqslant 600$ MeV. The velocity corresponding to this energy is given by $v_{ion} \leqslant v_K$, where v_K is the velocity of the orbital motion of K-electrons. This means that there is enough time for the electron shell to be formed (quasistatic process).

Experiments with uranium ions have not been carried out so far, although results of experiments with lighter ions $_{53}$I are already available. These ions ($E = 10$-60 MeV) were used to bombard $_{79}$Au, $_{90}$Th and $_{92}$U targets. In these experiments, radiation from quasiatoms with $Z = 132$, 143 and 145 was registered. Experiments of this type are very difficult to perform due to a low radiation yield and the continuous nature of the emission spectrum. The latter is due to the fact that the transition energies depend on the distance between ions and hence vary smoothly as the ions approach each other.

11.4. Interaction of Heavy Ions with Nuclei for $T_{ion} \geqslant B_C$

It was mentioned in Sec. 1.2 that for $T_{ion} \geqslant B_C$, there exists a limiting value of l_{gr} given by $l_{gr} = [(R_{nuc} + R_{ion})/\hbar] \times \sqrt{2\mu\,(T - Z_{nuc}Z_{ion}e^2)/(R_{nuc} + R_{ion})}$, which corresponds to grazing (peripheral) interaction. For all $l > l_{gr}$, only electromagnetic interaction is possible, while for $l \leqslant l_{gr}$, nuclear interaction can also take place besides electromagnetic one.

11.4.1. Elastic Scattering of Ions

Since electromagnetic interaction is a long-range interaction, $\rho\rho \simeq$ $\ldots$, where $0 \leqslant \rho < \infty$ indicates that $0 \leqslant l < \infty$. After scattering, however, waves with $l \leqslant l_{gr}$ must drop out of the amplitude of

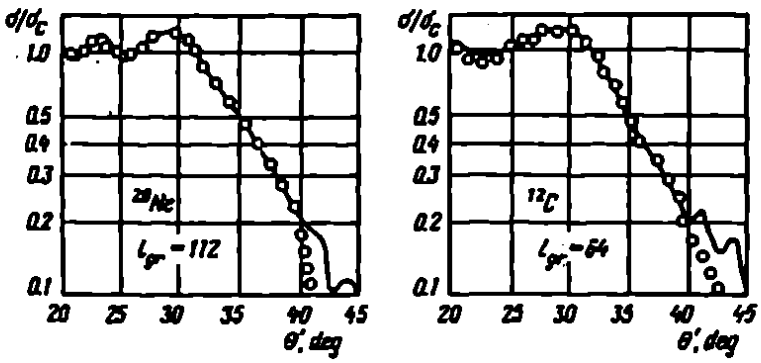

Fig. 312

elastic Coulomb scattering, since they are absorbed as a result of their participation in nuclear interaction. Hence in the theoretical interpretation of the elastic scattering of ions, these waves must be subtracted from the Coulomb amplitude, and the scattering cross section should be calculated for the remaining part. Figure 312 shows a comparison of such a calculation with the experimental result for $^{20}_{10}\mathrm{Ne} + {}^{197}_{79}\mathrm{Au}$ and $^{12}_{6}\mathrm{C} + {}^{197}_{79}\mathrm{Au}$ at an energy of 10 MeV/nucleon. The large value of l_{gr} is worth attention.

11.4.2. Transfer Reactions

When two nuclei come in a grazing contact, reactions involving the transfer of one nucleon are usually observed. For example,

$$^{9}\mathrm{Be}(^{14}\mathrm{N},\ ^{13}\mathrm{N})^{10}\mathrm{Be},\quad ^{23}\mathrm{Na}(^{14}\mathrm{N},\ ^{13}\mathrm{N})^{24}\mathrm{Na}, \qquad (11.4.1)$$

etc. Besides the above-mentioned reactions induced by $^{14}\mathrm{N}$ ions, other reactions of the same type were observed with $^{10}\mathrm{B}$, $^{14}\mathrm{N}$, $^{24}\mathrm{Mg}$,

^{25}Mg, ^{26}Mg, ^{12}C, ^{16}O, ^{27}Al and ^{32}S nuclei. The cross sections of these reactions attain values up to 5 mb.

If $l < l_{gr}$, the number of transferred nucleons increases, thus resulting in the formation of many different product nuclei. Some of the transfer reactions involving 4-6 nucleons are given below:

Stripping of four protons:

$$^{15}_{7}\mathrm{N} + ^{232}_{90}\mathrm{Th} \xrightarrow{-4p} ^{11}_{3}\mathrm{Li} + ^{236}_{94}\mathrm{Pu}^{*}, \qquad (11.4.2)$$

picking up of four neutrons

$$^{22}_{10}\mathrm{Ne} + ^{232}_{90}\mathrm{Th} \xrightarrow{+4n} ^{26}_{10}\mathrm{Ne} + ^{228}_{90}\mathrm{Th}, \qquad (11.4.3)$$

and exchange of nucleons

$$^{22}_{10}\mathrm{Ne} + ^{232}_{90}\mathrm{Th} \xrightarrow{-2p+4n} ^{24}_{8}\mathrm{O} + ^{230}_{92}\mathrm{U}^{*}. \qquad (11.4.4)$$

It can be easily seen that these reactions lead to the formation of light neutron-rich nuclei. This method was used at Dubna to obtain dozens of light neutron-rich nuclei, including such exotic nuclei as $^{8}_{2}$He, $^{11}_{3}$Li, $^{14}_{4}$Be, $^{15}_{5}$B, $^{21}_{7}$N, $^{20}_{8}$C, $^{24}_{8}$O, etc. Similar results were obtained by irradiating $^{232}_{90}$Th with ^{40}Ar ions ($^{29,30}_{12}$Mg, $^{31-33}_{13}$Al, $^{33-36}_{14}$Si, $^{35-38}_{15}$P, $^{39,40}_{16}$S, $^{41,42}_{17}$Cl). It should be noted that the method described above is not convenient for obtaining heavy neutron-rich nuclei, since protons are detached more easily from a light nucleus. This problem will be probably solved by using $^{48}_{20}$Ca for bombardment (since it has a large excess of neutrons), or the reaction $_{92}$U + $_{92}$U.

11.4.3. Complete Fusion Reactions

Complete fusion of nuclei takes place for $l \leqslant l_{cr}$, involving the formation of an excited compound nucleus which undergoes transformation as follows: emission of several fast nucleons, establishment of statistical equilibrium and fission or vaporization of nucleons.

The fusion reaction of light nuclei leads to the formation of neutron-deficient nuclei. For example, the reaction

$$^{40}_{20}\mathrm{Ca} + ^{40}_{20}\mathrm{Ca} \rightarrow ^{80}_{40}\mathrm{Zr}^{*} \qquad (11.4.5)$$

results in the formation of the nucleus $^{80}_{40}$Zr which has 10-12 neutrons fewer than the β-stable isotopes of this element. Further, if we take into account the fact that the compound nucleus in these reactions is formed in an excited state, and the oxcitation is removed by the emission of a few neutrons, it becomes clear that the deficiency of neutrons in product nuclei may be as high as 15-20 neutrons.

Investigation of the properties of neutron-deficient nuclei led to the discovery of delayed proton radioactivity.

11.5.1. Problems in the Physics of Relativistic Ions

Relativistic nuclei (ions) were first observed in 1948 in cosmic rays. Investigations were carried out by exposing emulsion stacks lifted to a height of about 30 km by balloons (see Sec. 7.1.1, Vol. II). At present, such investigations are made with the help of satellites. It is well known that the ionization losses of a charged particle are proportional to Z^2/β^2 (for $\beta < 0.8$). The major part of this energy is spent in the formation of δ-electrons whose number is proportional to Z^2. Thus the charge of a particle in the cosmic radiation can be determined from the number of δ-electrons.

Nuclei with different values of Z have quite different tracks. For $Z = 1$, the thickness of the track is about 0.5 μm and the track itself consists of individual black grains of silver reduced during developing. The grain density depends on the velocity β of the particle. If $\beta \simeq 0$, the track looks like a fine continuous black line. As Z increases, the track thickness and the grain density also increase. For $Z \simeq 90$, the track is a continuous black band whose width is nonuniform and varies between 50 and 70 μm.

The identification of nuclei in cosmic radiation led to a curve showing the relative abundance of various elements in cosmic radiation which can be compared with element abundance in the solar system. If both curves are normalized relative to the abundance of carbon, it is found that the cosmic radiation contains a large excess of light nuclei of Li, Be, B (whose relative abundances are 10^5, 10^6 and 10^4 times higher than in the solar system), as well as comparatively heavy nuclei of Sc (10^2), Ti (10^2), V (10^3), Cr (10^2) and Mn (10^2).

Assuming that the source of cosmic radiation has the same elemental composition as the solar system, the excess of light nuclei of Li, Be and B in cosmic radiation can be naturally attributed to the fragmentation of heavy nuclei upon their interaction with matter in the intergalactic medium. The extent of deformation of the spectrum and the density of intergalactic hydrogen (0.01 atom/cm^3) provide an estimate for the age of cosmic radiation. However, if this hypothesis were valid, the relative abundance of the heavy component of cosmic radiation (Sc, Ti, V, Cr and Mn) should be lower than in the solar system, and not higher as is borne out by actual comparison. Thus, it can be assumed that the source of cosmic radiation has an elemental composition quite different from that in the solar system. It may be that superdense stars composed of nuclear matter are the sources of this radiation. This conclusion, however, should not be treated as final, since the results obtained from the analysis of cosmic events are far from unambiguous due to considerable errors in the identification of nuclei and in the estimate of the value of fragmentation cross section. Hence it is very important to study the interaction of relativistic heavy ions under laboratory conditions.

Another important problem in the physics of relativistic particles involves the estimation of the contribution from multiply charged cosmic particles to the radiative processes taking place in spaceships and cosmic laboratories. It is difficult to obtain a complete solution of this problem directly on the spaceships due to a low intensity of the cosmic radiation and technical difficulties.

Another field of biomedical research requires the exploration of the possibility of using beams of relativistic nuclei in oncology. This seems to be a promising activity since with increasing mass of a relativistic ion the scattering radius of the beam decreases and the parameters of the Bragg peak at the end of the path are improved. This makes it possible to localize the action of the beam to a very small region.

Investigation of the interaction of nuclei at relativistic energies is very important for developing a theory of strong interactions. In quantum chromodynamics (see Sec. 9.1, Vol. II), each nucleon consists of three quarks lying in a deep potential "bag" which they cannot leave ("peripheral prison", confinement, captivity). However, quarks which are situated at close distances from each other inside the bag practically do not interact ("central" or asymptotic freedom). The parameters of the bags allow confinement of more than three (say, six) quarks in each of them. Such multiquark systems can appear in principle during interaction of relativistic nuclei, which must bring nuclei much closer to one another, and probably lead to a collectivization of the quarks contained in them. Thus, a study of the interaction of relativistic ions with nuclei may help in the development of quantum chromodynamics. In particular, this may correctly explain the confinement of quarks in larger numbers (i.e. at larger separations) than in a nucleon.

Multiquark systems are also interesting in that they must have a density of the nuclear matter comparable with the density of a nucleon, i.e. about twice or thrice the ordinary nuclear density. This provides a new approach to the problem of the existence of matter in superdense state (see also Sec. 2.1.3).

Finally, it is worth noting that the history of development of physics in general and nuclear physics in particular contains examples of many remarkable achievements which were not always in the offing.

11.5.2. First Results. Cumulative Effect

The first experiments with relativistic nuclei were carried out by using the Dubna accelerator. In 1971, Baldin and coworkers predicted and discovered the cumulative effect, according to which an escaping particle carries much higher energy than the average energy of each

nucleon in the incident nucleus. Thus, in the reaction $d + A \rightarrow \pi^- + \ldots$, in which the deuterons have an energy of 8 BeV, i.e. 4 BeV/nucleon, it is possible to obtain π-mesons with an energy of 5-7, or even about 8 BeV. This is a quite astonishing result, since the distance between nucleons in a nucleus is much larger than the radius of a nucleon, and hence it would seem that the nucleons must interact individually. Thus, the interaction of heavy relativistic ions can be used for investigating processes occurring in a region which is kinematically forbidden for collisions of free nucleons.

To explain the cumulative effect, a hypothesis was put forth according to which there exists a specific mechanism of collisions involving the transfer of large momenta. For example, we can assume that collisions between nuclei at relativistic energies take place in such a way that the escaping particle receives its energy not from one nucleon, but from several nucleons. In other words, it is possible that the cumulative effect is explained by the existence of a multiquark system belonging to several nucleons in a nucleus.

In the limit, a nucleus can be considered as a drop of a homogeneous hadronic matter for which the parameters (masses, form-factors) of nucleons and other particles become insignificant. Hence one particle of the target nucleus can interact with all the particles of the bombarding nucleus that lie inside the interaction tube. The number of such particles is approximately equal to $A^{1/3}$, where A is the mass number of the bombarding nucleus. Thus, for $A \simeq 30$, an escaping particle may attain a three-fold energy, while for $A \simeq 60$, the energy may be higher by a factor of four.

Another important result, which was also obtained at Dubna, is the discovery of a new type of interaction called multibaryon collisions. In this phenomenon, a large number of nucleons of the projectile nucleus interact with the target nucleus. Thus, in the collisions between carbon and tantalum nuclei, the average number of interacting nucleons in the carbon nucleus was found to be 6.0 ± 0.6.

It was shown that certain characteristics of multiple processes in the case of collisions between nuclei (for example, multiplicity distribution and distribution dispersion) are identical to the characteristics of collisions between nucleons at high energies. This makes it possible to analyze the results of collisions between nuclei by using methods worked out for particle interaction.

In nucleus-nucleus interactions, large values of cross section have been obtained for stripping and pick-up, which lead to the formation of nuclear fragments with velocities close to the velocity of the bombarding nucleus. Stripping and pick-up play an important role due to the low binding energy of nuclear fragments.

11.5.3. Anomalous Nuclei

As early as in 1954, experiments with cosmic rays revealed very rare events in which relativistic heavy ions with anomalously short nuclear ranges were registered. For a thorough investigation of this phenomenon under specific conditions (ions having a known charge and energy), a large body of experimental data was obtained by using Bevalac beams at the Lawrence Laboratory in Berkeley. Investigations were made by the emulsion chamber method (see Sec. 7.1.1, Vol. II) with stacks of special emulsion layers. One of the chambers was irradiated with $^{16}_{8}O$ ions having an energy of 2.1 BeV/nucleon, while the other chamber was irradiated with $^{56}_{26}Fe$ ions of 1.88-BeV/nucleon energy. Scanning and measuring both the stacks were made at two independent laboratories in Canada and the USA.

The detection and analysis of events was carried out as follows.[6] The track of a beam particle was followed from its entry into the photographic emulsion up to its escape or interaction. The path traversed was measured in both cases. From the point of interaction, tracks were followed for all relativistic particles (fragments) with $Z \geqslant 3$, escaping in the forward direction in a narrow cone. If these particles produced new fragments, the same process was repeated for the second-generation tracks, and so on. In some cases, up to seven generations of successively formed fragments were registered in nuclear cascades. The charge of each fragment was determined to within $\Delta Z = \pm 1$.

It is well known that the cross section of interaction of a particle with charge Z is equal to $\sigma_Z = 1/n\lambda_Z$, where n is the number density of nuclei in the medium and λ_Z is the mean free path of this particle before interaction. The dependence of λ_Z on charge Z can be described by the formula

$$\lambda_Z = \Lambda Z^{-b}, \tag{11.5.1}$$

where Λ and b are constants which are chosen empirically. For the photographic emulsion used in the above experiment, $\Lambda = 30.4 \pm 1.0$ cm and $b = -0.44 \pm 0.02$.

The value of λ_Z can be determined in two ways: from the ratio $\lambda_Z = S/N$, where S is the total length of all (interaction and non-interaction) tracks with a given Z, and N is the number of observed interactions, or from the distribution of distances x traversed before the interaction ($0 \leqslant x < \infty$):

$$f(x)\,dx = \exp(-x/\lambda_Z)\,\frac{dx}{\lambda_Z}, \tag{11.5.2}$$

[6] E.M. Friedlander *et al.*, *Phys. Rev. Lett.*, 45, 13, 1084 (1980).

where $\lambda_Z = \bar{x} = \int_0^\infty x f(x)\, dx$. The second method gives the value of λ_Z from the slope of the distribution curve $f(x)$ (without measuring the free paths of noninteracting fragments).

It was found as a result of measurements that in nuclear cascades containing several successive interactions, the particles formed after the second, third, etc. collision have on the average a shorter free path up to the next interaction than the beam particles with the same charge. A thorough analysis of about 1500 events showed that anomalously short free paths are observed for the first few centimetres of the path x covered ($x \leqslant 2.5$ cm) after the formation of particles (within the time of flight of 10^{-11} s). At large distances from the place of birth of a particle, its free path becomes normal. This effect is observed for fragments with a charge Z between 3 and 26. It was found that the mean free path decreases from generation to generation. In the third and subsequent generations, its value becomes 15% smaller than normal.

A computer analysis of the results showed that the observed effect cannot be attributed to a statistical spread of the results. Simulation by the Monte-Carlo method indicates that among the secondary fragments, a small portion (about 6%) of particles with an anomalously large interaction cross section, i.e. with an anomalously small mean free path $\lambda \simeq 2.5$ cm, is detected. The authors have not provided any explanation of the physical nature of the observed effect, but have simply confined themselves to the remark that it cannot be interpreted within the framework of conventional nuclear physics, since the mean free path $\lambda = 2.5$ cm corresponds to a nucleus with $Z \simeq 300$. Hence, if the results of this work are confirmed by subsequent experiments, their interpretation must have a nontrivial nature.

11.6. A Brief Resumé of Chapter 11

Accelerators capable of imparting energies of several megaelectron-volts per nucleon to heavy ions appeared in the 1950s. Later, the energy of accelerated ions increased to tens of MeV/nucleon, and at present heavy ions are accelerated to relativistic energies (2-5 BeV/nucleon). Accelerators are being constructed to impart energies of up to 10 BeV/nucleon to all types of nuclei (including uranium).

Nuclear reactions induced by heavy ions can produce nuclei with extremal values of density, angular momentum, mass, neutron-to-proton ratio, etc. Special methods were worked out to analyze these reactions (E, ΔE method, mechanical transport method, solid-state detector method, etc.).

For $T_{ion} < B_C$, the interaction of heavy ions with nuclei is electromagnetic in nature (elastic Coulomb scattering, inelastic Coulomb excitation of collective nuclear levels, etc.). The excitation of rotational levels with large angular momenta is one of typical features of this type of interaction. An investigation

of this process revealed the anomalous behaviour of rotational spectra for $I = 12$-16 (backbending).

For $T_{ion} \geqslant B_C$, the interaction of heavy ions with nuclei is determined by the angular momentum l. For $l > l_{gr}$, corresponding to the impact parameter $\rho > R_{ion} + R_{nuc}$, the interaction is purely electromagnetic. For $l = l_{gr}$ ($\rho = R_{ion} + R_{nuc}$), a grazing (peripheral) collision is observed, accompanied by the excitation of giant resonances, transfer of one nucleon, and other fast (about 10^{-22} s) direct processes. For $l < l_{gr}$ ($\rho < R_{ion} + R_{nuc}$) the extent of nuclear contact is increased, and highly inelastic processes involving the transfer of many nucleons are observed. In this case, the interacting nuclei form a non-equilibrium double nuclear system with a lifetime $\tau \simeq 10^{-21}$ s. For $l \leqslant l_{gr}$, the ion and the nucleus fuse into a compound system which gradually goes over to a state of statistical equilibrium followed by fission or emission of several nucleons. The lifetime of such a system is $\tau \simeq 10^{-16}$ s.

In recent years, studies have been undertaken on the interaction of heavy ions with nuclei at relativistic energies (2-5 BeV/nucleon). Among the first interesting results obtained in this field, the discovery of cumulative effect (Dubna) and the detection of fragments with anomalously short free paths (Berkeley) are worth mentioning.

Chapter 12

Nuclear Reactions Induced by Gamma-quanta

12.1. Simplest Reactions Induced by Gamma-quanta

Gamma-quanta are usually responsible for reactions of the types (γ, n), (γ, p) and (γ, α). All these reactions are similar to the photoelectric effect considered in Sec. 4.10, hence they are called *nuclear photoelectric effect*. The necessary condition for such a reaction to take place is that the energy of the γ-quanta must exceed the separation energy for the corresponding particle, i.e.

$$E_\gamma > \varepsilon_n \, (\varepsilon_p, \, \varepsilon_\alpha). \tag{12.1.1}$$

Nuclear photoelectric effect was first observed in 1934 by Chadwick and Goldhaber while considering the photodisintegration of deuteron, in which (γ, n)- and (γ, p)-reactions occur simultaneously:

$$\gamma + {}^2_1\mathrm{H} \rightarrow n + p. \tag{12.1.2}$$

In this experiment, γ-quanta emitted by a radioactive preparation of ThC″ ($E_\gamma = 2.62$ MeV) were used.[1] Protons with an energy of 0.2 MeV were detected in the photodisintegration of a deuteron. Since it was known at that time that the neutron mass is approximately equal to the proton mass, it could be concluded that the kinetic energy carried away by the neutron is also equal to 0.2 MeV (see Sec. 1.2.3 for details). Hence, the binding energy of the deuteron should be

$$\Delta W({}^2_1\mathrm{H}) = 2.62 - 2 \times 0.2 = 2.22 \text{ MeV}.^2$$

Later, another reaction induced by γ-quanta from natural radioactive elements was observed. It was found that γ-quanta from RaC ($E_\gamma = 1.78$ MeV) cause disintegration of the ${}^9_4\mathrm{Be}$ nucleus:

$$\gamma + {}^9_4\mathrm{Be} \rightarrow {}^8_4\mathrm{Be} + n, \quad {}^8_4\mathrm{Be} \rightarrow 2{}^4_2\mathrm{He}. \tag{12.1.3}$$

This exhausts the list of nuclear reactions induced by γ-quanta emitted by natural radioactive elements. For all the remaining

---

[1] According to modern terminology, ThC″ = ${}^{208}_{81}\mathrm{Tl}$, and RaC = ${}^{214}_{83}\mathrm{Bi}$

[2] The present value of the deuteron binding energy was obtained as a result of precise measurements of the energy of γ-quanta emitted in the reaction $p\,(n, \gamma){}^2_1\mathrm{H}$:

$$\Delta W\,({}^2_1\mathrm{H}) = 2.224667 \pm 0.000031 \text{ MeV}.$$

nuclei, the separation energy of a nucleon exceeds the energy of γ-quanta emitted by radioactive nuclei.

Gamma-quanta having higher energies are obtained in reactions of interaction of protons with nuclei. One such reaction was encountered by us while considering the interaction of protons with lithium. It should be recalled that an excited ${}_4^{8*}\mathrm{Be}$ nucleus goes over to the ground state by emitting γ-quanta of energy about 17.3 MeV. Other examples of such reactions are the reaction

$$ {}_5^{11}\mathrm{B}(p, \gamma){}_6^{12}\mathrm{C}, \qquad (12.1.4) $$

resulting in the emission of γ-quanta with energy 11.67 MeV, 16.10 MeV, etc., and the reaction

$$ p + {}_9^{19}\mathrm{F} \rightarrow {}_8^{16}\mathrm{O}^* + {}_2^4\mathrm{He}, \quad {}_8^{16}\mathrm{O}^* \rightarrow {}_8^{16}\mathrm{O} + \gamma, \qquad (12.1.5) $$

for which $E_\gamma = 6.13$ MeV.

12.2. Direct Emission of Protons Induced by Gamma-quanta

The possibility of obtaining high-energy γ-quanta paved the way for a systematic analysis of nuclear reactions induced by gamma radiation.

As a result of these investigations, it was revealed that the main types of reactions induced by gamma radiation are the (γ, n)- and (γ, p)-reactions. The absorption cross section of γ-quanta increases linearly with the nuclear charge. Separate studies of light and heavy nuclei led to the following results. It was found that the angular distribution of products in (γ, n)- and (γ, p)-reactions involving heavy nuclei ($A > 100$) is isotropic for neutrons and slow protons, and anisotropic for fast protons in the direction $\theta = 90°$. The ratio of the yields of (γ, p)- and (γ, n)-reactions has been obtained experimentally:

$$ \frac{Y(\gamma, p)}{Y(\gamma, n)} \simeq 10^{-3}. \qquad (12.2.1) $$

These results are in contradiction with Bohr's mechanism for nuclear reactions involving the formation of a compound nucleus. Indeed, if the reactions (γ, n) and (γ, p) occur with the formation of a compound nucleus, the emission of neutrons and protons must be characterized by a Maxwellian energy distribution with corresponding nuclear temperature. Moreover, the emission of protons must be less frequent due to the presence of the Coulomb barrier. Since the average energy of protons is considerably lower than the maximum value (on account of the fact that the product nucleus will be the more excited, the lower the energy of the emitted proton, and in the region of strong excitations the levels are more closely spaced

and hence the corresponding transition probability is higher), the barrier will exert a considerable influence. Estimates show that the ratio of the yields of the (γ, p)- and (γ, n)-reactions must be given by

$$\frac{Y(\gamma, p)}{Y(\gamma, n)} \simeq 10^{-3}\text{-}10^{-4}, \qquad (12.2.2)$$

which is much smaller than the experimental value.

To remove the discrepancy between the expected value and the experimental result, a new additional mechanism called *direct proton emission* was introduced.

This mechanism involves the absorption of a γ-quantum by a proton at the surface of the nucleus, followed by the flight of the proton until its energy is distributed among the remaining nucleons in the nucleus. The maximum energy of the proton in this case is given by

$$(T_p)_{max} = E_\gamma - \varepsilon_p, \qquad (12.2.3)$$

where ε_p is the binding energy of the proton.

The direct emission protons can also explain the relative increase in the yield of (γ, p)-reactions over the expected values from the compound nucleus model, as well as the anisotropy of angular distribution of emitted protons (transverse polarization of the electric vector of gamma radiation).

Direct proton emission is responsible for only a small part of the absorption cross section of γ-quanta. For the (γ, p)-reaction, however, it can have a considerable significance due to the smaller role of the barrier for high-energy "surface" protons in comparison to its role for evaporation protons.

The direct interaction mechanism is especially important for reactions involving heavy nuclei whose high Coulomb barrier obstructs the emission of low-energy evaporation protons.

12.3. Giant Electric Dipole Resonance

The limited choice of the energy values of γ-quanta emitted in reactions does not allow a systematic analysis of the cross sections of photodisintegration of nuclei as a function of energy. Such an analysis could be carried out only after the generation of γ-quanta with any energy became a reality. The source of such γ-quanta is the bremsstrahlung from electrons obtained in an accelerator. The spectrum of the gamma radiation obtained in this way is shown in Fig. 313*a*. The maximum energy of gamma radiation is equal to the kinetic energy of electrons being decelerated, while its intensity decreases approximately in inverse proportion to the energy. Thus, the deceleration of electrons may produce a continuous spectrum of

γ-quanta with a given maximum energy. Upon irradiation of nuclei by a continuous spectrum of gamma radiation, the overall effect due to γ-quanta of different energies will be observed. To single out the effect due to γ-quanta of a given energy, we must carry out two measurements with gamma radiation with different maximum energies:

$$(E_{\gamma_1})_{max} = T_{e_1} \text{ and } (E_{\gamma_2})_{max} = T_{e_2}.$$

Taking the difference effect of these two experiments, we can obtain the result for a quite narrow interval of the gamma radiation energy (Fig. 313*b*).

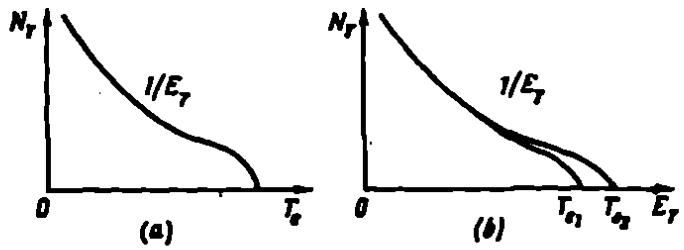

Fig. 313

By varying the energy of gamma radiation, we could study the dependence of the cross sections of (γ, *n*)- and (γ, *p*)-reactions on the energy of γ-quanta. A very interesting effect was discovered as a result of this analysis. It was found that σ (γ, *n*) and σ (γ, *p*) increase slowly from their threshold values and have a value of about 1 mb for $E_\gamma = 10$ MeV. For $E_\gamma \simeq 15$-25 MeV, however, a resonance pattern is observed, which is common to many investigated nuclei.

A typical feature of this resonance is its large half-width Γ and a regular variation of the resonance energy with the mass number A:

$$(E_\gamma)_{res} \propto A^{-0.2} \text{ MeV}. \qquad (12.3.1)$$

Table 35 contains the results of investigations for several nuclei. The values of threshold energies are given for each reaction. Apparently, these values are equal to the separation energies for the corresponding nucleons.[3] Besides, the table also lists the resonance energies E_{res} and the half-widths of the resonance curves. On account of large values of the half-widths, the phenomenon was termed *giant resonance*.

To explain the giant dipole resonance, nuclear oscillations induced by the electromagnetic field of γ-quanta were considered (in the USSR by Migdal, and abroad by Goldhaber, Teller and others).

[3] If the nucleon emission from the nucleus is not forbidden (say, by parity or spin).

Table 35

Reaction	$(E_\gamma)_{\min}=\varepsilon_N$, MeV	$(E_\gamma)_{res}$, MeV	Γ, MeV
$^{12}_{6}C(\gamma, n)^{11}_{6}C$	18.7	22.4	2.8
$^{27}_{13}Al(\gamma, n)^{26}_{13}Al$	14.0	19.2	4.7
$^{27}_{13}Al(\gamma, p)^{26}_{12}Mg$	7.4	21.2	5.4
$^{31}_{15}P(\gamma, n)^{30}_{15}P$	12.4	19.5	6.5
$^{63}_{29}Cu(\gamma, n)^{62}_{29}Cu$	10.9	17.5	6.0
$^{109}_{47}Ag(\gamma, n)^{108}_{47}Ag$	9.3	16.0	4.8
$^{181}_{73}Ta(\gamma, n)^{180}_{73}Ta$	8.0	13.5	5.5

Qualitatively, this phenomenon can be visualized as follows. Gamm quanta with energy E_γ have a wavelength

$$\lambda = \frac{hc}{E_\gamma} = \frac{1.2 \times 10^{-10}}{E_\gamma}, \qquad (12.3.$$

where λ is in cm and E_γ in MeV. This means that for $E_\gamma = 1$ 20 MeV, $\lambda \gg R_{nuc}$. As a result, all protons in the nucleus are fou to be in the same phase of the electromagnetic field of the γ-quant and the electric vector E must displace them in the same directio Two slightly differing mechanisms were specifically considered.

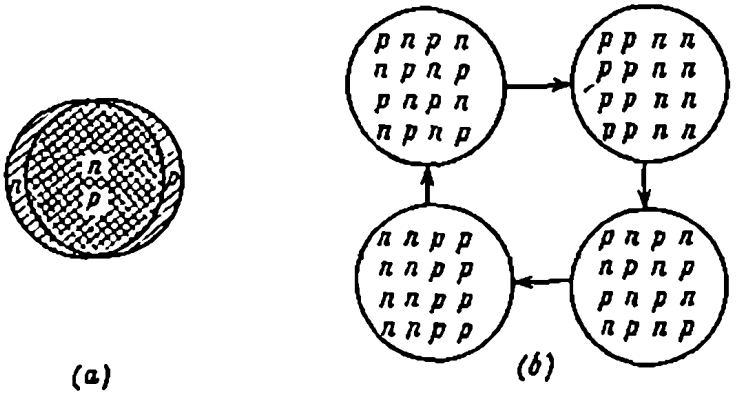

Fig. 314

According to the first mechanism, the entire proton part of tl nucleus is displaced relative to the entire neutron part, thus causir a polarization of the nucleus (Fig. 314a). Under the action of tl restoring elastic force, the nucleus is transformed into the opposi phase, and so on. This sets off dipole oscillations in the nucleu whose frequency can be estimated from the oscillator formula $\omega = \sqrt{K/M}$, where K is the modulus of elasticity and M is the ma

of the nucleus. In this mechanism, the role of the restoring elastic force is played by the interaction of displaced "bared" nucleons with the rest of the nucleus. Since the number of such nucleons is proportional to the surface area of the nucleus, $K \propto R^2$, and

$$\omega = \sqrt{\frac{K}{M}} \propto \sqrt{\frac{R^2}{R^3}} \propto \frac{1}{\sqrt{R}} \propto A^{-1/6}. \qquad (12.3.3)$$

Goldhaber and Teller obtained the value of 35 for the coefficient in this formula, which means that $E_\gamma^{res} = 35A^{-1/6}$ MeV.

According to the second mechanism, the giant dipole resonance can be imagined as an alternating mutual displacement of protons and neutrons to opposite ends of the nucleus, while the nucleon density remains unchanged (Fig. 314*b*). In this case, the restoring force is proportional to the distance which a nucleon must cover from one end of the nucleus to the other end, i.e. $K \propto R \propto A^{1/3}$. Hence for the oscillator frequency we obtain

$$\omega = \sqrt{K/M} \propto 1/R \propto A^{-1/3}. \qquad (12.3.4)$$

For the resonance energy, Migdal obtained the value (in MeV) $E_\gamma^{res} = 60A^{-1/3}$.

A comparison of the results with the experiment shows that the dependence of excitation energy on the mass number can be described correctly by a linear superposition of the two mechanisms:

$$W = 31.2A^{-1/3} + 20.6A^{-1/6}, \qquad (12.3.5)$$

where W is in MeV. According to this approximation, the position of the giant dipole resonance on the excitation energy scale varies from 25.5 to 13.5 MeV for the mass number A between 16 and 250. A simpler expression

$$W = 78A^{-1/3} \qquad (12.3.6)$$

(W is in MeV) is sometimes used for heavy nuclei.

In both mechanisms considered above, the protons and neutrons move in opposite phase and as if replace one another. Consequently, this resonance and other giant resonances (see Sec. 2.4.4) involving a similar motion of nucleons are called isovector resonances (the isospin of the nucleon changes by unity, i.e. $\Delta T = 1$).

A characteristic feature of the giant dipole resonance is that it covers a considerable part (up to 100%) of the energy-weighted sum rule (EWSR). Let us explain the meaning of this.

Each nucleus has a certain number of $E1$, $E2$, $M1$, . . . transitions. In other words, there is an upper bound for the dipole, quadrupole, and other nuclear forces. When applied to photoabsorption, this means that the absorption cross section of the dipole γ-quanta, integrated with respect to energy, must be equal to a definite value

depending on the nucleus. The same applies to the quadrupole γ-quanta and others. The sum of the contributions of all multipoles to the photoabsorption cross section, integrated up to the generation threshold for π-mesons (about 135 MeV) is given by the sum rule which thus sets the upper bound for the integral photoabsorption cross section. The sum rule for dipole photoabsorption was obtained by Gell-Mann *et al.* from quite fundamental concepts (causality principle, optical theorem, and Thomson's scattering formula). When expressed in MeV·mb, this relation has the form

$$\int_0^{m_\pi c^2} \sigma_A(\omega')\, d(\hbar\omega') = 60\frac{NZ}{A}(1+W), \qquad (12.3.7)$$

where $\sigma_A(\omega')$ is the photoabsorption cross section, N, Z and A are the number of neutrons, protons and the mass number respectively, while W is a correction factor, $W = 0.1A^2/NZ \simeq 0.4$.

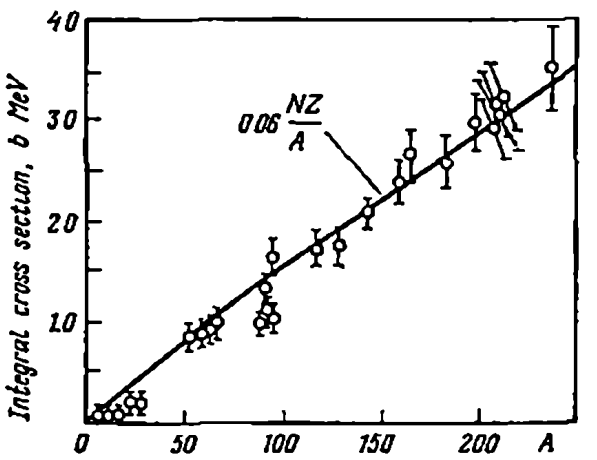

Fig. 315

A comparison of the sum rule with the experimental photoabsorption cross section shows that the giant dipole resonance practically consumes the entire transition energy for nuclei with mass numbers $50 \leqslant A \leqslant 240$ (Fig. 315).

Finally, it should be noted that a fine structure of the giant dipole resonance was observed (especially for light nuclei) in experiments permitting a high resolution. Thus, in the $\sigma(E_\gamma)$ dependence for the reaction ${}^{16}_{8}O(\gamma, p){}^{15}_{7}N$, three narrow peaks at energies 17, 22 and 25 MeV were observed instead of a single broad peak at $E_\gamma = 22$ MeV. The fine structure of the giant resonance was explained by single-particle transitions of nucleons between shells upon absorption of dipole γ-quanta. Later, these peaks were split into 10 (and subsequently even 18) narrower peaks. No satisfactory explanation for

this splitting has been offered so far. Apparently, the simplest interpretation for this effect is the particle-hole transitions corresponding to the capture of an $E1$ quantum, although it offers little prospects (nevertheless, the appearance of peaks at 22 and 25 MeV was explained in this way). It seems that the higher configurations and collective degrees of freedom must be taken into account. But this approach cannot be expected to provide a quantitative estimate on account of the large number of parameters involved.

12.4. A Brief Resumé of Chapter 12

In this chapter, we have briefly described the nuclear photoelectric effect, i.e. nuclear reactions induced by γ-quanta.

The simplest reaction of this type is the photodisintegration of deuteron:

$$\gamma + {}^{2}_{1}H \to n + p,$$

which is induced by gamma radiation from ThC'' ($E_\gamma = 2.62$ MeV). An analysis of this reaction, first made in 1934, led to the deuteron binding energy $\Delta W ({}^{2}_{1}H) \simeq 2.22$ MeV.

Usually, γ-quanta are responsible for reactions of the (γ, n), (γ, p) and (γ, α) types. The necessary condition for the occurrence of these reactions is written in the form

$$E_\gamma > s^n (s_p, s_\alpha).$$

The interaction of γ-quanta with nuclei usually takes place through Bohr's mechanism involving the formation of a compound nucleus and the subsequent emission of product particles. In this case, the emitted particles have a Maxwellian energy distribution. On account of the Coulomb barrier, the yield of the (γ, p)-reaction is lower than that of the (γ, n)-reaction by a factor of 10^3-10^4.

When γ-quanta interact with heavy nuclei, the (γ, p)-reaction may also occur through the mechanism of direct proton emission. In this mechanism, the energy of the γ-quantum is spent on knocking a proton from the surface of the nucleus instead of exciting the compound nucleus. The proton is emitted in this case at an angle close to 90° relative to the direction of the incident γ-quanta, and its energy may attain values up to $(T_p)_{max} = E_\gamma - s_p$.

The cross sections of photonuclear reactions of the type (γ, n) and (γ, p) in the energy interval of 15-25 MeV has a wide ($\Gamma = 3$-7 MeV) resonance peak (giant resonance). The resonance energy varies according to the law

$$(E_\gamma)_{res} \propto A^{-1/3}.$$

Studies of these reactions with increased resolving power instruments revealed that the giant resonance has a fine structure.

Chapter 13

Thermonuclear Reactions

13.1. Possibility of Self-sustained Fusion of Light Nuclei

It was shown in Sec. 1.3.2 that besides the fission of heavy nuclei, there exists another mechanism of liberation of nuclear energy, called the fusion of light nuclei. The binding energy per nucleon in light nuclei increases with the mass number A. Hence when two light nuclei are fused into a single heavier nucleus, energy equal to $A(\varepsilon - \bar{\varepsilon})$ must be released, where A is the total mass number of the fused nuclei, $\bar{\varepsilon}$ is the average binding energy per nucleon for these nuclei, and ε is the binding energy per nucleon for the heavier nucleus formed as a result of fusion [see formula (1.3.10b) and Fig. 21].

The amount of energy Q released during the fusion of two light nuclei is quite significant. When calculated for one nucleon, it usually exceeds the fission energy $q = Q_{fis}/A = 200/236 = 0.85$ MeV (Table 36).

Table 36

Reaction	Q, MeV	$q = Q/A$, MeV
${}_1^2H + {}_1^2H \rightarrow {}_2^3He + n$	3.25	0.8
${}_1^2H + {}_1^2H \rightarrow {}_1^3H + p$	4.03	1.0
${}_1^3H + {}_1^3H \rightarrow {}_2^4He + n$	17.6	3.5
$p + {}_3^7Li \rightarrow {}_2^4He + {}_2^4He$	17.3	2.2
$n + {}_3^6Li \rightarrow {}_2^4He + {}_1^3H$	4.8	0.7

Reactions listed in Table 36 can be easily accomplished. The only condition for the first four reactions to occur is that the deuterons and protons must have a sufficiently high energy (about 0.1 MeV) to overcome the Coulomb barrier. As regards the last reaction, it can be induced even by thermal neutrons. The only problem is to make these reactions self-sustained.

Let us recall the process of energy liberation in fission reactions. A neutron enters uranium nucleus which fissions and emits secondary neutrons. These neutrons enter new uranium nuclei which also undergo fission, and so on. As a result (if the number of neutrons

generated is larger than the number of neutrons absorbed), an exponential growth of the process is observed. Thus, in a self-sustained fission process, the nuclear fuel (uranium) is available in a sufficient quantity from the very beginning, while the neutrons required for "igniting" this fuel are produced during the reaction. It is a scheme of a chain fission reaction. Another type of fission, viz. nonchain reaction, is possible and can be considered as a single act if a large amount of uranium is irradiated at the same time by a high-intensity neutron flux (hydrogen bomb with a uranium shell).

The nature of fusion reactions is similar to the second process. The liberation of a large amount of energy in this case is ensured by a simultaneous participation of a large number of nuclei in the process. As has been mentioned above, all these nuclei must have a very high kinetic energy. The idea of a self-sustained fusion reaction involves the creation of high-energy particles at the expense of the reaction heat. If a gas of light nuclei, say, deuterons, is heated to a fairly high temperature, T, the kinetic energy $E = kT$ of the thermal motion of these nuclei can become comparable with the height of the Coulomb barrier.[1] This leads to the creation of favourable conditions for effective interaction of nuclei, accompanied by the release of a large amount of energy which, in turn, causes a further heating of the deuteron gas. Thus, fast deuterons are obtained in this scheme due to heat which is generated as a result of interaction between fast deuterons. It can be stated that in a way, the heat involved in this process plays the role of neutrons in a fission chain reaction. Hence reactions of this type are called thermonuclear reactions. Unlike in fission reactions, the neutrons produced in the thermonuclear reactions of the type $(d + d)$ or $(d + t)$ do not take part in the process. These neutrons can be used for obtaining useful energy.

It was mentioned in Sec. 6.7 that a large number of difficulties had to be overcome before putting into practice the simple idea of a fission chain reaction. The self-sustained fusion reaction also has its own problems which must be overcome. It can be easily calculated that heating to a temperature of 10^9° is required to obtain an average energy $E = 0.1$ MeV. At such (and even lower) temperatures, matter is in a state of completely ionized plasma, i.e. in the form of a mixture of nuclei (without electron shells) and electrons.[2] Plasma

---

[1] For the sake of convenience, we shall denote kinetic energy as E in this section.

[2] In general, plasma is a gas in which a considerable part (5-10%) of atoms is ionized. Plasma is the normal state of matter at temperatures of about 10^4°, just as solids, liquids and gases are normal forms of matter at lower temperatures. This is the fourth state of matter and is encountered in nature even more frequently than the remaining forms. The percentage of ionized atoms increases with temperature and at $T = (2\text{-}3) \times 10^4$°, the gas is almost com-

has some specific properties which must be taken into account while considering the problem of self-sustained fusion reactions.

Plasma components have a high kinetic energy and hence have a tendency to fly apart and carry energy with them. This gives rise to the problem of confining a plasma over a sufficiently long time. Plasma is hot and hence cannot be contained by conventional means in a reactor vessel. This raises the problem of isolating plasma from the reactor walls. Plasma consists of nuclei and electrons, and on account of the small mass of the electrons, the exchange of energy between nuclei and electrons takes place in small quantities. However, fast electrons lose energy through bremsstrahlung and synchrotron radiation. To compensate for these losses and to obtain an excess positive energy, a high density (10^{14}-10^{16} cm^{-3}) of the plasma is required. Finally, it is clear from general considerations that the relative losses decrease with increasing size of the reactor. Hence a thermonuclear reactor must have a large size in order to sustain an effective reaction.

Thus, a high temperature, a fairly long period of confinement of plasma, a reliable insulation, a high density and a large size of the reactor are the main features of a self-sustained fusion reaction. Let us consider these parameters in three different versions of self-sustained fusion, two of which (the Sun and the hydrogen bomb) are already in existence while the third (controlled thermonuclear fusion) has not been realized so far in practice.

13.2. Thermonuclear Reaction in the Sun and in a Hydrogen Bomb

To explain the glow of the Sun, Bethe proposed two cycles in 1938. These are the proton-proton and the carbon-nitrogen cycle. The principal chain[3] of the first cycle can be represented as follows:

$$\left.\begin{aligned} &2(p+p\to d+e^{+}+\nu),\\ &2(d+p\to {}^{3}\mathrm{He}+\gamma),\\ &{}^{3}\mathrm{He}+{}^{3}\mathrm{He}\to {}^{4}\mathrm{He}+2p. \end{aligned}\right\} \qquad (13.2.1)$$

This boils down to a transformation of protons into helium nuclei, accompanied by the liberation of a large amount of energy:

$$6p\to {}^{4}\mathrm{He}+2p+2e^{+}+2\nu+2\gamma, \qquad Q=26\ \mathrm{MeV}. \qquad (13.2.2)$$

---

pletely ionized, i.e. consists of ions (mainly single charged) and electrons, and does not contain any neutral components. Further increase in temperature leads to an increase in the fraction of doubly charged, triply charged, etc. ions, until a temperature of about 10^{7}°, when the gas is completely ionized, i.e. consists of a mixture of bare nuclei (stripped of all electron shells) and electrons.

[3] In other possible versions of the proton-proton cycle, the third reaction is replaced by several other reactions.

The first reaction, for which $T_{1/2} = 1.4 \times 10^{10}$ years, is the slowest reaction in the proton-proton cycle. Hence, in spite of the large value of Q, the energy liberation per unit mass of the proton-proton cycle is very low: $q = 2$ erg/(g·s). This is lower than even the energy liberation per unit mass of a human organism. However, by virtue of its enormous mass (2×10^{33} g), the Sun continuously emits a huge amount of energy, equivalent to the loss of mass $\Delta m = 4.3 \times 10^6$ t/s.

The carbon-nitrogen cycle is represented by a chain of six reactions, in which the ^{12}C nucleus serves as a catalyst:

$$\begin{aligned}
&^{12}C + p \rightarrow {}^{13}N + \gamma,\\
&^{13}N \rightarrow {}^{13}C + e^+ + \nu,\\
&^{13}C + p \rightarrow {}^{14}N + \gamma,\\
&^{14}N + p \rightarrow {}^{15}O + \gamma,\\
&^{15}O \rightarrow {}^{15}N + e^+ + \nu,\\
&^{15}N + p \rightarrow {}^{12}C + {}^4He\\
&\overline{4p \rightarrow {}^4He + 2e^+ + 2\nu + 3\gamma,\ Q = 23\text{MeV}.} \qquad (13.2.3)
\end{aligned}$$

The net result of this chain is practically the same as of the first chain. However, the carbon-nitrogen cycle has a much smaller characteristic time $T_{1/2} = 3 \times 10^8$ years, determined by the fourth reaction in the cycle.

Both cycles involve the production of neutrinos which can be detected on the Earth. From the number of neutrinos registered in the solar radiation, it can be concluded that the proton-proton cycle is the more likely process in the Sun, although the question assumes significance in view of the unexpectedly small number of neutrinos arriving on the Earth surface (see Sec. 5.4.5, Vol. II).

While considering the thermonuclear reaction in the Sun, it could be assumed that most of the problems listed at the end of the last section do not exist for this reaction. Indeed, the solar plasma is confined by the gravitational field and does not require any isolation; the density of the plasma is very high ($\rho \simeq 100$ g/cm^3 at the centre); and the energy losses are insignificant on account of the huge size (1.4×10^6 km) of the Sun.

The only problem requiring a detailed investigation is the temperature of the Sun. At first glance, the temperature appears to be too low for a thermonuclear reaction to take place. Indeed, the temperature at the centre of the Sun is estimated at $T^\circ = 14 \times 10^6$, corresponding to an average kinetic energy $\overline{E} = kT = 1.2$ keV of the protons. This is lower than the height of the Coulomb barrier $B_C \simeq 0.5$ MeV by more than two orders of magnitude. For such a low ratio $\overline{E}/B_C$, a reaction between nuclei is practically impossible under laboratory conditions. Hence the possibility of its occurrence

in the Sun can be questioned. The solution to this dilemma is provided by the fact that the energy spectrum of the plasma reveals the existence of particles with $E > \overline{E}$. The interaction of these particles determines the yield of the thermonuclear reaction.

This is schematically shown in Fig. 316. Here, $f = E \exp(-E/kT)$ is the Maxwellian curve for the flux of plasma particles with an average energy $\overline{E} = kT$; $\sigma(E)$ is the reaction cross section, and $J(E)$ is the reaction yield. It can be seen from the figure that for $E = \overline{E} = kT$, the reaction yield J is indeed equal to zero. However, in view of the sharp increase in the cross section, the product $f\sigma$ becomes nonzero for a certain effective energy $E_{eff} > \overline{E}$. It can be stated that the reaction yield in this energy region is determined by the tail of the Maxwellian curve. It is worth noting that due to the specific shape of the cross section curve (i.e. the Coulomb barrier), the ratio $\varepsilon = E_{eff}/\overline{E}$ is quite large at temperatures close to the temperature of the Sun, and decreases rapidly with increasing temperature. The value of E_{eff} can be determined as follows:

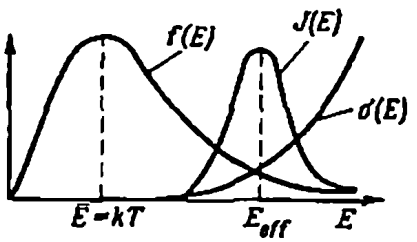

Fig. 316

$$f = E\exp(-E/kT) = \frac{\mu v^2}{2}\exp(-\mu v^2/2kT), \qquad (13.2.4)$$

$$\sigma = \pi\lambda^2 D = \frac{\pi\hbar^2}{\mu^2 v^2} D \qquad (13.2.5)$$

(at low energies), where

$$D = \exp(-2\pi Zze^2/\hbar v) \qquad \text{[see formula 9.1.7)]},$$

$$J = f\sigma = A\exp[-\varphi(v)], \qquad (13.2.6)$$

where

$$\varphi(v) = av^2 + b/v, \quad A = \pi\hbar^2/2\mu, \quad a = \mu/2kT, \quad b = 2\pi Zze^2/\hbar.$$

It is obvious from the shape of the function $\varphi(v)$ that it has a minimum at a certain $v = v_{eff}$. Consequently, the function $J = A\exp[-\varphi(v)]$ has a maximum. The position of this maximum is determined from the condition $d\varphi/dv = 0$:

$$v_{eff} = (b/a)^{1/3} = \left(\frac{2\pi Zze^2 kT}{\hbar\mu}\right)^{1/3}, \qquad \varphi(v_{eff}) = \frac{3}{2}\left(\frac{4\pi^2 Z^2 z^2 e^4 \mu}{\hbar^2 kT}\right)^{1/3}.$$

Thus,

$$J_{eff} = A\exp[-\varphi(v_{eff})] = A\exp(-C/T^{1/3}), \qquad (13.2.7)$$

where

$$C = \frac{3}{2}\left(\frac{4\pi^2 Z^2 z^2 e^4 \mu}{\hbar^3 k}\right)^{1/3}$$

and

$$E_{\text{eff}} = \frac{\mu v_{\text{eff}}^2}{2} = \frac{\mu}{2}\left(\frac{\pi Z z e^2 2kT}{\hbar\mu}\right)^{2/3}. \qquad (13.2.8)$$

Calculations made for a $(d + d)$-reaction yield the value

$$\varepsilon = E_{\text{eff}}/kT = 6.3T^{-1/3}, \qquad (13.2.9)$$

where T is in keV.

Table 37

T, keV	$\varepsilon = E_{\text{eff}}/kT$	E_{eff}, keV	T, keV	$\varepsilon = E_{\text{eff}}/kT$	E_{eff}, keV
0.125	12.6	1.58	27	2.1	56.7
1.0	6.3	6.3	64	1.58	101.0
8	3.15	25.2	125	1.26	158

The dependences $\varepsilon(T)$ and $E_{\text{eff}}(T)$ are shown in Table 37 and in Fig. 317. It can be seen that for the solar temperature $T = 14 \times 10^6 = 1.2$ keV, the energy gain $\varepsilon = E_{\text{eff}}/kT = 5.9$, i.e. $E_{\text{eff}} = 7.1$ keV. This energy is found to be sufficient for a fusion reaction to take place under conditions prevailing in the Sun. The fusion reaction in the Sun is characterized by a steady (continuous) regime.

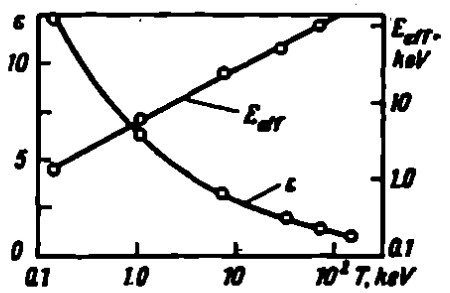

Fig. 317

The situation is quite different for a hydrogen bomb. Here, everything is determined by the problem of a rapid liberation of the fusion energy during a time $\tau = 10^{-6}$ s. Naturally, this circumstance simplifies the problems of confinement, thermal insulation, size and density. Insulation is just not required, since the plasma cannot become cold in 10^{-6} s; a premature flight can be prevented by using a solid shell (say, of uranium which also significantly increases the energy yield on account of its fission by fast neutrons); a high density and a small size are ensured by using a solid fuel,

say, *lithium deuteride* $^6Li^2H$. *Finally, a preliminary heating* to about 10^7° is provided by exploding an atomic bomb.

Apparently, the main reactions that determine a rapid liberation of energy in a hydrogen bomb are

$$^6Li + n \rightarrow {}^4He + {}^3H \qquad Q = 4.8\,MeV, \qquad (13.2.10)$$

$$^3H + {}^2H \rightarrow {}^4He + n, \qquad Q = 17.6\,MeV. \qquad (13.2.11)$$

These two reactions sort of sustain each other, and keep the number of neutrons and of ^3H nuclei constant. These particles are initially produced as a result of two other (slower) reactions:

$$^2H + {}^2H \rightarrow {}^3He + n. \qquad Q = 3.3\,MeV, \qquad (13.2.12)$$

$$^2H + {}^2H \rightarrow {}^3H + p, \qquad Q = 4.0\,MeV. \qquad (13.2.13)$$

Besides, neutrons are also produced during the explosion of the *atomic bomb.*

The hydrogen bomb explosion is a self-sustained thermonuclear reaction of transient type.

13.3. The Problem of Controlled Thermonuclear Fusion

Controlled fusion is much more difficult to realize than the self-sustained explosion reactions. The difficulties arise due to the fact that a sufficient energy gain (say, 100 W/cm^3) in controlled fusion requires heating of a concentrated plasma to a very high temperature (deuterium-tritium plasma with $n \simeq 10^{14}$ cm^{-3} to $T \simeq 10^8$°, or deuterium plasma with $n = 10^{16}$ cm^{-3} to $T = 10^9$°), and confining this plasma in such a state for a sufficiently long time τ within the volume of the thermonuclear reactor. The confinement time is determined by the energy content Q of the plasma, and by the energy losses W (due to heating of the walls, electron bremsstrahlung, neutron emission, etc.):

$$\tau = Q/W. \qquad (13.3.1)$$

The smaller the losses, the longer the confinement time.

The reaction intensity is determined by the product $n\tau$, called the confinement parameter (the higher the plasma density, the shorter the time required for a given number of nuclei to interact). For the energy released in a thermonuclear reactor to exceed the energy consumed, Lawson's criterion must be satisfied. This criterion involves a definite combination of the confinement parameter $n\tau$ and temperature T.

According to the latest estimates, the Lawson criteria for a deuterium-tritium plasma and a pure deuterium plasma are respectively

$$\left.\begin{aligned} n\tau &= (2\text{-}3)\times 10^{14}\ \text{cm}^{-3}\cdot\text{s}, \quad T = 10^{8}\,^{\circ},\\ n\tau &= 10^{16}\ \text{cm}^{-3}\cdot\text{s}, \quad T = 5\times 10^{8}\,^{\circ}. \end{aligned}\right\} \qquad (13.3.2)$$

The problem of obtaining controlled fusion reactions can in principle be solved in four ways:

(1) prolonged ($\tau \geqslant 0.1$ s) heating of a dense ($n \geqslant 10^{15}$ cm^{-3}) deuterium-tritium plasma in the reactor at a temperature of about $10^{8}\,^{\circ}$;

(2) superfast (about 10^{-9} s) heating of very small volumes of condensed thermonuclear materials;

(3) μ-catalysis, and

(4) hybrid atomic-thermonuclear reactor.

At present, the first of these methods is believed to be the most promising; hence we shall discuss it in detail.

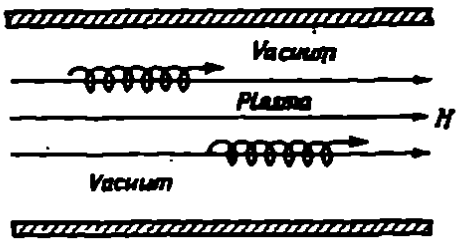

Fig. 318

The main difficulty involved in this method is a prolonged confinement of a dense high-temperature plasma within the reactor volume under conditions of thermal insulation. Hot plasma behaves as a highly compressed gas. In other words, the plasma moving inside the closed volume of the reactor will inevitably come in contact with the walls and get cooled by transferring heat to them (or melt and evaporate them, as in the case of a hydrogen bomb).

To confine plasma without letting it come in contact with the walls of the reactors, a method was proposed by Soviet scientists in 1950 and by American scientists in 1951, to concentrate plasma with the help of a magnetic field. All the components of a plasma (ions and electrons) are charged particles, hence they will move in a magnetic field in helical trajectories coiled round the lines of force of the magnetic field H (Fig. 318). Consequently, by confining the plasma to a hermetically sealed chamber with an appropriate magnetic field (magnetic trap), it can be expected that the plasma will move in this chamber without touching the walls. The pressure of the plasma will be perceived by the magnetic field, and in turn by the rigid construction of the current-carrying coils creating this

magnetic field. The condition for the confinement of plasma is that the magnetic pressure must exceed the plasma pressure:

$$H^2/8\pi > 2nkT. \qquad (13.3.3)$$

This condition can be satisfied for $n \leqslant 10^{17}$ cm^{-3}.

Various types of devices were constructed over nearly four decades that have elapsed since the investigations on controlled thermonuclear reactions were started. First devices for obtaining strongly heated plasma employed the discharge of condenser batteries of large capacitances (linear pinch effect). In this case, the magnetic field confining and heating plasma (by compression) is created by the discharge current flowing along the plasma column. This method led to the creation of a fairly hot (10^6 °) and dense (10^{12}-10^{13} cm^{-3}) plasma in which even neutrons (although of nonthermonuclear type) were observed. However, the solution of this problem posed another very serious problem, viz. that of the instability of plasma.

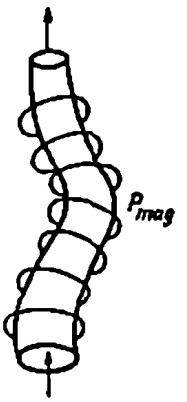

Fig. 319

The initial plasma column is found to be in a sort of unstable equilibrium with respect to compression and bending. Under the action of internal forces, the plasma rapidly (in about 10^{-6} s, at best in 10^{-4} s) gets deformed, breaks down and spreads to the reactor walls, where it quickly gets cooled (Fig. 319). In such a short time, a sufficient amount of thermonuclear energy cannot be liberated for maintaining the temperature, and hence the self-sustained process is not possible in this case. Attempts to obtain a stable hot plasma in devices for investigating the theta-pinch effect, i.e. heating of a plasma by its compression with the help of an increasing external magnetic field, also proved futile. In this case, the existence of a plasma at a high temperature and a large density is limited to a few microseconds due to its instability.

Similar difficulties were encountered in many other investigations aimed at the production of thermonuclear energy in a controlled process. However, a significant advancement was made in this direction in 1960s. In 1963, a group of scientists led by L.A. Artsimovich were able to produce at the Kurchatov Atomic Energy Institute a plasma with temperature 4×10^7 ° and density 10^{10} cm^{-3}, and to sustain it for a few hundredths of a second (up to 0.06 s) in a volume of tens of litres. This was made possible with the help of a toroidal magnetic trap with combined magnetic fields. Later, these devices

came to be known as Tokamaks (toroidal chamber with a stabilizing magnetic field). The parameters of plasma produced in 1968 in Tokamak-3, were $n\tau = 3\times10^{11}$ cm^{-3}·s and $T = 3\times10^{6}$°. Thermonuclear neutrons were obtained with the help of this device. In 1970, the parameters of the plasma generated in Tokamak-4 were improved to $n\tau = 6\times10^{11}$ cm^{-3}·s and $T = 4\times10^{6}$°.

Tokamaks began to be constructed in all countries engaged in fusion research by the beginning of the 1970s. Investigations carried out in these devices led to the conclusion that the plasma confinement time increases with the size of the device. Hence an improvement in the characteristics of the plasma requires Tokamaks of increased dimensions. This conclusion was finally confirmed in 1975 at the Atomic Energy Institute in Moscow, where Tokamak-10 with the following characteristics was constructed: power 200 MW, magnetic field strength up to 50 kOe, plasma volume 5 m^3 (larger radius 150 cm, smaller radius 39 cm), plasma current up to 800 kA, $T = (12\text{-}13)\times10^{7}$°, $\tau = 0.06\text{-}0.07$ s, $n = (7\text{-}8)\times10^{13}$ cm^{-3}, $n\tau = 6\times10^{13}$ cm^{-3}·s, neutron flux $(4\text{-}3)\times10^{9}$ neutrons/s. From the experiments carried out on T-10, it became clear that the size of the device must be enlarged by a factor of 4-5 in order to obtain the required values of $n\tau$ and T.

A temperature of 6×10^{7}° and $n\tau = 10^{13}$ cm^{-3}·s were obtained with the help of the PLT device (similar to Tokamak) built at Princeton (USA) in 1978. Tokamak-7 was commissioned in 1979 at the Moscow Atomic Energy Institute and had parameters similar to those of T-10. However, T-7 requires smaller amounts of energy for plasma confinement, since it utilizes superconducting systems for creating the toroidal magnetic field.

The next task is to create a demonstration reactor of the Tokamak type with such parameters that the fusion energy released in such a device is roughly equal to the energy imparted to the plasma. It is proposed to use such devices to demonstrate the feasibility of self-sustained fusion reactions and to carry out numerous investigations on plasma physics, heating technique, materials science, fuel regeneration, etc. For this purpose, it is proposed to construct Tokamak-15 (T-15) in the Soviet Union with a plasma volume of about 25 m^3 (larger radius 2.4 m, smaller radius 0.7 m). However, like its predecessors, T-15 will also serve as an experimental test bed for investigating the properties of plasma. To create a working model of a thermonuclear power plant, a device with a plasma volume of several hundred cubic metres is required.

The project for such a device (Tokamak-20) was worked out in the USSR in the 1970s. According to this project, this will be a very powerful (several hundred megawatts), complex and expensive device whose construction will require a lot of efforts and resources. In view of the fact that other developed countries also have their

Later, the followers of Zavoiskii led by L.I. Rudakov designed a high-power demonstration unit Angara-5 consisting of 48 modules of the Angara-1 type. The first module was constructed in September 1979. The new unit should generate more power than what will be required to put it into operation.

The third method for obtaining controlled fusion is the μ-catalysis of a thermonuclear reaction. This involves the initiation of fusion reactions through the formation of neutral systems of the type of μ-atoms and μ-molecules of a very small size (about 5×10^{-11} cm) which can come close to such an extent that nuclear interaction becomes possible through a tunneling transition (without heating). This is accompanied by the emission of a muon which can participate in a similar process with another nucleus, and so on. Thus, muon plays the role of a catalyst in this process, and hence the name of the method.

The process of μ-catalysis was first discussed as early as in 1947. However, it was shown shortly afterwards that the process is quite unsuitable from a practical point of view due to a low rate of μ-catalysis at low temperatures. The interest to this problem was renewed after it was shown by theoretical physicists at Dubna that a resonance acceleration of the μ-catalysis is possible with increasing temperature. In 1979, V.P. Dzhelepov and coworkers provided an experimental confirmation of this prediction. These experiments raised the hope that during its short lifetime (2.2×10^{-6} s), each muon will be able to interact about 100 times with nuclei, thus causing a liberation of energy comparable with the energy spent in the creation of the muon itself. Detailed investigations are being undertaken at present to prove the validity of this assumption.[4]

Finally, the fourth method of obtaining a fusion reaction is the creation of a hybrid thermonuclear-atomic reactor. The underlying idea is to use a natural uranium blanket as one of the components. Fast neutrons formed in a thermonuclear reaction will cause fission of ^{238}U nuclei, thus sharply increasing the output of the reactor. It can be assumed that the atomic part of the hybrid reactor will supply about 75-80% of the power, thus leaving only 20-25% power required from the thermonuclear part. Thus, a hybrid reactor can be constructed with less exacting design and plasma parameters. The fuel for such a reactor can be not only natural uranium, but even uranium depleted in the ^{235}U isotope, which is obtained as nuclear waste in atomic reactors.

The thermonuclear programme in the USSR is under the overall supervision of E.P. Velikhov.

---

[4] See Sec. 5.7.1, Vol. II for details on μ-catalysis

13.4. A Brief Resumé of Chapter 13

In this chapter, we have discussed the possibility of achieving self-sustained fusion of light nuclei, fusion reaction in the Sun and in a hydrogen bomb, as well as the problem of controlled thermonuclear fusion.

It is well known that the binding energy per nucleon in light nuclei increases with mass number. Hence the fusion of light nuclei is advantageous from the energy point of view and must be accompanied by the liberation of energy. The condition for the fusion process to take place is that the interacting nuclei must have a sufficiently high energy to overcome the Coulomb barrier. This energy can be obtained in the form of the energy of thermal motion as a result of a very intense heating.

Since the process of fusion is accompanied by the liberation of a very large amount of energy, a self-sustained thermonuclear reaction is theoretically possible for a large number density of the interacting nuclei. In this case, the thermal motion of the interacting nuclei is maintained due to the reaction energy, and the reaction is sustained due to the thermal motion of the interacting nuclei.

The temperature required for such reactions is determined by the size of the interacting system and the number density of the nuclei. Thus, the thermonuclear reaction in the Sun takes place at a temperature of about 1.4×10^7 °. An explosive thermonuclear reaction (hydrogen bomb) can be realized under terrestrial conditions at about the same temperature.

A much higher temperature (10^8-10^9 °) is required for controlled thermonuclear reactions. At such high temperatures, matter is in the state of hot and completely ionized plasma which consists exclusively of charged particles. The problem of realizing a controlled thermonuclear reaction is very complicated since it requires the generation of a dense, hot and long-lived plasma suspended inside an evacuated reactor of a limited size without coming in contact with the walls.

Estimates show that the thermonuclear reaction in a deuterium-tritium plasma heated to $T = 10^8$ ° will be advantageous from the energy point of view if $n\tau \geqslant (2\text{-}3) \times 10^{14}$ cm^{-3}·s, where n is the number density of the nuclei and τ is the confinement time for plasma in the reactor (in seconds). For a pure deuterium plasma, $T = 10^{8*}$, and $n\tau \geqslant 10^{15}$ cm^{-3}·s. The following plasma parameters were obtained in 1976 in Tokamak-10 device having a plasma volume of 5 m^3: $T = 1.3 \times 10^{7*}$, $n\tau = 5 \times 10^{13}$ cm^{-3}·s.

At present, Tokamak-15 with a plasma volume of 25 m^3 is under construction in the USSR. It is proposed to demonstrate the feasibility of a self-sustained fusion reaction on this unit. Besides, some fundamental investigations on plasma physics are also planned on this device. Tokamaks of the next generation will have a plasma volume of several hundred cubic metres and will serve as working models of thermonuclear power plants (T-20 project in the USSR and international project INTOR).

The second possible mechanism of releasing thermonuclear energy involves a superhigh rate (about 10^{-9} s) of all-round heating of miniaturized solid deuterium-tritium targets by high-power laser or electron beams. Other possible means of achieving controlled fusion are μ-catalysis and a hybrid reactor.

Appendix

I. Basic Formulas

1. $E = \sqrt{m^2c^4 + p^2c^2} = \frac{mc^2}{\sqrt{1-\beta^2}} = mc^2 + T,$

where E is the total energy, m is the mass, c is the velocity of light, $p = \frac{m\beta c}{\sqrt{1-\beta^2}}$ is the relativistic momentum, $\beta = v/c$, v is the velocity, $T = mc^2\left(\frac{1}{\sqrt{1-\beta^2}} - 1\right)$ is the relativistic kinetic energy.

2. $p^2c^2 = T(2mc^2 + T)$.

3. $\tau = \tau_0/\sqrt{1-\beta^2}$,

where τ_0 is the lifetime of the particle in the state of rest, and τ is the lifetime of the particle moving at a velocity β.

4. $E^2 - P^2c^2 = \text{inv}$,

where E is the total energy and P is the total momentum of a system of particles.

5. The equivalent energy of two particles with mass m having an energy T' in colliding beams:

$$T = 2mc^2\,[(1 + T'/mc^2)^2 - 1].$$

6. The uncertainty relations

$$\Delta E\,\Delta t \simeq \hbar,$$

$$\Delta r\,\Delta p \simeq \hbar.$$

7. The de Broglie wavelength for a nucleon

$$\lambda_N = 4.5 \times 10^{-13}/\sqrt{T},$$

where λ is in cm and T is in MeV.

8. Fine-structure constant

$$a = e^2/\hbar c = r_e/\lambda\!\!\!^{-}_{\text{Com}} \simeq 1/137,$$

where e is the electron charge, r_e is the classical radius of the electron and $\lambda\!\!\!^{-}_{\text{Com}}$ is the Compton wavelength of the electron.

9. The height of the Coulomb barrier (in MeV) for a particle with charge z relative to a nucleus with charge Z:

$$B_C = Zze^2/R \simeq Zz/A^{1/3}.$$

10. The height of centrifugal barrier (in MeV) for a nucleon relative to a nucleus with mass number A for a mutual angular momentum l:

$$B_0 = \hbar^2 l\,(l-1)/2mR^2 \simeq 10l\,(l+1)/A^{2/3}.$$

11. The law of radioactive decay:

$$N = N_0 \exp(-\lambda t),$$

where λ is the disintegration constant. The average lifetime $\tau = 1/\lambda$; the half-life

$$T_{1/2} = \ln 2/\lambda \simeq 0.69\tau.$$

12. Weizsäcker's formula

$$\Delta W = \alpha A - \beta A^{2/3} - \gamma \frac{Z^2}{A^{1/3}} - \zeta \frac{\left(\frac{A}{2} - Z\right)^2}{A} + \delta A^{-3/4},$$

where $\alpha = 15.75$ MeV, $\beta = 17.8$ MeV, $\gamma = 0.71$ MeV, $\zeta = 94.8$ MeV, $|\delta| = 34$ MeV,

$$\delta = \begin{cases} -|\delta| & \text{for even-even nuclei,} \\ 0 & \text{for odd nuclei,} \\ -|\delta| & \text{for odd-odd nuclei,} \end{cases}$$

A is the mass number and Z is the atomic number of the nucleus.

13. The Breit-Wigner formula for radiative capture and scattering of neutrons:

$$\sigma(n, \gamma) = A\pi\lambda^2 \frac{\Gamma_n \Gamma_\gamma}{(T - T_0)^2 + (\Gamma/2)^2},$$

$$\sigma(n, n) = A\pi\lambda^2 \frac{\Gamma_n^2}{(T - T_0)^2 + (\Gamma/2)^2},$$

where $A = \frac{2J+1}{(2I+1)(2s+1)}$, I, J, and s are the spins of the target nucleus, compound nucleus and the neutron respectively, λ is the de Broglie wavelength, Γ_n is the neutron width, Γ_γ is the radiation width, and T_0 is the resonance energy.

14. The nuclear radius

$$R = r_0 A^{1/3},$$

where $r_0 = (1.2\text{-}1.4) \times 10^{-13}$ cm.

15. The threshold of an endoergic reaction

$$T_{\min} = \frac{M+m}{M} |Q|,$$

where M is the mass of the nucleus, m is the mass of the bombarding particle, and Q is the reaction energy.

16. The Pauli matrices

$$\sigma_x = \begin{pmatrix} 0 & 1 \\ 1 & 0 \end{pmatrix}, \quad \sigma_y = \begin{pmatrix} 0 & -i \\ i & 0 \end{pmatrix}, \quad \sigma_z = \begin{pmatrix} 1 & 0 \\ 0 & -1 \end{pmatrix},$$

$$\hat{1} = \begin{pmatrix} 1 & 0 \\ 0 & 1 \end{pmatrix}, \quad \hat{0} = \begin{pmatrix} 0 & 0 \\ 0 & 0 \end{pmatrix}.$$

17. The γ-matrices

$$\gamma_1 = \begin{pmatrix} \hat{0} & \sigma_x \\ -\sigma_x & \hat{0} \end{pmatrix}, \quad \gamma_2 = \begin{pmatrix} \hat{0} & \sigma_y \\ -\sigma_y & \hat{0} \end{pmatrix},$$

$$\gamma_3 = \begin{pmatrix} \hat{0} & \sigma_z \\ -\sigma_z & \hat{0} \end{pmatrix}, \quad \gamma_4 = \begin{pmatrix} \hat{1} & \hat{0} \\ \hat{0} & -\hat{1} \end{pmatrix},$$

$$I = \begin{pmatrix} \hat{1} & \hat{0} \\ \hat{0} & \hat{1} \end{pmatrix}, \quad 0 = \begin{pmatrix} \hat{0} & \hat{0} \\ \hat{0} & \hat{0} \end{pmatrix}.$$

II. Basic Constants and Units *

1. The classical electron radius

$$r_e = e^2/m_e c^2 = 2.8 \times 10^{-13} \text{ cm}.$$

2. The Compton wavelength of the electron wave

$$\lambda\!\!\!^{-}{}_e^{\text{Com}} = \hbar/m_e c = 3.85 \times 10^{-11} \text{ cm}.$$

3. The Compton wavelength of the π-meson wave

$$\lambda\!\!\!^{-}{}_\pi^{\text{Com}} = \hbar/m_\pi c \simeq 1.4 \times 10^{-13} \text{ cm}.$$

4. The Compton wavelength of a nucleon wave

$$\lambda\!\!\!^{-}{}_N^{\text{Com}} = \hbar/m_N c \simeq 0.2 \times 10^{-13} \text{ cm}.$$

5. The nuclear time

$$\tau_{\text{nuc}} \simeq a/c = 1.4 \times 10^{-13}/(3 \times 10^{10}) \simeq 0.5 \times 10^{-23} \text{ s},$$

where a is the range of nuclear forces and c is the velocity of light.

6. Planck's constant

$$\hbar = 1.054 \times 10^{-27} \text{ erg·s} = 6.6 \times 10^{-16} \text{ eV·s}.$$

* Approximate values of the units and constants are given.

7. The velocity of light in vacuum

$$c \simeq 3 \times 10^{10} \text{ cm} \cdot \text{s}^{-1}.$$

8. The weak-interaction constant

$$g = 1.4 \times 10^{-49} \text{ erg} \cdot \text{cm}^3.$$

9. The atomic radius

$$R_{at} \simeq 10^{-8} \text{ cm}.$$

10. The nuclear radius

$$(2\text{-}8) \times 10^{-13} \text{ cm}.$$

11. The Bohr magneton

$$M_B = \frac{e}{m_e c} \frac{\hbar}{2} = 9.27 \times 10^{-21} \text{ erg/G}.$$

12. The nuclear Bohr magneton

$$\mu_B = \frac{e}{m_p c} \frac{\hbar}{2} = \frac{M_B}{1836} = 5.05 \times 10^{-24} \text{ erg/G}.$$

13. The neutron mass

$$m_n \simeq 1838.6 m_e = 1.008665 \text{ amu} = 939.55 \text{ MeV}.$$

14. The proton mass

$$m_p \simeq 1836.1 m_e = 1.007276 \text{ amu} = 938.26 \text{ MeV}.$$

15. The electron mass

$$m_e \simeq 9.1 \times 10^{-28} \text{ g} = 0.511 \text{ MeV}.$$

16. The electron charge

$$e \simeq 4.8 \times 10^{-10} \text{ CGSE units}.$$

17. The proton magnetic moment

$$\mu_p = 2.79 \mu_B.$$

18. The neutron magnetic moment

$$\mu_n \simeq -1.91 \mu_B.$$

19. The electron magnetic moment

$$\mu_e \simeq 1 M_B.$$

20. The energy of a thermal neutron

$$T_{therm} = kT^\circ$$

($kT^\circ \simeq 1/40$ eV at room temperature).

where M is the mass of the nucleus, m is the mass of the bombarding particle, and Q is the reaction energy.

16. The Pauli matrices

$$\sigma_x = \begin{pmatrix} 0 & 1 \\ 1 & 0 \end{pmatrix}, \quad \sigma_y = \begin{pmatrix} 0 & -i \\ i & 0 \end{pmatrix}, \quad \sigma_z = \begin{pmatrix} 1 & 0 \\ 0 & -1 \end{pmatrix},$$

$$\hat{1} = \begin{pmatrix} 1 & 0 \\ 0 & 1 \end{pmatrix}, \quad \hat{0} = \begin{pmatrix} 0 & 0 \\ 0 & 0 \end{pmatrix}.$$

17. The γ-matrices

$$\gamma_1 = \begin{pmatrix} \hat{0} & \sigma_x \\ -\sigma_x & \hat{0} \end{pmatrix}, \quad \gamma_2 = \begin{pmatrix} \hat{0} & \sigma_y \\ -\sigma_y & \hat{0} \end{pmatrix},$$

$$\gamma_3 = \begin{pmatrix} \hat{0} & \sigma_z \\ -\sigma_z & \hat{0} \end{pmatrix}, \quad \gamma_4 = \begin{pmatrix} \hat{1} & \hat{0} \\ \hat{0} & -\hat{1} \end{pmatrix},$$

$$I = \begin{pmatrix} \hat{1} & \hat{0} \\ \hat{0} & \hat{1} \end{pmatrix}, \quad 0 = \begin{pmatrix} \hat{0} & \hat{0} \\ \hat{0} & \hat{0} \end{pmatrix}.$$

II. Basic Constants and Units *

1. The classical electron radius

$$r_e = e^2/m_e c^2 = 2.8 \times 10^{-13} \text{ cm}.$$

2. The Compton wavelength of the electron wave

$$\lambda\!\!\!^{-}{}_e^{\text{Com}} = \hbar/m_e c = 3.85 \times 10^{-11} \text{ cm}.$$

3. The Compton wavelength of the π-meson wave

$$\lambda\!\!\!^{-}{}_\pi^{\text{Com}} = \hbar/m_\pi c \simeq 1.4 \times 10^{-13} \text{ cm}.$$

4. The Compton wavelength of a nucleon wave

$$\lambda\!\!\!^{-}{}_N^{\text{Com}} = \hbar/m_N c \simeq 0.2 \times 10^{-13} \text{ cm}.$$

5. The nuclear time

$$\tau_{\text{nuc}} \simeq a/c = 1.4 \times 10^{-13}/(3 \times 10^{10}) \simeq 0.5 \times 10^{-23} \text{ s},$$

where a is the range of nuclear forces and c is the velocity of light.

6. Planck's constant

$$\hbar = 1.054 \times 10^{-27} \text{ erg·s} = 6.6 \times 10^{-16} \text{ eV·s}.$$

* Approximate values of the units and constants are given.

Index

Actinides, 538
adiabatic demagnetization, 232
alpha decay, 173, 178, 186
americium, 526f
angle, mean multiple scattering, 317f
angular momentum
  intrinsic, 18, 75
  orbital, 91, 94, 98, 112, 368ff
  total, 178
antineutrino, 20, 214
  electron, 214
  muon, 215
atom(s), muonic, 66
atomic mass unit, 630

Backbending, 591
balance,
  alpha decay, 32, 36
  beta decay, 32, 37
barrier,
  fission, 468
  potential, 189f, 197
    centrifugal, 192f, 282, 547, 565
      height of, 369f
      penetrability, 282, 435
    Coulomb, 188, 282, 286, 364, 369f, 376, 379, 419, 546, 548, 551, 571, 605f, 611ff, 625
      height of, 626
      penetrability, 189
    penetrability, 546
  two-humped, 500, 520
baryons, 25
berkelium, 527f
beta decay, 204ff
  half-life, 237
  of neutrons, 237
  types of, 204
beta spectrometer, 209
beta spectrum, 209f
beta stability track, 42
Born approximation, 309
Bohr magneton, 18, 71
bremsstrahlung, 336, 353
Butler analysis, 575

Californium, 527f
capture,
  ϵ-, 21, 166, 205, 213f, 287, 505
  K-, 27
  radiative, of neutrons, 378
  resonance, of slow neutrons, 407, 478ff
charge,
  baryon, 27, 357
  electric, 26, 28, 357, 629
  nuclear, 28
chemical (isomeric) shift of nuclear levels, 273
C-invariance, violation of, 230
cluster(s), 581
coefficient,
  internal conversion, 252
  Mössbauer, 267
  transmission, 409
constant,
  beta interaction, 228
  Boltzmann, 630
  disintegration, 169f
  fine-structure, 623
  Gamow-Teller interaction, 239
  Planck, 628
  Rydberg, 16
  weak-interaction, 629
Coulomb excitation of nucleus, 355
Coulomb mixing, 374
counter,
  Geiger-Müller, 493
  Cherenkov, 331
  gaseous, 333
critical size, 471
cross section, differential effective, 308
  macroscopic, 309
Curie plot, 227
curium, 526f

Debye temperature, 268ff
decay,
  alpha, 166, 286
  beta, 166
  of K-mesons, 290
  $(\mu\text{-}e)$, 290
  $(\pi\text{-}\mu)$, 290
  proton, 278
    isomeric, 278, 281
delayed protons, 280
deuteron, 19
diagram,
  energy, 359ff
  momentum, 303f, 306, 353, 403
    for nuclear reactions, 364ff
dipole(s), 102
Dirac monopole, 12, 299
direct proton emission, 606
Doppler broadening, 259f, 267
Doppler shift, 259
Doppler width, 264f

Effect,
  Cherenkov, 330, 354
  Compton, 250, 290, 326, 344f, 347
    inverse, 348, 353
  cumulative, 599f
  density, 291
  Doppler, 262
  magnetocaloric, 232
  Mössbauer, 24, 74, 251, 258, 262ff, 269ff, 286, 288
  Paschen-Back, 76
  photoelectric, 250, 290f, 326, 338, 352, 354, 604, 611
  relativistic, 291
  shadow, 572, 589
  Zeeman, 76
    normal, 17
einsteinium, 528f
electrons
  Auger, 252, 288, 338
  Compton, 250f, 330
  delta-, 313ff
  internal conversion, 255
energy,
  of adhesion, 53
  alpha decay, 285
  average binding, per nucleon, 630
  average fission, of heavy nuclei, 630
  beta decay, 207, 223
  Coulomb, 116, 462, 460
  critical, 322, 353
  excitation, 31, 360, 508
    of compound nucleus, 570
  Fermi, 162
  fission, 456, 461f
    distribution of, 513
    utilization of, 470
  interaction, 72, 74f
  kinetic, of fission fragments, 457
  nuclear binding, 26, 41f, 45, 51f, 60, 63, 109, 117f, 122f, 125, 136, 163
    of deuterons, 604
    per nucleon, 42, 55, 119
  pairing, 57, 162
  reaction, 35, 358, 378
  relativistic kinetic, 30
  resonance, 479
  rest, 19, 29f
  separation, 511ff
    average, 55
    neutron, 56
    proton, 58
  of thermal neutron, 629
energy balance, 32
energy surface, 42f
equation,
  Dirac relativistic, 69, 594
  energy balance, 35, 403
  Hartree-Fock-Bogolyubov, 593
  Schrödinger, 95, 140, 163, 230
    one-dimensional, 452
    time-dependent, 97
  secular, 172
experiment,
  Chadwick, 40
  Cherenkov, 326
  Fermi, 383, 433
  Flyorov, 531
  Geiger and Marsden, 310
  Ghiorso, 531
  Ghoshal, 564
  Mössbauer, 261f
  Rutherford, 19, 131
  Stern and Gerlach, 76ff, 87
  Wu, 231

Factor
  Debye-Waller, 268
  forbiddenness, 197
  multiplication, for fast neutrons, 470, 480
  projection, 106
  structural amplification, 275
  thermal utilization, 480
fermium, 528f
fission, 50f
  by fast particles, 494
fission
  delayed, 166, 503

spontaneous, 59, 166
fission asymmetry, 494, 510
fission fragments, 50
force(s)
Coulomb, 122, 292, 302, 340, 465, 584
repulsion, 135
gravitational, 302
long-range, 302
nuclear, 44ff, 53, 302
saturation of, 122
formation of electron-positron pair, 348ff, 354
formula,
Bohr, for specific ionization, 291
Breit-Wigner, 412, 417f, 421, 431, 627
Born, 445
Fermi, 319
four-factor, 480
Klein-Nishina-Tamm, 346, 353
Mott, 311ff, 353
Rutherford, 307ff, 314, 353
Thomson scattering, 610
Weisskopf, 249
Weizsäcker semiempirical, 122, 126, 132, 136, 627
function, excitation, for reaction, 550
fusion,
controlled, 618, 624f
self-sustained, 612f, 625

Gamma-quanta, instantaneous, 493
gyromagnetic ratio, 71, 81, 88, 92

Half-life, 167, 627
hypothesis,
charge independence of nuclear forces, 111
charge symmetry of nuclear forces, 110
neutrino, 209ff

interaction,
Coulomb, 15, 222, 314, 320, 585
of charged particles with nuclei, 545
repulsive, 135
electromagnetic, 13, 25, 88, 95, 104, 114, 289f, 300, 352
electroweak, 12f
of gamma radiation with matter, 336, 351f
gravitational, 289
of heavy ions with nuclei, 591ff, 595ff
at relativistic energies, 597
internucleonic, 277
of neutrons with matter, 336ff
of neutrons with nuclei, 376ff
types of, 378ff
nuclear, 355ff
direct, 567
nucleon-nucleon, 12
pairing, 161
of particles and radiation with matter, 289ff
residual, 162, 164
spin-orbital, 120
strong, 25, 95, 104, 289, 352
tensor, 108
weak, 13, 24f, 104, 289f, 352
intrinsic line width, 258
ion-exchange chromatography, 523
isobar(s), 28, 43
isomerism, nuclear, 253, 258f, 288
isomerism islands, 164, 257
isotone(s), 28, 43
isotope(s), 28, 43
isotopic invariance, 113

Kurchatovium, 534f

Lanthanides, 538
Larmor frequency, 80, 85
Larmor precession, 80, 82
Law,
conservation,
of angular momentum, 113
of baryon number, 375
of electric charge, 357ff, 375
of energy, 19, 40, 358f, 375, 576
of isotopic spin, 116, 119, 178, 357, 373, 375
of momentum, 19, 212f, 304f, 358f, 375, 578
of parity, 119, 178, 200, 231, 284, 371ff, 375, 560, 580
Geiger-Nuttall, 62, 182, 184f, 196, 286
Law
Moseley, 310
1/v-, 392, 419, 431, 433, 453, 550
of radioactive decay, 169, 286, 411, 621
lawrencium, 534

Lawson criterion, 618
length,
  diffusion, 403
  radiation, 322
  scattering, 445
  slowing-down, 400, 404
lethargy of neutrons, 387
Loss(es),
  ionization, 291, 353
    for charged particles, 548
    dependence on medium, 296
    for monopole, 300
  radiation, for electrons, 319ff
  specific, 293

Magic numbers, 48, 185, 630
magneton,
  Bohr, 90, 629
  nuclear, 88, 629
mass,
  atomic, 29
  critical, 471
  electron, 629
  excess, 46
  neutron, 39, 41, 629
  nuclear, 29, 32
  nucleonic, 29
  proton, 41, 629
  relativistic, 29f
  rest, 29
mass defect, 46
mass number, 26f
mass spectrometer, 34
  Aston, 32
  Dempster, 33
mass spectrometry, 32
mendelevium, 529f
method,
  annular scattering, 438
  boron absorber, 432
  coincidence, 181
  crystal monochromator, 428ff
  magnetic resonance, 79f, 85
  mechanical monochromator, 421, 453
  mechanical selector, 423ff
  mechanical transport, 588
  molecular beam deflection, 76f
  perturbation theory, 101
  photoemulsion, 379
  projection, 588
  pulsed accelerator, 426ff
  Rabi, 79
  radiofrequency, 79f
  resonance absorption, 262
  Robson, 238
  Rose-Gorter, 231
  Szilard-Chalmerson, 383
  T, ΔT, 586
  time-of-flight, 420, 426
microwave radiospectroscopy, 37f
migration area, 405
model,
  of atom,
    Bohr, 441
    nuclear, 15f
    Rutherford, 15
    Thomson, 15, 309
  beta decay, 221
  nuclear,
    α-particle, 48, 583
    collective, 120
    electron-proton, 18f
    Fermi, 68, 120, 132, 135, 163
    four-quark, 13, 25
    generalized, 148f, 159f, 164
    independent-particle, 47, 49, 60, 132f, 161, 165
    liquid drop, 120, 123, 125, 127, 129, 132, 155, 163, 165, 185f, 407, 500
    optical, 121, 440ff, 454
    Schmidt one-nucleon, 87, 91, 94
    shell, 120, 133, 135f, 138, 140f, 145f, 148, 151, 155, 159, 163ff, 199, 247
    single-particle, 121, 147
    superfluid, 163, 165
  statistical, of compound nucleus, 116
moderating ratio, 402
moderation of neutrons, 383
moderator, 389f, 397, 399, 452
moment
  electric,
    dipole, 102ff
    quadrupole, 26, 28, 101f, 104ff, 117f, 136, 145, 148, 151, 154, 159f
  magnetic, 18f, 28
    dipole, 77
    effective, 92
    of electron, 71, 629
    of neutron, 83, 85, 629
    nuclear, 79, 89, 94f
    of nucleons and nuclei, 69ff, 92
    orbital, 89
    of proton, 70, 629
monochromator,
  mechanical, for neutrons, 421f
  Dunning, 421, 425
  gravitational, 450
μ-catalysis, 13, 624
multibaryon collisions, 600

p-nucleonic atoms, 13
muon(s), 23f

Neptunium family, 542
neutrino, 20f, 23, 211ff
  electron, 24, 214
  mass of, 24, 215
  muon, 24, 215
neutron(s),
  cold, 391, 453
  delayed, 474
  epicadmium, 394, 453
  epithermal, 391
  fast, 480
  fission, 405, 457, 460, 472, 498ff, 507, 520
  instantaneous, 520
  polarized, 88
  resonance, 393, 433, 453
  secondary, 457, 472, 481
  slow, 391, 394, 453
    diffraction by crystal, 428
  thermal, 40, 390f, 403
    diffusion of, 402f
  ultracold, 430, 444, 446ff, 454
neutron spectroscopy, 412, 431, 453
"nitrogen catastrophe", 89
nobelium, 530f
nuclear Fermi gas, 133ff
  degenerate, 135
nuclear fission, 455ff, 519
  cross section of, 477
  fragments of, 455ff, 484ff, 509
  induced, 519
  mechanism of, 463
  spontaneous, 467f, 496ff, 519
nuclear state,
  stationary, 410
  metastable, 410
nuclear time, 628
nucleon(s), 20
nucleon shell, 49
nucleus (i),
  anomalous, 601ff
  β-radioactive, 44, 53, 204
  β-stable, 20, 44f, 54
  compound, 355, 361, 406, 562ff
    angular momentum of, 417
    energy distribution, 411ff
    formation cross section, 413f
    levels of, 407f
  double, 594
  double magic, 49, 133, 136, 163
  isobar, 114
  isomer, 145
  magic, 49, 133
  mirror, 46, 62, 110
  neutron-deficient, 596
  nucleon-stable, 53f
  recoil, 553
  superdense, 130f
nuclide, 28

Operator, polarization, 129

Parameter, impact, 590
parity, 26, 95ff, 117
  combined, violation of, 24
  conservation of, 13, 95ff, 104
  G-, 13
  intrinsic, 99
  invariance of, 103
  nonconservation, 230, 233f, 241, 277, 287
    in beta-transitions, 274f
    in fission, 510
Pauli spin matrices, 220, 628
pion(s), 23f
plasma confinement, 618f
plutonium, 524ff
positron, 20
potential,
  centrifugal, 193f, 199
  Coulomb, 191, 193, 309, 443, 549
  interaction, 194
  intermolecular, 24
  ionization, 293f
  Nilsson, 161
  nonspherical (elliptic), 164
principle,
  detailed balancing, 415f
  Pauli exclusion, 114, 123, 138ff, 219, 442, 594
probability,
  beta decay, 237, 240, 245
  disintegration, 170
    of compound nucleus, 407
  gamma radiation, 253
  of gamma transitions, 247, 249
  of magnetic transition, 249
  of photoeffect, 340
proton, 19
Quantum number, orbital, 119
quasiatoms, 594

Radiation,
  alpha, 166
  beta, 166
  Cherenkov, 290, 294, 325ff, 354